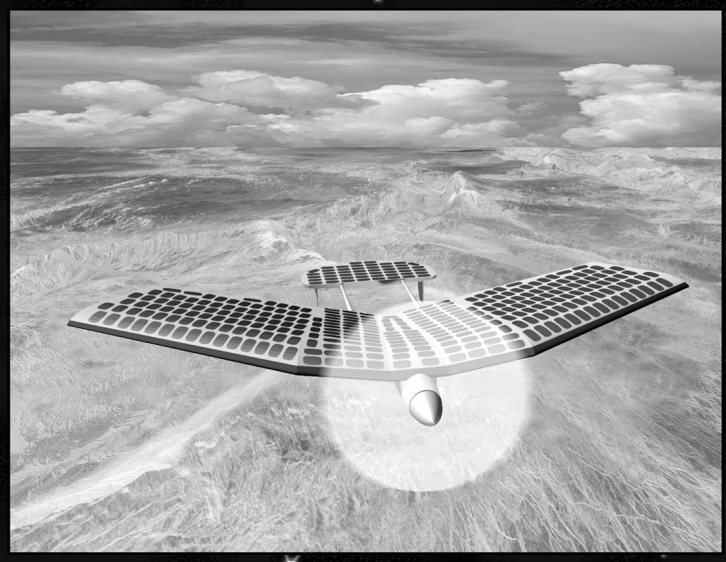

R&T

Research & Technology • 2003

NASA Glenn Research Center
at Lewis Field

Cleveland • Ohio

NASA/TM—2004-212729

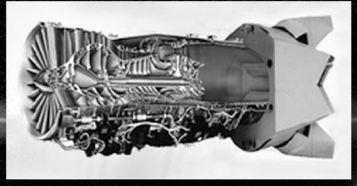

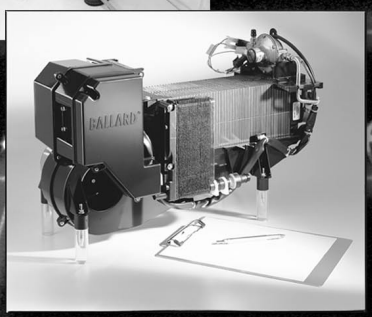

NASA

About the cover:

Top: Solar-powered Venus airplane shown over a computer-generated radar image of the surface of Venus. The surfaces of the wing and the horizontal tail are covered with solar cells. Artist's conception by Terence K. Condrich of InDyne, Inc.

Center: A prototype of the Hydrodynamic Focusing Bioreactor—Space (HFB–S) is free-floating inside NASA's KC–135 Reduced Gravity Research Aircraft. The HFB–S is being developed for possible use on the International Space Station to grow tissue cultures in microgravity.

Bottom left: NASA's Ultra-Efficient Engine Technology Project is developing and delivering revolutionary gas turbine propulsion technologies for increased performance and efficiency at the component or subsystem level, relying on strategic, cost-sharing partnerships and opportunities with the aerospace industry and other Government agencies for technology demonstration, maturation, and application. The engine shown here is a supersonic engine.

Bottom right: Fuel cells tested in conjunction with ultracapacitors as part of NASA's Hybrid Power Management (HPM) Program's emphasis in exploring new power applications.

Research & Technology 2003

National Aeronautics and
Space Administration

Glenn Research Center
Cleveland, Ohio 44135–3191

NASA/TM—2004-212729

Trade names or manufacturers' names are used in this report for identification only. This usage does not constitute an official endorsement, either expressed or implied, by the National Aeronautics and Space Administration.

Available from

NASA Center for Aerospace Information
7121 Standard Drive
Hanover, MD 21076

National Technical Information Service
5285 Port Royal Road
Springfield, VA 22100

Available electronically at http://www.grc.nasa.gov/WWW/RT

Introduction

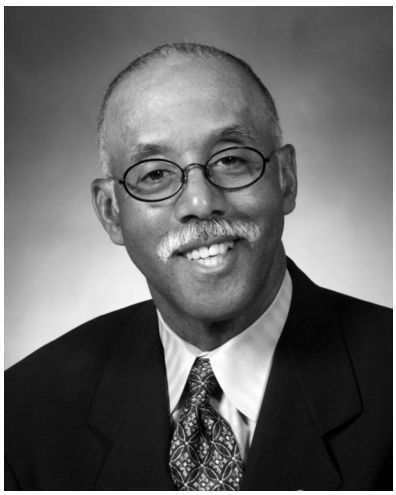

The NASA Glenn Research Center at Lewis Field, in partnership with U.S. industries, universities, and other Government institutions, is responsible for developing critical technologies that address national priorities in aeropropulsion and space applications. Our work is focused on research for new aeropropulsion technologies, aerospace power, microgravity science (fluids and combustion), electric propulsion, and communications technologies for aeronautics, space, and aerospace applications.

As NASA's premier center for aeropropulsion, aerospace power, and turbomachinery, our role is to conduct world-class research and to develop key technologies. We contribute to economic growth and national security through safe, superior, and environmentally compatible U.S. civil and military aircraft propulsion systems. Our Aerospace Power Program supports all NASA Enterprises and major programs, including the International Space Station, Advanced Space Transportation, and new initiatives in human and robotic exploration.

Glenn Research Center leads NASA's research in the microgravity science disciplines of fluid physics, combustion science, and acceleration measurement. Almost every space shuttle science mission has had an experiment managed by NASA Glenn, and we have conducted a wide array of similar experiments on the International Space Station.

The Glenn staff consists of over 3200 civil service employees and support service contractor personnel. Scientists and engineers comprise more than half of our workforce, with technical specialists, skilled workers, and an administrative staff supporting them. We aggressively strive for technical excellence through continuing education, increased diversity in our workforce, and continuous improvement in our management and business practices so that we can expand the boundaries of aeronautics, space, and aerospace technology.

Glenn Research Center is a unique facility located in northeast Ohio. Situated on 350 acres of land adjacent to the Cleveland Hopkins International Airport, Glenn comprises more than 140 buildings, including 24 major facilities and over 500 specialized research and test facilities. Additional facilities are located at Plum Brook Station, which is about 50 miles west of Cleveland. Plum Brook Station has four large, major, world-class facilities for space research available for Government and industry programs.

Knowledge is the end product of our activities. The R&T reports help make this knowledge fully available to potential users—the aircraft engine industry, the space industry, the energy industry, the automotive industry, the aerospace industry, and others. It is organized so that a broad cross section of the community can readily use it. Each article begins with a short introductory paragraph that should prove valuable for the layperson. These articles summarize the progress made during the year in various technical areas and portray the technical and administrative support associated with Glenn's technology programs.

We hope that this information is useful to all. If additional information is desired, readers are encouraged to contact the researchers identified at the end of each article and to visit Glenn on the World Wide Web at http://www.grc.nasa.gov.

Julian M. Earls
Director

NASA Glenn Research Center Senior Management

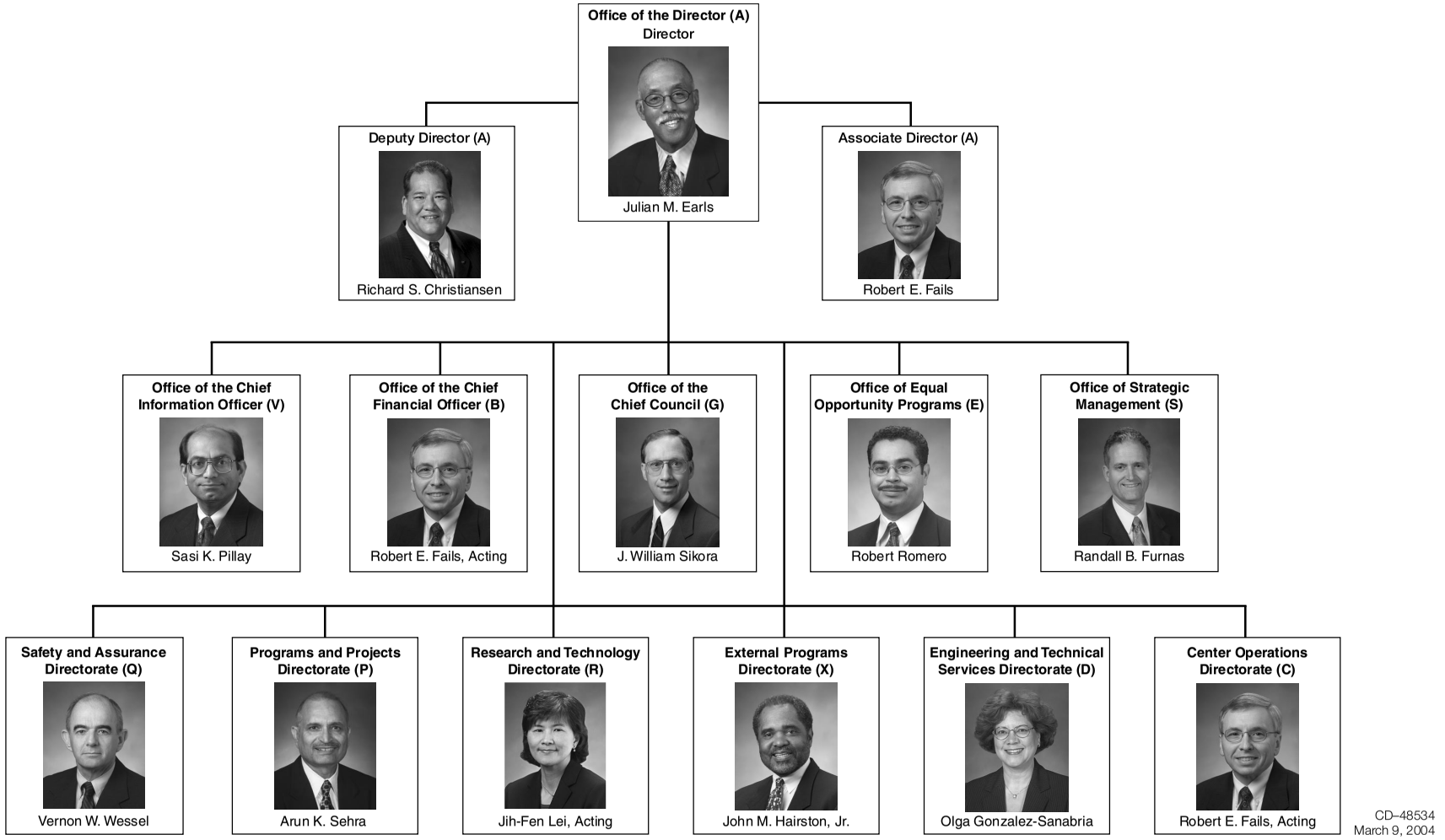

CD–48534
March 9, 2004

NASA Glenn Research Center at Lewis Field

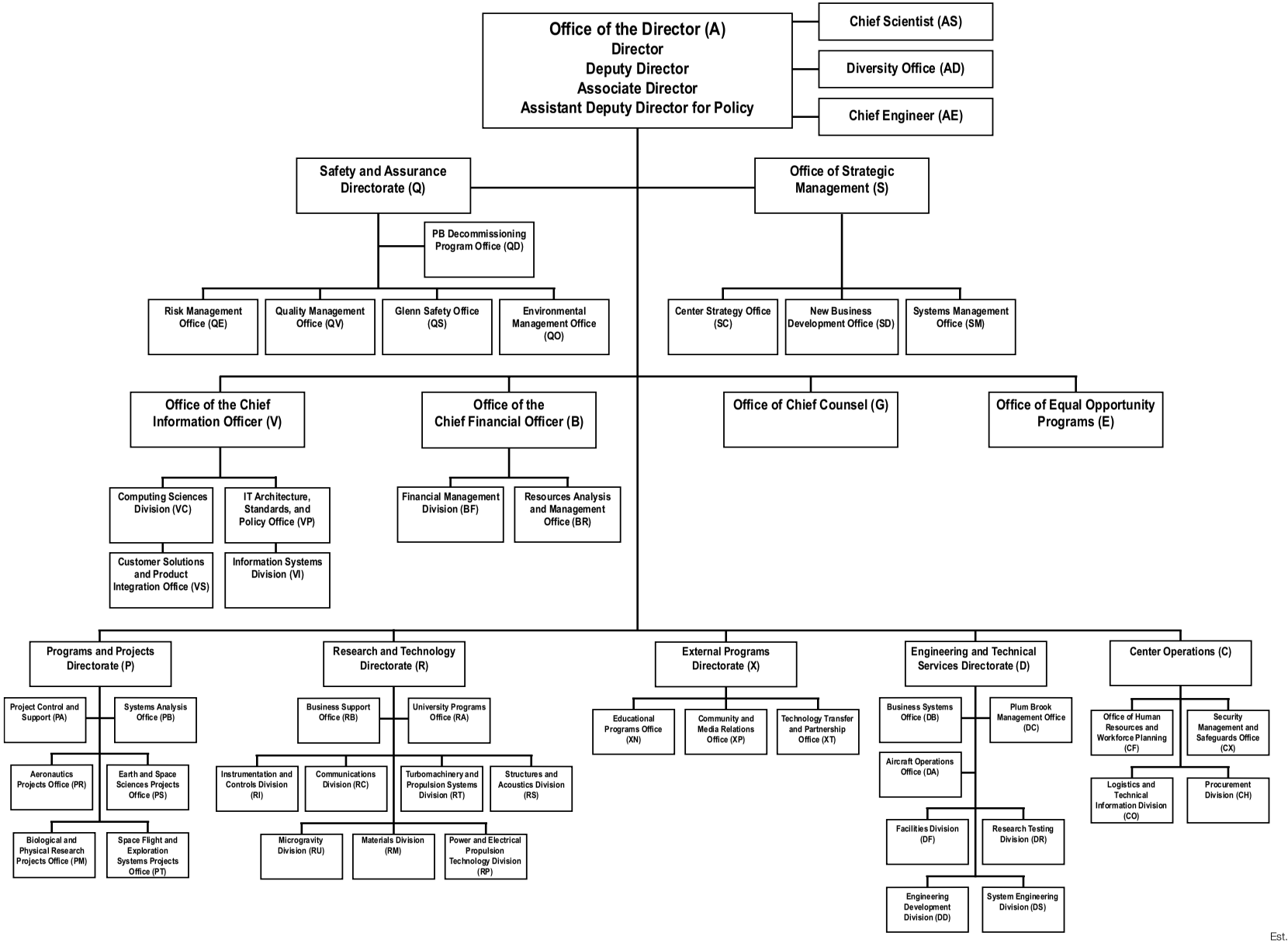

Est. 10–1–96
CD–44972
Rev. 3/25/04

Contents

Power and On-Board Propulsion Technology

Instrumentation and Controls

Communications Technology

Turbomachinery and Propulsion Systems

Structures and Acoustics

Space

Space Communications

Microgravity Science

Power and Propulsion

Engineering and Technical Services

Computer Services

Research Testing

Engineering Design and Analysis

Appendixes

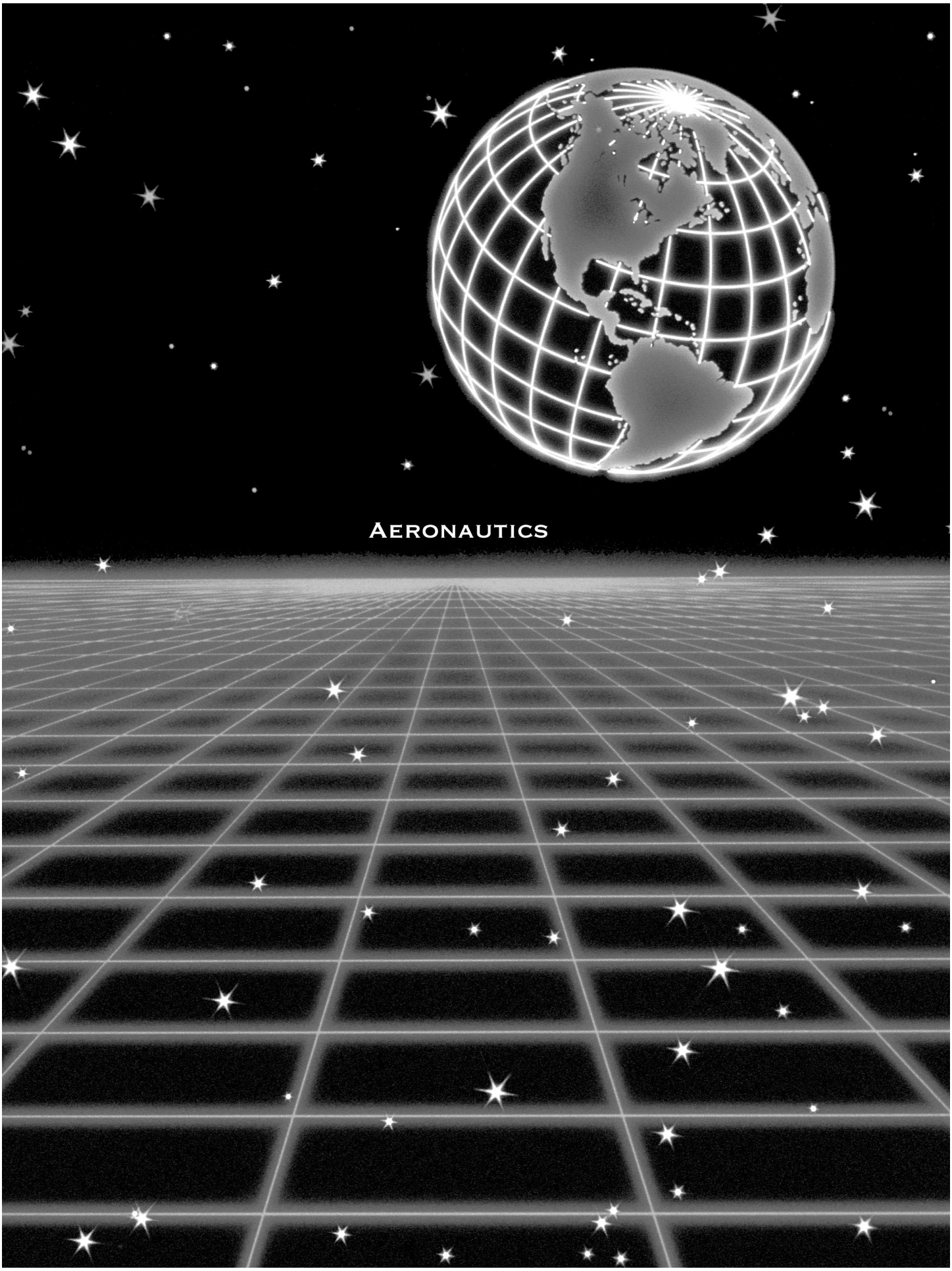
Aeronautics

Ultra-Efficient Engine Technology

Ultra-Efficient Engine Technology Project Integrated Into NASA's Vehicle Systems Program

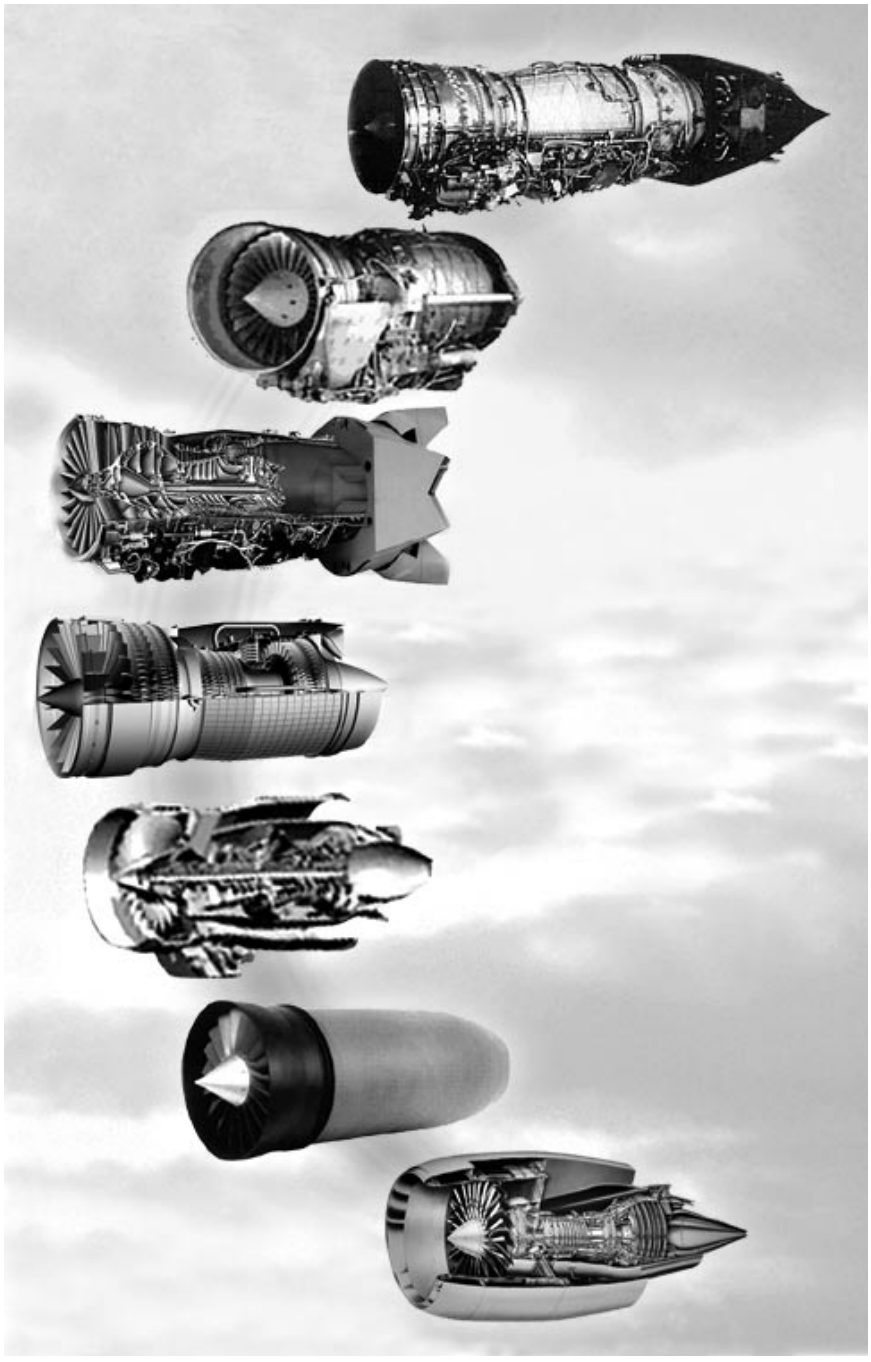

The UEET Project will develop and deliver revolutionary gas turbine propulsion technologies for increased performance and efficiency at the component or subsystem level, relying on strategic, cost-sharing partnerships and opportunities with the aerospace industry and other Government agencies for technology demonstration, maturation, and application.

The Ultra-Efficient Engine Technology (UEET) Project is formulated according to the Office of Aerospace Technology's objectives as outlined in the NASA Strategic Plan. It is directly related to the "protect the environment" objective and will make progress toward the "increase mobility" and "support national security" objectives as well. UEET technologies will impact future civil and military aircraft and will benefit the development of future space transportation propulsion systems. UEET Project success will, therefore, depend on developing revolutionary, but affordable, technology solutions that are inherently safe and reliable and thus can be incorporated in future propulsion system designs.

In fiscal year 2003, UEET became part of NASA's Vehicle Systems Program and continues to evolve its programmatic role. The Vehicle Systems Program aims to develop breakthrough technologies and methodologies, push the boundaries of flight through research on advanced vehicle concepts, respond quickly to industry and the Department of Defense on critical safety and other issues, and provide facilities and expert consultation for industry and other Government agencies during product development.

UEET's two primary goals make it viable within this framework: (1) develop propulsion technologies that will increase system efficiency and, therefore, reduce fuel burn by up to 15 percent (with equivalent reductions in carbon dioxide emissions) and (2) develop combustor technologies (configuration and materials) that will reduce landing and takeoff emissions of nitrogen oxides by 70 percent relative to 1996 International Civil Aviation Organization (ICAO) standards.

Long-range scenarios developed under ICAO auspices foresee continuing worldwide growth for commercial aviation through the middle of the next century. Given the current constraints on growth due to noise and emissions, propulsion will play a lead role in finding viable solutions. Propulsion also will play a critical role in enabling advanced aircraft designs and concepts required to achieve dramatic improvements in efficiencies of operations. Today's engine designs are limited by both the overall cycle pressure ratio and turbine inlet temperature levels that can be achieved. Increases in both parameters will be required to improve performance and efficiency, as well as reduce global climate impact.

UEET addresses potential ozone depletion concerns by demonstrating enabling aircraft combustor technologies that have little or no discernable impact on the ozone layer during cruise operation (up to a 90-percent reduction). This project will enable the United States to be competitive in developing propulsion systems with very low emissions. In addition, UEET will address the potential of climate impact on long-term aviation growth by providing critical gas turbine propulsion technologies that will increase efficiency dramatically to enable carbon dioxide reductions, on the basis of an overall fuel savings goal of about 15 percent for large subsonic transport and as much as 8 percent for supersonic and/or small aircraft. Fuel savings represent significant cost benefits to the traveling public.

UEET has continued to place top priority on exploring and developing meaningful partnerships with Department of Defense programs such as the Integrated High Performance Turbine Engine Technology (IHPTET) and Versatile Affordable Advanced Turbine Engine (VAATE) programs. Strategic partnerships have also been formed with the Department of Energy, the Environmental Protection Agency, and the Federal Aviation Administration on technology development and technology requirements definition. These partnerships will enable each program to leverage relevant technologies being developed in other programs as well as provide opportunities for joint technology development.

The overall UEET project includes research efforts at the NASA Glenn Research Center, the NASA Langley Research Center, and the NASA Ames Research Center, as well as at the following partner organizations: Air Force Research Laboratory, Allison/Rolls-Royce, Boeing Commercial Airplane Company, GE Aircraft Engines, Georgia Institute of Technology, Gulfstream, Honeywell, Lockheed Martin Corporation, Pratt & Whitney, and Williams International.

Glenn contact:
Dr. Robert J. Shaw, 216–977–7135, Robert.J.Shaw@nasa.gov

InDyne, Inc., contact:
Barbara L. Kakiris, 216–433–2513, Barbara.L.Kakiris@grc.nasa.gov

Author: Dr. Robert J. Shaw, UEET project manager

Headquarters program office: OAT

Programs/Projects:
VSP, UEET, IHPTET, VAATE

Air-Breathing Systems Analysis

Performance of a Fuel-Cell-Powered, Small Electric Airplane Assessed

Rapidly emerging fuel-cell-power technologies may be used to launch a new revolution of electric propulsion systems for light aircraft. Future small electric airplanes using fuel cell technologies hold the promise of high reliability, low maintenance, low noise, and—with the exception of water vapor—zero emissions. An analytical feasibility and performance assessment was conducted by NASA Glenn Research Center's Airbreathing Systems Analysis Office of a fuel-cell-powered, propeller-driven, small electric airplane based on a model of the MCR–01 two-place kitplane (Dyn'Aéro, Darois, France). This assessment was conducted in parallel with an ongoing effort by the Advanced Technology Products Corporation and the Foundation for Advancing Science and Technology Education. Their project—partially funded by a NASA grant—is to design, build, and fly the first manned, continuously propelled, nongliding electric airplane.

In our study, an analytical performance model of a proton exchange membrane (PEM) fuel cell propulsion system was developed and applied to a notional, two-place light airplane modeled after the MCR–01 kitplane. The PEM fuel cell stack was fed pure hydrogen fuel and humidified ambient air via a small automotive centrifugal supercharger. The fuel cell performance models were based on chemical reaction analyses calibrated with published data from the fledgling U.S. automotive fuel cell industry. Electric propeller

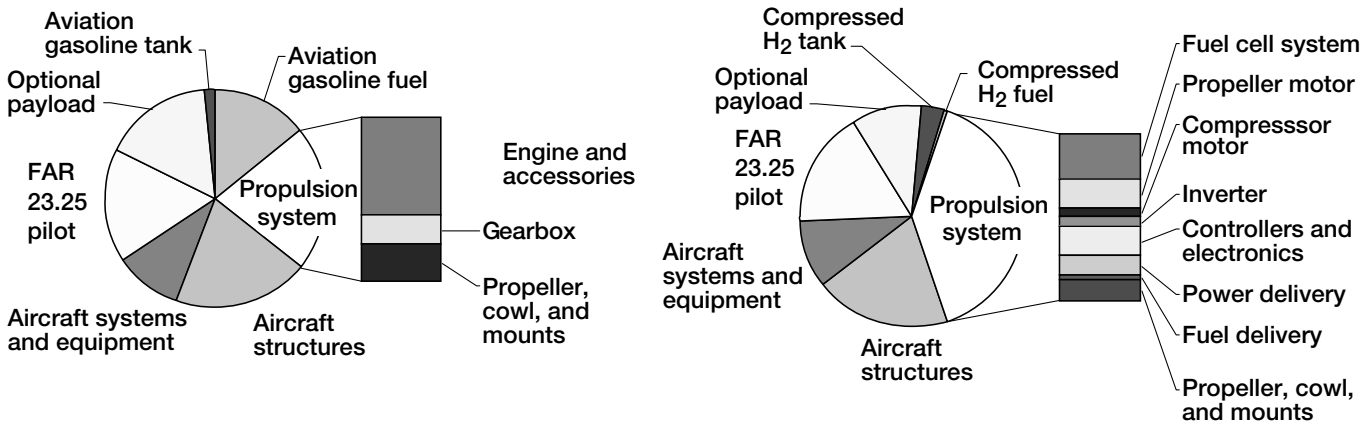

Takeoff gross weight breakdowns. Left: Conventional reciprocating-engine-powered airplane. Right: Fuel-cell-powered airplane. This figure is shown in color in the online version of this article (http://www.grc.nasa.gov/WWW/RT/2003/2000/2400berton.html).

motors, rated at two shaft power levels in separate assessments, were used to directly drive a two-bladed, variable-pitch propeller. Fuel sources considered were compressed hydrogen gas and cryogenic liquid hydrogen. Both of these fuel sources provided pure, contaminant-free hydrogen for the PEM cells.

Takeoff gross weight breakdowns are shown in the preceding pie charts for the conventional reciprocating-engine-powered MCR–01 (left), and for the fuel-cell-powered airplane (right). To reduce weight, designers sized the electric powerplant to provide much less power than for the original reciprocating engine. Such a small powerplant would result in lower airspeeds and ceilings, longer field lengths, and inferior climb rates; it is adequate only for a proof-of-concept, technology demonstration vehicle. Even so, the electric powerplant is much heavier than the reciprocating engine, in part because fuel cell technologies are not yet as mature as piston engine technologies.

The use of a payload-range diagram is one method to illustrate airplane performance as well as utility. These characteristics are shown in the following graph. The classic volume problem associated with most hydrogen vehicles applies here as well. Much more hydrogen fuel can be carried if it is stored as a liquid cryogen, resulting in greater range.

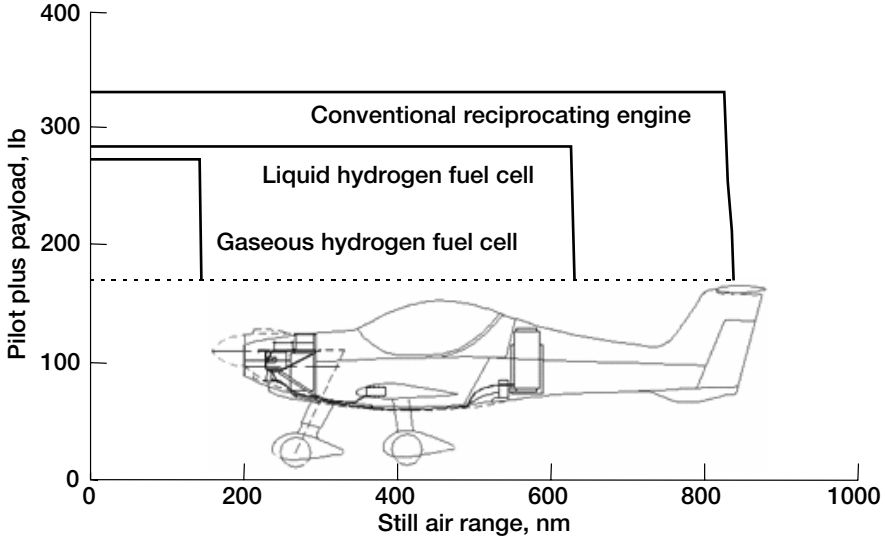

Payload-range performance diagrams for a fuel-cell-powered airplane equipped with compressed gaseous hydrogen fuel, a fuel-cell-powered airplane with cryogenic liquid hydrogen fuel, and a conventional reciprocating engine-powered airplane.

Electric flight appears possible using off-the-shelf fuel cell and power management technology levels, albeit at reduced speed, climb rate, range, and payload-carrying capability. Aircraft performance appears sufficient to fly a technology demonstration, proof-of-concept type vehicle using today's automotive-derived fuel cell and power systems. Only light aircraft are anticipated to be feasible with near-term technology because of their relatively low, automobile-like power requirements. Advanced fuel cell and power management technologies will be needed to achieve comparable reciprocating engine aircraft performance and utility and to enable the design of larger electric aircraft.

Find out more about this research:

Propulsion and Power Base Project:
http://www.grc.nasa.gov/WWW/AERO/base/psbase.htm

Fuel-celled-powered aircraft research:
http://gltrs.grc.nasa.gov/cgi-bin/GLTRS/browse.pl?2003/TM-2003-212393.html

Foundation for Advancing Science and Technology and Education:
http://www.fastecfund.org

Glenn contacts:
Jeffrey J. Berton, 216–977–7031, Jeffrey.J.Berton@nasa.gov;
Joshua E. Freeh, 216–433–5014, Joshua.E.Freeh@nasa.gov;
and Dean P. Petters, 216–433–6065, Dean.P.Petters@nasa.gov

Author: Jeffrey J. Berton

Headquarters program office: OAT

Programs/Projects: LEAP

Performance Benefits for a Turboshaft Engine Using Nonlinear Engine Control Technology Investigated

The potential benefits of nonlinear engine control technology applied to a General Electric T700 helicopter engine were investigated. This technology is being developed by the U.S. Navy SPAWAR Systems Center for a variety of applications. When used as a means of active stability control, nonlinear engine control technology uses sensors and small amounts of injected air to allow compressors to operate with reduced stall margin, which can improve engine pressure ratio. The focus of this study was to determine the best achievable reduction in fuel consumption for the T700 turboshaft engine. A customer deck (computer code) was provided by General Electric to calculate the T700 engine performance, and the NASA Glenn Research Center used this code to perform the analysis. The results showed a 2- to 5-percent reduction in brake specific fuel consumption (BSFC) at the three Sikorsky H–60 helicopter operating points of cruise, loiter, and hover.

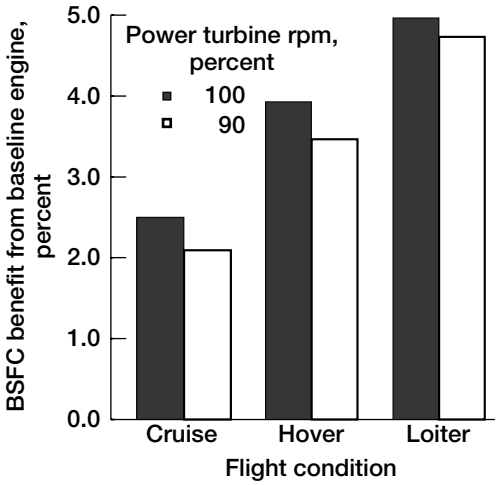

Improvement in brake specific fuel consumption (BSFC) at cruise, loiter, and hover for the T700 turboshaft engine using nonlinear engine control technology.

To simulate the technology, Glenn researchers varied the allowable flows into both the gas generator turbine and the power turbine to increase the compression system pressure ratio while maintaining gas generator revolutions per minute. In addition, the injected air could not be accurately modeled and thus was conservatively simulated by increasing the compressor bleed air extraction. Three engine operating conditions—cruise, loiter, and hover—were selected as being most relevant to the total fuel burn during a Sikorsky H–60 helicopter nominal mission. For these three operating points, the power turbine flow function was varied to maintain gas generator revolutions per minute at the baseline value as the stall margin changed. Shaft power output was also kept at the required (baseline) value for the flight condition.

The results show that the increased axial compressor pressure ratio (and by assumption, the decreased stall margin) allows an improvement in BSFC. The amount of the benefit appears to be inversely proportional to the power level or engine compression ratio—approximately 2.3 percent for cruise, 3.7 percent for hover, and 4.8 percent for loiter—as shown in the bar chart. The white and black bars indicate the relative BSFC benefit from the baseline value for output shaft speeds of 90 and 100 percent, respectively. The benefits shown include a 1-percent compressor bleed air penalty, but they are relatively insensitive to this amount of bleed. The combustor exit temperature was tracked during the study to see if it increased: varying the turbine flow scalars ultimately causes T4 to increase about 25 °C. This would be a potential concern at the cruise condition since the temperature is near its maximum at that point, perhaps requiring the use of the technology only at other conditions, such as hover and loiter.

Glenn contact:
Scott M. Jones, 216–977–7015,
Scott.M.Jones@nasa.gov

Author: Scott M. Jones

Headquarters program office: OAT

Programs/Projects: PR&T

Aeropropulsion Projects

Critical Low-Noise Technologies Being Developed for Engine Noise Reduction Systems Subproject

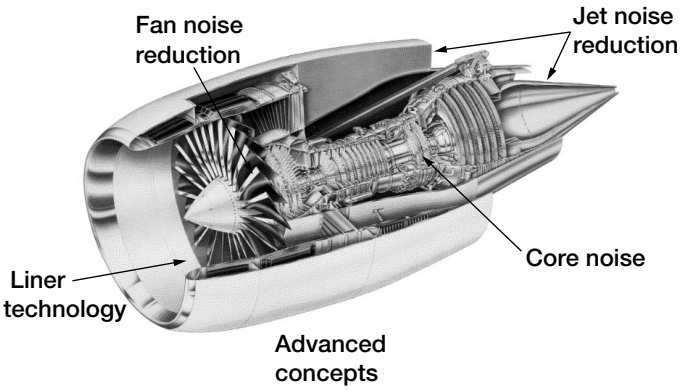

High-bypass-ratio turbofan engine cutaway showing the technology elements being pursued under the Engine Noise Reduction Systems (ENRS) subproject of the QAT project.

NASA's previous Advanced Subsonic Technology (AST) Noise Reduction Program delivered the initial technologies for meeting a 10-year goal of a 10-dB reduction in total aircraft system noise. Technology Readiness Levels achieved for the engine-noise-reduction technologies ranged from 4 (rig scale) to 6 (engine demonstration). The current Quiet Aircraft Technology (QAT) project is building on those AST accomplishments to achieve the additional noise reduction needed to meet the Aerospace Technology Enterprise's 10-year goal, again validated through a combination of laboratory rig and engine demonstration tests.

In order to meet the Aerospace Technology Enterprise goal for future aircraft of a 50-reduction in the perceived noise level, reductions of 4 dB are needed in both fan and jet noise. The primary objectives of the Engine Noise Reduction Systems (ENRS) subproject are, therefore, to develop technologies to reduce both fan and jet noise by 4 dB, to demonstrate these technologies in engine tests, and to develop and experimentally validate Computational Aero Acoustics (CAA) computer codes that will improve our ability to predict engine noise.

The ENRS subproject previously identified candidate fan- and jet-noise-reduction technologies with the potential to meet the QAT goal for engine noise reduction. ENRS is currently in a design-build-test phase that will culminate in engine (TRL 6) validation of these technologies in fiscal years 2006 to 2007, during which the noise-reduction benefit of each concept will be measured. In parallel with the development of noise-reduction technologies, more basic research is being conducted to understand the physics of engine noise sources. This work includes fan and jet source diagnostic tests as well as the development and application of advanced measurement technologies to characterize the flow fields in and around these components. These observations will be used to explain the physical mechanisms of dominant engine noise sources, and the test data will be used to validate CAA codes under development to predict fan and jet noise with increased accuracy and computational efficiency.

The ENRS subproject is organized into the five elements shown in the figure. The subproject includes research efforts at the NASA Glenn Research Center, the NASA Langley Research Center, and a number of universities and small businesses. The technologies under development will be accomplished in collaboration with GE Aircraft Engines, Pratt & Whitney, Honeywell, and Rolls Royce.

Glenn contact:
Dr. Joseph E. Grady, 216–433–6728, Joseph.E.Grady@nasa.gov

Authors: Dr. Joseph E. Grady and Kestutis C. Civinskas

Headquarters program office: OAT

Programs/Projects: VSP, QAT

Emerging Fuel Cell Technology Being Developed—Offers Many Benefits to Air Vehicles

Fuel cells, which have recently received considerable attention for terrestrial applications ranging from automobiles to stationary power generation, may enable new aerospace missions as well as offer fuel savings, quiet operations, and reduced emissions for current and future aircraft. NASA has extensive experience with fuel cells, having used them on manned space flight systems over four decades. Consequently, the NASA Glenn Research Center has initiated an effort to investigate and develop fuel cell technologies for multiple aerospace applications.

Two promising fuel cell types are the proton exchange membrane (PEM) and solid oxide fuel cell (SOFC). PEM technology, first used on the Gemini spacecraft in the sixties, remained unutilized thereafter until the automotive industry recently recognized the potential. PEM fuel cells are low-temperature devices offering quick startup time but requiring relatively pure hydrogen fuel. In contrast, SOFCs operate at high temperatures and tolerate higher levels of impurities. This flexibility allows SOFCs to use hydrocarbon fuels, which is an important factor considering our current liquid petroleum infrastructure. However, depending on the specific application, either PEM or SOFC can be attractive.

As only NASA can, the Agency is pursuing fuel cell technology for civil uninhabited aerial vehicles (UAVs) because it offers enhanced scientific capabilities, including enabling high-altitude, long-endurance missions. The NASA Helios aircraft demonstrated altitudes approaching 100,000 ft using solar power in 2001, and future plans include the development of a regenerative PEM fuel cell to provide nighttime power. Unique to NASA's mission, the high-altitude aircraft application requires the PEM fuel cell to operate on pure oxygen, instead of the air typical of terrestrial applications.

Fuel cells may also benefit conventional UAVs by providing greater power for payload and/or emergency backup. Adding power to current UAV platforms used for Earth science missions would allow more instrumentation, higher data-scan rates, and higher data-transmission rates to enhance scientific missions. Both PEM and SOFC are potential candidates, with SOFC offering the advantage of utilizing a single, conventional liquid fuel.

In addition, NASA is pursuing fuel cell technology for aircraft power generation on commercial transports. Power for systems necessary to fly the aircraft and accommodate passengers traditionally relies on auxiliary power units and power extracted from the main engines. Future commercial aircraft will incorporate more electric aircraft architectures and will use fuel cells. Challenges remain, however, to successfully apply the technology to commercial flight systems. Fuel processing is critical because the commercial transportation sector will depend on hydrocarbon fuel for the foreseeable future. High-temperature SOFCs are best suited because of the similarity in operating temperature with the fuel reformation process, and they enable hybrid configurations (SOFC and turboalternator) to increase efficiency. There are other challenges with unique aircraft requirements: improving the specific power of the stack, reducing the weight of the remaining components, and investigating flight-operation conditions.

Realizing the full benefits of fuel cells for aerospace applications will require a collaborative effort. Through workshops and technical/programmatic interchanges, Glenn has begun to facilitate and foster the required national partnership with the Department of Energy, the Department of Defense, State governments, academia, and the aerospace and fuel cell industries.

Glenn contacts:
Anita D. Liang, 216–977–7439, Anita.D.Liang@nasa.gov; and
Dr. Gary T. Seng, 216–433–3732, Gary.T.Seng@nasa.gov

Authors: James F. Walker and Kestutis C. Civinskas

Headquarters program office: OAT

Programs/Projects: VSP, LEAP

Computing and Interdisciplinary Systems

NASA Ground-Truthing Capabilities Demonstrated

NASA Research and Education Network (NREN) ground truthing is a method of verifying the scientific validity of satellite images and clarifying irregularities in the imagery. Ground-truthed imagery can be used to locate geological compositions of interest for a given area. On Mars, astronaut scientists could ground truth satellite imagery from the planet surface and then pinpoint optimum areas to explore. These astronauts would be able to ground truth imagery, get results back, and use the results during extravehicular activity without returning to Earth to process the data from the mission.

NASA's first ground-truthing experiment, performed on June 25 in the Utah desert, demonstrated the ability to extend powerful computing resources to remote locations. Designed by Dr. Richard Beck of the Department of Geography at the University of Cincinnati, who is serving as the lead field scientist, and assisted by Dr. Robert Vincent of Bowling Green State University, the demonstration also involved researchers from the NASA Glenn Research Center and the NASA Ames Research Center, who worked with the university field scientists to design, perform, and analyze results of the experiment.

As shown in the following figure, real-time Hyperion satellite imagery (data) is sent to a mass storage facility, while scientists at a remote (Utah) site upload ground spectra (data) to a second mass storage facility. The grid pulls data from both mass storage facilities and performs up to 64 simultaneous band ratio conversions on the data. Moments later, the results from the grid are accessed by local scientists and sent directly to the remote science team. The results are used by

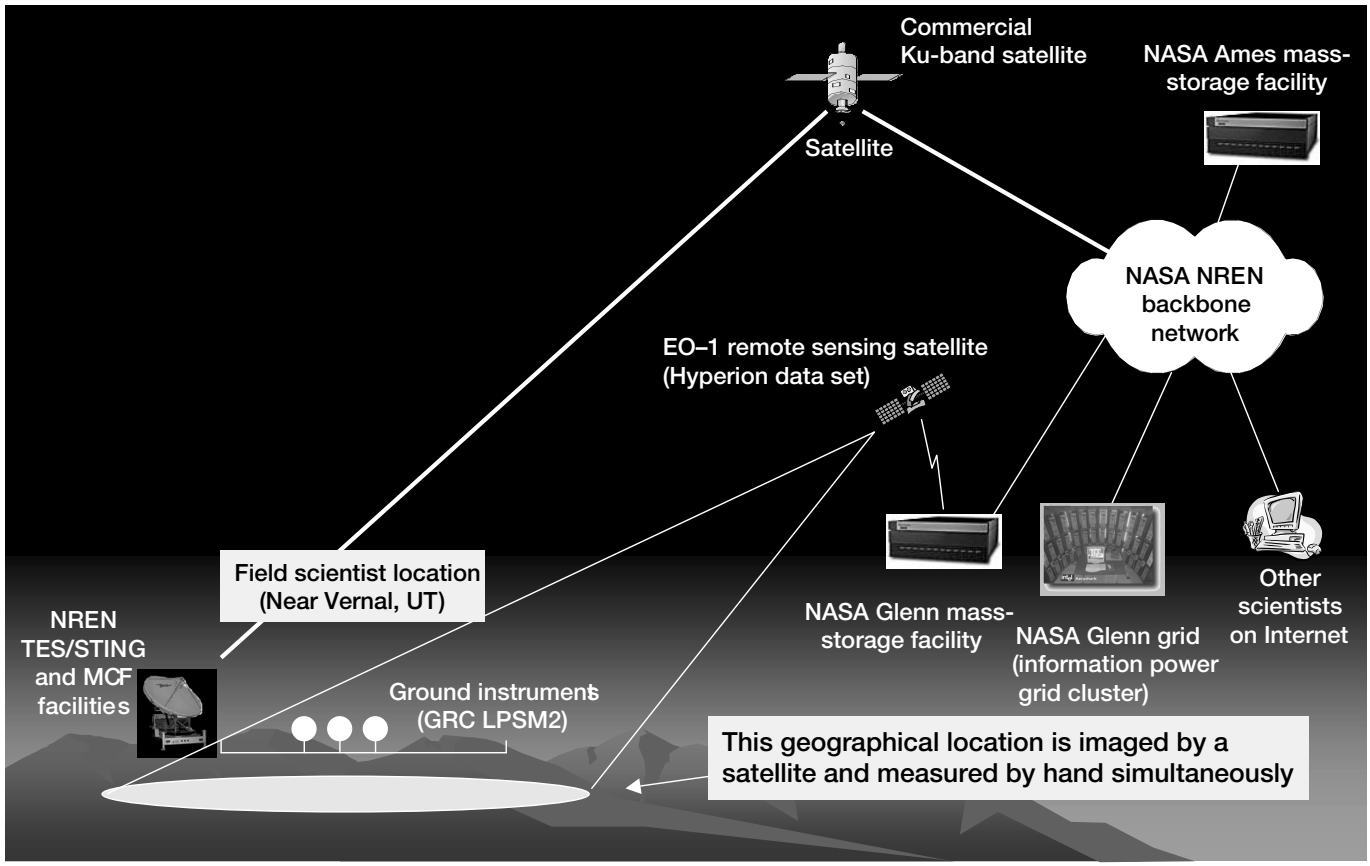

Experiment resource architecture of NREN ground-truthing experiment. TES, Transportable Earth Station; STING, Satellite Terminal for Internet Next Generation; MCF, Mobile Communication Facility; LPSM2, Lunar Planetary Science Module-2.

the remote science team to locate and explore new critical compositions of interest. The process can be repeated as required to continue to validate the data set or to converge on alternate geophysical areas of interest.

The experiment, which was the first attempt by a field team to ground truth satellite instrument data in real time, included simulated astronauts, a field geographer, and a geologist taking spectrum measurements on the ground while being imaged by a satellite (EO–1) from above. The scientists used a combination of field computing resources along with the NASA information power grid supercomputers and mass storage devices at Ames and Glenn to complete the ground-truthing experiment. The team connected to these NASA resources over the NREN hybrid networks, which include a wideband satellite link and wideband terrestrial networks.

The technology also can be applied to emergency settings or to scientists working just about anywhere in the field, including human missions to the Moon or Mars, where space will be limited but computational requirements will be high. This work is being funded by the Computing, Information and Communication Technology Program in the Office of Aerospace Technology.

U.S. Army Research Laboratory, Vehicle Technology Directorate at Glenn contact:
Isaac Lopez, 216–433–5893, Isaac.Lopez@grc.nasa.gov

Glenn contact:
Marc A. Seibert, 216–433–3535, Marc.A.Seibert@nasa.gov

Authors:
Isaac Lopez and Marc A. Seibert

Headquarters program office: OAT

Programs/Projects: CICT

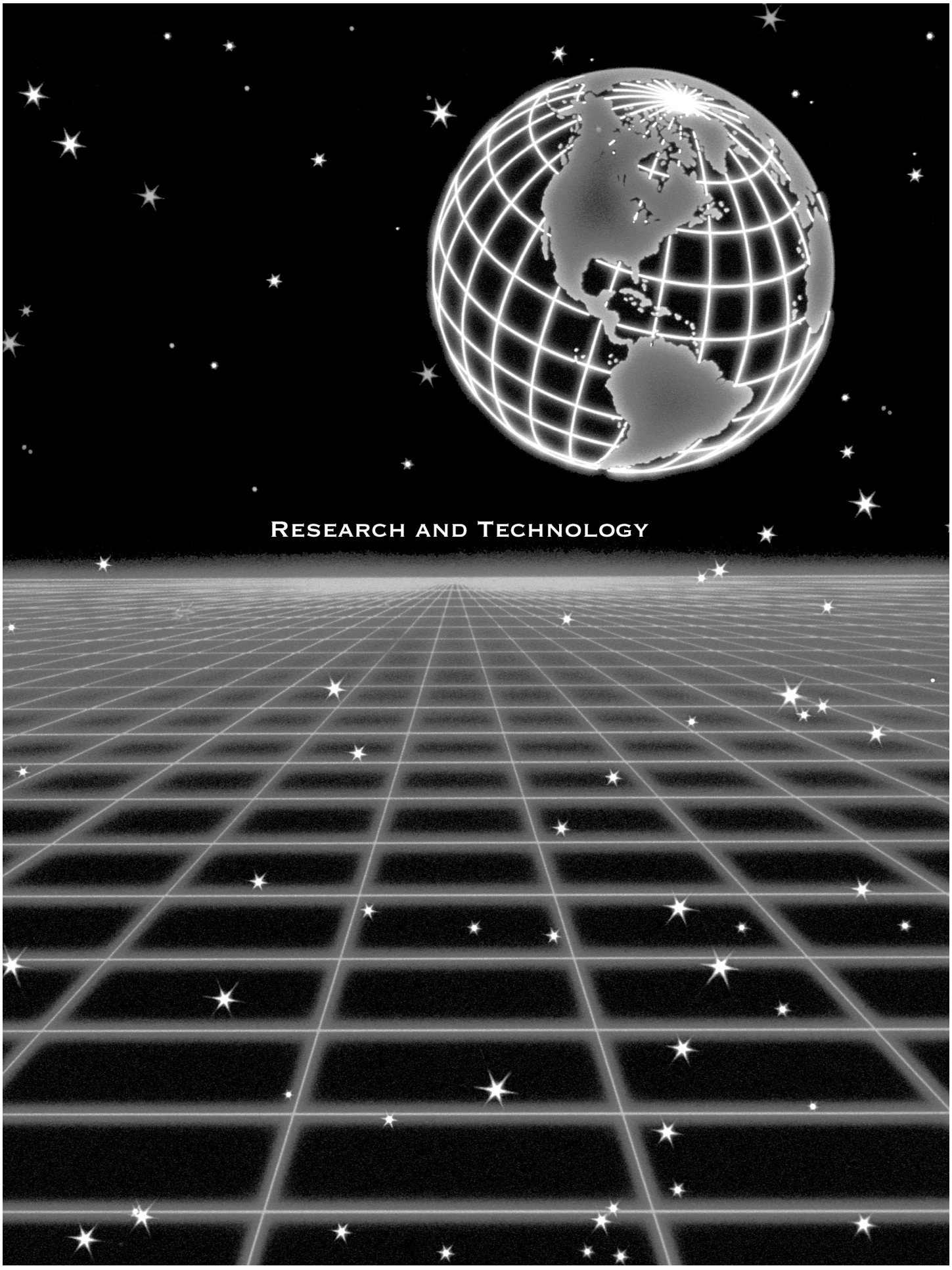

Research and Technology

Materials

High-Performance SiC/SiC Ceramic Composite Systems Developed for 1315 °C (2400 °F) Engine Components

As structural materials for hot-section components in advanced aerospace and land-based gas turbine engines, silicon carbide (SiC) ceramic matrix composites reinforced by high-performance SiC fibers offer a variety of performance advantages over current bill-of-materials, such as nickel-based superalloys. These advantages are based on the SiC/SiC composites displaying higher temperature capability for a given structural load, lower density (~30- to 50-percent metal density), and lower thermal expansion. These properties should, in turn, result in many important engine benefits, such as reduced component cooling air requirements, simpler component design, reduced support structure weight, improved fuel efficiency, reduced emissions, higher blade frequencies, reduced blade clearances, and higher thrust.

Under the NASA Ultra-Efficient Engine Technology (UEET) Project, much progress has been made at the NASA Glenn Research Center in identifying and optimizing two high-performance SiC/SiC composite systems. The table compares typical properties of oxide/oxide panels (ref. 1) and SiC/SiC panels formed by the random stacking of balanced 0°/90° fabric pieces reinforced by the indicated fiber types. The Glenn SiC/SiC systems A and B (shaded area of the table) were reinforced by the Sylramic-iBN SiC fiber, which was produced at Glenn by thermal treatment of the commercial Sylramic SiC fiber (Dow Corning, Midland, MI; ref. 2). The treatment process (1) removes boron from the Sylramic fiber, thereby improving fiber creep, rupture, and oxidation resistance and (2) allows the boron to react with nitrogen to form a thin in situ grown BN coating on the fiber surface, thereby providing an oxidation-resistant buffer layer between contacting fibers in the fabric and the final composite. The fabric stacks for all SiC/SiC panels were provided to GE Power Systems Composites for chemical vapor infiltration of Glenn-designed BN fiber

TYPICAL PROPERTIES FOR 0°/90° CERAMIC COMPOSITE PANELS FABRICATED FROM VARIOUS CONSTITUENTS WITH ~35- TO 40-PERCENT TOTAL FIBER FRACTION

Composite type	Oxide/Oxide (ref. 1)	SiC/SiC	SiC/SiC	SiC/SiC (system A)	SiC/SiC (system B)
Fiber type	Nextel 720[a]	Hi-Nicalon S	Sylramic	Sylramic-iBN (ref. 2)	Sylramic-iBN (ref. 2)
Fiber coating (or interphase)	None	BN	BN	BN (ref. 3)	BN (ref. 3)
Matrix type	Oxide (PIP)[b]	SiC-Si (CVI[c] + slurry + Si)	SiC-Si (CVI + slurry + Si)	SiC-Si (CVI + slurry + Si)	SiC-Si (CVI + ref. 4 + Si)
Ultimate tensile strength (UTS) at 20 °C, MPa	200	360	400	450	310
UTS at 20 °C after 100-hr burner exposure at 800 °C, MPa	200	170	240	450	300
Rupture strength after 100 hr at 800 °C in air, MPa	170	200	200	240	----
UTS at 1315 °C, MPa	<150	280	320	380	260
Rupture life at 105 MPa and 1315 °C in air, hr	<10	~500	~100	~500	>1000
Creep strain after 100 hr at 1315 °C and 105 MPa in air, percent	>0.2	0.05	0.2	0.05	0.02
Transverse thermal conductivity at 20 °C, W/m·°C	1.2	16	24	25	36

[a]Total fiber fraction, ~48 percent.
[b]PIP, polymer infiltration and pyrolysis.
[c]CVI, chemical vapor infiltration.

coatings (ref. 3) and conventional SiC matrices. Composite panels with system B were heat treated at Glenn (ref. 4), and the pores that remained open were filled by silicon melt infiltration (MI). Panels with system A and the other SiC/SiC systems were not heat treated, and remaining open pores in these systems were filled with SiC slurry and silicon MI.

The table clearly shows that the panels with the SiC/SiC system A have the best combination of properties needed for hot-section engine components: (1) especially ultimate tensile strength, a property needed for component damage tolerance; (2) rupture strength and retained strength after burner rig exposure near 800 °C, a temperature region where environmental attack of SiC/SiC composites is typically the greatest; (3) ultimate strength and rupture life at 1315 °C (2400 °F), a temperature well above the thermal capability of metal alloys (~1100 °C); (4) creep resistance, a key property needed for high-temperature dimensional control and intrinsic strength retention; and (5) thermal conductivity at 20 °C and higher, a property needed for reducing thermal gradients and stresses within the component. On the other hand, the panels with the Sylramic-iBN SiC/SiC system B, although they lose some ultimate strength during the composite treatment process, display state-of-the-art properties in terms of rupture life, creep resistance, and thermal conductivity. The microstructural sources for all these properties have been determined and modeled by Glenn researchers, and approaches for further improvements have been identified.

References

1. COI Ceramics, Inc.: OXIDE–OXIDE CMC Data Sheets, Nextel 720 CMC (AS–720N–0). http://www.coiceramics.com/datashts.htm Accessed Jan. 7, 2004.
2. DiCarlo, James A.; and Yun, Hee Mann: New High-Performance SiC Fiber Developed for Ceramic Composites. Research & Technology 2001, NASA/TM—2002-211333, 2002, pp. 8–9. http://www.grc.nasa.gov/WWW/RT2001/5000/5100dicarlo1.html
3. Morscher, Gregory N.; and Hurst, Janet B.: Ceramic Composite Intermediate Temperature Stress-Rupture Properties Improved Significantly. Research & Technology 2001, NASA/TM—2002-211333, 2002, pp. 22–23. http://www.grc.nasa.gov/WWW/RT2001/5000/5130morscher.html
4. Bhatt, R.T.; and DiCarlo, J.A.: Method Developed for Improving the Thermomechanical Properties of Silicon Carbide Matrix Composites. Research & Technology 2003, NASA/TM—2004-14254, 2004, pp. 20–21. http://www.grc.nasa.gov/WWW/RT/2003/5000/5130bhatt.html

Glenn contact:
Dr. James A. DiCarlo, 216–433–5514, James.A.DiCarlo@nasa.gov

Authors: Dr. James A. DiCarlo, Hee Mann Yun, Gregory N. Morscher, and Dr. Ramakrishna T. Bhatt

Headquarters program office: OAT

Programs/Projects: UEET

Third-Generation TiAl Alloy Tested—Exhibits Promising Properties for Rotating Components

The Revolutionary Turbine Accelerator/Turbine-Based Combined Cycle (RTA/TBCC) Program for the next-generation launch vehicle has targeted gamma titanium aluminide as a potential compressor and structural material. Because of the high compressor inlet and exit temperatures, the TBCC engine requires higher temperature materials than conventional Ti alloys, and because of its stringent thrust-to-weight requirements, the engine requires low-density material to be utilized wherever possible. Third-generation gamma alloys offer higher temperature capability along with low density and high stiffness. A high-temperature, high-strength γ-TiAl alloy with a high Nb-content (Gamma MET PX[1]) was selected for evaluation. The microstructure and mechanical properties of Gamma Met PX (GMPX) in both the as-extruded and a lamellar heat-treated

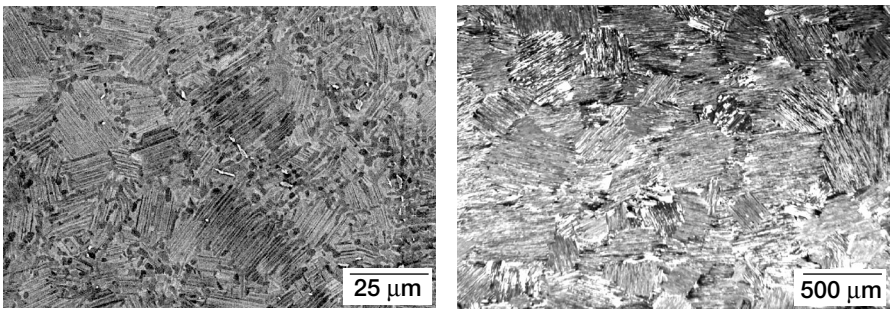

Microstructure of Gamma Met PX. Left: As-extruded condition. Right: After a lamellar heat treatment of 1340 °C for 40 min in vacuum.

[1]Gamma MET PX is a trademark of PLANSEE AG, Austria. Alloy composition is based on TNB alloys developed by GKSS Research Center, Germany.

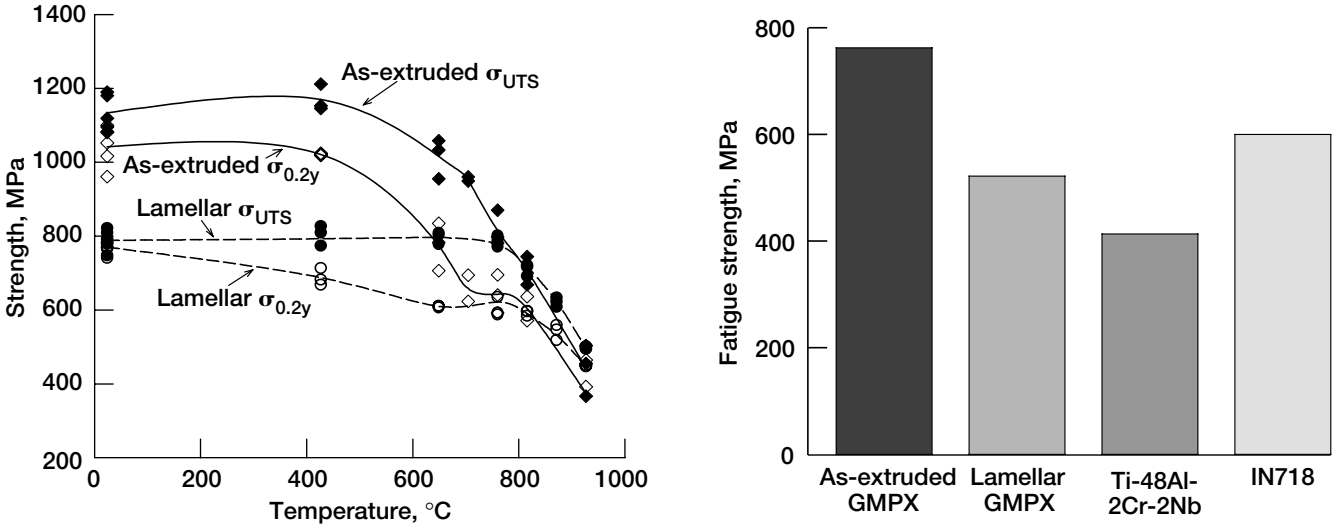

Left: Tensile strength of Gamma Met PX (GMPX), both as-extruded and after a lamellar heat treatment (σ_{UTS}, ultimate tensile strength; $\sigma_{0.2\%y}$, 0.2-percent yield strength). Right: As-extruded GMPX had a higher fatigue strength than a Ni-base superalloy, IN718 (ref. 2), even without correcting for density. The fatigue strength of both as-extruded and lamellar GMPX was significantly improved over that of a second-generation TiAl alloy, Ti-48Al-2Cr-2Nb.

condition and the influence of the microstructure on the tensile, creep, and fatigue properties were investigated in-house (ref. 1).

Triple vacuum arc-remelted Ti-45Al-X(Nb,B,C) (at.%) gamma TiAl ingots were extruded in two steps to a final extrusion ratio of 100:1. The as-extruded bars had a fine-grained, nearly lamellar microstructure. Heat treating at 1340 °C for 40 min in vacuum produced a fully lamellar microstructure with equiaxed lamellar colonies. The mechanical properties of GMPX depend on the microstructure. The tensile strength of the as-extruded microstructure was exceptionally high for a γ-TiAl alloy at all test temperatures. The as-extruded microstructure achieved room temperature total elongations slightly higher than 2 percent, traditionally considered the lower limit for component design. The tensile strength of the as-extruded material is on the order of forged superalloys. On a density-corrected basis, however, the specific strength would be double that of superalloys. Although still stronger than traditional γ-TiAl alloys, the lamellar heat-treated material had lower strengths than the as-extruded material from room temperature to 760 °C and also lower room-temperature ductility, typical for TiAl alloys. High-cycle-fatigue specimens, with both as-extruded and lamellar microstructures, were step fatigue tested at 650 °C with a load ratio of 0.05. The bar chart compares the fatigue strength of GMPX to a baseline TiAl alloy, Ti-48Al-2Cr, 2Nb and also a Ni-base superalloy, IN718 (ref. 2). Similar to the tensile strength, the fatigue strength of as-extruded GMPX was equivalent to a Ni-base superalloy even without correcting for density. The lamellar microstructure resulted in significantly lower fatigue strength because a lamellar microstructure is conducive to easy crack initiation (ref. 3). As-extruded and lamellar heat-treated GMPX samples were tested in both compression and tension to determine the creep behavior between 727 and 1027 °C. Creep strengths reached superalloy levels at fast strain rates and lower temperatures but deformation at slower strain rates and/or higher temperature indicated significant weakening for the as-extruded condition. At high temperatures and low stresses, the lamellar microstructure had improved creep properties. The microstructure can, thus, be altered to match the requirements for a particular application.

References

1. Draper, S.L., et al.: Microstructure and Mechanical Properties of Extruded Gamma MET PX. Gamma Titanium Aluminides 2003, Y.–W. Kim, H. Clemens, and H.H. Rosenberger, eds., TMS, 2004, pp. 207–212. To be published.
2. Metallic Materials and Elements for Aerospace Vehicle Structures, MIL–HDBK 5G. 1994.
3. Lerch, B.A., et al.: Durability Assessment of Various Gamma TiAl Alloys. Gamma Titanium Aluminides 2003, Y.–W. Kim, H. Clemens, and A.H. Rosenberger, eds., TMS, 2004, pp. 477–483. To be published.

Glenn contact:
Susan L. Draper, 216–433–3257,
Susan.L.Draper@nasa.gov

Authors:
Susan L. Draper, Dr. Ivan E. Locci,
Dr. J. Daniel Whittenberger, and
Dr. Bradley A. Lerch

Headquarters program office: OAT

Programs/Projects: NGLT, RTA/TBCC

TiAl Scramjet Inlet Flap Subelement Designed and Fabricated

Next-generation launch vehicles are being designed with turbine-based combined cycle (TBCC) propulsion systems having very aggressive thrust/weight targets and long lives. Achievement of these goals requires advanced materials in a wide spectrum of components. TiAl has been identified as a potential backstructure material for maintainable composite panel heat exchangers (HEX) in the inlet, combustor, and nozzle section of a TBCC propulsion system. Weight reduction is the primary objective of this technology. Design tradeoff studies have assessed that a TiAl structure, utilizing a high-strength, high-temperature TiAl alloy called Gamma MET PX,[1] reduce weight by 41 to 48 percent in comparison to the baseline Inconel 718 configuration for the TBCC propulsion system inlet, combustor, and nozzle (ref. 1). A collaborative effort between the NASA Glenn Research Center, Pratt & Whitney, Engineering Evaluation & Design, PLANSEE AG (Austria), and the Austrian Space Agency was undertaken to design, manufacture, and validate a Gamma-MET PX TiAl structure for scramjet applications.

The TiAl inlet flap was designed with segmented flaps to improve manufacturability, to better control thermal distortion and thermal stresses, and to allow for maintainable HEX segments. The design philosophy was to avoid excessively complicated shapes, to minimize the number of stress concentrations, to keep the part sizes reasonable to match processing capabilities, and to avoid risky processes such as welding. The conceptual design used a standard HEX approach with a double-pass coolant concept for centrally located manifolds. The flowpath side was actively cooled, and an insulation package was placed on the external side to save weight. The inlet flap was analyzed structurally, and local high-stress regions were addressed with local reinforcements.

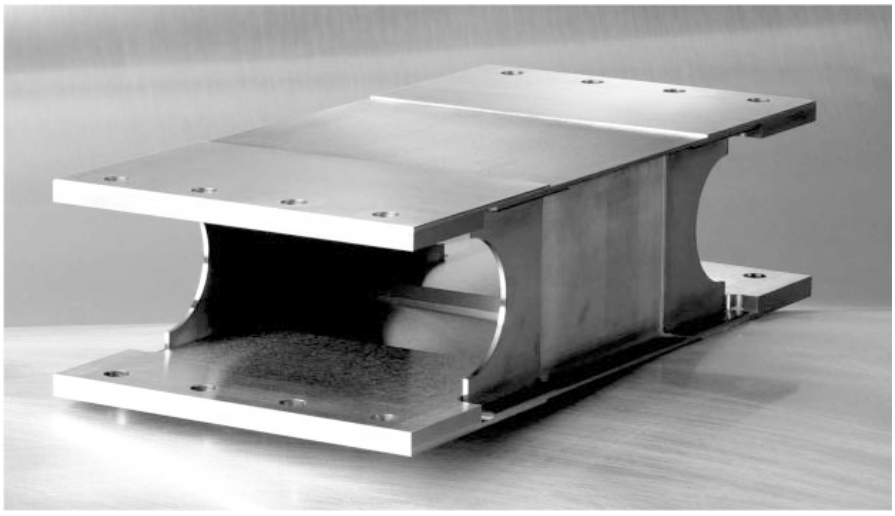

Gamma Met PX inlet flap subelement.

A Gamma MET PX subelement was designed to demonstrate full-scale manufacturing capability and to validate the design predictions and material properties. Three subelements were fabricated by one-pass brazing and were inspected by nondestructive evaluation with similar results. Brazes between the outer stiffener and the face sheet had good coverage, as did the majority of brazed joints. Subelement testing under anticipated mission conditions is scheduled for fiscal year 2004.

Considerable progress has been made on the design, fabrication, and testing of Gamma MET PX sheet structures. Gamma MET PX structures offer considerable weight savings, and with careful design they can be implemented successfully in aerospace applications.

Reference

1. Collier, Craig: Vehicle Structural Optimization Study, Informal Program Review, NASA Contract NAS3–01138, Nov. 2002. Available from the NASA Center for AeroSpace Information.

Glenn contact:
Susan L. Draper, 216–433–3257, Susan.L.Draper@nasa.gov

Author: Susan L. Draper

Headquarters program office: OAT

Programs/Projects: NGLT, RTA/TBCC

[1]Gamma MET PX is a trademark of PLANSEE AG, Austria. Alloy composition is based on TNB alloys developed by GKSS Research Center, Germany.

Conductivity of GRCop-42 Alloy Enhanced

GRCop-84, a material developed at the NASA Glenn Research Center, has shown considerable promise for staged combustion rocket engine cycles such as the Space Shuttle Main Engine. However, for an expander cycle rocket engine, the transfer of heat to the fuel is a paramount factor in determining the efficiency of the engine. Examples of current and potential future expander cycle rocket engines are the Pratt & Whitney RL–10, RL–60, and RLX engines. Development of a higher conductivity version of GRCop-84 was undertaken to meet these needs.

All expander cycle engines need a main combustion chamber liner with the maximum possible thermal conductivity. In an effort at Glenn to trade some of the greatly increased mechanical properties of GRCop-84 for improved thermal conductivity, the amounts of chromium and niobium were halved. The new Cu-4 at.% Cr-2 at.% Nb alloy was designated GRCop-42.

The top graph shows the result of lowering the alloying content on thermal conductivity. GRCop-42 has a sizeable improvement in thermal conductivity relative to GRCop-84. GRCop-42 also easily exceeds the thermal conductivity of the current Space Shuttle Main Engine liner alloy, NARloy-Z (Cu-3 wt%, Ag-0.5 wt%, Zr).

The cost of the improved thermal conductivity is minimal. The bottom graph shows the low-cycle-fatigue (LCF) lives of GRCop-42. LCF is generally the dominant failure mode for liners. There is a small, but statistically significant, decrease in the LCF life of GRCop-42 in comparison to that of GRCop-84. However, the lives are equivalent to that of NARloy-Z. Additional testing shows that the strength of the GRCop-42 is almost equal to that of GRCop-84 up to 800 °C (1472 °F) and much greater than that of NARloy-Z. However, the creep stress for a 15-hr life at 500 °C (932 °F), a typical value for a liner, is reduced by approximately 25 percent relative to GRCop-84. Even with the reduced creep stress, GRCop-42 retains an advantage in creep stress over NARloy-Z and most other alloys.

Additional testing is underway to generate a database similar to that already done for GRCop-84. Work will include characterizing the microstructural properties and determining the thermophysical and mechanical properties before and after the alloy is subjected to a simulated brazing thermal cycle. Following testing, the database will be made available to industry for their evaluation of GRCop-42 in potential high-heat-flux applications.

Glenn contacts:
Dr. David L. Ellis, 216–433–8736, David.L.Ellis@nasa.gov; and
Dr. Bradley A. Lerch, 216–433–5522, Bradley.A.Lerch@nasa.gov

Ohio Aerospace Institute (OAI) contact:
William S. Loewenthal, 216–433–2697, William.S.Loewenthal@grc.nasa.gov

Author: Dr. David L. Ellis

Headquarters program office: OAT

Programs/Projects: SLI, RLV

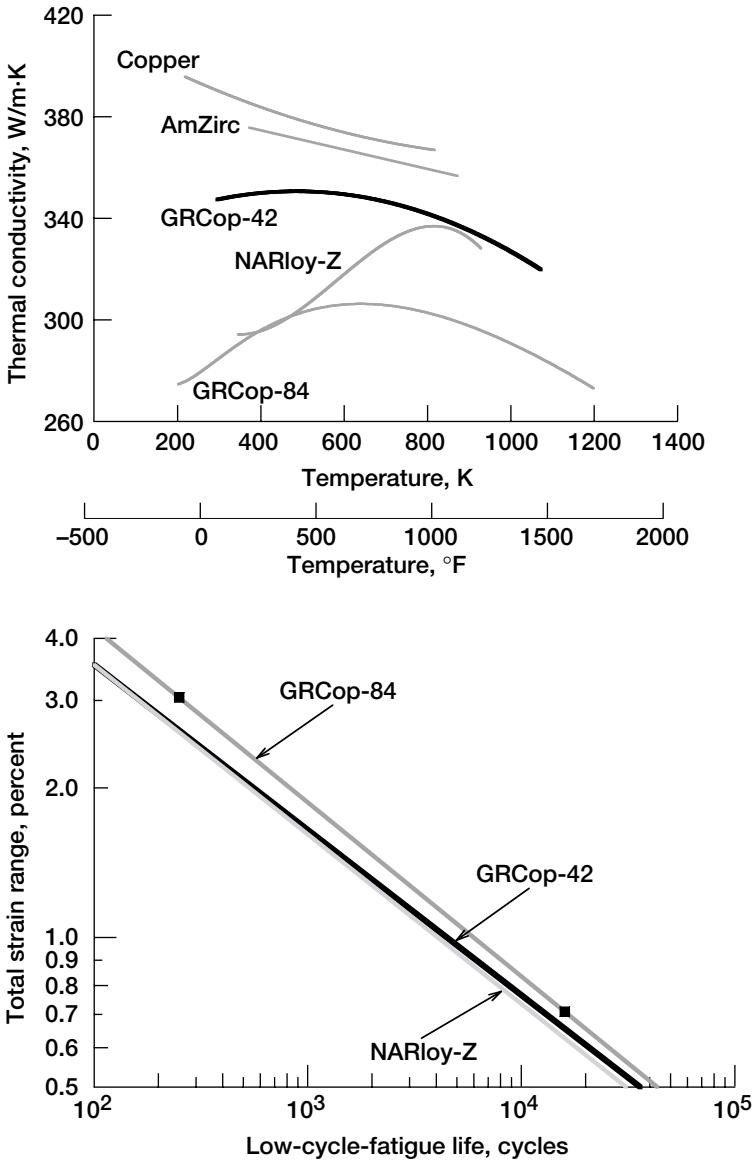

Top: Comparative thermal conductivity of GRCop-42. Bottom: Low-cycle-fatigue life comparison.

GRCop-84 Scaled Up for Production

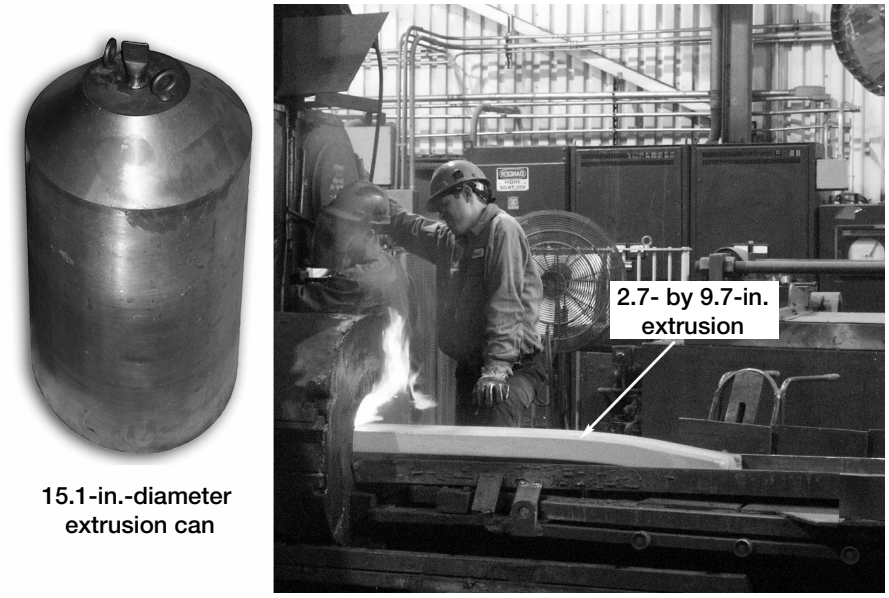

Extrusion of GRCop-84.

GRCop-84 (Cu-8 at.% Cr-4 at.% Nb) was developed at the NASA Glenn Research Center for use in regeneratively cooled rocket engine main combustion chamber liners. The alloy has demonstrated high elevated-temperature strength, excellent creep resistance, long low-cycle-fatigue lives, low thermal expansion, and good thermal conductivity on a laboratory scale. The combination of properties has led to interest from the Rocketdyne Division of Boeing, Aerojet, and Pratt & Whitney for their new engines. Under the Space Launch Initiative/Next Generation Launch Technology program, GRCop-84 is being taken out of the laboratory and put into a full-scale production environment.

Development work spans the entire process from powder production to finished liner preforms ready to be machined and integrated into test engines. Powder production has been increased to 1600 lb and larger production runs. Crucible Research, the producer, has identified and is currently weighing capital expenditures that would increase the production capacity 6 times while reducing the cost of the powder by 40 percent.

Extrusion is used to consolidate the powder into a solid form. As shown in the preceding photographs, the extrusion process has been successfully scaled up to 15.1-in.-diameter extrusion cans with 800 to 1000 lb of powder using the commercially available extrusion press at HC Starck. HC Starck has rolled the extruded GRCop-84 to a 24-in.-wide plate and a sheet as thin as 0.002 in. Additional commercial vendors have been identified to increase both the size of the extrusion can and the width of the rolled product.

Once the sheet and plate are produced, they are incorporated into two production processes to produce the liner preforms. In the first method, Aerojet uses their platelet technology to make the liners. Techniques similar to those used in integrated circuit chip production are used to remove material and make complex cooling passages in the thin sheets. The sheets are stacked and diffusion bonded together to produce liner sections such as the one shown in the photograph on the next page. The sections are electron beam welded together to make the final liner.

In a second method under development with Rocketdyne, a 0.5-in.-thick plate is formed and machined into two half cylinders. The half cylinders are friction stir welded (FSW) together at the NASA Marshall Space Flight Center to form a complete cylinder. Spin-Tech, the current producer of the Space Shuttle Main Engine liners, metal spins the cylinder into the hourglass-shaped liner preform. The preform can be machined to final dimensions and cooling channels added. The RS–84 program has expressed interest in hot fire testing one or more metal spun liners in fiscal year 2004.

Testing is underway to fully characterize the microstructure and mechanical properties of the rolled product, the FSW joints, and the platelet technology material. Results to date demonstrate that the commercially processed GRCop-84 retains at least 85 percent of the properties of the as-extruded bars examined under the Reusable Launch Vehicles focused program, and with moderate amounts of cold work, exceeds the as-extruded properties by up to 20 percent. This includes the properties of the FSW and platelet technology joints.

Although work remains to be done to optimize some of the processing steps, the basic ability to scale up GRCop-84 has been demonstrated. The appropriate databases are still being generated, but properties so far are comparable to prior results. Forming

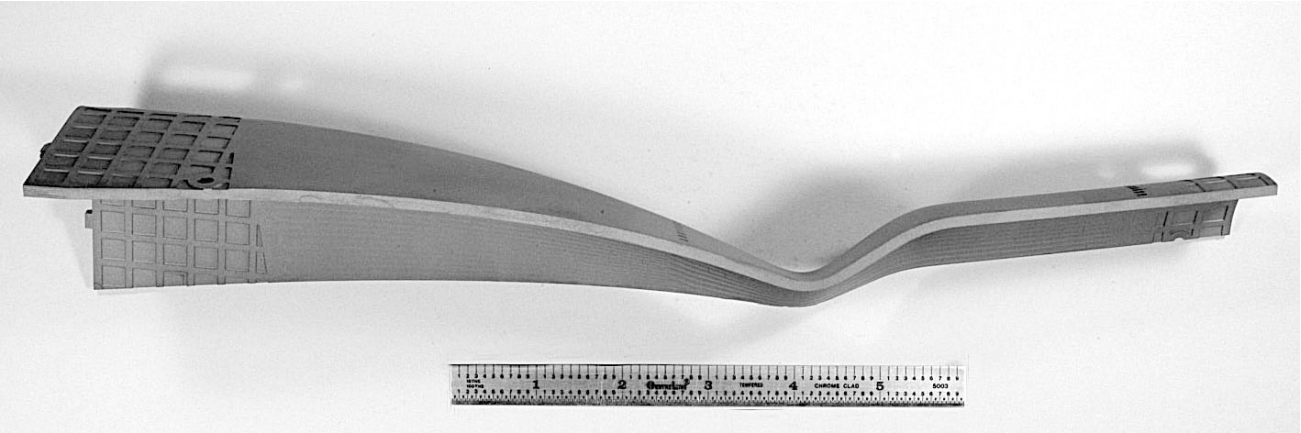

GRCop-84 platelet liner.

and joining technologies needed to make the liners have been demonstrated. With these successes, GRCop-84 is ready for full-scale production to meet the needs of the RS–84 and other engines.

Glenn contacts: Dr. David L. Ellis, 216–433–8736, David.L.Ellis@nasa.gov; and Dr. Bradley A. Lerch, 216–433–5522, Bradley.A.Lerch@nasa.gov

Ohio Aerospace Institute (OAI) contact:
William S. Loewenthal, 216–433–2697, William.S.Loewenthal@grc.nasa.gov

Author: Dr. David L. Ellis

Headquarters program office: OAT

Programs/Projects: SLI, NGLT, RLV

Special recognition: TGIR 2003

Potential High-Temperature Shape-Memory Alloys Identified in the Ti(Ni,Pt) System

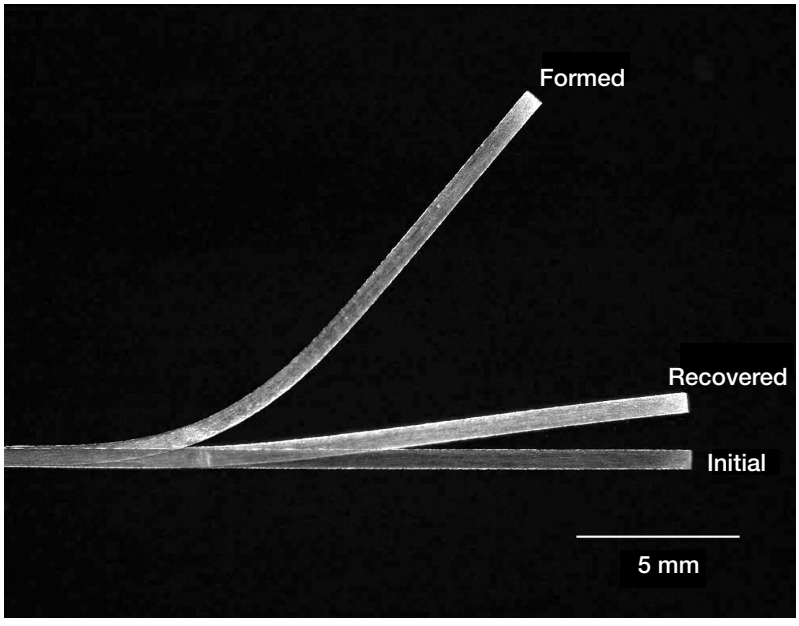

Demonstration of the shape-memory effect in a Ti(Ni,Pt) alloy. The superimposed images are of Ti-30Ni-20Pt rolled sheet, bent 38° at room temperature, and recovered to 8° by heating to 350 °C, resulting in a displacement of the sheet end of almost 10 mm.

"Shape memory" is a unique property of certain alloys that, when deformed (within certain strain limits) at low temperatures, will remember and recover to their original predeformed shape upon heating. It occurs when an alloy is deformed in the low-temperature martensitic phase and is then heated above its transformation temperature back to an austenitic state. As the material passes through this solid-state phase transformation on heating, it also recovers its original shape. An example of this behavior is shown in the photograph.

This behavior is widely exploited, near room temperature, in commercially available NiTi alloys for connectors, couplings, valves, actuators, stents, and other medical and dental devices. In addition, there are limitless applications in the aerospace, automotive,

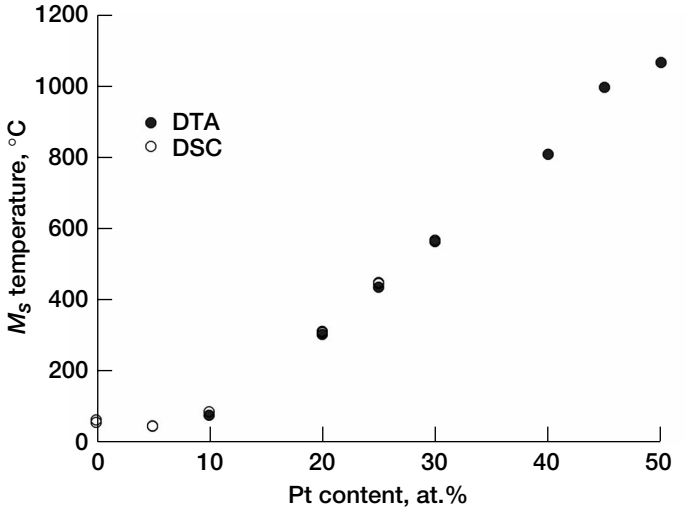

Martensitic start temperature, M_S, for $Ti_{50}Ni_{50-x}Pt_x$ alloys as a function of Pt content. The initial region of focus for high-temperature actuators for aerospace applications includes alloys containing 15 to 35 at.% Pt. DTA, differential thermal analysis; DSC, differential scanning calorimetry.

chemical processing, and many other industries for materials that exhibit this type of shape-memory behavior at higher temperatures. But for high temperatures, there are currently no commercial shape-memory alloys.

Although there are significant challenges to the development of high-temperature shape-memory alloys, at the NASA Glenn Research Center we have identified a series of alloy compositions in the Ti-Ni-Pt system that show great promise as potential high-temperature shape-memory materials. An example of the shape recovery achieved in one of these alloys is shown in the photograph on the preceding page. The graph on this page is a plot of the M_S temperature (a measure of the actuation temperature) as a function of Pt content from 0 to 50 at.%, when Pt is substituted for Ni in a series of $Ti_{50}Ni_{50-x}Pt_x$ alloys. There is a linear dependence of transformation temperature on Pt content for alloys containing 10 to 50 at.% Pt described by the following relation:

$$M_S\ (°C) = 25.2\ (\text{at.\% Pt}) - 182.7$$

with a correlation coefficient r^2 of 0.997. The alloys currently of most interest for aerospace applications (including combustor components, core exhaust chevrons, and other actuators) are those containing 15 to 35 at.% Pt.

One of the major challenges in developing shape-memory alloys for high-temperature actuators is achieving the long-term stability of the alloy, including its microstructure, phase structure, and resistance to oxidation. The reason is that the shape-memory process depends on the diffusionless transformation of the martensitic phase to the higher temperature austenite phase. For materials such as NiTi, where this diffusionless transformation occurs near room temperature, alloy stability is not an issue. But when this transformation occurs at elevated temperatures where decomposition, recovery, recrystallization, and other thermal processes are prevalent, alloy and microstructural stability are major concerns as is environmental resistance. These diffusional processes can retard the material's shape recovery and can also affect its transformation temperature. Moreover, since these actuators could be highly loaded, relaxation and creep are also concerns. Consequently, alloys in the composition range of interest are in the process of being fully characterized and optimized, and their potential as high-temperature shape-memory alloys demonstrated through subcomponent testing.

Glenn contact:
Dr. Ronald D. Noebe, 216–433–2093, Ronald.D.Noebe@nasa.gov

Authors: Dr. Ronald D. Noebe, Tiffany A. Biles, Dr. Anita Garg, and Dr. Michael V. Nathal

Headquarters program office: OAT

Programs/Projects: RAC

Method Developed for Improving the Thermomechanical Properties of Silicon Carbide Matrix Composites

Today, a major thrust for achieving engine components with improved thermal capability is the development of fiber-reinforced silicon-carbide (SiC) matrix composites. These materials are not only lighter and capable of higher use temperatures than state-of-the-art metallic alloys and oxide matrix composites (~1100 °C), but they can provide significantly better static and dynamic toughness than unreinforced silicon-based monolithic ceramics. However, for successful application in advanced engine systems, the SiC matrix composites should be able to withstand component service stresses and temperatures for the desired component lifetime. Since the high-temperature structural life of ceramic materials is typically controlled by creep-induced flaw growth, a key composite property requirement is the ability to display high creep resistance under these conditions. Also, because of the possibility of severe thermal gradients in the components, the composites should provide maximum thermal conductivity to minimize the development of thermal stresses.

State-of-the-art SiC matrix composites are typically fabricated via a three-step process: (1) fabrication of a component-shaped architectural preform reinforced by high-performance fibers, (2) chemical vapor infiltration of a fiber coating material such as boron nitride (BN) into the preform, and (3) infiltration of a SiC matrix into the remaining porous areas in the preform. Generally, the highest performing composites have matrices fabricated by the CVI process, which produces a SiC matrix typically more thermally stable and denser than matrices formed by other approaches. As such, the CVI SiC matrix is able to provide better environmental protection to the coated fibers, plus provide the composite with better resistance to crack propagation. Also, the denser CVI SiC matrix should provide optimal creep resistance and thermal conductivity to the composite. However, for adequate preform infiltration, the CVI SiC matrix process typically has to be conducted at temperatures below 1100 °C, which results in a SiC matrix that is fairly dense, but contains metastable atomic defects and is nonstoichiometric because of a small amount of excess silicon. Because these defects typically exist at the matrix grain boundaries, they can scatter thermal phonons and degrade matrix creep resistance by enhancing grain-boundary sliding.

To eliminate these defects and improve the thermomechanical properties of ceramic composites with CVI SiC matrices, researchers at the NASA Glenn Research Center developed a high-temperature treatment process that can be used after the CVI SiC matrix is deposited into the fiber preform. Using Glenn-developed Sylramic-iBN SiC fibers (ref. 1) and BN-based fiber coatings (ref. 2), which are stable in their functions under the treatment conditions, Glenn researchers observed minimal strength loss for composite panels formed from two-dimensional architectural preforms. More importantly, significant improvements were observed in composite thermal conductivity and creep resistance, as indicated in the left and right bar charts, respectively. For these panels, total fiber and coating volume fractions were ~35 and 5 vol%, respectively, and the CVI SiC matrices were deposited at ~50 and ~35 vol%. Porous areas that remained open in the 35 vol% CVI SiC matrices were filled either by repeated polymer infiltration and pyrolysis of a SiC yielding polymer, or by the melt infiltration of silicon near 1400 °C. The left bar chart also shows the detrimental effect of

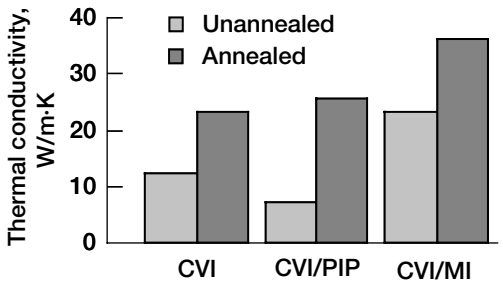

Effect of Glenn annealing treatment process on the room-temperature through-the-thickness thermal conductivity of Sylramic iBN SiC/BN/SiC composite panels containing full chemical vapor infiltration (CVI) (~50 vol%) SiC matrix, CVI (~35 vol%) plus polymer infiltration and pyrolysis (PIP) SiC matrix, and CVI (~35 vol%) plus melt infiltration (MI) SiC matrix.

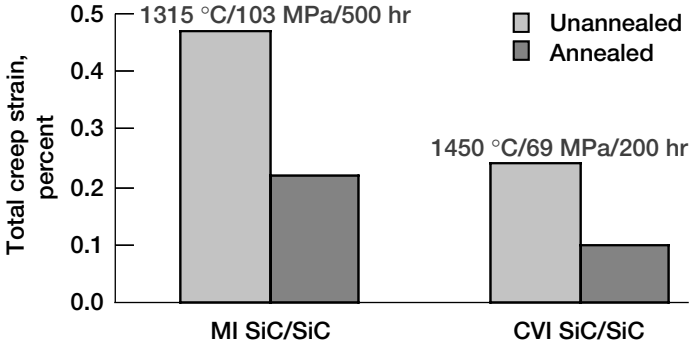

Effect of Glenn annealing treatment process on the tensile creep strain of Sylramic-iBN SiC/BN/SiC composite panels with a CVI (~35 vol%) plus MI SiC matrix and with a full CVI (~50 vol%) SiC matrix.

trapped porosity in the full CVI SiC matrix and the beneficial effect of pore filling for the hybrid CVI plus MI SiC matrix. However, the full CVI SiC matrix is best in creep resistance and allows temperature capability beyond 1400 °C (see the right bar chart on the preceding page), which is near the upper use temperature for the CVI plus MI SiC matrix (ref. 3).

Improvements in thermal conductivity of SiC/SiC CMCs will reduce thermal stresses in gas turbine engine components, such as combustor liner and turbine blades. Improvements in creep resistance will increase the life of CMC components in gas turbine engines.

References

1. DiCarlo, James A.; and Yun, Hee Mann: New High-Performance SiC Fiber Developed for Ceramic Composites, Research & Technology 2001, NASA/TM—2002-211333, 2002, pp. 8–9. http://www.grc.nasa.gov/WWW/RT2001/5000/5100dicarlo1.html
2. Morscher, Gregory N.; and Hurst, Janet B.: Ceramic Composite Intermediate Temperature Stress-Rupture Properties Improved Significantly. Research & Technology 2001, NASA/TM—2002-211333, 2002, pp. 22–23. http://www.grc.nasa.gov/WWW/RT2001/5000/5130morscher.html
3. Bhatt, R.T.; McCue, T.R.; and DiCarlo, J.A.: Thermal Stability of Melt Infiltrated SiC/SiC Composites. Ceram. Eng. Sci. Proc., vol. 24, no. 3, 2003, pp. 295–300.

U.S. Army Research Laboratory, Vehicle Technology Directorate at Glenn contact:
Dr. Ramakrishna T. Bhatt, 216–433–5513, Ramakrishna.T.Bhatt@grc.nasa.gov

Authors: Dr. Ramakrishna T. Bhatt and Dr. James A. DiCarlo

Headquarters program office: OAT

Programs/Projects: UEET

Processing Techniques Developed to Fabricate Lanthanum Titanate Piezoceramic Material for High-Temperature Smart Structures

Piezoelectric ceramic materials are potential candidates for use as actuators and sensors in intelligent gas turbine engines. For piezoceramics to be applied in gas turbine engines, they will have to be able to function in temperatures ranging from 1000 to 2500 °F. However, the maximum use temperature for state-of-the-art piezoceramic materials is on the order of 300 to 400 °F. Research activities have been initiated to develop high-temperature piezoceramic materials for gas turbine engine applications. Lanthanum titanate has been shown to have high-temperature piezoelectric properties with Curie temperatures of T_C = 1500 °C and use temperatures greater than 1000 °C (refs. 1 and 2). However, the fabrication of lanthanum titanate poses serious challenges because of the very high sintering temperatures required for densification.

Two different techniques have been developed at the NASA Glenn Research Center to fabricate dense lanthanum titanate piezoceramic material. In one approach, lower sintering temperatures were achieved by adding yttrium oxide to commercially available lanthanum titanate powder. Addition of only 0.1 mol% yttrium oxide lowered the sintering temperature by as much as 300 °C, to just 1100 °C, and dense lanthanum titanate was produced by pressure-assisted sintering. The lanthanum titanate containing 0.1 mol% yttria exhibited excellent piezoelectric properties, as shown in this graph, which displays a typical polarization response of lanthanum titanate as a function of applied electric field at 360 °C. In addition, this highly refractive material was able to sustain externally applied electric fields from 0.1 V/cm to 80 kV/cm without dielectric breakdown.

The second approach utilized the same commercially available powders but used an innovative sintering approach called differential sintering, which did not require any additive. Fully dense lanthanum titanate was produced by this technique, and the material did

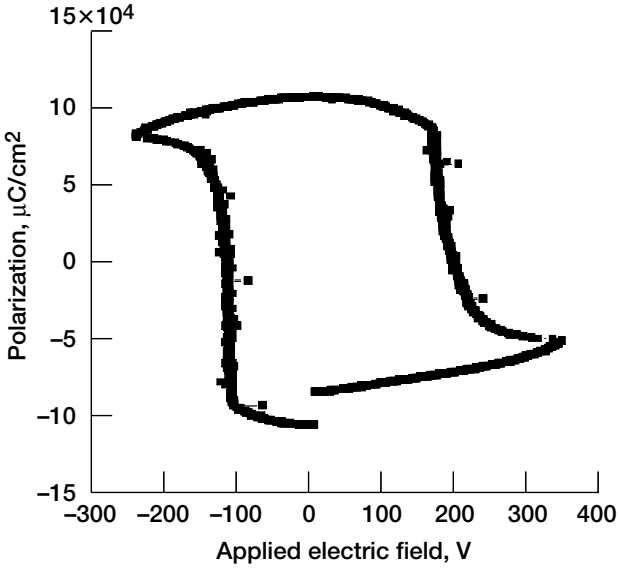

Electric polarization hysteretics of lanthanum titanate with 0.1 mol% of yttrium oxide taken at 360 °C.

not degrade over time. The material exhibited excellent piezoelectric properties at room temperature, as shown in the graph on this page. The displacement was significantly higher than anticipated for a moderate applied electric field. Future efforts are planned to concentrate on optimizing the piezoelectric properties of lanthanum titanate at elevated temperatures.

References

1. Scheunemann K.; and Muller-Bushbaum, H.K.: Crystal-Structure of $La_2Ti_2O_7$. J. Inorg. Nucl. Chem., vol. 37, no. 9, 1975, pp. 1879–1881.
2. Kimura M., et al.: Electro Optic and Piezoelectric Properties of $La_2Ti_2O_7$ Single-Crystal. Jpn. J. Appl. Phys., vol. 11, no. 6, 1972, p. 904.

Glenn contact: Dr. Jon C. Goldsby, 216–433–8250, Jon.C.Goldsby@nasa.gov

Authors: Dr. Jon C. Goldsby, Dr. Serene C. Farmer, and Dr. Ali Sayir

Headquarters program: OAT

Programs/Projects: Propulsion and Power

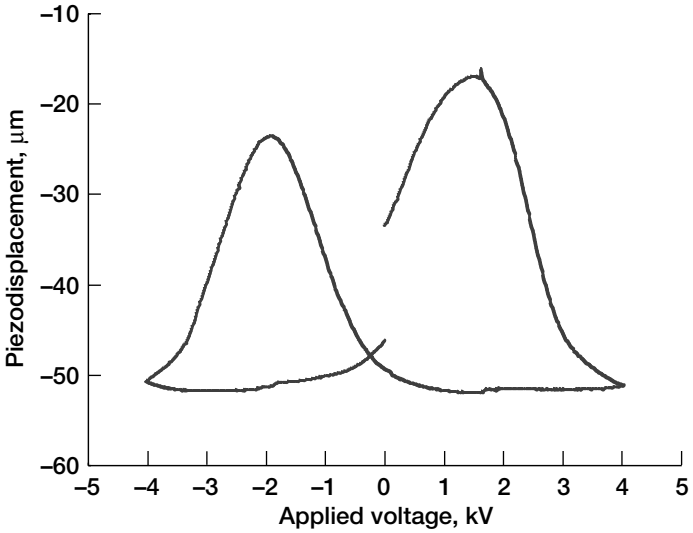

Displacement of differentially sintered lanthanum titanate as a function of an externally applied electric field.

Boron Nitride Nanotubes Synthesized by Pressurized Reactive Milling Process

Nanotubes, because of their very high strength, are attractive as reinforcement materials for ceramic matrix composites (CMCs). Recently there has been considerable interest in developing and applying carbon nanotubes for both electronic and structural applications. Although carbon nanotubes can be used to reinforce composites, they oxidize at high temperatures and, therefore, may not be suitable for ceramic composites. Boron nitride, because it has a higher oxidation resistance than carbon, could be a potential reinforcement material for ceramic composites. Although boron nitride nanotubes (BN-nT) are known to be structurally similar to carbon nanotubes, they have not undergone the same extensive scrutiny that carbon nanotubes have experienced in recent years. This has been due to the difficulty in synthesizing this material rather than lack of interest in the material. We expect that BN-nTs will maintain the high strength of carbon nanotubes while offering superior performance for the high-temperature and/or corrosive applications of interest to NASA.

At the NASA Glenn Research Center, several methods of preparing BN-nTs were investigated and compared. These include the arc jet process, the reactive milling process, and chemical vapor deposition. The most successful was a pressurized reactive milling process that synthesizes BN-nTs of reasonable quantities. Batch sizes of 6 g with over 90-percent yield have been successfully prepared by this method. The photomicrograph shows the as-synthesized BN-nTs. The temper-

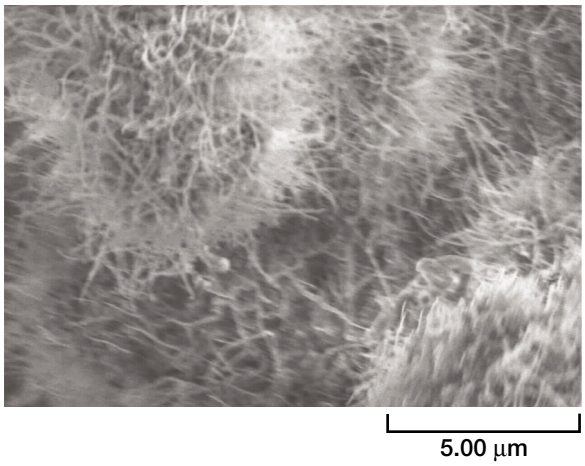

As-produced boron nitride nanotubes.

ature stability of these BN-nTs in air is significantly higher than that for commercially available carbon nanotubes, as shown in the graph. The carbon nanotubes lose weight rapidly at 400 °C because the carbon is oxidized. On the other hand, BN-nTs are stable in air up to 1000 °C, demonstrating the superior performance of the BN-nT. BN-nTs are currently being incorporated into composites to provide high-strength behavior at high temperatures.

Glenn contact: Janet B. Hurst, 216–433–3286, Janet.B.Hurst@nasa.gov

Author: Janet B. Hurst

Headquarters program office: OAT

Programs/Projects: Space Communications

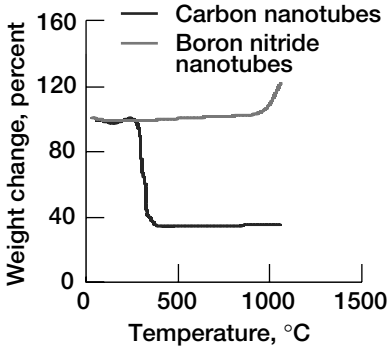

Superior temperature stability of boron nitride nanotubes in air relative to carbon nanotubes from weight loss data (thermogravimetric analysis).

Subscale Testing of a Ceramic Composite Cooled Panel Led to Its Design and Fabrication for Scramjet Engine Testing

In a partnership between the NASA Glenn Research Center and Pratt & Whitney, a ceramic heat exchanger panel intended for use along the hot-flow-path walls of future reusable launch vehicles was designed, fabricated, and tested. These regeneratively cooled ceramic matrix composite (CMC) panels offer lighter weight, higher operating temperatures, and reduced coolant requirements in comparison to their more traditional metallic counterparts. A maintainable approach to the design was adopted which allowed the panel components to be assembled with high-temperature

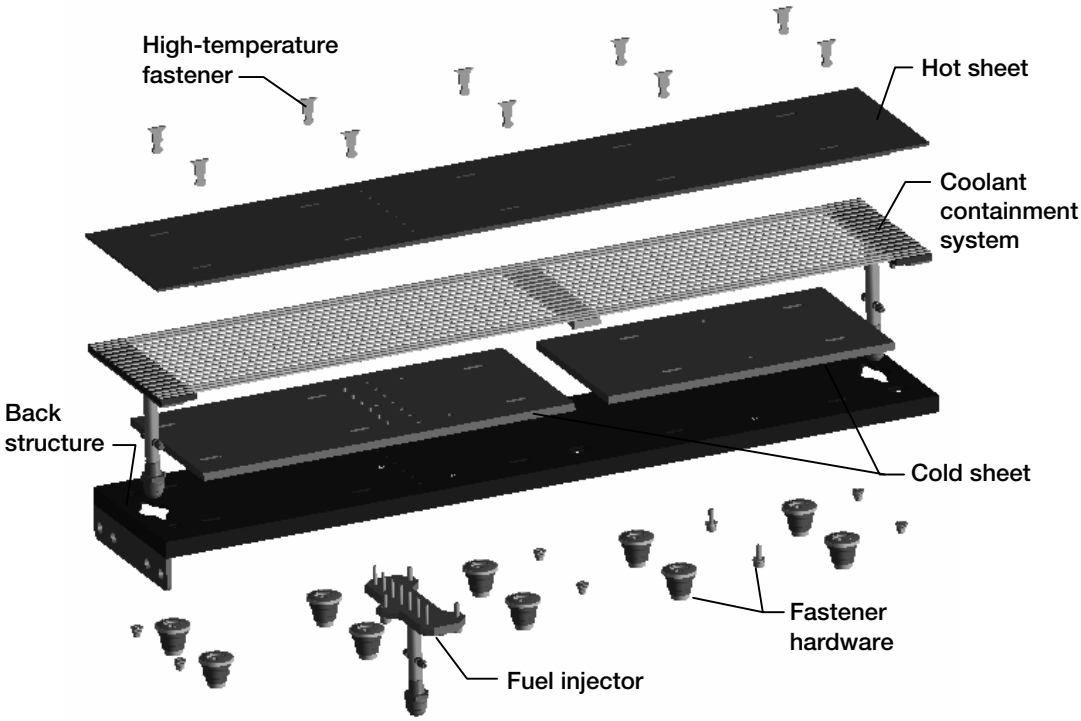

Exploded view of 6- by 30-in. maintainable panel design.

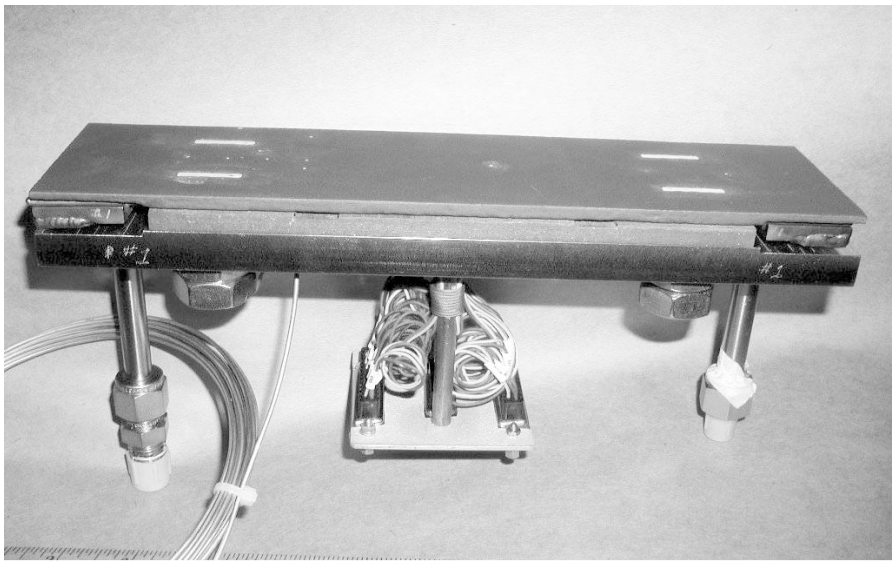

Subscale 2.5- by 10-in. maintainable panel assembly before testing in Glenn's Research Combustion Lab.

fasteners rather than by permanent bonding methods. With this approach, the CMC hot face sheet, the coolant containment system, and backside structure (see the illustration on the preceding page) were all fabricated separately and could be replaced individually as the need occurred during use. This maintainable design leads to both ease of fabrication and reduced cost.

During the first stage of the work, subscale panels were fabricated and tested to verify the predicted performance of the maintainable heat exchanger design and to demonstrate the fabricability of the components. For this stage, 1- by 6-in. cooled CMC samples were tested in a quartz lamp rig at United Technologies Research Center (UTRC) to verify model predictions at a lower heat flux. After heat exchanger performance of the panel assembly was verified with these results, 2.5- by 10-in. panels were fabricated and tested in Glenn's Research Combustion Lab (see the photograph). In addition to verifying the predictions of heat exchanger performance at higher heat fluxes, fabrication of the 2.5- by 10-in. panels identified processing and manifolding issues that needed to be addressed before the design could be scaled up to larger panel sizes. Fiber architectures and panel coatings were optimized to maximize thermal conductivity through the panel. Also surface coatings were identified which offered both improved oxidation resistance and durability under the extremes of the rocket engine tests. Three panels of this design were tested in the facility. The panels were either carbon-reinforced silicon carbide (C/SiC) or carbon-reinforced carbon (C/C) with a silicon carbide surface coating. Slight modifications to the panel and fastener design as the testing proceeded led to the third panel being tested for a cumulative time of 18.5 min with maximum surface temperatures sustained between 2400 to 2600 °F for 2-min durations.

In the final phase of this effort, the scale-up of the design and fabrication of a 6- by 30-in. maintainable CMC cooled panel was completed. The well-established system requirements for the Pratt & Whitney Hydrocarbon Scramjet Engine Technology (HySET) vehicle engine were chosen as the baseline requirements for the cooled CMC panel design. The design targeted the combustor section of the flow path panel with maximum heat and pressure loads at M8 and M5 in the vehicle trajectory. This section of the panel represented the highest heat flux section of the flow path that included operable fuel-injection ports. The effort originally focused on hydrocarbon fuels with a modified version added for hydrogen fuels. The heavily instrumented panel will be tested in fiscal year 2004 in the scramjet rig at UTRC. The objectives of the tests are to validate the materials and design in a representative combined aero/thermal/acoustic scramjet engine environment. The panel will be tested at conditions of Mach 7.0 and $q = 750$ psf cruise test point. It is anticipated that testing of the 6- by 30-in. panel in the scramjet facility will provide critical information on the performance of CMC heat exchangers, which will be needed for future engine demonstrator programs.

Bibliography

Jaskowiak, Martha H.; Dickens, Kevin W.; and Lawrence, Timothy W.: Actively Cooled Ceramic Matrix Composite Panels for Aerospace Propulsion Applications. Presented at the National Space & Missile Materials Symposium, San Diego, CA, 2003.

Glenn contact:
Martha H. Jaskowiak, 216–433–5515, Martha.H.Jaskowiak@nasa.gov

Author: Martha H. Jaskowiak

Headquarters program office: OAT

Programs/Projects: PR&T, NGLT

Prepreg and Melt Infiltration Technology Developed for Affordable, Robust Manufacturing of Ceramic Matrix Composites

Affordable fiber-reinforced ceramic matrix composites with multifunctional properties are critically needed for high-temperature aerospace and space transportation applications. These materials have various applications in advanced high-efficiency and high-performance engines, airframe and propulsion components for next-generation launch vehicles, and components for land-based systems. A number of these applications require materials with specific functional characteristics: for example, thick component, hybrid layups for environmental durability and stress management, and self healing and smart composite matrices. At present, with limited success and very high cost, traditional composite fabrication technologies have been utilized to manufacture some large, complex-shape components of these materials. However, many challenges still remain in developing affordable, robust, and flexible manufacturing technologies for large, complex-shape components with multifunctional properties. The prepreg and melt iInfiltration (PREMI) technology provides an affordable and robust manufacturing route for low-cost, large-scale production of multifunctional ceramic composite components.

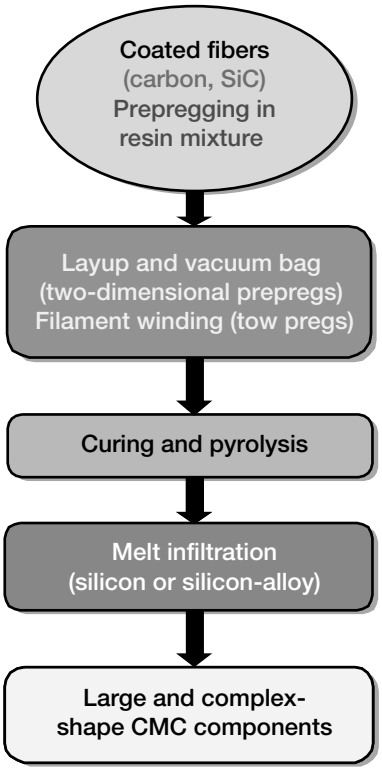

Various steps in the prepreg and melt infiltration (PREMI) process.

The PREMI technology for ceramic matrix composites fabrication, which was developed at the NASA Glenn Research Center, has four steps. These are shown in the figure to the right. In the first step, coated carbon and silicon carbide fibers are prepregged in a proprietary resin and particulate mixture and are B-staged to provide a tacky finish. Fiber tows can also be tow-pregged for filament winding. Flexible prepregs, shown in this photograph, can be used to fabricate large, complex shapes. In the second step, the prepreg cloths are laid up and vacuum bagged for curing. The third step is curing and pyrolysis, which yields an interconnected network of porosity in the matrix. In the final step of the process, the preform is infiltrated with molten silicon or refractory metal-silicon alloys in a furnace. This converts the carbon to silicon carbide. This process is also suitable for making composites with hybrid layups and two- or three-dimensional architectures by filament winding or other fiber placement techniques. This processing approach leads to dense composites, where matrix microstructure and composition can be tailored for optimum properties. It has a much lower processing cost (<50 percent) in comparison to other approaches to fabricating ceramic matrix composites. Thermomechanical and thermochemical characterization of these composites under the hostile environments that will be encountered in various aerospace applications is underway.

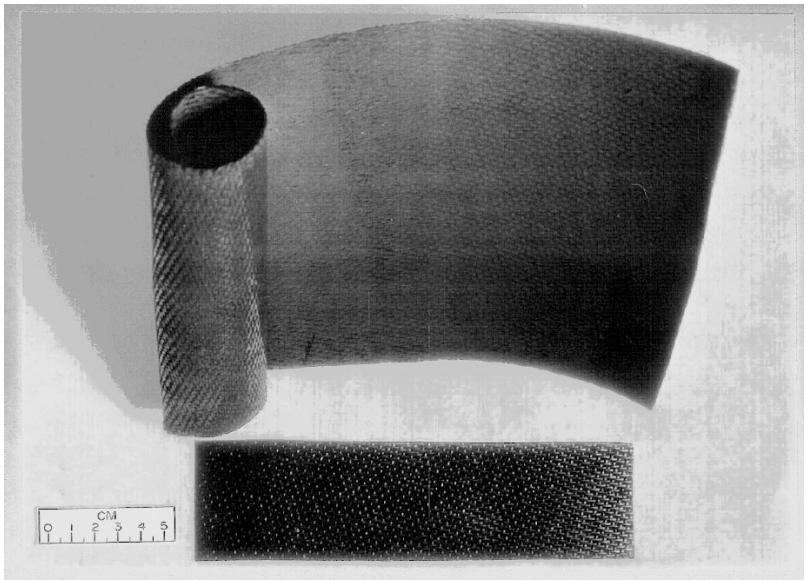

Flexible prepregs for the fabrication of large, complex shapes.

QSS contact:
Dr. Mrityunjay (Jay) Singh, 216–433–8883; Mrityunjay.Singh@grc.nasa.gov
Authors: Dr. Mrityunjay Singh and Jeannie F. Petko
Headquarters Program Office: OAT
Programs/Projects: NGLT

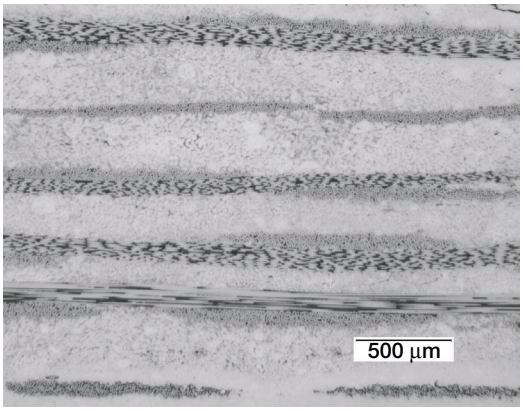

Dense SiC(Sylramic)/SiC ceramic composite fabricated by the PREMI process.

Polymer/Silicate Nanocomposites Used to Manufacture Gas Storage Tanks With Reduced Permeability

Over the past decade, there has been considerable research in the area of polymer-layered silicate nanocomposites. This research has shown that the dispersion of small amounts of an organically modified layered silicate improves the polymer strength, modulus, thermal stability, and barrier properties (ref. 1). There have been several reports on the dispersion of layered silicates in an epoxy matrix (ref. 2). Potential enhancements to the barrier properties of epoxy/silicate nanocomposites make this material attractive for low permeability tankage.

Polymer matrix composites (PMCs) have several advantages for cryogenic storage tanks. They are lightweight, strong, and stiff; therefore, a smaller fraction of a vehicle's potential payload capacity is used for propellant storage. Unfortunately, the resins typically used to make PMC tanks have higher gas permeability than metals. This can lead to hydrogen loss through the body of the tank instead of just at welds and fittings. One approach to eliminate this problem is to build composite tanks with thin metal liners. However, although these tanks provide good permeability performance, they suffer from a substantial mismatch in the coefficient of thermal expansion, which can lead to failure of the bond between the liner and the body of the tank. Both problems could be addressed with polymer-silicate nanocomposites, which exhibit reduced hydrogen permeability, making them potential candidates for linerless PMC tanks.

Polymer/silicate nanocomposite tanks tested for helium permeability.

Through collaboration with Northrop Grumman and Michigan State University, nanocomposite test tanks were manufactured for the NASA Glenn Research Center, and the helium permeability was measured. An organically modified silicate was prepared at Michigan State University and dispersed in an epoxy matrix (EPON 826/JeffamineD230). The epoxy/silicate nanocomposites contained either 0 or 5 wt% of the organically modified silicate. The tanks were made

by filament winding carbon fibers with the nanocomposite resin. Helium permeability was measured by Northrop Grumman, showing that the leak rate/day of the nanocomposite matrix tank was approximately 80-percent less than that of the neat epoxy matrix tank.

References

1. Burnside, S.D.; and Giannelis, E.P.: Synthesis and Properties of New Poly(Dimethylsiloxane). Chem. Mat., vol. 7, no. 9, 1995, pp. 1597–1600.
2. Shi, H.Z.; Lan, T.; and Pinnavaia, T.J.: Interfacila Effects on the Reinforcement Properties of Polymer-Organoclay Nanocomposites. Chem. Mat., vol. 8, no. 8, 1996, pp. 1584–1587.

Find out more about this research:
http://www.grc.nasa.gov/WWW/MDWeb/5150/Polymers.html

Glenn contacts:
Dr. Chris Johnston, 216–433–5029, James.C.Johnston-1@nasa.gov; and Sandi G. Campbell, 216–433–8489, Sandi.Campbell@nasa.gov

Authors: Sandi G. Campbell and Dr. Chris Johnston

Headquarters program office: OAT

Programs/Projects: AFFT

Development of DMBZ–15 High-Glass-Transition-Temperature Polyimides as PMR–15 Replacements Given R&D 100 Award

PMR–15, a high-temperature polyimide developed in the mid-1970's at the NASA Lewis Research Center,[1] offers the combination of low cost, easy processing, and good high-temperature performance and stability. It has been recognized as the leading polymer matrix resin for carbon-fiber-reinforced composites used in aircraft engine components. The state-of-the-art PMR–15 polyimide composite has a glass-transition temperature (T_g) of 348 °C (658 °F). Since composite materials must be used at temperatures well below their glass-transition temperature, the long-term use temperatures of PMR–15 composites can be no higher than 288 °C (550 °F). In addition, PMR–15 is made from methylene dianiline (MDA), a known liver toxin. Concerns about the safety of workers exposed to MDA during the fabrication of PMR–15 components and about the environmental impact of PMR–15 waste disposal have led to the industrywide implementation of special handling procedures to minimize the health risks associated with this material. These procedures have increased manufacturing and maintenance costs significantly and have limited the use of PMR–15 in commercial aircraft engine components.

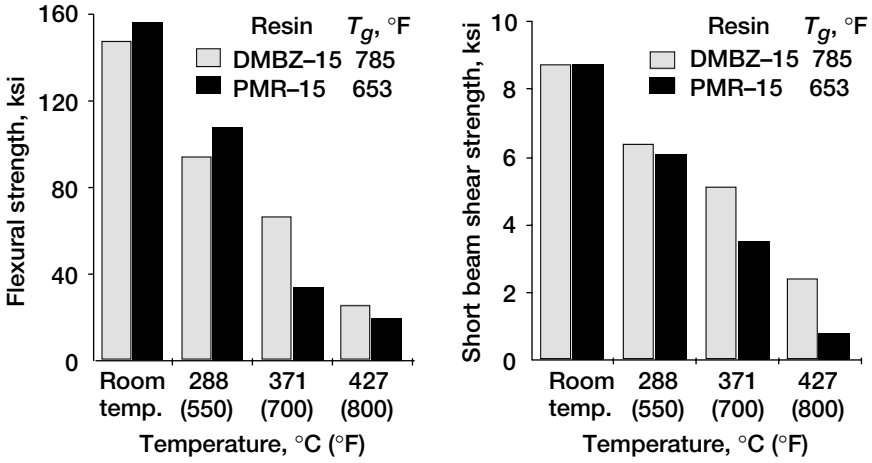

Elevated- and room-temperature mechanical properties of DMBZ–15 and PMR–15 T650–35 carbon fabric composites. T_g, glass-transition temperature. Left: Flexural strength; Right: Short-beam shear strength.

Efforts at the NASA Glenn Research Center to develop a PMR–15 replacement have yielded an alternative polyimide, DMBZ–15, which has a T_g of 418 °C (784 °F). Because of its unusually high T_g, DMBZ–15 can be used at temperatures as high as 343 °C (650 °F) (see the bar charts). This is an increase of 55 °C (100 °F) over the maximum temperature of PMR–15, which is the current state of the art. In addition, DMBZ–15 composites have been shown to have wear resistance superior to that of PMR–15. Potential aerospace applications for this ultra-high-temperature composite include aircraft engine components—such as bushings and bearings, cases, ducts, and fuel and lubricant lines—as well as

[1]Now called the NASA Glenn Research Center.

reusable-launch-vehicle (RLV) propulsion and airframe structures. Because of DMBZ's superior high-temperature stability and performance, use of this ultra-high-temperature composite in airframe components for RLVs would enable significant reductions in the thermal protection system (TPS) and its parasitic weight. Nonaerospace applications for DMBZ–15 include components for oil drilling equipment and replacements for oiled brass bearings in the rolling and printing industries.

Glenn contact:
Dr. Kathy Chuang, 216–433–3227, Kathy.Chuang@grc.nasa.gov

Author: Dr. Kathy Chuang

Headquarters program office: OAT

Programs/Projects:
HOTPC, Hypersonics Initiative, PR&T

Special recognition:
2003 R&D 100 Award

New High-Temperature Membranes Developed for Proton Exchange Membrane Fuel Cells

Fuel cells are receiving a considerable amount of attention for potential use in a variety of areas, including the automotive industry, commercial power generation, and personal electronics. Research at the NASA Glenn Research Center has focused on the development of fuel cells for use in aerospace power systems for aircraft, unmanned air vehicles, and space transportation systems. These applications require fuel cells with higher power densities and better durability than what is required for nonaerospace uses. In addition, membrane cost is a concern for any fuel cell application. The most widely used membrane materials for proton exchange membrane (PEM) fuel cells are based on sulfonated perfluorinated polyethers, typically Nafion 117, Flemion, or Aciplex. However, these polymers are costly and do not function well at temperatures above 80 °C. At higher temperatures, conventional membrane materials dry out and lose their ability to conduct protons, essential for the operation of the fuel cell. Increasing the operating temperature of PEM fuel cells from 80 to 120 °C would significantly increase their power densities and enhance their durability by reducing the susceptibility of the electrode catalysts to carbon monoxide poisoning. Glenn's Polymers Branch has focused on developing new, low-cost membranes that can operate at these higher temperatures.

A new series of organically modified siloxane (ORMOSIL) polymers were synthesized for use as membrane materials in a high-temperature PEM fuel cell (see the following figure). These polymers have an organic portion that can allow protons to transport through the polymer film and a cross-linked silica network that gives the polymers dimensional stability. These flexible xerogel polymer films are thermally stable, with decomposition onset as high as 380 °C (see the following figure).

Two types of proton conducting ORMOSIL films have been produced: (1) NASA–A, which can coordinate

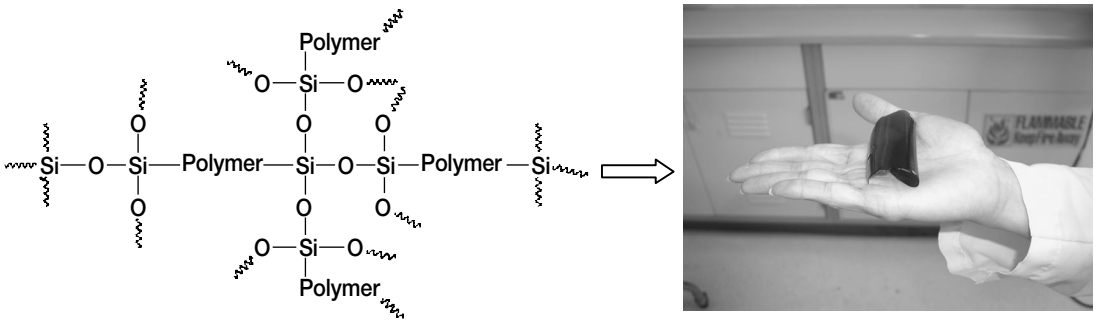

ORMOSIL polymer used in high-temperature proton exchange fuel cell. Left: structure. Right: polymer membrane of fuel cell.

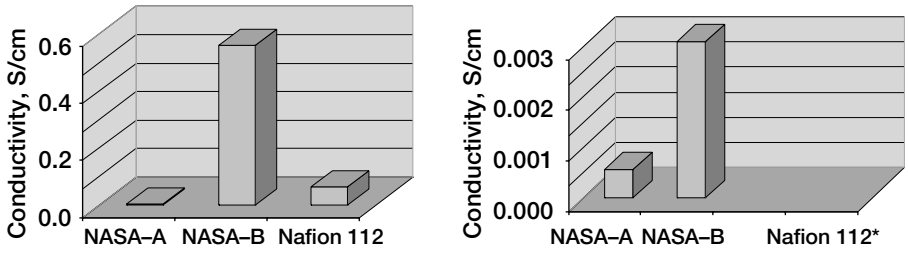

*Conductivity data. Left: At 100 °C and 47-percent relative humidity. Right: At 120 °C and 25-percent relative humidity. (*Below detection limit.)*

many highly acid inorganic salts that facilitate proton conduction and (2) NASA–B, which has been produced and which incorporates strongly acidic (proton donating) functional groups into the polymer backbone. Both of these polymer films have demonstrated significantly higher proton conductivity than Nafion at elevated temperatures and low relative humidities (see the bar charts). An added advantage is that these polymers are very inexpensive to produce because their starting materials are commodity chemicals that are commercially available in large volumes.

Find out more about this research:
http://www.grc.nasa.gov/WWW/MDWeb/5150/Polymers.html

Glenn contact:
Dr. James D. Kinder, 216–433–3149, James.D.Kinder@nasa.gov

Author: Dr. James D. Kinder

Headquarters program office: OAT

Programs/Projects: PR&T

Mechanically Strong Aerogels Formed by Templated Growth of Polymer Cross-Linkers on Inorganic Nanoparticles

In the search for materials with better mechanical, thermal, and electrical properties, it is becoming evident that oftentimes dispersing ceramic nanoparticles in plastics improves performance. Along these lines, chemical bonding (both covalent and noncovalent) between a filler and a polymer improves their compatibility, and thus enhances certain properties of the polymeric matrix above and beyond what is accomplished by simple doping with the filler. When a similarly sized dopant and matrix are used, elementary building blocks may also have certain distinct advantages (e.g., in catalysis). In this context, researchers at the NASA Glenn Research Center reasoned that in the extreme case, where the dopant and the matrix (e.g., a filler and a polymer) are not only sized similarly, but their relative amounts are comparable, the relative roles of the dopant and matrix can be reversed. Then, if the "filler," or a certain form thereof, possesses desirable properties of its own, such properties could be magnified by cross-linking with a polymer. We at Glenn have identified silica as such a filler in its lowest-density form, namely the silica aerogel.

Aerogels are used primarily in space applications as collectors of hypervelocity particles (STARDUST Program) or for thermal insulation in extreme environments (refer to the *Sojourner* Rover in 1997 or the two Mars Exploratory Rovers, *Spirit* and *Opportunity*, in 2003). For instance, it has been reported that if conventional thermal insulation had been used on the *Sojourner* Rover, 6 lb of the total 25-lb weight of the rover would have been lost for thermal insulation. Thus, it was reasoned that if the thermal insulator—the aerogel—was strong enough to comprise the building material of the entire space vehicle, more weight would be freed for useful payload.

With this in mind, we were able to "glue" together the nanoparticle building blocks of a conventional silica aerogel, by templated, directed growth of the polymer on those particles. Thus, the resulting material is ~3 times more dense than the underlying silica aerogel framework but takes more than 300 times the force to break. The preceding photograph shows such a cross-linked silica aerogel monolith just before its break point.

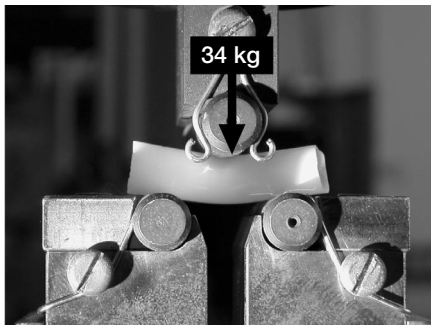

A cross-linked silica aerogel undergoing a three-point flexural bending test. The density of the monolith is ~0.55 g/cm^3. The density of the underlying silica is ~0.18 g/cm^3, and the silica has been cross-linked with polyhexamethylene diisocyanate.

The mechanism of cross-linking has been investigated carefully, and it has been discovered that the cross-linking chemistry is based on (1) a reaction between the cross-linker and the

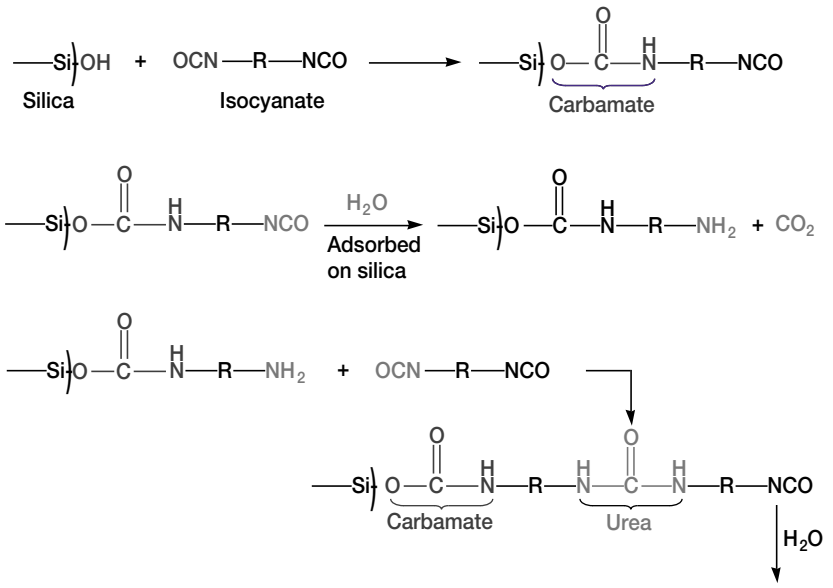

Cross-linking silica with a diisocyanate.

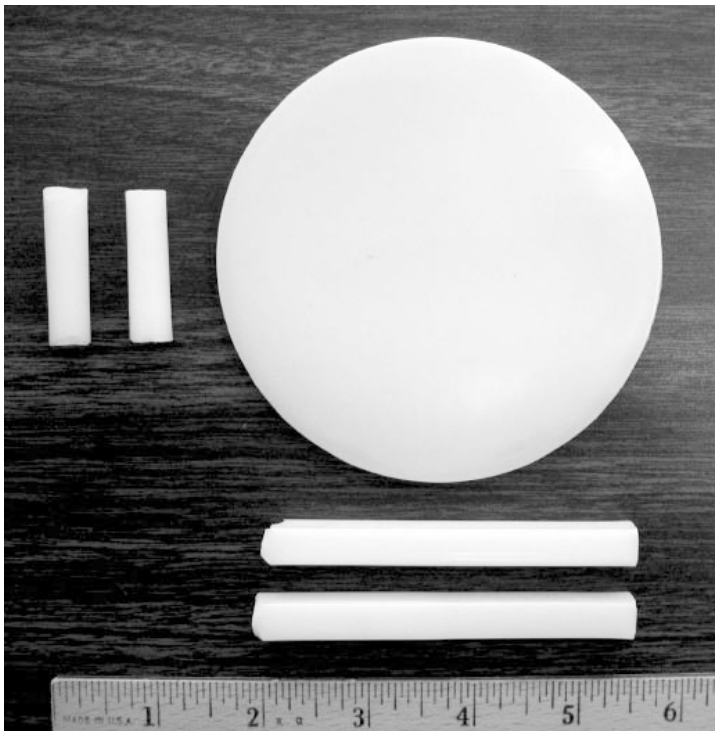

Aerogels produced by ambient pressure drying from pentane.

surface of the aerogel framework and (2) a reaction of the cross-linker with itself, either via a mechanism that is catalyzed by the surface of the aerogel framework or via a reagent that is confined on that surface. Thus diisocyanates react with the surface of the aerogel, forming urethanes, or they are hydrolyzed by adsorbed water, yielding amines, which then attack other diisocyanates, forming ureas (see the chemical diagram). In addition, epoxies containing two, three, or four reactive groups undergo a ring-opening cascade of reactions with themselves as well as with amino groups that have been deliberately placed on the aerogel surface.

Cross-linked aerogels are strong enough to withstand the surface tension forces developing around the residing meniscus of low-vapor-pressure liquids evaporating through their bulk. So it has been found that cross-linked hydrogels can be dried to aerogels from pentane under ambient pressure, thus eliminating the need for extractions with a supercritical fluid. As a result, objects with different shapes and sizes can be produced easily.

Find out more about this research:
http://www.grc.nasa.gov/WWW/MDWeb/5150/Polymers.html

Glenn contact:
Dr. Nicholas Leventis, 216–433–3202, Nicholas.Leventis@nasa.gov

Authors:
Dr. Nicholas Leventis, Dr. Eve F. Fabrizio, Dr. Chris Johnston, and Dr. Maryann Meador

Headquarters program office: OAT

Programs/Projects: PR&T

Erosion Coatings Developed to Increase the Life and Durability of Composites

Both the NASA Glenn Research Center and the Allison Advanced Development Company (AADC) have worked to develop and demonstrate erosion-resistant coatings that would increase the life and durability of composite materials used in commercial aircraft engines. These composite materials reduce component weight by 20 to 30 percent and result in less fuel burn and emissions and more fuel savings. Previously, however, their use was limited because of poor erosion resistance, which causes concerns about safety and leads to high maintenance costs. The coatings were tested by the University of Cincinnati, and the composites were manufactured by Texas Composites and coated by Engelhard and NASA Glenn.

Rolls-Royce Corporation uses composite materials, which are stronger and less dense than steel or titanium, to make bypass vanes for their AE3007 engines. These engines are widely used in regional jet aircraft (Embraer) and unmanned air vehicles such as the Northrop Grumman Global Hawk. Coatings developed by NASA/Rolls-Royce can reduce erosion from abrasive materials and from impurities in the air that pass over these vanes, allowing Rolls-Royce to take advantage of the benefits of composite materials over titanium without the added costs of increased maintenance and/or engine failure.

The Higher Operating Temperature Propulsion Components (HOTPC) Project developed cost-effective, durable coatings as part of NASA's goal to increase aviation system capacity growth. These erosion coatings will reduce the number of special inspections or instances of discontinued service due to erosion, allowing aircraft capacity to be maintained without inconveniencing the traveling public. A specific example of extending component life showed that these coatings increased the life of graphite fiber and polymer composite bypass vanes up to 8 times over that of the uncoated vanes. This increased durability allows components to operate to full design life without fear of wear or failure.

Recently, Rolls-Royce completed over 2000 hr of engine testing with the coated fan exit bypass vanes (see the photograph on the left). There was no loss of coating after nearly 5000 typical engine cycles. Midway through the engine tests, the coated vanes were removed from the engine during a scheduled maintenance and inspection period. The vanes were shipped back to Glenn, where they underwent further stress testing in the Structural Dynamics Lab, mimicking more extreme conditions than those typical of the AE3007 engine cycle. These vanes were then replaced in the AE3007 and subjected to another 1000 hr of engine tests. Once again, there was no loss of coating and only a minimal appearance of cracking (see the photograph on the right).

Find out more about this research:

Glenn's Polymers Branch:
http://www.grc.nasa.gov/WWW/MDWeb/5150/Polymers.html

Glenn's Structural Mechanics & Dynamics Branch:
http://structures.grc.nasa.gov/5930/

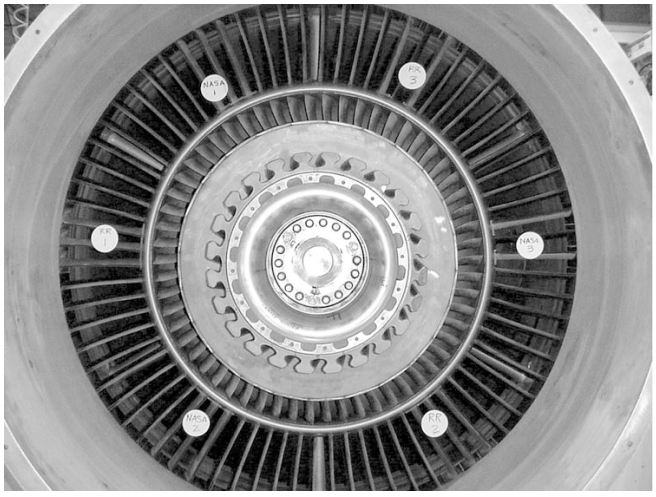

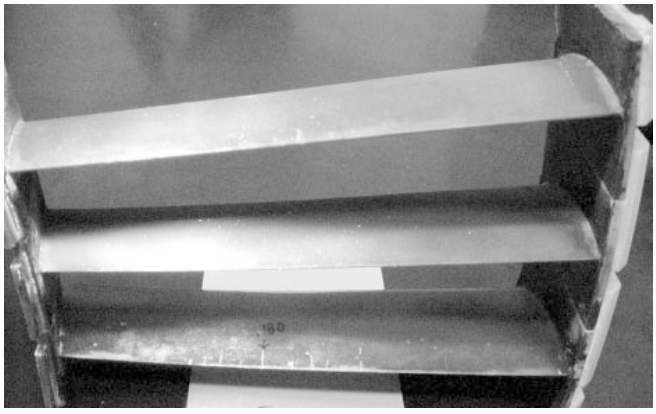

Left: AE3007 engine test of bypass vanes with erosion-resistant coatings. Right: Minor cracking shown by fluorescent dye penetrant.

Glenn's Structural Dynamics Laboratory:
http://www.grc.nasa.gov/WWW/Facilities/int/sdl/

Glenn contacts: Dr. James K. Sutter, 216–433–3226, James.K.Sutter@nasa.gov; Dr. Cheryl L. Bowman, 216–433–8462, Cheryl.L.Bowman@nasa.gov; Dr. Kazuhisa Miyoshi, 216–433–6078, Kazuhisa.Miyoshi-1@nasa.gov; and Gail P. Perusek, 216–433–8729, Gail.P.Perusek@nasa.gov

Rolls-Royce contact:
Subhash K. Naik, 317–230–5756, subhash.k.naik@rolls-royce.com

AADC contact: Robert Siefker, 317–230–2260, bob.g.siefker@aadc.com

Authors:
Dr. James K. Sutter, Subhash K. Naik, Dr. Cheryl L. Bowman, Robert Siefker, Dr. Kazuhisa Miyoshi, and Gail P. Perusek

Headquarters program office: OAT

Programs/Projects:
Propulsion and Power, HOTPC

Depth-Penetrating Measurements Developed for Thermal Barrier Coatings Incorporating Thermographic Phosphors

The insulating properties of thermal barrier coatings (TBCs) provide highly beneficial thermal protection to turbine engine components by reducing the temperature sustained by those components. Therefore, measuring the temperature beneath the TBC is critical for determining whether the TBC is performing its insulating function. Currently, noncontact temperature measurements are performed by infrared pyrometry, which unfortunately measures the TBC surface temperature rather than the temperature of the underlying component. To remedy this problem, the NASA Glenn Research Center, under the Information Rich Test Instrumentation Project, developed a technique to measure the temperature beneath the TBC by incorporating a thin phosphor layer beneath the TBC. By performing fluorescence decay-time measurements on light emission from this phosphor layer, Glenn successfully measured temperatures from the phosphor layer up to 1100 °C. This is the first successful demonstration of temperature measurements that penetrate beneath the TBC.

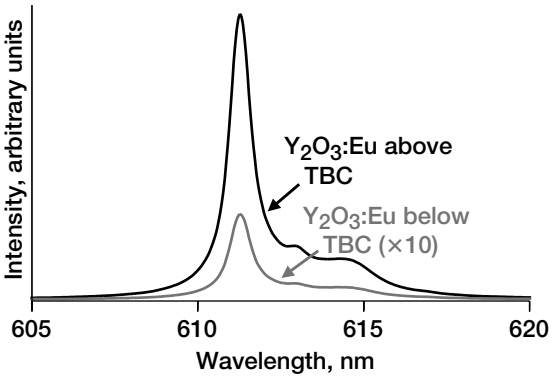

Comparison of the phosphor emission intensity for the Y_2O_3:Eu phosphor layer above the 100-μm-thick thermal barrier coating (TBC) versus the layer below it. The emission spectrum for the phosphor layer below the TBC has been multiplied by 10 for easier comparison.

Thermographic phosphors have a history of providing noncontact surface temperature measurements. Conventionally, a thermographic phosphor is applied to the material surface and temperature measurements are performed by exciting the phosphor with ultraviolet light and then measuring the temperature-dependent decay time of the phosphor emission at a longer wavelength. The innovative feature of the new approach is to take advantage of the relative transparency of the TBC (composed of yttria-stabilized zirconia) in order to excite and measure the phosphor emission beneath the TBC. The primary obstacle to achieving depth-penetrating temperature measurements is that the TBCs are completely opaque to the ultraviolet light usually employed to excite the phosphor. The strategy that Glenn pursued was to select a thermographic phosphor that could be excited and emit at wavelengths that could be transmitted through the TBC. The phosphor that was selected was yttria doped with europia (Y_2O_3:Eu), which has a minor excitation peak at 532 nm (green) and an emission peak at 611 nm (red)—both are wavelengths that exhibit significant transmission through the TBC.

The measurements were performed on specimens consisting of a 25-μm-thick phosphor layer beneath a 100-μm-thick TBC. The 532-nm (green) excitation light was provided by a frequency-doubled YAG:Nd (yttrium-aluminum-garnet:neodymium) laser, and the fluorescence decay time measurements were acquired with a modified Raman microscope. The preceding graph compares the intensity of the phosphor emission of the phosphor layer above the TBC versus that of the phosphor layer beneath the TBC. Although there was considerable attenuation of the

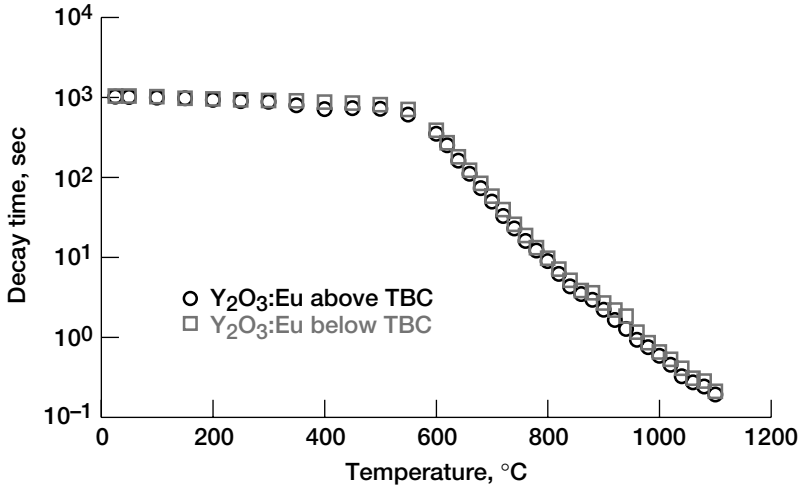

The fluorescence decay time as a function of temperature for the Y_2O_3:Eu phosphor layer above the TBC versus the layer below it.

phosphor signal (a factor of 30), the phosphor emission at the reduced intensity was more than sufficient to perform fluorescence decay time measurements. The graph on the left shows the fluorescence lifetime temperature dependency for the Y_2O_3:Eu phosphor layers both above and below the TBC. These curves show an excellent match and indicate that despite the attenuation due to the overlying TBC, the phosphor layer beneath the TBC still functions as an effective temperature indicator.

Glenn contact:
Dr. Jeffrey I. Eldridge, 216–433–6074, Jeffrey.I.Eldridge@nasa.gov

Authors: Dr. Jeffrey I. Eldridge and Timothy J. Bencic

Headquarters program office: OAT

Programs/Projects:
Information Rich Test Instrumentation

New Effective Material Couple—Oxide Ceramic and Carbon Nanotube—Developed for Aerospace Microsystem and Micromachine Technologies

The prime driving force for using microsystem and micromachine technologies in transport vehicles, such as spacecraft, aircraft, and automobiles, is to reduce the weight, power consumption, and volume of components and systems to lower costs and increase affordability and reliability (refs. 1 and 2). However, a number of specific issues need to be addressed with respect to using microsystems and micromachines in aerospace applications—such as the lack of understanding of material characteristics; methods for producing and testing the materials in small batches; the limited proven durability and lifetime of current microcomponents, packaging, and interconnections; a cultural change with respect to system designs; and the use of embedded software, which will require new product assurance guidelines.

In regards to material characteristics, there are significant adhesion, friction, and wear issues in using microdevices. Because these issues are directly related to surface phenomena, they cannot be scaled down linearly and they become increasingly important as the devices become smaller (ref. 2). When microsystems have contacting surfaces in relative motion, the adhesion and friction affect performance, energy consumption, wear damage, maintenance, lifetime and catastrophic failure, and reliability. Ceramics, for the most part, do not have inherently good friction and wear properties. For example, coefficients of friction in excess of 0.7 have been reported for ceramics and ceramic composite materials (e.g., ref. 3).

Under Alternate Fuels Foundation Technologies funding, two-phase oxide ceramics (ref. 4) developed for superior high-temperature wear resistance in NASA's High Operating Temperature Propulsion Components (HOTPC) project and new two-layered carbon nanotube (CNT) coatings (CNT topcoat/iron bondcoat/quartz substrate) developed in NASA's Revolutionary Aeropropulsion Concepts (RAC) project have been chosen as a materials couple for

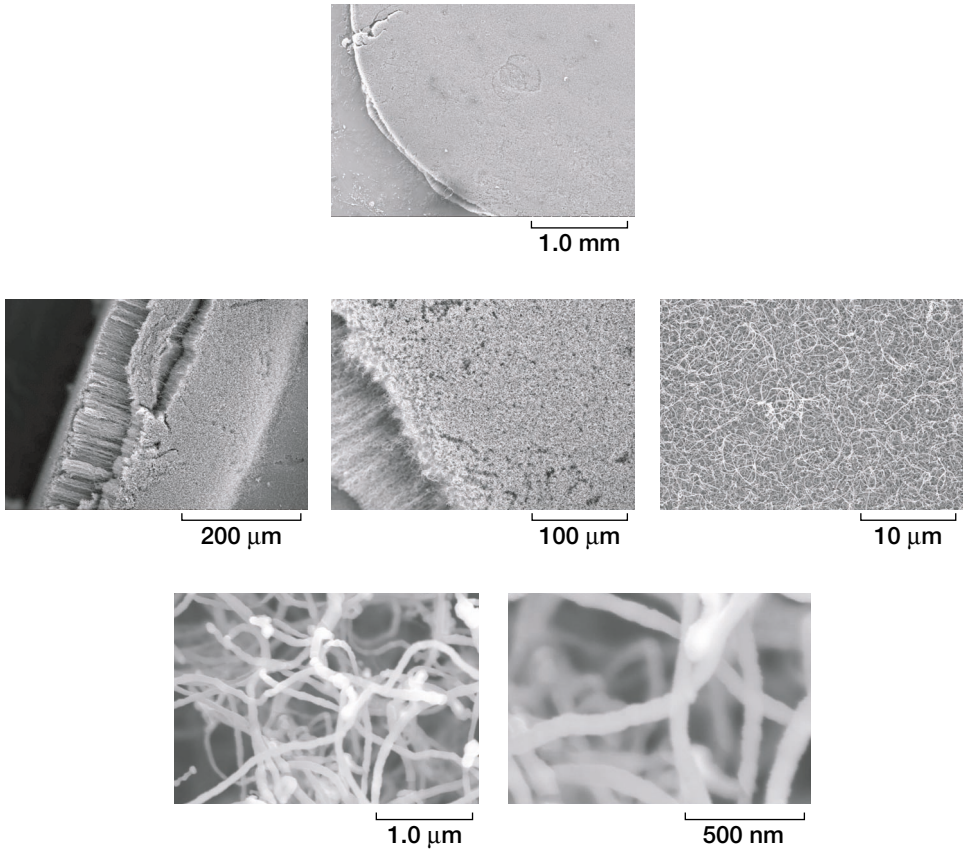

Carbon nanotube materials showing oriented growth.

aerospace applications, including micromachines, in the nanotechnology lubrication task because of their potential for superior friction and wear properties in air and in an ultrahigh vacuum, spacelike environment. At the NASA Glenn Research Center, two-phase oxide ceramic eutectics, Al_2O_3/ZrO_2 (Y_2O_3), were directionally solidified using the laser-float-zone process (ref. 5), and carbon nanotubes were synthesized within a high-temperature tube furnace at 800 °C (ref. 6). Physical vapor deposition was used to coat all quartz substrates with 5-nm-thick iron as catalyst and bondcoat, which formed iron islands resembling droplets and serving as catalyst particles on the quartz.

The preceding figure presents a series of scanning electron micrographs showing multiwalled carbon nanotubes directionally grown as aligned "nanograss" on quartz. Unidirectional, sliding friction experiments were conducted at Glenn with the two-layered CNT coatings in contact with the two-phase Al_2O_3/ZrO_2 (Y_2O_3) eutectics in air and in ultrahigh vacuum (see the graphs on the next page). The main criteria for judging the performance of the materials couple for solid lubrication and antistick applications in a space environment were the coefficient of friction and the wear resistance (reciprocal of wear rate), which had to be less than 0.2 and greater than 10^5 N·m/mm^3, respectively, in ultrahigh vacuum.

In air, the coefficient of friction for the CNT coatings in contact with Al_2O_3/ZrO_2 (Y_2O_3) eutectics was 0.04, one-fourth of that for quartz. In an ultrahigh vacuum, the coefficient of friction for CNT coatings in contact with Al_2O_3/ZrO_2 (Y_2O_3) was one-third of that for quartz. The two-phase Al_2O_3/ZrO_2 (Y_2O_3) eutectic coupled with the two-layered CNT coating met the coefficient of friction and wear resistance criteria both in air and in an ultrahigh vacuum, spacelike environment. This material's couple can dramatically improve the stiction (or adhesion), friction, and wear resistance of the contacting surfaces, which are major issues for microdevices and micromachines.

References

1. Stark, Brian, ed.: MEMS Reliability Assurance Guidelines for Space Applications. JPL Publication 99–1, 1999.
2. Hermans, L.: MEMS R&D in Europe. Tribology Issues and Opportunities in MEMS, Kluwer Academic Publishers, Dordrecht, Netherlands, 1998, pp.1–16. Available from Kluwer Academic Publishers.

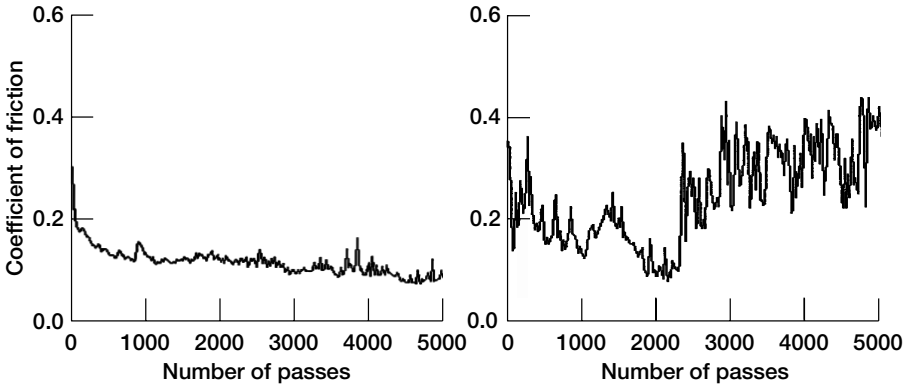

Coefficient of friction for carbon nanotube coating and quartz substrate in sliding contact with an Al_2O_3/ZrO_2 (Y_2O_3) eutectic (two-phase oxide ceramic) hemispherical pin in ultrahigh vacuum. Left: Carbon nanotube coating on quartz (CNT/iron/quartz). Right: Uncoated quartz.

3. Jahanmir, Said: Friction and Wear of Ceramics. Marcel Dekker, New York, NY, 1994.
4. Sayir, Ali; Miyoshi, Kazuhisa; and Farmer, Serene C.: New Oxide Ceramic Developed for Superior High-Temperature Wear Resistance. Research & Technology 2002, NASA/TM—2003-211990, 2003, pp. 39–40. http://www.grc.nasa.gov/WWW/RT2002/5000/5160miyoshi1.html
5. Sayir, A.; and Farmer, S.C.: The Effect of the Microstructure on Mechanical Properties of Directionally Solidified Al_2O_3/ZrO_2 (Y_2O_3) Eutectic. Acta Mater., vol. 48, nos. 18–19, 2000, pp. 4691–4697.
6. Vander Wal, R.L.; and Hall, L.J.: Carbon Nanotube Synthesis Upon Stainless Steel Meshes. Carbon, vol. 41, no. 4, 2003, pp. 659–672.

Glenn contacts:
Dr. Kazuhisa Miyoshi, 216–433–6078, Kazuhisa.Miyoshi-1@nasa.gov; and Dr. Serene C. Farmer, 216–433–3289, Serene.C.Farmer@nasa.gov

National Center for Microgravity Research contacts:
Dr. Randy L. Vander Wal, 216–433–9065, Randall.L.VanderWal@grc.nasa.gov; and Aaron J. Tomasek, 216–433–9628, Aaron.J.Tomasek@grc.nasa.gov

Case Western Reserve University contact:
Dr. Ali Sayir, 216–433–6254, Ali.Sayir@grc.nasa.gov

Authors:
Dr. Kazuhisa Miyoshi, Dr. Randall L. Vander Wal, Aaron J. Tomasek, Dr. Ali Sayir, and Dr. Serene C. Farmer

Headquarters program office: OAT

Programs/Projects: LEAP, VSP, AFFT

Coating Development for GRCop-84 Liners for Reusable Launch Vehicles Aided by Modeling Studies

The design of the next generation of reusable launch vehicles calls for using GRCop-84 copper alloy liners based on a composition invented at the NASA Glenn Research Center (ref. 1). Despite its considerable advantage over other copper alloys, it is expected that GRCop-84 will suffer from environmental degradation depending on the type of rocket fuels used and on thermomechanical fatigue (refs. 2 to 4). Applying protective coatings on GRCop-84 substrates can minimize or eliminate many of these problems and extend the operational life of the combustion liner. This could increase component reliability, shorten depot maintenance turnaround times, and lower operating costs. Therefore, Glenn is actively pursuing the development of advanced coatings technology for GRCop-84 liners. Technology is being developed in four major areas: (1) new metallic coating compositions, (2) application techniques, (3) test methods, and (4) life prediction design methodology using finite element analysis. The role of finite element analysis in guiding the coating effort is discussed in this report.

Thermal analyses were performed at Glenn for different combinations of top- and bond-coat compositions to determine the temperature variation across the coated cross section with the thickness of the top coat. These calculations were conducted for simulated LH_2/LO_2 booster engine conditions assuming that the bond coat had a constant thickness of 50 μm. The graphs on the next page show the predicted temperatures at the outer surface of the top coat (hot wall), at the top-coat/bond-coat interface, at the bond-coat/GRCop-84 interface, and at the GRCop-84 cold wall as a function of top-coat thickness for Cu-26(wt%)Cr top coat (top graph), Ni-17(wt%)Cr-6%Al-0.5%Y top coat and Cu-26%Cr bond coat (center graph), and NiAl top coat and Ni bond coat (bottom graph). In all cases, the temperature of the top coat at the hot wall increased with increasing top-coat thickness and with corresponding decreases in the temperatures at the two interfaces and the cold wall. These temperatures are

not acutely sensitive to the thermal conductivity of the top coat when it exceeds 25 and 50 W/m/K for low and high heat flux engines (see the graphs at the top of the next page). This observation is significant for two reasons. First, several different top-coat compositions can be evaluated as potential protective coatings without loss in the heat-transfer efficiency of the coated system. Second, materials with thermal conductivities less than the critical values of 25 or 50 W/m/K are more likely to act as thermal barrier coatings.

The deposition of overlay coatings on GRCop-84 substrates results in the development of residual stresses (ref. 5). The presence of these residual stresses influences the probability of coating spallation, the thermal cycling life, and the fatigue properties of the coated substrate during use. Since it is important to understand how these stresses develop during the vacuum-plasma-spraying coating deposition process, the nature and magnitudes of the cool-down residual stresses were calculated and compared with experimentally determined values across the coated cross section of a disk specimen. The calculations were conducted assuming that the specimen cools down to room temperature from vacuum-plasma-spraying temperatures of either 250 or 650 °C. The effects of coating the substrate with and without grit blasting were also theoretically examined. The bottom graph on the next page compares the predicted and the experimental results for a GRCop-84 disk coated with about a 50-μm-thick Ni bond coat and a 75- to 100-μm NiAl top coat, where the curves for NASA–2 assume the presence of a prior residual stress generated by grit blasting under conditions similar to the experimental situation. The predicted cool-down in-plane stresses were compressive in both the NiAl top coat and the Ni bond coat. They were also compressive in the substrate to a depth of about 0.25 mm from the Ni/GRCop-84 interface when the vacuum-plasma-spraying temperature was low. However, using a higher plasma spraying temperature is likely to leave the substrate under a small tensile stress to counter the compressive stresses in the bond and top coats because of the relaxation of residual stresses generated in the substrate during the grit blasting of its surface prior to spraying. These results suggest that the NiAl and Ni coatings are unlikely to spall after spraying as confirmed by the microstructural observations shown in the photomicrograph (next page) of an as-sprayed specimen. Finally, it is noted that the calculated and experimental results are not in complete agreement, which indicates that both the experimental and modeling techniques need further refinement.

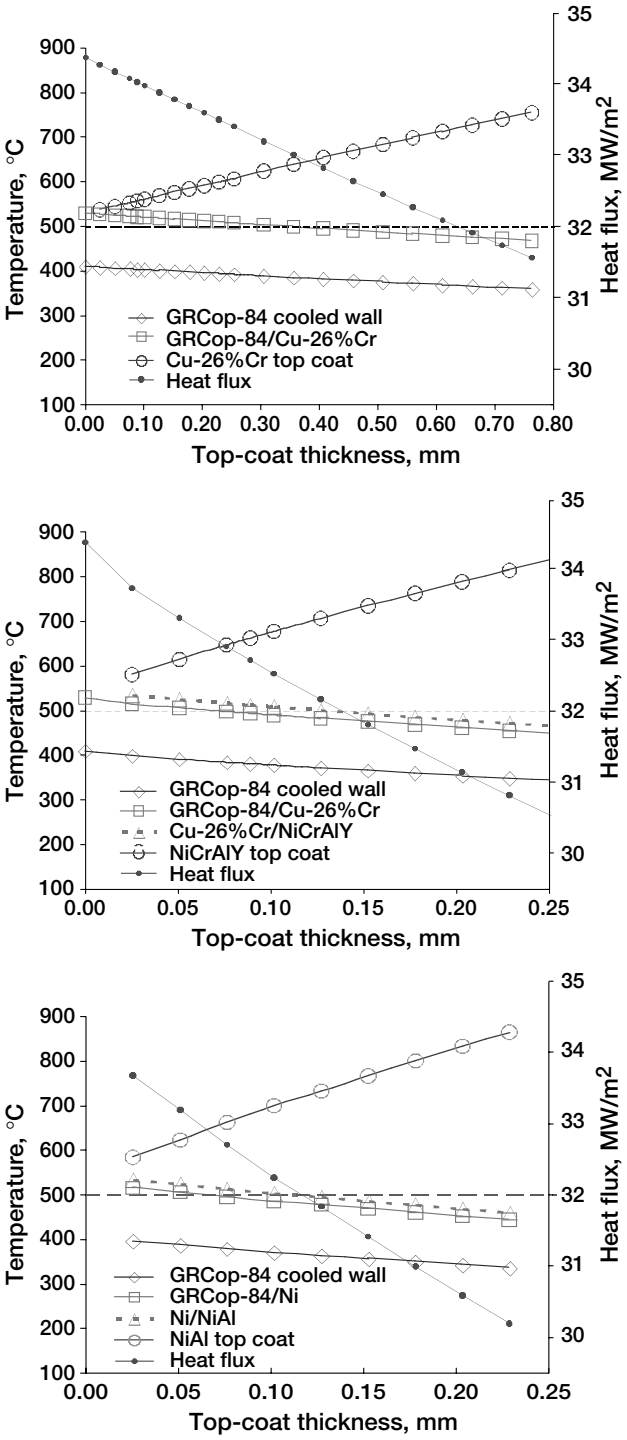

Effect of different coatings on the expected temperature distribution of the GRCop-84 liner in a rocket engine environment for a bond-coat thickness of 50 μm. The temperature of the hot gas was assumed to be 3277 °C; the coolant temperature, –176 °C; the convective heat transfer coefficient of the hot gas, 12.4 kW/m^2/K; and the convective heat transfer coefficient of the coolant, 58.2 MW/m^2/K. Left: Cu-26Cr/GRCop-84. Center: NiCrAlY/Cu-26Cr/GRCop-84. Right: NiAl/Ni/GRCop-84.

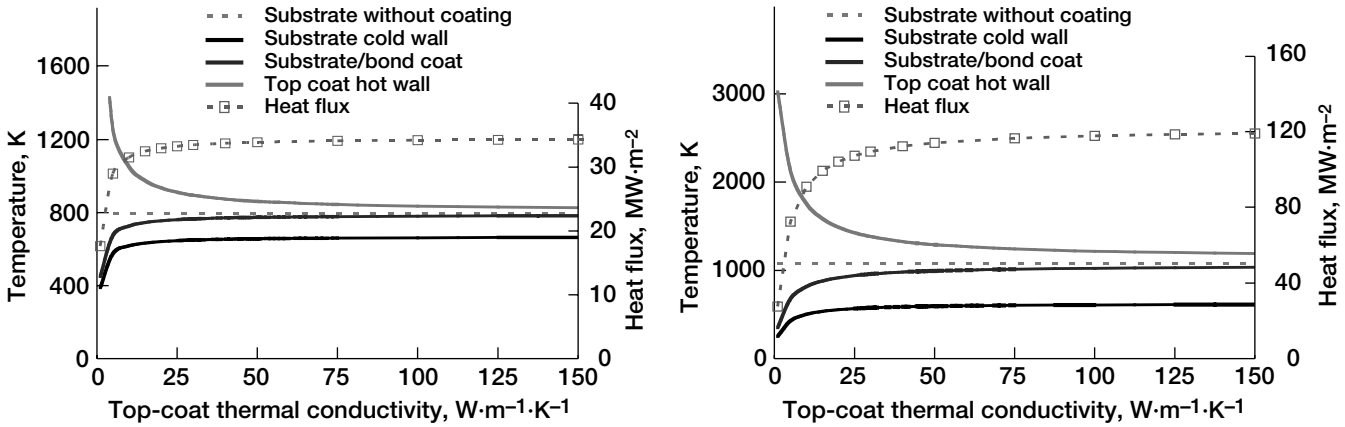

Predicted temperature variation across the cross section of coated GRCop-84 substrates in a rocket engine environment for top coats with different thermal conductivities. The thicknesses of the bond coat, top coat, and liner were assumed to be 50 μm, 100 μm, and 1.0 mm, respectively. Left: Low-heat-flux rocket engine. Right: High-heat-flux rocket engine.

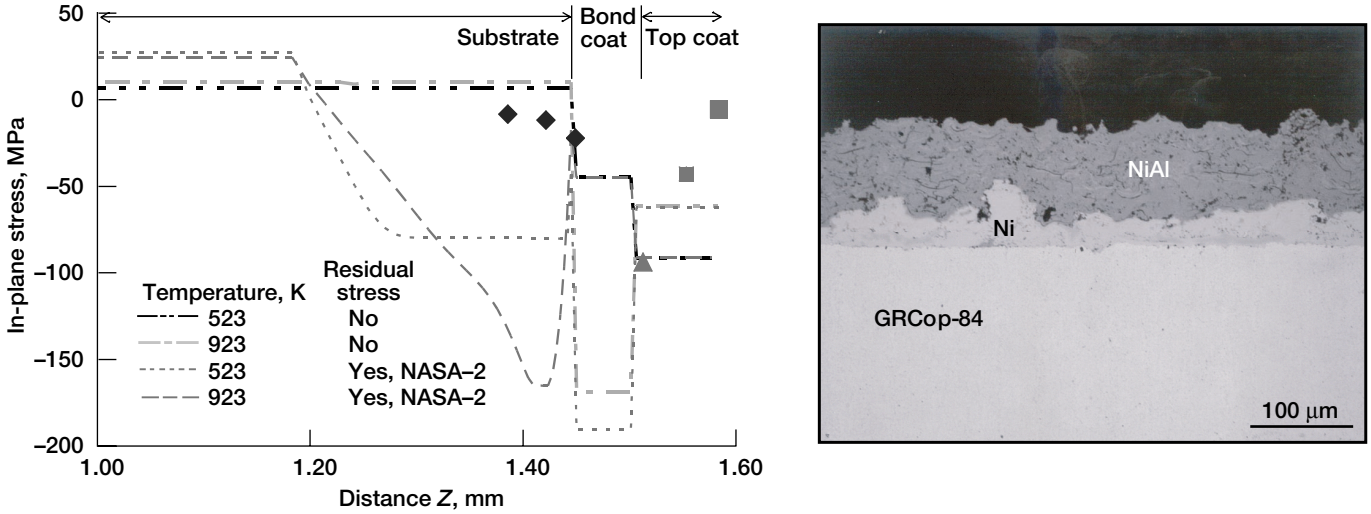

Left: Comparison of experimental and calculated residual stresses at different points across the NiAl/Ni/GRCop-84 cross section, assuming that the initial specimen temperatures soon after vacuum plasma spraying were 523 and 923 K for substrates with and without a prior residual stress history. Right: Micrograph of the cross section of an as-sprayed GRCop-84 substrate showing the microstructures of the NiAl top and the Ni bond coats, respectively.

References

1. Ellis, David L.; and Michal, Gary M.: Mechanical and Thermal Properties of Two Cu-Cr-Nb Alloys and NARloy-Z. NASA CR–198529, 1996.
2. Morgan, D.B.; and Kobayashi, A.C.: Main Chamber Combustion and Cooling Technology Study. NASA CR–184345, 1989. Available from the NASA Center for AeroSpace Information.
3. Rosenberg, S.D., et al.: Hydrocarbon-Fuel Copper Combustion-Chamber Liner Compatibility, Corrosion Prevention, and Refurbishment. J. Propul. P., vol. 8, no. 6, 1992, pp. 1200–1207.
4. Quentmeyer, R.J.: Experimental Fatigue Life Investigation of Cylindrical Thrust Chambers. NASA–TM–X–73665, 1977.
5. Tsui, Y.C.; and Clyne, T.W.: An Analytical Model for Predicting Residual Stresses in Progressively Deposited Coatings. I. Planar Geometry. Thin Solid Fi., vol. 306, no.1, 1997, pp. 23–33.

Glenn contact:
Dr. Sai V. Raj, 216–433–8195, Sai.V.Raj@nasa.gov

Authors:
Dr. Sai V. Raj and Dr. Louis J. Ghosn

Headquarters program office: OAT

Programs/Projects: Gen 2 and Gen 3

New Screening Test Developed for the Blanching Resistance of Copper Alloys

NASA's extensive efforts towards more efficient, safer, and more affordable space transportation include the development of new thrust-cell liner materials with improved capabilities and longer lives. For rocket engines fueled with liquid hydrogen, an important metric of liner performance is resistance to blanching, a phenomenon of localized wastage by cycles of oxidation-reduction due to local imbalance in the oxygen-fuel ratio. The current liner of the Space Shuttle Main Engine combustion chamber, a Cu-3Ag-0.5Zr alloy (NARloy-Z) is degraded in service by blanching. Heretofore, evaluating a liner material for blanching resistance involved elaborate and expensive hot-fire tests performed on rocket test stands. To simplify that evaluation, researchers at the NASA Glenn Research Center developed a screening test that uses simple, in situ oxidation-reduction cycling in a thermogravimetric analyzer (TGA). The principle behind this test is that resistance to oxidation or to the reduction of oxide, or both, implies resistance to blanching. Using this test as a preliminary tool to screen alloys for blanching resistance can improve reliability and save time and money.

In this test a small polished coupon is hung in a TGA furnace at the desired (service) temperature. Oxidizing and reducing gases are introduced cyclically, in programmed amounts. Cycle durations are chosen by calibration, such that all copper oxides formed by oxidation are fully reduced in the next reduction interval. The sample weight is continuously acquired by the TGA as usual.

The graph shows the oxidation-reduction responses of two types of materials: One type (group I) is distinguished by a flat weight-change profile, whereas the other type (group II) exhibits a steady increase of weight with exposure time. (Only the trends are significant in this figure, not the relative heights: the plots have been spaced out vertically to avoid overlap.) Group I, at the bottom of the chart, includes pure Cu and three of its alloys. They all share one characteristic: upon oxidation, they form a nonprotective Cu_2O/CuO scale. The two Cu-Cr-Nb alloys at the top are in group II; they also form Cu_2O/CuO, but are further characterized by a compact layer of protective Cr-Nb oxides beneath the Cu_2O/CuO scale. In both groups, the Cu_2O/CuO scale formed during oxidation is removed during reduction in each cycle. That should result in zero weight change—and does for group I, but not for group II. For the latter, the additional layer of protective oxides is also resistant to reduction and its continuous growth leads to the monotonic

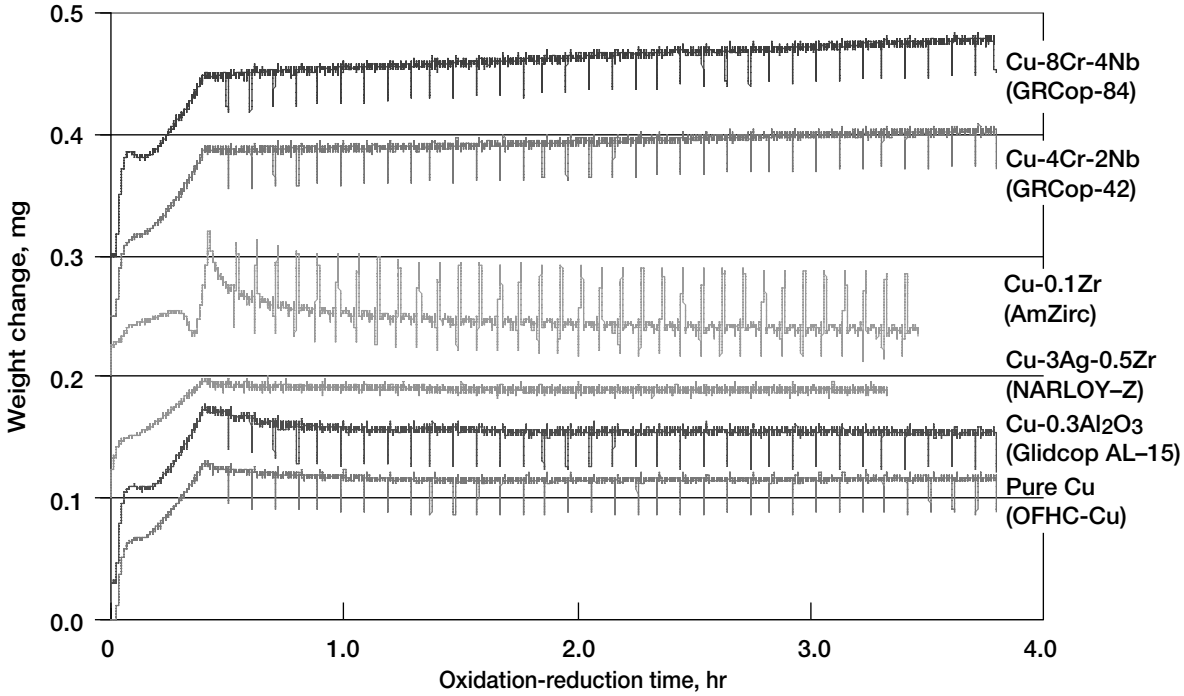

Oxidation-reduction behavior of copper and its aerospace alloys. A horizontal trend (bottom four curves) suggests susceptibility to degradation by blanching, while a rising trend (top two curves) indicates resistance to blanching due to the growth of protective oxide.

weight increase seen in the figure. SEM examination after exposure reveals that the surfaces of group I samples are grooved and pitted with scars of incipient blanching attack, whereas group II samples are covered and protected by the Cr-Nb oxides. Cu-Cr coating compositions were observed to fall into group II, with a Cr_2O_3 subscale providing extra protection for blanching resistance.

The clear contrast in response between the two groups makes this test a reliable discriminant of blanching tendencies. These results indicate that Cu, NARloy-Z, and AmZirc should blanch (as they are known to do in service, ref. 1); in contrast, GRCop-84 should not—and hot-fire tests recently performed elsewhere indicate that GRCop-84 is resistant to blanching, as predicted by the graph. The simplicity of this test makes it a useful tool for screening. Results are read from weight-gain charts, rather than interpreted from visual signs of damage (as was done heretofore). Hence, with some precaution the test results can be used to rank alloys semiquantitatively on the basis of specific weight gains from a prescribed duration of oxidation-reduction cycling.

Reference

1. Morgan, Deena B.; and Kobayashi, A.C.: Main Chamber Combustion and Cooling Technology Study. Final Report. NASA CR—184345, 1989. Available from the NASA Center for AeroSpace Information.

QSS Group, Inc., contact:
Linus U. Thomas-Ogbuji, 216–433–6463, Linus.U.Thomas-Ogbuji@grc.nasa.gov

Author: Linus U. Thomas-Ogbuji

Headquarters program office: OAT

Programs/Projects: RLV, Gen 2

Ceramic Matrix Composite Vane Subelements Tested in a Gas Turbine Environment

The use of ceramic matrix composites (CMCs) as vanes for the next generation of turbine engines is under evaluation for improving engine performance, such as lowering emissions and enabling higher cycle efficiency, relative to today's engines with superalloy hot section components. Because of the high-temperature capability of this class of materials, CMC vanes would be able to operate with higher combustion exit temperatures than today's engines can. Alternatively, a potential vane cooling requirement reduction of 15 to 25 percent for a CMC, such as SiC/SiC, relative to a single-crystal superalloy would be realized if the combustion operation was not altered.

Vane subelements were fabricated from a silicon carbide fiber-reinforced silicon carbide matrix (SiC/SiC) composite and were coated with an advanced environmental barrier coating (EBC). So that the critical design features of a turbine airfoil could be addressed, the vane subelement geometry was derived from an aircraft engine vane. A fabrication technique was developed that enables vanes to be constructed using a high-strength silicon carbide fiber in the form of woven cloth. A unique cloth configuration was used to provide continuous fiber reinforcement at the sharp trailing edge, the most challenging feature for fabrication from a continuous-fiber-reinforced composite. A completed vane subelement is shown in this photograph.

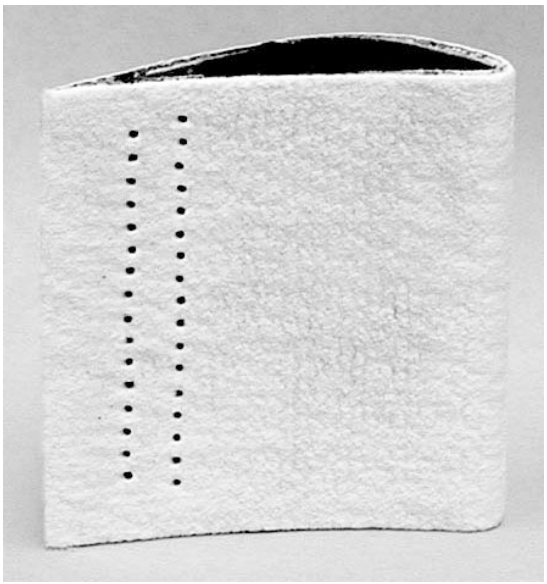

SiC/SiC vane subelement coated with an advanced environmental barrier coating and containing cooling holes in the trailing edge.

A test configuration for the vanes in a high-pressure gas turbine environment was designed and fabricated for the High Pressure Burner Rig at the NASA Glenn Research Center. Vane surface temperatures are measured using optical pyrometry, as shown in the illustration on the next page. Test conditions include combustion flow at 60 m/sec and 6 atm, and temperatures above 1200 °C.

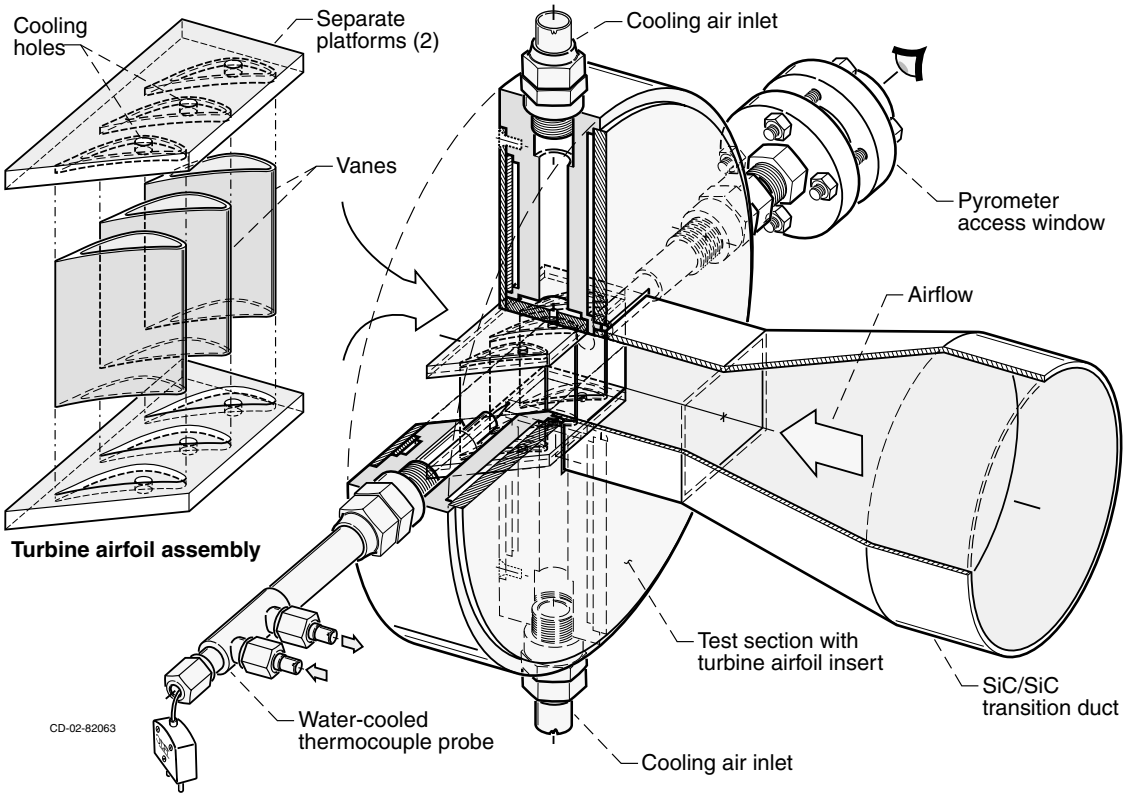

Configuration for testing SiC/SiC vanes in the High Pressure Burner Rig. (Illustration by Richard J. Czentorycki of InDyne, Inc.)

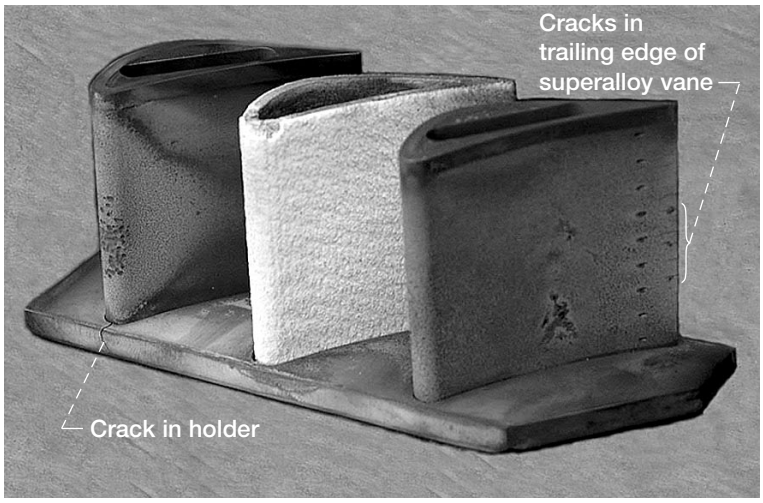

SiC/SiC vane with environmental barrier coating (center) after 20 hr of rig testing. Note the damage in the metal vanes and rig hardware.

Over 50 hr of rig testing on a SiC/SiC vane subelement have been completed. As shown in the final photograph, no degradation of the EBC-coated SiC/SiC vane occurred after testing at material temperatures up to 1200 °C. Metal vanes and rig hardware that were exposed to the same conditions had damage in the form of cracks and deformation, demonstrating the improved high-temperature capability of this ceramic composite over the metals used in today's gas turbine engines.

Find out more about this research:

Glenn's Environmental Durability Branch:
http://www.grc.nasa.gov/WWW/EDB/

Glenn's Materials Division:
http://www.grc.nasa.gov/WWW/MDWeb/

Glenn contacts:
Michael J. Verrilli, 216–433–3337, Michael.J.Verrilli@nasa.gov; and Dr. Anthony M. Calomino, 216–433–3311, Anthony.M.Calomino@nasa.gov

QSS Group, Inc., contact:
R. Craig Robinson, 216–433–5547, Raymond.C.Robinson@grc.nasa.gov

Authors:
Michael J. Verrilli, R. Craig Robinson, and Dr. Anthony M. Calomino

Headquarters program office: OAT

Programs/Projects: UEET

Hafnia-Based Materials Developed for Advanced Thermal/Environmental Barrier Coating Applications

Thermal and environmental barrier coatings (T/EBCs) will play a crucial role in advanced gas turbine engine systems because of their ability to significantly increase engine operating temperatures and reduce cooling requirements, and thus help achieve engine goals of low emissions and high efficiency. Under the NASA Ultra-Efficient Engine Technology (UEET) Project, advanced T/EBCs are being developed for low-emission SiC/SiC ceramic matrix composite (CMC) combustor applications by extending the CMC liner and vane temperature capability to 1650 °C (3000 °F) in oxidizing and water-vapor-containing combustion environments. The coating system is required to have increased phase stability, lower lattice and radiation thermal conductivity, and improved sintering and thermal stress resistance under high-heat-flux and thermal-cycling engine conditions. Advanced heat-flux testing approaches (refs. 1 to 4) have been established at the NASA Glenn Research Center for 1650 °C coating developments. The simulated combustion water-vapor environment is also being incorporated into the heat-flux test capabilities (ref. 3).

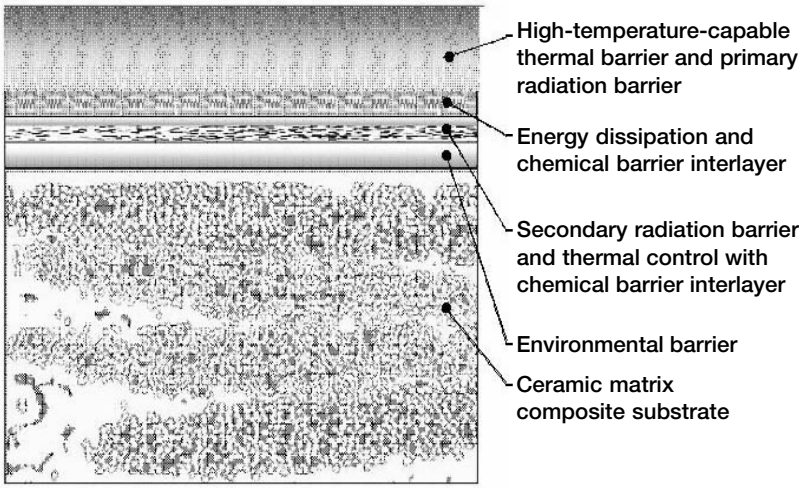

An advanced coating design concept for the 1650 °C T/EBC system for ceramic matrix composite combustor applications.

An advanced coating concept for the 1650 °C T/EBC system for CMC combustor applications is shown in the schematic to the left (ref. 5). The top layer is a high-temperature-capable thermal barrier coating, designed to provide the major thermal protection for the subcoating systems and the CMC substrate, and also to act as the first-stage radiation barrier by reducing the transmission of the infrared thermal radiations from the combustion gas environment and the higher temperature coating surface. In addition, the energy dissipation, secondary radiation barrier, and environmental barrier layers also will be incorporated to provide strain tolerance, further reduce radiation energy penetration, and ensure environmental protection. The HfO_2-based oxides are being developed as potential candidate 1650 °C coating materials for advanced thermal/environmental barrier top coating applications.

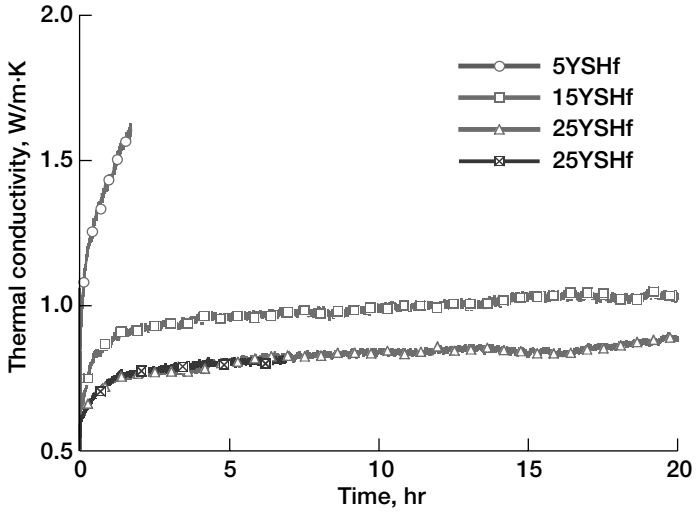

Thermal conductivity of plasma-sprayed HfO_2-Y_2O_3 coatings tested at 1650 °C as a function of time (test pass-through heat flux (95 to 100 W/cm^2).

The graph on the left shows the thermal conductivity change kinetics of plasma-sprayed HfO_2-Y_2O_3 coatings as a function of time tested at 1650 °C. It can be seen that the conductivity of HfO_2-5mol%Y_2O_3 (5YSHf) increased significantly upon 1650 °C thermal exposure. On the other hand, the HfO_2-15mol%Y_2O_3 (15YSHf) and HfO_2-25mol%Y_2O_3 (25YSHf) coatings showed lower initial and 20-hr

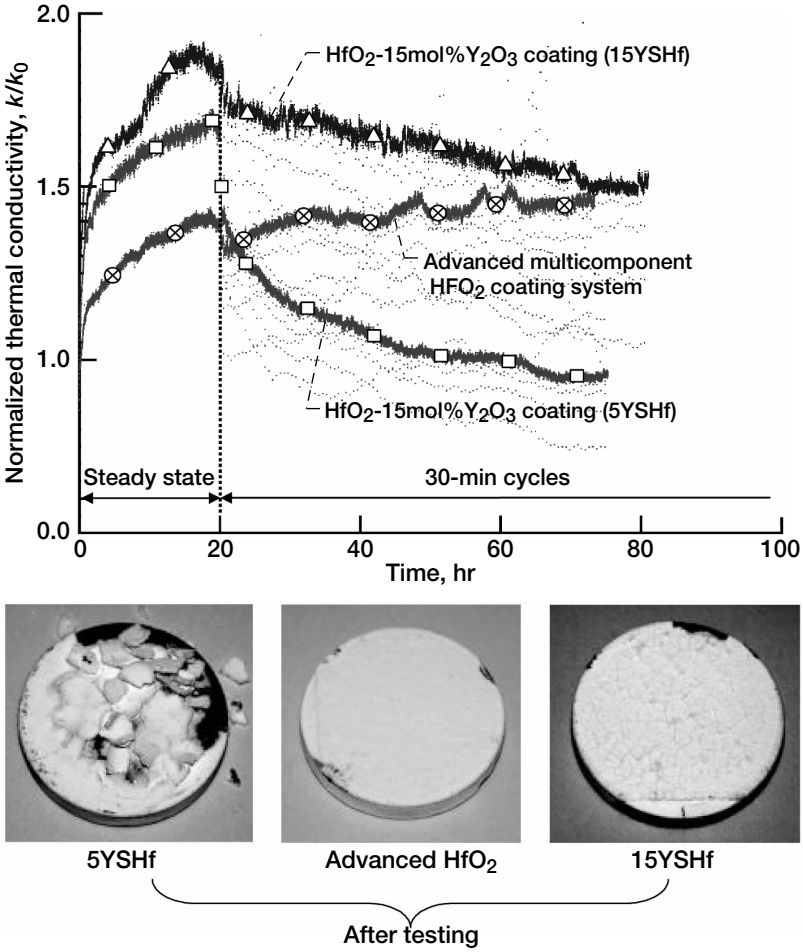

The 1650 °C sintering and cyclic behavior of a multicomponent HfO_2-Y_2O_3-Gd_2O_3-Yb_2O_3 coating on mullite-based EBC/Si on SiC substrates in comparison to the baseline 5YSHf and 15YSHf coatings.

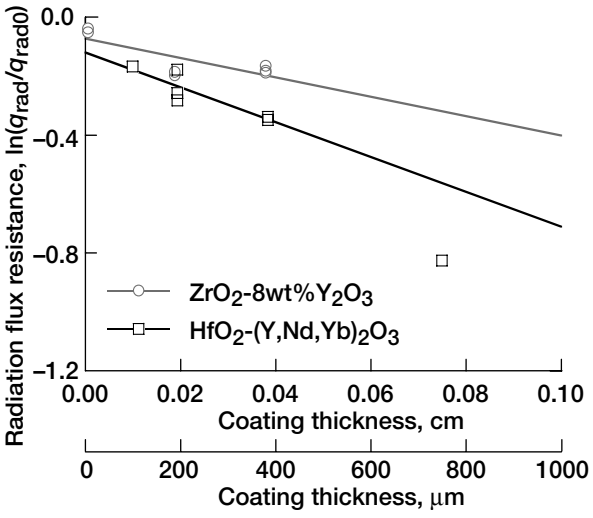

Significantly improved radiation resistance is demonstrated for an advanced plasma-sprayed HfO_2-Y_2O_3-Nd_2O_3-Yb_2O_3 coating in comparison to a baseline plasma-sprayed ZrO_2-8wt%Y_2O_3 coating.

sintered thermal conductivity, indicating better temperature stability. The x-ray diffraction results showed that the as-sprayed 5YSHf initially had a partially stabilized tetragonal phase structure with a small amount of the monoclinic phase (2 to 3 mol%), and the as-sprayed 15YSHf and 25YSHf had a fully stabilized cubic structure. The monoclinic phase content in the 5YSHf increased to 12 mol% after the testing, indicating the substantial destabilization of the low-ytttria-dopant coating system. Thermal conductivity generally decreased with an increase in Y_2O_3 dopant. The more stable cubic-structured 15YSHf and 25YSHf showed lower conductivity and less conductivity increases in comparison to the tetragonal 5YSHf. Advanced multicomponent rare-earth-doped HfO_2-Y_2O_3-Gd_2O_3 (Nd_2O_3)-Yb_2O_3 coatings have achieved even lower thermal conductivity and better thermal stability (ref. 5).

The figure at the top of this page shows the 1650 °C sintering and cyclic behavior of a multicomponent HfO_2-Y_2O_3-Gd_2O_3-Yb_2O_3 coating that was coated on the mullite-based EBC/Si on SiC substrates. The advanced multicomponent HfO_2 coating had a relatively low conductivity increase during the first 20 hr of steady-state testing. It also showed essentially no cracking and delamination during subsequent testing for 100 30-min cycles at 1650 °C, indicating excellent sintering resistance and cyclic durability. In contrast, the HfO_2 baseline coatings showed significant conductivity increases during the initial 20-hr steady-state sintering test, and later conductivity reductions because the coating had cracked and delaminated. The 5YSHf showed severe spallation partially because of the large amount of monoclinic phase formation (>25 mol%) and the phase destabilization (ref. 3).

The final graph shows the radiation flux resistance ln (q_{rad}/q_{rad0}), defined as the ratio of the pass-through radiation heat flux q_{rad} to the imposed radiation flux q_{rad0}, of a plasma-sprayed HfO_2-Y_2O_3-Nd_2O_3-Yb_2O_3 coating as a function of coating thickness, as determined by a laser-activated emitting-source flux technique.

It can be seen that, in comparison to the baseline plasma-sprayed ZrO_2-8wt%Y_2O_3 coating, the advanced HfO_2-Y_2O_3-Nd_2O_3-Yb_2O_3 coating improved radiation resistance significantly. The advanced high-stability, low-conductivity 1650 °C HfO_2 coatings will affect NASA's UEET low-emission combustor technology significantly.

References

1. Zhu, Dongming; and Miller, Robert A.: Thermal Conductivity Change Kinetics of Ceramic Thermal Barrier Coatings Determined by the Steady-State Laser Heat Flux Technique. Research & Technology 1999, NASA/TM—1999-209639, 2000, pp. 29–31. http://www.grc.nasa.gov/WWW/RT1999/5000/5160zhu.html
2. Zhu, D.M.; and Miller, R.A.: Thermal Conductivity and Elastic Modulus Evolution of Thermal Barrier Coatings Under High Heat Flux Conditions. J. Thermal Spray Technol., vol. 9, 2000, pp. 175–180.
3. Zhu, Dongming; and Miller, Robert A.: Development of Advanced Thermal and Environmental Barrier Coatings Using a High-Heat-Flux Testing Approach. Presented at the 27th Annual International Conference on Advanced Ceramics and Composites, Cocoa Beach, FL, 2003.
4. Zhu, D., et al.: Thermal Conductivity of Ceramic Coating Materials Determined by a Laser Heat Flux Technique. Proceedings of the 4th High Temperature Ceramic Matrix Composites Conference (HT–CMC4), Walter Krenkel, R. Naslain, and H. Schneider, eds., Wiley-VCH, Weinheim, Germany, 2001, pp. 262–267.
5. Zhu, Dongming; Bansal, Narottam P.; and Miller, Robert A.: Thermal Conductivity and Stability of HfO_2-Y_2O_3 and $La_2Zr_2O_7$ Evaluated for 1650 °C Thermal/Environmental Barrier Coating Applications. NASA/TM—2002-212544, 2003.

U.S. Army Research Laboratory, Vehicle Technology Directorate at Glenn contact:
Dr. Dongming Zhu, 216–433–5422, Dongming.Zhu@grc.nasa.gov

Glenn contact:
Dr. Robert A. Miller, 216–433–3298, Robert.A.Miller@nasa.gov

Authors: Dr. Dongming Zhu and Dr. Robert A. Miller

Headquarters program office: OAT

Programs/Projects: UEET (Advanced 3000 °F coatings concepts)

Power and On-Board Propulsion Technology

Nanostructured Materials Developed for Solar Cells

There has been considerable investigation recently regarding the potential for the use of nanomaterials and nanostructures to increase the efficiency of photovoltaic devices. Efforts at the NASA Glenn Research Center have involved the development and use of quantum dots and carbon nanotubes to enhance inorganic and organic cell efficiencies. Theoretical results have shown that a photovoltaic device with a single intermediate band of states resulting from the introduction of quantum dots offers a potential efficiency of 63.2 percent. A recent publication extended the intermediate band theory to two intermediate bands and calculated a limiting efficiency of 71.7 percent. The enhanced efficiency results from converting photons of energy less than the band gap of the cell by an intermediate band. The intermediate band provides a mechanism for low-energy photons to excite carriers across the energy gap by a two-step process. Quantum dots offer the potential to control the intermediate band energies since the individual quantum energy levels associated with isolated quantum dots are a function of their size and material composition. Placing the appropriate quantum dot material of the necessary size into an organized matrix within an ordinary *p-i-n* structure solar cell should result in the formation of accessible energy levels within what would normally be the forbidden band of the device.

In preparation for their insertion into a *p-i-n* amorphous silicon cell structure, we have been investigating depositing quantum dots of $CuInS_2$ and $CuInSe_2$. $CuInS_2$ quantum dots were coated with hexanethiol and a sequential exchange of the hexanethiol coating by triocytlphosphine oxide (TOPO), pyridine, and mercaptoacetic acid was performed to render the dots dispersible in water. The figure to the right shows tapping mode atomic force microscope (AFM) of these dots arrayed on a glass substrate by electrostatic layer-by-layer assembly. The remaining issues regarding the best procedure for introducing these dots into a *p-i-n* amorphous silicon cell structure are currently being addressed.

Thin-film polymeric solar cells may also benefit from the introduction of quantum dots. Solar cells that utilize conjugated polymers such as poly-3-octyl-thiophene (P3OT) or poly-3-hexyl-thiophene (P3HT) making junctions with indium tin oxide (ITO) have suffered from low conversion efficiencies because of the low transport

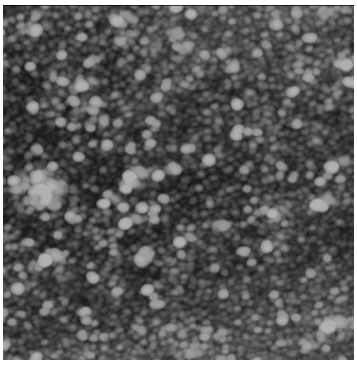

1- by 1-μm tapping-mode atomic force microscope image of colloidal $CuInS_2$ (mercaptoacetic acid) quantum dots on glass.

mobility of the photogenerated carriers. The light that is absorbed in the conjugated polymers creates excitons or bound electron/hole pairs. Before these charges can contribute to any photocurrent, they must first be separated. It has been shown that semiconducting quantum dots introduced into the polymeric matrix will serve as disassociation centers and improve overall device efficiency. However, even with the disassociation of the carriers, their mobility in these materials is still quite low. This can be addressed to a certain extent by the use of nanorods instead of the spheroidal quantum dots.

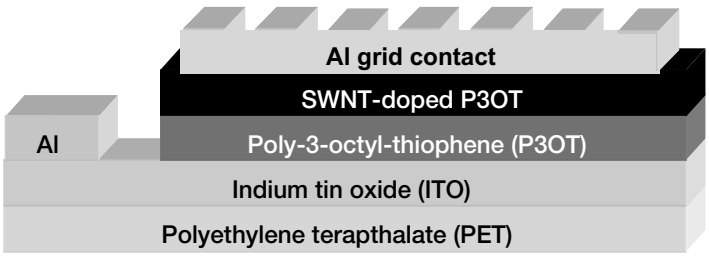

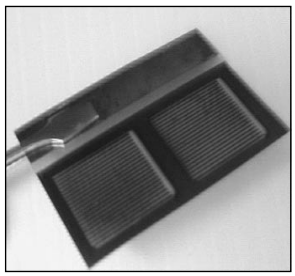

Carbon nanotube polymeric solar cell.

The problem of low carrier mobility in thin-film polymeric solar cells may be addressed through the use of single-walled carbon nanotubes (SWNTs). It has been demonstrated that even a small weight percent doping of SWNTs in a polymeric thin film can dramatically improve the film's electrical conductivity. In addition, SWNTs can themselves be semiconducting and are very good absorbers in the visible range. They may serve a similar role to that of the quantum dots when introduced into the conjugated polymers used in photovoltaic development.

Photovoltaic devices have been constructed at Glenn using P3OT doped with high-purity SWNTs produced by laser vaporization. The composite solution (1 wt% SWNTs in P3OT) was applied to ITO-coated glass substrates. The cell structure can be seen in the figure at the bottom of the preceding page. A simple 1.0-μm-thick Al grid contact was deposited onto the P3OT surface via thermal evaporation. The SWNT–P3OT diode response produced an open-circuit voltage V_{OC} in the range of 0.7 to 0.9 V, and the short-circuit current I_{SC} was observed to double for the composite solar cells in comparison to those that contained P3OT without the SWNTs. It is typically the case that the work function difference between Al and ITO (i.e., 4.3 and 4.7 eV, respectively) is responsible for determining the V_{OC} in these types of devices. However, the relatively higher V_{OC} measured here is presumably due to the influence of the SWNTs. We suggest that for an MIM-type junction the ITO-polymer-SWNTs account for the measured potential.

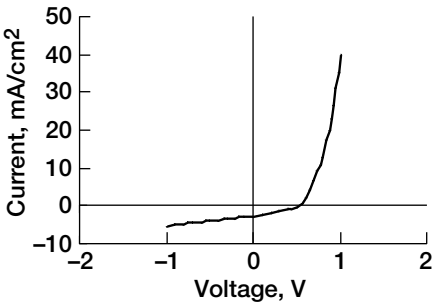

Current-versus-voltage response of an SWNT-doped P3OT/ITO solar cell.

Glenn contact:
Dr. Sheila G. Bailey, 216–433–2228, Sheila.G.Bailey@nasa.gov

Authors:
Dr. Sheila G. Bailey, Stephanie L. Castro, Ryne P. Raffaelle, Stephen D. Fahey, Thomas Gennett, and Padetha Tin

Headquarters program office: OAT

Programs/Projects: anything that requires space power

Scanning Tunneling Optical Resonance Microscopy Developed

The ability to determine the in situ optoelectronic properties of semiconductor materials has become especially important as the size of device architectures has decreased and the development of complex microsystems has increased. Scanning Tunneling Optical Resonance Microscopy, or STORM, can interrogate the optical bandgap as a function of its position within a semiconductor microstructure. This technique uses a tunable solid-state titanium-sapphire laser whose output is "chopped" using a spatial light modulator and is coupled by a fiber-optic connector to a scanning tunneling microscope in order to illuminate the tip-sample junction. The photoenhanced portion of the tunneling current is spectroscopically measured using a lock-in technique. The capabilities of this technique were verified using semiconductor microstructure calibration standards that were grown by organometallic vapor-phase epitaxy. Bandgaps characterized by STORM measurements were found to be in good agreement with the bulk values determined by transmission spectroscopy and photoluminescence and with the theoretical values that were based on x-ray diffraction results.

Combining the localized spectroscopic illumination provided by a fiber-optically coupled solid-state Ti:S laser with the imaging and electronic characterization capabilities of scanning tunneling microscopy provides a technique for determining the in situ semiconductor optical bandgaps of these small systems. The scanning tunneling microscope (STM) can be used to identify small semiconducting regions of a material or system by monitoring the change in tunneling current as a function of position. It is possible to enhance the tunneling current in these semiconducting regions by illuminating the semiconductor surface with light of sufficient energy. The photoenhancement results when the wavelength or energy of the illuminating photons is such that the valence electrons in the sample can absorb these photons and be promoted into the conduction band where they can contribute to the tunneling current. The use of a tunable solid-state laser allows the wavelength of the illumination to be continuously tuned and directed into the system via a fiber-optic device that can be directed onto

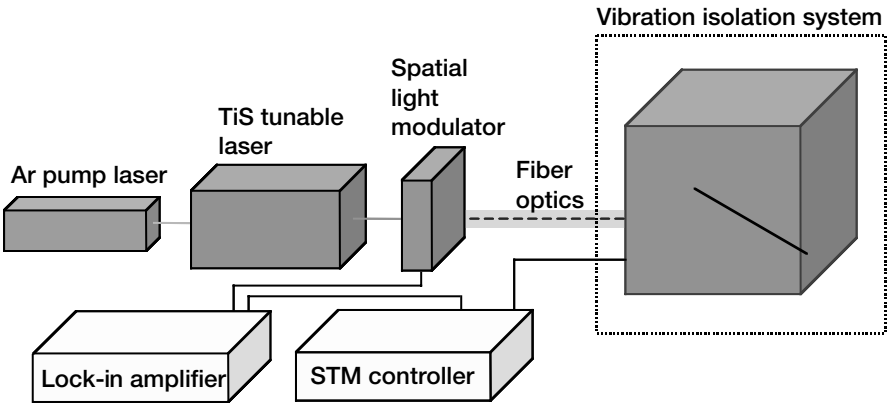

Schematic of STORM setup. STM, scanning tunneling microscope.

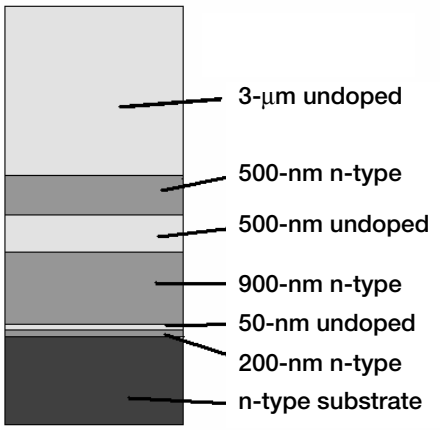

Growth profile of layered InP sample.

the tip-sample region. By chopping the laser light with a spatial light modulator (SLM), one can measure a voltage proportional to the tunneling current by a lock-in amplifier at the SLM chopping frequency. The output of the lock-in is then monitored as a function of the wavelength of the illumination. The onset of the photoenhanced tunneling current then provides a direct measurement of the optoelectronic bandgap of the material (i.e., the individual quantum dot, carbon nanotube, semiconductor quantum well, etc.) or region of the material that is being imaged in the STM. See the STORM apparatus in the schematic on the left.

The scanning capability of STORM was investigated at the NASA Glenn Research Center using samples grown with a number of layers with varying doping concentrations. The figure on the right shows the growth profile of the layered InP sample. The following figure shows an enhancement in the bandgap differences between the individual layers when the sample was illuminated with white light. The direct-current illumination was initiated in the middle of the scan shown in this figure.

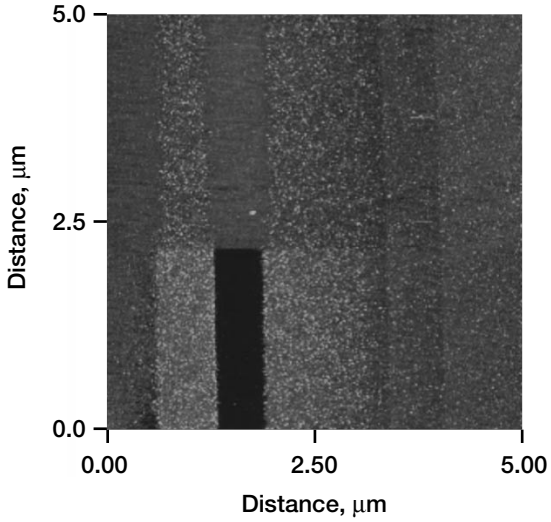

Cross-sectional STM image of layered InP sample. The top half of the image has no illumination, and the bottom half is illuminated with white light.

Other areas of investigation that will be enhanced by an increased capability to probe optoelectronic properties at the nanoscale include the combination of multiple nanomaterials in close proximity to each other. We have sought to covalently couple semiconductor quantum dots with single-wall carbon nanotubes. By taking advantage of the dangling bonds produced on the ends of the carbon nanotubes during purification of the raw soot, we can introduce organic functional groups at these sites. Standard covalent coupling techniques can then be used to create a bond between the carbon nanotube and a complementary functional group introduced on the surface of the quantum dot.

Glenn contact:
Dr. Sheila G. Bailey, 216–433–2228, Sheila.G.Bailey@nasa.gov

Authors:
Dr. Sheila G. Bailey, Ryne P. Raffaelle, Janis E. Lau, Phillip P. Jenkins, Stephanie L. Castro, Padetha Tin, David M. Wilt, Anna Maria Pal, and Stephen D. Fahey

Headquarters program office: OAT

Programs/Projects:
Microsystem analysis

Solar Airplane Concept Developed for Venus Exploration

An airplane is the ideal vehicle for gathering atmospheric data over a wide range of locations and altitudes, while having the freedom to maneuver to regions of scientific interest.

Solar energy is available in abundance on Venus. Venus has an exoatmospheric solar flux of 2600 W/m^2, compared with Earth's 1370 W/m^2. The solar intensity is 20 to 50 percent of the exoatmospheric intensity at the bottom of the cloud layer, and it increases to nearly 95 percent of the exoatmospheric intensity at 65 km. At these altitudes, the temperature of the atmosphere is moderate, in the range of 0 to 100 °C, depending on the altitude.

A Venus exploration aircraft, sized to fit in a small aeroshell for a "Discovery" class scientific mission, has been designed and analyzed at the NASA Glenn Research Center. For an exploratory aircraft to remain continually illuminated by sunlight, it would have to be capable of sustained flight at or above the wind speed, about 95 m/sec at the cloud-top level. The analysis concluded that, at typical flight altitudes above the cloud layer (65 to 75 km above the surface), a small aircraft powered by solar energy could fly continuously in the atmosphere of Venus. At this altitude, the atmospheric pressure is similar to pressure at terrestrial flight altitudes.

For exploration at lower altitudes, the aircraft could glide down for periods of several hours and then climb back to higher altitudes, allowing the cloud layers to be probed. Analysis of a flight using battery storage shows that it is not feasible to keep the aircraft aloft on battery power during the passage across the night side of the planet.

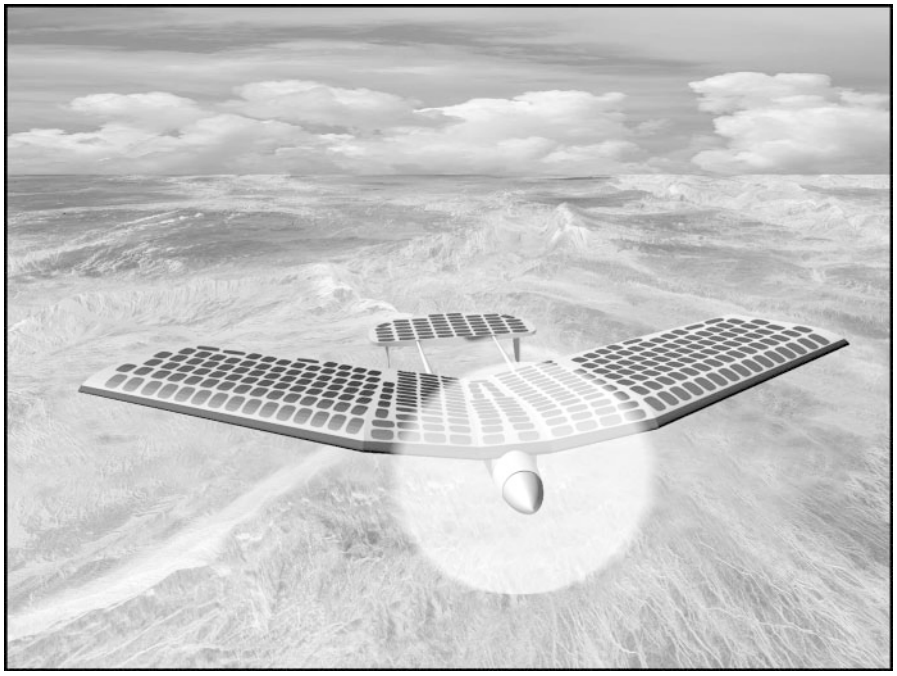

Solar-powered Venus airplane shown over a computer-generated radar image of the surface of Venus. (Artist's conception by Terence K. Condrich of InDyne, Inc.)

The planet Venus has a number of fundamental scientific mysteries, both in its atmosphere and in its surface. An aircraft-based probe could measure the volatile inventory of Venus and the isotope ratio in the atmosphere, helping to determine whether early Venus once had an atmosphere and to determine the process and timing by which the planet lost its primordial inventory of water. The aircraft mission could also, by "sniffing" the sulfur content of the atmosphere as a function of position on the surface, determine whether the sulfur abundance in the atmosphere is correlated with specific surface features (such as volcanoes or fumaroles).

The atmospheric dynamics of Venus are also not yet understood. At the cloud tops, the atmosphere moves around the planet 60 times faster than at the surface. The mechanism that supports this atmospheric superrotation is not well understood. To address this problem, an aircraft would measure the infrared absorption and the horizontal and vertical components of atmospheric motion as a function of the altitude, latitude, and subsolar longitude. Detailed modeling of the atmosphere also will require knowledge of the atmospheric correlation, using two aircraft flying with a known separation. Even the nature of the absorbing particles in the clouds remains enigmatic. These could be characterized by chemical and physical sensors in the atmosphere.

The primary tool for aircraft-based investigation of the surface of Venus would likely be radar. Because the aircraft would observe the surface from a distance of 10's of kilometers, rather than the 100's of kilometers altitude of an orbiting probe, resolution will be improved by a factor of 10, and the required power will be reduced by a

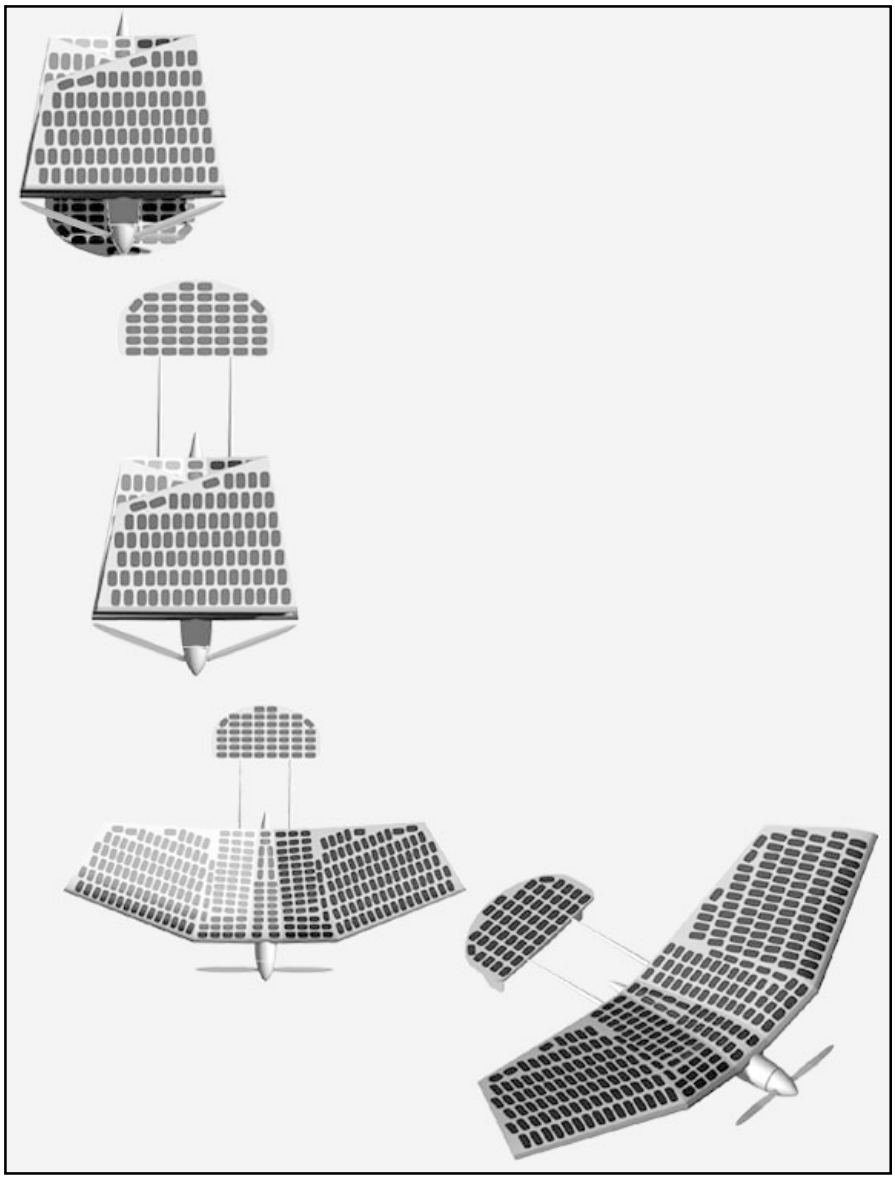

Venus airplane as it arrives at the atmosphere of Venus in a folded configuration, and unfolds its wings and tail to fly. (Artist's visualization by Terence K. Condrich of InDyne, Inc.)

factor of a 100. Such an aircraft would also be able to circle over particular spots of interest, allowing detailed study of those areas, rather than uniformly covering all regions of the planet.

An aircraft such as the one analyzed here would be a powerful tool for exploration. By learning how Venus can be so similar to Earth, and yet so different, we will learn to better understand the climate and geological history of the Earth. The success of a prototype solar airplane could lead to the development of a fleet of solar-powered airplanes flying across the Venus cloud tops, taking simultaneous measurements to develop a "snapshot" of the climate across the face of the planet.

Bibliography

Landis, G.A.; Colozza, A.; and LaMarre, C.M.: Atmospheric Flight on Venus: A Conceptual Design. J. Spacecr. Rockets, (NASA/TM—2002-211467), vol. 40, no. 5, 2003, pp. 672–677. http://gltrs.grc.nasa.gov/cgi-bin/GLTRS/browse.pl?2002/TM-2002-211467.html

Landis, Geoffrey; LaMarre, C.; and Colozza, A.: Venus Atmospheric Exploration by Solar Aircraft. IAC–02–Q.4.2.03, Proceedings of the 53rd International Astronautical Congress/2002 World Space Congress, 2002.

Landis, G.A.: Exploring Venus by Solar Airplane. AIP Conf. Proc., vol. 552, 2001, pp. 16–18.

Find out more about this research:
http://powerweb.grc.nasa.gov/pvsee/publications/

Glenn contact:
Dr. Geoffrey A. Landis, 216–433–2238, Geoffrey.A.Landis@nasa.gov

Analex contact:
Anthony J. Colozza, 216–433–5293, Anthony.Colozza@grc.nasa.gov

Author: Dr. Geoffrey A. Landis

Headquarters program office: OAT

Programs/Projects:
Planetary exploration, Aeronautics

Special recognition: ASM/AIAA Best Paper of 2002 award for best paper, atmospheric flight mechanics

Thermionic Emission of Single-Wall Carbon Nanotubes Measured

Researchers at the NASA Glenn Research Center, in collaboration with the Rochester Institute of Technology, have investigated the thermionic properties of high-purity, single-wall carbon nanotubes (SWNTs) for use as electron-emitting electrodes. Carbon nanotubes are a recently discovered material made from carbon atoms bonded into nanometer-scale hollow tubes. Such nanotubes have remarkable properties. An extremely high aspect ratio, as well as unique mechanical and electronic properties, make single-wall nanotubes ideal for use in a vast array of applications. Carbon nanotubes typically have diameters on the order of 1 to 2 nm. As a result, the ends have a small radius of curvature. It is these characteristics, therefore, that indicate they might be excellent potential candidates for both thermionic and field emission.

Three techniques for synthesizing such carbon nanotubes are arc discharge, chemical vapor deposition, and laser vaporization. The laser vaporization process was chosen in this study because of the large degree of control that can be exhibited on the final nanotube products. Variations in parameters such as target catalyst composition, laser beam power density, and synthesis temperature can influence the SWNT diameter distribution, production rate, and yield within the as-produced material.

Production of efficient thermionic devices depends on the use of low-work-function materials as electron emitters. For single-wall nanotubes, work function has been determined using a number of techniques. Ab initio calculations predict a work function of 3.75 eV for closed-ended single-wall nanotubes. In these studies, we used the thermionic emission of purified laser-vaporization-produced single-walled nanotubes to experimentally measure their work function.

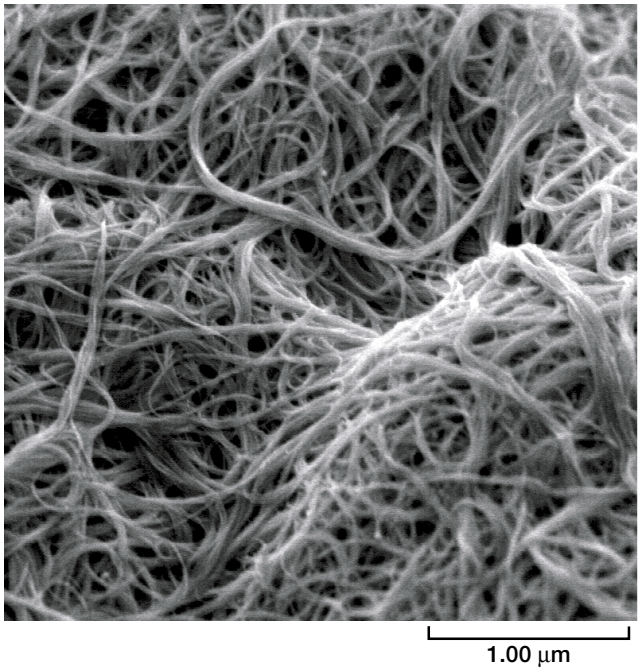

SEM micrograph of purified nanotube paper.

All materials were synthesized using pulsed-laser synthesis with a 755-nm Alexandrite laser. Laser pulse duration was set at 100 μsec with a repetition rate of 10 Hz, and the nanotubes produced were purified to remove metal catalyst impurities and extraneous carbonaceous material by reflux in nitric acid, followed by thermal oxidation in 20-percent O_2 ambient and annealing in argon at 1200 °C. The purification procedure results in a "paper" in which the nanotubes are the fibers. A representative scanning electron microscope (SEM) image of the resultant SWNTs is shown in the figure on this page.

So that the thermal emission could be measured, the nanotube paper was used as the electron emitter in a parallel plate configuration with a tantalum collector. The nanotube paper was held in good thermal contact to a ceramic boron nitride heater capable of providing measurement temperatures up to 1300 °C. All measurements were taken in a vacuum chamber with a pressure of 1×10^{-8} torr or lower. The tantalum anode was brought to a distance of 0.5 mm from the single-walled nanotube paper. Potentials ranging from 0 to 1100 V were applied in ascending 10-V increments. Emission was studied for temperatures ranging from 25 to 1207 °C.

The emission plots obtained from a purified nanotube paper are shown in the top graph on the next page. Significant thermionic emission is observed starting at around 700 °C.

By fitting the Richardson-Laue-Dushman equation for thermionic emission current to the experimental data, one can obtain a value for the work function of single-wall carbon nanotubes. Using this equation,

$$J = AT^2 e^{(-e\varphi/kT)}$$

where J is the saturation current density, A is a universal constant (120 $A \cdot cm^{-2} \cdot K^{-2}$), T is temperature in kelvin, $e\varphi$ is the effective work function, and k is Boltzman's constant, one can obtain the work function by plotting $\ln(J/T^2)$ versus $-1/kT$. The effective work function is then equal to the slope of the resultant line. The Richardson-Laue-Dushman plot for the SWNT paper is shown in the final graph. This plot indicates that the single-wall carbon nanotubes have an effective work function of 3.46 eV.

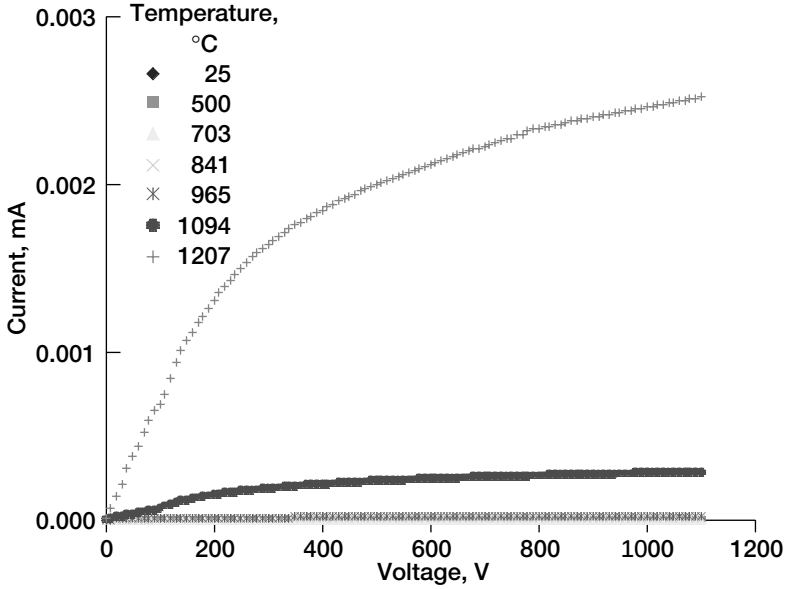

Thermionic emission from purified carbon-nanotube paper.

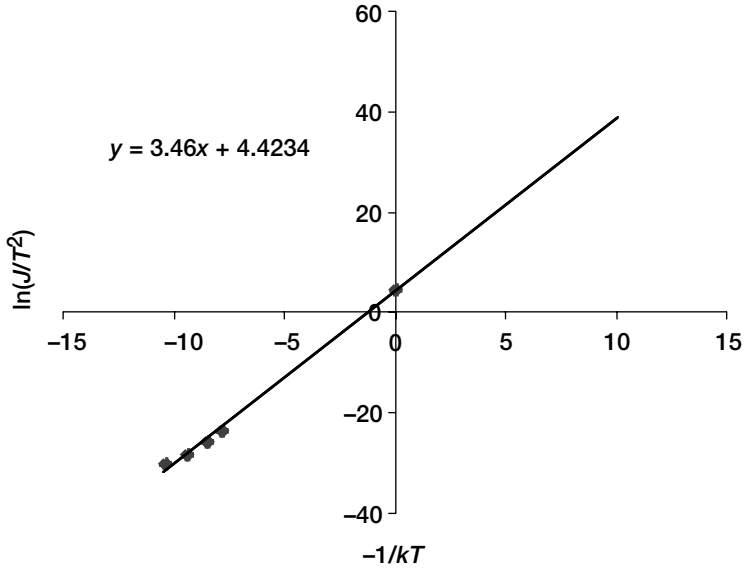

Richardson-Laue-Dushman plot for the purified laser-vaporized single-wall nanotube paper.

There are a large number of possible applications for carbon-nanotube-based electron emitters, including use as lightweight, low-power emission sources for electron-beam displays, x-ray sources, vacuum tubes for high-power microwave communication systems, and energy-generation devices. By developing a technique to produce a thin sheet of highly purified nanotube emitter and measuring the electron emission as a function of temperature and applied field strength, we are making significant progress toward the development of higher efficiency and greater power devices for NASA and commercial applications.

Bibliography

Elich, Jeffrey, et al.: Single Wall Carbon Nanotube Thermionic Emitters. Paper presented at the 3rd Conference on Thin Films and Nanotechnology for Energy Conversion, Brook Park, OH, 2003. To be published in a special issue of Materials Science and Engineering B, summer 2004.

Glenn contacts:

Dr. Geoffrey A. Landis, 216–433–2238, Geoffrey.A.Landis@nasa.gov;
Dr. Isay L. Krainsky, 216–433–3509, Isay.L.Krainsky@nasa.gov; and
Dr. Sheila G. Bailey, 216–433–2228, Sheila.G.Bailey@nasa.gov

Authors: Dr. Geoffrey A. Landis, Dr. Isay L. Krainsky, Dr. Sheila G. Bailey, Jeffrey M. Elich, Brian J. Landi, Thomas Gennett, and Ryne P. Raffaelle

Headquarters program office: OAT

Programs/Projects:

Propulsion and Power, Aeropropulsion Project Office, Communications, RAC, Alternate Fuels Foundation Technologies

Stirling Cooler Designed for Venus Exploration

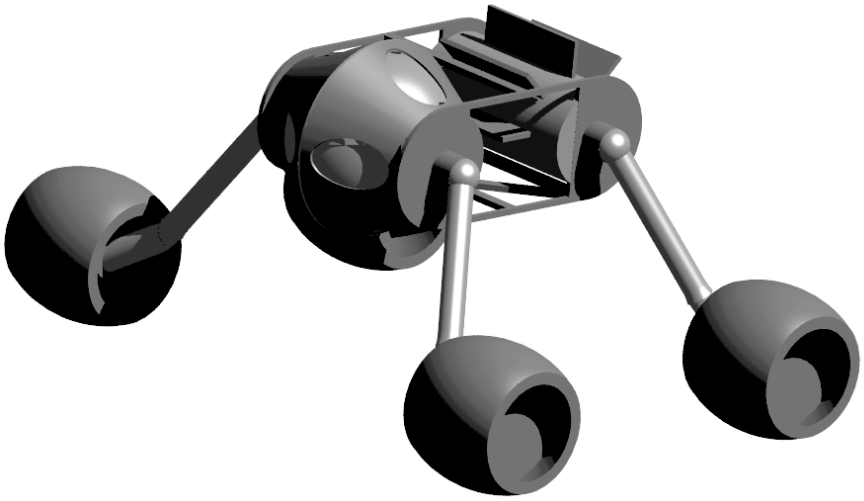

Artist's conception of a robotic rover for the exploration of Venus, incorporating a spherical electronics enclosure and a Stirling cooler for heat rejection (CAD visualization by Shawn A. Krizan of Analytical Mechanics Associates, Inc.).

Exploring the surface of Venus is a daunting task. With Venus having an average surface temperature of 460 °C (about 860 °F) and an atmosphere 150 times denser than the Earth's atmosphere, designing a robot to merely survive on the surface to do planetary exploration is an extremely difficult task. This temperature is hundreds of degrees higher than the maximum operating temperature of currently existing microcontrollers, electronic devices, and circuit boards.

To meet the challenge of Venus exploration, researchers at the NASA Glenn Research Center studied methods to keep a pressurized electronics package cooled, so that the operating temperature within the electronics enclosure would be cool enough for electronics to run, to allow a mission to operate on the surface of Venus for extended periods.

In the Venus electronics package design, the electronics are located inside a 25-cm-diameter spherical thermal enclosure. The design uses a Stirling engine to serve as a heat pump to eject heat through a heat pipe away from the interior of the thermal enclosure. The cold side of the heat pipe (inside the thermal enclosure) is at 473 K (200 °C). This temperature was chosen so that a currently available high-temperature silicon-based microcontroller could operate. The Stirling cooler transfers the waste heat to convective radiators, which efficiently reject heat to the Venus atmosphere at a temperature of 500 °C, 40 °C above the surface ambient temperature.

The cooling requirement to keep the heat pipe cold-side temperature at 475 K is 105 W of heat pumping. As calculated using the Stirling heat-engine design tool SAGE, the configuration that was modeled effectively pumps 100 W of heat across the required 300 °C of temperature differential with an operating coefficient of performance of 0.44, requiring approximately 240 W of input power, which can be provided by an isotope power system. The cooler operates with a working fluid of 46 bar nominal pressure (4.6 MPa) of gaseous helium. The estimated mass of the cooler is 1.6 kg.

Because this new heat pump design keeps the thermal enclosure at a moderate temperature, it is now possible to plan missions to explore the most hostile environment in our Solar System: the surface of Venus. With some modifications, the electronics cooling system design may be able to be adapted to other missions, such as near-Sun missions, Mercury surface robots, and volcano exploration.

Find out more about this research:
http://rasc.larc.nasa.gov/

Glenn contacts:
Dr. Geoffrey A. Landis, 216–433–2238, Geoffrey.A.Landis@nasa.gov; and Kenneth D. Mellott, 216–433–3347, Kenneth.D.Mellott@nasa.gov

Authors: Dr. Geoffrey A. Landis and Kenneth D. Mellott

Headquarters program office: OAT

Programs/Projects: Space Science, Propulsion and Power, RASC

Stretched Lens Array Photovoltaic Concentrator Technology Developed

Solar arrays have been and continue to be the mainstay in providing power to nearly all commercial and government spacecraft. Light from the Sun is directly converted into electrical energy using solar cells. One way to reduce the cost of future space power systems is by minimizing the size and number of expensive solar cells by focusing the sunlight onto smaller cells using concentrator optics. The stretched lens array (SLA) is a unique concept that uses arched Fresnel lens concentrators to focus sunlight onto a line of high-efficiency solar cells located directly beneath. The SLA concept is based on the Solar Concentrator Array with Refractive Linear Element Technology (SCARLET) design that was used on NASA's New Millennium Deep Space 1 mission. The highly successful asteroid/comet rendezvous mission (1998 to 2001) demonstrated the performance and long-term durability of the SCARLET/SLA solar array design and set the foundation for further improvements to optimize its performance.

Although SLA uses the same basic concept as SCARLET (an arched-linear refractive concentrator to focus light onto solar cells below), a number of refinements have been made that dramatically decrease the weight and stowed volume of the design. The linear concentrator lenses, made from a flexible, space-qualified clear silicone can now be stowed flat against the solar cells, greatly reducing weight and complexity. As the individual panels of the solar array are deployed for in-space operation, the concentrator lenses are "stretched" at the proper position above the cells, providing excellent operational performance with minimal excess hardware or mechanical complexity. A deployed four-panel prototype wing is shown in the photograph. The reduction in concentrator weight and deployment mechanisms has also enabled further weight reductions to the inboard honeycomb panels. These improvements, combined with additional features such as high-voltage operational capability and minimal degradation high-radiation environments, have led to the demonstration of 3- to 4-fold specific power improvements over the previous SCARLET design and other state-of-the-art solar arrays. These technology advancements were accomplished under a NASA Glenn Research Center contract with Entech, Inc., with support from AEC-Able Engineering.

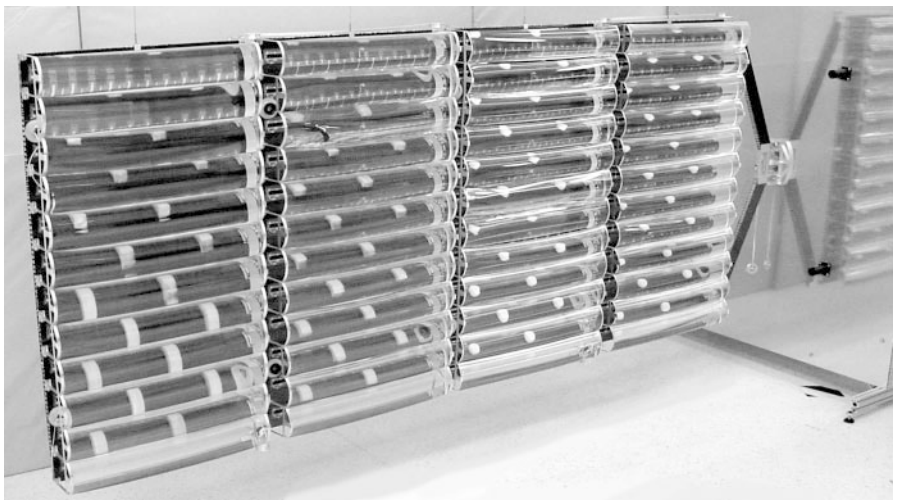

Four-panel prototype wing of the stretched lens array (SLA) in deployed mode. On the second panel from the left, lines of concentrator solar cells can be seen beneath the linear concentrator lenses.

The near-term design demonstrated in the photograph supports a wide variety of NASA missions. The radiation-tolerant and high-voltage capabilities are particularly applicable to deep-space science missions and those using solar electric propulsion technology. The cost-reduction benefits of photovoltaic concentrator arrays also make the SLA technology appealing for a number of commercial and other Government space systems. Concepts for very high power (>100 kW) SLA systems are currently being studied. These designs have the potential to enable various future NASA missions and would help further the commercial development of space.

Find out more about this research:
http://www.entechsolar.com

Glenn contact:
Michael F. Piszczor, Jr.; 216–433–2237, Michael.F.Piszczor@nasa.gov

Authors: Michael F. Piszczor, Jr., and Mark J. O'Neill

Headquarters program office: OAT

Programs/Projects: Energetics, SSP

Materials International Space Station Experiment (MISSE) 5 Developed to Test Advanced Solar Cell Technology Aboard the ISS

The testing of new technologies aboard the International Space Station (ISS) is facilitated through the use of a passive experiment container, or PEC, developed at the NASA Langley Research Center. The PEC is an aluminum suitcase approximately 2 ft square and 5 in. thick. Inside the PEC are mounted Materials International Space Station Experiment (MISSE) plates that contain the test articles. The PEC is carried to the ISS aboard the space shuttle or a Russian resupply vehicle, where astronauts attach it to a handrail on the outer surface of the ISS and deploy the PEC, which is to say the suitcase is opened 180°. Typically, the PEC is left in this position for approximately 1 year, at which point astronauts close the PEC and it is returned to Earth. In the past, the PECs have contained passive experiments, principally designed to characterize the durability of materials subjected to the ultraviolet radiation and atomic oxygen present at the ISS orbit. The MISSE5 experiment is intended to characterize state-of-art (SOA) and beyond photovoltaic technologies. The photograph to the right shows PEC1 attached to the ISS.

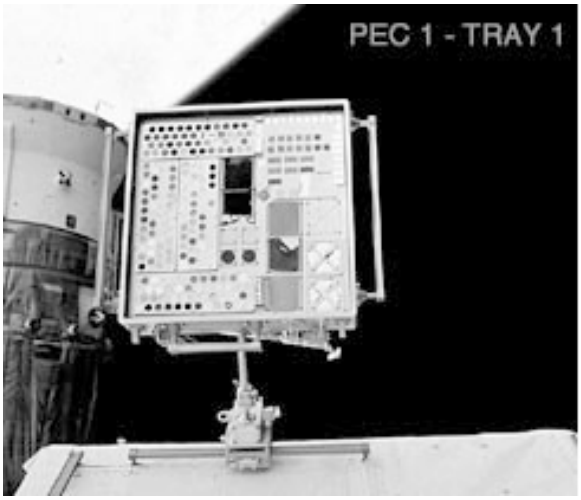

MISSE1 aboard the ISS.

The MISSE5 experiment differs from previous versions by virtue of the active nature of the payload. MISSE5 includes a photovoltaic power system and an onboard data acquisition and storage system, which was designed and fabricated by engineers from the Optical Instrumentation Technology Branch at the NASA Glenn Research Center and the Ohio Aerospace Institute (OAI). The electronic characterization system will measure the individual current-voltage characteristics of the 36 test solar cells as well as collect data from numerous other sensors (temperatures, Sun angle, etc.). The primary focus of MISSE5 is the characterization of commercial SOA multijunction solar cells from Emcore and Spectrolab. The data collected will be stored onboard as well as transmitted to Earth approximately once every 4 min, where it will be autonomously collected by ground stations.

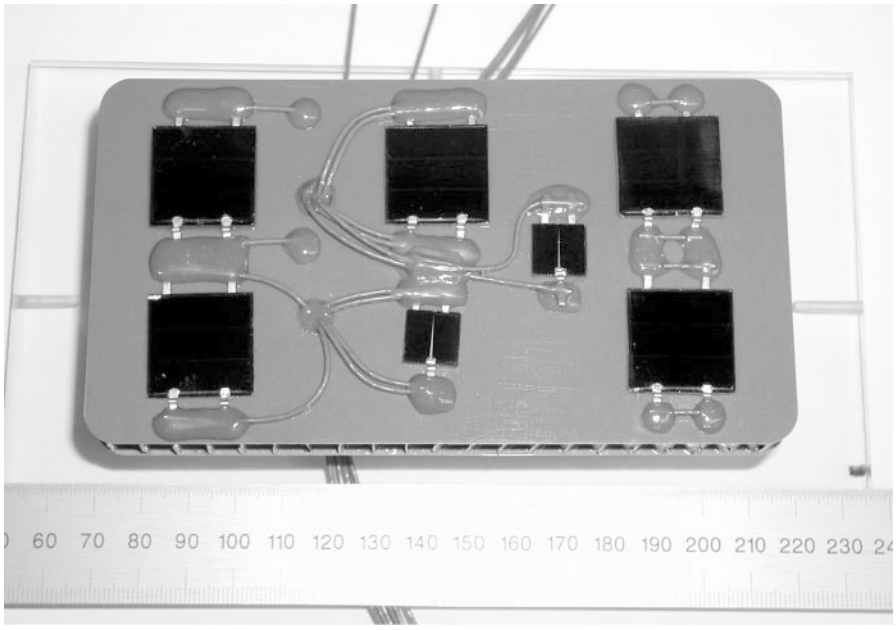

MISSE5 gallium arsenide on silicon (GaAs/Si) solar cell flight article developed by Glenn, the Ohio State University, and MIT.

Glenn, in collaboration with the Ohio State University and the Massachusetts Institute of Technology (MIT), has developed advanced high-efficiency gallium-arsenide- (GaAs-) based solar cells on silicon (Si) substrates. The use of Si substrates offers significant mass, area, and thermal benefits, although significant technical challenges have had to be addressed. Glenn was asked by the Naval Research Laboratory (NRL—the primary MISSE5 experiment integrator) to supply MISSE5 with GaAs/Si test articles. The MISSE5 GaAs/Si experiment plate (see the photograph to the left) was fabricated

at Glenn. It contains five GaAs/Si cells, three of which will be electrically characterized on-orbit. In addition, a GaAs/GaAs control cell will be characterized on-orbit. The remaining samples will be measured after flight to compare with their preflight characteristics.

MISSE5 is being assembled at the Naval Research Laboratory and is scheduled to launch aboard a Russian resupply vehicle (fall 2004). This mission will provide valuable in-flight data for SOA technologies as well as promising new technologies, such as the GaAs/Si technology and advanced thin-film technologies. Finally, the cell characterization electronics developed by Glenn for MISSE5 are already being considered for use in future spacecraft.

Find out more about this research:

Photovoltaic & Space Environments Branch at Glenn:
http://powerweb.grc.nasa.gov/pvsee/

MISSE: http://misse1.larc.nasa.gov

Glenn contacts:
David M. Wilt, 216–433–6293, David.M.Wilt@nasa.gov; and
Michael J. Krasowski, 216–433–3729, Michael.J.Krasowski@nasa.gov

Ohio Aerospace Institute (OAI) contact:
Phillip P. Jenkins, 226–433–2233, Phillip.P.Jenkins@grc.nasa.gov

Author: David M. Wilt

Headquarters program office: OAT

Programs/Projects:
All of NASA's solar-powered space missions and projects

Systems Analysis Developed for All-Electric Aircraft Propulsion

There is a growing interest in the use of fuel cells as a power source for all-electric aircraft propulsion as a means to substantially reduce or eliminate environmentally harmful emissions. Among the technologies under consideration for these concepts are advanced proton exchange membrane (PEM) and solid oxide fuel cells (SOFCs), alternative fuels and fuel processing, and fuel storage. A multidisciplinary effort is underway at the NASA Glenn Research Center to develop and evaluate concepts for revolutionary, nontraditional fuel cell power and propulsion systems for aircraft applications. As part of this effort, system studies are being conducted to identify concepts with high payoff potential and associated technology areas for further development.

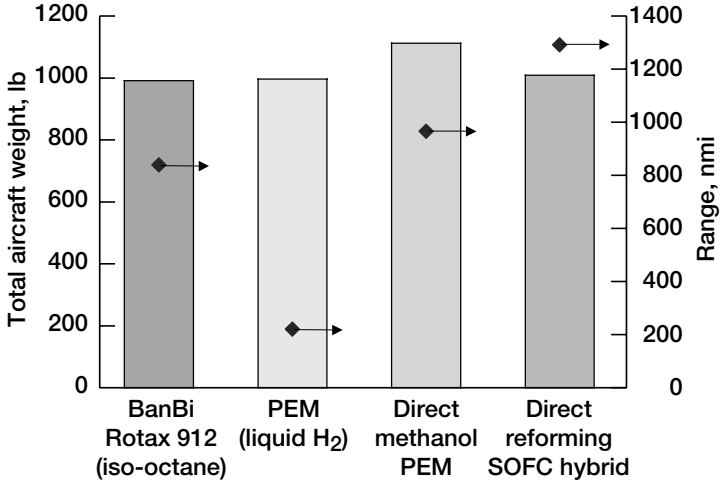

Comparison of proton exchange membrane and solid oxide fuel cell/ hybrid systems.

To support this effort, a suite of component models was developed to estimate the mass, volume, and performance for a given system architecture. These models include a hydrogen-air PEM fuel cell; an SOFC; balance-of-plant components (compressor, humidifier, separator, and heat exchangers); compressed gas, cryogenic, and liquid fuel storage tanks; and gas turbine/generator models for hybrid system applications.

First-order feasibility studies were completed for an all-electric personal air vehicle utilizing a fuel-cell-powered propulsion system. A representative aircraft with an internal combustion engine was chosen as a baseline to provide key parameters to the study, including engine power and subsystem mass, fuel storage volume and mass, and aircraft range. The engine, fuel tank, and associated ancillaries were then replaced with a fuel cell subsystem. Various configurations were considered including a PEM fuel cell with liquid hydrogen storage, a direct methanol PEM fuel cell, and a direct internal reforming SOFC/

turbine hybrid system using liquid methane fuel. Each configuration was compared with the baseline case on a mass and range basis. A comparison of the study results is shown in the bar chart on the preceding page. On the basis of the study methodology, the SOFC-hybrid system appeared to offer the most potential in terms of achieving an acceptable takeoff weight and range. This was due to a number of factors, including the use of a hydrocarbon fuel, which is more volumetrically efficient than liquid hydrogen storage; direct internal reforming of the fuel, thus eliminating the need for an external fuel processor; and the ability to extract energy from the hot fuel cell exhaust streams by expanding the gas in a turbine.

Bibliography

Kohout, Lisa L.; and Schmitz, Paul C.: Fuel Cell Propulsion Systems for an All-Electric Personal Air Vehicle. NASA/TM—2003-212354 (AIAA Paper 2003–2867), 2003. http://gltrs.grc.nasa.gov/cgi-bin/GLTRS/browse.pl?2003/TM-2003-212354.html

Glenn contact:
Lisa L. Kohout, 216–433–8004,
Lisa.L.Kohout@nasa.gov

Power Computing Solutions, Inc., contact:
Paul C. Schmitz, 216–433–6174,
Paul.C.Schmitz@grc.nasa.gov

Author: Lisa L. Kohout

Headquarters program office: OAT

Programs/Projects:
Propulsion and Power, RAC

Testing Conducted for Lithium-Ion Cell and Battery Verification

The NASA Glenn Research Center has been conducting in-house testing in support of NASA's Lithium-Ion Cell Verification Test Program, which is evaluating the performance of lithium-ion cells and batteries for NASA mission operations. The test program is supported by NASA's Office of Aerospace Technology under the NASA Aerospace Flight Battery Systems Program, which serves to bridge the gap between the development of technology advances and the realization of these advances into mission applications.

During fiscal year 2003, much of the in-house testing effort focused on the evaluation of a flight battery originally intended for use on the Mars Surveyor Program 2001 Lander. Results of this testing will be compared with the results for similar batteries being tested at the Jet Propulsion Laboratory, the Air Force Research Laboratory, and the Naval Research Laboratory. Ultimately, this work will be used to validate lithium-ion battery technology for future space missions.

The Mars Surveyor Program 2001 Lander battery was characterized at several different voltages and temperatures before life-cycle testing was begun. During characterization, the battery displayed excellent capacity and efficiency characteristics across a range of temperatures and charge/discharge conditions. Currently, the battery is undergoing life-cycle testing at 0 °C and 40-percent depth of discharge under low-Earth-orbit (LEO) conditions.

LEO conditions simulate the operations on orbit. An orbit is approximately 90 min long and consists of 55 min of charge time while the satellite is in the Sun and 35 min of discharge time during the portion of the orbit when the Earth casts a shadow on the satellite. The battery is the main source of power during the dark portion of the orbit. The goal is to demonstrate 5 years of life, or 30,000 cycles, under LEO conditions.

An additional in-house effort involves the cycling of several single lithium-ion cells that are being used as test articles to provide critical data necessary to define parameters and test conditions for NASA's Lithium-Ion Cell Verification Test Program. This testing will be used to develop wakeup procedures for cells that have been in storage and cell-matching procedures for selecting multiple cells for a single pack.

The purpose of this program is to evaluate the performance of cells from

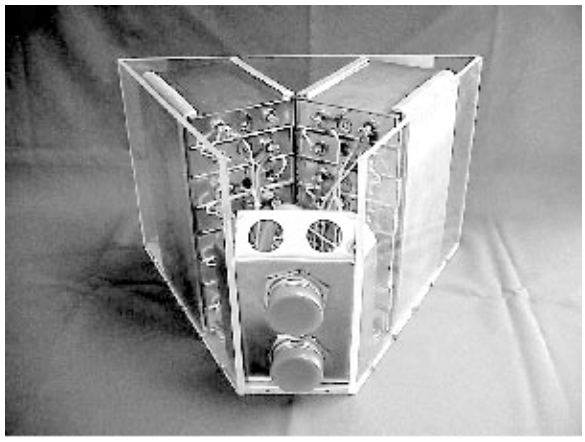

Mars 2001 lander battery.

several different vendors at different temperatures, depths of discharge, and charge cutoff voltages. The resulting database of information will be essential for predicting performance and establishing the capabilities of lithium-ion batteries for aerospace missions. The Lithium-Ion Cell Verification Test Program is a NASA-led effort headed by Glenn with participation from the other NASA centers involved in space programs, the Central Intelligence Agency, the National Reconnaissance Organization, the Air Force, the Navy, and the Aerospace Corporation.

The in-house testing discussed is being conducted in the Electrochemical Cell and Battery Test Facility, a newly renovated facility of Glenn's Electrochemistry Branch dedicated to the characterization and testing of aerospace cells and batteries. It supports cell and battery development and validation efforts for future NASA missions. It is equipped to perform testing on lithium-ion cells and batteries and other battery chemistries.

The facility is equipped with three Arbin Instruments battery testing units and four environmental chambers. Cells and batteries with capacities up to 200 A-hr and voltages as high as 45 V can be tested in inert environments at controlled temperatures of –40 to 120 °C. Different charge and discharge regimes can be simulated, including LEO, geosynchronous-Earth-orbit, mission profiles, and other predefined load profiles.

Find out more about this research:
http://www.grc.nasa.gov/WWW/Electrochemistry/

Glenn contact:
Concha M. Reid, 216–433–8943, Concha.M.Reid@nasa.gov

Authors:
Concha M. Reid, Thomas B. Miller, and Michelle A. Manzo

Headquarters program office: OAT

Programs/Projects: NASA Aerospace Flight Battery Systems, Energetics, RLV, Propulsion and Power, Mars Program

High-Power Krypton Hall Thruster Technology Being Developed for Nuclear-Powered Applications

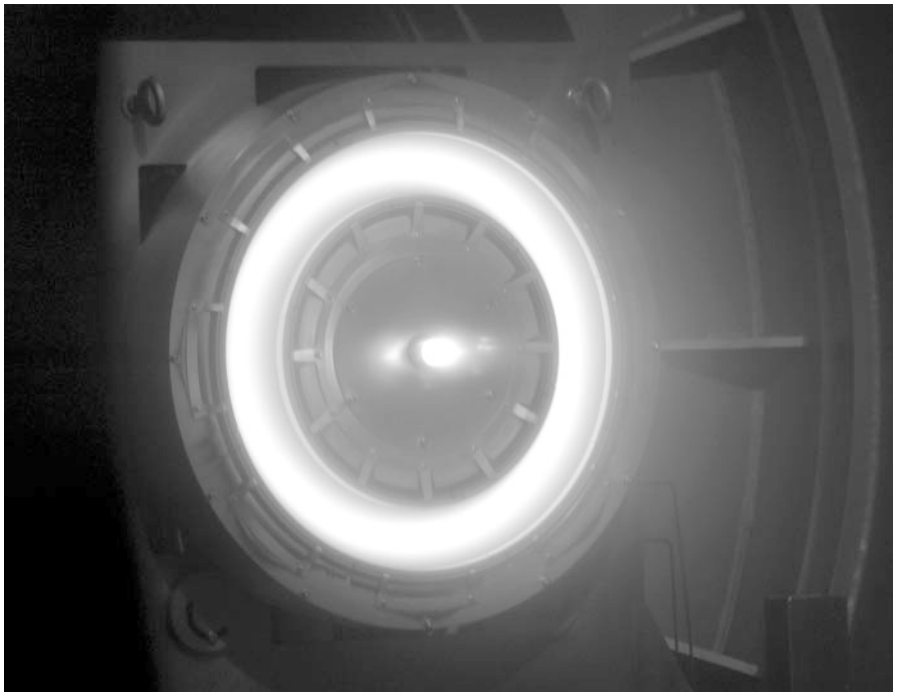

NASA–457M Hall thruster operating at 65 kW on krypton propellant.

The NASA Glenn Research Center has been performing research and development of moderate specific impulse, xenon-fueled, high-power Hall thrusters for potential solar electric propulsion applications. These applications include Mars missions, reusable tugs for low-Earth-orbit to geosynchronous-Earth-orbit transportation, and missions that require transportation to libration points. This research and development effort resulted in the design and fabrication of the NASA–457M Hall thruster that has been tested at input powers up to 95 kW. During project year 2003, NASA established Project Prometheus to develop technology in the areas of nuclear power and propulsion, which are enabling for deep-space science missions. One of the Project-Prometheus-sponsored Nuclear Propulsion Research tasks is to investigate alternate propellants for high-power Hall thruster electric propulsion.

The motivation for alternate propellants includes the disadvantageous cost and availability of xenon propellant for extremely large scale, xenon-fueled propulsion systems and the potential system performance benefits of using alternate propellants. The alternate propellant krypton was investigated because of its low cost relative to xenon. Krypton propellant also has potential performance benefits for deep-space missions because the theoretical specific impulse for a given voltage is 20 percent higher than for xenon because of krypton's lower molecular weight. During project year 2003, the performance of the high-power NASA–457M Hall thruster was measured using krypton as the propellant at power levels ranging from 6.4 to 72.5 kW. The thrust produced ranged from 0.3 to 2.5 N at a discharge specific impulse up to 4500 sec.

Glenn contact:
David T. Jacobson, 216–433–3691, David.T.Jacobson@nasa.gov

Authors: David T. Jacobson and David H. Manzella

Headquarters program office: OSS

Programs/Projects:
Project Prometheus, Nuclear Propulsion Research

Ion Thruster Power Levels Extended by a Factor of 10

In response to two NASA Office of Space Science initiatives, the NASA Glenn Research Center is now developing a 7-kW-class xenon ion thruster system for near-term solar-powered spacecraft and a 25-kW ion engine for nuclear-electric spacecraft. The 7-kW ion thruster and power processor can be throttled down to 1 kW and are applicable to 25-kW flagship missions to the outer planets, asteroids, and comets. This propulsion system was scaled up from the 2.5-kW ion thruster and power processor that was developed successfully by Glenn, Boeing, the Jet Propulsion Laboratory (JPL), and Spectrum Astro for the Deep Space 1 spacecraft. The 7-kW ion thruster system is being developed under NASA's Evolutionary Xenon Thruster (NEXT) project, which includes partners from JPL, Aerojet, Boeing, the University of Michigan, and Colorado State University.

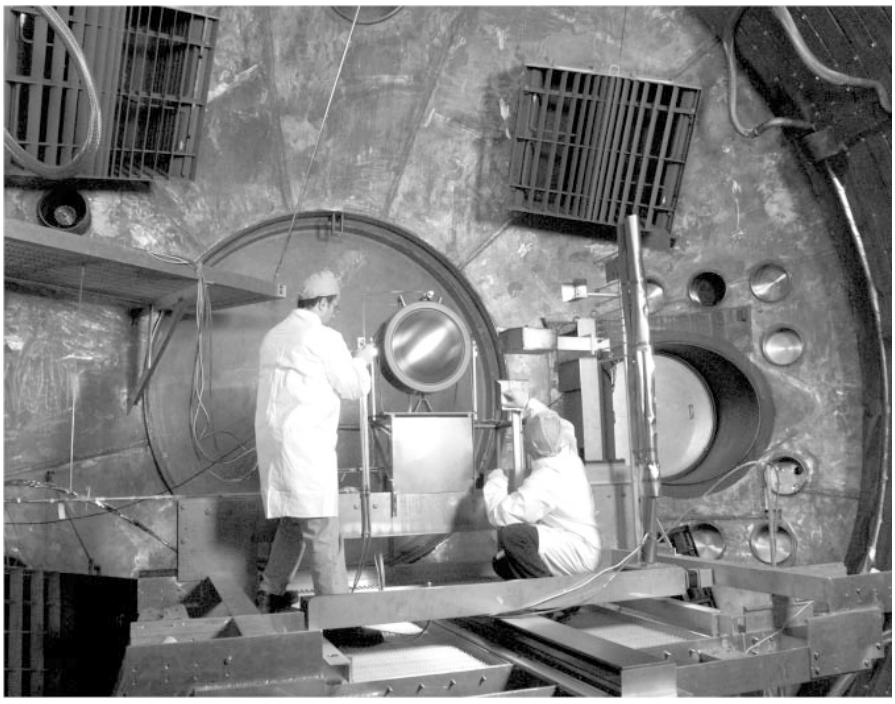

Integration of an engineering model ion thruster in a Glenn test bed prior to wear testing.

Engineering model thrusters have been built along with a breadboard power processor, a single-string xenon feed system, and a controller. Recently, a single-string system of this hardware was tested successfully at a Glenn test-bed facility that includes a suite of ion current probes, charge-state analyzers, and plasma potential diagnostics. In another vacuum facility at Glenn, an engineering model thruster completed more than 1500 hr of a scheduled 2000-hr wear test. Posttest analyses of the 7-kW thruster will be performed prior to the construction of a prototype thruster capable of not only delivering the required performance and lifetime but also satisfying all environmental and multistring system-level test requirements. In addition, the power processor and xenon feed system will be upgraded to operate in the desired vibration and thermal-vacuum environments. This system is scheduled to be flight-ready by 2006.

Glenn's 25-kW ion-thruster development project, High Power Electric Propulsion (HiPEP), features a 41- by 91-cm rectangular ion thruster that employs a microwave discharge for plasma generation and ion beam neutralization with carbon-based ion-extraction grids. This is the largest inert gas ion thruster ever developed.

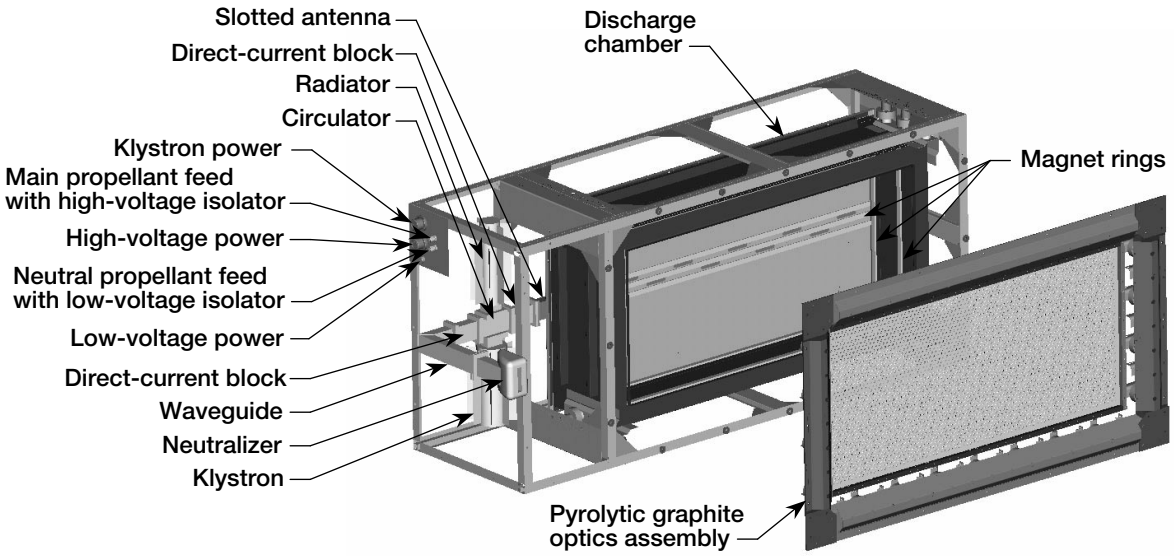

Xenon plasma generated by microwaves in a large, rectangular ion thruster instrumented with plasma probes.

Glenn's partners in the HiPEP development effort include Aerojet, Boeing, the University of Michigan, Colorado State University, and the University of Wisconsin. Eventually, this type of ion thruster along with power-conversion systems and a nuclear reactor will be part of a spacecraft dedicated to demanding missions such as a Jupiter grand tour, a Pluto orbiter, or a Jupiter icy moon orbiter. A vacuum facility test bed for the large, rectangular thruster has been built up, and uniform plasmas have been generated using a slotted-antenna microwave discharge. Software models have been exercised to determine the design of the ion-extraction grids, grid system performance, expected wear rates, and lifetime estimates. In addition, preliminary power processor design studies have been completed based on an alternating current power bus at about 500 V and ~1.5 kHz. A breadboard of the 25-kW-class power processor is planned to be built and tested in 2004. A 25-kW ion thruster, power processor, and xenon feed system is planned to be ready for advanced flight development in 2006.

Find out more about this research:
http://www.grc.nasa.gov/WWW/ion/

Glenn contact:
Michael J. Patterson, 216–977–7481, Michael.J.Patterson@nasa.gov

Author: Michael J. Patterson

Headquarters program office: OSS

Programs/Projects:
NEXT, HiPEP, JIMO, Project Prometheus

Special recognition:
2001Turning Goals Into Reality Award, 2001 R&D 100 Award, NASA Invention of the Year, 2002 Hollow Cathode Assembly Award

Lorentz Force Accelerator Technology Investigated

The NASA Glenn Research Center is developing Lorenz force accelerators (LFAs) for a wide variety of space applications. These range from the precision control of formation-flying spacecraft to the primary propulsion system for very high power interplanetary spacecraft. The specific thruster technologies being addressed are pulsed plasma thrusters (PPT) and magnetoplasmadynamic (MPD) thrusters.

The PPT mounted on the Earth Observing-1 spacecraft was operated successfully in orbit in 2002. The two-axis thruster system is fully incorporated in the attitude determination and control system and is being used to automatically counteract disturbances in the pitch axis of the spacecraft. Since the first successful functionality demonstration, the effects of thruster emissions on communication systems have been examined. X-band communications data packages were transmitted during thruster operation and analyzed for data corruption. The analysis verified that there was no measurable increase in bit error rates during thruster operation. Such benign interactions reduce user concerns and pave the way for electric propulsion applications on future Earth-imaging satellites.

Laboratory magnetoplasmadynamic thruster is prepared for operation.

Future applications of pulsed plasma thrusters will include longer life, higher precision, multiaxis thruster configurations for three-axis attitude control systems or high-precision, formation-flying systems. Advanced components, such as a "dry" mica-foil capacitor, a wear-resistant spark plug, and a multichannel power processing unit have been developed under contract with Unison Industries, General Dynamics, and C.U. Aerospace. A life test has demonstrated over 18 million pulses on these components, which approaches the near-term life requirements for deep-space interferometry demonstrator missions. Additional in-house research has included the performance evaluation of additives to polytetrafluoroethylene (PTFE) propellants, which indicated that adding small amounts of carbon to PTFE significantly reduced propellant ablation rates, resulting in a 20- to 50-percent improvement in specific impulse depending on thruster conditions.

High-power, steady-state LFAs are being considered as primary propulsion options for robotic and piloted interplanetary and deep-space missions. Glenn's LFA team is developing megawatt-class MPD thrusters to meet these demanding future mission requirements. MPD system models have been developed, a thruster has been built to parametrically consider new thruster geometries, and Glenn's high-power test facility has been utilized to evaluate megawatt-class MPD thruster performance (see the photograph). The initial quasi-steady data demonstrated 35-percent efficiency with argon propellant, with thruster models showing a path to 50-percent efficiency. Future plans include the numerical modeling and design of more efficient thruster geometries and experiments to demonstrate improved efficiency and assess thruster lifetime.

Find out more about this research:

Earth Observing-1 PPT experiment:
http://space-power.grc.nasa.gov/ppo/projects/eo1/

Earth Observing-1:
http://eo1.gsfc.nasa.gov

Glenn contact:
Eric J. Pencil, 216–977–7463,
Eric.J.Pencil@nasa.gov

Authors: Eric J. Pencil, Dr. Michael R. LaPointe, Lynn A. Arrington, Dr. Hani Kamhawi, Scott W. Benson, and W. Andrew Hoskins

Headquarters program offices:
OSS, OSF, OAT, OES

Programs/Projects: Energetics, Prometheus, New Millennium Program

Multikilowatt Power Module Designed and Fabricated for High-Power Hall Thrusters

Previous efforts to develop power processing units (PPUs) for Hall thruster systems were targeted for the 1- to 5-kW power range and an output voltage of approximately 300 V. The NASA Glenn Research Center is developing new high-power Hall thrusters with a favorable combination of thrust, specific impulse, and efficiency to enable Earth-orbiting and Mars missions. These thrusters require up to 100 kW of power and a discharge voltage in excess of 800 V.

The implementation of power processors for this power level typically requires modular designs. Processing power in smaller blocks allows the use of more efficient semiconductors, and it simplifies packaging and thermal management. In addition, it reduces voltage and current stresses in components like MOSFETs, capacitors, and transformers. Modular PPUs can be easily scaled up to higher power or made redundant, connecting parallel or series combinations of modules. This can significantly reduce PPU development time and cost.

During program year 2003, a high-power breadboard power module for Hall thrusters was designed and fabricated. This high-frequency power converter, shown in the photograph, was operated from an unregulated 100-V input to a regulated 500-V output up to an output power of 10 kW. Efficiencies in excess of 95 percent were measured. Mass projections indicate the possibility of this power module yielding 10-kW-class PPUs with a specific mass of ≤2 kg/kW, which is lower than the state-of-the-art PPU. The breadboard multikilowatt power module was used to study the issues of high-power PPU design. We plan to integrate it with a NASA–457M high-power Hall thruster and use it as a building block for higher power PPUs.

Find out more about this research:
http://www.grc.nasa.gov/WWW/onboard/onboard.html

Glenn contact:
Luis R. Pinero, 216–977–7428, Luis.R.Pinero@nasa.gov

Author: Luis R. Pinero

Headquarters program office:
OAT, OSS, OES, OSF

Programs/Projects: Energetics

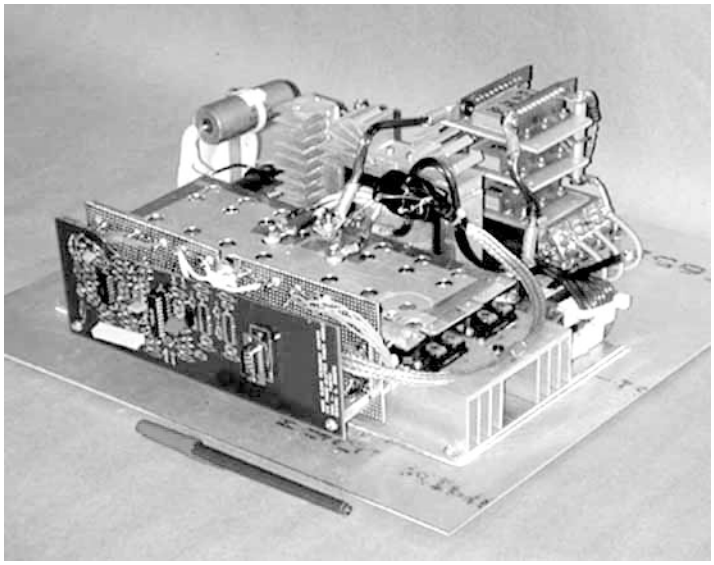

10-kW power module for Hall thrusters.

High-Performance Monopropellants and Catalysts Evaluated

The NASA Glenn Research Center is sponsoring efforts to develop advanced monopropellant technology. The focus has been on monopropellant formulations composed of an aqueous solution of hydroxylammonium nitrate (HAN) and a fuel component. HAN-based monopropellants do not have a toxic vapor and do not need the extraordinary procedures for storage, handling, and disposal required of hydrazine (N_2H_4). Generically, HAN-based monopropellants are denser and have lower freezing points than N_2H_4. The performance of HAN-based monopropellants depends on the selection of fuel, the HAN-to-fuel ratio, and the amount of water in the formulation. HAN-based monopropellants are not seen as a replacement for N_2H_4 per se, but rather as a propulsion option in their own right. For example, HAN-based monopropellants would prove beneficial to the orbit insertion of small, power-limited satellites because of this propellant's high performance (reduced system mass), high density (reduced system volume), and low freezing point (elimination of tank and line heaters).

Early technology efforts centered on a HAN-glycine formulation that had a relatively low performance but was compatible with state-of-art catalysts. More recent work has been oriented toward HAN formulations that perform better than N_2H_4, with a specific impulse I_{sp} goal of 250 sec. The combustion environment of high-performance HAN formulations is both high-temperature (>1700 °C) and corrosive (nitric acid, steam). State-of-art catalysts have not lasted more than a few seconds in this aggressive combustion environment. The developmental challenge is to develop catalysts (carrier and active coating) that can survive longer in the HAN combustion environment.

Under a Glenn-contracted effort, Aerojet Redmond Rocket Center conducted testing to provide the foundation for the development of monopropellant thrusters with an $I_{sp} \geq 250$ sec. A modular, workhorse reactor (representative of a 1-lbf thruster) was used to evaluate HAN formulations with catalyst materials. Stoichiometric, oxygen-rich, and fuel-rich formulations of HAN-methanol and HAN-tris(aminoethyl)amine trinitrate were tested to investigate the effects of stoichiometry on combustion behavior. Aerojet found that fuel-rich formulations degrade the catalyst and reactor faster than oxygen-rich and stoichiometric formulations do. A HAN-methanol formulation with a theoretical I_{sp} of 269 sec (designated HAN269MEO) was selected as the baseline. With a combustion efficiency of at least 93 percent demonstrated for HAN-based monopropellants, HAN269MEO will meet the $I_{sp} \geq 250$ sec goal.

Various ceramic carrier materials were evaluated in laboratory testing and the workhorse reactor. These high-temperature ceramics generally have lower surface areas than state-of-art catalysts but are more thermally stable at high temperatures. One catalyst material, using a relatively low-cost carrier, demonstrated the longest lifetime (over 5 min) and throughput (900 g) ever accomplished with high-performance monopropellants.

The Aerojet test program identified a baseline formulation and catalyst material for a monopropellant with an $I_{sp} > 250$ sec, and it provided fundamental insights to HAN combustion and catalyst behavior. These efforts have established a firm foundation for the development of high-performance monopropellant thrusters.

Glenn contact:
Brian D. Reed, 216–977–7489,
Brian.D.Reed@nasa.gov

Author: Brian D. Reed

Headquarters program office: OAT

Programs/Projects:
Earth Science, Space Science

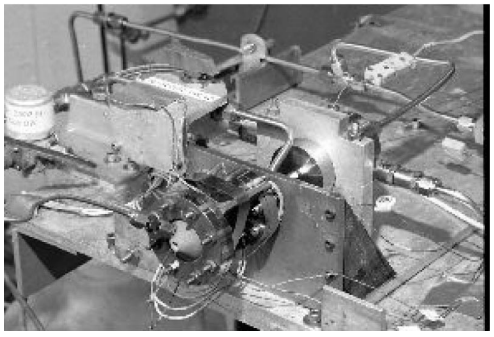

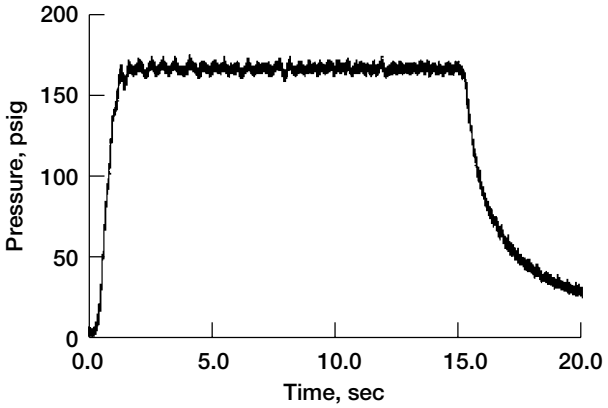

Left: Workhorse reactor used for HAN-based monopropellant testing, Right: typical chamber pressure trace for baseline propellant formulation and catalyst.

Soft-Fault Detection Technologies Developed for Electrical Power Systems

The NASA Glenn Research Center, partner universities, and defense contractors are working to develop intelligent power management and distribution (PMAD) technologies for future spacecraft and launch vehicles. The goals are to provide higher performance (efficiency, transient response, and stability), higher fault tolerance, and higher reliability through the application of digital control and communication technologies. It is also expected that these technologies will eventually reduce the design, development, manufacturing, and integration costs for large, electrical power systems for space vehicles.

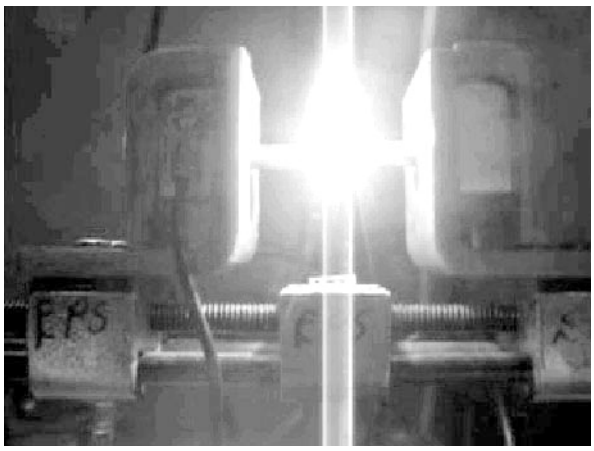

Arc fault detection research.

The main focus of this research has been to incorporate digital control, communications, and intelligent algorithms into power electronic devices such as direct-current to direct-current (dc-dc) converters and protective switchgear. These technologies, in turn, will enable revolutionary changes in the way electrical power systems are designed, developed, configured, and integrated in aerospace vehicles and satellites. Initial successes in integrating modern, digital controllers have proven that transient response performance can be improved using advanced nonlinear control algorithms.

One technology being developed includes the detection of "soft faults," those not typically covered by current systems in use today. Soft faults include arcing faults, corona discharge faults, and undetected leakage currents. Using digital control and advanced signal analysis algorithms, we have shown that it is possible to reliably detect arcing faults in high-voltage dc power distribution systems (see the photograph above). Another research effort has shown that low-level leakage faults and cable degradation can be detected by analyzing power system parameters over time. This additional fault detection capability will result in higher reliability for long-lived power systems such as reusable launch vehicles and space exploration missions.

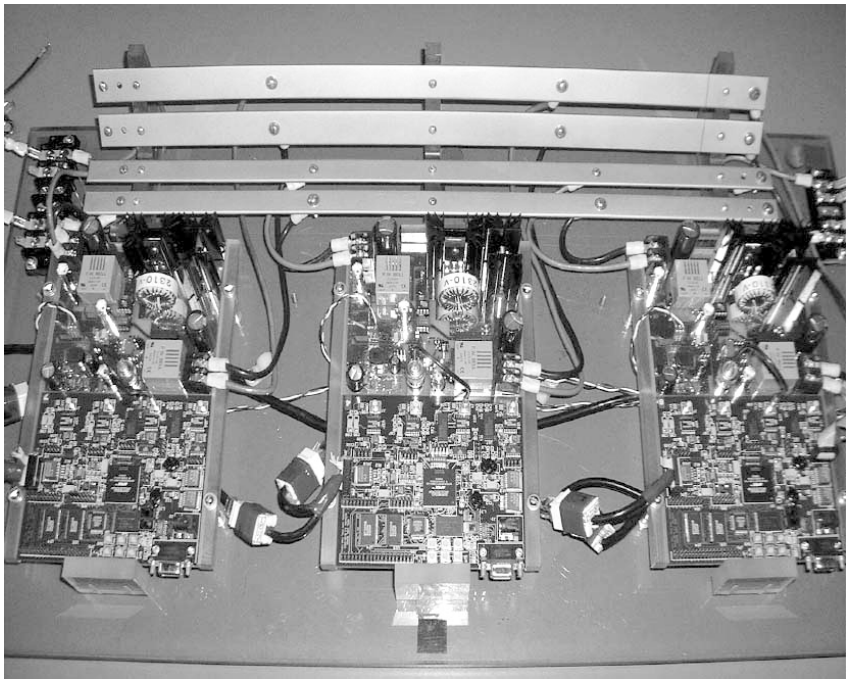

Multimodule, digital control of dc-dc converters.

An extension of the digital technology being developed is to provide active "collaboration" among modular components to improve performance and enable the use of common modules, thereby reducing costs. The performance improvement goals include active current sharing, load efficiency optimization, and active power quality control. The challenge is to make these modules truly stand alone—with no central controller—thereby eliminating sources of single-point failures. The current technology demonstrator (see the photograph to the left) has high-speed serial communication between the modular controllers, and it can actively control the switching phase between three paralleled dc-dc converters, thereby greatly improving power quality.

Future technologies to be developed include active stability control, health monitoring, and prognostics of power electronic hardware. Finally a highly reconfigurable distribution topology is being developed that will greatly increase system reliability and enable autonomous reconfiguration of the electrical power system in response to system failures or changes in mission priorities.

Find out more about this research: http://powerweb.grc.nasa.gov/elecsys/

Glenn contact:
Robert M. Button, 216–433–8010, Robert.M.Button@nasa.gov

Author: Robert M. Button

Headquarters program office: OAT

Programs/Projects: Enabling Concepts & Technologies, Energetics

Advanced Electrical Materials and Components Being Developed

All aerospace systems require power management and distribution (PMAD) between the energy and power source and the loads. The PMAD subsystem can be broadly described as the conditioning and control of unregulated power from the energy source and its transmission to a power bus for distribution to the intended loads. All power and control circuits for PMAD require electrical components for switching, energy storage, voltage-to-current transformation, filtering, regulation, protection, and isolation. Advanced electrical materials and component development technology is a key technology to increasing the power density, efficiency, reliability, and operating temperature of the PMAD.

The primary means to develop advanced electrical components is to develop new and/or significantly improved electronic materials for capacitors, magnetic components, and semiconductor switches and diodes. The next important step is to develop the processing techniques to fabricate electrical and electronic components that exceed the specifications of presently available state-of-the-art components. The NASA Glenn Research Center's advanced electrical materials and component development technology task is focused on the following three areas:

(1) New and/or improved dielectric materials for the development of power capacitors with increased capacitance volumetric efficiency, energy density, and operating temperature.
(2) New and/or improved high-frequency, high-temperature soft magnetic materials for the development of transformers and inductors with increased power density, energy density, electrical efficiency, and operating temperature.
(3) Packaged high-temperature, high-power density, high-voltage, and low-loss SiC diodes and switches.

The accomplishments for each of these areas follow:

For the power capacitor area, candidate high-temperature ceramic dielectrics with dielectric and electrical properties suitable for use up to 300 °C were identified and evaluated along with dopant materials that increased the bulk resistivity and decreased the average grain size in the fired, multilayer ceramic capacitors (MLCCs). In addition, MLCCs of different compositions and sizes were fabricated, tested, and evaluated using the candidate dielectric and dopant materials that exhibited the best dielectric (dielectric constant) and electrical (resistivity and dielectric strength) properties for long-term, high-temperature use.

The capability to deposit up to 25 ft of wrinkle-free diamondlike-carbon (DLC) film on both sides of aluminum foil was demonstrated for capacitor construction. Five different types of aluminum foils, two different types of metalized polymer films, and three different types of polymer films were demonstrated as substrates for diamondlike-carbon films and were evaluated in terms of surface roughness, adhesion, wrinkle-free characteristics, and film thickness and uniformity.

In the magnetic materials research area, Glenn's core loss and dynamic hysteresis loop measurement system was upgraded to measure the electrical and magnetic characteristics of high quality factor (Q) inductor-type magnetic materials. These core loss tests were conducted on $Co_{50}(SiO_2)_{50}$ and $(Fe_{50}Ni_{50})_{90}(SiO_2)$ nanocomposite magnetic materials at room temperature over frequencies ranging from 100 kHz to 1 MHz. In addition, a 2.5-kVA/kg, 200 °C transformer was demonstrated. Compacted, noncoated NiFe nanoparticles were investigated extensively to study the magnetic-moment-exchange coupling mechanism. In addition, their seven soft, magnetic, FeCo-based nanocrystalline alloys were designed, processed, and fabricated, and their physical and direct-current magnetic properties were characterized.

In the semiconductor switch and diode area, experimental methods and procedures were investigated for measuring the dynamic characteristics of Si, GaA, and SiC Schottky diodes. The room-temperature current-voltage characteristics of Si, GaA, and SiC Schottky diodes with similar rated Si pn junction diodes were investigated for comparative purposes, and the effects of NO passivation on the radiation responses of gate oxides for 4H-SiC power MOSFETS were investigated. High-quality GaN and AlGaN/GaN epitaxial films were grown on SiC and sapphire substrates using metal organic vapor deposition, and the growth of defect-free 3C-SiC on 4H- and 6H-SiC mesas was demonstrated using step-free surface heteroepitaxy.

Find out more about this research:
http://powerweb.grc.nasa.gov/elecsys/

Glenn contact:
Gene E. Schwarze, 216–433–6117,
Fax: 216–433–8311,
Gene.E.Schwarze@nasa.gov

Author: Gene E. Schwarze

Headquarters program office: OAT

Programs/Projects: Space Power

Flywheel Single-Axis Integrated Momentum and Power Control System Demonstrated

On July 10, 2003, the NASA Glenn Research Center flywheel team experimentally demonstrated a two-flywheel-module system that simultaneously provided attitude control in a single axis and regulated power. The test was conducted using the D1 flywheel module and the high-speed shaft (HSS) in the High Energy Flywheel Facility (HEFF). Both of these flywheel modules consist of a magnetically levitated rotor with an integral motor/generator, a vacuum housing, and mechanical touchdown bearings. Energy is stored kinetically in the rotor. The motor/generator allows energy to be added to or withdrawn from the rotor, and magnetic bearings and a vacuum enclosure are used to minimize losses.

D1 and HSS flywheels on air table.

The modules are both located on a common table that is mounted on an air bearing, allowing the table to rotate (see the photograph). When a command is issued to move the table to a new angle, the attitude control system commands opposite torques on each module, resulting in a net torque on the air table. The table moves, and the position is fed back to the controller. We were only able to move the air table through an angle of ±0.1° because of cable drag in our test setup (see the graph on the next page). This is functionally similar to a momentum control system on a satellite. In addition to providing attitude control, the system simultaneously provides energy storage and electrical bus regulation. The bus voltage was regulated at 125 V during charge and discharge. Charge-discharge and discharge-charge transitions were demonstrated by changing the amount of power that the power supply provided. In a satellite system, this would be the equivalent of changing the amount of energy that the solar array provides to the spacecraft.

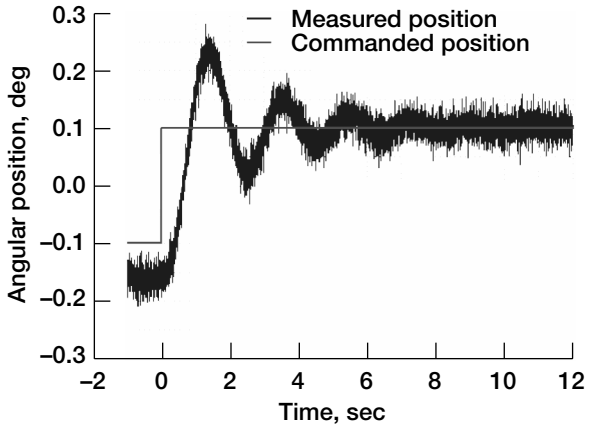

Air table tracking-angle command.

Glenn contacts:
Jim Soeder, 216–433–5328, Jim.Soeder@nasa.gov;
Kerry McLallin, 216–433–5389, Kerry.L.McLallin@nasa.gov; and
Ralph Jansen, 216–433–6038, Ralph.Jansen@nasa.gov

Author: James F. Soeder

Headquarters program office: OAT

Programs/Projects: Aerospace Flywheel Technology, Energetics

Hubble Space Telescope Degradation Data Used for Ground-Based Durability Projection of Insulation on the International Space Station

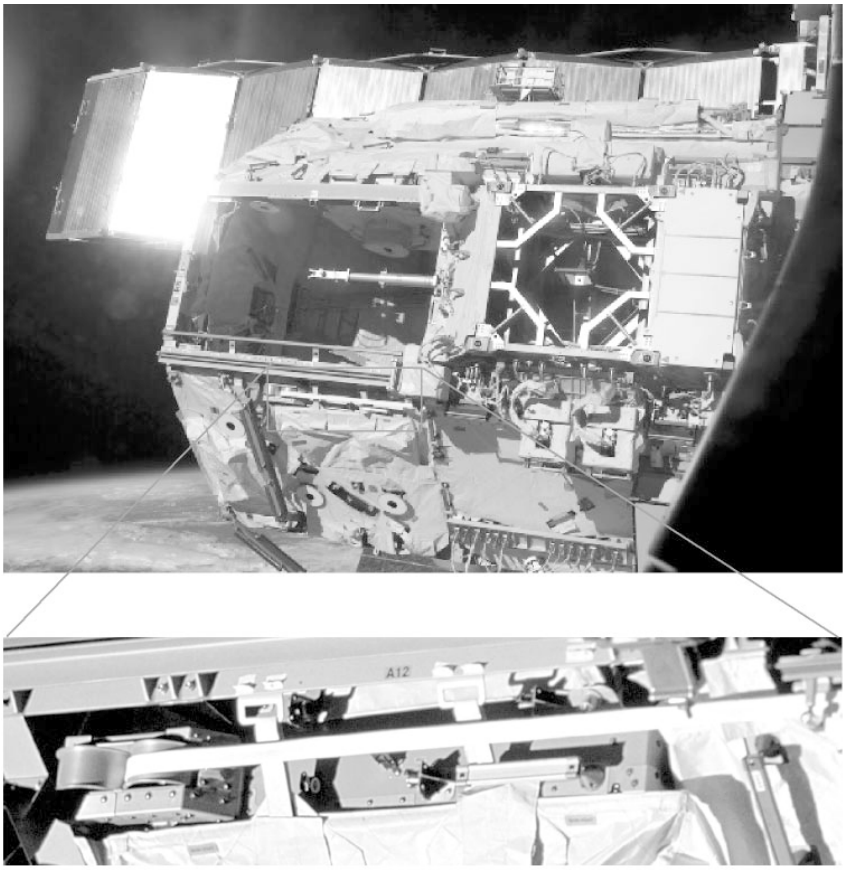

S-Zero (S0) truss on the International Space Station. Top: Mobile transporter (MT) on the S0 truss during shuttle mission STS–110. Bottom: Closeup photograph of the MT trailing umbilical system cable during STS–111.

Ground-based environmental durability tests have indicated that exposing materials in accelerated tests to known spacecraft mission degradation sources predicted by an environmental model does not simulate the extent of damage that occurs in the space environment. The reasons for this may include the complex nature of the space environment, which is not simulated completely in any ground-based facility, the extreme differences in exposure rates in space and in ground tests, and inaccuracies in environmental models. One approach to overcoming the difficulties in simulating the space environment using ground-based testing is to calibrate the facility using data from actual space-exposed materials to determine exposure levels required to replicate degraded properties observed in space. Research was conducted at the NASA Glenn Research Center to develop a ground-to-space correlation method that determines the durability of Teflon-based insulation for the International Space Station (ISS) by using data obtained in a ground facility and degraded Teflon thermal insulation retrieved from the Hubble Space Telescope.

The mobile transporter (MT), also called the ISS railcar, was installed on the ISS S-Zero (S0) truss during STS–110 in April 2002. The MT trailing umbilical system (TUS) contains two cables that provide redundant power, video, and communication conductors to the MT. Each cable is contained within a mechanical reel assembly that deploys and retracts the cable as the MT translates. The space-exposed TUS cable insulation is made of an outer jacket and inner core of expanded polytetrafluoroethylene (ePTFE). The outer jacket is composed of six layers of ePTFE (a total thickness of 50±10 mils) that is heated and pressed during cable fabrication. After fabrication, the outer jacket ePTFE varies in thickness and is approximately 43±3 mils (0.11±0.008 cm) thick. The inner core is 7 to 10 mils (0.018 to 0.0254 cm) thick. The TUS cable has a mission life of 10 years and is estimated to thermal cycle from –100 to 130 °C on orbit. The bottom photograph (previous page) shows a closeup of one of the TUS cables, as photographed in June 2002 during STS–111. Polytetrafluoroethylene, from which ePTFE is made, is known to be significantly more susceptible to radiation degradation than fluorinated ethylene propylene (FEP). Hubble Space Telescope Teflon FEP thermal insulation of 2- and 5-mil (0.0051- and 0.0125-cm) thicknesses has become extremely brittle in the space environment. Therefore, we desired to test the durability of the ePTFE for the TUS application on the ISS.

The ground-to-space correlation method developed uses a multiple-step process to determine the durability of ePTFE for ISS applications based on ground-based x-ray irradiation and heating exposure that simulates the bulk embrittlement that occurs in the 5-mil- (0.0125-cm-) thick FEP thermal insulation covering the Hubble Space Telescope. The method was designed to damage the back surface of equivalent thickness ePTFE to the same amount of scission damage as occurred in FEP retrieved from the Hubble Space Telescope after 9.7 years in space (based on elongation data) and then correct for differences in ground test ionizing radiation versus space radiation effects, temperature variations, space ionizing radiation environment variations (spacecraft altitude, inclination, and duration), and thickness variations.

The analysis for this application indicates that after a 10-year mission, the ISS ePTFE will have an extremely embrittled front surface, with surface cracks induced under any given strain, and a very ductile back surface. This study also found that a thermal-induced strain of 0.1 will develop in the ePTFE, and under this strain condition, microscopic cracks will start developing very early in the mission at the exposed surface and could develop to a depth of ≈0.030 cm after 10 years.

The test method developed can be applied to other materials and space flight environments, and thus can improve durability predictions of spacecraft materials based on ground testing.

Find out more about this research:
http://www.grc.nasa.gov/WWW/epbranch/

Glenn contacts:
Kim K. de Groh, 216–433–2297, Fax: 216–433–2221, Kim.K.deGroh@nasa.gov;
Bruce A. Banks, 216–433–2308, Fax: 216–433–2221, Bruce.A.Banks@nasa.gov; and
Joyce A. Dever, 216–433–6294, Fax: 216–433–2221, Joyce.A.Dever@nasa.gov

Authors:
Kim K. de Groh, Bruce A. Banks, Joyce A. Dever, and Janet C. Hodermarsky

Headquarters program office: OAT

Programs/Projects:
ISS, Earth Observing Systems, DOD, Future spacecraft

Effects of Various Wavelength Ranges of Vacuum Ultraviolet Radiation on Teflon FEP Film Investigated

Teflon FEP films (DuPont) have been widely used for spacecraft thermal control and have been observed to become embrittled and cracked upon exposure to the space environment (refs. 1 and 2). This degradation has been attributed to a synergistic combination of radiation and thermal effects (refs. 1 and 3). A research study was undertaken at the NASA Glenn Research Center to examine the effects of different wavelength ranges of vacuum ultraviolet (VUV) radiation on the degradation of the mechanical properties of FEP. This will contribute to an overall understanding of space radiation effects on Teflon FEP, and will provide information necessary to determine appropriate techniques for using laboratory tests to estimate space VUV degradation. Research was conducted using in-house facilities at Glenn and was carried out, in part, through a grant with the Cleveland State University.

Samples of Teflon FEP film of 50.8-μm thickness were exposed to radiation from a VUV lamp from beneath different cover windows to provide different exposure wavelength ranges: MgF_2 (115 to 400 nm), crystalline quartz (140 to 400 nm), and fused silica (FS, 155 to 400 nm). Following exposure, FEP film specimens were tensile tested to determine the ultimate tensile strength and elongation at failure as a function of the exposure duration for each wavelength range. The graphs show the effect of ultraviolet exposure on the mechanical properties of the FEP samples.

In order to interpret the effects of exposure to the various wavelength ranges, it is important to understand the nature of the interaction of ultraviolet radiation with Teflon FEP. Teflon PTFE, which is chemically similar to FEP, has been found to have an absorption peak at approximately 160 nm (ref. 4). VUV radiation of wavelengths in this absorption peak are absorbed significantly within a very thin slice of the Teflon thickness, resulting in a concentration of photoreactions near the surface. One consequence of surface-concentrated photoreactions is erosion. Surface erosion was observed upon exposure of FEP to both broad spectrum VUV (115 to 400 nm) and monochromatic VUV (147 nm) (ref. 5). In comparison, mechanical properties degradation of FEP was caused by 115- to 400-nm VUV, but not by 147-nm VUV (ref. 5). This implies that wavelengths that cause erosion cannot penetrate into the polymer deeply enough to embrittle the bulk material. Typical laboratory VUV sources have a peak output at approximately 160 nm, which matches the absorption peak of Teflon but which is not representative of a peak in the solar spectrum. Therefore, it is likely that laboratory VUV exposure with these sources would cause greater surface erosion than would occur in

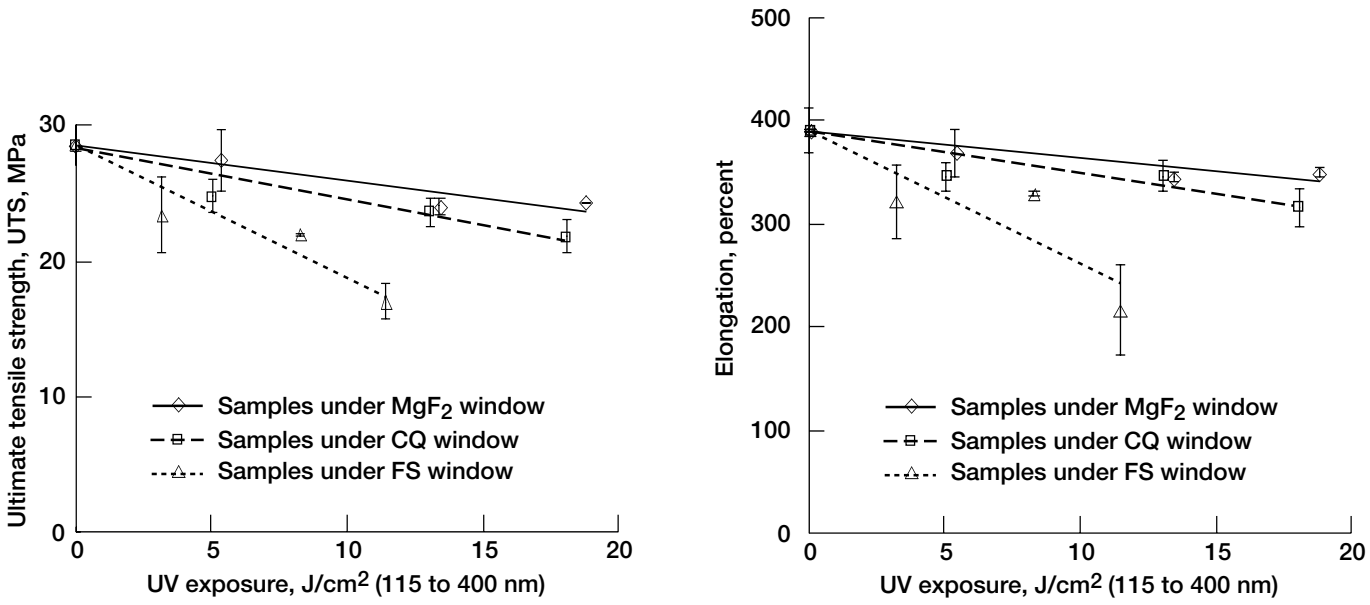

Effects of ultraviolet radiation on 50.8-μm FEP, where UV was provided by broad spectrum VUV lamps transmitted through cover-windows of MgF_2 (115 to 400 nm), CQ (140 to 400 nm), and FS (155 to 400 nm). Left: Effects of ultraviolet radiation on ultimate tensile strength. Right: Effects of ultraviolet radiation on elongation to failure.

space (ref. 6), and may lead to inaccuracies in interpreting the results of ground laboratory tests of Teflon materials in terms of expected degradation in the space environment.

Examining the data in the graphs, we see that the fastest rate of mechanical properties degradation is for FEP exposed to 155- to 400-nm wavelengths (from beneath fused silica). Whereas the cut-on wavelength for fused silica is 155 nm, transmittance through fused silica does not approach a maximum until approximately 180 nm, so the vast majority of the VUV lamp's output peak centered at 160 nm is not transmitted through fused silica to the sample. Both the crystalline quartz (CQ) and magnesium fluoride (MgF_2) windows allow the 160-nm output peak to be transmitted with minimal attenuation, and therefore, provide a significant fluence of surface-eroding wavelengths of VUV in addition to wavelengths that can cause degradation deeper in the material. The apparent slower rate of mechanical properties degradation for samples exposed from beneath the CQ and MgF_2 windows is due to the fact that the total VUV fluence for these cases includes fluence that only thins the material and does not lead to embrittlement, and, in fact, may remove an embrittled layer. When the eroding wavelengths are excluded from the VUV exposure test, laboratory testing results are expected to produce a more conservative estimate of in-space degradation and may be appropriate for determining worst-case effects. The results of this research study are presented in reference 6.

References

1. Townsend, J.A., et al.: Ground-Based Testing of Replacement Thermal Control Materials for the Hubble Space Telescope. High Per. Polym., vol. 11, no. 1, 1999, pp. 63–79.
2. Dever, J.A., et al.: Mechanical Properties of Teflon® FEP Retrieved From the Hubble Space Telescope. High Per. Polym., vol. 13, no. 3, 2001, pp. S373–S390.
3. de Groh, K.K., et al.: Thermal Contributions to the Degradation of Teflon® FEP on the Hubble Space Telescope. High Per. Polym., vol. 13, no. 3, 2001, pp. S401–S420.
4. Seki, K., et al.: Electronic-Structure of Poly(Tetrafluoroethylene) Studied by UPS, VUV Absorption, and Band Calculations. Phys. Scr., vol. 41, no. 1, 1990, pp. 167–171.
5. Skurat, V.E., et al.: The Separate and Combined Effects of VUV Radiation and Fast Atomic Oxygen on Teflon® FEP and Silicon Carbide. ESA SP 399, 1997, pp. 267–279.
6. Dever, Joyce A.; and McCracken, Cara A.: Effects of Various Wavelength Ranges of Vacuum Ultraviolet Radiation on Teflon® FEP Film. ESA SP 540, 2003, pp. 367–373.

Find out more about this research:
http://www.grc.nasa.gov/WWW/epbranch/

Glenn contact:
Joyce A. Dever, 216–433–6294, Joyce.A.Dever@nasa.gov

Authors:
Joyce A. Dever and Cara A. McCracken

Headquarters program office: OAT

Programs/Projects:
Energetics, Hubble Space Telescope, ultra-lightweight space structures

Resistivity of Carbon-Carbon Composites Halved

Carbon-carbon composites have become the material of choice for applications requiring strength and stiffness at very high temperatures (above 2000 °C). These composites comprise carbon or graphite fibers embedded in a carbonized or graphitized matrix. In some applications, such as shielding sensitive electronics in very high temperature environments, the performance of these materials would be improved by lowering their electrical resistivity.

One method to lower the resistivity of the composites is to lower the resistivity of the graphite fibers, and a proven method to accomplish that is intercalation. Intercalation is the insertion of guest atoms or molecules into a host lattice. In this study (ref. 1) the host fibers were highly graphitic pitch-based graphite fibers, or vapor-grown carbon fibers (VGCF), and the intercalate was bromine. Intercalation compounds of graphite are generally thought of as being only metastable, but it has been shown that the residual bromine graphite fiber intercalation compound is remarkably stable, resisting decomposition even at temperatures at least as high as 1000 °C (ref. 2). The focus of this work was to fabricate composite preforms, determine whether the fibers they were made from were still intercalated with bromine after processing, and determine the effect on composite resistivity. It was not expected that the resistivity would be lowered as dramatically as with graphite polymer composites because the matrix itself would be much more conductive, but it was hoped that the gains would be substantial enough to warrant its use in high-performance applications.

In a collaborative effort supporting a Space Act Agreement between the NASA Glenn Research Center and Applied Sciences, Inc. (Cedarville, OH), laminar preforms were fabricated with pristine and bromine-intercalated

pitch-based fibers (P100 and P100-Br) and VGCF (Pyro I and Pyro I-Br). The green preforms were carbonized at 1000 °C and then heat treated to 3000 °C. To determine whether the fibers in the samples were still intercalated after composite fabrication, they were subjected to x-ray diffraction. The composites containing intercalated graphite fibers showed much higher background scatter than that of pristine fibers, indicating the presence of bromine in the samples. More importantly, faint features indicative of intercalation were visible in the diffraction pattern, showing that the fibers were still intercalated.

The resistivity as a function of density of the composites is shown in the graph. As expected, the resistivity of the VGCF composites was lower than that of the pitch-based fiber composites. The resistivity of the bromine-intercalated fiber composites of both types was lower than their pristine counterparts by a factor of 2. This is compelling evidence that the fibers remained intercalated, though the composite resistivity was not lowered by as large a factor as the fiber resistivity was lowered. However, the resistivities of the composites were comparable to that of polymer composites (ref. 3) in spite of the fact that the matrix was not fully graphitized, and so fiber-to-fiber contacts were less than ideal. Thus, a new route to making highly conductive, high-temperature, low-weight materials has been demonstrated.

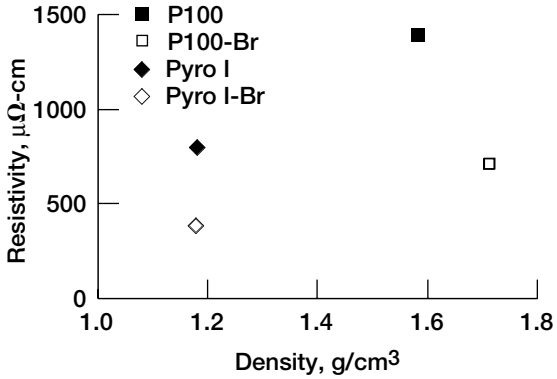

Resistivity of carbon-carbon composites made from pitch-based fibers (P100), bromine-intercalated pitch-based fibers (P100-Br), vapor-grown carbon fibers (Pyro I), and bromine-intercalated vapor-grown carbon fibers (Pyro I-Br).

Glenn contact:
Dr. James R. Gaier, 216–433–6686, James.R.Gaier@nasa.gov

Author: Dr. James R. Gaier

Headquarters program office: OAT

Programs/Projects:
High-temperature, high-conductivity, low-weight applications such as shielding engine sensors

References

1. Gaier, James R., et al.: The Resistivity of Intercalated Graphite-Carbon Composite Preforms. Proceedings of the Tenth International Conference on Composites/Nano Engineering, David Hui, ed., ICCE, New Orleans, LA, 2003, p. 195.
2. Gaier, James R.; Croy, Carla; and Stueben, Heather: High Temperature Stability of Bromine Intercalated Graphite Fibers. Paper presented at Carbon '01: An International Conference on Carbon. American Carbon Society, St. Marys, PA, 2001. (Proceedings available on CD–ROM only.)
3. Gaier, J.R.; Hambourger, P.D.; and Slabe, M.E.: Resistivity of Pristine and Intercalated Graphite Fiber Epoxy Composites. Carbon, vol. 29, no. 3, 1991, pp. 313–320.

Solar Absorptance of Cermet Coatings Evaluated

Cermet coatings, molecular mixtures of metal and ceramic, are being considered for the heat inlet surface of solar Stirling convertors. In this application, the key role of the cermet coating is to absorb as much of the incident solar energy as possible. To achieve this objective, the cermet coating has a high solar absorptance value. Cermet coatings are manufactured utilizing sputter deposition, and many different metal and ceramic combinations can be created. The ability to mix metal and ceramic at the atomic level offers the opportunity to tailor the composition, and hence, the optical properties of these coatings. The NASA Glenn Research Center has prepared and characterized a wide variety of cermet coatings utilizing different metals deposited in an aluminum oxide ceramic matrix. In addition, the atomic oxygen durability of these coatings has been evaluated.

The cermet coatings are typically 250 nm thick, and they are purposely made to be metal rich at the substrate-coating interface and ceramic rich at the surface, with the composition of metal and ceramic changing through the thickness of the coating. As a consequence of the changing composition, islands of metal form in the ceramic matrix. Diffusion of the metal atoms plays an important role in island

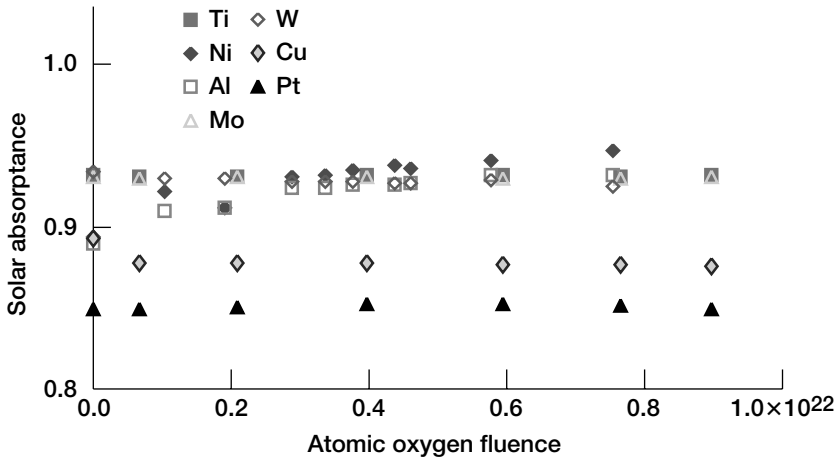

Solar absorptance of several cermet coatings as a function of effective atomic oxygen fluence.

formation, whereas the ceramic plays an important role in locking the islands in place as-formed. Much of the solar spectrum is absorbed as it passes through the labyrinth.

The following metals were utilized to make cermet coatings, in conjunction with an aluminum oxide ceramic: aluminum, nickel, titanium, platinum, copper, and molybdenum. Tungsten was used to make a cermet coating in conjunction with an aluminum nitride ceramic. Of the cermet coatings evaluated to-date, the titanium/aluminum oxide combination and the molybdenum/aluminum oxide combination offer the best optical properties, having a solar absorptance value of 0.93. Both coatings are durable to atomic oxygen, as indicated in the graph, and additional testing is underway to identify coating durability with respect to vacuum ultraviolet radiation and high temperatures.

Find out more about this research:
http://www.grc.nasa.gov/WWW/epbranch/

Glenn contact:
Dr. Don A. Jaworske, 216–433–2312, Donald.A.Jaworske@nasa.gov

Author: Dr. Donald A. Jaworske

Headquarters program office: OAT

Programs/Projects:
Energetics, Stirling Convertor Space Power Systems

Generation of Electrical Power From Stimulated Muscle Contractions Evaluated

This project is a collaborative effort between NASA Glenn Research Center's Revolutionary Aeropropulsion Concepts (RAC) Project, part of the NASA Aerospace Propulsion and Power Program of the Aerospace Technology Enterprise, and Case Western Reserve University's Cleveland Functional Electrical Stimulation (FES) Center. The RAC Project foresees implantable power requirements for future applications such as organically based sensor platforms and robotics that can interface with the human senses. One of the goals of the FES Center is to develop a totally implantable neural prosthesis. This goal is based on feedback from patients who would prefer a system with an internal power source over the currently used system with an external power source.

The conversion system under investigation would transform the energy produced from a stimulated muscle contraction into electrical energy. We hypothesize that the output power of the system will be greater than the input power necessary to initiate, sustain, and control the electrical conversion system because of the stored potential energy of the muscle. If the system can be made biocompatible, durable, and with the potential for sustained use, then the biological power source will be a viable solution.

The requirements for this project have been identified and include (1) the system must be completely implantable, (2) the system must have a maximum power-output-to-volume ratio, and (3) the system must have long-term durability and life expectancy. Two concepts have been developed and are under investigation: (1) attach piezoelectric material to a tendon and generate electricity by deforming the material with the force produced during muscle contractions, as shown in the top figure on the next page, and (2) attach a magnet to a tendon and have the motion produced during muscle contraction cause the magnet to move through a coil to produce electricity, as shown in the bottom figure on the next page. Preliminary theoretical output power calculations for these two options have been made, and further analysis will be done to determine which option to investigate fully. Workbench studies will investigate

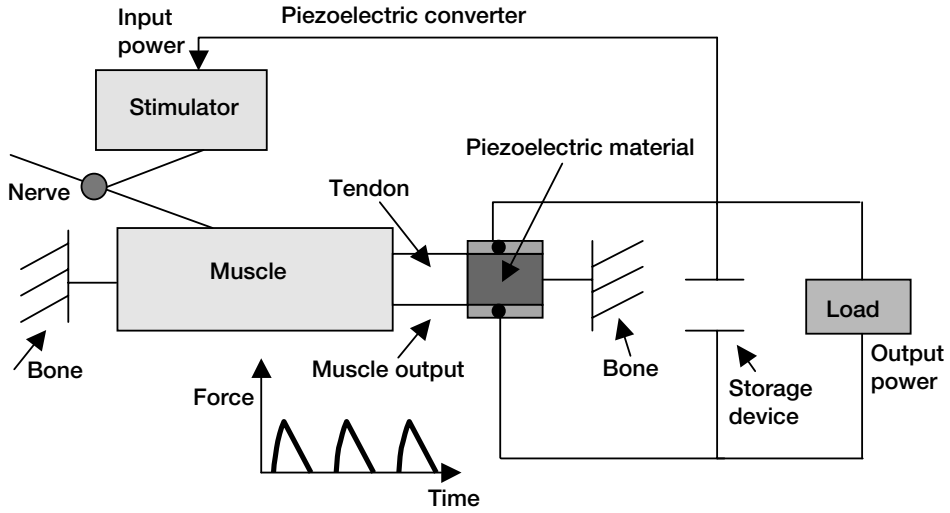

Diagram of the piezoelectric converter idea. A piece of piezoelectric material is attached between a tendon and bone. The muscle contraction stretches the piezoelectric material, causing a charge to build up on it. A capacitor or battery is used to store the generated electricity. Some of the generated power is used to stimulate the muscle to cause the contraction.

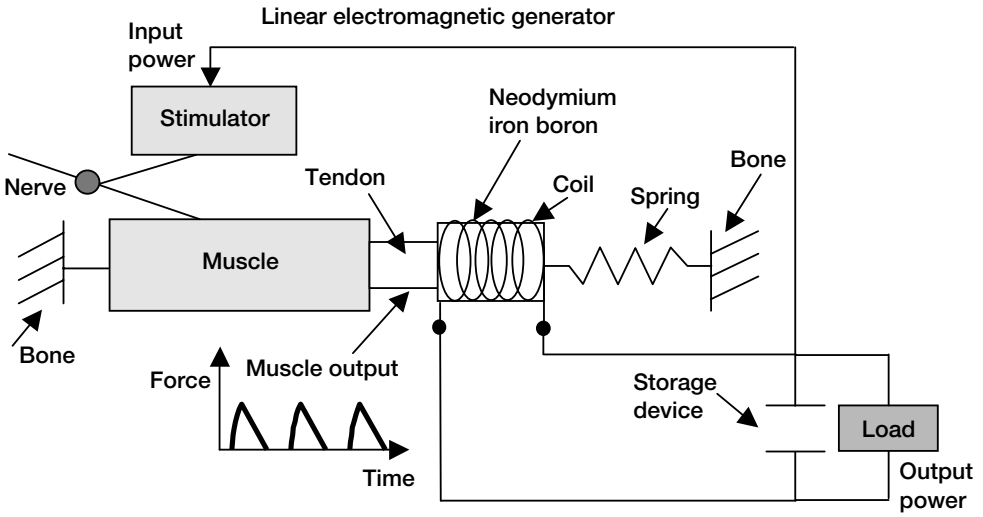

Diagram of the linear electromagnetic generator idea. A magnet and spring are attached between a tendon and bone. A coil is wound around the magnet and tendon leaving room for the magnet to slide in and out of the coil. The muscle contraction causes the magnet to move, causing voltage induction across the coils. A capacitor or battery is used to store the generated electricity. Some of the generated power is used to stimulate the muscle to cause the contraction.

the experimental power characteristics of one or more power-conversion systems, and animal studies will investigate the ability to generate power when driven by the physiological process.

Find out more about this research:
http://www.grc.nasa.gov/WWW/AERO/base/rac.htm

Glenn contacts: Beth Lewandowski, 216–433–8873, Beth.E.Lewandowski@nasa.gov; and David Ercegovic, 216–977–7009, David.B.Ercegovic@nasa.gov

Cleveland Functional Electrical Stimulation Center contact:
Kevin Kilgore, 216–778–3801, klk4@po.cwru.edu

Authors: Beth Lewandowski, Kevin Kilgore, and David B. Ercegovic

Headquarters program office: OAT

Programs/Projects:
Propulsion and Power, RAC

Atomic Oxygen Used to Restore Artworks

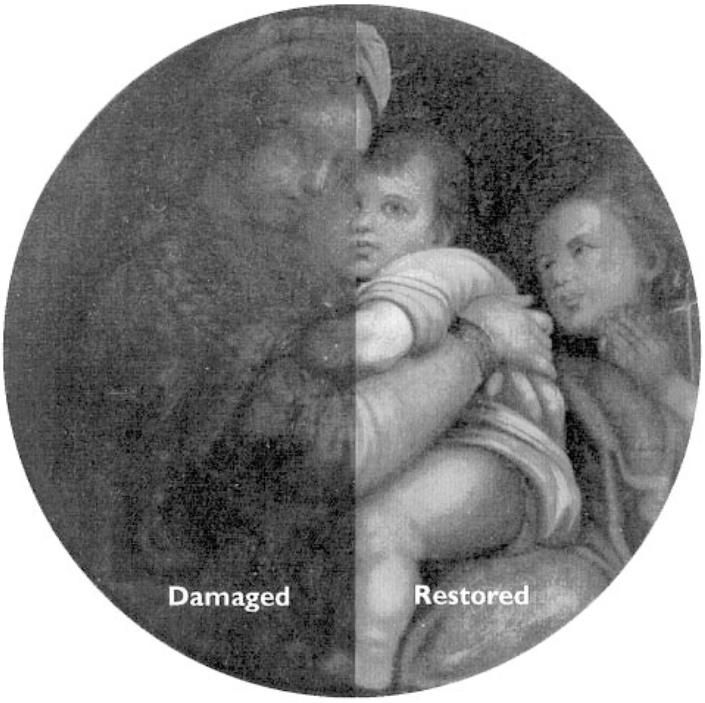

Painting "Madonna of the Chair" damaged in a 1989 fire at St. Alban's Church in Cleveland, Ohio. Left: Before restoration with atomic oxygen. Right: After restoration with atomic oxygen. This figure is shown in color in the online version of this article (http://www.grc.nasa.gov/WWW/RT/2003/5000/5480miller1.html).

Techniques developed at the NASA Glenn Research Center to produce atomic oxygen in order to simulate the low-Earth-orbit environment for spacecraft materials testing can also be applied in the field of art restoration. Defaced or fire-damaged artwork can be treated with atomic oxygen to remove the damage and enable restoration that could not be accomplished with conventional methods. The process has been patented (U.S. Patents 5,560,781 and 5,693,241) and has been used to restore several works of art.

Atomic oxygen reacts readily with compounds containing carbon, typically converting them to carbon monoxide or carbon dioxide, which leaves as a gas from the surface in trace amounts, making the process more environmentally "green" than traditional solvent cleaning techniques. The reaction is generally limited to the surface such that penetration of the atomic oxygen into the underlying surface is improbable. When artwork is damaged in a fire or defaced using pencil, crayon, some types of pen, or lipstick, there is typically a layer of carbon-containing material on the surface that a conservator wishes to remove without disturbing the underlying pigments. In many cases of fire damage, the paint binder intermixed with the pigment underneath the layer of soot can be charred as well. Unless this is removed, the paint pigment cannot be made visible and the artwork will remain dark and for the most part featureless. The use of atomic oxygen to treat the artwork allows soot, char, and other unwanted marks to be gently removed through chemical reaction in a dry, noncontact process. Since most of the paint pigments are oxides or metal complexes that are already oxides or are not as easily oxidized as carbon, the chemical reaction slows or stops when the paint pigment becomes exposed. In many cases this allows the removal of charred binder from between pigment particles, thereby allowing the surface to be restored to the point that a replacement binder can be applied by a conservator to bring the painting back to near its original state. Surfaces with organic pigments can be treated through careful timing of the exposure to atomic oxygen and/or masking so as not to remove too much of the pigment.

Atomic oxygen treatment provides a way in which many artworks, believed to be unrecoverable by conventional wet chemical techniques, can be restored to again allow the art to be viewed, studied, and enjoyed. The ability to restore artwork treasured by cultural groups and to restore national art treasures allows cultural history to be preserved and provides great benefit to the public. This technology was given the R&D 100 Award for 2002 and was selected for the "best of the best" of the 2002 R&D 100 award winners, receiving the Editor's Choice Award for Most Innovative New Technology.

Find out more about this research:
http://www.grc.nasa.gov/WWW/epbranch/

Glenn contacts:
Bruce A. Banks, 216–433–2308, Bruce.A.Banks@nasa.gov; and Sharon K. Miller, 216–433–2219, Sharon.K.Miller@nasa.gov

Authors:
Bruce A. Banks and Sharon K. Miller

Headquarters program office:
OAT (TTPO)

Programs/Projects: Microgravity Science for cleaning of contaminants from experiment hardware, cleaning of spacecraft surfaces by removal of organics or biocontaminants

Special recognition:
2002 R&D 100 Award 2002, The Best of the Best of the R&D 100—Editor's Choice Award for Most Innovative New Technology

Monte Carlo Technique Used to Model the Degradation of Internal Spacecraft Surfaces by Atomic Oxygen

Atomic oxygen is one of the predominant constituents of Earth's upper atmosphere. It is created by the photodissociation of molecular oxygen (O_2) into single O atoms by ultraviolet radiation. It is chemically very reactive because a single O atom readily combines with another O atom or with other atoms or molecules that can form a stable oxide. The effects of atomic oxygen on the external surfaces of spacecraft in low Earth orbit can have dire consequences for spacecraft life, and this is a well-known and much-studied problem. Much less information is known about the effects of atomic oxygen on the internal surfaces of spacecraft. This degradation can occur when openings in components of the spacecraft exterior exist that allow the entry of atomic oxygen into regions that may not have direct atomic oxygen attack but rather scattered attack. Openings can exist because of spacecraft venting, microwave cavities, and apertures for Earth viewing, Sun sensors, or star trackers.

The effects of atomic oxygen erosion of polymers interior to an aperture on a spacecraft were simulated at the NASA Glenn Research Center by using Monte Carlo computational techniques. A two-dimensional model was used to provide quantitative indications of the attenuation of atomic oxygen flux as a function of the distance into a parallel-walled cavity. The model allows the atomic oxygen arrival direction, the Maxwell Boltzman temperature, and the ram energy to be varied along with the interaction parameters of the degree of recombination upon impact with polymer or nonreactive surfaces, the initial reaction probability, the reaction probability dependence upon energy and angle of attack, degree of specularity of scattering of reactive and nonreactive surfaces, and the degree of thermal accommodation upon impact with reactive and nonreactive surfaces to be varied to allow the model to produce atomic oxygen erosion geometries that replicate actual experimental results from space. The degree of erosion of various interior locations was compared with the erosion that would occur external to the spacecraft.

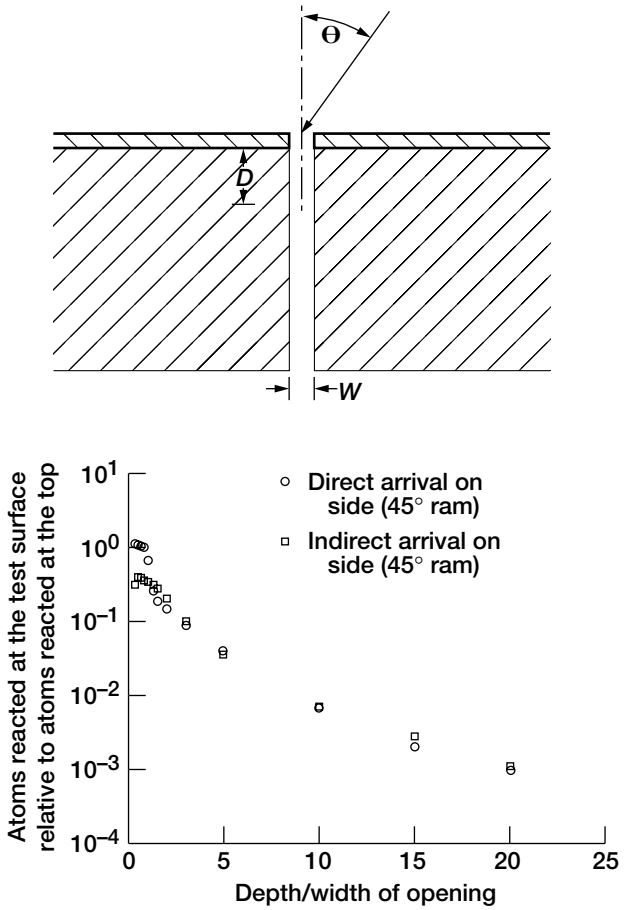

Atomic oxygen erosion on the sides of a cavity relative to the top surface of the cavity as a function of the depth-to-width ratio.

Results of one cavity model indicate that, at depths into a two-dimensional cavity that are equal to 10 cavity widths, the erosion on the walls of the cavity is less than that on the top surface by over 2 orders of magnitude. Wall erosion near the surface of a cavity depends on which wall is receiving direct atomic oxygen attack. However, deep in the cavity little difference is present. Testing of various cavity models such as these gives spacecraft designers an indication of the level of threat to sensitive interior surfaces for different geometries. Even though the Monte Carlo model is two-dimensional, it can be used to provide qualitative information about spacecraft openings that are three-dimensional by offering reasonable insight as to the nature of the attenuation of damage that occurs within a spacecraft in low Earth orbit.

Find out more about this research: http://www.grc.nasa.gov/WWW/epbranch/

Glenn contacts:
Bruce A. Banks, 216–433–2308, Bruce.A.Banks@nasa.gov; and
Sharon K. Miller, 216–433–2219, Sharon.K.Miller@nasa.gov

Authors: Bruce A. Banks and Sharon K. Miller

Headquarters program office: OSS

Programs/Projects: All spacecraft flying in low Earth orbit

Prototype Motor Controllers Demonstrated for the James Webb Space Telescope Cryogenic Environment

NASA is in the process of designing the James Webb Space Telescope. This telescope will investigate images of objects in deep space (stars, galaxies, etc.) by using light in the infrared region of the light spectrum. To make such observations, the telescope must have light sensors that operate at very cold temperatures, near absolute zero. To achieve this low-temperature tolerance, designers must place the light sensors behind a Sun shield that will prevent sunlight, and its heat, from reaching the sensors.

In this cold region inside the telescope, electric motors and some motor controls must operate at temperatures near 40 K (40 degrees above absolute zero). These motors will be used to position light filters needed by the telescope. There are motors that operate at the low temperatures, but there is little technology for low-temperature motor-control electronics. The drawing shows how the motors and their controls are positioned behind the Sun shield.

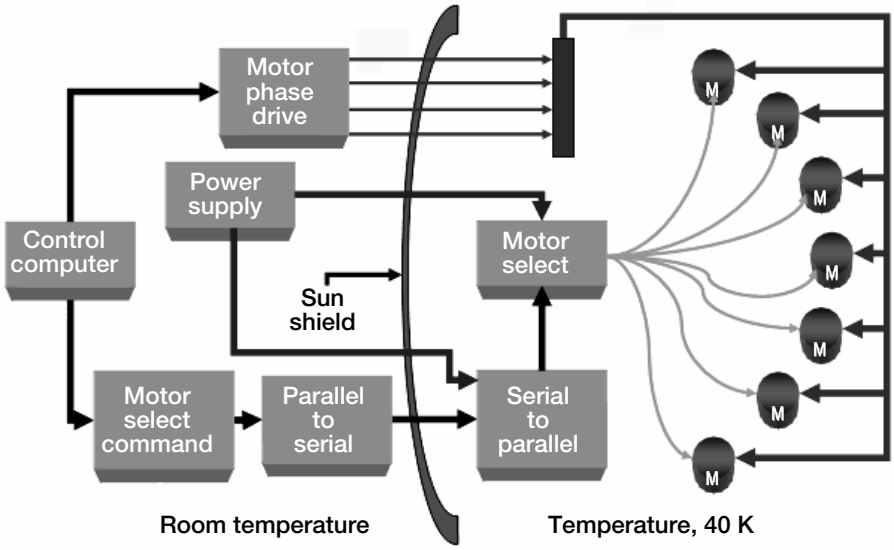

Simplified layout of motors and controller electronics on the James Webb Space Telescope.

The Low Temperature Electronics Group at the NASA Glenn Research Center has been working to develop motor control electronics that will operate at a temperature of 40 K. The group conducted tests to determine which electronic components will operate at such very low temperatures. Then, components that were determined to operate successfully at the low temperatures were used to design low-temperature motor-controller circuits. A prototype motor controller circuit was built, evaluated, and demonstrated to operate at 70 K. Next, Glenn researchers plan to determine circuit performance at much colder temperatures—down to 40 K.

This low-temperature program was supported by the James Webb Space Telescope Electrical Systems Design Group at the NASA Goddard Space Flight Center and by the NASA Electronic Parts and Packaging Program at NASA Headquarters and the Jet Propulsion Laboratory.

Find out more about this research:
http://www.grc.nasa.gov/WWW/epbranch/

Glenn contact:
Richard L. Patterson, 216–433–8166, Richard.L.Patterson@nasa.gov

Authors: Richard L. Patterson and Ahmad Hammoud

Headquarters program office: OSS

Programs/Projects: JWST, NEPP, NEPAG, Mars 07, JIMO, Europa Lander

Regenerative Fuel Cell Test Rig Completed and Operational at Glenn Research Center

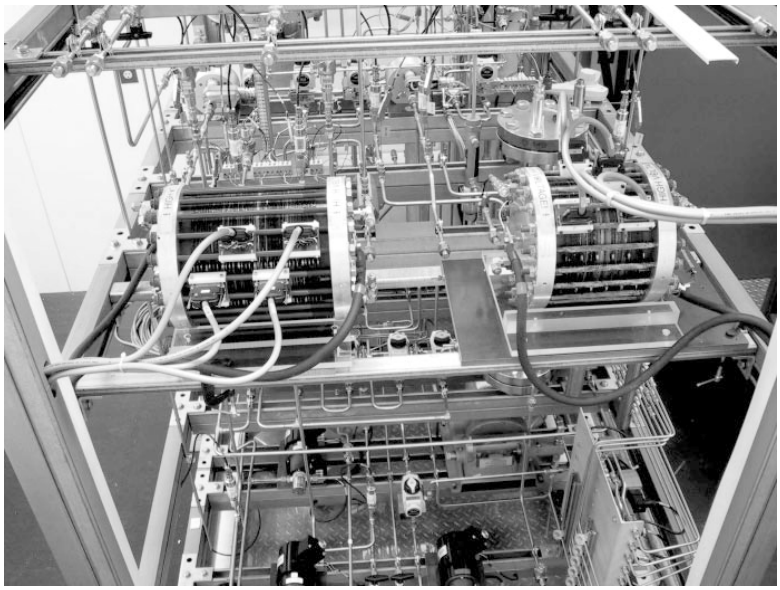

RFC-integrated equipment assembly at Glenn.

The NASA Glenn Research Center has completed construction of its first closed-cycle hydrogen-oxygen regenerative fuel cell (RFC). The RFC is an electrochemical system that collects and stores solar energy during the day then releases that energy at night, thus making the Sun's energy available all 24 hours. It consists of a dedicated hydrogen-oxygen fuel cell stack and an electrolyzer stack, the interconnecting plumbing and valves, cooling pumps, water transfer pumps, gas recirculation pumps, phase separators, storage tanks for oxygen (O_2) and hydrogen (H_2), heat exchangers, isolation valves, pressure regulators, nitrogen purge provisions, instrumentation, and other components. It includes all the equipment required to (1) absorb electrical power from an outside source and store it as pressurized hydrogen and oxygen and (2) make electrical power from the stored gases, saving the product water for reuse during the next cycle.

The Glenn RFC is a "brassboard" test rig built from off-the-shelf hardware components. It will be used to

(1) Test fuel cells and fuel cell components under repeated closed-cycle operation (nothing escapes; everything is used over and over again).
(2) Simulate diurnal charge-discharge cycles.
(3) Observe long-term system performance and identify degradation and loss mechanisms.
(4) Develop safe and convenient operation and control strategies leading to the successful development of mission-capable, flight-weight, closed-cycle aerospace RFCs for spacecraft and high-altitude aircraft.

Construction was sponsored by the Environmental Research Aircraft and Sensor Technology (ERAST) project of the Flight Research Base Program. The ERAST charter included the development and demonstration of new technologies for unmanned aircraft that are suitable for Earth science, including RFC-equipped solar-electric aircraft with potentially unlimited endurance. Although ERAST was an aeronautics project, RFC energy storage is applicable to a wide variety of space and planetary surface missions in addition to high-altitude solar-electric flight; hence, there is widespread interest throughout NASA to bring this technology to a flight demonstration. Potentially the highest storage capacity and lowest weight of any nonnuclear device, a flight-weight RFC aboard a solar-electric aircraft that is flown continuously through several successive day-night cycles will provide the most convincing demonstration that this technology's widespread potential has been realized. Leading up to the flight demonstration are several laboratory and full-scale demonstrations of key components and subsystems, including the coordinated operation of a hydrogen-oxygen fuel cell and electrolyzer as an energy storage system in a sealed, closed-loop environment (the venue provided by this brassboard RFC).

The Glenn RFC was built up over calendar years 2002 to 2003 and was operated as an end-to-end energy storage system for the first time in September 2003. Additional characterization tests, and the next generation of fuel cell and electrolyzer stacks, will take place during 2004 and 2005. The photograph shows the integrated equipment assembly (IEA) at Glenn, with fuel cell and electrolyzer stacks shown in the foreground.

Find out more about NASA Glenn:
http://www.grc.nasa.gov

Glenn contact:
David J. Bents, 216–433–6135,
David.J.Bents@nasa.gov

Author: David J. Bents

Headquarters program office: OAT

Programs/Projects: VSP, ERAST, LEAP, AFCPS, Regenerative Fuel Cell

Power-Conversion Concept Designed for the Jupiter Icy Moons Orbiter

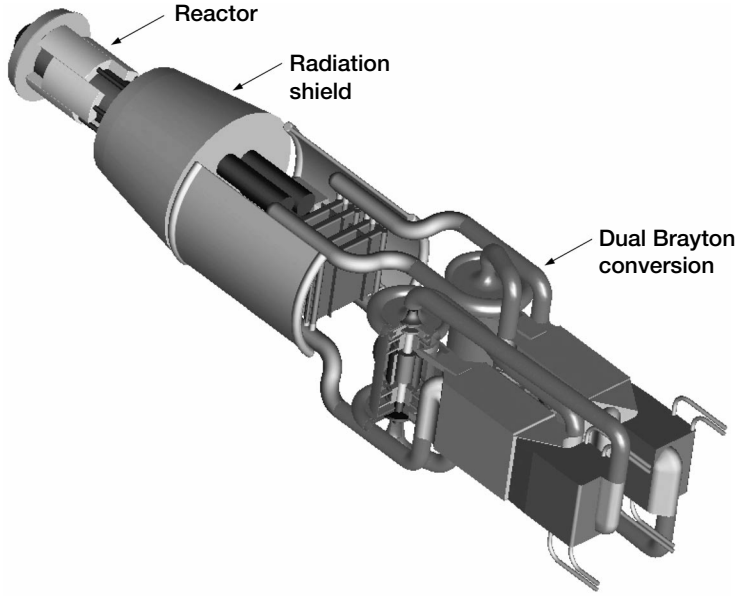

Dual 100-kWe Brayton conversion system with liquid-metal-cooled reactor.

The Jupiter Icy Moons Orbiter (JIMO) is a bold new mission being developed by NASA's Office of Space Science under Project Prometheus. JIMO is examining the potential of nuclear electric propulsion (NEP) technology to efficiently deliver scientific payloads to three of Jupiter's moons: Callisto, Ganymede, and Europa. A critical element of the NEP spacecraft is the space reactor power system (SRPS), consisting of the nuclear reactor, power conversion, heat rejection, and power management and distribution (PMAD).

The NASA Glenn Research Center participated in a joint NASA/Department of Energy study examining SRPS design options for missions such as JIMO. Glenn developed a potential SRPS architecture based on closed-Brayton-cycle power-conversion technology. For the study, researchers assumed a power level of 100 kWe for the NEP spacecraft and a liquid-metal-cooled reactor concept, although both heat-pipe and gas-cooled reactors are possible alternatives. The reactor subsystem includes a conical radiation shield to protect the spacecraft from reactor-induced gamma and neutron radiation. The power-conversion subsystem consists of two independent 100-kWe closed-Brayton-cycle converters (see the illustration) that provide 100-percent power-generation redundancy. The converter design is based on state-of-the-art superalloy hot-end construction that permits turbine inlet temperatures of 1150 K and cycle efficiencies in excess of 20 percent. The only moving part is a single-shaft, radial turbocompressor that is supported by gas foil bearings.

High-voltage, three-phase alternating current is delivered by the rotary alternator to the PMAD subsystem, which includes two completely redundant modules, each capable of delivering 100 kWe to the spacecraft. Each PMAD module includes a 400-Vac bus for the high-power electric thruster loads and a 120-Vdc bus for the low-power spacecraft and science loads. Within the PMAD, a parasitic load radiator regulates the Brayton alternator speed by maintaining a constant load on the alternator regardless of spacecraft power demands. The waste-heat-rejection subsystem includes a pumped liquid-metal heat-transport loop and water heat-pipe radiator panels. The heat-transport loop interfaces with the Brayton gas coolers, allowing either or both Brayton units to utilize the full radiator surface. The radiator consists of two planar wings, each having a series of staircased, deployable rectangular panels that are contained within the radiation shield half-angle and that provide two-sided heat rejection.

Many tradeoff studies were performed in arriving at this candidate power system concept. System-level studies examined design and off-design operating modes, determined startup requirements, evaluated subsystem redundancy options, and quantified the mass and radiator area of space reactor power systems from 20 to 200 kWe. For the Brayton converter subsystem, studies investigated converter packaging options and assessed the torque effects induced on spacecraft dynamics by rotating machinery. For the heat-rejection subsystem, design tradeoff studies were conducted on heat-transport approaches, material and fluid options, and deployed radiator geometries. For the PMAD subsystem, the overall electrical architecture was defined and tradeoff studies examined distribution approaches, voltage levels, and cabling options.

Find out more about this research:
http://www.grc.nasa.gov/WWW/tmsb/

Glenn contact:
Lee S. Mason, 216–977–7106,
Lee.S.Mason@nasa.gov

Author: Lee S. Mason

Headquarters program office: OSS

Programs/Projects: Prometheus, JIMO

Stirling Microregenerators Fabricated and Tested

A mesoscale Stirling refrigerator patented by the NASA Glenn Research Center is currently under development. This refrigerator has a predicted efficiency of 30 percent of Carnot and potential uses in electronics, sensors, optical and radiofrequency systems, microarrays, and microsystems. The mesoscale Stirling refrigerator is most suited to volume-limited applications that require cooling below the ambient or sink temperature. Primary components of the planar device include two diaphragm actuators that replace the pistons found in traditional-scale Stirling machines and a microregenerator that stores and releases thermal energy to the working gas during the Stirling cycle.

Diaphragms are used to eliminate frictional losses and bypass leakage concerns associated with pistons, while permitting reversal of the hot and cold sides of the device during operation to allow precise temperature control. Three candidate microregenerators were fabricated under NASA grants for initial evaluation: two constructed of porous ceramic, which were fabricated by Johns Hopkins Applied Physics Laboratory, and one made of multiple layers of nickel and photoresist, which was fabricated by Polar Thermal Technologies.

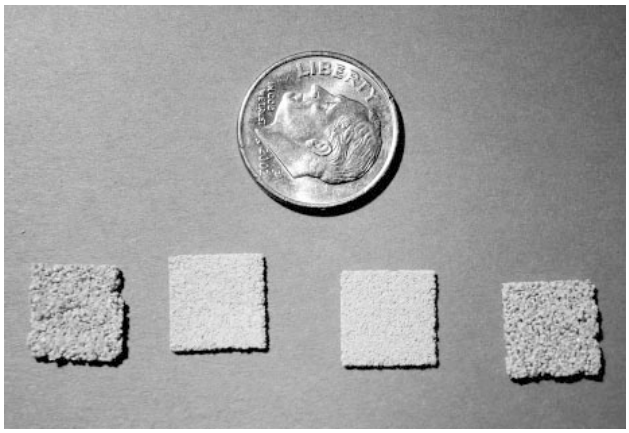

Porous ceramic microregenerators.

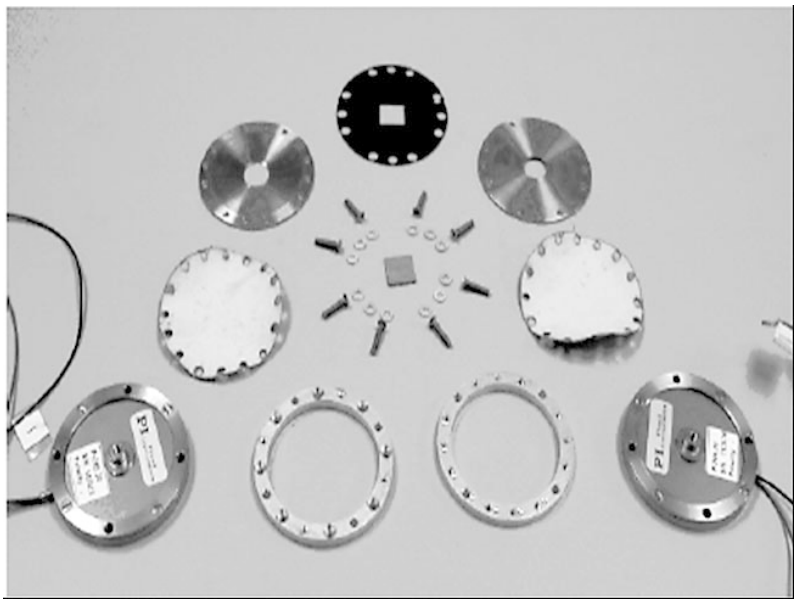

Apparatus parts for testing the microregenerators.

The candidate regenerators are being tested by Johns Hopkins Applied Physics in a custom piezoelectric-actuated test apparatus designed to produce the Stirling refrigeration cycle. In parallel with the regenerator testing, Johns Hopkins is using deep reactive ion etching to fabricate electrostatically driven, comb-drive diaphragm actuators. These actuators will drive the Stirling cycle in the prototype device.

The top photograph shows the porous ceramic microregenerators. Two microregenerators were fabricated with coarse pores and two with fine pores. The bottom photograph shows the test apparatus parts for evaluating the microregenerators, including the layered nickel-and-photoresist regenerator fabricated using LIGA[1] techniques.

Bibliography

Wilt, David; Hepp, Aloysius; and Moran, Matt: Integrated Micro-Power System (IMPS) Development at NASA Glenn Research Center. Proceedings of the International Micropower and Microdevices Symposium, vol. 2002–25, Electrochemical Society, Inc., Pennington, NJ, 2003, pp. 194–202.

Moran, Matthew E.: Micro-Scale Avionics Thermal Management. NASA/TM—2001-211095, 2001. http://gltrs.grc.nasa.gov/cgi-bin/GLTRS/browse.pl?2001/TM-2001-211095.html

Moran, Matthew E.: Micro-Scalable Thermal Control Device. U.S. Patent 6,385,973 B1, May 2002.

Moran, Matthew E.: Multidisciplinary Analysis of a Microsystem Device for Thermal Control. NASA/CP—2002-211486, Proceedings of the 11th Thermal and Fluids Analysis Workshop, 2002, pp. 173–186. http://gltrs.grc.nasa.gov/cgi-bin/GLTRS/browse.pl?2002/CP-2002-211486.html

[1] LIGA is a German acronym meaning lithography, electroplating, and molding.

Glenn contact:
Matthew E. Moran, 216–433–8324, Matthew.E.Moran@nasa.gov

Author: Matthew E. Moran

Headquarters program office: OAT

Programs/Projects: Enabling Concepts & Technologies, Energetics

Special recognition:
Best paper in session, 34th International Symposium on Microelectronics (IMAPS)

Development of Electronic Load Controllers for Free-Piston Stirling Convertors Aided by Stirling Simulation Model

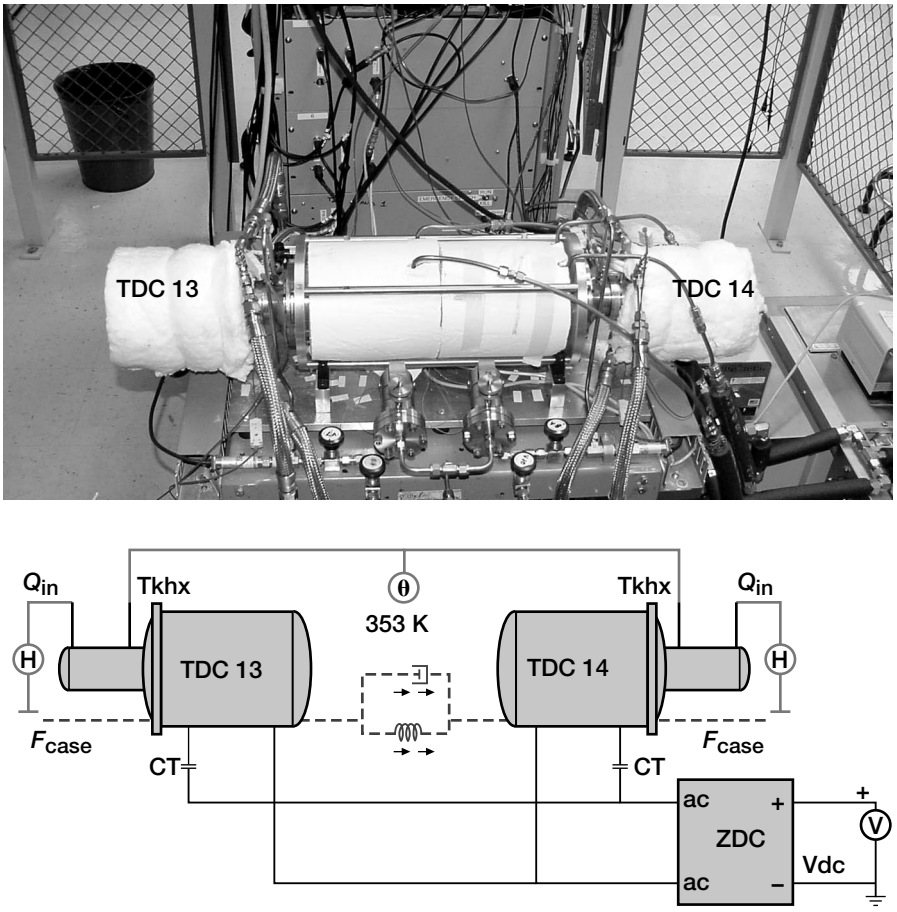

Technology Demonstration Convertors (TDC) 13 and 14 on the test stand (top) and in the simulation model (bottom). Heat flux applied to these Stirling convertors is connected to the Q_{in} nodes. The rejection temperature is connected to the nodes labeled Tkhx. The alternating current (ac) electrical power output of the TDCs is connected to the Zener diode controller (ZDC) through tuning capacitors labeled CT. The stainless steel rods connecting the two convertors in the photograph are modeled by the dashed line in the simulation diagram, and F_{case} is a node through which the net force on the convertor case can be accessed.

The free-piston Stirling convertor end-to-end modeling effort at the NASA Glenn Research Center has produced a software-based test bed in which free-piston Stirling convertors can be simulated and evaluated. The simulation model includes all the components of the convertor: the Stirling cycle engine, heat source, linear alternator, controller, and load. So far, it has been used in evaluating the performance of electronic controller designs. Three different controller design concepts were simulated using the model:

(1) Controllers with parasitic direct current loading.
(2) Controllers with parasitic alternating current loading.
(3) Controllers that maintain a reference current.

The free-piston Stirling convertor is an electromechanical device that operates at resonance. It is the function of the electronic load controller to ensure that the electrical load seen by the machine is always great enough to keep the amplitude of the piston and alternator oscillation at the rated value. This is done by regulating the load on the output bus. The controller monitors the instantaneous voltage, regulating it by switching loads called parasitic loads onto the bus whenever the bus voltage is too high and remov-

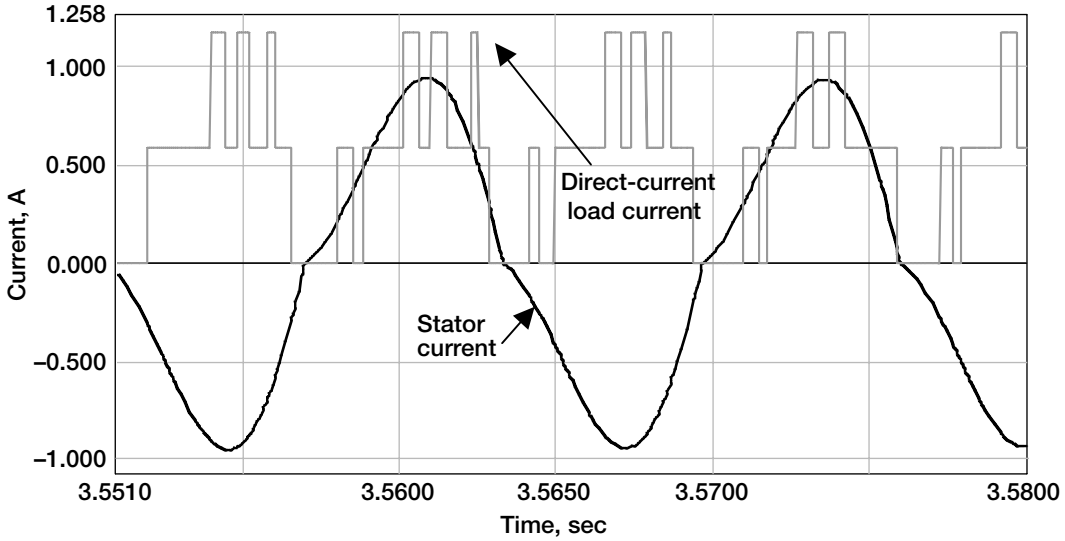

Typical output waveform of the simulation model. This shows the ac flowing through the stator windings of TDC 14 and the direct current (dc) dissipated in the ZDC.

ing them whenever the voltage is too low. In the first type of controller, the monitoring and switching are done on the direct-current (dc) bus. In the second type, the alternating-current bus is used. The model allows designers to test a controller concept before investing time in hardware. The simulation code used to develop the model also offers detailed models of digital and analog electronic components so that the resulting designs are realistic enough to translate directly into hardware circuits.

Sest, Inc., contact:
Timothy F. Regan, 216–433–2086, Timothy.F.Regan@grc.nasa.gov

Author: Timothy F. Regan

Headquarters program office: OSS

Programs/Projects: Prometheus, SRG

Find out more about this research:
http://www.grc.nasa.gov/WWW/tmsb/stirling.html

Stirling Convertor for the Stirling Radioisotope Generator Tested as a Prelude to Transition to Flight

The Stirling Radioisotope Generator (SRG) is currently being developed by Lockheed Martin Astronautics (Valley Forge, PA) under contract to the Department of Energy (Germantown, MD). In support of this project, the NASA Glenn Research Center has established a near-term technology effort to provide some of the critical data to ensure a successful transition to flight for what will be the first dynamic power system to be used in space. The generator will be a high-efficiency electric power source for potential use on NASA space science missions. The generator will be able to operate in the vacuum of deep space or in an atmosphere such as on the surface of Mars. High system efficiency is obtained through the use of free-piston Stirling power-conversion technology. The power output of the generator will be greater than 100 W at the beginning of life, with the slow decline in power being largely due to decay of the plutonium heat source. Previously, Glenn's supporting technology efforts focused only on the most critical technical issues. Now, however, they have been expanded to cover a more comprehensive range of technical issues. The tasks include Stirling convertor and controller testing, materials evaluations, heater head life assessment, magnet aging characterization, linear alternator analysis, structural dynamics analysis, electromagnetic interference and compatibility, organics evaluation, mechanical design evaluation, and reliability analysis.

Many of the tests conducted at Glenn use the 55-We Technology Demonstration Convertor (TDC) developed by the Stirling Technology Company (Kennewick, WA). There have been

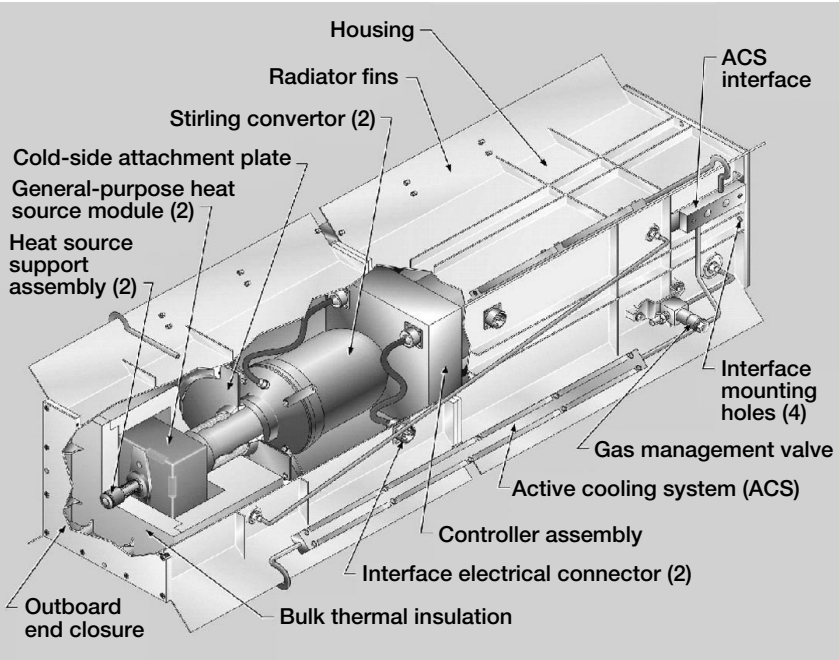

Conceptual design of the SRG by Lockheed Martin.

multiple controller tests that support the LMA flight controller design effort. Preparation is continuing for a system-level demonstration of TDC's operating in a thermal/vacuum environment. Recently, a pair of flight prototype TDC's were placed on an extended test with unattended, continuous operation. Heater head life assessment efforts continue, with the material data being refined, heater head structural testing beginning, and the analysis of life including more details of the integrated system. Long-term magnet aging tests are continuing to characterize any possible aging in the permanent magnets used in the linear alternator, including changes in magnetic strength or demagnetization resistance. The epoxy bond between the magnets and the stator lamination stock in the linear alternator is being evaluated in terms of lifetime and adhesion strength.

In a parallel effort, higher performance magnets are also being evaluated. A reliability effort is being initiated that will help to guide the development activities with a focus on the key components and subsystems. There is also an advanced technology effort that is complementary to the near-term technology effort.

Bibliography

Thieme, Lanny G.; and Schreiber, Jeffrey G.: NASA GRC Stirling Technology Development Overview. NASA/TM—2003-212454, 2003. http://gltrs.grc.nasa.gov/cgi-bin/GLTRS/browse.pl?2003/TM-2003-212454.html

Schreiber, J.G.; and Thieme, L.T.: Overview of NASA GRC Stirling Technology Development. Proceedings of the 1st International Energy Conversion Engineering Conference, Portsmouth, VA, Aug. 17–21, 2003.

Find out more about this research:
http://www.grc.nasa.gov/WWW/tmsb/stirling.html

Glenn contacts:
Jeffrey G. Schreiber, 216–433–6144, Jeffrey.G.Schreiber@nasa.gov; and Lanny G. Thieme, 216–433–6119, Lanny.G.Thieme@nasa.gov

Authors: Jeffrey G. Schreiber and Lanny G. Thieme

Headquarters program office: OSS

Programs/Projects: Prometheus, SRG

NASA Multidimensional Stirling Convertor Code Developed

A high-efficiency Stirling Radioisotope Generator (SRG) for use on potential NASA Space Science missions is being developed by the Department of Energy, Lockheed Martin, Stirling Technology Company, and the NASA Glenn Research Center. These missions may include providing spacecraft onboard electric power for deep space missions or power for unmanned Mars rovers. Glenn is also developing advanced technology for Stirling convertors, aimed at substantially improving the specific power and efficiency of the convertor and the overall power system. Performance and mass improvement goals have been established for second- and third-generation Stirling radioisotope power systems. Multiple efforts are underway to achieve these goals, both in house at Glenn and under various grants and contracts. These efforts include the development of a multidimensional Stirling computational fluid dynamics code, high-temperature materials, advanced controllers, an end-to-end system dynamics model, low-vibration techniques, advanced regenerators, and a lightweight convertor.

Under a NASA grant, Cleveland State University (CSU) and its subcontractors, the University of Minnesota (UMN) and Gedeon Associates, have developed a two-dimensional computer simulation of a CSUmod Stirling convertor. The CFD–ACE commercial software developed by CFD Research Corp. of Huntsville, Alabama, is being used. The CSUmod is a scaled version of the Stirling Technology Demonstrator Convertor (TDC), which was designed and fabricated by the Stirling Technology Company and is being tested by NASA. The schematic illustrates the structure of this model. Modeled are the fluid-flow and heat-transfer phenomena that occur in the expansion space, the heater, the regenerator, the cooler, the compression space, the surrounding walls, and the moving piston and displacer. In addition, the overall heat transfer, the indicated power, and the efficiency can be calculated. The CSUmod model is being converted to a two-dimensional model of the TDC at NASA Glenn.

Validation of the multidimensional Stirling code is an important part of the grant effort. UMN has been generating data in an oscillating-flow test facility using two different test sections: a 90° turn and a cooler/regenerator/heater test section. CSU has created computational fluid dynamics models of both these test sections and has been making comparisons with the data, then improving their models to improve the agreement with the test data. CSU has also been using data available in the literature for code validation. UMN is now preparing to begin fabrication of a new 180° turn test section that will be more representative of certain portions of the Stirling engine geometry.

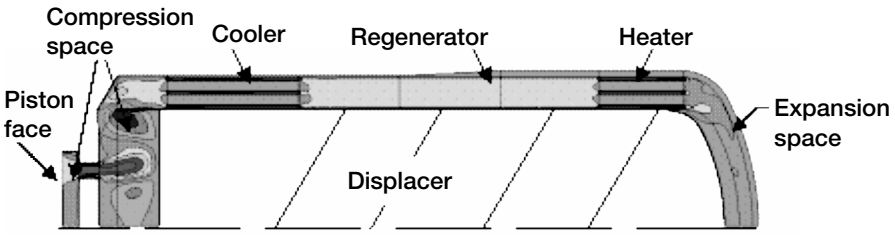

Schematic showing velocity contours generated by a two-dimensional axisymmetric CFD–ACE model of a Stirling convertor working space.

Simulations to almost periodic steady state with the two-dimensional CSUmod model indicate that, to reach periodic steady state on a single 2-GHz desktop computer, 75 to 100 complete simulation cycles would be required and between 1 and 2 months of computer time. Therefore, Glenn has purchased the first 8 computers, of a 64-computer cluster, to be run in parallel to accelerate the simulation. On the basis of CFD Research Corp.'s experience with running the parallelized version of CFD–ACE on their clusters, we estimate that the complete 64-computer cluster will reduce simulation computing time by a factor of about 40.

Plans are to continue development of these multidimensional Stirling codes and to use them to study the fluid-flow and heat-transfer phenomena that occur inside Stirling convertors. This is expected to lead to improved thermodynamic loss understanding, one-dimensional design and performance codes, and engine performance.

Find out more about this research:
http://www.grc.nasa.gov/WWW/tmsb/stirling.html

Glenn contacts:
Dr. Roy C. Tew, 216–433–8471, Roy.C.Tew@nasa.gov; and
Lanny G. Thieme, 216–433–6119, Lanny.G.Thieme@nasa.gov

Sest, Inc., contact:
Scott D. Wilson, 216–433–6681, Scott.D.Wilson@grc.nasa.gov

Authors:
Dr. Roy C. Tew and Lanny G. Thieme

Headquarters program offices:
OAT, OSS

Programs/Projects:
Energetics, Prometheus, SRG

Instrumentation and Controls

Passive Acoustic Tomography Tested for Measuring Gas Temperatures

The requirements of higher performance, better fuel economy, and lower emissions place an increasing premium on knowing the internal operating parameters of jet engines. One of the most important is the gas temperature in the post combustor section of the engine. Typically the gas temperature is measured with a thermocouple probe or by some optical technique such as Rayleigh scattering.

Probes, while providing valuable information, have several limitations. The probe signal must be corrected for radiation and conduction losses, probes provide only a point measurement, and probes must be constructed of materials whose melting points are lower than the temperature of the environment into which they are inserted.

Some of the disadvantages of probes are overcome by various optical techniques. Nothing needs to be inserted into the flow, and the temperature can be directly related to the signal by known physical laws. However, optical techniques require optical access (i.e., a window) and a light source (such as a laser), and they are very sensitive to the presence of particles in the flow.

To overcome these problems, researchers from the NASA Glenn Research Center and The University of Nevada are developing a technique that uses sound instead of light to measure gas temperature. Like optical techniques, it is nonintrusive—no probe need be exposed to the combustion environment—and the temperature is directly related to a measured quantity—the speed of sound, which is proportional to the square root of the absolute temperature.

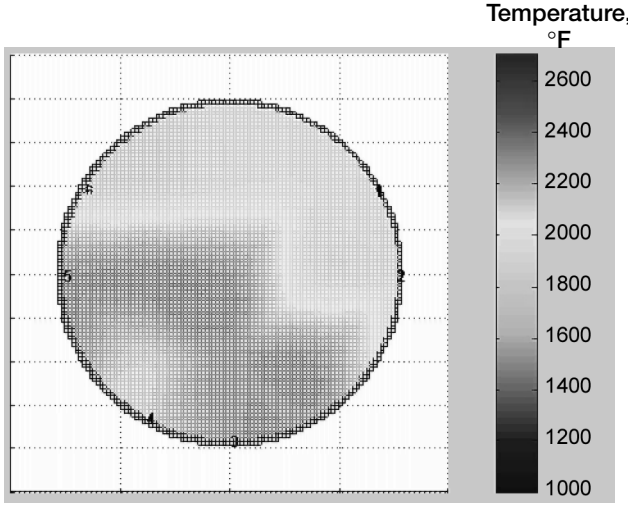

Temperature distribution inside Glenn's High Pressure Burner Rig, as measured using passive acoustic tomography. This illustration is shown in color in the online version of this article (http://www.grc.nasa.gov/WWW/RT/2003/5000/5510fralick.html).

The temperature profile inside the engine is constructed from the differences in arrival time between correlated signals from an array of microphones placed around the circumference of the engine. In much the same way as a complete picture of the inside of your body can be constructed from an array of x-ray photographs taken at different angles, the temperature profile in the engine is constructed from the angular array of microphones. It is tomography by sound waves.

Active acoustic tomography, in which a sound pulse is injected into the flow and the time delays between members of an array of microphones are used to construct the temperature field has been used successfully in the stacks of power plants. However, the flow field inside a jet engine is much too noisy for it to be possible to detect an externally injected sound pulse. Instead we are developing passive acoustic tomography, which uses the sound already present in the flow.

The figure shows the temperature distribution inside Glenn's High Pressure Burner Rig. The data were taken from an array of six microphones spaced roughly equally around the circumference of the ~8-in.-diameter duct. The data were reduced using a new frequency domain algorithm that we expect will provide the temperature distribution in real time, making passive acoustic tomography a candidate control sensor for both the combustor operating point and the burner pattern factor. These expectations are reinforced by the fact that, during the course of testing, it was discovered that the frequency content of the signal was correlated with the rig fuel air ratio. Further development of passive

acoustic tomography includes plans to reduce the burner factor data taken last year in a burner rig at Rolls-Royce U.S. and to test an engine during calendar year 2004 or 2005.

Glenn contact: Gus Fralick, 216–433–3645, Gustave.C.Fralick@nasa.gov

University of Nevada (principal investigator):
Prof. John Kleppe, 775–784–6944, kleppe@ee.unr.edu

Author: Gustave C. Fralick

Headquarters program office: OAT

Programs/Projects: UEET

Web Growth Used to Confine Screw Dislocations to Predetermined Lateral Positions in 4H-SiC Epilayers

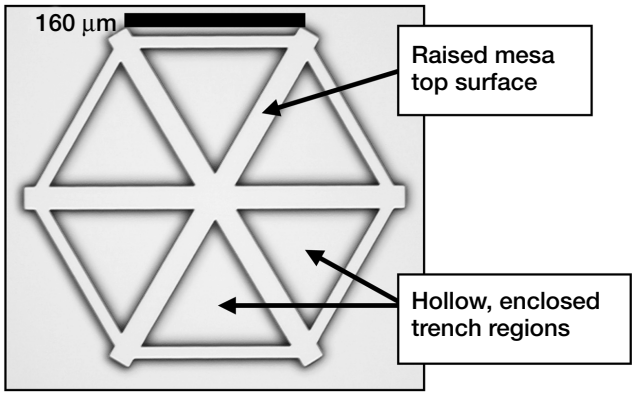

Pregrowth mesa etched into SiC wafer surface with enclosed trench regions.

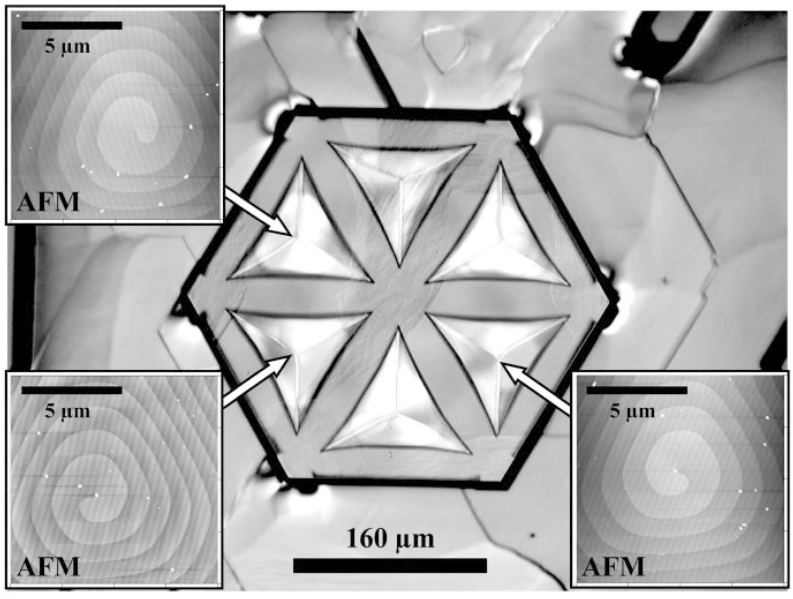

Homoepitaxial web growth carried out on the mesa of the image on the left. Insets show AFM measurements of screw dislocation spirals where cantilever films coalesce.

Silicon-carbide- (SiC-) based power devices could enable substantial aerospace electronics benefits over today's silicon-based electronics. However, present-day SiC wafers contain electrically harmful dislocations (including micropipes) that are unpredictably distributed in high densities across all commercial 4H- and 6H-SiC wafers. The NASA Glenn Research Center recently demonstrated a crystal growth process that moves SiC wafer dislocations to predetermined lateral positions in epitaxial layers so that they can be reproducibly avoided during subsequent SiC electronic device fabrication.

The process starts by reactive ion etching mesa patterns with enclosed trench regions into commercial on-axis (0001) 4H- or 6H-SiC substrates. An example of a pregrowth mesa geometry with six enclosed triangular-shaped trench regions is shown in the microscopic image in the top figure. After the etch mask is stripped, homoepitaxial growth is carried out in pure stepflow conditions that enable thin cantilevers to grow laterally from the tops of mesas whose pregrowth top surfaces are not threaded by substrate screw dislocations (ref. 1). The image in the bottom figure shows the postgrowth structure that forms after the lateral cantilevers expand to coalesce and completely roof over each of the six triangular trench regions. Atomic force

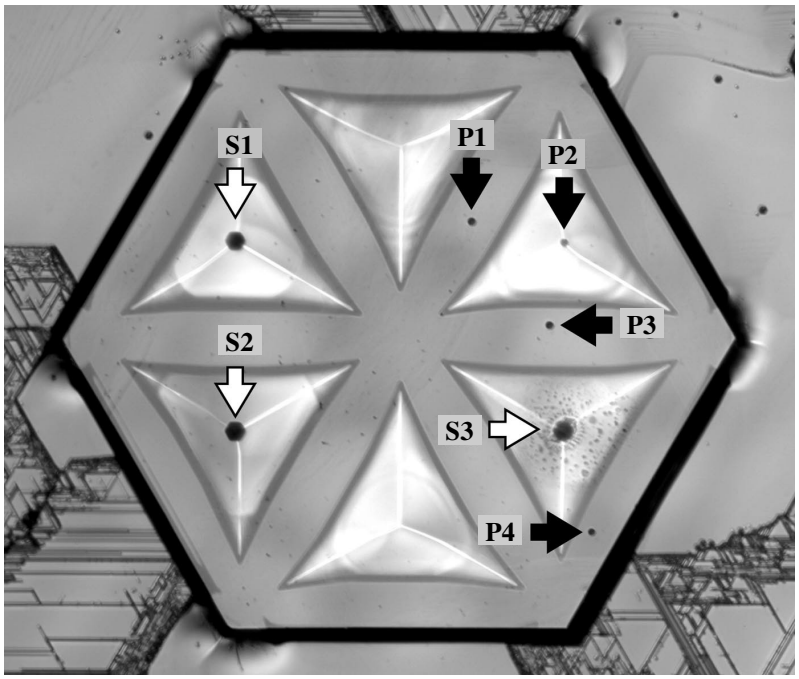

Etch pits formed on the structure in the preceding image on the right following KOH etching reveal that all dislocations are confined to the pregrowth mesa region and to points of final cantilever coalescence.

microscope (AFM) measurements of the roof revealed that three elementary screw dislocation growth spirals, each shown in the AFM insets of the bottom image on the previous page, formed in the film roof at three respective points of cantilever film coalescence. The image above shows the structure following an etch in molten potassium hydroxide (KOH) that produced surface etch pits at the dislocation defects. The larger KOH etch pits—S1, S2, and S3—shown in this image correspond to screw dislocations relocated to the final points of cantilever coalescence. The smaller KOH etch pits are consistent with epilayer threading edge dislocations from the pregrowth substrate mesa (P1, P3, and P4) and a final cantilever coalescence point (P2). No defects (i.e., no etch pits) are observed in other cantilevered portions of the film surface.

On the basis of the principle of dislocation Burgers vector conservation, we hypothesize that all vertically propagating substrate dislocations in an enclosed trench region become combined into a single dislocation in the webbed film roof at the point of final roof coalescence. The point of final roof coalescence, and therefore the lateral location of a webbed roof dislocation, can be designed into the pregrowth mesa pattern. Screw dislocations with predetermined lateral positions can then be used to provide the new growth steps necessary for growing a 4H/6H-SiC epilayer with a lower dislocation density than the substrate. Devices fabricated on top of such films can be positioned to avoid the preplaced dislocations.

Find out more about this research:

A formal technical paper describing this work in more detail:
http://www.grc.nasa.gov/WWW/SiC/publications/MRSPGN2002.pdf

SiC electronics research:
http://www.grc.nasa.gov/WWW/SiC/SiC.html

Reference

1. Neudeck, Philip G.: Improved Silicon Carbide Crystals Grown From Atomically Flat Surfaces. Research & Technology 2002, NASA/TM—2003-211990, 2003, p. 75. http://www.grc.nasa.gov/WWW/RT2002/5000/5510neudeck.html

Glenn contact: Dr. Philip G. Neudeck, 216–433–8902, Neudeck@nasa.gov

Ohio Aerospace Institute (OAI) contact:
Andrew J. Trunek, 216–433–6736, Andrew.J.Trunek@grc.nasa.gov

Sest, Inc., contact:
J. Anthony Powell, 216–433–3652, J.A.Powell@nasa.gov

Authors:
Dr. Philip G. Neudeck, David J. Spry, Andrew J. Trunek, J. Anthony Powell, and Dr. Glenn M. Beheim

Headquarters program office: OAT

Programs/Projects: UEET, Energetics

Thin-Film Ceramic Thermocouples Fabricated and Tested

The Sensors and Electronics Technology Branch of the NASA Glenn Research Center is developing thin-film-based sensors for surface measurement in propulsion system research. Thin-film sensors do not require special machining of the components on which they are mounted, and they are considerably thinner than wire- or foil-based sensors. One type of sensor being advanced is the thin-film thermocouple, specifically for applications in high-temperature combustion environments. Ceramics are being demonstrated as having the potential to meet the demands of thin-film thermocouples in advanced aerospace environments.

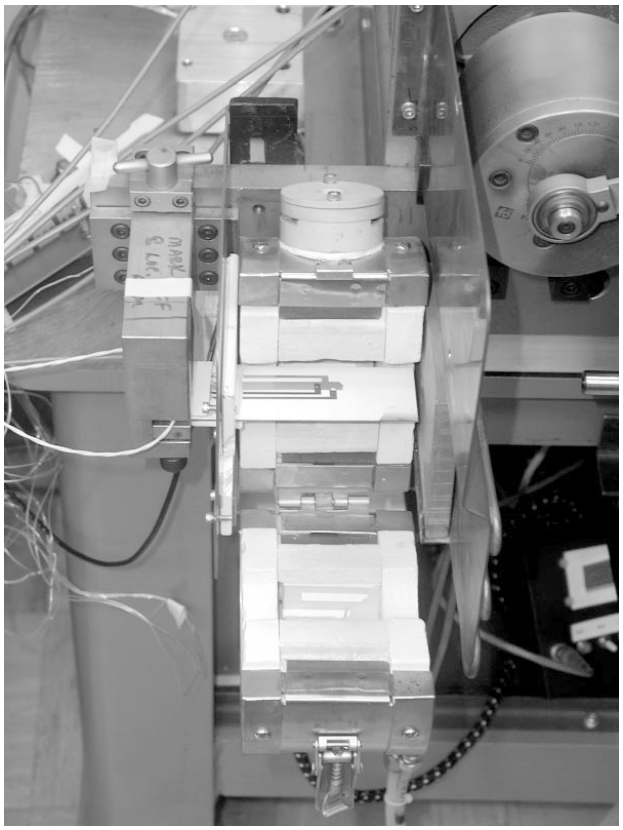

Test fixture in Glenn's Thin Film Sensors Laboratory with the CrSi-TaC test sample in place.

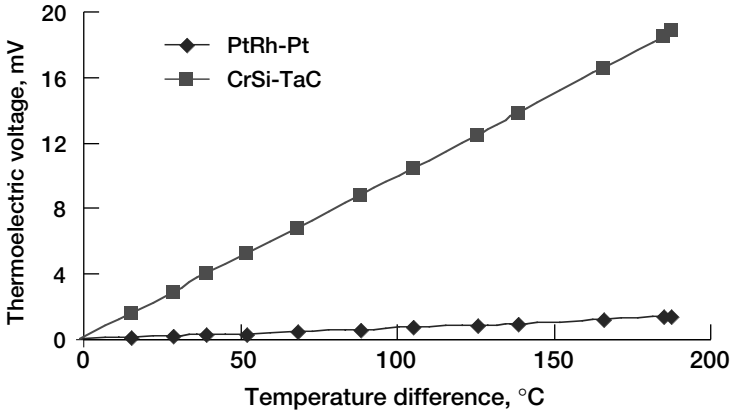

Relative thermoelectric voltage output of the CrSi-TaC thermocouple compared with the PtRh-Pt (standard type R) thermocouple on the test sample.

The maximum-use temperature of noble metal thin-film thermocouples, 1500 °C (2700 °F), may not be adequate for components used in the increasingly harsh conditions of advanced aircraft and next-generation launch vehicles. Ceramic-based thermocouples are known for their high stability and robustness at temperatures exceeding 1500 °C, but are typically in the form of bulky rods or probes. As part of ASTP, Glenn's Sensors and Electronics Technology Branch is leading an in-house effort to apply ceramics as thin-film thermocouples for extremely high-temperature applications as part of ASTP.

Since the purity of the ceramics is crucial for the stability of the thermocouples, Glenn's Ceramics Branch and Case Western Reserve University are developing high-purity ceramic sputtering targets for fabricating high-temperature sensors. Glenn's Microsystems Fabrication Laboratory, supported by the Akima Corporation, is using these targets to fabricate thermocouple samples for testing. The first of the materials used were chromium silicide (CrSi) and tantalum carbide (TaC). These refractory materials are expected to survive temperatures in excess of 1500 °C. Preliminary results indicate that the thermoelectric voltage output of a thin-film CrSi versus TaC thermocouple is 15 times that of the standard type R (platinum-rhodium versus platinum) thermocouple, producing 20 mV with a 200 °C temperature gradient. The photograph on this page shows the CrSi-TaC thermocouple in a test fixture at Glenn, and the resulting

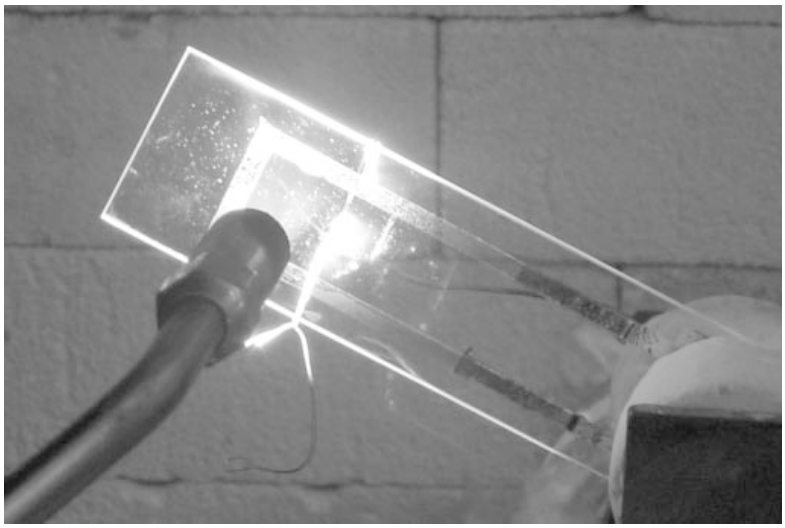

ITO ceramic thermocouple deposited onto a quartz substrate and tested in an open flame at the University of Rhode Island.

output signal is shown on the graph on the preceding page. The temperature differential across the sample, from the center of the sample inside the oven to the sample mount outside the oven, is measured using a type R thermocouple on the sample.

Glenn's Sensors and Electronics Technology Branch has enlisted the Thin Films and Interfacial Research Center of the University of Rhode Island in ceramic-based thermocouple research. The initial results of their thermocouple research have been promising. At the University of Rhode Island, two thin-film indium-tin-oxide- (ITO-) based thermocouples have been fabricated and tested to 1500 °C, and the thermoelectric voltage outputs are consistently similar to that of type R thermocouples. The photograph to the left shows the ITO thermocouple being tested.

This merging of the high-temperature capabilities of ceramics with the nonintrusiveness of thin films is ongoing. NASA has shown that a new class of ceramic thin films can be used as high-temperature thermocouples and intends to apply this technology to strain gauges as well. This research advances the effort that Glenn is leading to develop a complete sensor package to enable the use of ceramics as thin-film sensors in environments where standard metal sensors would not survive.

Glenn contacts:
John D. Wrbanek, 216–433–2077, John.D.Wrbanek@nasa.gov; and Gus Fralick, 216–433–3645, Gustave.C.Fralick@nasa.gov

Authors:
John D. Wrbanek, Gustave C. Fralick, Dr. Serene C. Farmer, Dr. Ali Sayir, Otto J. Gregory, and Charles A. Blaha

Headquarters program office: OAT

Programs/Projects: ASTP, HOTPC

Applicability of a Crack-Detection System for Use in Rotor Disk Spin Test Experiments Being Evaluated

Engine makers and aviation safety government institutions continue to have a strong interest in monitoring the health of rotating components in aircraft engines to improve safety and to lower maintenance costs. To prevent catastrophic failure (burst) of the engine, they use nondestructive evaluation (NDE) and major overhauls for periodic inspections to discover any cracks that might have formed. The lowest cost fluorescent penetrant inspection NDE technique can fail to disclose cracks that are tightly closed during rest or that are below the surface. The NDE eddy current system is more effective at detecting both crack types, but it requires careful setup and operation and only a small portion of the disk can be practically inspected. So that sensor systems can sustain normal function in a severe environment, health-monitoring systems require the sensor system to transmit a signal if a crack detected in the component is above a predetermined

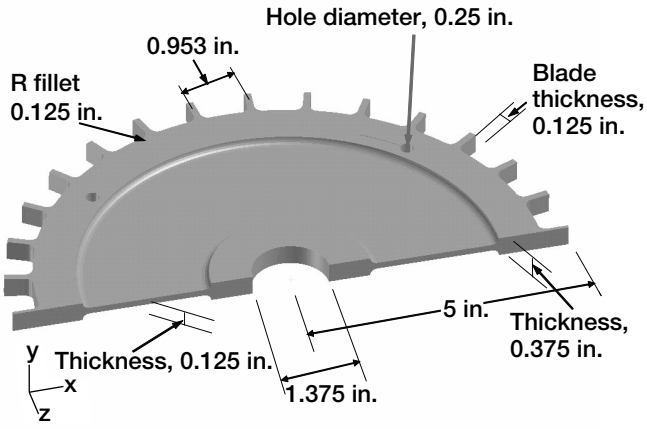

Flat disk geometry and dimensions.

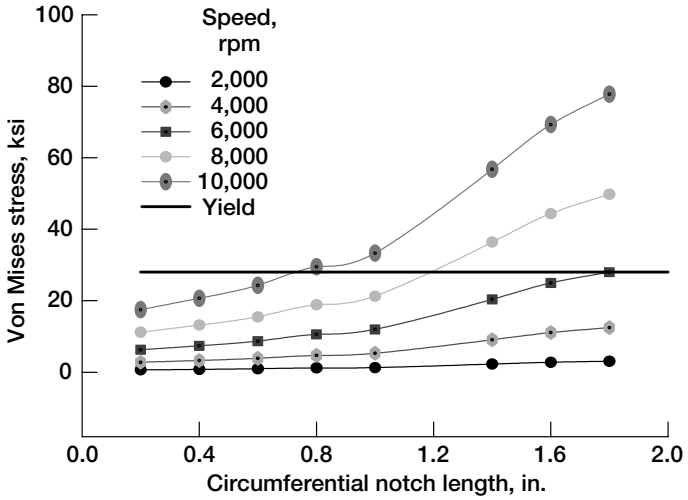

Von Mises stress as a function of crack or notch size.

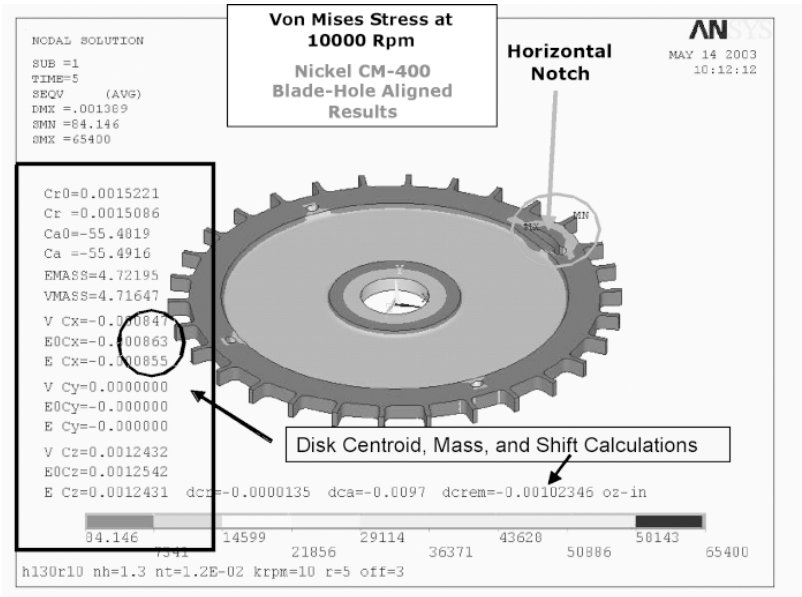

Von Mises stress contour plot at 10,000 rpm for a 1.3-in.-long notch located in the rim region of the disk. This figure is shown in color in the online version of this article (http://www.grc.nasa.gov/WWW/RT/2003/5000/5520abdulaziz2.html).

length (but below the length that would lead to failure) and lastly to act neutrally upon the overall performance of the engine system and not interfere with engine maintenance operations. Therefore, more reliable diagnostic tools and high-level techniques for detecting damage and monitoring the health of rotating components are very essential in maintaining engine safety and reliability and in assessing life.

These concerns are high priorities in the NASA Aviation Safety Program, whose intention is to develop and demonstrate technologies that will help reduce the aviation fatal accident rate by a factor of 5 by the year 2007. This ambitious program is a partnership that includes NASA, the Federal Aviation Administration, the aviation industry, and the Department of Defense (ref. 1). The program's objectives are twofold: (1) to develop and demonstrate technologies that will reduce aircraft accident rates and (2) to develop technologies that will reduce aviation injuries and fatalities when accidents do occur. As a result and in support of the latter aim, the NDE Group at the NASA Glenn Research Center is actively involved in developing combined experimental and analytical health-monitoring technologies to detect rotor damage prior to any catastrophic events (ref. 2). This work is focused on presenting finite element results of a 25.4-cm-(10-in.-) diameter flat turbinelike disk used to evaluate crack-detection techniques. The illustration on the preceding page shows the geometry. The solutions are focused on finding the changes in maximum radial deflections and changes in the center of mass as a function of the rotational speed and crack characteristics (crack size and location) to make detection feasible in the subscale flat test disk. The study is motivated by data showing that cracks as small as 1.27 mm (0.05 in.) have been detected in jet engine rotors tested in spin pits (Drumm, M.J.: Personal communication, 1998.) by monitoring the radial vibration amplitude and phase and detecting changes in the center of mass associated with a minute unbalance of the distorted strain field of a developing crack (ref. 3). The current analytical work is seeking an optimized disk design that can be tested to evaluate the functionality of the health monitoring and its applicability in the spin test facility. Data pertaining to the results obtained are shown in the figures on this page, where the maximum stress (ref. 4) due to the applied rotational speed and the notch size are shown.

References

1. General Aviation Propulsion Program. http://www.grc.nasa.gov/WWW/AST/GAP/
2. Gyekenyesi , Andrew L.; Sawicki, Jerzy T.; and Baaklini, George Y.: Application of Vibration Monitoring Techniques for Damage Detection in Rotating Disks. Paper presented at the 9th International Symposium on Transport Phenomena and Dynamics of Rotating Machinery, Honolulu, HI, 2002, pp. 1–6.

3. Sonnichsen, H.E.: Real-Time Detection of Developing Cracks in Jet Engine Rotors. IEEE Aerosp. Conf. Proc., vol. 6, 2000, pp. 173–184. http://www.testdevices.com
4. ANSYS Finite Element Program. ANSYS Release 7.1, ANSYS, Inc., Canonsburg, PA, 2003.

Cleveland State University contact:
Dr. Ali Abdul-Aziz, 216–433–6729, Ali.Abdulaziz@grc.nasa.gov

Glenn contacts: Dr. George Y. Baaklini, 216–433–6016, George.Y.Baaklini@nasa.gov; and Don Roth, 216–433–6017, Donald.J.Roth@nasa.gov

Authors: Dr. Ali Abdul-Aziz, Dr. George Y. Baaklini, and Don J. Roth

Headquarters program office: OAT

Programs/Projects: AvSP

Reannealed Fiber Bragg Gratings Demonstrated High Repeatability in Temperature Measurements

Fiber Bragg gratings (FBGs) are formed by periodic variations of the refractive index of an optical fiber. These periodic variations allow an FBG to act as an embedded optical filter, passing the majority of light propagating through a fiber while reflecting back a narrow band of the incident light. The peak reflected wavelength of the FBG is known as the Bragg wavelength. Since the period and width of the refractive index variation in the fiber determines the wavelengths that are transmitted and reflected by the grating, any force acting on the fiber that alters the physical structure of the grating will change the wavelengths that are transmitted and reflected by it. Both thermal and mechanical forces acting on the grating will alter its physical characteristics, allowing the FBG sensor to detect both the temperature variations and the physical stresses and strains placed upon it. This ability to sense multiple physical forces makes the FBG a versatile sensor.

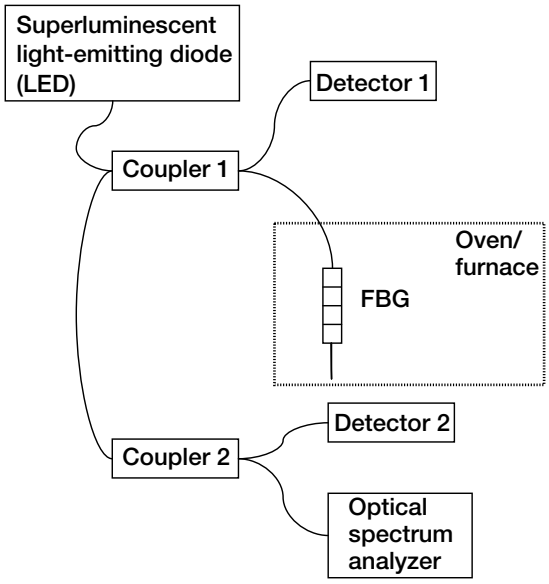

Setup used for reannealing and thermal cycling of FBGs.

To assess the feasibility of using Bragg gratings as temperature sensors for propulsion applications, researchers at the NASA Glenn Research Center evaluated the performance of Bragg gratings at elevated temperatures for up to 300 °C. For these purposes, commercially available polyimide-coated high-temperature gratings were used that were annealed by the manufacturer to 300 °C. To assure the most thermally stable gratings at the operating temperatures, we reannealed the gratings to 400 °C at a very slow rate for 12 to 24 hr until their reflected optical powers were stabilized. The reannealed gratings were then subjected to periodic thermal cycling from room temperature to 300 °C, and their peak reflected wavelengths were monitored.

This schematic diagram shows the setup used for reannealing and thermal cycling the FBGs. Signals from the photodetectors and the spectrum analyzer were fed into a computer (not shown in the diagram) equipped with LabVIEW software. The software synchronously monitored the oven/furnace temperature and the optical spectrum analyzer as well as processed the data. Experimental results presented in the graph on the next page show typical wavelength versus temperature dependence of a reannealed FBG through six thermal cycles (80 hr).

The average standard deviation of the temperature-to-wavelength relationship ranged from 1.86 to 2.92 °C over the six thermal cycles each grating was subjected to. This is an error of less than 1.0 percent of full scale throughout the entire evaluation temperature range from ambient to 300 °C.

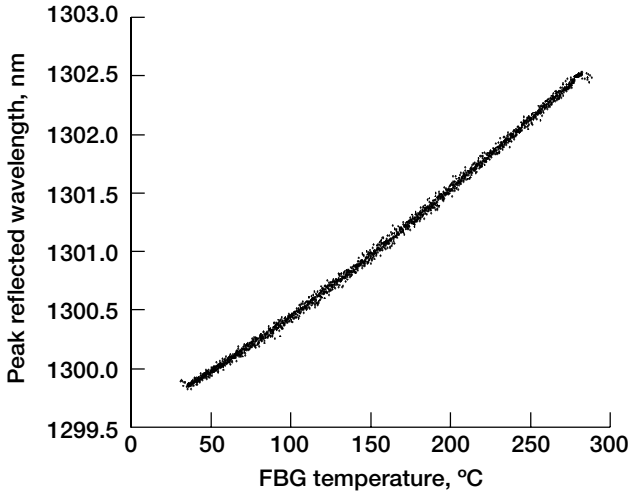

Experimentally obtained typical wavelength versus temperature dependency of a reannealed FBG through six thermal cycles from room temperature to 300 °C.

Bibliography

Adamovsky, G.; and Juergens, J.: Performance Evaluation of Fiber Bragg Gratings at Elevated Temperatures. SPIE 5272A, Proceedings of the Fiber Optic Sensor Technology and Applications II Conference, 2003.

Glenn contacts:

Dr. Grigory Adamovsky, 216–433–3736, Grigory.Adamovsky-1@nasa.gov; and Jeffrey R. Juergens, 216–433–5460, Jeffrey.R.Juergens@nasa.gov

Authors: Dr. Grigory Adamovsky and Jeffrey R. Juergens

Headquarters program office: OAT

Programs/Projects: PR&T, RAC

Sandwich Panels Evaluated With Ultrasonic Spectroscopy

Enhanced, lightweight material systems, such as 17–4PH stainless steel sandwich panels are being developed for use as fan blades and fan containment systems for next-generation engines. The bond strength between the core and face sheets is critical in maintaining the structural integrity of the sandwich structure. To improve the inspection and production of these systems, researchers at the NASA Glenn Research Center are using nondestructive evaluation (NDE) techniques, such as ultrasonic spectroscopy, to evaluate the brazing quality between the face plates and the metallic foam core. The capabilities and limitations of a swept-frequency approach to ultrasonic spectroscopy were evaluated with respect to these sandwich structures (ref. 1). This report discusses results from three regions of a sandwich panel representing different levels of brazing quality between the outer face plates and a metallic foam core. Each region was investigated with ultrasonic spectroscopy. Then, on the basis of the NDE results, three shear specimens sectioned from the sandwich panel to contain each of these regions were mechanically tested.

The graphs below depict the ultrasonic spectroscopy responses from

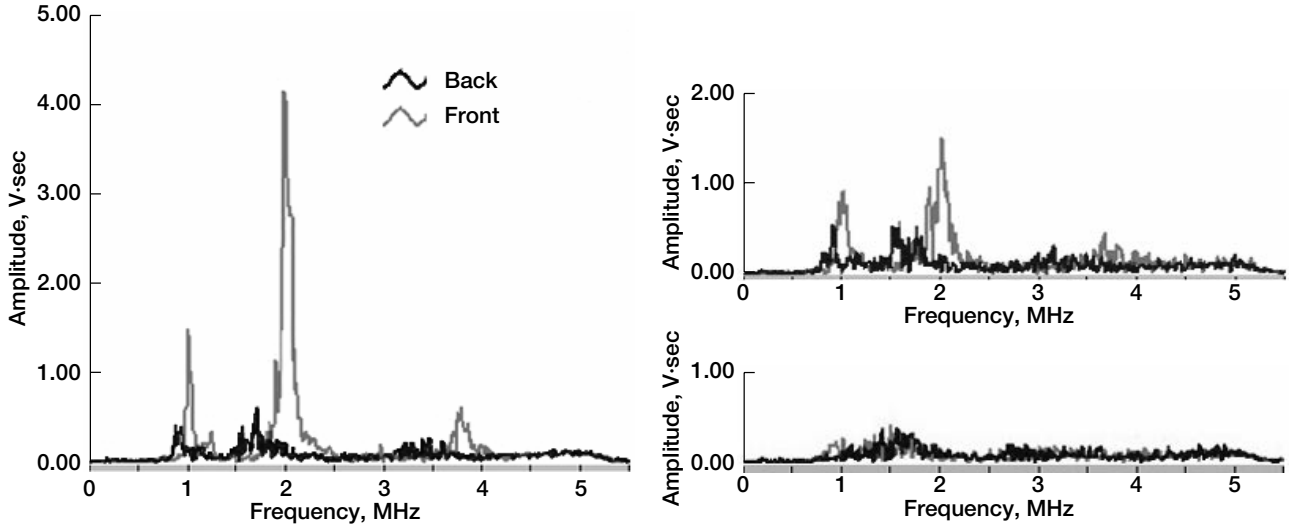

Frequency spectra plots from the front and back of regions A, B, and D. Left: Region A with poor brazing on the front face plate and presumed good brazing on the back face plate. Top right: Region B with intermediate brazing on the front face plate and presumed good brazing between the back face plate and the foam core. Bottom right: Region D with good brazing conditions between both face plates and the foam core.

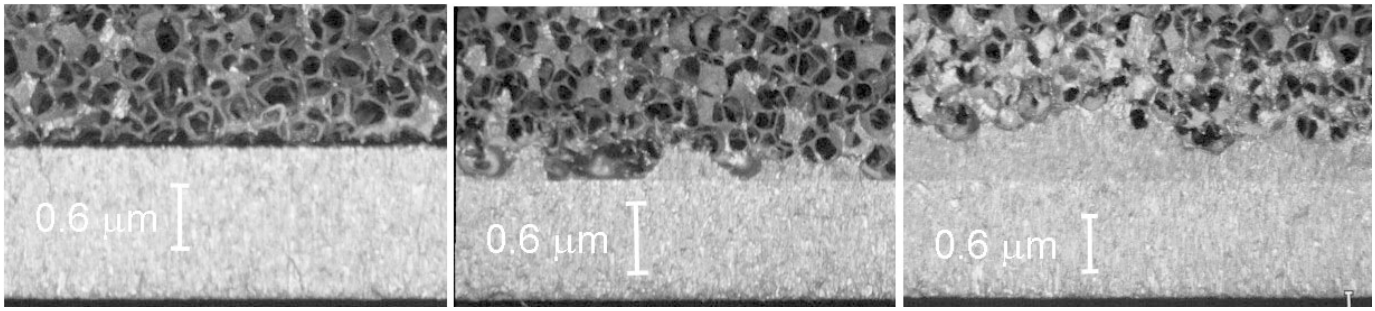

Optical photographs of three brazing conditions investigated in this study. Left: Front of shear specimen A with poor brazing. Center: Front of specimen B with intermediate brazing. Right: Front of specimen D with good brazing between the outer face plate and the foam core.

the front and back of each of the three regions. After the sectioning, optical photographs illustrating the braze conditions investigated (see the figure on this page) were taken from the gauge region of each of the shear specimens. When braze did not wet the surface of the plate (left photograph), a resonance corresponding to the thickness of the face sheet was produced, as in the ultrasonic spectroscopy response from the front of shear specimen A (left graph on previous page). Intermediate brazing conditions (center photograph) produced a resonance with much lower amplitude, as shown in the top right graph (previous page). With the presence of good braze between the face sheet and the metallic foam (right photograph), the ultrasonic spectroscopy signal was attenuated so that no resonance was produced, as in the responses depicted in the bottom right graph (previous page).

Ultrasonic spectroscopy successfully characterized each of the braze conditions shown in the optical photographs. However, the results of the shear tests indicated that possible cracks in the foam near the braze interface or small amounts of braze wetting the surface of the face sheet, but not the foam core, represented more critical manufacturing defects than having very little or no braze wet the surface of the plate. This conclusion came from the actual failures of shear specimens A and B, which occurred near the interfaces with good brazing conditions instead of at the interfaces with poor or intermediate brazing conditions. Shear specimen D failed through the foam thickness as expected.

Ultrasonic spectroscopy demonstrated capabilities in examining braze quality between stainless steel foam cores and face sheets at the panel level. These results can be extended to the evaluation of manufactured components made from these sandwich structures because ultrasonic spectroscopy signals corresponding to various levels of brazing quality were identified. However, the technique demonstrated limitations with respect to evaluating the condition of the metallic foam beyond the braze interface. To further improve the manufacturing and inspection methods, we need a better understanding of the failure mechanisms occurring in these sandwich structures. Additional NDE techniques are being investigated to further understand these sandwich structures and their failure mechanisms.

Reference

1. Cosgriff, L.M., et al.: Ultrasonic Spectroscopy of Stainless Steel Sandwich Panels. To be published in the proceedings for the 35th International SAMPE Technical Conference, SAMPE, Covina, CA, 2003.

Cleveland State University contact:
Laura M. Cosgriff, 216–433–3866, Laura.M.Cosgriff@grc.nasa.gov

Author: Laura M. Cosgriff

Headquarters program office: OAT

Programs/Projects: Ultra Safe

Optical Calibration Process Developed for Neural-Network-Based Optical Nondestructive Evaluation Method

A completely optical calibration process has been developed at Glenn for calibrating a neural-network-based nondestructive evaluation (NDE) method. The NDE method itself detects very small changes in the characteristic patterns or vibration mode shapes of vibrating structures as discussed in many references (refs. 1 and 2). The mode shapes or characteristic patterns are recorded using television or electronic holography and change when a structure experiences, for example, cracking, debonds, or variations in fastener properties. An artificial neural network can be trained to be very sensitive to changes in the mode shapes, but quantifying or calibrating that sensitivity in a consistent, meaningful, and deliverable manner has been challenging. The standard calibration approach has been difficult to implement, where the response to damage of the trained neural network is compared with the responses of vibration-measurement sensors. In particular, the vibration-measurement sensors are intrusive, insufficiently sensitive, and not numerous enough. In response to these difficulties, a completely optical alternative to the standard calibration approach was proposed and tested successfully. Specifically, the vibration mode to be monitored for structural damage was intentionally contaminated with known amounts of another mode, and the response of the trained neural network was measured as a function of the peak-to-peak amplitude of the contaminating mode. The neural-network calibration technique essentially uses the vibration mode shapes of the undamaged structure as standards against which the changed mode shapes are compared. The published response of the network can be made nearly independent of the contaminating mode, if enough vibration modes are used to train the net. The sensitivity of the neural network can be adjusted for the environment in which the test is to be conducted.

The graph on the left shows the response of a neural network trained with measured vibration patterns for use on a vibration isolation table in the presence of various sources of laboratory noise. The output of the neural network is called the degradable classification index. The curve was generated by a simultaneous comparison of means, and it shows a peak-to-peak sensitivity of about 100 nm. The graph on the right uses model-generated data from a compressor blade to show that much higher sensitivities are possible when the environment can be controlled better. The peak-to-peak sensitivity here is about 20 nm. The training procedure was modified for the second graph, and the data were subjected to an intensity-dependent transformation called folding. All the measurements for this approach to calibration were optical. The peak-to-peak amplitudes of the vibration modes were measured using heterodyne interferometry, and the modes themselves were recorded using television (electronic) holography.

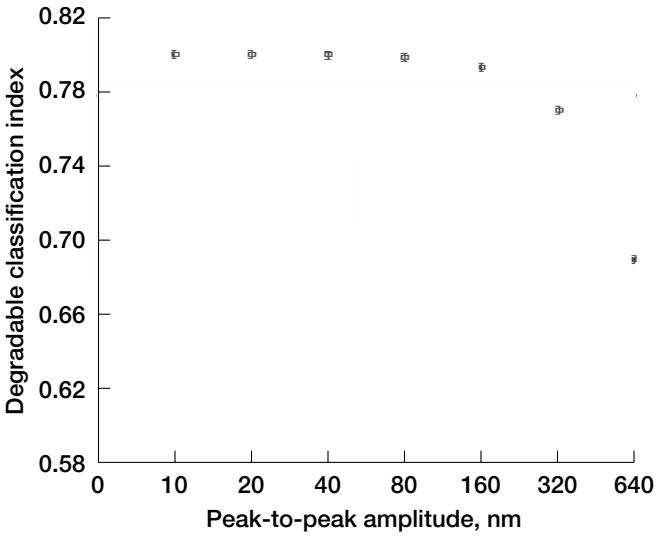

Response of a measured-data-trained neural network versus the peak-to-peak amplitude of a contamination mode.

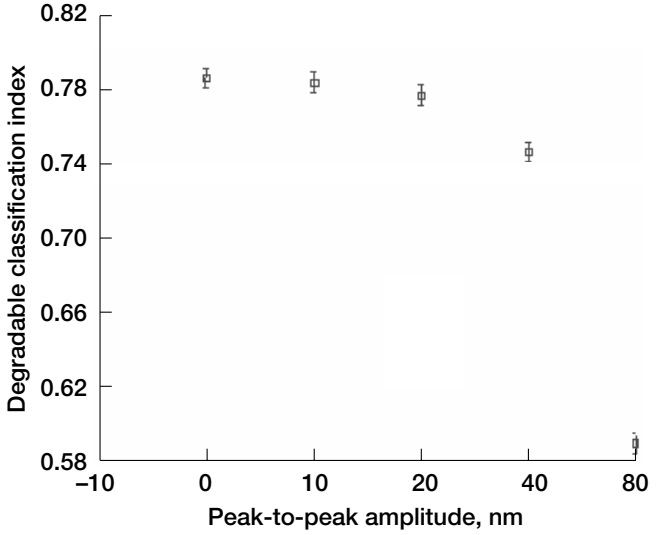

Response of a calculated-data-trained neural network versus the peak-to-peak amplitude of a contamination mode showing a potential sensitivity limit.

References
1. Decker, A.J.: Sensitivity and Calibration of Non-Destructive Evaluation Method That Uses Neural-Net Processing of Characteristic Fringe Patterns. SPIE 5191, Proceedings of the Optical Diagnostics for Fluids, Solids, and Combustion II Conference, 2003.
2. Decker, Arthur J.: Damage Detection Using Holography and Interferometry. Optical Metrology for Fluids, Combustion and Solids, ch. 14, Carolyn R. Mercer, ed., Kluwer Academic Publishers, Boston, MA, 2003.

Glenn contact: Dr. Arthur J. Decker, 216–433–3639, Arthur.J.Decker@nasa.gov

Author: Dr. Arthur J. Decker

Headquarters program office:
OSMA (Safety in Operation of Ground Test Facilities)

Programs/Projects:
PR&T, UEET, operation of any facility where the nonintrusive detection of structural changes or damage is of value

Vibration-Based Data Used to Detect Cracks in Rotating Disks

Rotor health monitoring and online damage detection are increasingly gaining the interest of aircraft engine manufacturers. This is primarily due to the fact that there is a necessity for improved safety during operation as well as a need for lower maintenance costs. Applied techniques for the damage detection and health monitoring of rotors are essential for engine safety, reliability, and life prediction. Recently, the United States set the ambitious goal of reducing the fatal accident rate for commercial aviation by 80 percent within 10 years (ref. 1). In turn, NASA, in collaboration with the Federal Aviation Administration, other Federal agencies, universities, and the airline and aircraft industries, responded by developing the Aviation Safety Program. This program provides research and technology products needed to help the aerospace industry achieve their aviation safety goal. The Nondestructive Evaluation (NDE) Group of the Optical Instrumentation Technology Branch at the NASA Glenn Research Center is currently developing propulsion-system-specific technologies to detect damage prior to catastrophe under the propulsion health management task.

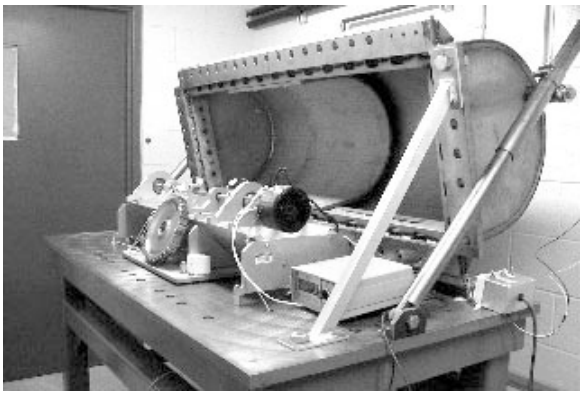

Subscale disk spin simulation system.

Currently, the NDE group is assessing the feasibility of utilizing real-time vibration data to detect cracks in turbine disks. The data are obtained from radial blade-tip clearance and shaft-clearance measurements made using capacitive or eddy-current probes. The concept is based on the fact that disk cracks distort the strain field within the component. This, in turn, causes a small deformation in the disk's geometry as well as a possible change in the system's center of mass. The geometric change and the center of mass shift can be indirectly characterized by monitoring the amplitude and phase of the first harmonic (i.e., the 1× component) of the vibration data. Spin pit experiments and full-scale engine tests have been conducted while monitoring for crack growth with this detection methodology (ref. 2). Even so, published data are extremely limited, and the basic foundation of the methodology has not been fully studied.

The NDE group is working on developing this foundation on the basis of theoretical modeling as well as experimental data by using the newly constructed subscale spin system shown in this photograph. This, in turn, involved designing an optimal subscale disk that was meant to represent a full-scale turbine disk; conducting finite element analyses of undamaged and damaged disks to define the disk's deformation and the resulting shift in center of mass; and creating a rotordynamic model of the complete disk and shaft assembly to confirm operation beyond the first critical

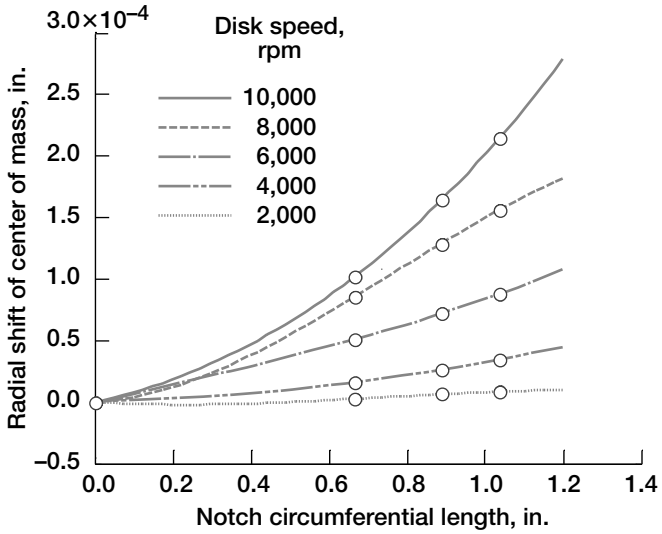

Radial shift of the center of mass as a function of notch length and disk revolutions per minute.

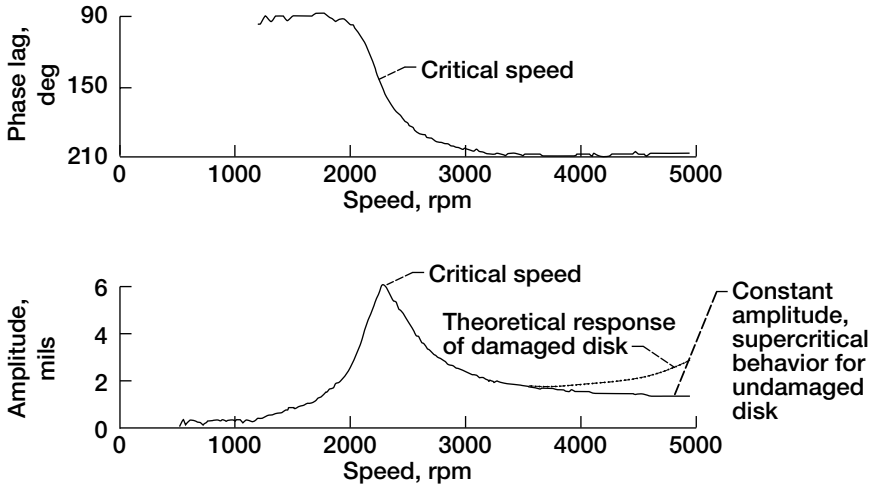

Experimental vibration response of the 1× component. Also indicated is the theoretical response of a damaged disk.

concerning the subscale experimental setup. The finite element analysis data, defining the center of mass shift due to disk damage, are shown in the top figure. As an example, the change in the center of mass for a disk spinning at 8000 rpm with a 0.963-in. notch was 1.3×10^{-4} in. The bottom figure shows the actual vibration response of an undamaged disk as well as the theoretical response of a cracked disk.

Experiments with cracked disks are continuing, and new approaches for analyzing the captured vibration data are being developed to better detect damage in a rotor. In addition, the subscale spin system is being used to test the durability and sensitivity of new NDE sensors that focus on detecting localized damage. This is designed to supplement the global response of the crack-detection methodology described here.

References

1. Shin, Jaiwon: The NASA Aviation Safety Program: Overview. NASA/TM—2000-209810, 2000. http://gltrs.grc.nasa.gov/cgi-bin/GLTRS/browse.pl?2000/TM-2000-209810.html
2. Gyekenyesi, Andrew L.; Sawicki, Jerzy T.; and Baaklini, George Y.: Vibration Based Crack Detection in a Rotating Disk: Part 1—An Analytical Study. NASA/TM—2003-212624, 2003. http://gltrs.grc.nasa.gov/cgi-bin/GLTRS/browse.pl?2003/TM-2003-212624.html

Ohio Aerospace Institute contact:
Dr. Andrew L. Gyekenyesi, 216–433–8155, Andrew.L.Gyekenyesi@grc.nasa.gov

Glenn contact:
Dr. George Y. Baaklini, 216–433–6016, George.Y.Baaklini@nasa.gov

Authors: Dr. Andrew L. Gyekenyesi, Prof. Jerzy T. Sawicki, Richard E. Martin, and Dr. George Y. Baaklini

Headquarters program office: OAT

Programs/Projects: AvSP

Automated Guided-Wave Scanning Developed to Characterize Materials and Detect Defects

The Nondestructive Evaluation (NDE) Group of the Optical Instrumentation Technology Branch at the NASA Glenn Research Center has developed a scanning system that uses guided waves to characterize materials and detect defects. The technique uses two ultrasonic transducers to interrogate the condition of a material. The sending transducer introduces an ultrasonic pulse at a point on the surface of the specimen, and the receiving transducer detects the signal after it has passed through the material. The aim of the method is to correlate certain parameters in both the time and frequency domains of the detected waveform to characteristics of the material between the two transducers.

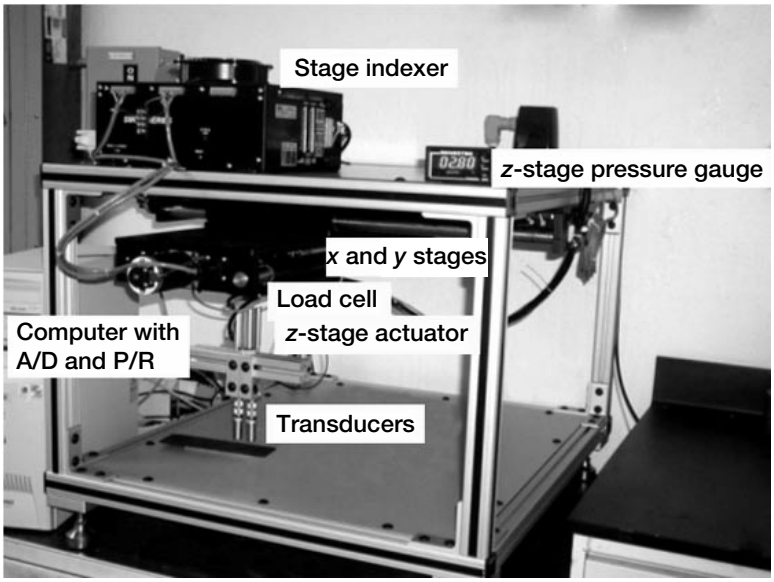

Guided wave scanner setup. A/D, analog-to-digital converter; P/R, pulser–receiver.

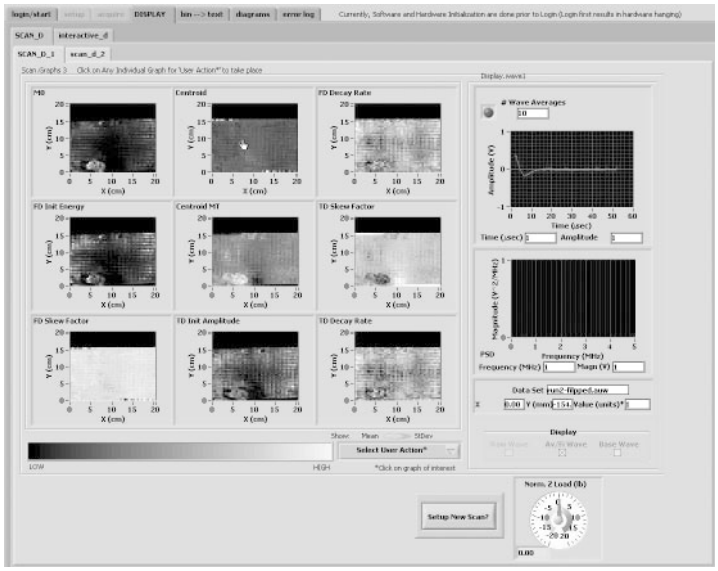

Front panel display of results for a guided wave scan of a composite plate. Each subimage represents a different guided wave parameter.

This photograph shows the scanning system. The waveform parameters of interest include the attenuation due to internal damping, waveform shape parameters, and frequency shifts due to material changes. For the most part, guided waves are used to gauge the damage state and defect growth of materials subjected to various mechanical or environmental loads. The technique has been applied to polymer matrix composites, ceramic matrix composites, and metal matrix composites as well as metallic alloys. Historically, guided wave analysis has been a point-by-point, manual technique with waveforms collected at discrete locations and postprocessed. Data collection and analysis of this type limits the amount of detail that can be obtained. Also, the manual movement of the sensors is prone to user error and is time consuming. The development of an automated guided-wave scanning system has allowed the method to be applied to a wide variety of materials in a consistent, repeatable manner. Experimental studies have been conducted to determine the repeatability of the system as well as compare the results obtained using more traditional NDE methods. The screen capture to the left shows guided-wave scan results for a ceramic matrix composite plate, including images for each of nine calculated parameters. The system can display up to 18 different wave parameters. Multiple scans of the test specimen demonstrated excellent repeatability in the measurement of all the guided-wave parameters, far exceeding the traditional point-by-point technique. In addition, the scan

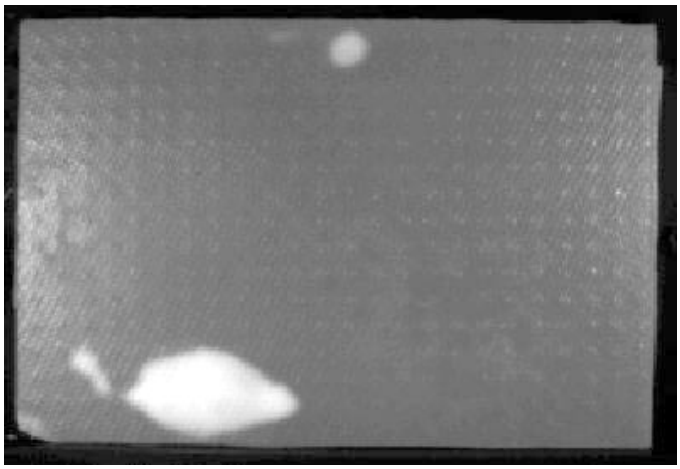

Pulsed thermography results for a ceramic composite plate. The lighter area indicates the location of a subsurface flaw.

was able to detect a subsurface defect that was confirmed using flash thermography (see the image above).

This technology is being further refined to provide a more robust and efficient software environment. Future hardware upgrades will allow for multiple receiving transducers and the ability to scan more complex surfaces. This work supports composite materials development and testing under the Ultra-Efficient Engine Technology (UEET) Project, but it also will be applied to other material systems under development for a wide range of applications.

Glenn contact:
Don Roth, 216–433–6017,
Donald.J.Roth@nasa.gov

Authors: Richard E. Martin, Dr. Andrew L. Gyekenyesi, and Don J. Roth

Headquarters program office: OAT

Programs/Projects: UEET, PR&T

Ultrasonic Guided-Wave Scan System Used to Characterize Microstructure and Defects in Ceramic Composites

Ceramic matrix composites (CMCs) are being developed for advanced aerospace propulsion applications to save weight, improve reuse capability, and increase performance. However, mechanical and environmental loads applied to CMCs can cause discrete flaws and distributed microdamage, significantly reducing desirable physical properties. Such microdamage includes fiber/matrix debonding (interface failure), matrix microcracking, fiber fracture and buckling, oxidation, and second phase formation. A recent study (ref. 1) of the durability of a C/SiC CMC discussed the requirement for improved nondestructive evaluation (NDE) methods for monitoring degradation in these materials. Distributed microdamage in CMCs has proven difficult to characterize nondestructively because of the complex microstructure and macrostructure of these materials. This year, an ultrasonic guided-wave scan system developed at the NASA Glenn Research Center was used to characterize various microstructural and flaw conditions in SiC/SiC (silicon carbide fiber in silicon carbide matrix) and C/SiC (carbon fiber in silicon carbide matrix) CMC samples.

Ultrasonic guided-wave inspection can be an attractive alternative to scanning because a single transducer, or a line of transducers can be used to excite guided waves at one location of a structure, with returning echoes indicating the presence of defects (ref. 2). This type of inspection has successfully detected flaws and degradation in many types of materials and components, and in some applications, over significant distances. The guided-wave signal in raw form is very complex (many dispersive and interfering modes traveling at different velocities) with

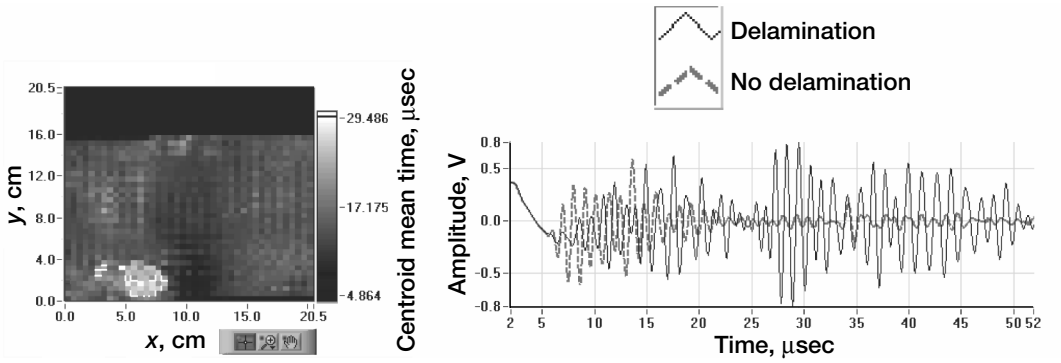

Left: Centroid mean time image (in μsec) of SiC/SiC sample. The lower left whitish area is delaminated. Right: Time-domain waveforms associated with delaminated and nondelaminated areas. This figure is shown in color in the online version of this article (http://www.grc.nasa.gov/WWW/RT/5000/5520roth.html).

significant coherent noise that cannot be averaged out. As a result, guided-wave methods seem to be most successful when they control coherent noise by tuning for a minimally dispersive or nondispersive mode of ultrasound, at a particular excitation frequency, in just one direction. The guided-wave method used at Glenn takes a different approach by utilizing the total (multimode) ultrasonic response in a scanning configuration and by employing specialized signal-processing routines to extract parameters of the time- and frequency-domain signals. These parameters, which have proven to be sensitive to changes in microstructural conditions and to the presence of defects, appear promising in monitoring the degradation in CMCs.

Guided-wave scanning may have several further advantages over conventional ultrasonic methods.

(1) Guided-wave scanning can be performed directionally, allowing correlations to be made between ultrasonic parameters and directionally dependent material properties (such as for unidirectional composites or in testing the nondirectionality of properties).
(2) The sample under test does not have to be immersed in fluid (as for most conventional ultrasonic characterization).
(3) Guided-wave scanning is potentially applicable to components with mildly curved surfaces.
(4) Guided-wave scanning is potentially more versatile in characterizing local modulus changes than resonant frequency methods since the resonant frequency methods require nodal excitation and generation and, thus, are not applicable for scanning.

The figure shows an ultrasonic guided-wave scan image of a SiC/SiC composite sample containing delamination. The delamination was most easily discriminated in the centroid mean time image (whitish areas in image; the signal processing performed allows over 20 parameters of the time and frequency domains to be calculated for image formation). Centroid mean time can be thought of as the time in the raw waveform demarcating the location of energy balance. The time-domain waveforms associated with the delaminated and nondelaminated areas are shown in the figure. The shift in the centroid mean time away from the origin is quite apparent for the delamination.

References

1. Verrilli, M.J.; Kantzos, P.T.; and Telesman, J.: Characterization of Damage Accumulation in a C/SiC Composite Subjected to Mechanical Loadings at Elevated Temperature. Proceedings of Environmental, Mechanical, and Thermal Properties and Performance of Continuous Fiber Ceramic Composite (CFCC) Materials and Components, ASTM STP–1392, M.G. Jenkins, ed., American Society for Testing and Materials, West Conshohocken, PA, 2000.
2. Roth, D.J., et al.: Microstructural and Defect Characterization in Ceramic Composites Using an Ultrasonic Guided Wave Scan System. NASA/TM—2003-212518, 2003. http://gltrs.grc.nasa.gov/cgi-bin/GLTRS/browse.pl?2003/TM-2003-212518.html

Glenn contact:
Don Roth, 216–433–6017, Donald.J.Roth@nasa.gov

Authors: Don J. Roth, Laura M. Cosgriff, Richard E. Martin, Michael J. Verrilli, and Dr. Ramakrishna T. Bhatt

Headquarters program office: OAT

Programs/Projects: UEET, RLV

Vibration-Based Method Developed to Detect Cracks in Rotors During Acceleration Through Resonance

In recent years, there has been an increasing interest in developing rotating machinery shaft crack-detection methodologies and online techniques. Shaft crack problems present a significant safety and loss hazard in nearly every application of modern turbomachinery. In many cases, the rotors of modern machines are rapidly accelerated from rest to operating speed, to reduce the excessive vibrations at the critical speeds. The vibration monitoring during startup or shutdown has been receiving growing attention (ref. 1), especially for machines such as aircraft engines, which are subjected to frequent starts and stops, as well as high speeds and acceleration rates. It has been recognized that the presence of angular acceleration strongly affects the rotor's maximum response to unbalance and the speed at which it occurs. Unfortunately, conventional nondestructive evaluation (NDE) methods have unacceptable limits in terms of their application for online crack detection. Some of these techniques are time consuming and inconvenient for turbomachinery service testing. Almost all of these techniques require that the vicinity of the damage be known in advance, and they can provide only local information, with no indication of the structural strength at a component or system level. In addition, the effectiveness of these experimental techniques is affected by the high measurement noise levels existing in complex turbomachine structures. Therefore, the use of vibration monitoring along with vibration analysis has been receiving increasing attention.

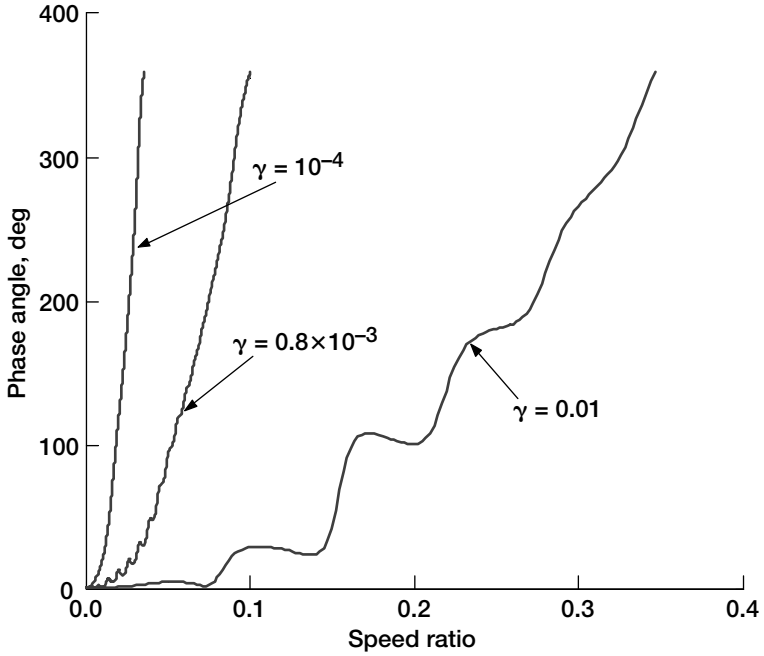

Phase angle of the accelerated rotor passing through the critical speed for angular acceleration ratios, γ, of 0.01, 0.8×10^{-3}, and 10^{-4}; γ, crack depth, 0.4.

A new analytical model for detecting shaft cracks was developed (refs. 2 and 3) on the basis of the Jeffcott rotor model with transverse crack assumed at the middle of the shaft. The criterion for the opening and closing of the crack were based on the angle between the crack centerline and the shaft vibration vector, so the rotor weight-dominance assumption can be ignored. The stiffness-weakening effects of a cracked rotor in both the strong and weak axes were taken into consideration for deep cracks.

The nonlinear responses of a rotor passing through the critical speed with several values of constant angular acceleration ratios γ and different crack depths ΔK were evaluated. For all cases, we assumed that the damping ratio ζ was 0.05 and the normalized unbalance eccentricity was 0.05. This graph presents the change in the rotor phase response due to the acceleration and crack. In general, a crack causes the amplitude of the phase response to decrease for the given speed ratio and acceleration rate. It induces significant oscillations in the rotor phase response, especially for higher acceleration rates. The characteristic "saw-cut" pattern of the phase waveform can be used in the online crack-detection systems.

The graph on the next page illustrates the response of a cracked rotor subjected to constant torque, when the rotor was locked in the stalled condition; that is, it failed to accelerate beyond the critical speed. For this case, the normalized unbalance eccentricity was assumed to be 0.85×10^{-3}, the nondimensional

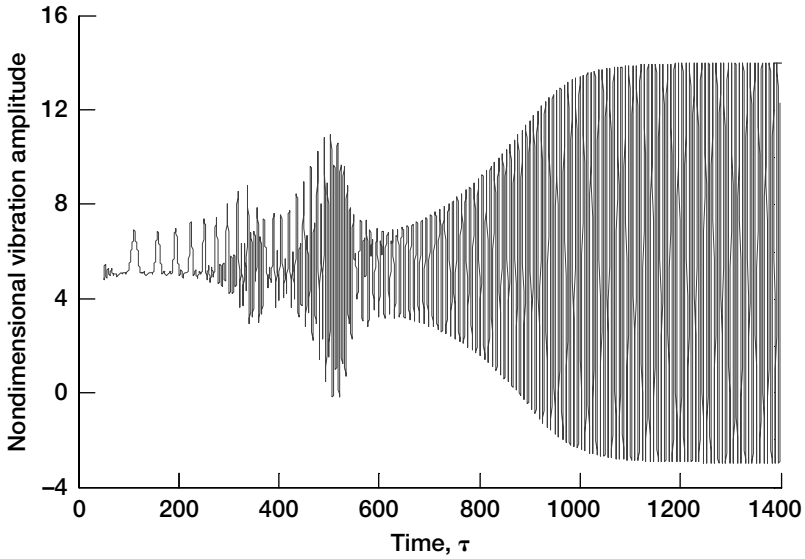

Time history of normalized vibration amplitude for a rotor with a crack with a nondimensional crack depth, ΔK, of 0.25 at the stalled condition for a nondimensional driving torque, T, of 0.001.

weight of the rotor was 5, and the damping ratio ζ was 0.005. The crack caused one-third and one-half subharmonic peaks in the rotor response and significantly increased the fundamental vibration response of the "stalling" rotor. In this case, the large vibration amplitudes of the stalling cracked rotor might well have exceeded the rotor static deflection and, therefore, violated the common weight dominance assumption made in the study of rotors with breathing cracks. It was shown that for the stalled rotor the maximum vibration amplitude grows parabolically as the crack depth increases and the corresponding rotor stalling speed decreases almost linearly. We plan to verify these results experimentally.

References

1. Sawicki, Jerzy T.: Some Advances in Diagnostics of Rotating Machinery Malfunctions. Proceedings of the International Symposium on Machine Condition Monitoring and Diagnosis, The Japan Society of Mechanical Engineers, Tokyo, Japan, 2002, pp. 138–144.
2. Sawicki, J.T., et al.: Vibration-Based Crack Diagnosis in Rotating Shafts During Acceleration Through Resonance. Proc. Soc. Photo Opt. Instrum. Eng., vol. 5046, 2003, pp. 1–10.
3. Sawicki, Jerzy T., et al.: Dynamic Behavior of Cracked Flexible Rotor Subjected to Constant Driving Torque. Proceedings of the Second International Symposium on Stability Control of Rotating Machinery, Gdansk, Poland, 2003, pp. 231–241.

Cleveland State University contact:
Prof. Jerzy T. Sawicki, 216–687–2565, j.sawicki@csuohio.edu

Glenn contact:
Dr. George Y. Baaklini, 216–433–6016, George.Y.Baaklini@nasa.gov

Authors:
Prof. Jerzy T. Sawicki, Dr. George Y. Baaklini, and Dr. Andrew L. Gyekenyesi

Headquarters program office: OAT

Programs/Projects: AvSP

Planar Particle Imaging Doppler Velocimetry Developed

Two current techniques exist for the measurement of planar, three-component velocity fields. Both techniques require multiple views of the illumination plane in order to extract all three velocity components. Particle image velocimetry (PIV) is a high-resolution, high-accuracy, planar velocimetry technique that provides valuable instantaneous velocity information in aeropropulsion test facilities. PIV can provide three-component flow-field measurements using a two-camera, stereo viewing configuration. Doppler global velocimetry (DGV) is another planar velocimetry technique that can provide three-component flow-field measurements; however, it requires three detector systems that must be located at oblique angles from the measurement plane. The three-dimensional configurations of either technique require multiple (DGV) or at least large (stereo PIV) optical access ports in the facility in which the measurements are being conducted. Optical access is extremely limited in aeropropulsion test facilities. In many cases, only one optical access port is available. A hybrid measurement technique has been developed at the NASA Glenn Research Center, planar particle image and Doppler velocimetry (PPIDV), which combines elements from both the PIV and DGV techniques into a single detection system that can measure all three components of velocity across a planar region of a flow field through a single optical access port.

In the standard PIV technique, a pulsed laser is used to illuminate the flow field at two closely spaced instances in time, which are recorded on a "frame-straddling" camera, yielding a pair of single-exposure image frames. The PIV camera is oriented perpendicular to the light sheet, and the processed PIV data yield the two-component velocity field in the plane of the light sheet. In the standard DGV technique, an injection-seeded Nd:YAG pulsed laser light sheet illuminates the seeded

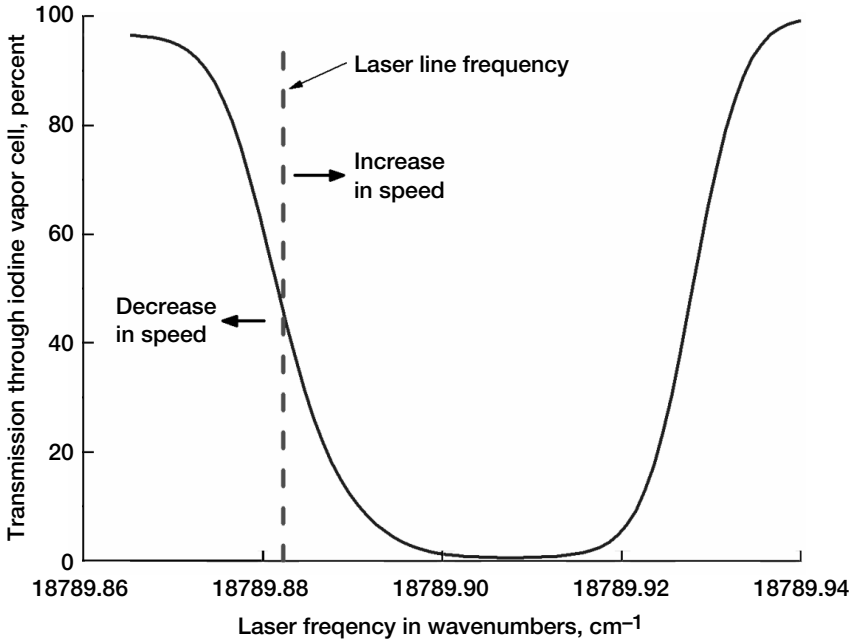

Iodine vapor cell absorption feature showing percent transmission through the cell versus frequency. Also shown is the illumination laser line position relative to the iodine absorption profile. Any increase in velocity will result in an upshift in frequency and a decrease in the amount of transmitted light. A decrease in velocity will cause a downshift in frequency and a resultant increase in the amount of transmitted light.

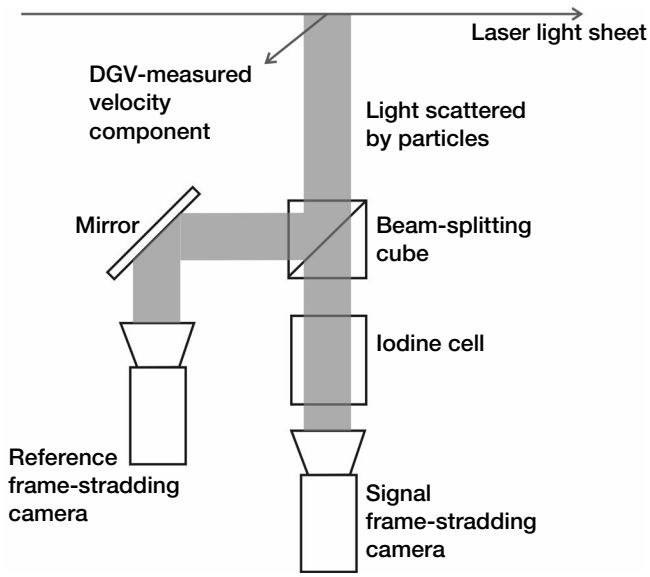

Layout of the planar particle imagery and Doppler velocimetry receiver head. The collected light passes through a beam-splitting cube. Half of the light goes to a reference camera, while the other half goes through the iodine vapor cell before reaching the signal camera. Taking the ratio of the intensity-modulated signal image to the reference image yields an intensity map that is proportional to the gas velocity in the plane of the light sheet. The component of the velocity measured via the Doppler shift (DGV) is depicted by the arrow that lies 45° out of the plane of the light sheet. The Doppler-shifted out-of-plane measurement is combined with the in-plane two-dimensional PIV measurements to compute the full three-component velocity field across the illuminated plane of the flow.

flow field, and three receiver systems are used to measure three components of velocity. The receiver systems are oriented at oblique angles to the light sheet in order to accurately resolve the three-component velocity. Each DGV receiver system contains two cameras, which share a common view of the illuminated flow through a beam-splitting cube. One camera views the illuminated flow directly (reference camera) and the second camera images the illuminated flow through an iodine vapor cell (signal camera). The laser frequency (wavelength) is adjusted so that the Doppler-shifted light from particles in the flow falls on an iodine absorption feature, see the graph. The iodine vapor cell acts as a frequency-to-velocity filter by modulating the intensity of the transmitted light as a function of the flow velocity (Doppler shift). The ratio of the signal and reference images yields the component of the flow velocity along the bisector of the laser sheet propagation direction and the receiver system observation direction.

The hybrid system employs a single-component DGV receiver system configured to simultaneously acquire PIV image data, as shown in the diagram. The cameras used in the DGV receiver are replaced with PIV frame-straddling cameras, and the receiver system views the illuminated light sheet plane at 90° (as in the standard PIV configuration).

Find out more about this research:
http://www.grc.nasa.gov/WWW/OptInstr/piv/

Glenn contact:
Dr. Mark P. Wernet, 216–433–3752, Mark.P.Wernet@nasa.gov

Author: Dr. Mark P. Wernet

Headquarters program office: OAT

Programs/Projects:
UEET, CVCCE, QAT

Active Closed-Loop Stator Vane Flow Control Demonstrated in a Low-Speed Multistage Compressor

Closed-loop flow control was successfully demonstrated on the surface of stator vanes in NASA Glenn Research Center's Low-Speed Axial Compressor (LSAC) facility. This facility provides a flow field that accurately duplicates the aerodynamics of modern highly loaded compressors. Closed-loop active flow control uses sensors and actuators embedded within engine components to dynamically alter the internal flow path during off-nominal operation in order to optimize engine performance and maintain stable operation.

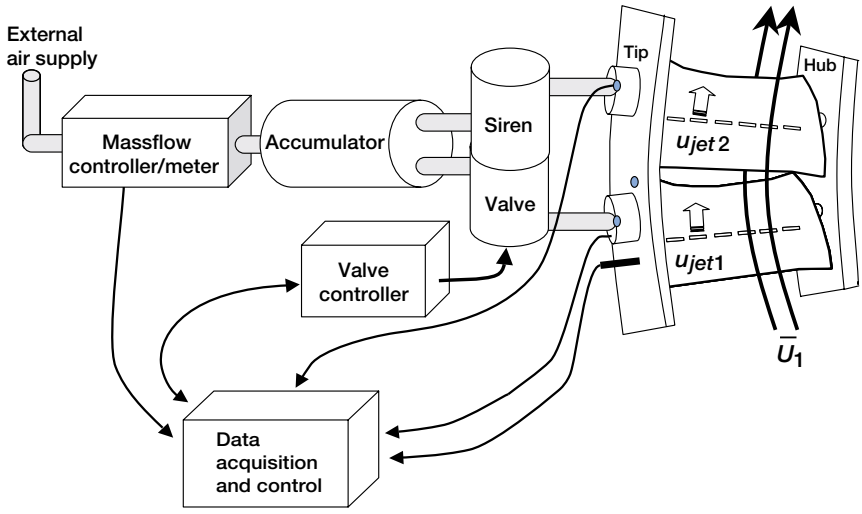

Flow-control actuation system. $\bar{U}_1$ free-stream velocity; u_{jet}, jet velocity out of the vane.

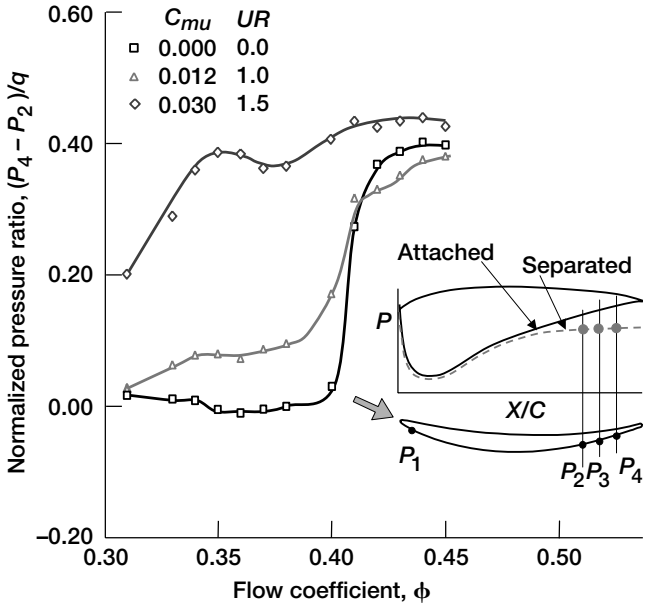

Sensing separation from blade surface sensors. Surface static pressure gradient usable as control input. P_1, P_2, P_3, and P_4, pressures along vanes; C_{mu}, momentum coefficient; UR, velocity ratio.

In highly loaded modern compressors, the flow tends to separate from the stator airfoils under conditions of low mass flow and distortion. These conditions are often encountered during takeoff, landing, and (for military aircraft) the extreme maneuvers encountered during combat operations. Flow separation acts as a blockage in the flow path that limits pressure recovery and may even trigger the severe mechanical stress conditions known as stall and surge. Closed-loop active flow control uses sensors and actuators to sense and delay the onset of separation by injecting air ahead of the separation line. The diagram on the left shows the experimental configuration for the system, including surface static pressure taps to monitor separation along the stator, an unsteady pressure transducer in the compressor casing to monitor velocity perturbations from the downstream rotor, and a control computer to perform closed-loop detection of the pressure signals and to command the injection through the stator vane.

As part of this closed-loop control system, two methods were developed to determine separation along the vane. The first method employs suction-surface static pressure taps located at 70- and 85-percent chord and at 56-percent span. The pressure rise between these two locations provides the controller with the pressure gradient over the rear of the vane. The bottom figure on the left shows the pressure rise measurements that were acquired over the vane with and without steady air injection. As the flow coefficient through the compressor decreased, separation occurred across the vane, which is shown as a drop in pressure rise at flow coefficients below 0.40. With the use of steady

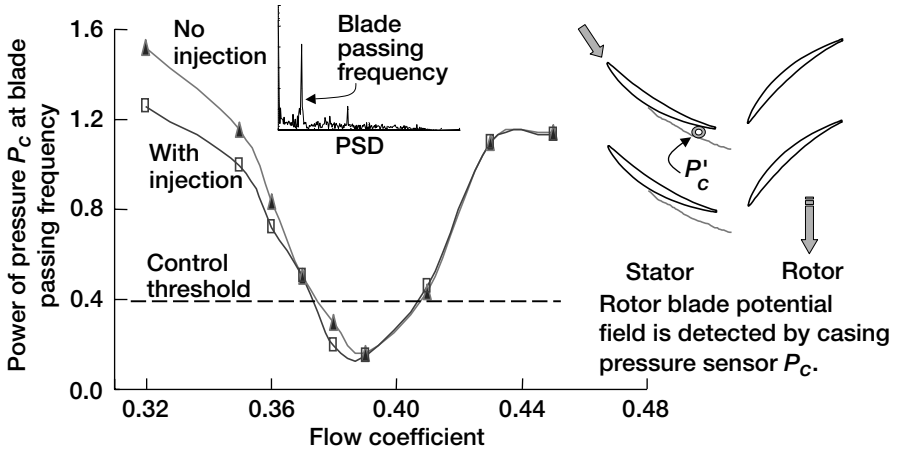

Sensing separation from casing static pressure. The rotor blade potential field is detected by the casing pressure sensor. PSD, power spectral density.

injection, this pressure rise was maintained across the vane. This strategy thus uses the pressure difference across the vane to monitor separation. When the pressure difference across the vane is greater than 0.3, a control command turns on injection.

The second separation detection scheme (figure above) uses a pressure transducer located in the casing next to the vane suction surface at 85-percent chord. This scheme is based on time-series analysis of casing static pressure. The wake shed from the vane causes an unsteady loading on the downstream rotor. The first Fourier harmonic of the rotor blade passing frequency is a measure of the wake-induced pressure variation generated by the rotor. Since vane surface separation increases wake strength, separation can be detected from the casing static pressure signal by monitoring the power in the first harmonic (see the figure above). In a control strategy for the vane, the power of the first Fourier harmonic of the pressure signal is used to determine when to switch injection on. Both these strategies are detailed further in reference 1.

This work describes two successful active flow-control strategies for compressors. Modern compressors must be designed to accommodate a broad range of operating conditions in a safe and efficient manner. Since overall engine performance is driven by compressor performance, advances in compressor technology that reduce weight and parts count, reduce fuel consumption, and lower maintenance costs will decrease the cost of aircraft ownership significantly. Active flow-control strategies may deliver such advances.

This work was partially funded by the Defense Advanced Research Program Agency and was performed in collaboration with Honeywell and the Illinois Institute of Technology. Presently, all work is being conducted as part of Glenn's in-house support of the Ultra-Efficient Engine Technology Project.

Reference

1. Culley, Dennis E., et al.: Active Flow Separation Control of a Stator Vane Using Surface Injection in a Multistage Compressor Experiment. NASA/TM—2003-212356, 2003. http://gltrs.grc.nasa.gov/cgi-bin/GLTRS/browse.pl?2003/TM-2003-212356.html

Glenn contacts:
Dr. Michelle M. Bright, 216–433–2304, Michelle.M.Bright@nasa.gov;
Dennis E. Culley, 216–433–3797, Dennis.E.Culley@nasa.gov; and
Dr. Anthony J. Strazisar, 216–433–5881, Anthony.J.Strazisar@nasa.gov

Authors:
Dr. Michelle M. Bright, Dennis E. Culley, and Dr. Anthony J. Strazisar

Headquarters program office: OAT

Programs/Projects:
PR&T, UEET, DARPA

Probabilistic Study Conducted on Sensor-Based Engine Life Calculation

Turbine engine life management is a very complicated process to ensure the safe operation of an engine subjected to complex usage. The challenge of life management is to find a reasonable compromise between the safe operation and the maximum usage of critical parts to reduce maintenance costs. The commonly used "cycle count" approach does not take the engine operation conditions into account, and it oversimplifies the calculation of the life usage. Because of the shortcomings, many engine components are regularly pulled for maintenance before their usable life is over. And, if an engine has been running regularly under more severe conditions, components might not be taken out of service before they exceed their designed risk of failure.

The NASA Glenn Research Center and its industrial and academic partners have been using measurable parameters to improve engine life estimation. This study was based on the Monte Carlo simulation of 5000 typical flights under various operating conditions. First a closed-loop engine model was developed to simulate the engine operation across the mission profile and a thermomechanical fatigue (TMF) damage model was used to calculate the actual damage during takeoff, where the maximum TMF accumulates. Next, a Weibull distribution was used to estimate the implied probability of failure for a given accumulated cycle count. Monte Carlo simulations were then employed to find the profiles of the TMF damage under different operating assumptions including parameter uncertainties. Finally, probabilities of failure for different operating conditions were analyzed to demonstrate the importance of a sensor-based damage calculation in order to better manage the risk of failure and on-wing life.

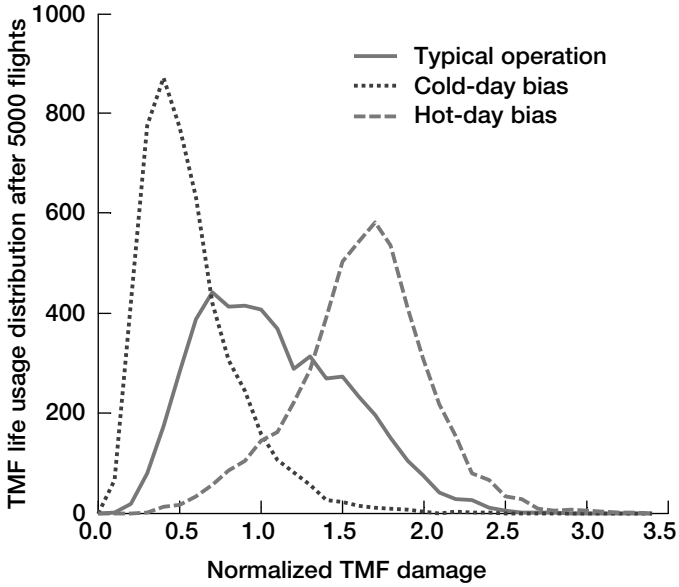

TMF damage distribution for different operating conditions.

The table (next page) compares the different study cases. In the typical usage study, where system uncertainties, as well as different ambient temperatures and altitudes, were considered, the average risk of failure was 48-percent higher than the design point. In the hot-day-biased case, the ambient temperatures were consistently higher than for the standard condition. The 5000 simulated flights were actually equivalent to 7892 standard flights. This has a corresponding risk of failure of 0.062 percent, or 6.2 times the original value. An engine operated under these extreme conditions should be taken out of service much sooner than the nominal 5000 cycles if the same risk of failure is to be maintained. On the other hand, in the cold-day-biased case, much less engine life was consumed, and the risk of failure at the 5000 flight point was only a fraction of the original designed value. An engine operated at this condition could be allowed to extend its on-wing service life without any safety concerns. The graph shows the TMF life usage distribution of 5000 flights based on the Monte Carlo simulation for normal, hot-day, and cold-day operation. In conclusion, this study clearly shows the necessity of sensor-based life monitoring in order to avoid the high risk of failure when an engine is operated under severe conditions, or to do unnecessary maintenance on the engine when the engine is still safe statistically.

ENGINE OPERATING CONDITIONS

Case	System parameter uncertainties	Change from ambient temperature (standard deviation), °F	Airport elevation, ft	Number of equivalent standard flights after 5000 flights	Probability of failure after 5000 flights, percent
Design point	None	0	0	5000	0.01
Normal operation	Yes	Normal (30)	Uniform, 0 to 1000	5501	.0148
Hot-day-biased	Yes	Bias = 30 (20)	Uniform, 0 to 1000	7892	.062
Cold-day-biased	Yes	Bias = –30 (20)	Uniform, 0 to 1000	3172	.0016

Bibliography

Guo, Ten-Huei; and Chen, Philip: Sensor Based Engine Life Calculation—A Probabilistic Perspective. NASA/TM—2003-212499 (ISABE–2003–1147), 2003. http://gltrs.grc.nasa.gov/cgi-bin/GLTRS/browse.pl?2003/TM-2003-212499.html

Guo, Ten-Huei: A Roadmap for Aircraft Engine Life Extending Control. Proceedings of the 2001 American Control Conference, vol. 5, IEEE, Piscataway, NJ, 2001, pp. 3702–3705.

Find out more about this research:
http://www.grc.nasa.gov/WWW/cdtb/

Glenn contact:
Dr. Ten-Huei Guo, 216–433–3734, Ten-Huei.Guo-1@nasa.gov

Author: Dr. Ten-Huei Guo

Headquarters program office: OAT

Programs/Projects: CICT

Adaptive Controls Method Demonstrated for the Active Suppression of Instabilities in Engine Combustors

This year, an adaptive feedback control method was demonstrated that suppresses thermoacoustic instabilities in a liquid-fueled combustor of a type used in aircraft engines. Extensive research has been done to develop lean-burning (low fuel-to-air ratio) combustors that can reduce emissions throughout the mission cycle to reduce the environmental impact of aerospace propulsion systems. However, these lean-burning combustors are susceptible to thermoacoustic instabilities (high-frequency pressure waves), which can fatigue combustor components and even the downstream turbine blades. This can significantly decrease the safe operating lives of the combustor and turbine. Thus, suppressing the thermoacoustic combustor instabilities is an enabling technology for lean, low-emissions combustors under NASA's Propulsion and Power Program. This control methodology has been developed and tested in a partnership of the NASA Glenn Research Center, Pratt & Whitney, United Technologies Research Center, and the Georgia Institute of Technology. Initial combustor rig testing of the controls algorithm was completed during 2002. Subsequently, the test results were analyzed and improvements to the method were incorporated in 2003, which culminated in the final status of this controls algorithm.

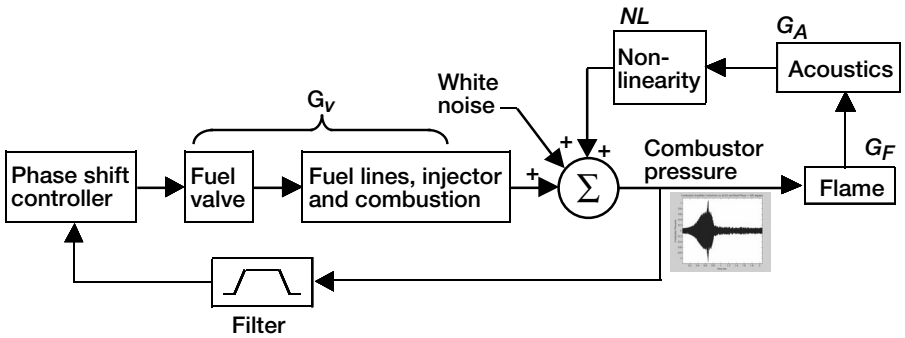

Combustion instability control block diagram. G_V, G_F, and G_A are transfer functions of the associated combustion processes reflected in the figure; NL is a damping nonlinearity that restricts the amplitude of the opened-loop self-excited instability.

This control methodology is based on adaptive phase shifting. The combustor pressure oscillations are sensed and phase shifted, and a high-frequency fuel valve is actuated to put pressure oscillations into the combustor to cancel pressure oscillations produced by the instability.

Combustor instability suppression poses a challenging feedback controls problem due to unmodeled dynamics, large dead-time phase shift in excess of 1000°, large-amplitude wide-band noise in comparison to the amplitude of the instability (~ 6/1 ratio for the combustor rig), severe amplitude modulations, frequency and phase-shift randomness, and a system that continuously transitions through inherently unstable operation at increased suppression levels. To overcome these difficulties, NASA researchers developed a sophisticated controls method that does not depend on detailed modeling of system dynamics. The controls method is named "adaptive sliding phasor averaged control." The controller phase continuously slides back and forth inside the boundaries of an effective stability region that lies within a restricted control region in a stationary frame of reference. In this control algorithm, the combustor pressure oscillations are sensed through a band-pass filter to isolate the instability from noise. Then, the filtered pressure oscillations are continuously phase shifted at a rate of 40 Hz in the direction that suppresses the instability and are output to the fuel actuator at a rate of 10 kHz in order to suppress the instability. Also, discontinuous exponential gain modulation and control parameter adaptation is employed.

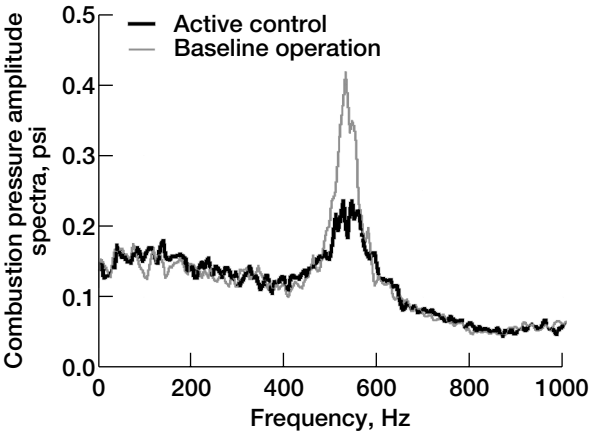

Amplitude spectral density of uncontrolled versus controlled instability.

This active combustion instability control method was shown to reduce thermoacoustic-driven combustor pressure oscillations and was demonstrated for a high-frequency (530 Hz) instability on a single-nozzle combustor rig at United Technologies Research Center. This is the first known successful demonstration of high-frequency combustion instability suppression in a realistic aircraft engine environment. This rig, which emulates an actual engine instability experience, has many of the complexities of a real engine combustor (i.e., an actual fuel nozzle and swirler, dilution cooling, etc.).

Bibliography

Kopasakis, George; and DeLaat, John C.: Adaptive Instability Suppression Controls in a Liquid-Fueled Combustor. NASA/TM—2002-211805 (AIAA Paper 2002–4075), 2002. http://gltrs.grc.nasa.gov/cgi-bin/GLTRS/browse.pl?2002/TM-2002-211805.html

Kopasakis, George: High Frequency Adaptive Instability Suppression Controls in a Liquid-Fueled Combustor. NASA/TM—2003-212535 (AIAA Paper 2003–4491), 2003. http://gltrs.grc.nasa.gov/cgi-bin/GLTRS/browse.pl?2003/TM-2003-212535.html

Kopasakis, G.: Systems Characterization of Combustor Instabilities With Controls Design Emphasis. AIAA–2004–0638, To be presented at the 42nd AIAA Aerospace Sciences Meeting and Exhibit, Reno, NV, 2004.

Find out more about this research:

Active Combustion Control:
http://www.grc.nasa.gov/WWW/cdtb/projects/combustor/

Glenn's Combustion Branch:
http://www.grc.nasa.gov/WWW/combustion/

Glenn contact:
George Kopasakis, 216–433–5327, George.Kopasakis-1@nasa.gov

Author: George Kopasakis

Headquarters program office: OAT

Programs/Projects:
Propulsion and Power, SEC, UEET

Autonomous Propulsion System Technology Being Developed to Optimize Engine Performance Throughout the Lifecycle

The goal of the Autonomous Propulsion System Technology (APST) project is to reduce pilot workload under both normal and anomalous conditions. Ongoing work under APST develops and leverages technologies that provide autonomous engine monitoring, diagnosing, and controller adaptation functions, resulting in an integrated suite of algorithms that maintain the propulsion system's performance and safety throughout its life.

Engine-to-engine performance variation occurs among new engines because of manufacturing tolerances and assembly practices. As an engine wears, the performance changes as operability limits are reached. In addition to these normal phenomena, other unanticipated events such as sensor failures, bird ingestion, or component faults may occur, affecting pilot workload as well as compromising safety. APST will adapt the controller as necessary to achieve optimal performance for a normal aging engine, and the safety net of APST algorithms will examine and interpret data from a variety of onboard sources to detect, isolate, and if possible, accommodate faults. Situations that cannot be accommodated within the faulted engine itself will be referred to a higher level vehicle management system. This system will have the authority to redistribute the faulted engine's functionality among other engines, or to replan the mission based on this new engine health information.

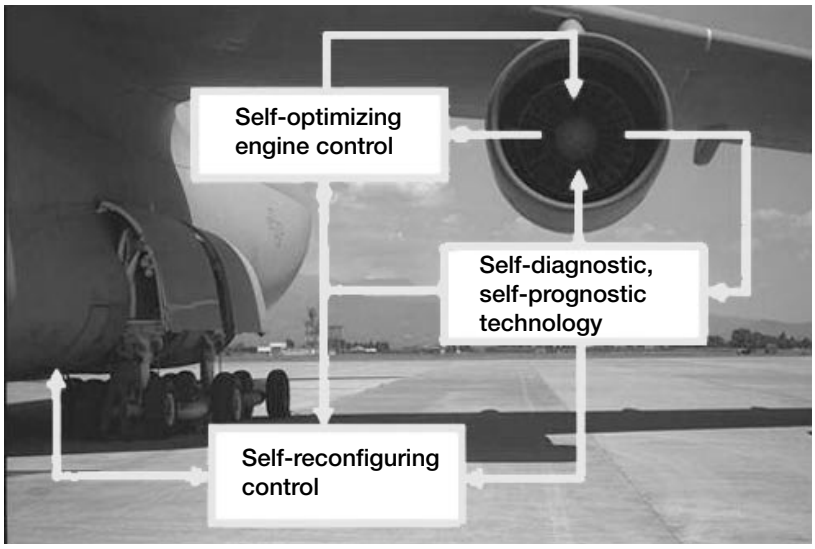

Autonomous Propulsion System Technology architecture.

Work is currently underway in the areas of adaptive control to compensate for engine degradation due to aging, data fusion for diagnostics and prognostics of specific sensor and component faults, and foreign object ingestion detection. In addition, a framework is being defined for integrating all the components of APST into a unified system.

A multivariable, adaptive, multimode control algorithm has been developed that accommodates degradation-induced thrust disturbances during throttle transients. The baseline controller of the engine model currently being investigated has multiple control modes that are selected according to some performance or operational criteria. As the engine degrades, parameters shift from their nominal values. Thus, when a new control mode is swapped in, a variable that is being brought under control might have an excessive initial error. The new adaptive algorithm adjusts the controller gains on the basis of the level of degradation to minimize the disruptive influence of the large error on other variables and to recover the desired thrust response.

Once fully developed and implemented, APST will (1) adapt the controller to a specific engine in the "nominal" range; (2) adapt the controller to slow changes in engine dynamics due to aging and component degradation; (3) identify potential engine problems before they occur, accurately diagnose the cause of

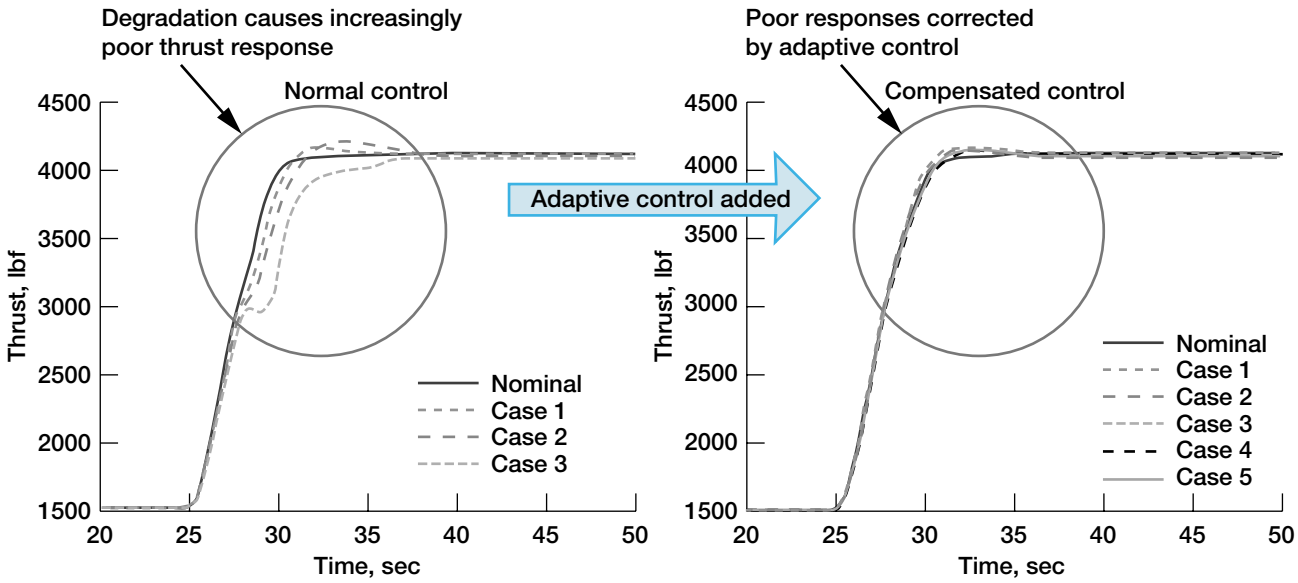

Adaptive control compensates for deteriorated thrust response due to aging and degradation across the flight envelope.

the problem, and recommend control action needed to keep the engine operating safely; (4) reconfigure the engine control for "optimal" achievable performance to accommodate sudden dynamic changes; and (5) optimize engine performance throughout the lifecycle while ensuring safety of operation and enabling true autonomous vehicle operation.

U.S. Army Research Laboratory, Vehicle Technology Directorate at Glenn contact:
Jonathan S. Litt, 216–433–3748, Jonathan.S.Litt@grc.nasa.gov

Author: Jonathan S. Litt

Headquarters program office: OAT

Programs/Projects: ECS

Propulsion Integrated Vehicle Health Management Technology Experiment (PITEX) Conducted

The Propulsion Integrated Vehicle Health Management (IVHM) Technology Experiment (PITEX) is a continuing NASA effort being conducted cooperatively by the NASA Glenn Research Center, the NASA Ames Research Center, and the NASA Kennedy Space Center. It was a key element of a Space Launch Initiative risk-reduction task performed by the Northrop Grumman Corporation in El Segundo, California. PITEX's main objectives are the continued maturation of diagnostic technologies that are relevant to second-generation reusable launch vehicle (RLV) subsystems and the assessment of the real-time performance of the PITEX diagnostic solution.

The PITEX effort has considerable legacy in the NASA IVHM Technology Experiment for X-vehicles (NITEX) that was selected to fly on the X–34 subscale RLV that was being developed by Orbital Sciences Corporation. NITEX, funded through the Future-X Program Office, was to advance the technology-readiness

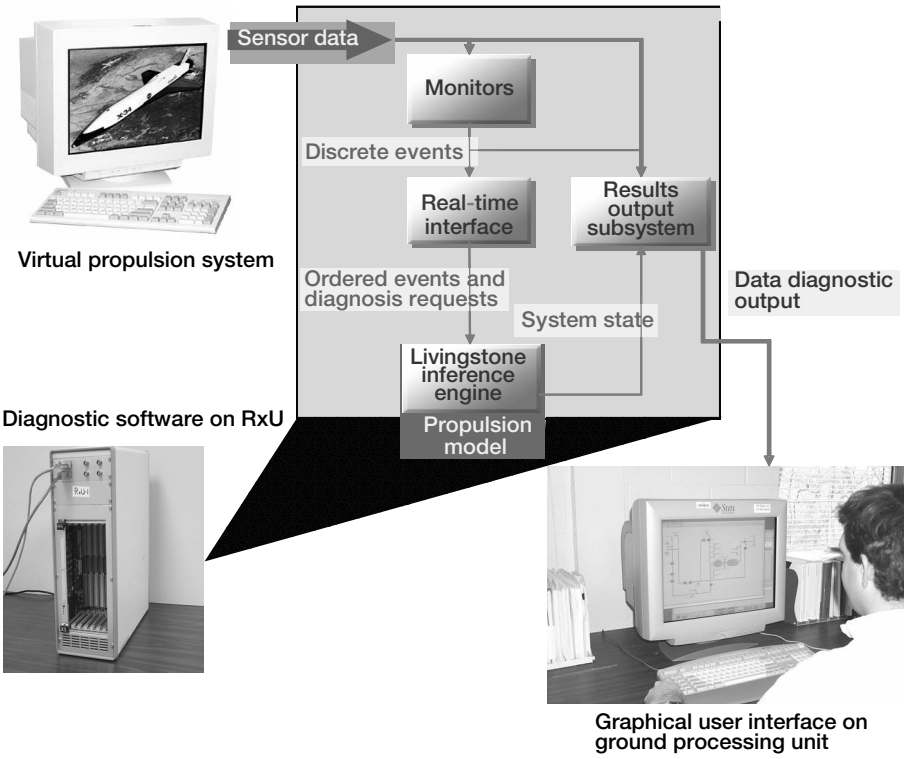

PITEX demonstration architecture.

level of selected IVHM technologies within a flight environment and to begin the transition of these technologies from experimental status into RLV baseline designs. The experiment was to perform real-time fault detection and isolation and suggest potential recovery actions for the X–34 main propulsion system (MPS) during all mission phases by using a combination of system-level analysis and detailed diagnostic algorithms.

The overall PITEX demonstration system architecture is shown in the top figure. The demonstration system was designed to test a subset of software components from the NITEX flight experiment architecture. The software package consists of the telemetry input system, the monitors, the real-time interface, Livingstone and the results output system (which are all contained on a real-time flightlike box called the RxU), and the ground processing unit. The virtual propulsion system simulated the sensor data associated with a particular mission phase and nominal or failure scenario.

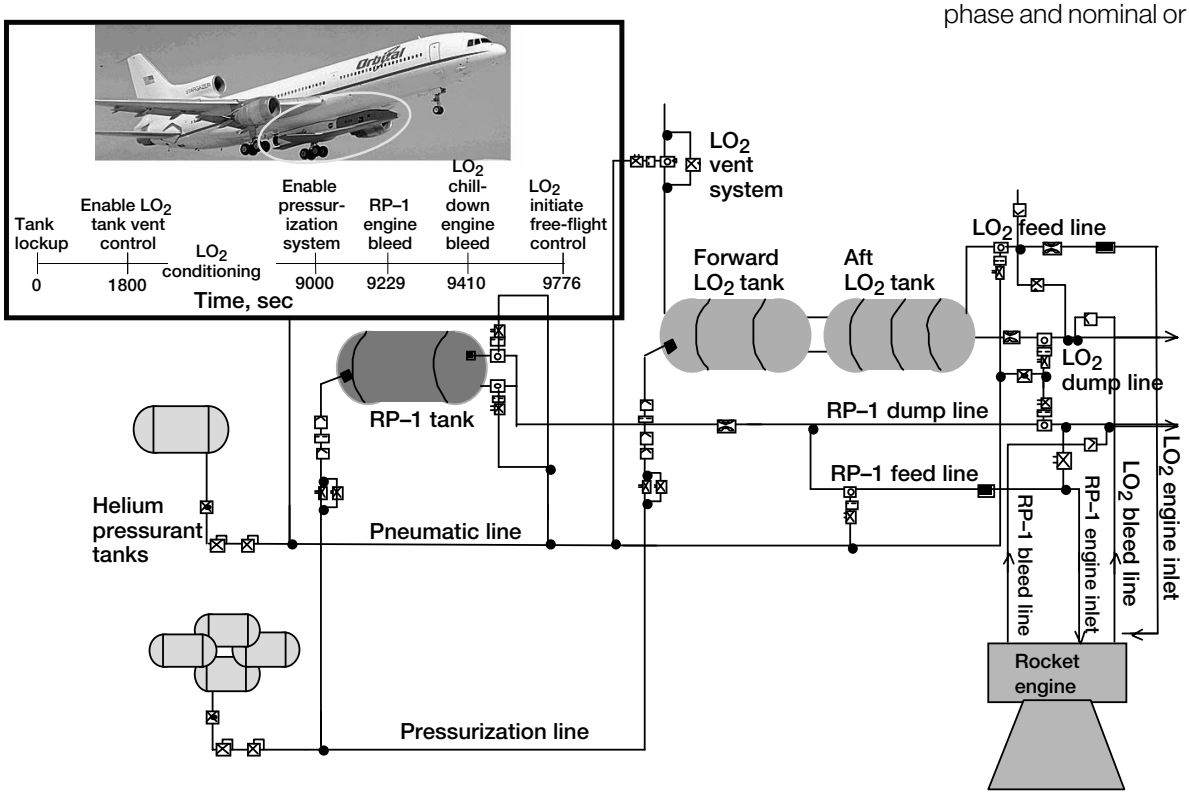

Design reference mission and MPS schematic tested by PITEX. RP–1, jet fuel; LO_2, liquid oxygen.

These data would be input to the monitors, where pertinent features of the propulsion system would be extracted and the quantitative information of the system transformed into qualitative information. This information would then be passed through the real-time interface to Livingstone, where the system-level diagnostics would be performed using a high-level qualitative model of the system. From there, the output would be collected by the results output system and displayed on the ground processing unit.

The selected design reference mission for the X–34 MPS was the captive carry mission phase. This phase was selected because of crew safety considerations of the piloted L–1011. During this phase of operation, the X–34 would be carried to the required launch altitude of 38,000 ft while it was attached to the underside of an L–1011 aircraft. The engine would not be running, and most of the other subsystems of the MPS would be in a quasi-static state, except for the liquid oxidizer (liquid oxygen) and RP–1 (jet fuel) subsystems. The bottom figure on the preceding page captures both the scope of the X–34 mission and the components in the MPS that were used in demonstrations of PITEX.

As part of the second-generation RLV risk-reduction effort, PITEX successfully demonstrated real-time model-based fault detection of a virtual MPS. Realistic propulsion system failures involving valves, regulators, and sensors were simulated and correctly diagnosed by PITEX. Simulated scenarios focused on providing the diagnostic system with realistic data signals, which included random sensor noise, resolution and bias, and build-to-build data variations. During testing of the software on flightlike hardware, system resources—CPU and memory—were found to be largely underutilized. This indicated that more complex applications could be handled by the PITEX diagnostic solution. The current results are summarized in reference 1. The PITEX project continues to address challenges aimed at improving the speed, efficiency, and timeliness of the diagnoses and is exploring other potential applications.

Reference

1. Meyer, C.M., et al.: Propulsion IVHM Technology Experiment Overview. Proceedings of the 2003 IEEE Aerospace Conference, vol. 2, 2003, pp. 2859–2868.

Find out more about this research:
http://www.grc.nasa.gov/WWW/cdtb/

Analex Corporation contacts:
William A. Maul, 216–977–7496, William.A.Maul@grc.nasa.gov; and Amy K. Chicatelli, 216–433–3613, Amy.K.Chicatelli@grc.nasa.gov

Authors:
William A. Maul, Amy K. Chicatelli, and Christopher E. Fulton

Headquarters program office: OAT

Programs/Projects:
NGLT, OSP, SLEP, SLI

Simplified Dynamic Model of Turbine Clearance Developed for Active Clearance Control Studies

A simplified analytical model was developed and implemented to simulate changes in turbine tip clearance during the operation of a commercial gas turbine engine. The clearance model is an enabling technology for the fast-response active turbine tip-clearance control being developed by the NASA Glenn Research Center under the Ultra-Efficient Engine Technology Project.

As shown in the top figure on the next page, fast-response active turbine tip clearance control is an attempt to improve engine efficiency and reduce peak exhaust gas temperatures by manipulating both transient and steady-state clearances during engine operation. A fast-acting clearance control system would provide minimal clearance throughout the flight profile as shown by the dashed line. Existing clearance control systems are based on slow thermal processes that cannot mitigate reacceleration transients. Recent studies equate a 10-mil reduction in turbine tip clearance to a reduction in engine exhaust gas temperature of up to 10 °C and an increase in turbine efficiency of up to 1 percent. Reductions of 10 to 30 mils at cruise are expected with a fast-acting clearance control.

One of the critical technology gaps in the development of a fast-acting clearance control system is a dynamic model of the clearance phenomena. Although models of the clearance dynamics are alluded to in the open literature, they tend to be proprietary in nature and, as a result, are not published in the open literature. In order to address this gap, Glenn, in partnership with the University of Texas Pan American, is developing a generic model to simulate the clearance dynamics. A first-principles approach is used to estimate the clearance by modelling the thermal and mechanical

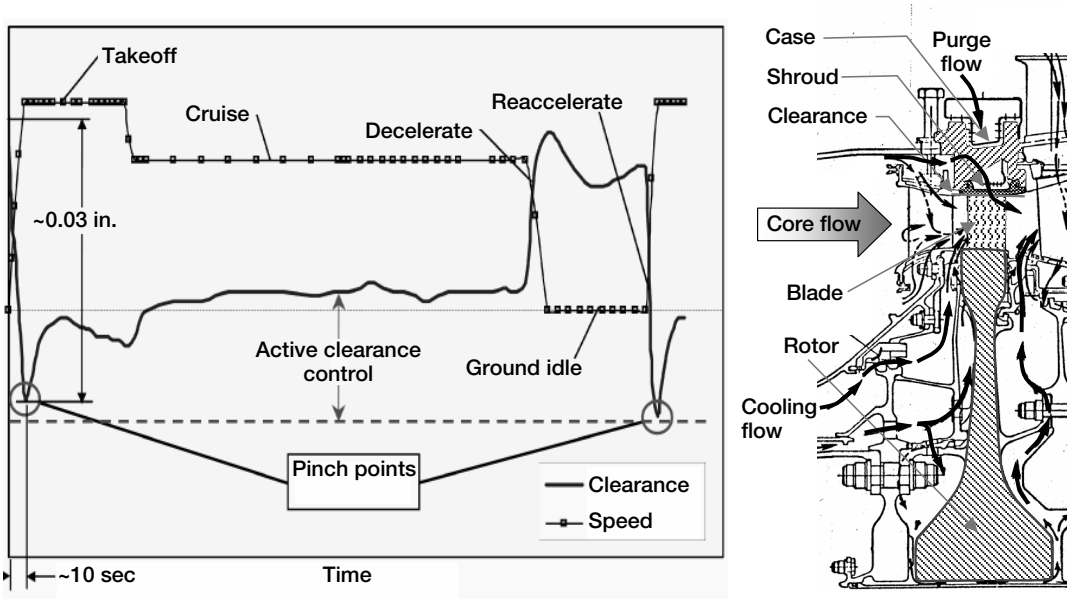

Changes in tip clearance during a notional mission profile and turbine stage cross section.

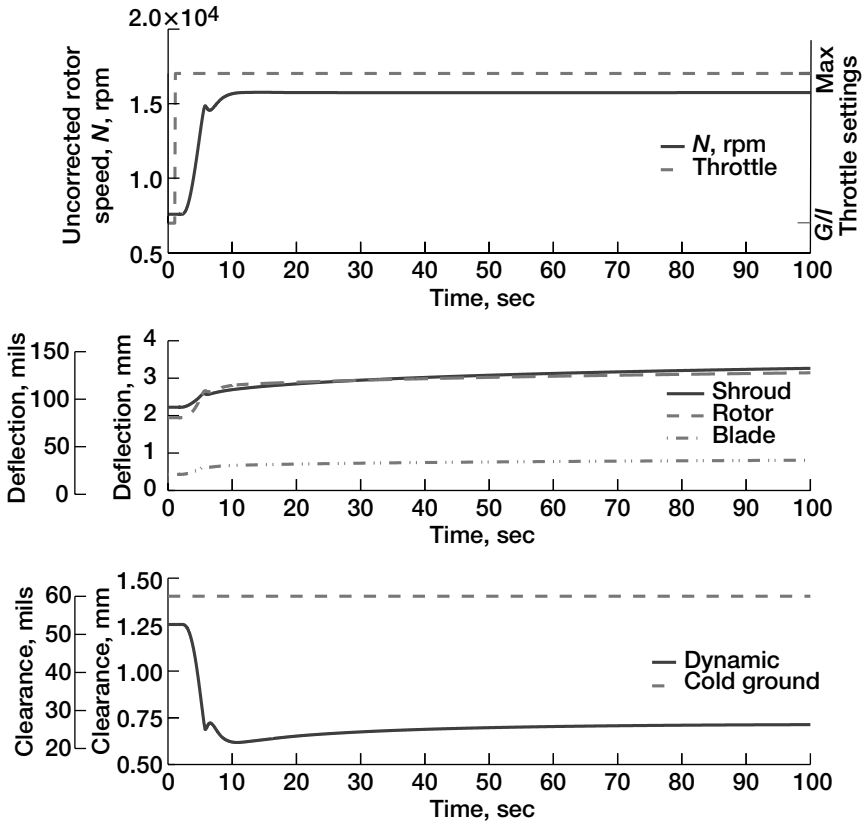

Results from dynamic simulation of the turbine clearance model. G/I, ground idle.

effects of engine operating conditions on the radial deformation of the turbine subcomponents—blade, rotor, and shroud—at each point in time. The model uses engine speed, temperatures, and pressures with thermal and mechanical constants to compute the deformation of the turbine subcomponents at each point in time. The mechanical and thermal deformation of each subcomponent is then added to the cold-build radius (or length for the blade) to obtain the deformed radius. The clearance then becomes the difference between the deformed radius of the shroud and that of the rotor plus the blade.

Partnership researchers implemented the model in a graphical simulation environment, using the speeds, temperatures, and pressures from the simulation of an engine representative of modern fighter aircraft as input. The graphs to the left show results from the simulation. The pinch point is clearly visible on the lower axis. Ongoing efforts are focused on improving and validating the model.

Bibliography
Melcher, K.J.; and Kypuros, J.A.: Toward a Fast-Response Active Turbine Tip Clearance Control, Proceedings of the XVI International Symposium on Air Breathing Engines, Cleveland, OH, Aug. 31–Sep. 5, 2003, ISABE 2003–1102 (NASA/TM—2003-212627), 2003. http://gltrs.grc.nasa.gov/cgi-bin/GLTRS/browse.pl?2003/TM-2003-212627.html

Kypuros, Javier A.; and Melcher, Kevin J.: A Reduced Model for Prediction of Thermal and Rotational Effects on Turbine Tip Clearance. NASA/TM—2003-212226, 2003. http://gltrs.grc.nasa.gov/cgi-bin/GLTRS/browse.pl?2003/TM-2003-212226.html

Lattime, Scott B.; and Steinetz, Bruce M.: Turbine Engine Clearance Control Systems: Current Practices and Future Directions. AIAA Paper 2002–3790 (NASA/TM—2002-211794), 2002. http://gltrs.grc.nasa.gov/cgi-bin/GLTRS/browse.pl?2002/TM-2002-211794.html

Find out more about this research:
http://www.grc.nasa.gov/WWW/cdtb/

Glenn contact:
Kevin J. Melcher, 216–433–3743, Kevin.J.Melcher@nasa.gov

Author: Kevin J. Melcher

Headquarters program office: OAT

Programs/Projects:
Propulsion and Power, UEET

Turbofan Engine Simulated in a Graphical Simulation Environment

Recently, there has been an increase in the development of intelligent engine technology with advanced active component control. The computer engine models used in these control studies are component-level models (CLM), models that link individual component models of state space and nonlinear algebraic equations, written in a computer language such as Fortran. The difficulty faced in performing control studies on Fortran-based models is that Fortran is not supported with control design and analysis tools, so there is no means for implementing real-time control. It is desirable to have a simulation environment that is straightforward, has modular graphical components, and allows easy access to health, control, and engine parameters through a graphical user interface. Such a tool should also provide the ability to convert a control design into real-time code, helping to make it an extremely powerful tool in control and diagnostic system development.

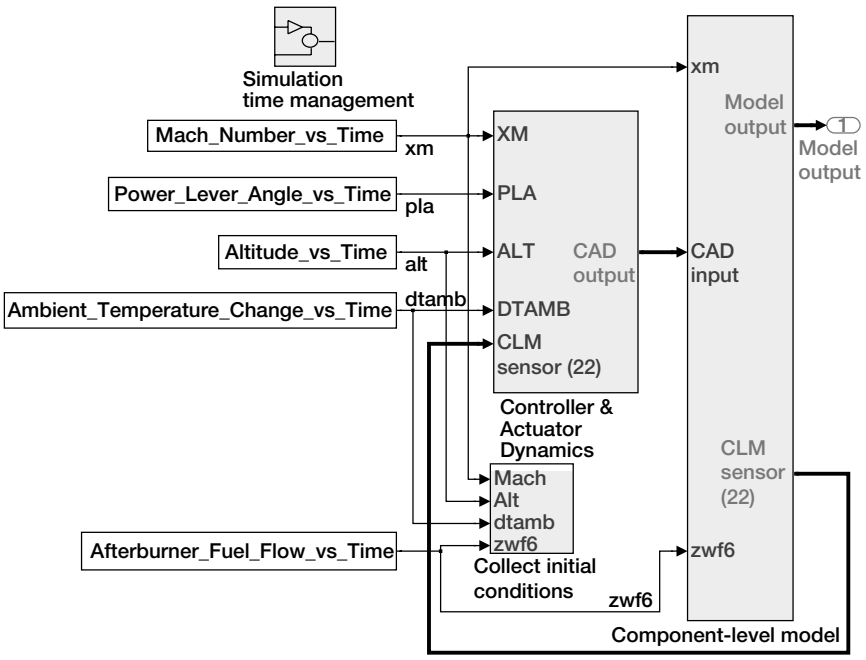

MAPSS block diagram showing the CAD module and the CLM.

The Controls and Dynamics Technologies Branch at the NASA Glenn Research Center has developed and demonstrated a flexible, generic turbofan engine simulation platform that can meet these objectives, known as the Modular Aero-Propulsion System Simulation (MAPSS). MAPSS is a Simulink-based implementation of a Fortran-based, modern high-pressure ratio, dual-spool, low-bypass, military-type variable-cycle engine with a digital controller. Simulink (The Mathworks, Natick, MA) is a computer-aided control design and simulation package allows the graphical representation of dynamic systems in a block diagram form. MAPSS is a nonlinear, non-real-time system composed of controller and actuator dynamics (CAD) and component-level model (CLM) modules (see the diagram to the left). The controller in the CAD module

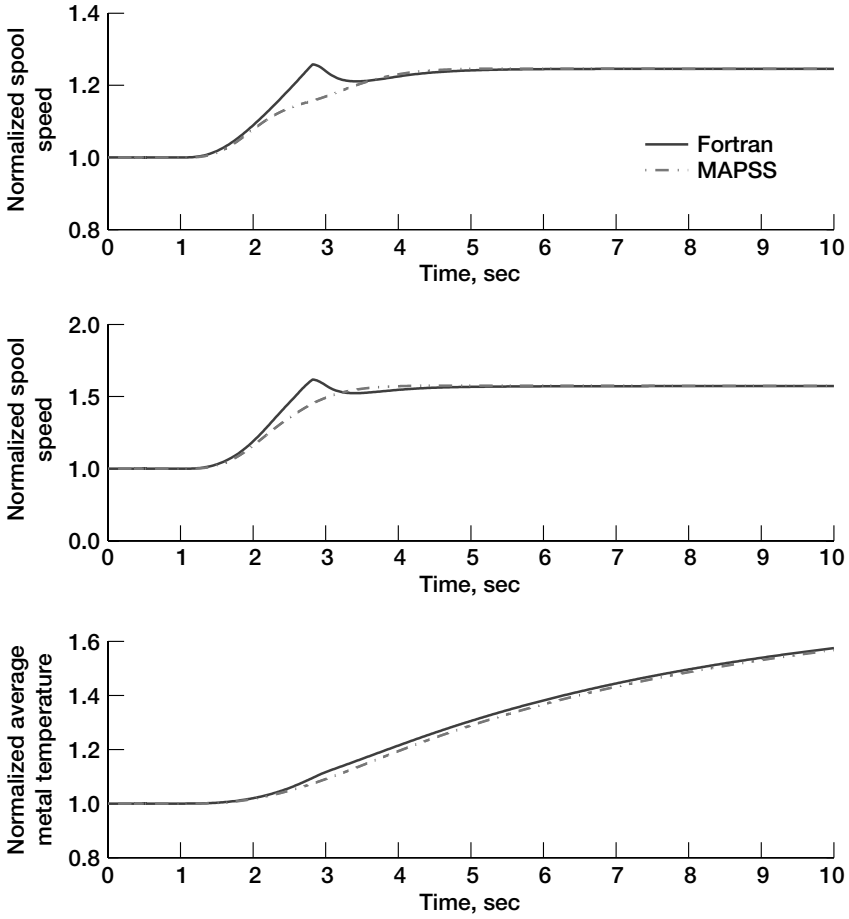

Very good closed-loop comparison between Fortran and MAPSS simulations. Top: Low-pressure spool speed. Center: High-pressure spool speed. Bottom: Average metal temperature between combustor and nozzle.

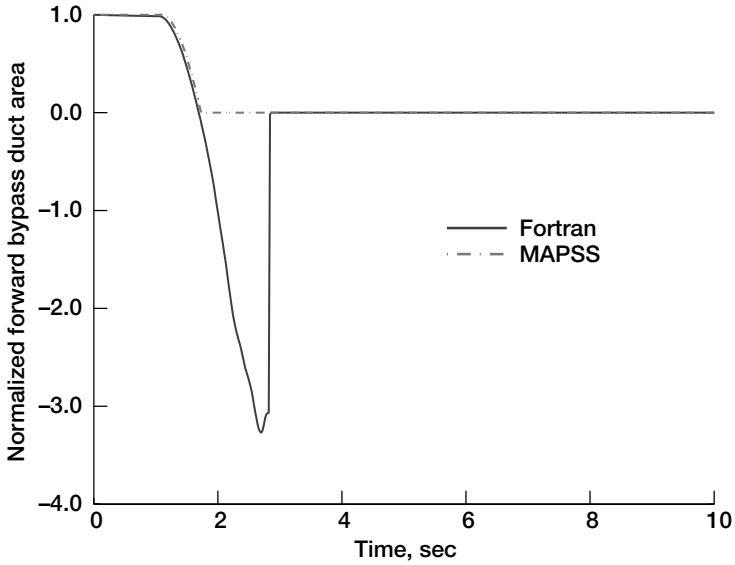

Negative flow prevention in a bypass duct inlet for power lever angles greater than 35°.

emulates the functionality of a digital controller, which has a typical update rate of 50 Hz. The CLM module simulates the dynamics of the engine components and uses an update rate of 2500 Hz, which is needed to iterate to balance mass and energy among system components. The actuators in the CAD module use the same sampling rate as those in the CLM.

MAPSS was validated via open-loop and closed-loop comparisons with the Fortran simulation. The plots to the left show the normalized results of a closed-loop comparison looking at three states of the model: low-pressure spool speed, high-pressure spool speed, and the average metal temperature measured from the combustor to the high-pressure turbine. In steady state, the error between the simulations is less than 1 percent. During a transient, the difference between the simulations is due to a correction in MAPSS that prevents the gas flow in the bypass duct inlet from flowing forward instead of toward the aft end, which occurs in the Fortran simulation. The final graph is a comparison between MAPSS and the Fortran model of the bypass duct inlet flow for power lever angles greater than 35°.

Bibliography

Parker, Khary I.; and Guo, Ten-Heui: Development of a Turbofan Engine Simulation in a Graphical Simulation Environment. NASA/TM—2003-212543, 2003. http://gltrs.grc.nasa.gov/cgi-bin/GLTRS/browse.pl?2003/TM-2003-212543.html

Find out more about Intelligent Life Extending Control:
http://www.grc.nasa.gov/WWW/cdtb/projects/ilec/

Glenn contact:
Khary I. Parker, 216–433–8442, Khary.I.Parker@nasa.gov

Authors:
Khary I. Parker and Dr. Ten-Huei Guo

Headquarters program office: OAT

Programs/Projects: ICDPS/ICD

Starting Vortex Identified as Key to Unsteady Ejector Performance

Unsteady ejectors are currently under investigation for use in some pulse-detonation-engine-based propulsion systems. Experimental measurements made in the past, and recently at the NASA Glenn Research Center, have demonstrated that thrust augmentation can be enhanced considerably when the driver is unsteady. In ejector systems, thrust augmentation ϕ is defined as $\phi = T^{Total}/T^{j}$, where T^{Total} is the total thrust of the combined ejector and driving jet and T^{j} is the thrust due to the driving jet alone.

The exact mechanism behind the enhanced performance is unclear; however, it is believed to be related to the powerful vortex emitted with each pulse of the unsteady driver. As such, particle imaging velocimetry (PIV) measurements were obtained for three unsteady drivers: a pulsejet, a resonance tube, and a speaker-driven jet. All the drivers were tested with ejectors, and all exhibited performance enhancement over similarly sized steady drivers. The characteristic starting vortices of each driver are shown in these images. The images are color contours of measured instantaneous vorticity. Each image is an ensemble-average of at least 150 phase-locked measurements. The flow is from right to left. The shape and location of each driver is shown on the far right of each image. The rectangle shown in each image represents the ejector diameter that was found experimentally to yield the highest thrust augmentation. It is apparent that the optimal ejector diameter is that which just "captures" the vortex: that is, the diameter bounding the outermost edge of the vortex structure.

Although not shown, it was observed that the emitted vortex spread as it traveled downstream. The spreading rate for the pulsejet is shown as the dashed lines in the top image. A tapered ejector was fabricated that matched this shape. When tested, the ejector demonstrated superior performance to all those previously tested at Glenn (which were essentially of straight, cylindrical form), achieving a remarkable thrust augmentation of 2. The measured thrust augmentation is shown in the graph on the next page as a function of ejector length. Also shown on the plot are the thrust augmentation values achieved with the straight, cylindrical ejectors of varying diameters.

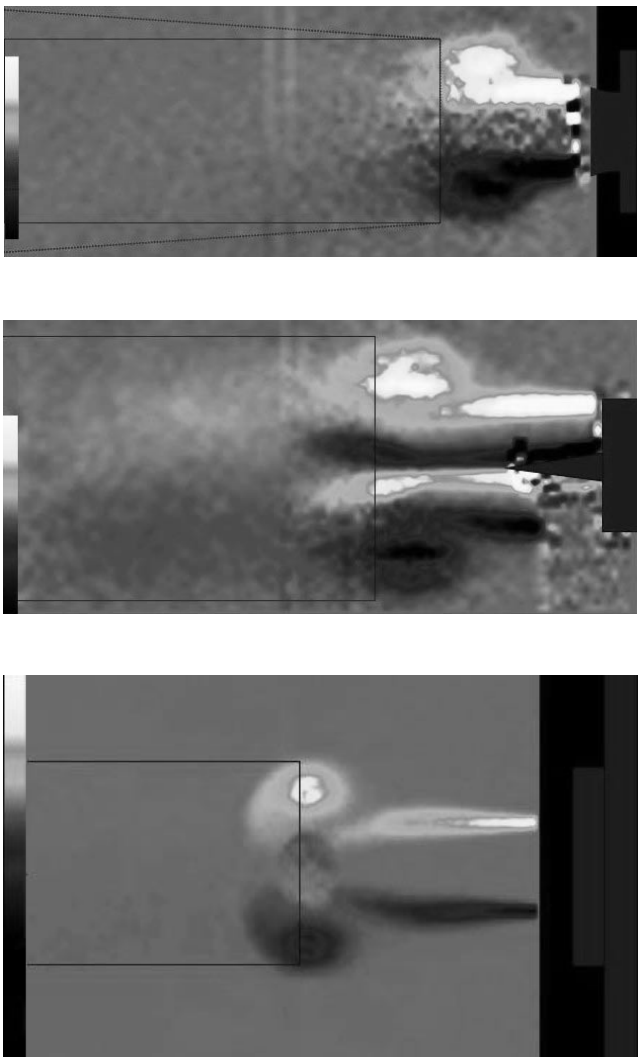

Ensemble-averaged contours of measured instantaneous vorticity for three pulsed thrust sources. Measurements were made using digital particle imaging velocimetry. These images are shown in color in the online version of this article (http://www.grc.nasa.gov/WWW/RT/5000/5530paxson.html). Top: 220-Hz pulsejet. Center: 275-Hz resonance tube. Bottom: 50-Hz speaker-driven jet.

That the cross-sectional dimensions of optimal ejectors scaled precisely with the vortex dimensions on three separate pulsed thrust sources demonstrates that the action of the vortex is responsible for the enhanced ejector performance. The result also suggests that, in the absence of a complete understanding of the entrainment and augmentation mechanisms, methods of characterizing starting vortices may be useful for correlating and predicting unsteady ejector performance.

Bibliography

Paxson, Daniel E.; Wilson, Jack; and Dougherty, Kevin T.: Unsteady Ejector Performance: An Experimental Investigation Using a Pulsejet Driver. AIAA Paper 2002–3915 (NASA/TM—2002-211711), 2002. http://gltrs.grc.nasa.gov/cgi-bin/GLTRS/browse.pl?2002/TM-2002-211711.html

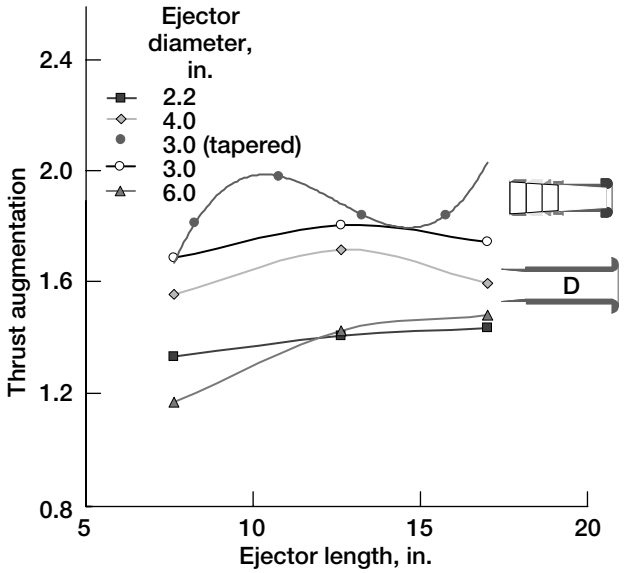

Measured thrust augmentation as a function of ejector length for the tapered and straight ejectors. Each curve represents a different ejector diameter. The driver is a pulsejet.

Wilson, Jack; Paxson, Daniel E.; and Dougherty, Kevin T.: Unsteady Ejector Performance: An Experimental Investigation Using Resonance Tube Driver. AIAA Paper 2002–3632 (NASA/TM—2002-211474), 2002. http://gltrs.grc.nasa.gov/cgi-bin/GLTRS/browse.pl?2002/TM-2002-211474.html

John, Wentworth T.; Paxson, Daniel; and Wernet, Mark P.: Conditionally Sampled Pulsejet Driven Ejector Flow Field Using DPIV. AIAA–2002–3231, 2002.

Paxson, D.; Wernet, M.; and John, W.: An Experimental Investigation of Unsteady Thrust Augmentation Using a Speaker-Driven Jet. AIAA–2004–0092, 2004.

Glenn contact:
Dr. Daniel E. Paxson, 216–433–8334, Daniel.E.Paxson@nasa.gov

Author: Dr. Daniel E. Paxson

Headquarters program office: OAT

Programs/Projects:
Propulsion and Power, Pulse Detonation Engine Technology

Strategy Developed for Selecting Optimal Sensors for Monitoring Engine Health

Sensor indications during rocket engine operation are the primary means of assessing engine performance and health. Effective selection and location of sensors in the operating engine environment enables accurate real-time condition monitoring and rapid engine controller response to mitigate critical fault conditions. These capabilities are crucial to ensure crew safety and mission success. Effective sensor selection also facilitates postflight condition assessment, which contributes to efficient engine maintenance and reduced operating costs. Under the Next Generation Launch Technology program, the NASA Glenn Research Center, in partnership with Rocketdyne Propulsion and Power, has developed a model-based procedure for systematically selecting an optimal sensor suite for assessing rocket engine system health. This optimization process is termed the systematic sensor selection strategy.

Engine health management (EHM) systems generally employ multiple diagnostic procedures including data validation, anomaly detection, fault-isolation, and information fusion. The effectiveness of each diagnostic component is affected by the quality, availability, and compatibility of sensor data. Therefore systematic sensor selection is an enabling technology for EHM.

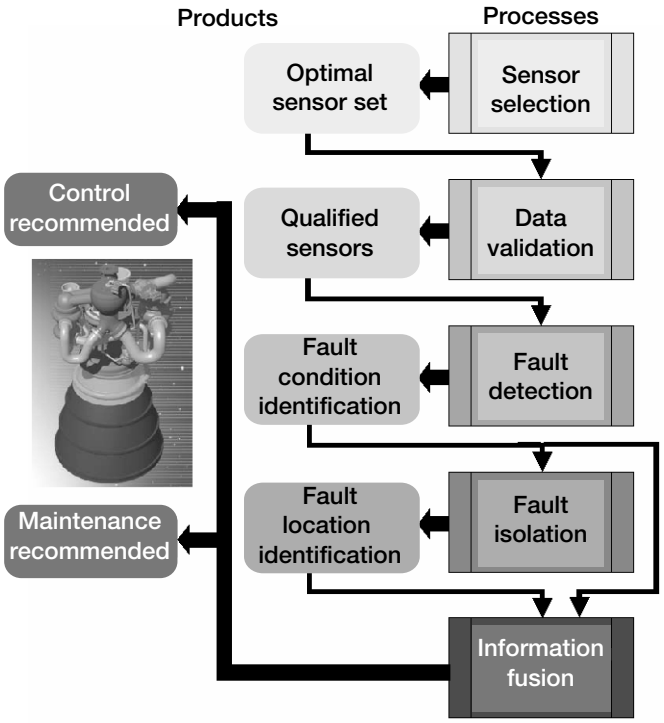

Sensor selection enables diagnostics for engine health management.

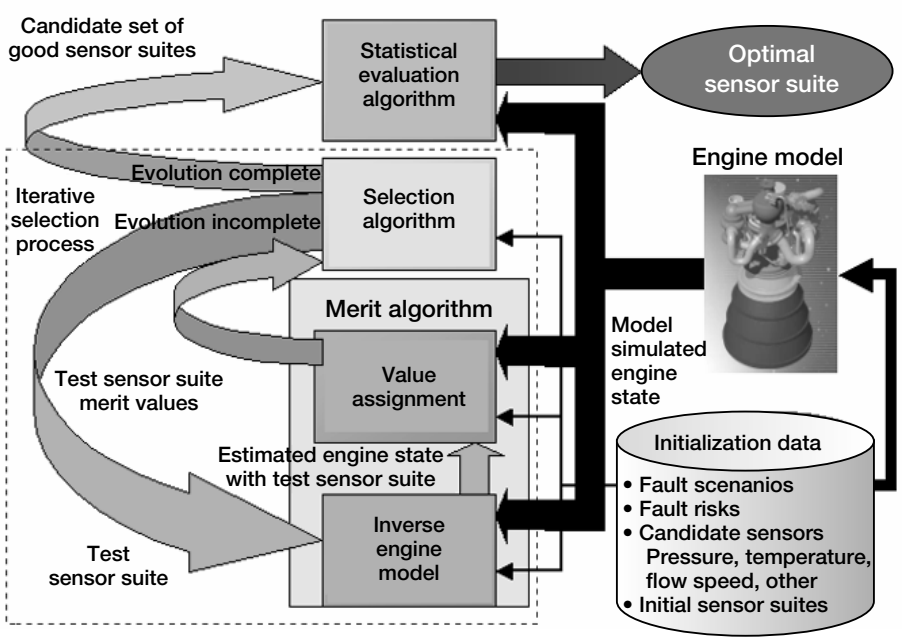

Systematic sensor selection strategy.

Information in three categories is required by the systematic sensor selection strategy. The first category consists of targeted engine fault information; including the description and estimated risk-reduction factor for each identified fault. Risk-reduction factors are used to define and rank the potential merit of timely fault diagnoses. The second category is composed of candidate sensor information; including type, location, and estimated variance in normal operation. The final category includes the definition of fault scenarios characteristic of each targeted engine fault. These scenarios are defined in terms of engine model hardware parameters. Values of these parameters define engine simulations that generate expected sensor values for targeted fault scenarios. Taken together, this information provides an efficient condensation of the engineering experience and engine flow physics needed for sensor selection.

The systematic sensor selection strategy is composed of three primary algorithms. The core of the selection process is a genetic algorithm that iteratively improves a defined quality measure of selected sensor suites. A merit algorithm is employed to compute the quality measure for each test sensor suite presented by the selection process. The quality measure is based on the fidelity of fault detection and the level of fault source discrimination provided by the test sensor suite. An inverse engine model, whose function is to derive hardware performance parameters from sensor data, is an integral part of the merit algorithm. The final component is a statistical evaluation algorithm that characterizes the impact of interference effects, such as control-induced sensor variation and sensor noise, on the probability of fault detection and isolation for optimal and near-optimal sensor suites.

The strategy outlined herein is an advanced technique for specifying sensor types and reference locations that optimize the fidelity of EHM diagnostics. It is currently being used to enable robust health diagnostics for engine systems being developed under the Next Generation Launch Technology program. Extension of the selection technique to consider sensor response times in the overall suite quality measure is planned.

Glenn contact:
Louis M. Santi, 216–433–3521,
Louis.M.Santi@grc.nasa.gov

Authors:
Louis M. Santi and Thomas S. Sowers

Headquarters program office: OAT

Programs/Projects: NGLT

Communications Technology

Advanced Communications Architecture Demonstration Made Significant Progress

The Advanced Communications Architecture Demonstration (ACAD) is a concept architecture to provide high-rate Ka-band (27-GHz) direct-to-ground delivery of payload data from the International Space Station. This new concept in delivering data from the space station targets scientific experiments that buffer data onboard. The concept design provides a method to augment the current downlink capability through the Tracking Data Relay Satellite System (TDRSS) Ku-band (15-GHz) communications system. The ACAD concept pushes the limits of technology in high-rate data communications for space-qualified systems. Research activities are ongoing in examining the various aspects of high-rate communications systems including (1) link budget parametric analyses, (2) antenna configuration trade studies, (3) orbital simulations (figure to the left), (4) optimization of ground station contact time (top graph on next page), (5) processor and storage architecture definition, and (6) protocol evaluations and dependencies.

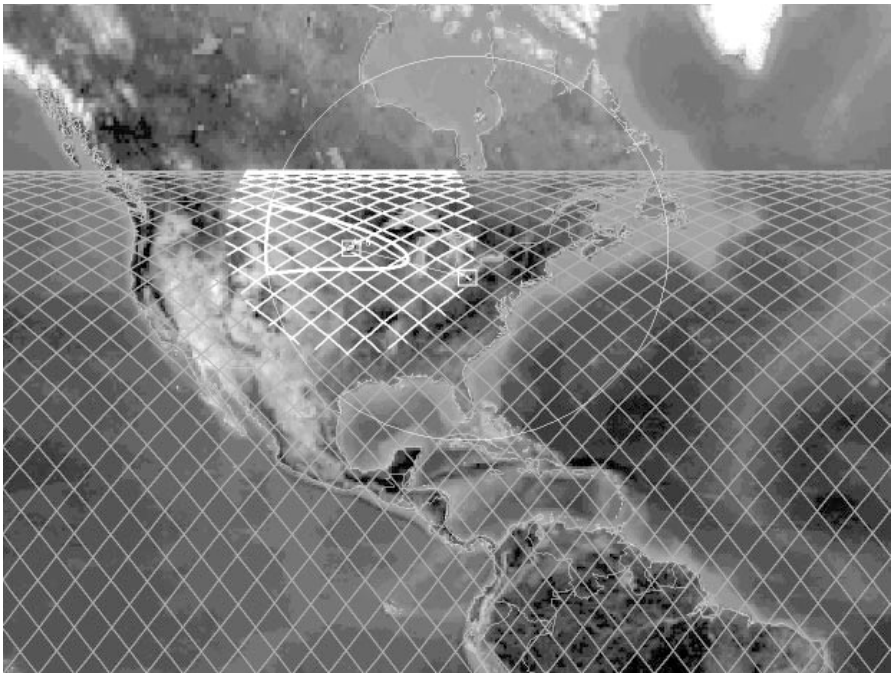

Access simulation for a sample ground station.

Current satellite communications research efforts are focusing on delivering data at high transmission rates to accommodate increased data volume needs. However, the technology available for NASA missions still appears to be limited when data transmission rates are above 150 million bits per second (Mbps). ACAD provides a system capable of delivering high-rate data at an information rate of at least 622 Mbps, and coding and protocol overhead can easily drive the required modulation to gigabit rates. ACAD focuses on assessing the state of the art in high-rate, space-qualified communication systems and is pushing to close existing technology gaps.

Although packet-based protocols such as Transmission Control Protocol/Internet Protocol (TCP/IP) have become pervasive in terrestrial communications systems, inefficiencies may exist when they are used over satellite networks. Several findings

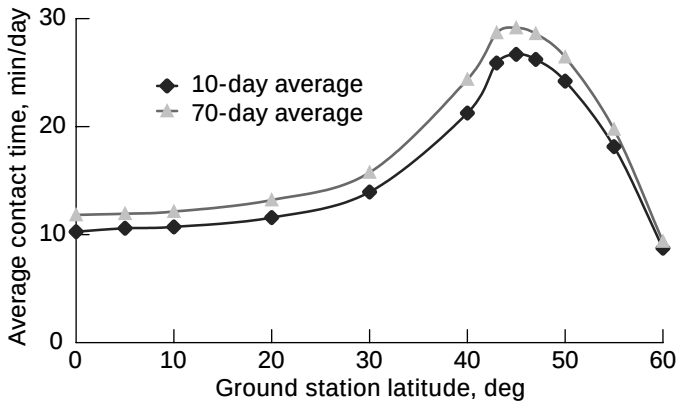

Ground station latitude versus average contact time.

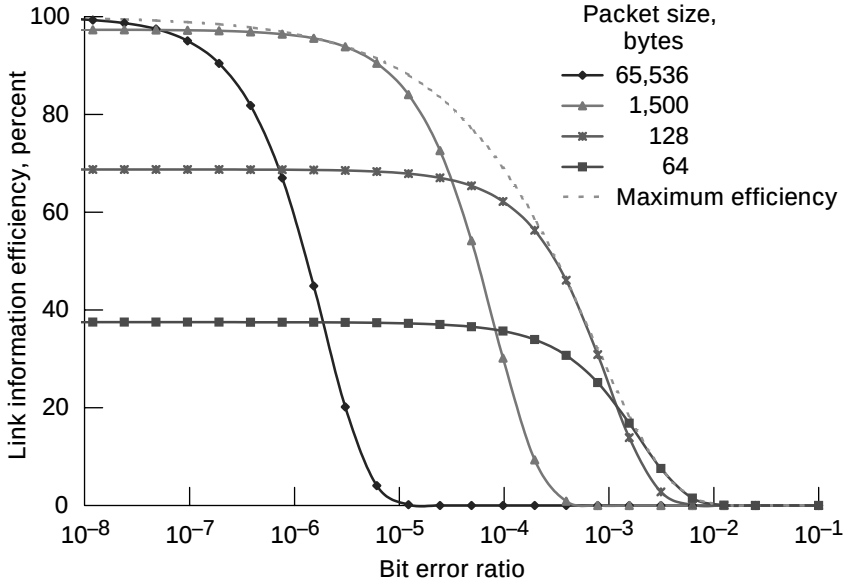

Link bit error ratio versus information efficiency.

were made regarding the implications of these protocols when used over highly bandwidth asymmetric radio networks with high error conditions. As part of this effort, formulations have been derived to optimize the efficiency of packet-based protocols by tuning packet sizes on the basis of link conditions (see the bottom graph). These findings have wide application to both low-Earth-orbit satellite communications architectures and aeronautics communications architectures.

Satellite communications systems are typically designed to provide a link margin for the worst-case scenario. However, the findings uncovered with this research may allow future systems to be designed with less margin, thereby conserving spacecraft power as well as reducing signal interference. In addition, these findings can be applied to standards-based protocols to allow communications to be maintained under much worse error conditions than have been permissible in the past.

The ACAD project is managed under the Space Communications Applied Systems & Technologies Program of the Space Communications Office and is being developed as a collaborative team effort among members of the Space Communications Office and researchers in the NASA Glenn Research Center's Communications Technology Division, including its Satellite Networks and Architectures Branch.

Find out more about this research:
http://ctd.grc.nasa.gov/5610/5610.html

Glenn contact:
David Andrew Carek, 216–433–8396,
David.A.Carek@nasa.gov

Author: David Andrew Carek

Headquarters program office: OSF

Programs/Projects:
ISS, Earth Science, space shuttles

Internet-Protocol-Based Satellite Bus Architecture Designed

NASA is designing future complex satellite missions ranging from single satellites and constellations to space networks and sensor webs. These missions require more interoperability, autonomy, and coordination than previous missions; in addition, a desire exists to have scientists retrieve data directly from the satellite rather than a central distribution source. To meet these goals, NASA has been studying the possibility of extending the Transmission Control Protocol/Internet Protocol (TCP/IP) suite for space-based applications.

The objective of this research at the NASA Glenn Research Center was to develop a generic IP-based satellite bus architecture as shown in the diagram. The onboard architecture includes command and control, housekeeping, and science instruments to take measurements and data recorders to store the data until download. The bus also provides a standard interface to connect each of these components. The goal was to leverage the advances made in the terrestrial Internet while providing a flexible architecture to meet the requirements of different satellite missions.

IP can provide a number of benefits for a satellite mission. First, IP can provide end users with simple access to satellite platforms using standard terrestrial Internet tools (e.g., telnet, ftp, ssh, scp, etc.). Second, IP can permit the integration of heterogeneous platforms by standardizing the communication protocols. These platforms can be developed by universities, foreign governments, or private industries. Finally, it can free NASA from developing and maintaining the communication infrastructure and allow the agency to focus on new missions. NASA will have the flexibility to incorporate research by universities, private industries, and other Government agencies.

Using terrestrial Internet concepts, the generic bus contains four different subnets, as follows: (1) the Satellite Status & Maintenance Subnet, which contains the command, control, and housekeeping instruments; (2) the Instrument Subnet, which contains the science instruments; (3) the Recorder Subnet, which is the central repository for the data collected by the satellite for download; and (4) Additional Subnet(s), which represents one or more subnet(s) that are needed to meet specific mission requirements.

Leveraging terrestrial security concepts, the architecture includes both a firewall and a router. The firewall scrutinizes packets on the basis of rules implemented by the missions (e.g., IP addresses or port numbers). The router is responsible for routing data packets to their correct destination, keeping the satellite and instrument commands on separate subnets. Together, these components function as the interface between the local onboard network and the ground. All communications are required to pass through this interface before reaching any module on the satellite. If additional security is required, the mission can implement a Virtual Private Network between the ground and satellite.

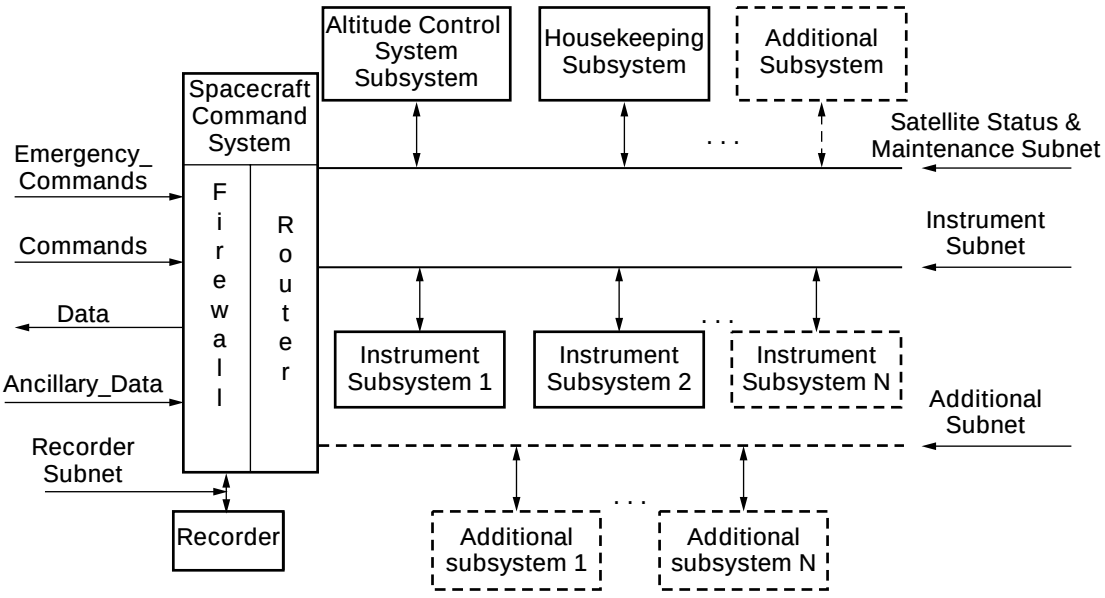

Generic satellite bus architecture.

Although this study focused on the satellite bus architecture, it, along with other NASA research, shows that true IP connectivity from the ground station to the satellite is a possibility. However, a detailed design is needed for the bus architecture to ensure that each component can be easily and seamlessly integrated. Then, the design must be applied to more complex missions that are coming on the horizon.

Find out more about this research:
http://ctd.grc.nasa.gov/5610/5610.html

Glenn contact:
Rich Slywczak, 216–433–3493,
Richard.A.Slywczak@nasa.gov

Author: Richard A. Slywczak

Headquarters program office:
OSF (SCDS)

Programs/Projects: Earth Sciences

Silicon-Germanium Films Grown on Sapphire for Ka-Band Communications Applications

NASA's vision in the space communications area is to develop a broadband data network in which there is a high degree of interconnectivity among the various satellite systems, ground stations, and wired systems. To accomplish this goal, we will need complex electronic circuits integrating analog and digital data handling at the Ka-band (26 to 40 GHz). The purpose of this project is to show the feasibility of a new technology for Ka-band communications applications, namely silicon germanium (SiGe) on sapphire. This new technology will have several advantages in comparison to the existing silicon-substrate-based circuits. The main advantages are extremely low parasitic reactances that enable much higher quality active and passive components, better device isolation, higher radiation tolerance, and the integration of digital and analog circuitry on a single chip.

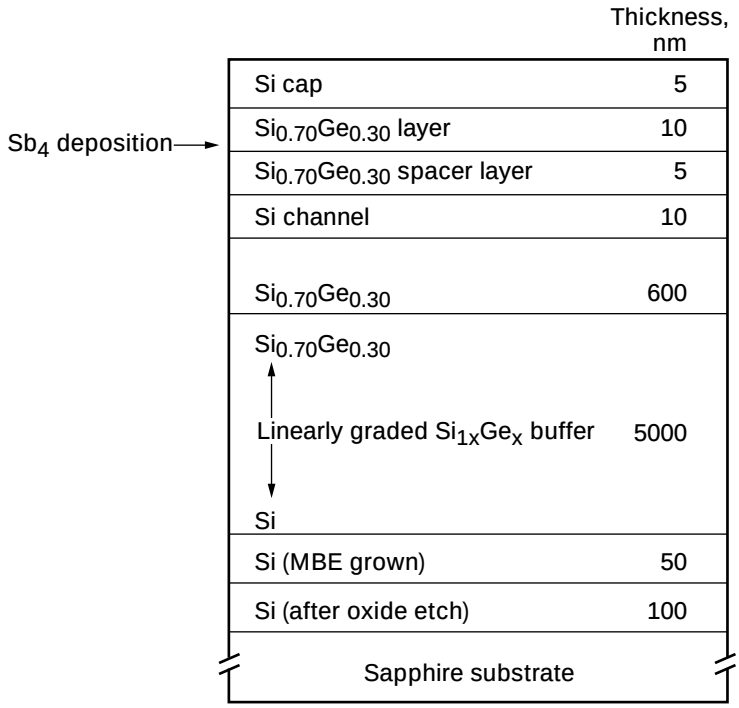

Schematic diagram of SiGe transistor structure on a sapphire substrate, including the virtual SiGe substrate, the graded buffer, and the top active channel layers.

Specifically, the purpose of this research was to grow, for the first time, SiGe films on sapphire suitable for electron conduction transistors and to evaluate whether or not the quality of these films will prove adequate for high-frequency applications. To date, these films have not been reported in the literature for SiGe electronic conduction devices at any frequency. All the work except the molecular beam epitaxy (MBE) step was performed at the NASA Glenn Research Center. MBE growth was done at HRL Laboratories LLC.

Actual work included three steps: device modeling, material fabrication, and material characterization. The first step in the work was the modeling of various SiGe film structures and transistors for their Ka-band performance. The results of this step set the starting values for the layer structure needed for the SiGe transistor and the required electron mobility for Ka-band operation, namely a mobility of at least 700 cm^2/V-sec. The fabrication step included substrate preparation and MBE film growth. Researchers started

with 4-in. commercial silicon-on-sapphire wafers. Then, the top Si layer on each wafer was amorphized, recrystallized, and thinned down to roughly 100 nm. The MBE growth used several buffer layers and virtual substrates, with one example of a final structure shown in the diagram on the preceding page. Several structures were investigated in this study. In the characterization step, the following techniques were used: Hall effect, high-resolution x-ray diffractometry, secondary ion mass spectroscopy, atomic force microscopy, and transmission electron microscopy. The results showed high-quality crystalline SiGe and strained Si active layers, with the correct dopings and Ge concentrations. Most importantly, measurements at room temperature showed electron mobilities as high as 1300 cm^2/V-sec. This result proved that this material is now ready to be used for SiGe transistors working in the Ka-band and fabricated on sapphire substrates.

Glenn contact:
Dr. Samuel A. Alterovitz, 216–433–3517, Samuel.A.Alterovitz@nasa.gov

Analex contact:
Dr. Carl H. Mueller, 216–433–8853, Carl.H.Mueller@grc.nasa.gov

Authors:
Dr. Samuel A. Alterovitz, Dr. Carl H. Mueller, and Dr. Edward T. Croke

Headquarters program office: DDF

Programs/Projects:
Space Communications

Bibliography

Mueller, C.H.; Croke, E.T.; and Alterovitz, S.A.: High Electron Mobility in SiGe/Si n-MODFET Structures on Sapphire Substrates. Electron. Lett., vol. 39, no. 18, 2003, pp. 1353–1354.

High-Temperature Probe Station Developed to Characterize Microwave Devices Through 500 °C

A high-temperature measurement system capable of performing on-wafer microwave testing of semiconductor devices has been developed at the NASA Glenn Research Center. This high-temperature probe station can characterize active and passive devices and circuits at temperatures ranging from room temperature to above 500 °C. The heating system uses a ceramic heater mounted on an insulating block of NASA shuttle tile material. The temperature is adjusted by a simple graphical computer interface and is automatically controlled by the software-based feedback loop. The system is used with a Hewlett-Packard 8510C Network Analyzer (Palo Alto, CA) to measure scattering parameters over a frequency range of 1 to 50 GHz. The microwave probes, cables, and inspection microscope are all shielded to protect from heat damage. The high-temperature probe station has been used successfully to characterize gold transmission lines on silicon carbide (SiC) at temperatures up to 540 °C.

Photograph of high-temperature probe station and instrumentation.

The ability to perform microwave tests at high temperatures is becoming necessary. There is now a need for sensors and communication circuits that can operate at 500 °C and above for aircraft engine development and monitoring during flight. To address this need, researchers have fabricated devices using wide bandgap semiconductors such as SiC with targeted operating temperatures of 500 to 600 °C. However, the microwave

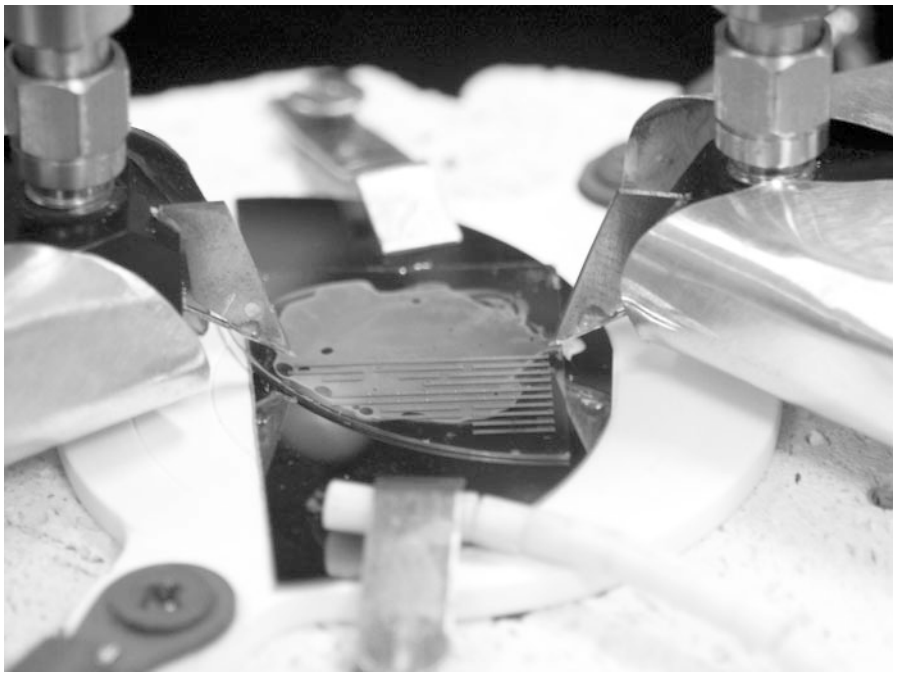

Microwave probes and test circuit on heater.

properties of these devices often change drastically with temperature, so any designs that are intended to be used in such an environment must be characterized at high temperatures. For some reliability, lifetime, and direct-current testing, the device under test can be packaged and characterized in an oven. However, for RF and microwave measurements, it is usually not possible to establish a calibrated reference plane at the device terminals within a package. In addition, the characteristics of the package would vary over a 500 °C temperature range, and this would have to be accounted for when the data were analyzed. A high-temperature probe station allows circuits and devices to be characterized through on-wafer measurements across a broad temperature range with a known reference plane.

The conventional, commercially available thermal wafer-probe stations that are used to evaluate microwave devices across a controlled temperature range have a typical upper limit of 200 °C. Standalone thermal heating chucks are available with an extended upper temperature range of 300 to 400 °C. To effectively characterize devices at temperatures up to and surpassing 500 °C, Glenn researchers developed a custom probe station. In the past, custom probe stations have been developed to test devices under other extreme environments, such as cryogenic temperatures as low as 37 K. Similarly, this custom probe station was specifically modified for high-temperature use. It allows devices to be measured quickly and flexibly, without the use of wire bonds and test fixtures.

Glenn contact:
Alan N. Downey, 216–433–3508, Alan.N.Downey@nasa.gov

Authors: Alan N. Downey and Zachary D. Schwartz

Headquarters program office: OAT

Programs/Projects:
UEET, Intelligent Propulsion Controls

Novel Biomedical Device Utilizing Light-Emitting Nanostructures Developed

A novel biomedical device is being developed at the NASA Glenn Research Center in cooperation with the University of Michigan. This device uses nanostructured quantum dots that emit light in the near-infrared (IR) region. The nanostructured quantum dots are used as a source and excite fluorochrome polymers coupled with antibodies that seek out and attach to specific bacteria and viruses. The fluorochrome polymers/antibodies fluoresce at specific wavelengths in the near-IR spectrum, but these wavelengths are offset from the excitation wavelength and can be detected with a tunable spectrometer. The device will be used to detect the presence of viruses and bacteria in simple fluids and eventually in more complex fluids, such as blood.

Current state-of-the-art devices are limited to single bacteria or virus detection and a considerable amount of time and effort is required to prepare samples for analysis. Most importantly, the devices are quite large and cumbersome, which prohibits them from being used on the International Space Station and the space shuttles. This novel device uses nanostructured quantum dots which, through molecular beam epitaxy and highly selective annealing processes, can be developed into an illumination source that could potentially generate hundreds of specific wavelengths. As a result, this device will be able to excite hundreds of antibody/

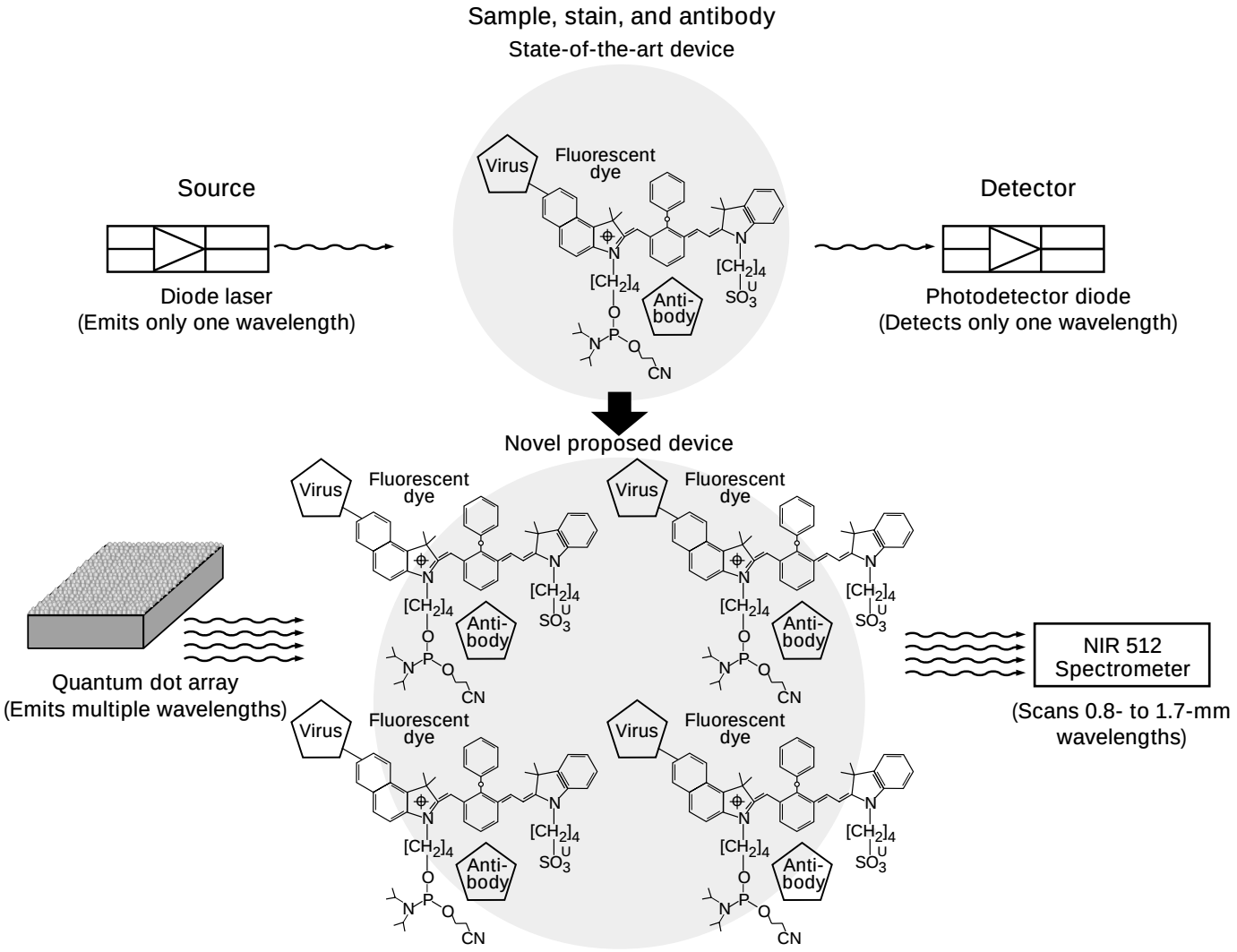

Novel biomedical device versus current state-of-the-art device.

fluorochrome polymer combinations, which in turn could be used to detect hundreds of bacteria and viruses in fluids (see the figure). A novel sample preparation technique that exploits micromembrane filtration and centrifugation methods has been developed for this device. The technique greatly reduces the time required to prepare the sample and the amount of sample needed to perform an accurate and comprehensive analysis. Last, and probably most important, because of the nano-light-emitting source and the novel sample preparation technique, the overall size of the device could be reduced dramatically.

This device will serve as a nanoscale lab-on-a-chip for in situ microorganism detection and will enable tests to be performed on a time scale of minutes rather than days. Thus, it is ideally suited for monitoring the environmental conditions onboard the International Space Station and the space shuttles, thereby enhancing the safety of the astronauts. In addition, the device has important commercial applications, such as detecting the presence of bacteria and viruses in water at food- and beverage-processing centers, water treatment plants, and restaurants. Also, this technology has the potential to be used to detect bacteria and viruses in more complex fluids, such as blood—which in all likelihood would revolutionize blood analysis as it is performed today. This project was made possible through the Director's Discretionary Fund and is ongoing. In addition, this project provides funding to Dr. Rachel Goldman of the University of Michigan for the research and development of nanostructured quantum dots.

Glenn contact:
Max Scardelletti, 216–433–9704,
Maximilian.C.Scardelletti@nasa.gov

Authors: Maximilian C. Scardelletti and Dr. Rachel Goldman

Headquarters program office: OBPR

Programs/Projects: DDF

Flat Lens Focusing Demonstrated With Left-Handed Metamaterial

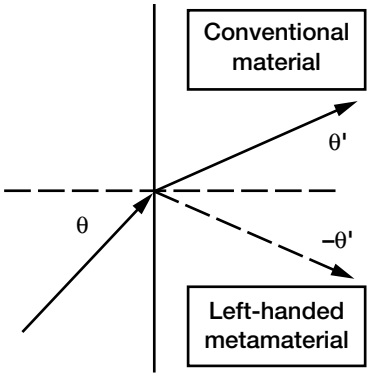

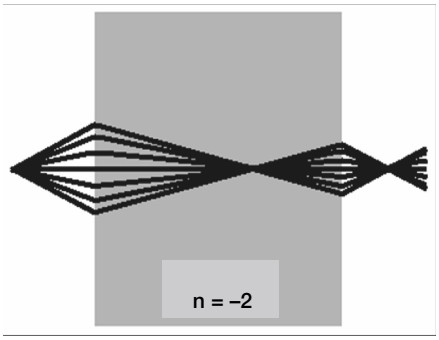

Left: An incident electromagnetic wave from free space entering a material at the boundary indicated by the lower left arrow refracts as shown by the solid upper right arrow when entering a conventional material and as shown by the dashed lower right arrow when entering a left-handed metamaterial. Right: Electromagnetic radiation is focused by a flat slab of left-handed metamaterial (n, index of refraction).

Left-handed metamaterials (LHM's) are a new media engineered to possess an effective negative index of refraction over a selected frequency range. This characteristic enables LHMs to exhibit physical properties never before observed. In particular, a negative index of refraction should cause electromagnetic radiation to refract or bend at a negative angle when entering an LHM, as shown in the figure above on the left. The right side of the figure above shows that this property could be used to bring radiation to a focus with a flat LHM lens. The advantage of a flat lens in comparison to a conventional curved lens is that the focal length could be varied simply by adjusting the distance between the lens and the electromagnetic wave source. In this in-house work, researchers at the NASA Glenn Research Center developed a computational model for LHMs with the three-dimensional electromagnetic commercial code Microwave Studio, constructed an LHM flat lens, and used it to experimentally demonstrate the reversed refraction and flat lens focusing of microwave radiation.

The LHM configuration is a periodic array of metallic rings and wires based on work by researchers at the University of California at San Diego (refs. 1 and 2). A schematic representation of an array is shown in the left side of the figure below, and a photograph of the flat lens array of LHM cells that we have constructed is shown on the right side. For microwave radiation at wavelengths about 10 times a cell length, this configuration provides negative effective values of electric permittivity and magnetic permeability, resulting in a negative value for the index of

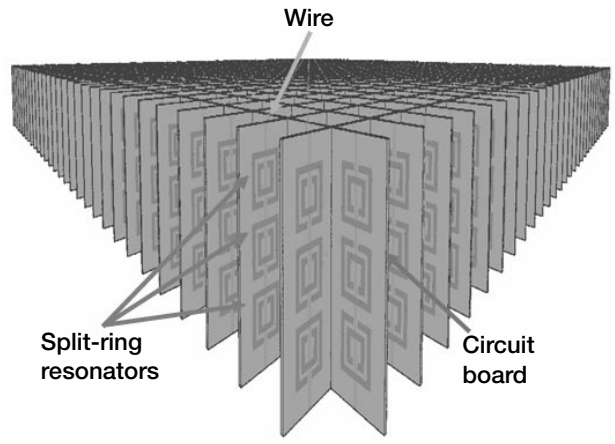

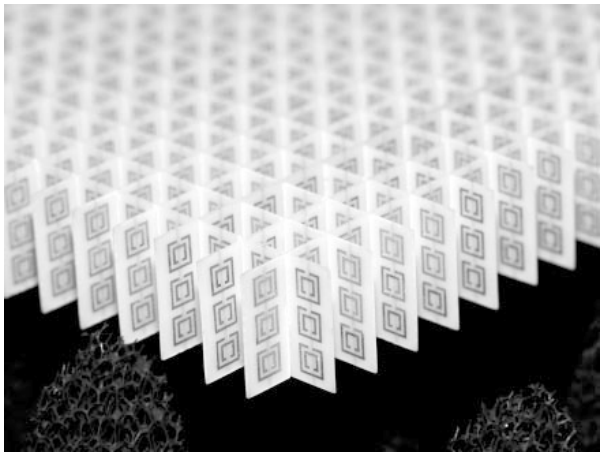

Left: Left-handed metamaterial array configuration consisting of copper split-ring resonators and wires mounted on interlocking sheets of fiberglass circuit board. Right: Left-handed metamaterial flat lens consisting of an array of 3 by 20 by 20 unit cells. With a unit cell width of 5 mm, this geometry shows reversed refraction and left-handed focusing properties at microwave frequencies between 10 and 11 GHz.

refraction. Preliminary testing has demonstrated a reversed refraction effect with focusing of the microwave radiation. Finite element models are being developed and an optics ray tracing code is being used to create new lens designs. We plan to create, design, and test other LHM configurations that are more amenable for operation at higher frequencies and investigate applications of a flat lens for biomedical imaging and detection and other applications.

References

1. Smith, D.R., et al.: Composite Medium With Simultaneously Negative Permeability and Permittivity. Phys. Rev. Lett., vol. 84, no. 18, 2000, pp. 4184–4187.
2. Shelby, R.A., et al.: Microwave Transmission Through a Two-Dimensional, Isotropic, Left-Handed Metamaterial. Appl. Phys. Lett., vol. 78, no. 4, 2001, pp. 489–491.

Find out more about this research:
http://microgravity.grc.nasa.gov/grcbio/SRF.html

Glenn contact:
Dr. Jeffrey D. Wilson, 216–433–3513, Jeffrey.D.Wilson@nasa.gov

Authors:
Dr. Jeffrey D. Wilson, Zachary D. Schwartz, Christine T. Chevalier, Alan N. Downey, and Karl R. Vaden

Headquarters program office: DDF

Programs/Projects: BEGIN

Novel High-Voltage, High-Power Piezoelectric Transformer Developed and Demonstrated for Space Communications Applications

Improvements in individual piezoelectric transformer (PT) performance and the combination of these PTs in a unique modular topology under a Phase I contract with the NASA Glenn Research Center have enabled for the first time the simultaneous achievement of both high voltage and high power at much higher levels than previously obtained with any PT. Feasibility was demonstrated by a prototype transformer (called a Tap-Soner), which is shown in the photograph to the right as part of a direct-current to direct-current (dc-dc) converter having two outputs rated at 1.5 kV/5 W and 4.5 kV/20 W. The power density of 3.5 W/cm^3 is significantly lower than for magnetic transformers with the same voltage and power output. This development, which is being done under a Small Business Innovation Research (SBIR) contract by Face Electronics, LC (Norfolk, VA), is based on improvements in the materials and design of Face's basic patented Transoner-T3 PT, shown in the top left figure on the next page. The T3 PT is most simply described as a resonant multilayer transducer where electrical energy at the input section is efficiently mechanically coupled to the output section, which then vibrates in a fundamental longitudinal mode to generate a high gain in voltage. The piezoelectric material used is a modified lead-zirconium-titanate-based ceramic. One of the significant improvements in PT design was the incorporation of a symmetrical double input layer, shown in the top right figure on the next page, which eliminated the lossy bending vibration modes characteristic of a single input layer. The performance of the improved PT was optimized to 1.5 kV/5 W. The next step was devising a way to combine the individual PTs in a modular circuit topology needed to achieve the desired high voltage and power output. Since the optimum performance of the individual PT occurs at resonance, the most efficient operation of the modular transformer was

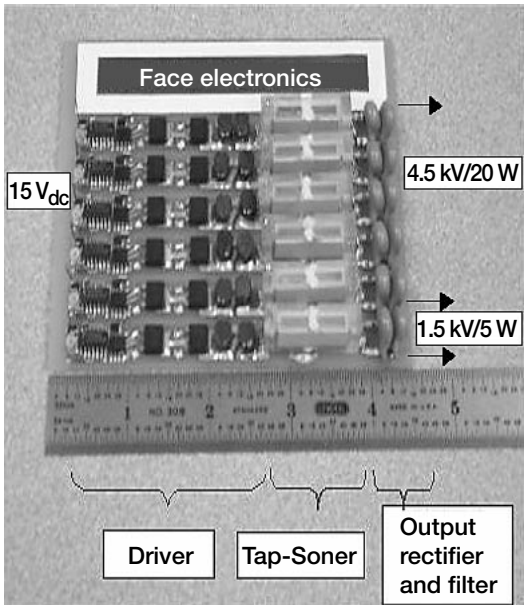

A dc-dc converter showing a prototype high-voltage, high-power piezoelectric transformer used to demonstrate the feasibility of a modular approach.

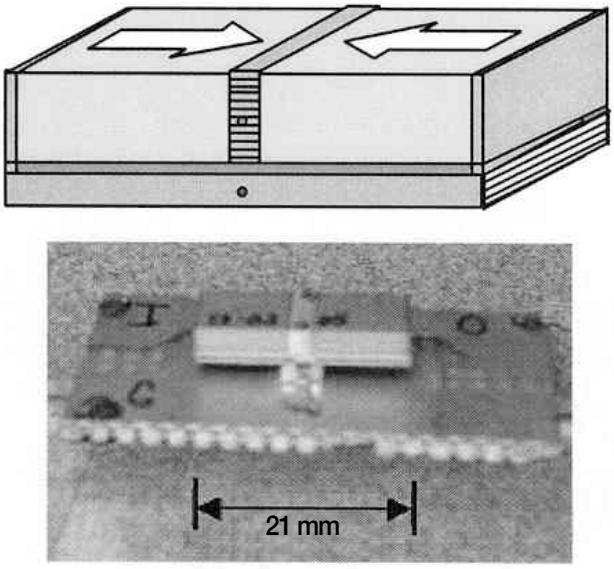

Basic Transoner piezoelectric transformer used as starting point for developing a modular high-voltage, high-power piezoelectric transformer.

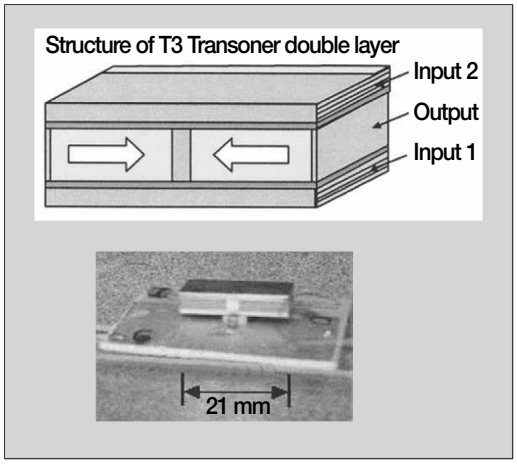

Improved double-layer, symmetric Transoner piezoelectric transformer.

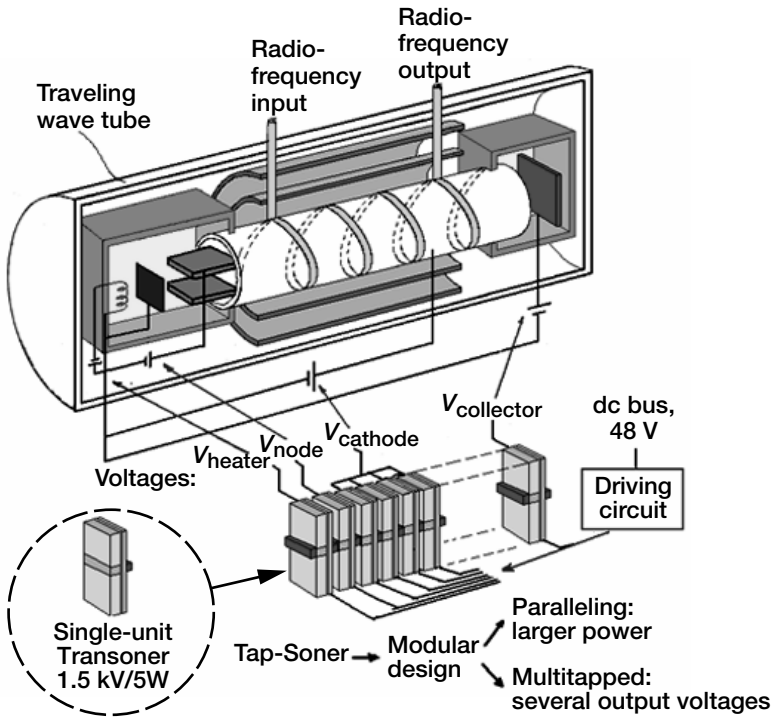

Operation of a traveling wave tube using a high-voltage, high-power piezoelectric transformer to replace the magnetic transformer in an electronic power conditioner.

achieved by using a separate drive circuit for each PT. The output section consists of a separate output rectifier for each PT connected in series.

Piezoelectric transformers are being developed as a potential replacement for the high-voltage, high-power magnetic transformers now used in power modules such as electronic power conditioners, as shown in the bottom figure, for traveling wave tubes used in space communications. Among the advantages offered by the piezoelectric transformer are significant reductions in mass and volume, no electromagnetic noise, and inherent high-voltage isolation. The performance goals of the current ongoing development are a 6-kV, 100-W four-output transformer, with an efficiency greater than 95 percent, suitable for operation in current state-of-the-art electronic power conditioners.

Find out more about this research:

Glenn's Communications Technology Division: http://ctd.grc.nasa.gov

The FACE Companies:
http://www.faceco.com

Glenn contact:
Edwin G. Wintucky, 216–433–3510, Edwin.G.Wintucky@nasa.gov

Face Electronics contact:
Dr. Alfredo V. Carazo (principal investigator), 757–624–2121, alfredo@fraeco.com

Author: Edwin G. Wintucky

Headquarters program office: OAT

Programs/Projects: Space Communications, electric propulsion

Field Effect Transistor Behavior in Electrospun Polyaniline/ Polyethylene Oxide Demonstrated

Novel transistors and logic devices based on nanotechnology concepts are under intense development. The potential for ultra-low-power circuitry makes nanotechnology attractive for applications such as digital electronics and sensors. For NASA applications, nanotechnology offers tremendous opportunities for increased onboard data processing, and thus autonomous decisionmaking ability, and novel sensors that detect and respond to environmental stimuli with little oversight requirements. Polyaniline/polyethylene oxide (PANi/PEO) nanofibers are of interest because they have electrical conductivities that can be changed from insulating to metallic by varying the doping levels and conformations of the polymer chain.

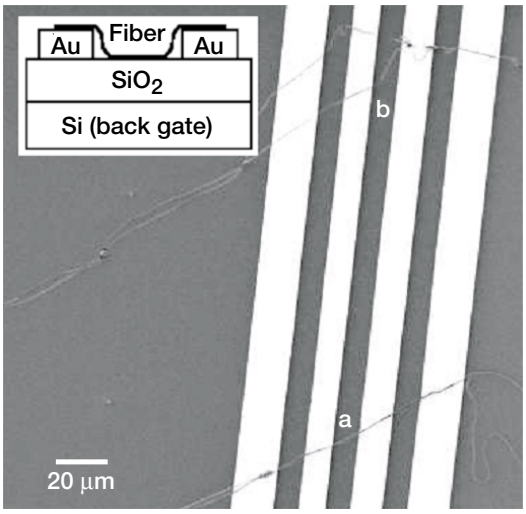

Scanning electron microscope image of electrospun PANi/PEO fibers over a prepatterned Si/SiO_2 substrate.

At the NASA Glenn Research Center, we have observed field effect transistor (FET) behavior in electrospun PANi/PEO nanofibers doped with camphorsulfonic acid. The nanofibers were deposited onto Au electrodes, which had been prepatterned onto oxidized silicon substrates. The scanning electron image to the right shows the device used in the transistor measurements. Saturation channel currents are observed at surprisingly low source/drain voltages (see the following graph). The hole mobility in the depletion regime is 1.4×10^{-4} $cm^2/V\cdot sec$, whereas the one-dimensional charge density (at zero gate bias) is calculated to be approximately 1 hole per 50 two-ring repeat units of polyaniline, consistent with the rather high channel conductivity (~10^{-3} S/cm). Reducing or eliminating the PEO content in the fiber is expected to enhance device parameters. Electrospinning is thus proposed as a simple method of fabricating one-dimensional polymer FET's.

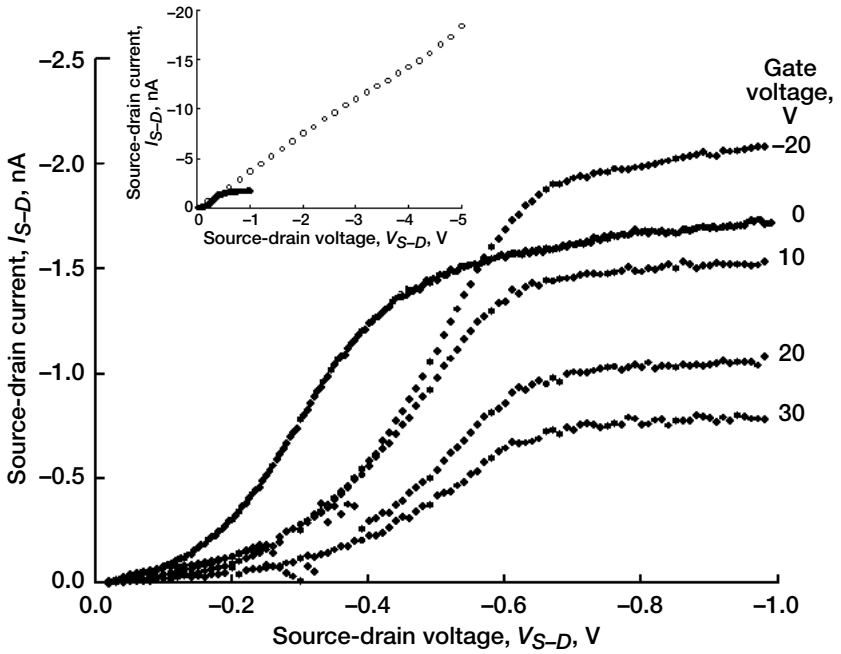

Current-voltage characteristics of the FET device. Inset: Current-voltage characteristics of the device with no applied back gate voltage.

Glenn contacts:
Noulie Theofylaktos, 216–433–2702, Onoufrios.Theofylaktos-1@nasa.gov; Daryl C. Robinson, 216–433–3553, Daryl.C.Robinson@nasa.gov; and Dr. Félix A. Miranda, 216–433–6589, Felix.A.Miranda@nasa.gov

Analex contact:
Dr. Carl H. Mueller, 216–433–8853, Carl.H.Mueller@grc.nasa.gov

Authors:
Dr. Carl H. Mueller, Onoufrios Theofylaktos, Daryl C. Robinson, and Dr. Félix A. Miranda

Headquarters program office: OAT

Programs/Projects: DDF, Space Science—such as Magnetospheric Constellation, Deep Space Probes (e.g., missions to Mars and Jupiter)

Robust Sliding Window Synchronizer Developed

The development of an advanced robust timing synchronization scheme is crucial for the support of two NASA programs—Advanced Air Transportation Technologies and Aviation Safety. A mobile aeronautical channel is a dynamic channel where various adverse effects—such as Doppler shift, multipath fading, and shadowing due to precipitation, landscape, foliage, and buildings—cause the loss of symbol timing synchronization.

Tests from a ground-based mobile vehicle through a geosynchronous communications satellite, using the EB200 direct-sequence spread spectrum modem, lost synchronization at a signal-to-noise ratio E_b/N_0 as high as 11 dB. At this signal-to-noise ratio, the modulations could still maintain an adequate bit error rate of about 1×10^{-6} if the synchronization was not lost.

Consequently, a novel non-data-aided symbol timing synchronizer for M-ary phase-shift-keying (MPSK) modulation schemes was studied at the NASA Glenn Research Center. It calculates the postdemodulation baseband signal energy in a sliding window. If the symbol timing is correct, the average signal energy will be the maximum. On the basis of this principle, the synchronizer detects the phase errors and/or frequency errors. The synchronizer structure is designed and simulated using MATLAB/Simulink. The following block diagram shows the robust sliding-window average (SWA) synchronizer. The *I* (in-phase) and *Q* (quadrature-phase) channel baseband signals are digitized by the analog-to-digital converter (ADC) and sent to two shift registers, respectively. The sampling clock is generated by the voltage-controlled oscillator (VCO), and the shift registers act as two simultaneous sliding windows. At the symbol rate, the *K* samples of *I* and *Q* channels in the window are summed and squared, and the results are added to form the signal *W*(*n*) at the adder output. When the local symbol clock and the incoming data symbol clock are synchronized, the output of the adder is the maximum. The control algorithm computes the control signal (+ or –) to send to the VCO as it attempts to obtain the maximum *W*(*n*).

A simulation model of the SWA synchronizer is shown in the diagram on the next page. The performance is evaluated in an added white gaussian noise (AWGN) channel. The synchronizer model consists of an eight-tap delay line for the *I* and *Q* baseband channels. The output of the delay line is summed and squared each sample time. Then, these data are added and fed into a serial-to-parallel converter. Each sample period, the parallel data are forwarded to the SWA of length 128. The data are then sent to the control algorithm, which in turn adjusts the VCO to achieve phase and frequency lock with the incoming data.

Simulations for 45° and 90° phase errors are shown in the graphs on the next page. The synchronizer can achieve phase lock for a ratio of symbol energy to noise energy E_s/N_0 as low as 0 dB ($E_b/N_0 = -3$ dB for quadrature phase shift keying, QPSK) with a convergence time less than 100 symbols. For comparison, when the old popular early-late-gate symbol timing synchronizer was simulated, the minimum working E_b/N_0 was 3 dB, which is 6 dB higher than for the SWA synchronizer with about the same convergence time. Because the sliding-window symbol timing synchronizer can work at a very low signal-to-noise ratio, the modem can work in unconventionally noisy environments, which include aeronautical satellite communications.

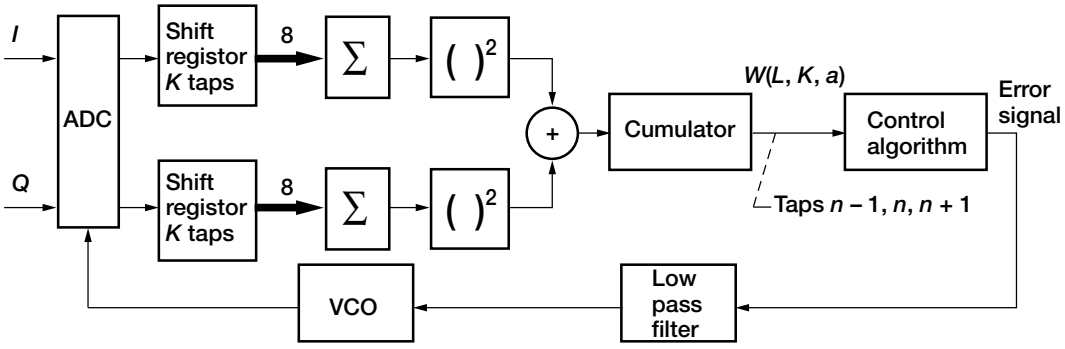

Sliding-window symbol synchronizer.

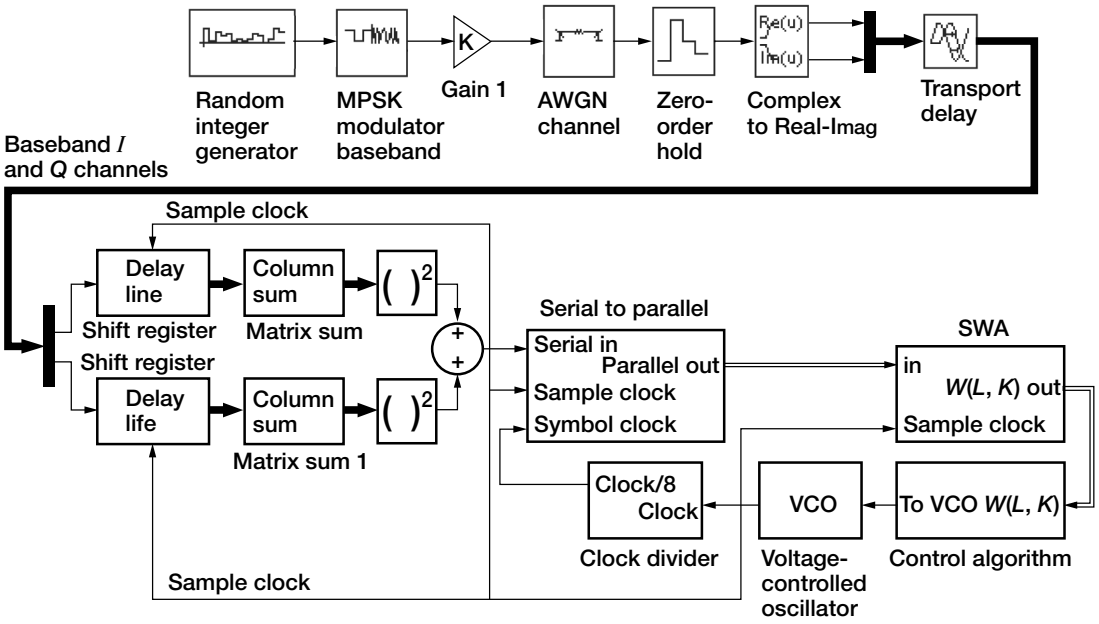

MATLAB-Simulink simulation program for the sliding-window symbol synchronizer.

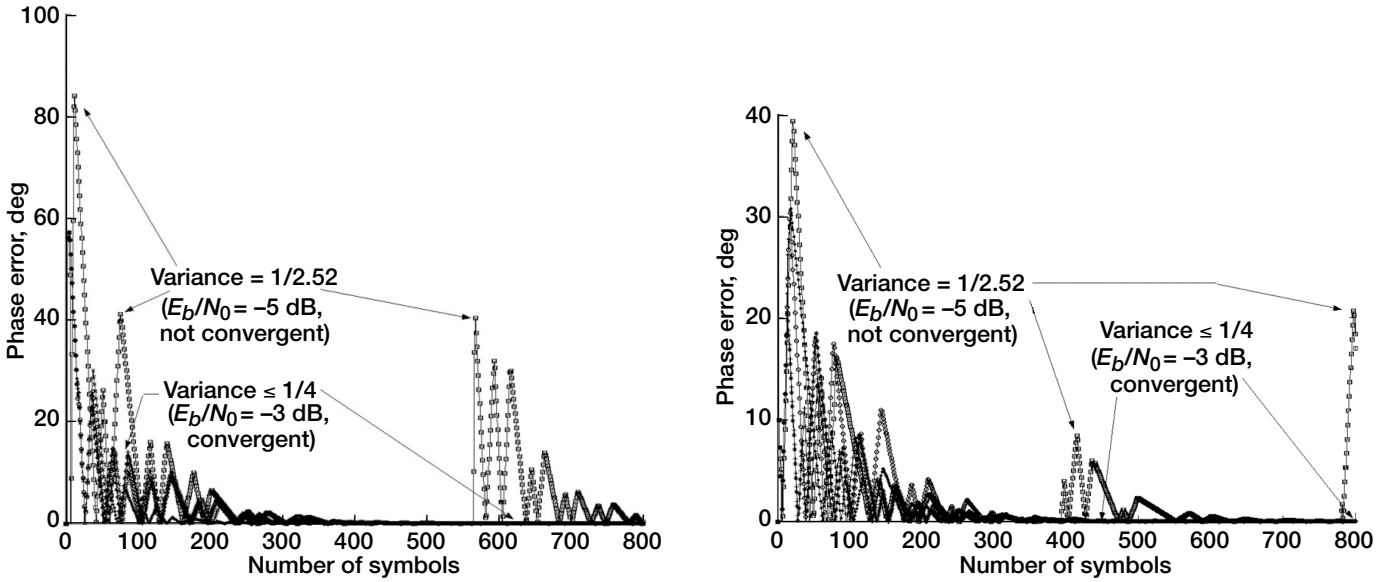

Left: Phase error versus symbol count for initial phase error of 1 tap (45°). Right: Phase error versus symbol count for initial phase error of 2 taps (90°).

Research on robust carrier synchronization and pseudonoise (PN) code acquisition and tracking is needed to further improve the robustness of a code division multiple access (CDMA) communications satellite for aeronautical applications. The SWS will be useful in the development of the new PN code tracking scheme. This research will support the newly initiated NASA Exploratory Technology for National Air Space (NExTNAS).

Glenn contact:
Kue S. Chun, 216–433–3624,
Kue.S.Chun@nasa.gov

Authors: Kue S. Chun, Fuqin Xiong, and Stanley Pinchak

Headquarters program office: OAT

Programs/Projects:
AATT, AvSP, NExTNAS

Space Network Devices Developed

The NASA Glenn Research Center through a contract with Spectrum Astro, Inc., has been developing space network hardware as an enabling technology using open systems interconnect (OSI) standards for space-based communications applications. The OSI standard is a well-recognized layered reference model that specifies how data should be sent node to node in a communications network. Because of this research and technology development, a space-qualifiable Ethernet-based network interface card (similar to the type found in a networked personal computer) and the associated four-port hub were designed and developed to flight specifications. During this research and development, there also have been many lessons learned for determining approaches for migrating existing spacecraft architectures to an OSI-network-based platform. Industry has recognized the benefits of targeting hardware developed around OSI standards such as Transmission Control Protocol/Internet Protocol (TCP/IP) or similar protocols for use in future generations of space communication systems. Some of these tangible benefits include overall reductions in mission schedule and cost and in system complexity. This development also brings us a step closer to the realization of a principal investigator on a terrestrial Internet site being able to interact with space platform assets in near real time.

To develop this hardware, Spectrum Astro first conducted a technology analysis of alternatives study. For this analysis, they looked at the features of three protocol specifications: Ethernet (IEEE 802.3), Firewire (IEEE 1394), and Spacewire (IEEE 1355). A thorough analysis was performed on the basis of criteria such as current protocol performance and suitability for future space applications. Spectrum Astro also projected future influences such as cost, hardware and software availability, throughput performance, and integration procedures for current and transitive space architectures. After a thorough analysis, Ethernet was chosen because it was seen as the best longer term fit because of the prevalent commercial market; the current and projected availability of hardware, software, and development tools; and the ease of architecture integration.

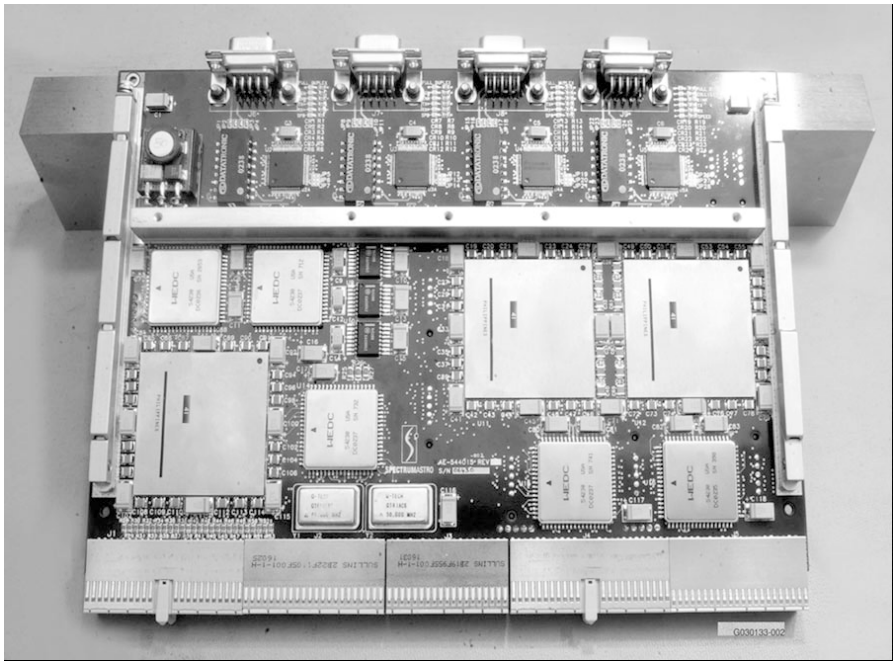

Ethernet multipurpose board.

On the basis of the results of this study, Spectrum Astro designed and developed the Ethernet network interface and four-port hub around the IEEE 802.3–2000 specification for supporting 10BASE–T/100BASE–T (10 Mbps and 100 Mbps) data rates, which are prevalent in industry today. Spectrum Astro used an Ethernet multipurpose board (see the photograph), peripheral component interconnect, and compact peripheral component interconnect interfaces as development bases for the hardware. The design was made scaleable to accommodate future projected 1-Gbps rates and can be migrated to the 3U form factor board, which already exists in versions of space-qualified products. Military and space components were specified and included in the design where possible. Design techniques were targeted to flight specifications such as random access memory (RAM) scrubbing and cyclic redundancy error check of packets. This minimized the effects of radiation, such as latchup and single-event upset, and augmented overall radiation-hardened qualities. Total ionizing dose testing was performed on the chips used in the design as part of the verification, and the final hardware and software functionality was verified using accepted industry standard benchmarks.

This development is an enabling technology that will be useful in a variety of space communications applications including point-to-point links, onboard instrument control, and command and data handling. In addition, valuable lessons were learned during this development about migrating existing spacecraft architectures to future configurations using OSI network products.

Find out more about this research: http://ctd.grc.nasa.gov/5650/5650.html

Glenn contact: Robert E. Jones, 216–433–3457, Robert.E.Jones@nasa.gov

Author: Robert E. Jones

Headquarters program office: OAT

Programs/Projects: CICT

Ka-Band Multibeam Aperture Phased Array Being Developed

Phased-array antenna systems offer many advantages to low-Earth-orbiting satellite systems. Their large scan angles and multibeam capabilities allow for vibration-free, rapid beam scanning and graceful degradation operation for high rate downlink of data to users on the ground. Technology advancements continue to reduce the power, weight, and cost of these systems to make phased arrays a competitive alternative in comparison to the gimbled reflector system commonly used in science missions. One effort to reduce the cost of phased arrays is the development of a Ka-band multibeam aperture (MBA) phased array by Boeing Corporation under a contract jointly by the NASA Glenn Research Center and the Office of Naval Research. The objective is to develop and demonstrate a space-qualifiable dual-beam Ka-band (26.5-GHz) phased-array antenna. The goals are to advance the state of the art in Ka-band active phased-array antennas and to develop and demonstrate multibeam transmission technology compatible with spacecraft in low Earth orbit to reduce the cost of future missions by retiring certain development risks. The frequency chosen is suitable for space-to-space and space-to-ground communication links.

The phased-array antenna has a radiation pattern designed by combining a set of individual radiating elements, optimized with the type of radiating elements used, their positions in space, and the amplitude and phase of the currents feeding the elements. This arrangement produces a directional radiation pattern that is proportional to the number of individual radiating elements. The arrays of interest here can scan the main beam electronically with a computerized algorithm.

The antenna is constructed using electronic components with no mechanical parts, and the steering is performed electronically, without any resulting vibration. The speed of the scanning is limited primarily by the control electronics. The radiation performance degrades gracefully if a portion of the elements fail. The arrays can be constructed to conform to a mounting surface, and multibeam capability is integral to the design. However, there are challenges for mission designers using monolithic-microwave-integrated-circuit- (MMIC-) based arrays because of reduced power efficiency, higher costs, and certain system effects that result in link degradations. The multibeam aperture phased-array antenna development is attempting to address some of these issues, particularly manufacturing, costs, and system performance.

A performance requirements and specifications document was developed in-house at Glenn to provide all relevant performance, interface, and environmental specifications for successful operation in the space environment. The array architecture proposes a multi-element module providing a scalable array architecture that addresses both small low-rate and large high-rate users. Systems engineering has provided array antenna pattern analysis, radiofrequency performance predictions against projected link analysis, and power management. MMIC designs for the power amplifier, phase shifter, and buffer amplifier have been completed. Radiofrequency link analysis through the array has been conducted to address waveform and performance specifications. Fabrication of a 16-element prototype array is scheduled for the middle of fiscal year 2004, with a full-scale 256-element array in the middle of fiscal year 2005.

Find out more about this research:

Glenn's Digital Communications Technology Branch: http://ctd.grc.nasa.gov/5650/5650.html

Office of Naval Research: http://www.onr.navy.mil/

Boeing Phantom Works: http://www.boeing.com/phantom/atp.html

Glenn contacts:
Richard C. Reinhart, 216–433–6588, Richard.C.Reinhart@nasa.gov;
Dr. Félix A. Miranda, 216–433–6589, Felix.A.Miranda@nasa.gov;
Dr. Roberto J. Acosta, 216–433–6640, Roberto.J.Acosta@nasa.gov;
Sandy K. Johnson, 216–433–8016, Sandra.K.Johnson@nasa.gov; and
Dr. Scott Sands, 216–433–2607, Obed.S.Sands@nasa.gov

Authors: Richard C. Reinhart and Thomas J. Kacpura

Headquarters program office: OSF

Programs/Projects: SCDS

Reconfigurable Transceiver and Software-Defined Radio Architecture and Technology Evaluated for NASA Space Communications

The NASA Glenn Research Center is investigating the development and suitability of a software-based open-architecture for space-based reconfigurable transceivers (RTs) and software-defined radios (SDRs). The main objectives of this project are to enable advanced operations and reduce mission costs. SDRs are becoming more common because of the capabilities of reconfigurable digital signal processing technologies such as field programmable gate arrays and digital signal processors, which place radio functions in firmware and software that were traditionally performed with analog hardware components.

Features of interest of this communications architecture include nonproprietary open standards and application programming interfaces to enable software reuse and portability, independent hardware and software development, and hardware and software functional separation. The goals for RT and SDR technologies for NASA space missions include prelaunch and on-orbit frequency and waveform reconfigurability and programmability, high data rate capability, and overall communications and processing flexibility. These operational advances over current state-of-art transceivers will be provided to reduce the power, mass, and cost of RTs and SDRs for space communications. The open architecture for NASA communications will support existing (legacy) communications needs and capabilities while providing a path to more capable, advanced waveform development and mission concepts (e.g., ad hoc constellations with self-healing networks and high-rate science data return).

A study was completed to assess the state of the art in RT architectures, implementations, and technologies. In-house researchers conducted literature searches and analysis, interviewed Government and industry contacts, and solicited information and white papers from industry on space-qualifiable RTs and SDRs and their associated technologies for space-based NASA applications. The white papers were evaluated, compiled, and used to assess RT and SDR system architectures and core technology elements to determine an appropriate investment strategy to advance these technologies to meet future mission needs.

The use of these radios in the space environment represents a challenge because of the space radiation suitability of the components, which drastically reduces the processing capability. The radios available for space are considered to be RTs (as opposed to SDRs), which are digitally programmable radios with selectable changes from an architecture combining analog and digital components. The limited flexibility of this design contrasts against the desire to have a power-efficient solution and open architecture.

The project team has two major upcoming activities, developing a space transceiver open-architecture for NASA missions and establishing an in-house test bed. The study and associated modeling effort are planned to explore the technologies, cost, benefits, and risks to establish an open-architecture for RTs and SDRs for NASA, possibly leveraging the Joint Tactical Radio System Software Communication Architecture (JTRS SCA) or its approach for use in space. The JTRS SCA is an example of an open-architecture SDR system being developed for terrestrial-based, tactical radios. It is part of a Department of Defense program to develop a family of multimode, multiband programmable radios with ad hoc, mobile networking and cross-banding capabilities based on a common, open architecture. Currently, this program has requirements for systems operating from 2 MHz to 2 GHz with recent extensions to 55 GHz for satellite communications terminals with wideband waveforms. The second activity is the establishment of a test bed that will be used for architectures and technologies testing and evaluation. The trade-off between reconfigurability versus traditional performance (speed, size, weight, power) will be examined. Specifically, architectures capable of high data rates will be investigated.

Find out more about this research:

Glenn's Digital Communications Technology Branch:
http://ctd.grc.nasa.gov/5650/5650.html

Joint Tactical Radio System:
http://jtrs.army.mil

Glenn contact:
Richard C. Reinhart, 216–433–6588,
Richard.C.Reinhart@nasa.gov

Authors: Richard C. Reinhart and Thomas J. Kacpura

Headquarters program office: OSF

Programs/Projects: SCDS

Turbomachinery and Propulsion Systems

Single-Stage, 3.4:1-Pressure-Ratio Aspirated Fan Developed and Demonstrated

Researchers are constantly pursuing technologies that will increase the performance of gas turbine engines. The aspirated compressor concept discussed here would allow the compression system to perform its task with about one-half of the compressor blades. To accomplish this, the researchers applied boundary layer control to the blades, casing, and hub. This method of boundary layer control consisted of removing small amounts of air from the main flow path at critical areas of the compressor. This bleed air could be used by other systems such as engine cooling or could be reinjected into lower pressure areas that require air for enhanced performance.

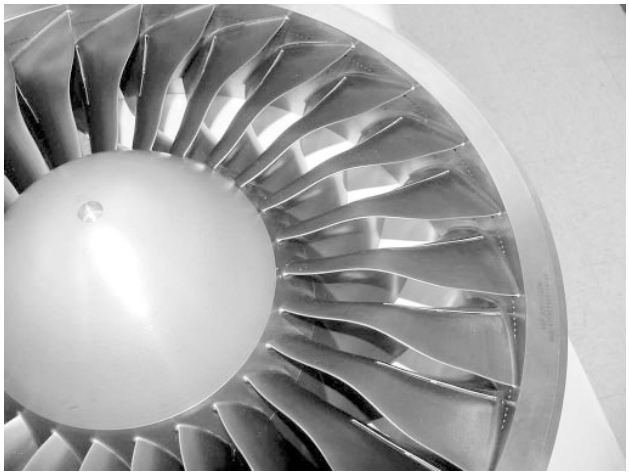

Tip shrouded aspirated rotor with bleed slots on blade surfaces and bleed holes in shroud.

This effort was initiated by the Massachusetts Institute of Technology (MIT) in response to a solicitation from the Defense Advanced Research Projects Agency (DARPA) who sought to advance research in flow control technology. The NASA Glenn Research Center partnered with MIT (principal investigator), Honeywell Aircraft Engines (cycle analysis, structural analysis, and mechanical design), and Pratt & Whitney (cycle analysis and aeroanalysis) to conceptualize, design, analyze, build, and test the aspirated fan stage. The aerodesign and aeroanalysis of this fan stage were jointly executed by MIT and Glenn to minimize the amount of bleed flow needed and to maintain the highest efficiency possible (ref. 1). Mechanical design issues were complicated by the need to have a shrouded rotor with hollow blades, with rotor stress levels beyond the capabilities of titanium. The high stress issues were addressed by designing a shroud that was filament wound with a carbon fiber/epoxy matrix, resulting in an assembly that was strong enough to handle the high stresses. Both the rotor (photographs on this page) and stator (photograph on the next page) were fabricated in two halves and then bolted together at the hub and tip, permitting the bleed passages to be machined into each half before assembly.

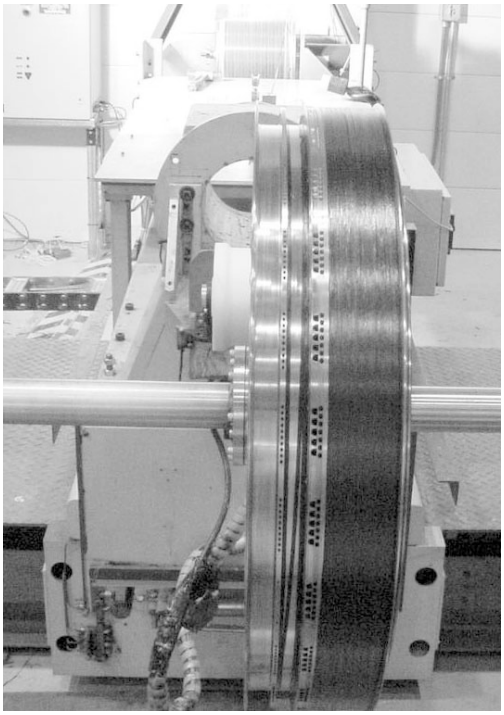

Aspirated rotor 50-percent wound with carbon fiber/epoxy matrix. Holes in the shroud are exit paths for bleeds taken from blades and shroud.

The aspirated fan stage was successfully tested at Glenn in December 2002 from 0 to 100 percent of the design speed and from 0 to 100 percent of the design mass flow rate. The stage pressure ratios and mass flow rates agreed very well with the pretest predicted values obtained from an in-house turbomachinery flow analysis code. This is a significant accomplishment given the complexity involved in the aerodynamic design of the blading and suction slot placements. The fan stage delivered a pressure ratio 50-percent higher than for conventional designs operating at the same speeds. This effort validates both the aerodesign and aeroanalysis codes used in this project. The aerodesign

code known as MISES was developed by MIT, and the aeroanalysis code applied was APNASA, a Glenn in-house-developed code. Research in this area continues by NASA, academia, and industry.

Reference

1. Merchant, A.A., et al.: Aerodynamic Design and Analysis of a High Pressure Ratio Aspirated Compressor Stage. ASME Paper 2000–GT–619, 2000.

Glenn contact: Edward Braunscheidel, 216–433–6298, Edward.P.Braunscheidel@nasa.gov

Author: Edward P. Braunscheidel

Headquarters program office: OAT

Programs/Projects: PR&T, UEET

Aspirated stator with bleed slots on blade surfaces, bleed holes along the stator hub, and pitchwise bleed slot between blades.

Pulsed Ejector Thrust Amplification Tested and Modeled

There is currently much interest in pulsed detonation engines for aeronautical propulsion. This, in turn, has sparked renewed interest in pulsed ejectors to increase the thrust of such engines, since previous, though limited, research had indicated that pulsed ejectors could double the thrust in a short device. An experiment has been run at the NASA Glenn Research Center, using a shrouded Hartmann-Sprenger tube as a source of pulsed flow, to measure the thrust augmentation of a statistically designed set of ejectors. A Hartmann-Sprenger tube directs the flow from a supersonic nozzle (Mach 2 in the present experiment) into a closed tube. Under appropriate conditions, an oscillation is set up in which the jet flow alternately fills the tube and then spills around flow emerging from the tube. The tube length determines the frequency of oscillation. By shrouding the tube, the flow was directed out of the shroud as an axial stream. The set of ejectors comprised three different ejector lengths, three ejector diameters, and three nose radii. The thrust of the jet alone, and then of the jet plus ejector, was measured using a thrust plate. The arrangement is shown in this photograph. Thrust augmentation is defined as the thrust of the jet with an ejector divided by the thrust of the jet alone. The experiments exhibited an optimum ejector diameter and length for maximizing the thrust augmentation, but little dependence on nose radius. Different frequencies were produced by changing the length of the Hartmann-Sprenger tube, and the experiment was run at a total of four frequencies. Additional

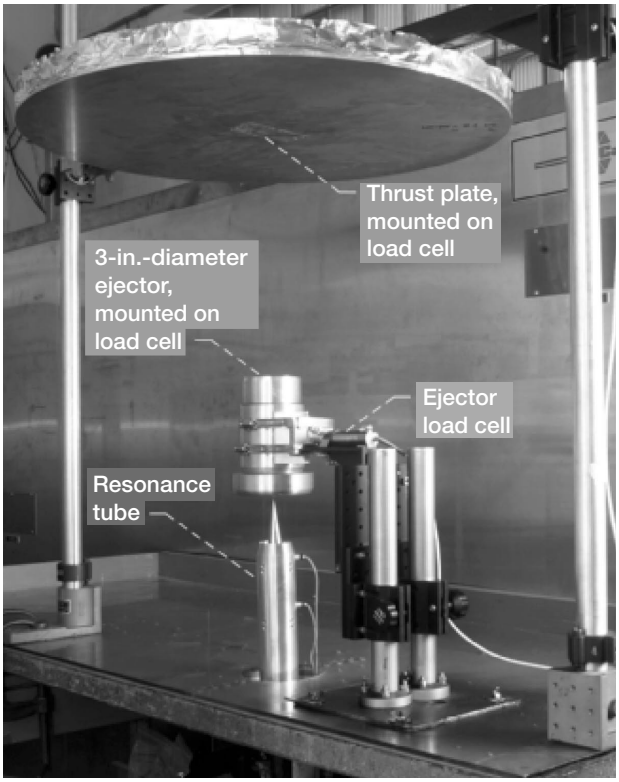

Photograph of the apparatus, showing the thrust plate at the top, the shrouded Hartmann-Sprenger (resonance) tube at the bottom, and an ejector above it.

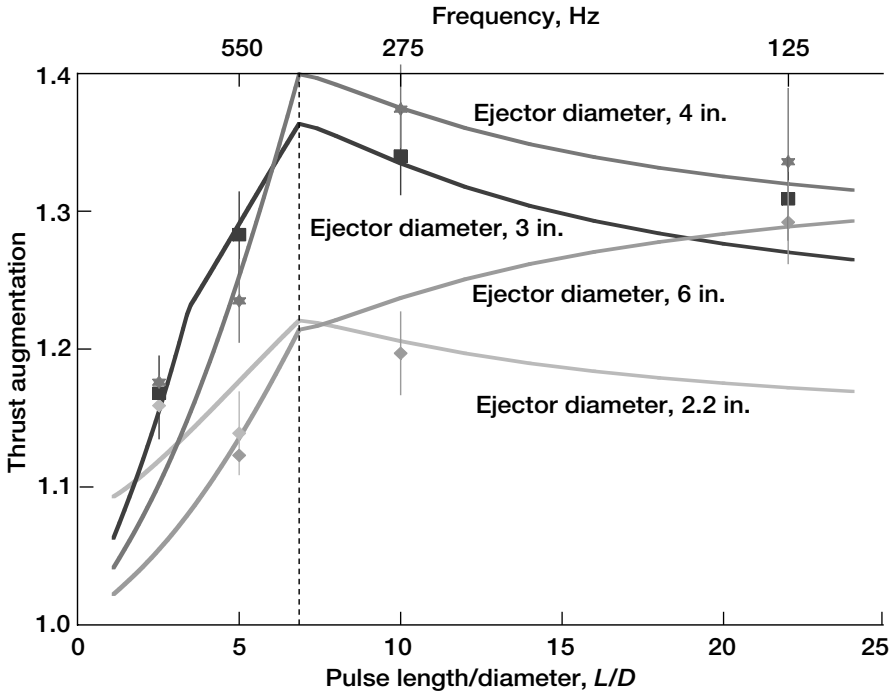

Graph of the calculated thrust augmentation (lines) versus the experimental thrust augmentation (points) as a function of pulse frequency, for four different ejector diameters.

measurements showed that the major feature of the pulsed jet was a starting vortex ring. The size of the vortex ring depended on the frequency, as did the optimum ejector diameter.

It is well known that the so-called slug model of vortex ring formation, which uses the ratio of the jet pulse length *L* to its diameter *D*, provides information on the vortex ring properties. For the present experiment, the value of *L/D* is inversely related to the pulse frequency. A calculation of the vortex ring diameter, core size, and velocity, using a modified version of the slug model, gave good agreement with experimental measurements of these quantities. From that, a model of the flow in the ejector allowed the thrust augmentation to be calculated, using a fit to the data for unknown parameters. The model shows the dependence on ejector diameter correctly, but it does not predict the ejector length. Calculated values of thrust augmentation for different ejector diameters, together with experimental values, are given in this graph, showing that there is reasonable agreement between them. Complete details on this work can be found in reference 1.

Reference

1. Wilson, Jack; and Deloof, Richard A.: A Simple Model of Pulsed Ejector Thrust Augmentation: Final Report. NASA/CR—2003-212541, 2003. http://gltrs.grc.nasa.gov/cgi-bin/GLTRS/browse.pl?2003/CR-2003-212541.html

QSS Group, Inc., contact:
Jack Wilson, 216–977–1204,
Jack.Wilson@grc.nasa.gov

Author: Jack Wilson

Headquarters program office: OAT

Programs/Projects:
Pulse Detonation Engine Technology

Glow Discharge Plasma Demonstrated for Separation Control in the Low-Pressure Turbine

Flow separation in the low-pressure turbine (LPT) is a major barrier that limits further improvements of aerodynamic designs of turbine airfoils. The separation is responsible for performance degradation, and it prevents the design of highly loaded airfoils. The separation can be delayed, reduced, or eliminated completely if flow control techniques are used. Successful flow control technology will enable breakthrough improvements in gas turbine performance and design.

The focus of this research project was the development and experimental demonstration of active separation control using glow discharge plasma (GDP) actuators in flow conditions simulating the LPT. The separation delay was shown to be successful, laying the foundation for further development of the technologies to practical application in the LPT.

In a fluid mechanics context, the term "flow control" means a technology by which a very small input results in a very large effect on the flow. In this project, the interest is to eliminate or delay flow separation on LPT airfoils by using an active flow control approach, in which disturbances are dynamically inserted into the flow, they interact with the flow, and they delay separation. The disturbances can be inserted using a localized, externally powered, actuating device, examples are acoustic, pneumatic, or mechanical devices that generate vibrations, flow oscillations, or pulses. A variety of flow control devices have been demonstrated in recent years in the context of the external aerodynamics of aircraft wings and airframes, where the incoming flow is quiescent or of a very low turbulence level. However, the flow conditions in the LPT are significantly different because there are high levels of disturbances in the incoming flow that are characterized by high free-stream turbulence intensity. In addition, the Reynolds number, which characterizes the viscous forces in the flow and is related to the flow speed, is very low in the LPT passages.

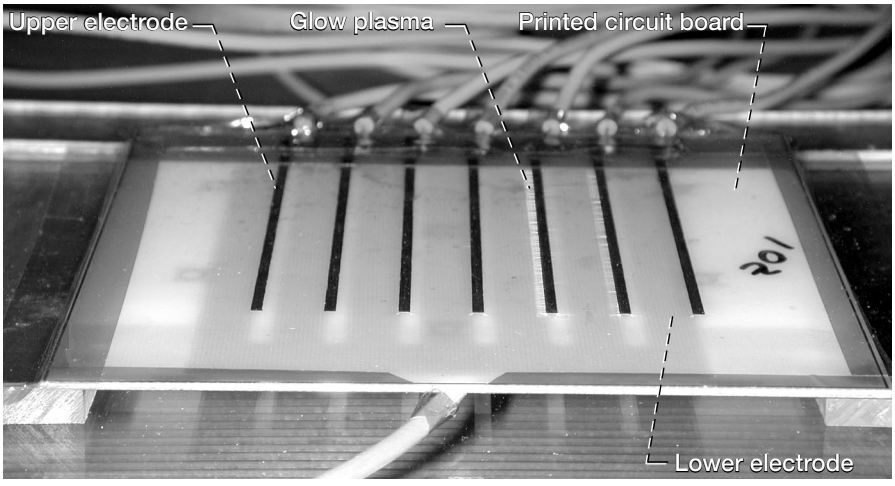

Glow discharge plasma actuator. More details can be seen in the color online version of this figure (http://www.grc.nasa.gov/WWW/RT/2003/5000/5820ashpis.html).

This work focused on using GDP actuators. These are innovative devices that generate flow disturbances. Electrodes on the surface, powered by high alternating-current voltage, create a type of plasma called glow-discharge plasma. The plasma creates a body force in the air near the surface. By proper design and operation of the electrodes, flow disturbances are inserted into the flow. A GDP actuator was fabricated on an electronic circuit board and was flush mounted on a test flat plate in Glenn's CW–7 transition research wind tunnel, which was equipped with an insert to simulate the pressure distribution on the suction surface of an LPT airfoil. A computer-controlled electronic driver system was designed and built. It employs operational amplifiers and custom transformers and can supply eight channels with 12 kV at up to 15 KHz. The actuator, which was operated as a phased array, was based on an idea developed by Corke (ref. 1). It generated an oscillating wall jet at a frequency in the range of instability waves associated with a separation bubble. The boundary layer was measured using surface pressure taps and hot-wire anemometry. Using hot-wire anemometry in the presence of ionized air required special attention. The system was protected from electric charge associated with the GDP by using optical links and a custom low-capacitance isolation transformer and by floating all the electrical grounds. Measurements were made for several Reynolds numbers and free-stream turbulence levels.

This project was the first to demonstrate that GDP phased-array actuators are an effective technique for separation delay in LPT flow conditions. In addition, it was the first time that hot-wire measurements were made in presence of glow discharge plasma.

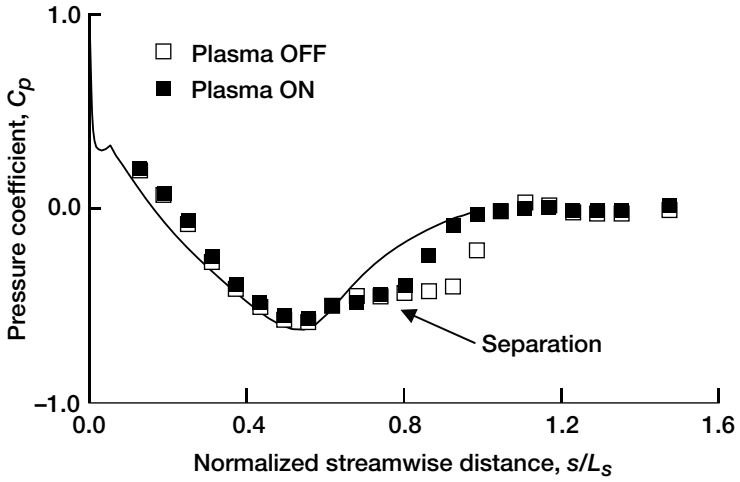

Pressure distribution on surface, indicating that when the plasma is ON the separated region is decreased. Reynolds number, Re, 50,000; turbulence intensity, TI, 0.2 percent; streamwise coordinate, s; reference length, L_s.

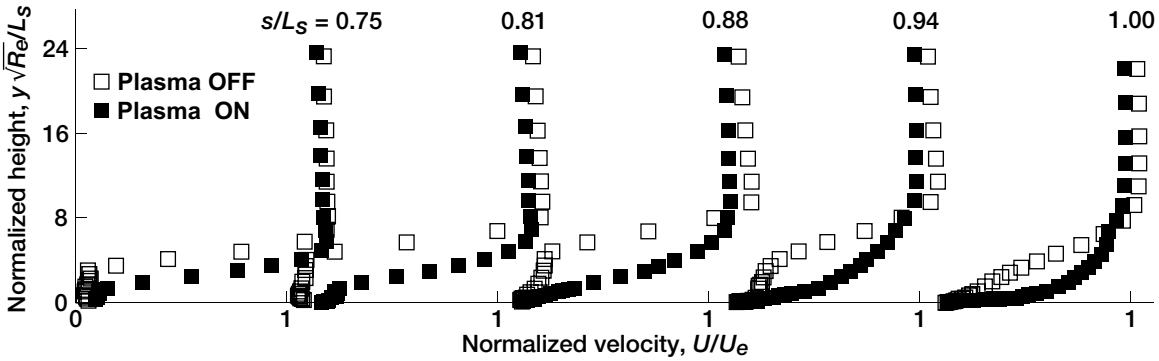

Velocity profiles at selected stations. The inflected profiles with white symbols indicate separated flow without control. The profiles with GDP actuators ON (black symbols) are full profiles indicating attached flow. Reynolds number, Re, 50,000; turbulence intensity, TI, 0.2 percent; normal coordinate, y; streamwise coordinate, s; reference length, L_s; velocity, U; free-stream velocity, U_e.

It was first set of direct measurements inside the boundary layer verifying the effect of GDP actuators. The work is described in detail in Hultgren and Ashpis (refs. 2 and 3). It represents Glenn's contribution to a cooperative agreement with the University of Notre Dame. The results are being used in experiments with GDP flow control on an LPT cascade there (ref. 4).

References

1. Corke, Thomas C.; and Matlis, Eric: Phased Plasma Arrays for Unsteady Flow Control. AIAA Paper 2000–2323, 2000.
2. Hultgren, Lennart S.; and Ashpis, David E.: Glow Discharge Plasma Active Control of Separation at Low Pressure Turbine Conditions. Bull. Am. Phys. Soc., vol. 47, no. 10, 2002, pp. 167–168.
3. Hultgren, Lennart S.; and Ashpis, David E.: Demonstration of Separation Delay With Glow-Discharge Plasma Actuators. AIAA Paper 2003–1025 (NASA/TM—2003-212204), 2003. http://gltrs.grc.nasa.gov/cgi-bin/GLTRS/browse.pl?2003/TM-2003-212204.html
4. Huang, J.; Corke, T.; and Thomas, F.: Plasma Actuators for Separation Control of Low Pressure Turbine Blades. AIAA Paper 2003–1027, 2003.

Glenn contact: Dr. David E. Ashpis, 216–443–8317, ashpis@nasa.gov

Authors: Dr. David E. Ashpis and Dr. Lennart S. Hultgren

Headquarters program office: OAT

Programs/Projects: SEC, DDF, UEET, Propulsion and Power, VSP, Twenty-first Century Aircraft Technology

TopMaker: Technique Developed for Automatic Multiblock Topology Generation Using the Medial Axis

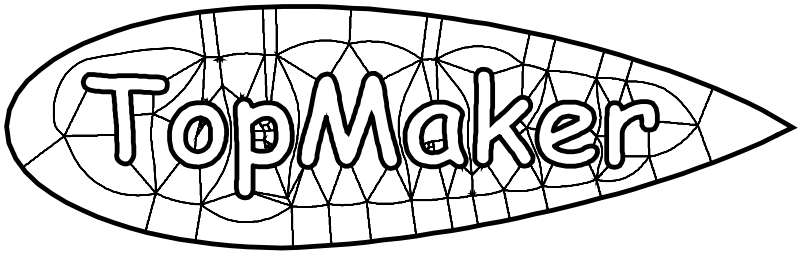

Automatically generated blocking topology between the word TopMaker and an airfoil shape.

The TopMaker technique was developed in an effort to reduce the time required for grid generation in complex numerical studies. Topology generation accounts for much of the man-hours required for structured multiblock grids. With regard to structured multiblock grids, topology refers to how the blocks are arranged and connected.

A two-dimensional multiblock topology generation technique has been developed at the NASA Glenn Research Center. Very general configurations can be addressed by the technique. A configuration is defined by a collection of nonintersecting closed curves, which will be referred to as loops. More than a single loop implies that holes exist in the domain, which poses no problem. This technique requires only the medial vertices and the touch points that define each vertex. From the information about the medial vertices, the connectivity between medial vertices is generated. The physical shape of the medial edge is not required. By applying a few simple rules to each medial edge, a multiblock topology can be generated without user intervention. The resulting topologies contain only the level of complexity dictated by the configurations. Grid lines remain attached to the boundary except at sharp concave turns, where a change in index family is introduced as would be desired. Keeping grid lines attached to the boundary is especially important in computational fluid dynamics, where highly clustered grids are used near no-slip boundaries. This technique is simple and robust and can easily be incorporated into the overall grid-generation process.

In the bottom left figure, the dashed lines show the medial axis for the configuration defined by the black lines. The gray circles show the defining circle for each medial vertex. Notice that each circle touches the black lines at three locations. In two dimensions, the medial axis is found easily by using available software. In the bottom center figure, outlines of the resulting blocks are shown as dashed lines.

The bottom right figure shows an example of a more complicated configuration. This configuration is a schematic meant to evoke the idea of a turbine blade with measuring probes inserted. The “probes” are artificially large for clarity in showing the block structure. Work is continuing in an effort to extend this technique to three-dimensional configurations.

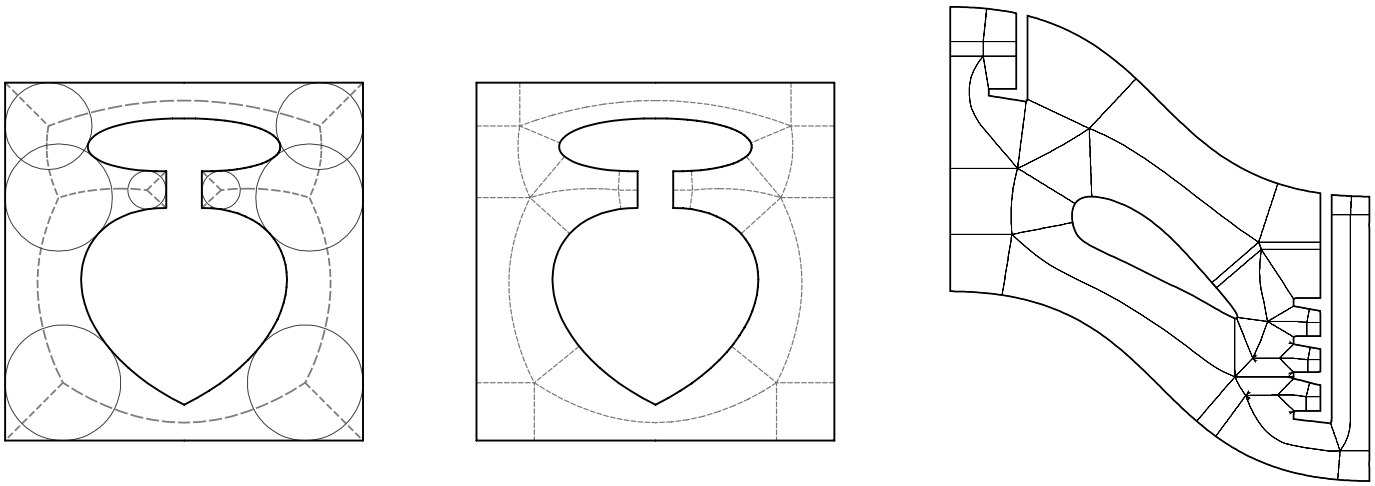

Left: The medial axis for the region between a square and a more complex toplike shape is shown by the dashed lines. Circles are drawn with centers at the medial vertices. Center: Automatically generated blocking topology for the region between the square and the toplike shape. Right: Automatically generated blocking topology for a turbine blade with probes in the flowfield.

Bibliography
Rigby, David: TopMaker: A Technique for Automatic Multiblock Topology Generation Using the Medial Axis. Proceedings of FEDSM'03 4th ASME–JSME Joint Fluids Engineering Conference, FEDSM2003–45527, 2003.

Find out more about this research:
http://www.grc.nasa.gov/WWW/TURBINE/Turbine.htm

QSS Group, Inc., contact:
Dr. David L. Rigby, 216–433–5965, David.L.Rigby@grc.nasa.gov

Glenn contact:
Dr. Raymond E. Gaugler, 216–433–5882, Raymond.E.Gaugler@nasa.gov

Author: Dr. David L. Rigby

Headquarters program office: OAT

Programs/Projects: PR&T, UEET

Supersonic Rocket Thruster Flow Predicted by Numerical Simulation

Despite efforts in the search for alternative means of energy, combustion still remains the key source. Most propulsion systems primarily use combustion for their needed thrust. Associated with these propulsion systems are the high-velocity hot exhaust gases produced as the byproducts of combustion. These exhaust products often apply uneven high temperature and pressure over the surfaces of the appended structures exposed to them. If the applied pressure and temperature exceed the design criteria of the surfaces of these structures, they will not be able to protect the underlying structures, resulting in the failure of the vehicle mission.

An understanding of the flow field associated with hot exhaust jets and the interactions of these jets with the structures in their path is critical not only from the design point of view but for the validation of the materials and manufacturing processes involved in constructing the materials from which the structures in the path of these jets are made.

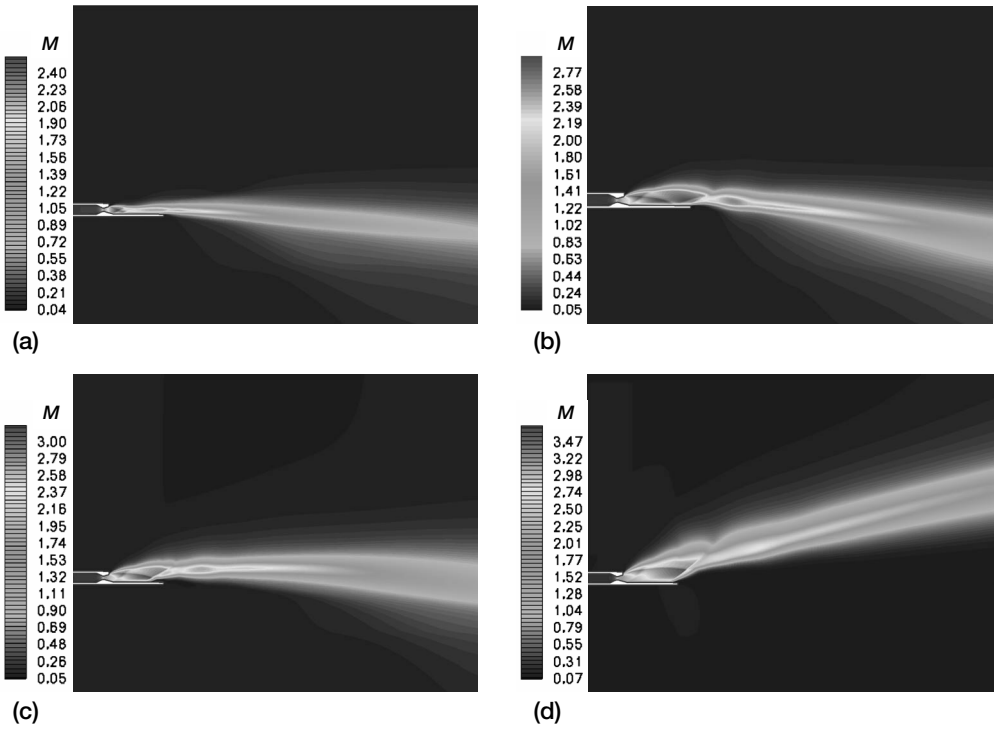

Plume prediction of a rocket thruster operating at four different combustion chamber pressures (M, Mach number). This figure is shown in color in the online verson of this article (http://www.grc.nasa.gov/WWW/RT/5000/5830davoudzadeh.html). (a) 130 psia. (b) 250 psia. (c) 300 psia. (d) 500 psia.

The hot exhaust gases often flow at supersonic speeds, and as a result, various incident and reflected shock features are present. These shock structures induce abrupt changes in the pressure and temperature distribution that need to be considered. In addition, the jet flow creates a gaseous plume that can easily be traced from large distances.

To study the flow field associated with the supersonic gases induced by a rocket engine, its interaction with the surrounding surfaces, and its effects on the strength and durability of the materials exposed to it, NASA Glenn Research Center's Combustion Branch teamed with the Ceramics Branch to provide testing and analytical support.

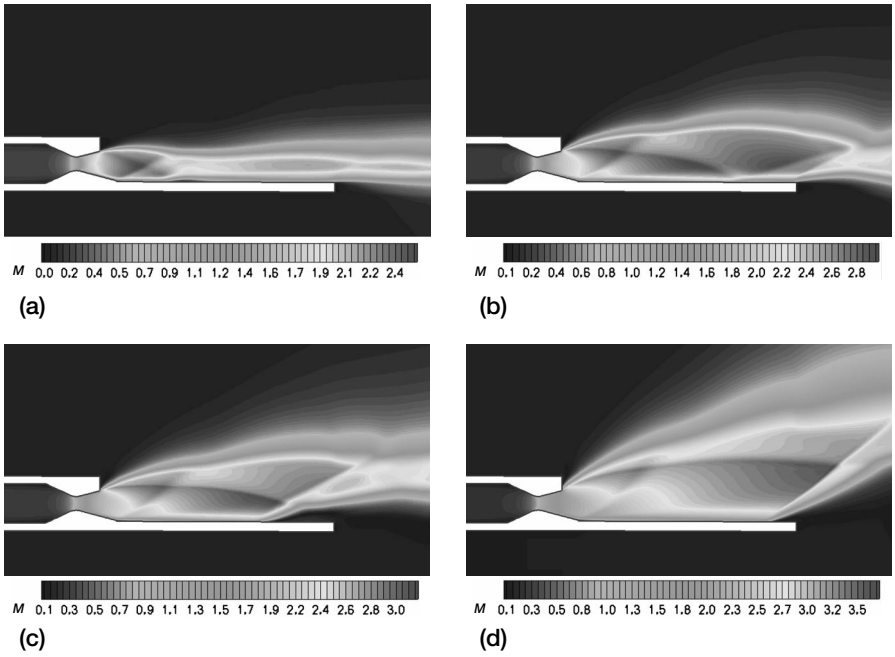

Numerical simulation of shock waves and their interaction in a supersonic rocket engine operating at different chamber pressures (M, Mach number). This figure is shown in color in the online verson of this article (http://www.grc.nasa.gov/WWW/RT/5000/5830davoudzadeh.html). (a) 130 psia. (b) 250 psia. (c) 300 psia. (d) 500 psia.

The experimental work included the full range of heat flux environments that the rocket engine can produce over a flat specimen. Chamber pressures were varied from 130 to 500 psia and oxidizer-to-fuel ratios (*o/f*) were varied from 1.3 to 7.5.

The computational work used the National Combustion Code (NCC) to produce numerical results for several operating conditions. The accompanying figures show the computational results obtained with this code. The figures on the preceding page show the plumes predicted by the Reynolds average Navier-Stokes numerical simulations for the supersonic flow field induced by a H_2-O_2 rocket thruster with an attached panel, under a variety of operating conditions. The plume direction was controlled by the shocks. It moved from a straight and slightly downward direction to an upward direction as the combustion chamber pressure was increased from 130 to 500 psia. The 500-psia case exhibits the highest plume angle, where the Mach number remains very high past the initial shock, aft of the inclined ramp, and over the flat panel. The figures on this page show the Mach number distributions, demonstrating the structure of the shocks beyond the nozzle exit. The geometry is asymmetric about the nozzle centerline; hence, the shock patterns are not symmetric. The degree of asymmetry in the shock pattern is a function of the velocity of the jet exiting the nozzle. In the 130-psia case shown in part (a), the exit velocity is not high enough to create excessive asymmetry about the centerline of the nozzle. The typical diamond-shaped shock pattern can still be recognized. As the chamber pressure and, consequently, the exit velocity increases, the asymmetry becomes more pronounced, as in part (b). Eventually, the asymmetry increases to the degree that the shock emanating from the top edge of the nozzle exit is directed away from the panel, as in the 300-psia case shown in part (c). Finally, it is parallel to the flat panel, as in the 500-psia case shown in part (d).

The simulations have captured details of the supersonic flow field, such as the plume formations, the direction and expansion of the plumes, the formation of the shock waves, and the effects of the shock waves on the temperature and pressure distributions on the walls. A comparison showed that the results of the simulations are consistent with related measurements obtained from rig tests.

References

1. Davoudzadeh, Farhad; and Liu, Nan-Suey: Shock Waves and Plume Prediction of a Rocket Thruster With an Attached Panel. Proceedings of FEDSM'03 4th ASME–JSME Joint Fluids Engineering Conference, FEDSM2003–45077, 2003.
2. Davoudzadeh, Farhad; and Liu, Nan-Suey: Simulation of the Flow Field Associated With a Rocket Thruster Having an Attached Panel. NASA/TM—2003-212347, 2003. http://gltrs.grc.nasa.gov/cgi-bin/GLTRS/browse.pl?2003/TM-2003-212347.html
3. Liu, Nan-Suey: On the Comprehensive Modeling and Simulation of Combustion Systems. AIAA Paper 2001–0805, 2001.

University of Toledo contact:
Dr. Farhad Davoudzadeh, 216–433–8876, Farhad.Davoudzadeh@grc.nasa.gov

Glenn contact:
Dr. Nan-Suey Liu, 216–433–8722, Nan-Suey.Liu-1@nasa.gov

Author: Dr. Farhad Davoudzadeh

Headquarters program office: OAT

Programs/Projects: PR&T, RLV

ThermoBuild: Online Method Made Available for Accessing NASA Glenn Thermodynamic Data

The new Web site program "ThermoBuild" allows users to easily access and use the NASA Glenn Thermodynamic Database of over 2000 solid, liquid, and gaseous species. A convenient periodic table allows users to "build" the molecules of interest and designate the temperature range over which thermodynamic functions are to be displayed. ThermoBuild also allows users to build custom databases for use with NASA's Chemical Equilibrium with Applications (CEA) program or other programs that require the NASA format for thermodynamic properties.

The NASA Glenn Research Center has long been a leader in the compilation and dissemination of up-to-date thermodynamic data, primarily for use with the NASA CEA program, but increasingly for use with other computer programs. The NASA Glenn Thermodynamic Database, available at http://www.grc.nasa.gov/WWW/CEAWeb/, contains accurate, frequently updated thermodynamic data for over 2000 solid, liquid, and gaseous species (ref. 1). The data are presented as nine coefficients to an empirical formula in temperature for heat capacity, enthalpy, and entropy.

ThermoBuild is available as a link to the CEA Web site. It guides the user through the steps necessary to produce tabulated thermodynamic functions for one or several species without complicated calculations or interpolations. The user selects the constituent atoms from ThermoBuild's periodic table and is prompted for a temperature schedule. Heat capacity, enthalpy, entropy, Gibbs energy, heat of formation, and logK values are tabulated for the user's selected species. Equations and data references are conveniently available at the Web site.

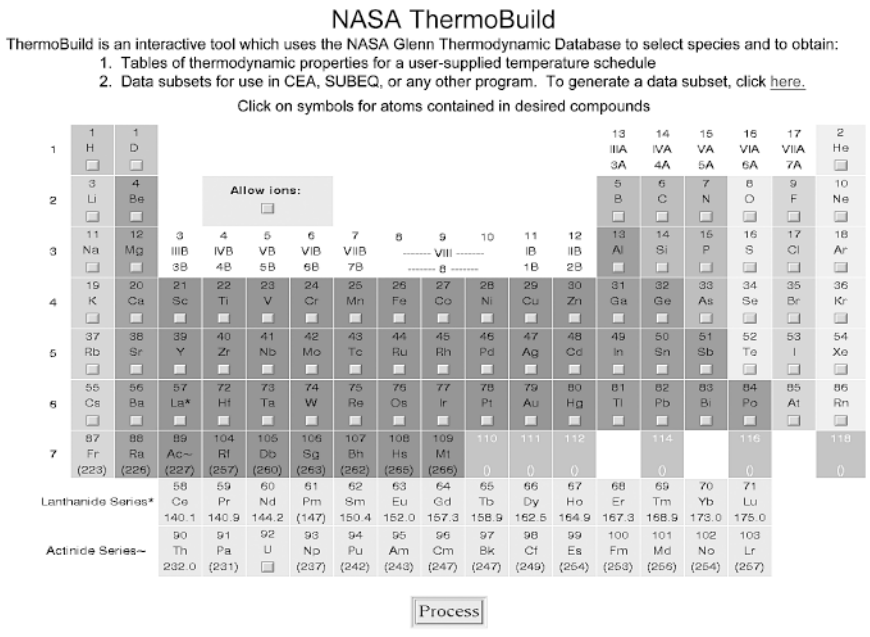

NASA ThermoBuild.

Another useful feature of ThermoBuild allows users to create custom databases by downloading a subset of the NASA data. These custom databases can be used for specialty CEA applications, or for any program that requires the NASA empirical formula for thermodynamic properties.

ThermoBuild was made fully operational during fiscal year 2003. It was produced as part of a continuing program at Glenn to provide high-quality, easily accessible thermodynamic information to the scientific community.

Access the NASA Glenn Thermodynamic Database:
http://www.grc.nasa.gov/WWW/CEAWeb/

Reference

1. McBride, Bonnie J.; Zehe, Michael J.; and Gordon, Sanford: NASA Glenn Coefficients for Calculating Thermodynamic Properties of Individual Species. NASA/TP—2002-211556, 2002. http://gltrs.grc.nasa.gov/cgi-bin/GLTRS/browse.pl?2002/TP-2002-211556.html

Glenn contacts:
Bonnie McBride, 216–433–5870, Bonnie.J.McBride@nasa.gov;
Dr. Michael Zehe, 216–433–5833, Michael.J.Zehe@nasa.gov; and
Russell W. Claus, 216–433–5869, Russell.W.Claus@nasa.gov

Authors: Dr. Michael J. Zehe and Bonnie J. McBride

Headquarters program office: OAT

Programs/Projects:
UEET, RTA, NGLT, NPSS

Low-Cost, User-Friendly, Rapid Analysis of Dynamic Data System Established

An issue of primary importance to the development of new jet and certain other air-breathing combined-cycle powered aircraft is the advancement of airframe-integrated propulsion technologies. Namely, engine inlets and their systems and subsystems are required to capture, convert, and deliver the atmospheric airflow demanded by such engines across their operating envelope in a form that can be used to provide efficient, stable thrust. This must be done while also minimizing aircraft drag and weight. Revolutionary inlet designs aided by new technologies are needed to enable new missions. An unwanted byproduct of pursuing these inlet technologies is increased time-variant airflow distortion. Such distortions reduce propulsion system stability, performance, operability, and life.

To countermand these limitations and fully evaluate the resulting configurations, best practices dictate that this distortion be experimentally measured at large scale and analyzed. The required measurements consist of those made by an array of high-response pressure transducers located in the flow field at the aerodynamic interface plane (AIP) between the inlet and engine. Although the acquisition of the necessary pitot-pressure time histories is relatively straightforward, until recent years, the analysis has proved to be very time-consuming, tedious, and expensive.

To transform the analysis of these data into a tractable and timely proposition, researchers at the NASA Glenn Research Center created and established the Rapid Analysis of Dynamic Data (RADD) system. The system provides complete, near real-time analysis of time-varying inlet airflow distortion datasets with report quality output. This fully digital approach employs Institute of Electrical and Electronics Engineers (IEEE) binary data file format standardization to establish data-acquisition-system-independent processing on low-cost personal computers. Features include invalid instrumentation code-out, logging, and multiple replacement schemes as needed for each channel of instrumentation. The AIP pressure distribution can be interpolated to simulate measurements by alternate AIP probe arrays, if desired. In addition, the RADD system provides for the application of filters that can be used to focus the analysis on the frequency range of interest.

The most important capability of the RADD system is its ability to analyze

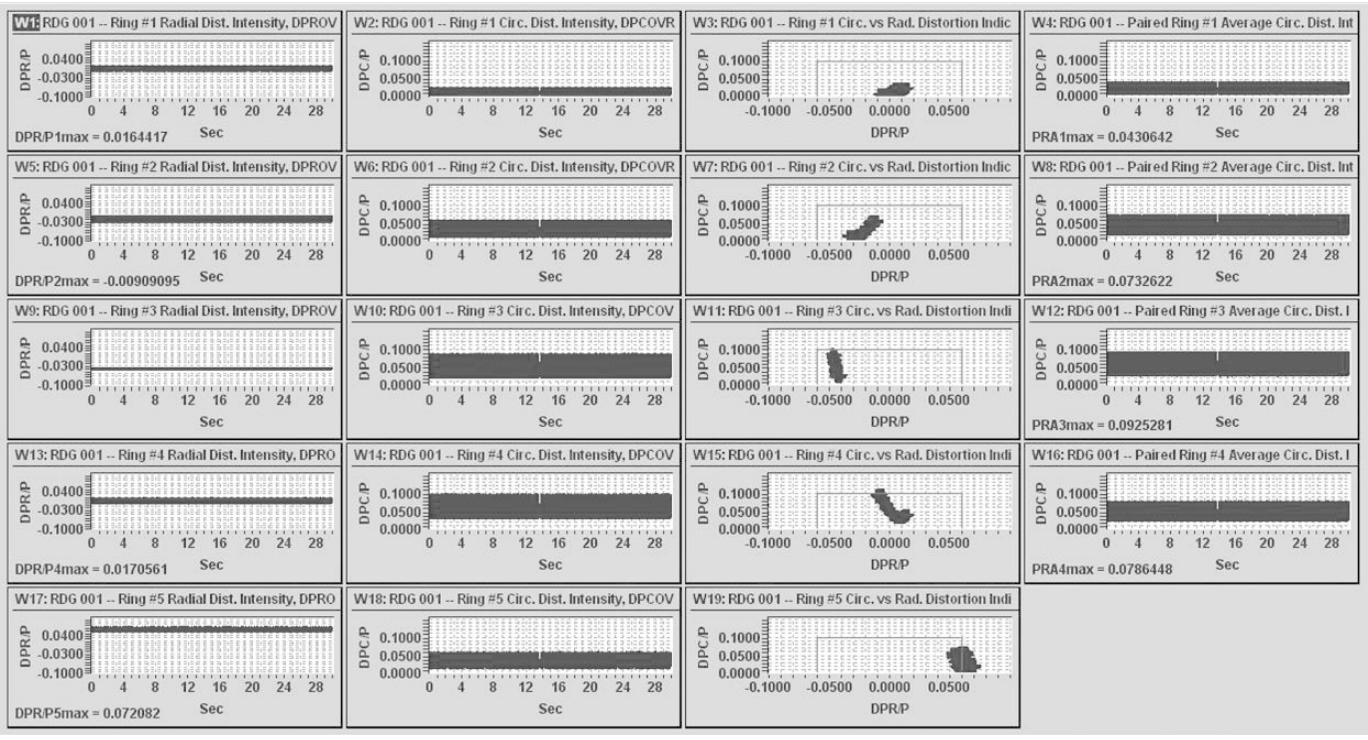

Typical screen-displayed summary output of a fully processed simulated dynamic inlet airflow distortion dataset provided by the RADD system.

dynamic inlet distortion in accordance with the Society of Automotive Engineers' (SAE) Aerospace Recommended Practice 1420 (ARP1420) guidelines (ref. 1). Off-the-shelf DADiSP (DSP Development Corporation, MA) digital signal analysis software is used to provide a full range of data management, processing, and presentation capabilities. In this way, users are provided with a very powerful suite of relevant capabilities that require only a minimum of programming effort. Fully validated, the RADD system has greatly enhanced and accelerated the processing of a wide array of dynamic inlet and other test data over previous capabilities. Opportunities for further development, such as the ability to generate color contour plots of selected scans of the AIP pressure distribution and in situ production of Moving Picture Experts Group (MPEG) dynamic distortion movies, have been identified.

Reference

1. Gas Turbine Engine Inlet Flow Distortion Guidelines. Aerospace Recommended Practice 1420—Rev. B, Society of Automotive Engineers, 2002.

Glenn contact:
David J. Arend, 216–433–2387, David.J.Arend@nasa.gov

Author: David J. Arend

Headquarters program office: OAT

Programs/Projects:
UEET, PR&T, AvSP

Contact Angle Influence on Geysering Jets in Microgravity Investigated

Microgravity poses many challenges to the designer of spacecraft tanks. Chief among these are the lack of phase separation and the need to supply vapor-free liquid or liquid-free vapor to the spacecraft processes that require fluid. One of the principal problems of phase separation is the creation of liquid jets. A jet can be created by liquid filling, settling of the fluid to one end of the tank, or even closing a valve to stop the liquid flow. Anyone who has seen a fountain knows that jets occur in normal gravity also. However, in normal gravity, the gravity controls and restricts the jet flow. In microgravity, with gravity largely absent, surface tension forces must be used to contain jets.

To model this phenomenon, a numerical method that tracks the fluid motion and the surface tension forces is required. Jacqmin (ref. 1) has developed a phase model that converts the discrete surface tension force into a barrier function that peaks at the free surface and decays rapidly away. Previous attempts at this formulation were criticized for smearing the interface. This can be overcome by sharpening the phase function, double gridding the fluid function, and using a higher-order solution for the fluid function. The solution of this equation can be rewritten as two coupled Poisson equations that also include the velocity.

Using this code, researchers at the NASA Glenn Research Center investigated the effect of changing the wall contact angle. This value can be changed with a single input into the code. It is of interest because it varies greatly in the liquids used in spacecraft (water, 60°; cryogens, 0°). It also gives a range of free-surface forces (90°, no force, 0°, maximum force.) This change enables us to study how changes in the equilibrium shape, without changes in the jet, influence the final geyser shape. The graph to the right compares the shapes. The graph on the next page shows the free-surface pressures for each of these runs. Although the graph on this page shows that the free-surface shapes are different, the forces acting from the free surface seem to be quite similar.

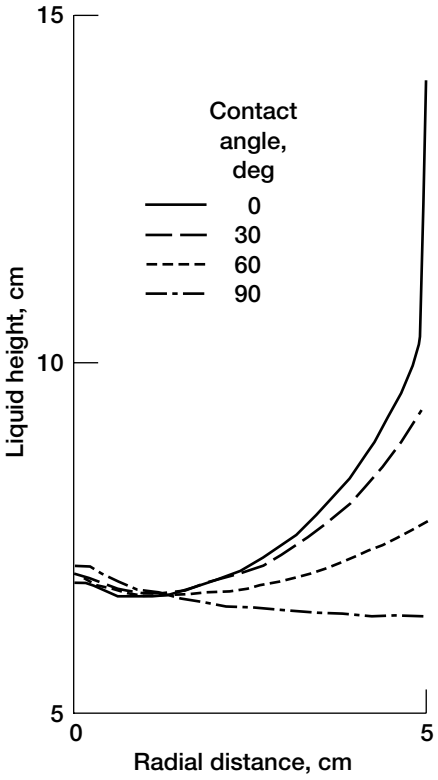

Comparison of free surface shape as a function of contact angle.

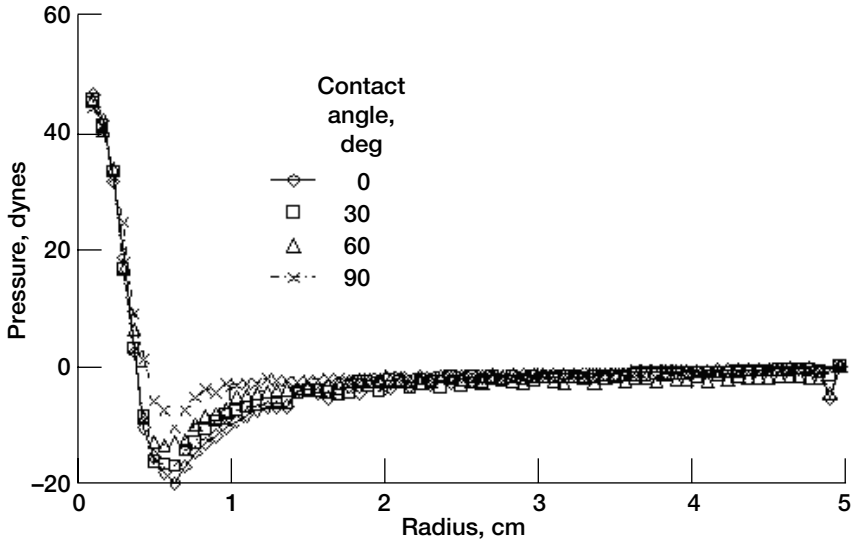

Pressure at the free surface as a function of contact angle.

Reference

1. Jacqmin, David: Calculation of Two-Phase Navier-Stokes Flows Using Phase-Field Modeling. J. Comput. Phys., vol. 155, no. 1, 1999, pp. 96–127.

Glenn contact:
David J. Chato, 216–977–7488, David.J.Chato@nasa.gov

Author: David J. Chato

Headquarters program office: OAT

Programs/Projects:
PR&T, NGLT, Microgravity Science

Cryogenic Nitrogen Thermosyphon Developed and Characterized

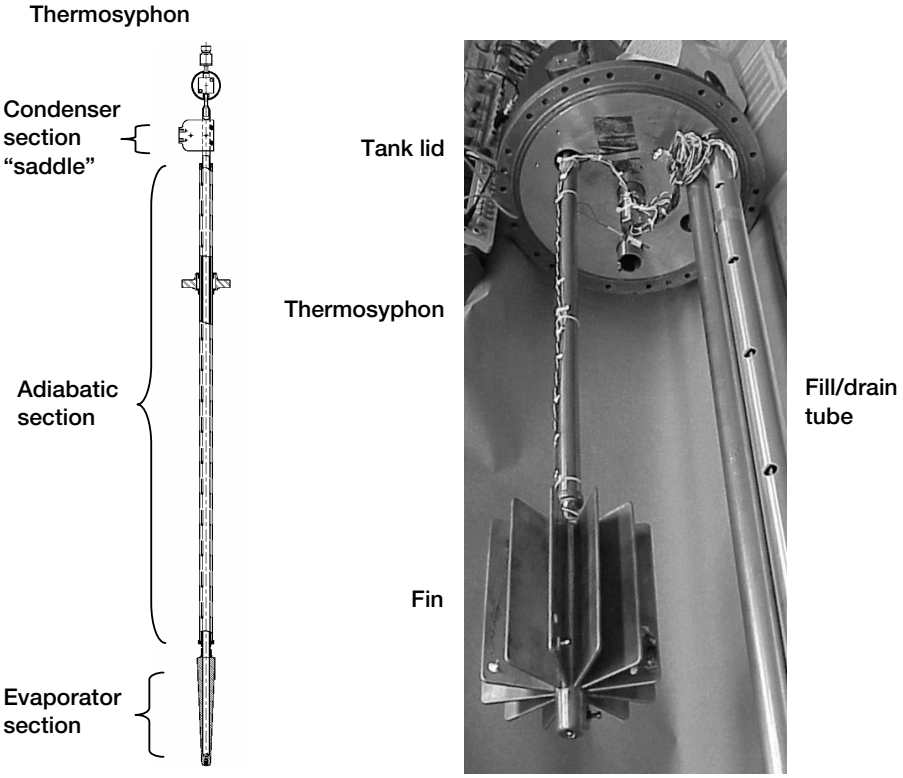

Left: A thermosyphon schematic is shown. Near the top is the condenser saddle, which is where the cryocooler was coupled. Right: Picture of the as-built hardware. The tank lid shown is toward the top of the adiabatic section of the thermosyphon. The fin is the heat exchanger coupled to the evaporator. It was where the heat entering the cryogenic test tank was removed.

A two-phase nitrogen thermosyphon was developed at the NASA Glenn Research Center to efficiently integrate a cryocooler into an insulated liquid-nitrogen-filled tank as part of an advanced development zero-boiloff (ZBO) ground test. NASA Marshall Space Flight Center's (MSFC) Advanced Space Transportation Program supported this test to improve the performance of in-space propulsion system concepts. Recent studies (ref. 1) have shown significant mass reductions and other advantages when incorporating active cooling in a ZBO configuration, enabling consideration of high-performing cryogenic propellants for long-duration applications in space. Active cooling was integrated via a thermosyphon, made of copper, 42 in. (1070 mm) long with an inner diameter of 0.436 in. (11 mm). It was charged with nitrogen to 225 psia at 300 K, which provided a fill ratio of 15 percent. The temperatures and heat flows through the thermosyphon were monitored during the startup phase of the ZBO test, and steady-state tests were conducted over a range of

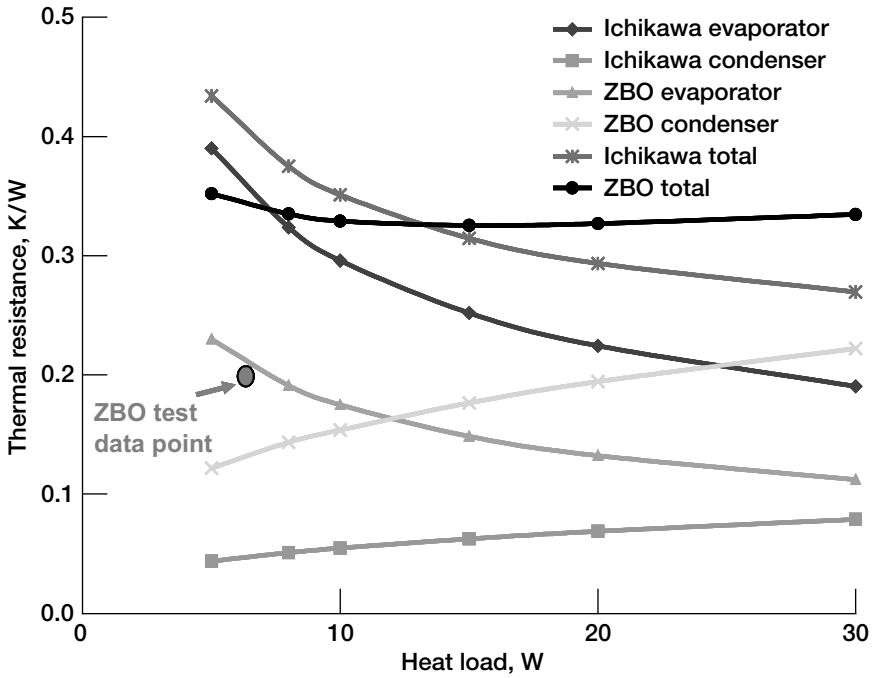

This figure shows that the Ichikawa (best reference available) total resistance was strongly influenced by the evaporator; the large condenser did not add much to the total resistance. The ZBO thermosyphon thermal total resistance is relatively constant, caused by a decreasing evaporator resistance counteracted by an increasing condenser resistance. The ZBO test data point shows that the built thermosyphon had much less resistance than predicted.

increasing and decreasing heat flows. The results also were compared with the initial design calculations and with results for a similar thermosyphon. They show that the thermal resistance of the thermosyphon was one-half of that expected—0.2 K/W at a heat flow of 8.0 W. The design calculations also showed that this resistance can be made relatively constant over a wider range of heat flows by making the ratio of evaporator area to condenser area 3:1. The better-than-expected results will translate into reduced integration loss for the ZBO concept. Analysis and test details are described in reference 2.

References

1. Plachta, David; and Kittel, Peter: An Updated Zero Boil-Off Cryogenic Propellant Storage Analysis Applied to Upper Stages or Depots in an LEO Environment. NASA/TM—2003-211691, (AIAA Paper 2002–3589), 2003. http://gltrs.grc.nasa.gov/cgi-bin/GLTRS/browse.pl?2003/TM-2003-211691.html
2. Christie, R.; Robinson, D.; and Plachta, D.W.: Design and Operating Characteristics of a Cryogenic Nitrogen Thermosyphon. Paper presented at the Cryogenic Engineering Conference, C3–C–07, 2003.

Glenn contact:
David W. Plachta, 216–977–7126, David.W.Plachta@nasa.gov

Authors:
David W. Plachta and Robert Christie

Headquarters program office: OSS

Programs/Projects:
In-Space Propulsion, ASTP

Structures and Acoustics

Distribution of Inclusion-Initiated Fatigue Cracking in Powder Metallurgy Udimet 720 Characterized

In the absence of extrinsic surface damage, the fatigue life of metals is often dictated by the distribution of intrinsic defects. In powder metallurgy (PM) alloys, relatively large defects occur rarely enough that a typical characterization with a limited number of small-volume fatigue test specimens will not adequately sample inclusion-initiated damage. Counterintuitively, inclusion-initiated failure has a greater impact on the distribution in PM alloy fatigue lives because they tend to have fewer defects than their cast and wrought counterparts. Although the relative paucity of defects in PM alloys leads to higher mean fatigue lives, the distribution in observed lives tends to be broader. In order to study this important failure initiation mechanism without expending an inordinate number of specimens, a study was undertaken at the NASA Glenn Research Center where known populations of artificial inclusions (seeds) were introduced to production powder. Fatigue specimens were machined from forgings produced from the seeded powder. Considerable effort has been expended in characterizing the crack growth rate from inclusion-initiated cracks in seeded PM alloys. A rotating and translating positioning system, with associated software, was devised to map the surface inclusions in low-cycle fatigue (LCF) test bars and to monitor the crack growth from these inclusions. The graph below illustrates

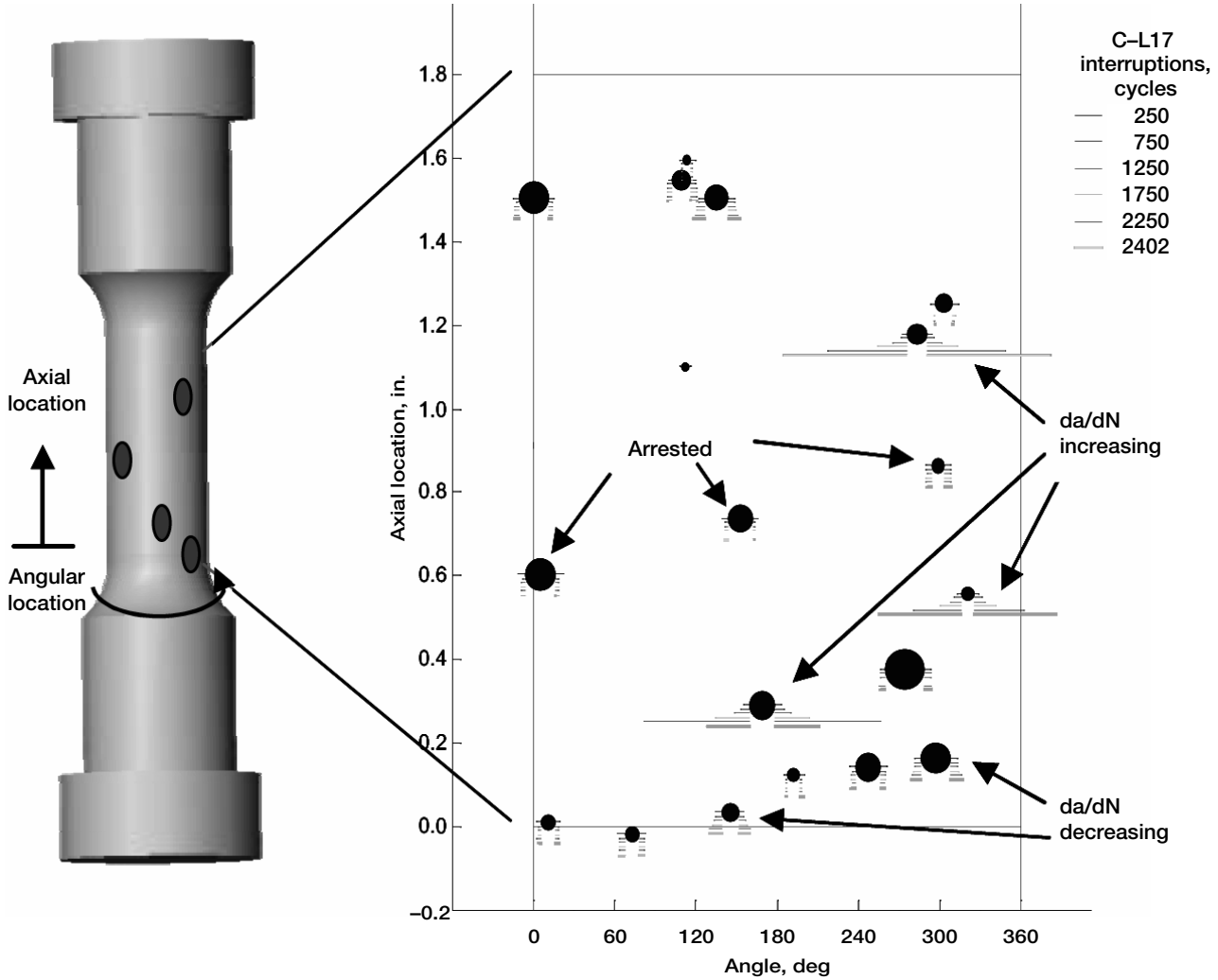

Map of a low-cycle fatigue (LCF) specimen surface showing the relative sizes of observed surface inclusions and crack lengths observed at intervals during interrupted fatigue testing; da/dN, crack growth rate. Details are shown in color in the online version of this article (http://www.grc.nasa.gov/WWW/RT/2003/5000/5920bonacuse.html).

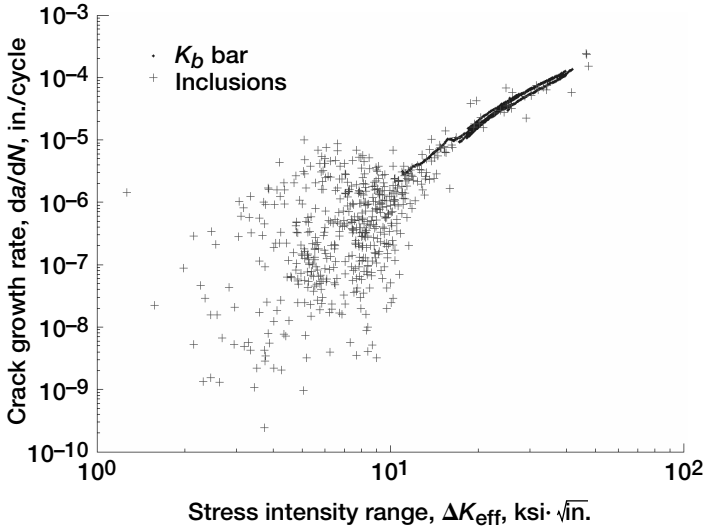

Distribution of measured growth rates of inclusion-initiated cracks in seeded Udimet 720 LCF test bars. K_b bar data represent large-crack propagation behavior.

the measured extension in fatigue cracks from inclusions on a seeded LCF test bar subjected to cyclic loading at a strain range of 0.8 percent and a strain ratio ($\varepsilon_{max}/\varepsilon_{min}$) of zero. Notice that the observed inclusions fall into three categories: some do not propagate at all (arrest), some propagate with a decreasing crack growth rate, and a few propagate at increasing rates that can be modeled by fracture mechanics. The graph above shows the measured inclusion-initiated crack growth rates from 10 interrupted LCF tests plotted against stress intensities calculated for semielliptical cracks with the observed surface lengths. The expected scatter in the crack growth rates for stress intensity ranges near threshold is observed. These data will be used to help determine the distribution in growth rates of cracks emanating from inclusions as well as the proportion of cracks that arrest under various loading conditions.

References

1. Bonacuse, Peter J.; and Kantzos, Peter T.: Scanning Electron Microscope Mapping System Developed for Detecting Surface Defects in Fatigue Specimens. Research and Technology 2001, NASA/TM—2002-211333, p. 136. http://www.grc.nasa.gov/WWW/RT2001/5000/5920bonacuse.html
2. Bonacuse, P.J., et al.: Modeling Ceramic Inclusions in Powder Metallurgy Alloys. Fatigue 2002, Proceedings of the Eighth International Fatigue Congress, A.F. Blom, ed., vol. 2/5, Engineering Materials Advisory Services, Ltd., West Midlands, U.K., 2002, pp. 1339–1346.
3. Gabb, T.P., et al.: Initial Assessment of the Effects of Nonmetallic Inclusions on Fatigue Life of Powder-Metallurgy-Processed Udimet™ 720. NASA/TM—2002-211571, 2002. http://gltrs.grc.nasa.gov/cgi-bin/GLTRS/browse.pl?2002/TM-2002-211571.html

Glenn contacts:
Jack Telesman, 216–433–3310, Ignacy.Telesman-1@nasa.gov; and Tim Gabb, 216–433–3272, Timothy.P.Gabb@nasa.gov

U.S. Army Research Laboratory, Vehicle Technology Directorate at Glenn contacts:
Pete Bonacuse, 216–433–3309, Peter.J.Bonacuse@grc.nasa.gov; and Robert Barrie, 216–433–5090, Robert.L.Barrie@grc.nasa.gov

Ohio Aerospace Institute (OAI) contacts:
Pete Kantzos, 216–433–5202, Pete.T.Kantzos@grc.nasa.gov; and Louis J. Ghosn, 216–433–3822, Louis.J.Ghosn@grc.nasa.gov

Authors: Peter J. Bonacuse, Dr. Pete T. Kantzos, Robert L. Barrie, Dr. Jack Telesman, Dr. Louis J. Ghosn, and Dr. Tim P. Gabb

Headquarters program office: OAT

Programs/Projects: AvSP, Ultra Safe

Associative Flow Rule Used to Include Hydrostatic Stress Effects in Analysis of Strain-Rate-Dependent Deformation of Polymer Matrix Composites

Procedures for modeling the high-strain-rate impact of composite materials are needed for designing reliable composite engine cases that are lighter than the metal cases in current use. The types of polymer matrix composites that are likely to be used in such an application have a deformation response that is nonlinear and that varies with strain rate. The nonlinearity and the strain-rate dependence of the composite response are due primarily to the matrix constituent. Therefore, in developing material models to be used in the design of impact-resistant composite engine cases, the deformation of the polymer matrix must be correctly analyzed. However, unlike in metals, the nonlinear response of polymers depends on the hydrostatic stresses, which must be accounted for within an analytical model. By applying micromechanics techniques along with given fiber properties, one can also determine the effects of the hydrostatic stresses in the polymer on the overall composite deformation response. First efforts to account for the hydrostatic stress effects in the composite deformation applied purely empirical methods that relied on composite-level data. In later efforts, to allow polymer properties to be characterized solely on the basis of polymer data, researchers at the NASA Glenn Research Center developed equations to model the polymers that were based on a nonassociative flow rule, and efforts to use these equations to simulate the deformation of representative polymer materials were reasonably successful. However, these equations were found to have difficulty in correctly analyzing the multiaxial stress states found in the polymer matrix constituent of a composite material. To correct these difficulties, and to allow for the accurate simulation of the nonlinear strain-rate-dependent deformation analysis of polymer matrix composites, in the efforts reported here Glenn researchers reformulated the polymer constitutive equations from basic principles using the concept of an associative flow rule. These revised equations were characterized and validated in an experimental program carried out through a university grant with the Ohio State University, wherein tensile and shear deformation data were obtained for a representative polymer for strain rates ranging from quasi-static to high rates of several hundred per second. Tensile deformation data also were obtained over a variety of strain rates and fiber orientation angles for a representative polymer matrix composite composed using the polymer.

To obtain the material data, Glenn's researchers designed and fabricated test specimens of a representative toughened epoxy resin and a representative polymer matrix composite. Quasi-static tests at low strain rates and split Hopkinson bar tests at high strain rates were then conducted at the Ohio State University. To analyze the polymer, Glenn researchers modified state-variable constitutive equations previously used for the

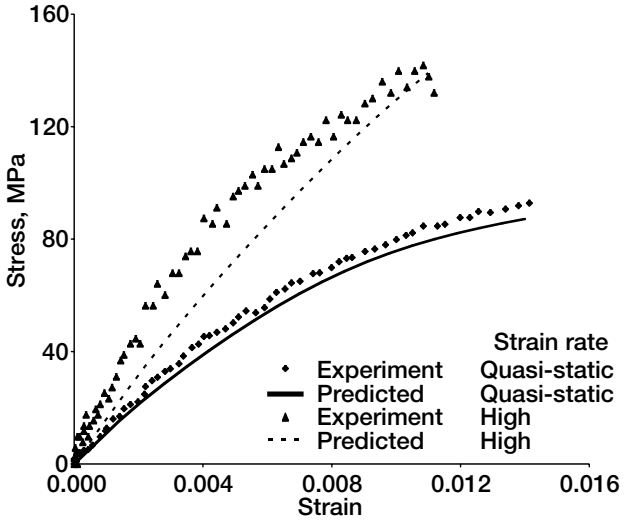

Experimental and predicted tensile stress-strain curves for a representative [45°] polymer matrix composite at quasi-static and high strain rates.

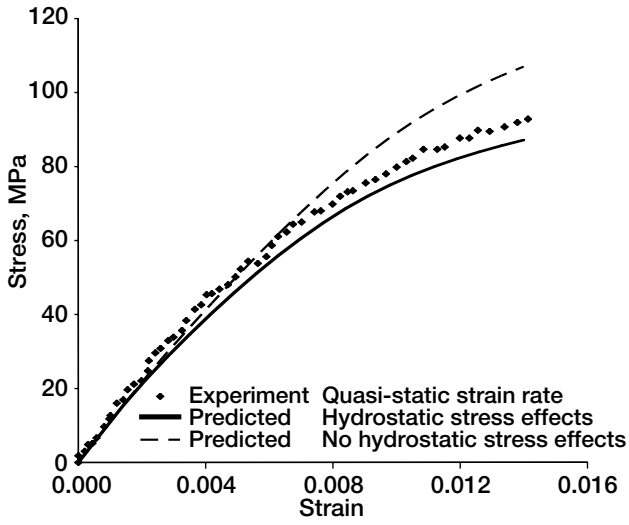

Effects of hydrostatic stresses on the predicted tensile stress-strain curve for a representative [45°] polymer matrix composite under quasi-static strain-rate loading conditions.

viscoplastic analysis of metals to allow for the analysis of the nonlinear, strain-rate-dependent polymer deformation. Specifically, to account for the effects of hydrostatic stresses, the equations were modified using first principles, with an associative flow rule, a concept developed in basic plasticity theory. This revision modified the calculations of the effective stress and effective inelastic strain from their original definitions and appropriately modified the inelastic flow law. To predict the overall composite deformation, researchers applied a Glenn-developed micromechanics approach in which the predicted response of the composite was computed on the basis of the properties of the individual constituents.

The graph on the left (previous page) shows the experimental and computed tensile stress-strain curves for both quasi-static and high strain rates for a unidirectional [45°] composite. As can be seen in the figure, the nonlinearity and the strain-rate dependence of the composite deformation are correctly computed. The graph on the right shows the effects of correctly accounting for the hydrostatic stress effects in the polymer on the composite deformation for the quasi-static case. As can be seen in the figure, if the hydrostatic stresses in the polymer are not correctly accounted for, the computed tensile stresses are significantly higher than their experimental values in the nonlinear portion of the stress-strain curve. However, if the hydrostatic stress effects in the polymer matrix are correctly accounted for, the comparison between the experimental and computed curves is reasonably good.

Glenn contacts:
Dr. Robert K. Goldberg, 216–433–3330, Robert.K.Goldberg@nasa.gov; and
Dr. Gary D. Roberts, 216–433–3244, Gary.D.Roberts@nasa.gov

Authors: Dr. Robert K. Goldberg and Dr. Gary D. Roberts

Headquarters program office: OAT

Programs/Projects: PR&T, Ultra Safe

Probability Distribution Estimated From the Minimum, Maximum, and Most Likely Values: Applied to Turbine Inlet Temperature Uncertainty

Modern engineering design practices are tending more toward the treatment of design parameters as random variables as opposed to fixed, or deterministic, values. The probabilistic design approach attempts to account for the uncertainty in design parameters by representing them as a distribution of values rather than as a single value. The motivations for this effort include preventing excessive overdesign as well as assessing and assuring reliability, both of which are important for aerospace applications.

However, the determination of the probability distribution is a fundamental problem in reliability analysis. A random variable is often defined by the parameters of the theoretical distribution function that gives the best fit to experimental data. In many cases the distribution must be assumed from very limited information or data. Often the types of information that are available or reasonably estimated are the minimum, maximum, and most likely values of the design parameter. For these situations the beta distribution model is very convenient because the parameters that define the distribution can be easily determined from these three pieces of information. Widely used in the field of

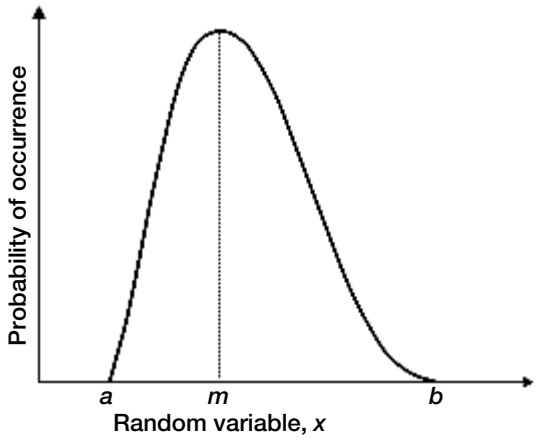

Example of a beta probability distribution with minimum value, a; maximum value, b; and most likely value, m. A new approach was developed for determining the beta distribution given a, b, and m.

operations research, the beta model is very flexible and is also useful for estimating the mean and standard deviation of a random variable given only the aforementioned three values. However, an assumption is required to determine the four parameters of the beta distribution from only these three pieces of information (some of the more common distributions, like the normal, lognormal, gamma, and Weibull distributions, have two or three parameters). The conventional method assumes that the standard deviation is a certain fraction of the range. The beta parameters are then determined by solving a set of equations simultaneously. A new method developed in-house at the NASA Glenn Research Center assumes a value for one of the beta shape parameters based on an analogy with the normal distribution (ref.1). This new approach allows for a very simple and direct algebraic solution without restricting the standard deviation. The beta parameters obtained by the new method are comparable to the conventional method (and identical when the distribution is symmetrical). However, the proposed method generally produces a less peaked distribution with a slightly larger standard deviation (up to 7 percent) than the conventional method in cases where the distribution is asymmetric or skewed. The beta distribution model has now been implemented into the Fast Probability Integration (FPI) module used in the NESSUS computer code for probabilistic analyses of structures (ref. 2).

This work was motivated by the problem of modeling the uncertainty in turbine inlet temperature for aeroengines given the minimum, maximum, and most likely temperature values (ref. 3). The method, therefore, offers enhanced probabilistic assessment of aeropropulsion components and systems subject to nondeterministic thermal loads. However, the method is applicable to the general problem of estimating the parameters of the beta distribution for any random variable where the minimum, maximum, and most likely values are available. Furthermore, this work demonstrated the utility of the beta distribution for these types of problems in probabilistic engineering analyses.

References

1. Holland, Frederic A., Jr.: A Simple Method for Estimating the Parameters of the Beta Distribution Applied to Modeling Uncertainty in Gas Turbine Inlet Temperature. ASME Paper GT–2002–30295, 2002, pp. 627–633.
2. Tong, Michael T.: A Probabilistic Assessment of Advanced Aeropropusion Technologies. ASME Paper GT–2004–53485, 2004.
3. Tong, Michael T.: A Probabilistic Approach to Aeropropulsion System Assessment. NASA/TM—2000-210334, 2000. http://gltrs.grc.nasa.gov/cgi-bin/GLTRS/browse.pl?2000/TM-2000-210334.html

Glenn contact:
Frederic A. Holland, Jr., 216–433–8367, Frederic.A.Holland@nasa.gov

Author: Frederic A. Holland, Jr.

Headquarters program office: OAT

Programs/Projects: HOTPC

Structural Benchmark Testing of Superalloy Lattice Block Subelements Completed

A multitude of benchmark tests on superalloy lattice block structural specimens gave promising results for this new high-performance material system that utilizes alloys with a 50-plus-year history in gas turbine engine use. The testing was performed in-house at the NASA Glenn Research Center (http://www.grc.nasa.gov) Structural Benchmark Test Facility, where the subelement-sized beam specimens were loaded at room and elevated temperatures to observe their elastic and plastic behavior, strength, and fatigue resistance.

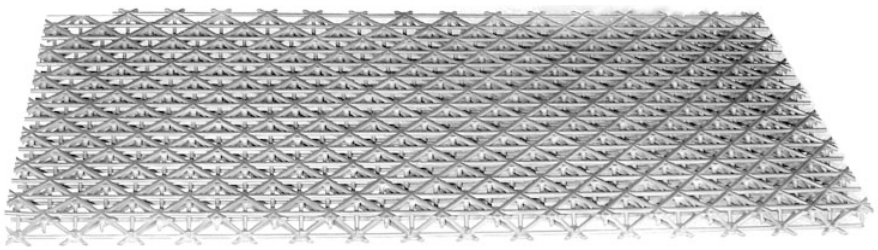

Cast Inconel 718 lattice block panel, approximately 140 by 300 by 11 mm (5.5 by 12 by 0.44 in.).

Superalloy lattice block panels, which are produced directly by investment casting, are composed of thin ligaments arranged in three-dimensional triangulated trusslike structures (see the figure to the left). Optionally, solid panel face sheets can be formed integrally during casting. In either form, lattice block panels can easily be produced with weights less than 25 percent of the mass of a solid panel. Inconel 718 (IN 718) and MarM-247 superalloy lattice block panels have been developed under NASA's Ultra-Efficient Engine Technology Project (http://www.ueet.nasa.gov) and Higher Operating Temperature

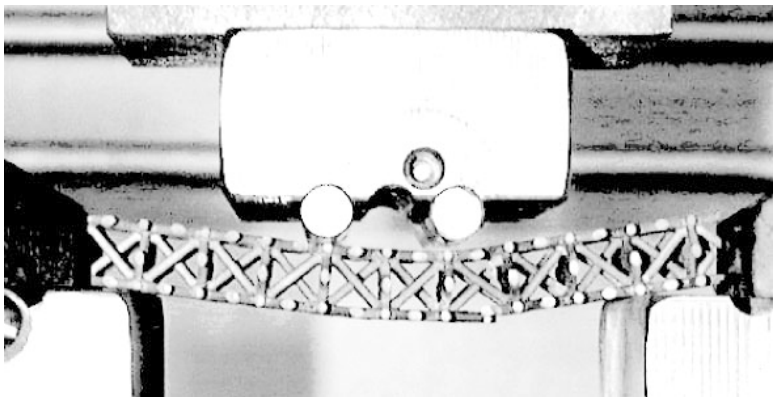

Open-cell lattice block beam specimen following strength testing in a 75-mm-span four-point bend test fixture.

Propulsion Components Project (http://www.grc.nasa.gov/WWW/AERO/base/hotpc.htm) to take advantage of the superalloys' high strength and elevated temperature capability with the inherent light weight and high stiffness of the lattice architecture (ref. 1). These characteristics are important in the future development of turbine engine components.

Casting quality and structural efficiency were evaluated experimentally using small beam specimens machined from the cast and heat treated 140- by 300- by 11-mm panels. The matrix of specimens included samples of each superalloy in both open-celled and single-face-sheet configurations, machined from longitudinal, transverse, and diagonal panel orientations. Thirty-five beam subelements were tested in Glenn's Life Prediction Branch's (http://www.grc.nasa.gov/WWW/LPB/) material test machine at room temperature and 650 °C under both static (see the photograph above) and cyclic load conditions. Surprisingly, test results exceeded initial linear elastic analytical predictions. This was likely a result of the formation of plastic hinges and redundancies inherent in lattice block geometry, which was not considered in the finite element models. The value of a single face sheet was demonstrated by increased bending moment capacity, where the face sheet simultaneously increased the gross section modulus and braced the compression ligaments against early buckling as seen in open-cell specimens. Preexisting flaws in specimens were not a discriminator in flexural, shear, or stiffness measurements, again because of redundant load paths available in the lattice block structure. Early test results are available in references 2 and 3; more complete analyses are scheduled for publication in 2004.

This experimental work supports the value of superalloy lattice block technology for damage-tolerant structures and for lightweight components under low and moderate pressure loadings at elevated temperatures. Potential aeropropulsion uses for this technology include turbine engine actuated panels, exhaust nozzle flaps, side-panel structures, and rotating hardware containment rings.

References

1. Hebsur, Mohan G.: Processing of IN–718 Lattice Block Castings. Processing of IN–718 Lattice Block Castings, NASA/CR—2002-211332, 2002. http://gltrs.grc.nasa.gov/cgi-bin/GLTRS/browse.pl?2002/CR-2002-211332.html
2. Krause, David L., et al.: Mechanical Testing of IN718 Lattice Block Structures. Processing and Properties of Lightweight Cellular Metals and Structures. Third Global Symposium on Materials Processing and Manufacturing, Amit K. Ghosh, T.H. Sanders, and T.D. Claar, eds., TMS, Warrendale, PA, 2002, pp. 233–242.
3. Krause, D.L., et al.: Mechanical Testing of IN718 Lattice Block Structures. NASA/TM—2002-211325, 2002. http://gltrs.grc.nasa.gov/cgi-bin/GLTRS/browse.pl?2002/TM-2002-211325.html

Find out more about this research:

Ultra-Efficient Engine Technology:
http://www.ueet.nasa.gov

Higher Operating Temperature Propulsion Components Project:
http://www.grc.nasa.gov/WWW/AERO/base/hotpc.htm

NASA Glenn Research Center:
http://www.grc.nasa.gov

Life Prediction Branch:
http://www.grc.nasa.gov/WWW/LPB/

Glenn contact:
David L. Krause, 216–433–5465, David.L.Krause@nasa.gov

Authors:
David L. Krause, Dr. J. Daniel Whittenberger, Dr. Pete T. Kantzos, and Dr. Mohan G. Hebsur

Headquarters program office: OAT

Programs/Projects: UEET, HOTPC

Benchmark Tests for Stirling Convertor Heater Head Life Assessment Conducted

A new in-house test capability has been developed at the NASA Glenn Research Center (http://www.grc.nasa.gov), where a critical component of the Stirling Radioisotope Generator (SRG) is undergoing extensive testing to aid the development of analytical life prediction methodology (ref. 1) and to experimentally aid in verification of the flight-design component's life. The new facility includes two test rigs that are performing creep testing of the SRG heater head pressure vessel test articles at design temperature and with wall stresses ranging from operating level to seven times that (see the following photograph).

The SRG is being developed for multimission use, including electric power supply for deep space missions (ref. 2). For this application, the heater head component must endure high temperature for a long time, but at low stress. These conditions impose the life-limiting failure mechanism of material creep, a slow, gradual increase in strain that could eventually end in rupture of the pressure vessel. Because the SRG is required to operate for more than 10 years, creep testing the heater head under prototypical conditions alone would not provide enough timely data to fully complement the analytical effort, nor would it provide the basis for experimental life prediction. Therefore, increasing the test pressure to levels higher than design raises the stress levels of the test articles and accelerates the creep results. In addition, although creep-limited components have been designed satisfactorily using material properties generated from traditional uniaxial tests, the heater head is subjected to a highly biaxial state of stress. To supplement the ongoing uniaxial creep tests on flight heat Inconel 718 (IN 718) material (ref. 3), the benchmark test program has been designed to experimentally evaluate the response to this specific biaxial stress condition.

New facility includes two pneumatic test rigs for elevated temperature creep testing of SRG pressure vessel test articles.

Beginning with calibration runs, short-term, high-stress benchmark tests have been conducted on geometrically simplified test vessels fabricated from a heat of flight material to provide early test results; additional calibration runs of 6 months to 1 year in duration are planned for test articles of flight design geometry (see the photograph on the next page). Also, one "full-up" test will be performed for a flight-design specimen with all structurally significant attachments. This test will be conducted with prototypical internal pressure and additional externally applied axial stress to duplicate actual flight loading.

The new test facility is located at the Life Prediction Branch's (http://www.grc.nasa.gov/WWW/LPB/) Structural Benchmark Test Facility. The test stand includes two independently operated test rigs with argon pressurization systems capable of 3000 psig, although the test article limit is 1500 psig. Two 3-kW induction power supplies and water-cooled induction coils provide even heating and temperature profiling. A custom data acquisition and control system is employed to safely conduct tests and record results.

This ongoing testing is being performed for the Thermo-Mechanical Systems Branch (http://www.grc.nasa.gov/WWW/tmsb/) and the Power and Propulsion Office (http://www.space-power.grc.nasa.gov/ppo/) as part of a Glenn in-house project supporting the development of the SRG. The overall SRG project is managed by the Department of Energy. Lockheed Martin and Stirling Technology Company are developing the SRG for the Department of Energy. NASA's Office of Space Science is providing technical support to the project through Glenn.

IN 718 heater head at 650 °C (1200 °F) with an induction heater coil.

References

1. Halford, G.R., et al.: Structural Analyses of Stirling Power-Convertor Heater Head for Long-Term Reliability, Durability, and Performance. AIP Conf. Proc. 608, 2002, pp. 880–887.
2. Thieme, Lanny G.; and Schreiber, Jeffrey G.: NASA GRC Stirling Technology Development Overview. NASA/TM—2003-212454, 2003. http://gltrs.grc.nasa.gov/cgi-bin/GLTRS/browse.pl?2003/TM-2003-212454.html
3. Bowman, R.R.: Long-Term Creep Assessment of a Thin-Walled Inconel 718 Stirling Power-Convertor Heater Head. Proceedings of the 36th Intersociety Energy Conversion Engineering Conference, vol. 1, ASME, New York, NY, 2001, pp. 435–440.

Find out more about this research:

NASA Glenn Research Center:
http://www.grc.nasa.gov/

Glenn's Thermo-Mechanical Systems Branch:
http://www.grc.nasa.gov/WWW/tmsb/

Glenn's Power and Propulsion Office:
http://space-power.grc.nasa.gov/ppo/

Glenn's Life Prediction Branch:
http://www.grc.nasa.gov/WWW/LPB/

Glenn contacts:
David L. Krause, 216–433–5465, David.L.Krause@nasa.gov; and
Dr. Gary R. Halford, 216–433–3265, Gary.R.Halford@nasa.gov

Authors:
David L. Krause, Dr. Gary R. Halford, and Dr. Randy R. Bowman

Headquarters program office: OSS

Programs/Projects:
SRG, Mars Exploration

Scatter in Carbon/Silicon Carbide (C/SiC) Composites Quantified

Carbon-fiber-reinforced silicon carbide matrix (C/SiC) composites processed by chemical vapor infiltration are candidate materials for aerospace thermal structures. Carbon fibers can retain properties at very high temperatures, but they are known to have poor oxidation resistance in adverse, high-temperature environments. Nevertheless, the combination of CVI-SiC matrix with higher stiffness and oxidation resistance, the interfacial coating, and additional surface-seal coating provides the necessary protection to the carbon fibers, and makes the material viable for high-temperature space applications operating under harsh environments. Furthermore, C/SiC composites, like other ceramic matrix composites (CMCs), exhibit graceful noncatastrophic failure because of various inherent energy-dissipating mechanisms. The material exhibits nonlinearity in deformation even at very low stress levels. This is the result of the severe matrix microcracking present in the as-processed composite because of large differences between the coefficients of thermal expansion of the fiber and the matrix.

Utilization of these advanced composites in next generation space vehicles will require innovative structural configurations, updated materials, and refined analyses. Structural safety issues for these vehicles are in direct competition with performance and cost. One would have to quantify the uncertainties associated with the design using formal probabilistic

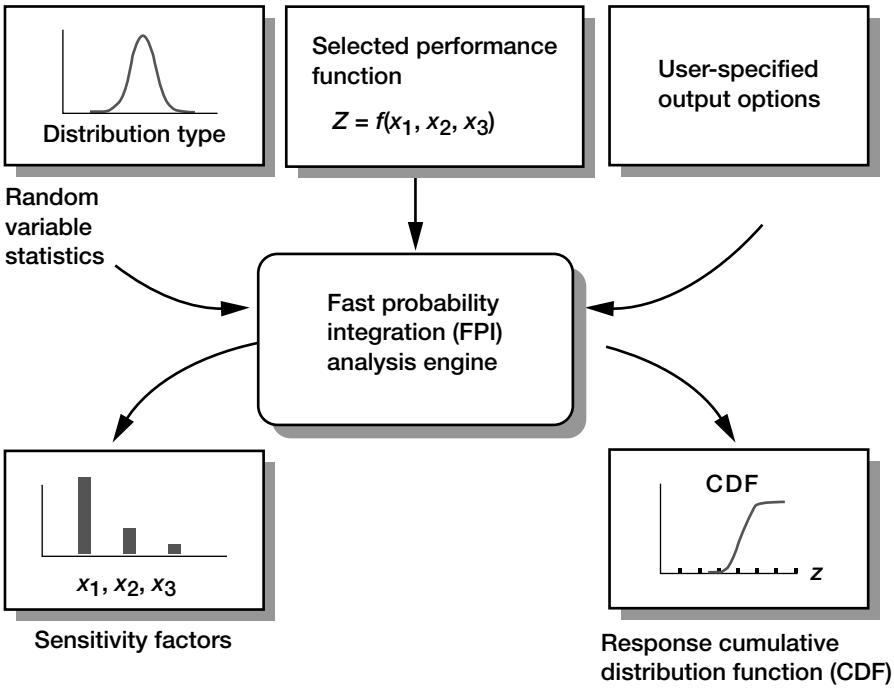

Integrated approach to computational simulation of probabilistic CMC behavior.

methods. Specifically four fundamental aspects on which analyses are based—(1) loading conditions, (2) material behavior, (3) geometrical configurations, and (4) structural connections between the composite components and baseline structure—are stochastic in nature. A direct way to formally account for uncertainties is to develop probabilistic structural analysis methods where all participating variables are described by appropriate probability density functions. The present work, however, focuses on analyzing the stochastic material behavior of these advanced composites using formal probabilistic analysis methods.

Often, some of the desirable property characteristics that allow composites to offer advantages over conventional structural materials (like tailoring of composite properties) and the complexity are in fact responsible for their greater statistical variability and the requirements for more characterization tests. Composite properties are anisotropic as well, having different properties in different directions. This means that characterization of a property such as stiffness—which will vary greatly depending on the orientation of the fiber relative to the direction of the testing—must be repeated for several different directions and loading conditions. The fabrication process for composites also introduces statistical variations in properties and geometry. A composite part is produced in a number of steps, each of which introduces statistical variability. The matrix is usually produced from a combination of raw materials; and the fiber, which has its own set of properties, is often coated or surface treated, introducing yet another source of variability. The processes are usually performed by various vendors and are not under the control of the fabricator of the composite part. Additional irregularities are introduced by the influence of temperature and moisture. Composites are usually more susceptible to environmental conditions. Changes in environmental conditions produce a significant change in properties, leading not only to a source of property variability, but also to a requirement for additional testing to characterize the effects of these variables. In general, CMCs are complex, have brittle constituents, and are potentially flaw-sensitive materials. They inherently have considerable scatter in their properties. It is important to note that because of the flaw-sensitivity of brittle materials, additional characterization is required to characterize the "volume effect." Thus, the advantages that composites bring must be weighed against increased material testing costs. Any CMC material characterization effort based solely on a large test matrix is simply impractical because of time and cost considerations.

The primary objective of the present work is to develop an efficient computational design tool that could account for all the uncertainties in the constituent properties in a more rigorous manner, and predict the overall composite properties and their probabilistic distributions. Such information could then be used to design structural components to meet the necessary life requirements at an assured level of reliability. In addition to providing more rigor to the analysis than the so-called safety factor approach, such procedures would enhance the interpretation of experimentally observed data, which usually exhibit a wide range of scatter. Furthermore, the procedure would help identify the dominant variables, those that most influence scatter in a specific response, thereby providing guidelines for quality control as well as guidance for data collection resource allocation. It is important to realize that not all variability can be controlled. Thus the methodology could be applied not only in designing with these materials but in designing better CMCs as well.

The approach taken here is to combine the woven CMC analysis in the W–CEMCAN (Woven Ceramic Matrix Composites Analyzer, ref. 1) program with the Fast Probability Integration (FPI) techniques available in the NESSUS computer code (ref. 2). The W–CEMCAN computer program provides functional relationships (micromechanics and macromechanics) that tie the constituent

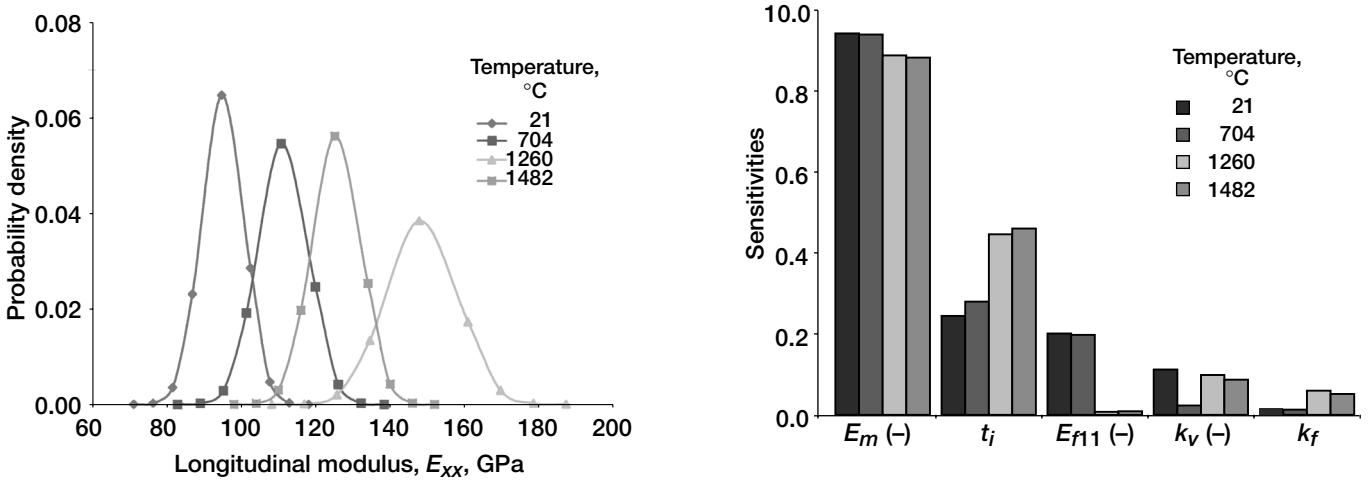

Left: Probability density function of in-plane tensile modulus. Right: Sensitivity factors of in-plane tensile modulus at probability level 0.001. E_m, matrix material modulus; t_i, coating thickness; E_{f11}, fiber longitudinal modulus; k_v (–), void volume ratio; k_f, fiber volume ratio.

properties and woven composite architecture to the overall composite properties. FPI performs probabilistic analyses by utilizing composite properties generated by W–CEMCAN. The results are cumulative distribution functions of the composite properties. A CDF is a relationship defined by the value of a property (response variable) with respect to its cumulative probability of occurrence. These can easily be converted to probability density functions of the response variable. As a byproduct of the probabilistic analyses, probabilistic sensitivities of response variables to the inherent scatter in the primitive variables are also obtained. As previously mentioned, an integrated approach is adopted in the present work. This approach is a synergistic combination of two methodologies developed in-house at the NASA Glenn Research Center. The first methodology is concerned with woven CMC micromechanics and macromechanics (refs. 1 and 3). The second methodology consists of an FPI technique that takes into account the uncertainties occurring at various scales in a composite material and computes the cumulative probability density functions of composite global behavior. A schematic of the integrated approach is shown in the figure on the preceding page.

Typical results for a carbon-fiber-reinforced silicon carbide matrix (C/SiC) woven CMC manufactured by Honeywell Advanced Composites, Inc., are shown in the graphs on this page (ref. 4). These show the probability density functions of the in-plane tensile modulus and their corresponding sensitivity factors to various primitive variables at a 0.001 probability level and four different use temperatures.

References

1. Mital, Subodh K.; Murthy, Pappu L.N.; and Chamis, Christos C.: Simplified Micromechanics of Plain Weave Composites. J. Adv. Mater., vol. 33, no. 3, 2001, pp. 10–17.
2. NESSUS/FEM User's Manual. Computer Code, version 6.2, Southwest Research Institute, Nov. 1995.
3. Murthy, Pappu L.N., et al.: Computational Simulation of Continuous Fiber-Reinforced Ceramic Matrix Composites Behavior. NASA TP–3602, 1996.
4. Mital, Subodh K.; and Murthy, Pappu L.N.: Characterizing the Properties of a C/SiC Composite Using Micromechanics Analysis. AIAA Paper 2001–1363, 2001.

Glenn contact:
Dr. Pappu L.N. Murthy, 216–433–3332, Pappu.L.Murthy@nasa.gov

University of Toledo contact:
Dr. Subodh K. Mital, 216–433–3261, Subodh.K.Mital@grc.nasa.gov

Authors:
Dr. Pappu L.N. Murthy, Dr. John P. Gyekenyesi, and Dr. Subodh K. Mital

Headquarters program office: OSS

Programs/Projects: RLV

Integrity of Ceramic Parts Predicted When Loads and Temperatures Fluctuate Over Time

Brittle materials are being used, and being considered for use, for a wide variety of high-performance applications that operate in harsh environments, including static and rotating turbine parts for unmanned aerial vehicles, auxiliary power units, and distributed power generation. Other applications include thermal protection systems, dental prosthetics, fuel cells, oxygen transport membranes, radomes, and microelectromechanical systems (MEMS). In order for these high-technology ceramics to be used successfully for structural applications that push the envelope of materials capabilities, design engineers must consider that brittle materials are designed and analyzed differently than metallic materials. Unlike ductile metals, brittle materials display a stochastic strength response because of the combination of low fracture toughness and the random nature of the size, orientation, and distribution of inherent microscopic flaws. This plus the fact that the strength of a component under load may degrade over time because of slow crack growth means that a probabilistic-based life-prediction methodology must be used when the tradeoffs of failure probability, performance, and useful life are being optimized. The CARES/*Life* code (which was developed at the NASA Glenn Research Center) predicts the probability of ceramic components failing from spontaneous catastrophic rupture when these components are subjected to multiaxial loading and slow crack growth conditions. Enhancements to CARES/*Life* now allow for the component survival probability to be calculated when loading and temperature vary over time. This capability is referred to as transient reliability analysis and can be used to predict component reliability (probability of survival) for situations such as thermal shock, startup and shutdown conditions in heat engines, and cyclic loading. The methodology has been developed with the following features:

- Transient cyclic fatigue modeling
- Ability to efficiently compute transient reliability for any number of loading cycles
- Transient proof-testing analysis capability
- Ability to account for fatigue and Weibull parameters that change over the operating temperature range

This technology is considerably more sophisticated than the common approach of making predictions based on a maximum stressed point at some snapshot in time. Instead, in predicting the probability of survival, it considers the whole history of loading and the multiaxial stress distribution throughout the entire component. The probability-of-survival algorithm uses results from transient finite element analysis, where loading profiles are broken into discrete time steps.

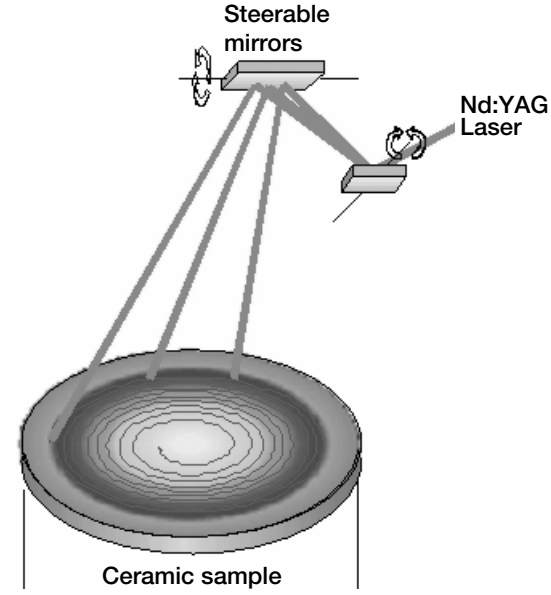

Example of a thin silicon nitride disk under thermal shock. The schematic is of the laser upshock technique (experimental data from the literature). Copyright Uwe Rettig; used with permission.

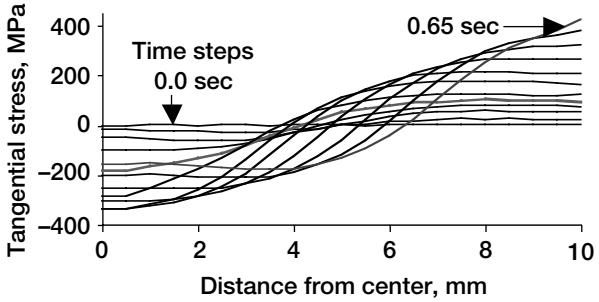

Transient tangential stress profile of a silicon nitride disk under thermal shock. Time steps range from 0.0 to 0.65 sec. Not all time steps are shown.

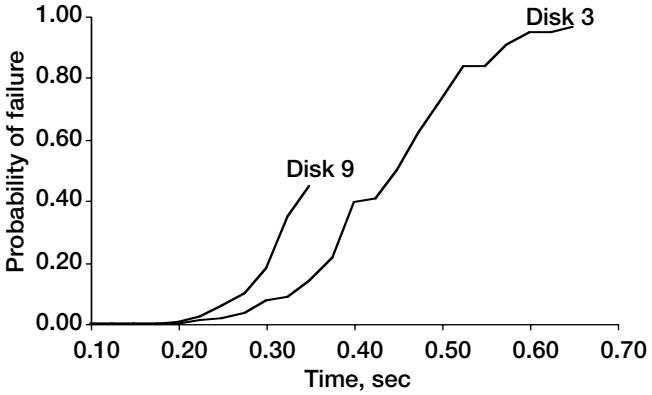

CARES/Life predicted failure probability as a function of time for disk specimens 3 and 9. The predictions are based on the transient stress profile (see the right figure on the preceding page) and a finite element model of the disk. Shown are predictions for each discrete time step (which are connected by straight line segments).

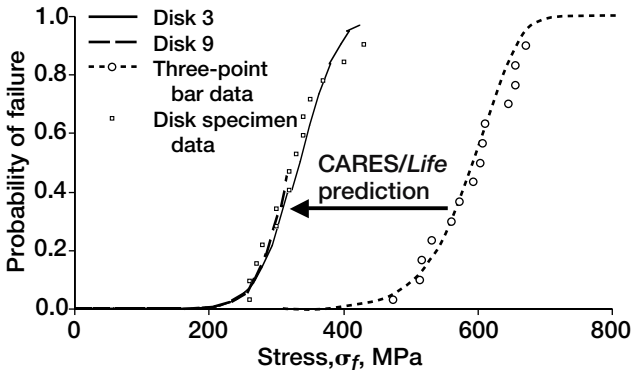

Silicon nitride disks under thermal shock. Failure probability of disk versus maximum stress predicted using CARES/Life finite element analysis and experimental results from three-point flexure bar data. Experimental rupture data are shown as discrete points. The disk prediction shown was based on the analysis of disks 3 and 9.

The figures show two examples that demonstrate some of these capabilities: the first four figures show thermal shocked silicon nitride disks in fast-fracture (where material strength does not degrade over time because of slow crack growth), and the last two figures show a silicon nitride turbine vane experiencing engine startup/shutdown conditions. These figures are described in more detail in the following paragraphs.

The preceding figures are an example of thin silicon nitride disks (20 mm diameter by 0.3 mm) rapidly heated by a laser. The experimental data were taken from the literature. The left figure on the preceding page is a schematic of the laser heating method. Starting at the center of the disk, the laser spirals out towards the edge of the disk over a time interval of approximately 1 sec. The heating of the central portion of the disk causes high tangential stresses along the edge of the disk. The right figure on the preceding page shows the transient tangential stresses versus distance as a function of time for a particular disk. The top left figure on this page shows the CARES/*Life* predictions as a function of time for two of the ruptured disks. These predictions result from a finite element model of the disk loaded with the measured thermal profile of a given disk (in this case, disks 3 and 9) as a function of time. The top right figure shows the transient CARES/*Life* predictions as a function of stress compared with experimental data. The disk prediction shown is based on an analysis of disks 3 and 9. The three-point flexure bar data were used to calibrate (characterize the material stochastic fracture behavior of) the CARES/*Life* probabilistic models.

The figures below show the transient reliability analysis for a silicon nitride stator vane during the turbine startup/shutdown cycle. The figure on the left

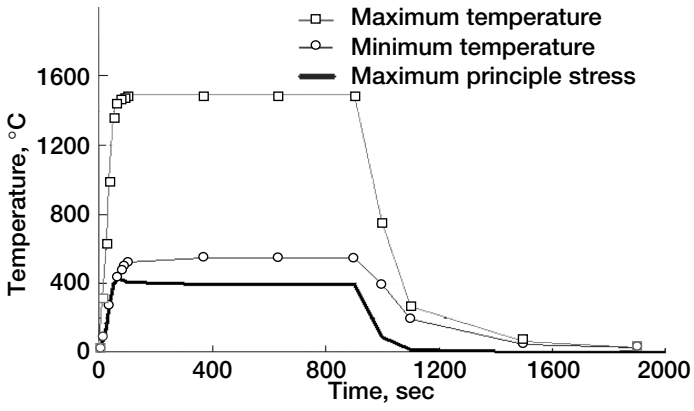

Maximum temperatures and stresses versus time for a simulated startup-shutdown cycle of a ceramic turbine vane.

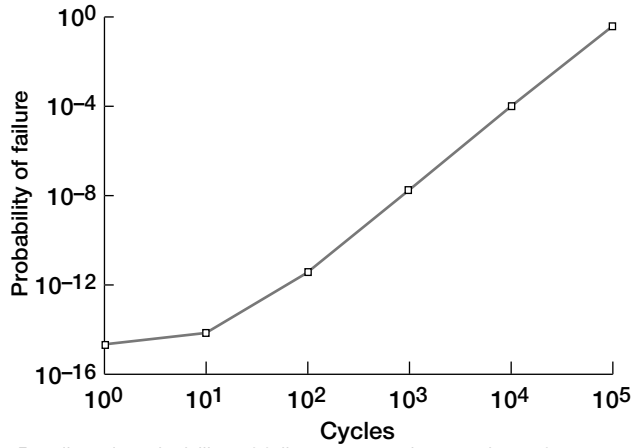

Predicted probability of failure versus the number of startup-shutdown cycles for the ceramic turbine vane.

shows the maximum vane temperatures and stresses over the startup-shutdown cycle. The figure on the right is the predicted (power law) failure probability versus the number of startup-shutdown cycles. The significance of this example is that it shows the ability to make lifetime predictions for situations where fatigue and strength modeling parameters are changing (with temperature) over the loading cycle.

Glenn contact: Noel N. Nemeth, 216–433–3215, Noel.Nemeth@nasa.gov

Author: Noel N. Nemeth

Headquarters program office: OAT

Programs/Projects: HOTPC

Particulate Titanium Matrix Composites Tested—Show Promise for Space Propulsion Applications

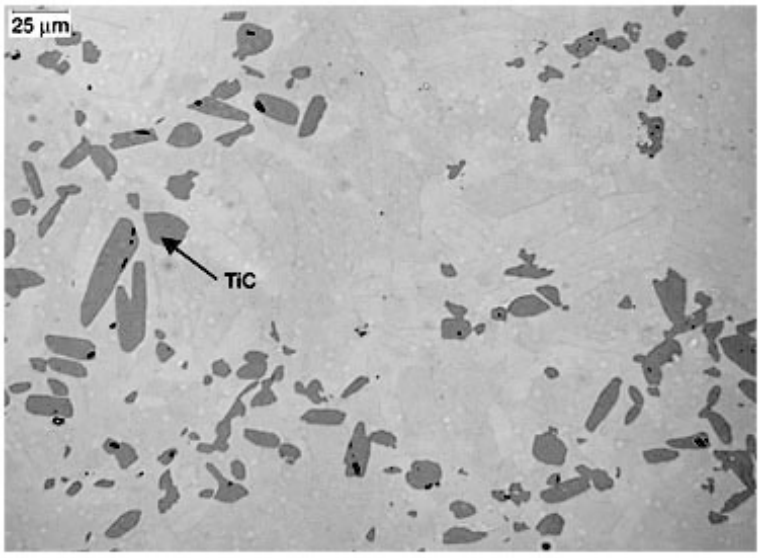

Distribution of titanium carbide particles in a matrix of Ti-6Al-4V.

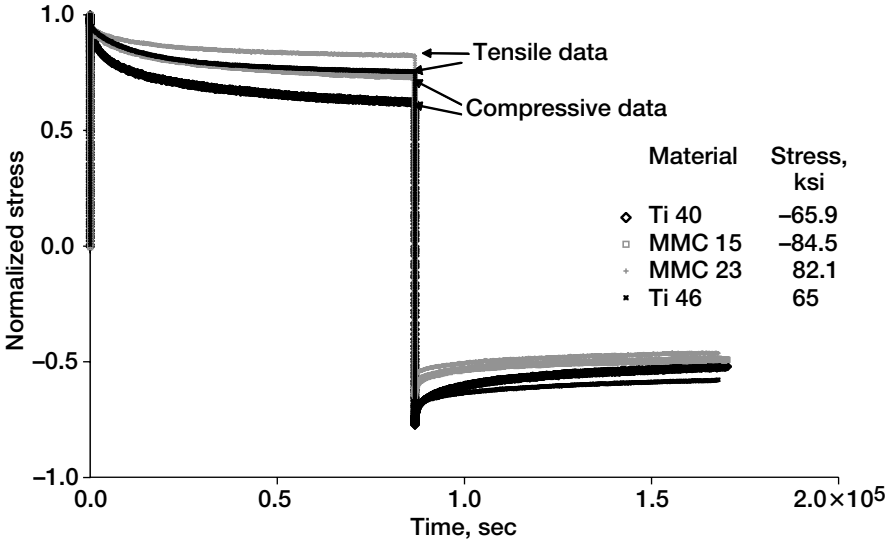

Stress relaxation behavior in tension and compression for both the composite and the neat Ti-6Al-4V alloy. MMC, metal matrix composite.

Uniformly distributed particle-strengthened titanium matrix composites (TMCs) can be manufactured at lower cost than many types of continuous-fiber composites. The innovative manufacturing technology combines cold and hot isostatic pressing procedures to produce near-final-shape components. Material stiffness is increased up to 26-percent greater than that of components made with conventional titanium materials at no significant increase in the weight. The improved mechanical performance and low-cost manufacturing capability motivated an independent review to assess the improved properties of ceramic titanium carbide (TiC) particulate-reinforced titanium at elevated temperature.

Researchers at the NASA Glenn Research Center creatively designed and executed deformation and durability tests to reveal operating regimes where these materials could lower the cost and weight of space propulsion systems. The program compares the elevated-temperature performance of titanium alloy Ti-6Al-4V matrix material to an alloy containing 10 wt% of TiC particles (see the photograph).

Initial experiments showed that at these relatively low particle concentrations the material stiffness of the TMC was improved 20 percent over that of the plain Ti-6Al-4V alloy when tested at 427 °C. The proportional limit and

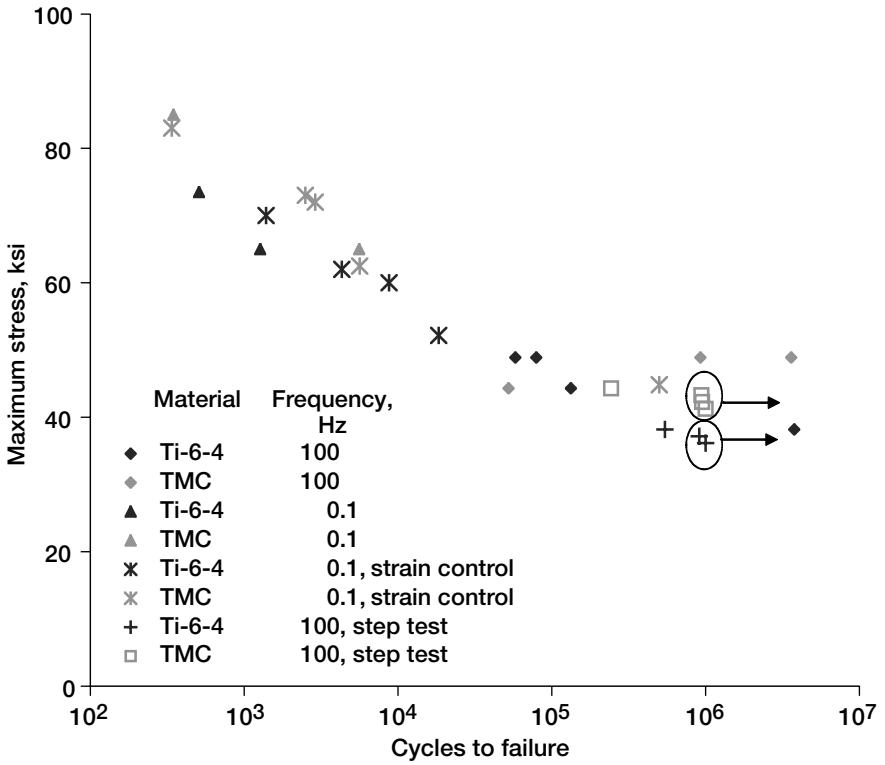

Slightly improved low-cycle fatigue response of the composite in comparison to the neat Ti-6Al-4V alloy.

ultimate strength of the composite in tension are 21- and 14-percent greater than those of the plain alloy. Compression tests showed that the proportional limit is about 30 percent greater for TMC than for the plain alloy.

The enhanced deformation resistance of the TMC was also evident in a series of tensile and compressive stress relaxation tests that were made. Specimens were subjected to tensile or compressive strain amplitudes of 0.75 percent for 24 hr followed by a return to zero strain imposed for 24 hr. The stress relaxation data were normalized with respect to the maximum stress for each case and plotted as a function of time in the graph on the preceding page. Tensile stresses relaxed 19 percent for the TMC and 25 percent for the plain Ti-6Al-4V alloy. Compressive stresses relaxed 25 percent for the TMC and 39 percent for the plain Ti-6Al-4V alloy. The superior deformation resistance of the TMC extends to a creep rate that is 28-percent slower for the TMC when it is loaded to stress levels that are 26-percent higher than for the plain Ti-6Al-4V alloy.

However, the composite's greater deformation resistance and strength is offset by a ductility reduced by one-fifth and a strain-controlled fatigue life reduced by one-third of that of the plain alloy at 427 °C. This prompted a more detailed study of the stress-controlled, low- and high-cycle fatigue response of the TMC. The graph to the left presents a master plot of new fatigue data, generated in either stress or strain control, plotting maximum stress as a function of cycles to failure. On this basis, TMC fatigue durability appears to be neutral to slightly better than that for the plain Ti-6Al-4V alloy. Furthermore, material stiffness is maintained over the entire life of the TMC specimen.

In conclusion, even a low-concentration particulate-reinforced composite can enhance strength and deformation resistance significantly with no weight penalty and no durability penalty in stress control. These experiments demonstrate that TMC's may reduce the weight and cost of space propulsion components in stress-loaded and stiffness-driven operating regimes. Continuing experiments will examine the fatigue durability of notched samples.

Find out more about this research:
http://www.grc.nasa.gov/WWW/LPB/

Ohio Aerospace Institute (OAI) contact:
Dr. John C. Thesken, 216–433–3012, John.C.Thesken@grc.nasa.gov

Glenn contacts:
Dr. Bradley A. Lerch, 216–433–5522, Bradley.A.Lerch@nasa.gov; and Dr. Steven M. Arnold, 216–433–3334, Steven.M.Arnold@nasa.gov

Authors: Dr. John C. Thesken, Dr. Bradley A. Lerch, Dr. J. Rodney Ellis, and Dr. Steven M. Arnold

Headquarters program office: OAT

Programs/Projects: HOTPC, Gen 3

Probabilistic Residual Strength Model Developed for Life Prediction of Ceramic Matrix Composites

For the next generation of reusable launch vehicles, NASA is investigating introducing ceramic matrix composites (CMCs) in place of current superalloys for structural propulsion applications (e.g., nozzles, vanes, combustors, and heat exchangers). The higher use temperatures of CMCs will reduce vehicle weight by eliminating and/or reducing cooling system requirements. The increased strength-to-weight ratio of CMCs relative to superalloys further enhances their weight savings potential. However, in order to provide safe designs for components made of these new materials, a comprehensive life-prediction methodology for CMC structures needs to be developed.

A robust methodology for lifing composite structures has yet to be adopted by the engineering community. Current industry design practice continues to utilize deterministic empirically based models borrowed from metals design for predicting material life capabilities. The deterministic nature of these models inadequately addresses the stochastic character of brittle composites, and their empirical reliance makes predictions beyond the experimental test conditions a risky extrapolation.

A team of engineers at the NASA Glenn Research Center has been developing a new life-prediction engineering model. The Probabilistic Residual Strength (PRS) model uses the residual strength of the composite as its damage metric. Expected life and material strength are both considered probabilistically to account for the observed stochastic material response. Extensive experimental testing has been carried out on C/SiC (a candidate aerospace CMC material system) in a controlled 1000 ppm O_2/argon environment at elevated temperatures of 800 and 1200 °C. The test matrix was established to allow observation of the material behavior, characterization of the model, and validation of the model's predictive capabilities. Sample results of the validation study are illustrated in the graphs.

Research in this area is ongoing with current efforts focusing on improving the representation of environmental effects within the PRS model. A testing program with SiC/SiC (a material proposed for aerocombustor and aerovane applications) in high-temperature air is also underway.

Bibliography

Verrilli, Michael J.; Calomino, Anthony; and Thomas, David J.: Stress/Life Behavior of a C/SiC Composite in a Low Partial Pressure of Oxygen Environment. I—Static Strength and Stress Rupture Database. Proceedings of the 26th Annual Conference on Composites, Advanced Ceramics, Materials, and Structures: A, American Ceramic Society, Westerville, OH, 2002, pp. 435–442.

Calomino, Anthony; Verrilli, Michael J.; and Thomas, David J.: Stress/Life Behavior of C/SiC Composites in a Low Partial Pressure of Oxygen Environment. II—Stress Rupture Life and Residual Strength Relationship. Proceedings of the 26th Annual Conference on Composites, Advanced Ceramics, Materials, and Structures: A, American Ceramic Society, Westerville, OH, 2002, pp. 443–451.

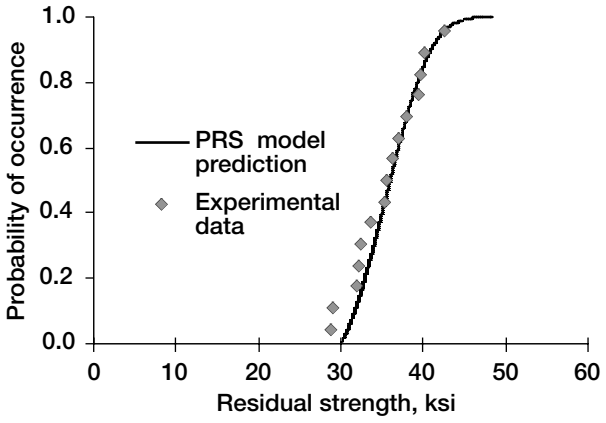

Residual strength of C/SiC after 15 hr, 30 ksi, 1200 °C, 1000-ppm O_2 exposure.

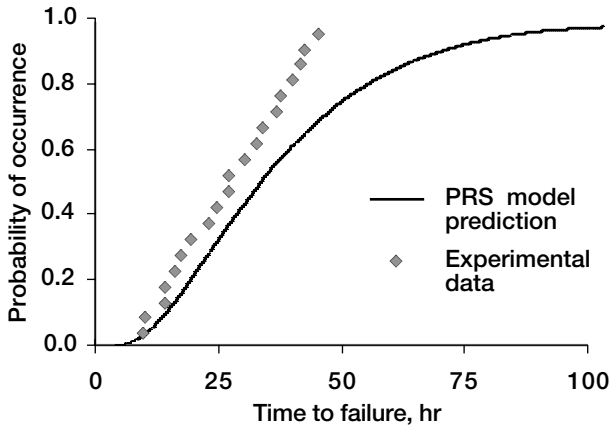

Time to failure of C/SiC under 30 ksi, 1200 °C, 1000-ppm O_2 exposure.

Thomas, David J.; Calomino, Anthony M.; and Verrilli, Michael J.: Stress/Life Behavior of C/SiC Composites in a Low Partial Pressure of Oxygen Environment. III—Life Prediction Using Probabilistic Residual Strength Model. Proceedings of the 26th Annual Conference on Composites, Advanced Ceramics, Materials, and Structures: A, American Ceramic Society, Westerville, OH, 2002, pp. 453–460.

Ohio Aerospace Institute (OAI) contact:
Dr. David J. Thomas, 216–433–5664, David.J.Thomas@grc.nasa.gov

Authors:
Dr. David J. Thomas, Michael J. Verrilli, Dr. Anthony M. Calomino

Headquarters Program Office: OAT

Programs/Projects: UEET, NGLT

Flutter Stability of the Efficient Low Noise Fan Calculated

The TURBO–AE aeroelastic code has been used to verify the flutter stability of the Efficient Low Noise Fan (ELNF), which is also referred to as the trailing-edge blowing fan. The ELNF is a unique technology demonstrator being designed and fabricated at the NASA Glenn Research Center for testing in Glenn's 9- by 15-Foot Low-Speed Wind Tunnel. In the ELNF, air can be blown out of slots near the trailing edges of the fan blades to fill in the wakes downstream of the rotating blades. This filling of the wakes leads to a reduction of the rotor-stator interaction (tone) noise that results from the interaction of wakes with the downstream stators. The ELNF will demonstrate a 1.6-EPNdB[1] reduction in tone noise through wake filling, without increasing the broadband noise. Furthermore, the reduced blade row interaction will decrease the possibility of forced response and enable closer spacing of blade rows, thus reducing engine length and weight.

During the design of the ELNF, the rotor blades were checked for flutter stability using the detailed aeroelastic analysis capability of the three-dimensional Navier-Stokes TURBO–AE code. The aeroelastic calculations were preceded by steady calculations in which the blades were not allowed to vibrate. For each rotational speed, as the backpressure was increased, the mass flow rate decreased, and the operating point moved along the constant-speed characteristic (speed-line) from choke to stall as shown on the fan map.

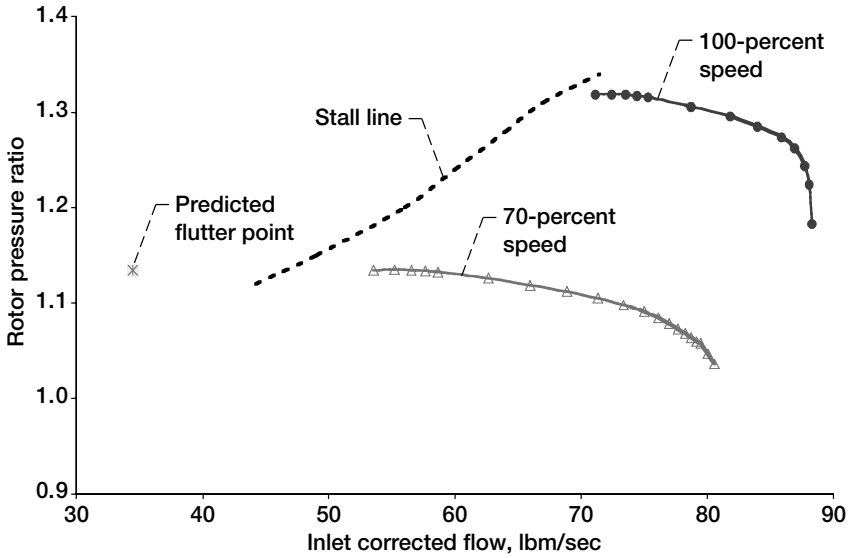

Fan map for the Efficient Low Noise Fan (ELNF) showing constant-speed characteristics, or speed lines, and the flutter point calculated using the TURBO–AE aeroelastic analysis code.

The TURBO–AE aeroelastic analyses were performed separately for the first two vibration modes (bending and torsion) and covered the complete range of interblade phase angles or nodal diameters at which flutter can occur. The results indicated that the ELNF blades would not encounter flutter at takeoff conditions. The calculations were then repeated for a part-speed condition (70-percent rotational speed), and the results again showed no flutter in the operating region. On the fan map (shown), the predicted flutter point at part-speed condition was located beyond the stall line, which means that the ELNF will not encounter flutter since it will never operate beyond the stall line. All the calculations done so far have been for the nonblowing case, and selected calculations will be repeated with air blowing from the trailing edge of the fan.

[1]Effective perceived noise level.

The completion of the TURBO–AE flutter calculations for the ELNF with trailing edge blowing will verify that there will not be unexpected flutter problems during wind tunnel testing of this unique technology demonstrator. The aeroelastic calculations described here were performed under a contract by University of Toledo researchers in collaboration with Glenn researchers. This work was supported by the Quiet Aircraft Technology Project and the Ultra-Efficient Engine Technology Project.

Glenn contact:
Dr. Milind A. Bakhle, 216–433–6037, Milind.A.Bakhle@nasa.gov

University of Toledo contact:
Dr. Rakesh Srivastava, 216–433–6045, Rakesh.Srivastava@grc.nasa.gov

Authors: Dr. Milind A. Bakhle and Dr. Rakesh Srivastava

Headquarters program office: OAT

Programs/Projects: QAT, UEET

TURBO–AE Code Used to Redesign the Quiet High-Speed Fan

The NASA/Honeywell Quiet High-Speed Fan (QHSF) was designed with aggressive goals for performance and noise reduction. During testing in NASA Glenn Research Center's 9- by 15-Foot Low-Speed Wind Tunnel, this forward-swept fan performed very well at design speed, and it also accomplished its goal of decreasing noise (6 dB measured) from the baseline fan used in current engines. However, an unexpected, severe flutter problem was encountered at part-speed conditions.

Honeywell and Glenn used the flutter analysis capability of the TURBO–AE code to redesign the QHSF. The TURBO–AE code was included in Honeywell's design cycle. During the redesign effort, more than 30 airfoil geometries were analyzed in the design-of-experiments approach and more than 600 TURBO–AE flutter analyses were performed. The redesigned QHSF II, which is predicted to be flutter-free throughout its operating range, is being fabricated and will be tested in Glenn's 9- by 15-ft wind tunnel in the near future. Engine validation of the TURBO–AE flutter predictions for the QHSF II will be conducted on Honeywell's AS–907 advanced technology demonstrator engine in 2005. This work contributes directly to NASA's 10-year goal of reducing noise in future aircraft by 50 percent (10 dB) from current levels. It also enables aircraft engine blade rows to be checked for flutter stability during design with realistic physics modeling, thus eliminating added costs ($5 to $30 million) and delays (1 to 3 months) in engine development due to unexpected flutter vibrations. If a flutter analysis tool such as TURBO–AE had been available during the original QHSF design effort, the entire QHSF redesign may have been avoided, with an estimated saving of $2.4 million. The flutter calculations described here were performed under a contract by University of Toledo researchers in collaboration with Glenn and Honeywell researchers. All of this work was funded by the Quiet Aircraft Technology project (Dr. Joseph Grady, project manager).

Glenn contact:
Dr. Milind A. Bakhle, 216–433–6037, Milind.A.Bakhle@nasa.gov

University of Toledo contact:
Dr. Rakesh Srivastava, 216–433–6045, Rakesh.Srivastava@grc.nasa.gov

Authors: Dr. Milind A. Bakhle and Dr. Rakesh Srivastava

Headquarters program office: OAT

Programs/Projects: QAT, QHSF

Testing of Composite Fan Vanes With Erosion-Resistant Coating Accelerated

The high-cycle fatigue of composite stator vanes provided an accelerated life-state prior to insertion in a test stand engine. The accelerated testing was performed in the Structural Dynamics Laboratory at the NASA Glenn Research Center under the guidance of Structural Mechanics and Dynamics Branch personnel. Previous research on fixturing and test procedures developed at Glenn determined that engine vibratory conditions could be simulated for polymer matrix composite vanes by using the excitation of a combined slip table and electrodynamic shaker in Glenn's Structural Dynamics Laboratory. Bench-top testing gave researchers the confidence to test the coated vanes in a full-scale engine test.

Coated stator vane on the shaker slip table. Total vane height is approximately 15 cm (6 in.).

Bypass fan stator vanes from the AE3007 (Rolls-Royce Corporation, Indianapolis, IN) gas turbine engine were coated by Engelhard (Windsor, CT) with compliant bond coatings and hard ceramic coatings. The coatings were developed collaboratively by Glenn and Allison Advanced Development Company (AADC)/Rolls-Royce Corporation (Indianapolis, IN) through research sponsored by the Advanced High-Temperature Engine Materials Technology Program (HITEMP) and the Higher Operating Temperature Propulsion Components (HOTPC) Project. High-cycle fatigue was performed through high-frequency vibratory testing on a shaker table.

At the request of Rolls Royce engineers, four stator vane segments were preconditioned by high-cycle fatigue using Glenn's facilities. The bypass stator vanes for the AE3007 engine were assembled as segments consisting of three vanes. Two of the vane segments were cycled for 30 million cycles at a maximum strain amplitude of 300 to 400 microstrain. This fatigue condition is comparable to the loading on the vanes during nominal engine conditions. The other two vane segments were tested for 5 million cycles at a maximum strain amplitude of 600 to 700 microstrain—a level estimated to correspond to an aerodynamic engine overload condition. The vanes were instrumented with both lightweight accelerometers and strain gauges to establish resonant frequencies, deflection mode shape, and strain amplitudes. Inspection with a fluorescent-dye penetrant indicated that at the higher strain amplitude the bench-top fatigue had initiated small cracks in the vanes from one of the segments tested. No obvious damage was found on the vanes from the other three vane segments.

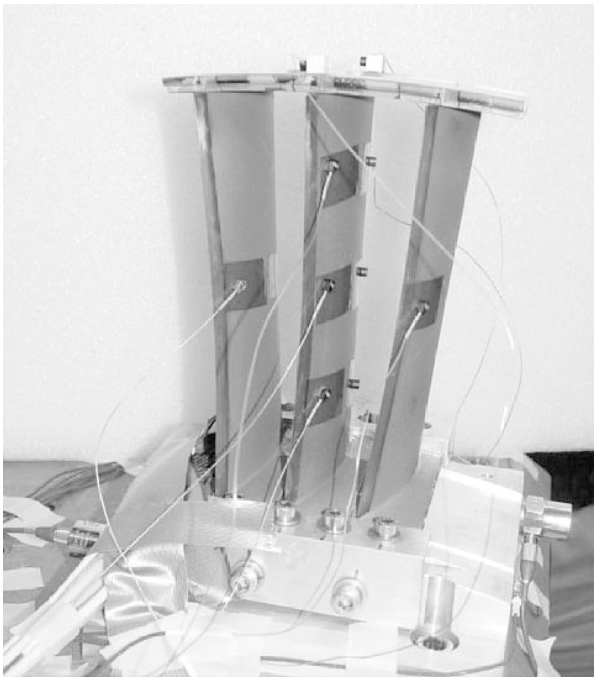

Bypass fan vane segment instrumented for accelerated life testing via high-cycle fatigue.

The four preconditioned vane segments were inserted into a test-stand, AE3007 engine at Rolls Royce America in Indianapolis, Indiana. Also in the engine were vane segments that had not experienced accelerated testing, as well as baseline, uncoated production vanes. The coated vanes were successfully engine tested for 4750 engine cycles (1663 hr). The coating remained intact (did not spall or come off the vanes) even though some cracking occurred. The segments that had been preconditioned to the higher-than-normal strain amplitudes were the first

to show damage or coating crack growth when inspected during interruptions in the engine testing. The damage on the preconditioned vanes was similar to that on the vanes that were not preconditioned. Therefore, bench-top testing is a useful means for developing accelerated life history on the vanes.

Find out more about this research:

Glenn's Structural Mechanics and Dynamics Branch:
http://structures.grc.nasa.gov/5930/

Glenn's Polymers Branch:
http://www.nasa.gov/WWW/MDWeb/5150/Polymers.html

Glenn's Structural Dynamics Laboratory:
http://www.grc.nasa.gov/WWW/Facilities/int/sdl/

Glenn contacts:
Dr. Cheryl L. Bowman, 216–433–8462, Cheryl.L.Bowman@nasa.gov;
Dr. James K. Sutter, 216–433–3226, James.K.Sutter@nasa.gov; and
Gail P. Perusek, 216–433–8729, Gail.P.Perusek@nasa.gov

Analex contact:
Kim D. Otten, 216–433–2224, Kim.D.Otten@grc.nasa.gov

Zin Technologies contact:
Sergey Samorezov, 216–433–5294, Sergey.Samorezov@grc.nasa.gov

Authors: Dr. Cheryl L. Bowman, Dr. James K. Sutter, Kim D. Otten, Sergey Samorezov, and Gail P. Perusek

Headquarters program office: OAT

Programs/Projects: HOTPC

Cryogenic Electric Motor Tested

Technology for pollution-free "electric flight" is being evaluated in a number of NASA Glenn Research Center programs. One approach is to drive propulsive fans or propellers with electric motors powered by fuel cells running on hydrogen. For large transport aircraft, conventional electric motors are far too heavy to be feasible. However, since hydrogen fuel would almost surely be carried as liquid, a propulsive electric motor could be cooled to near liquid hydrogen temperature (–423 °F) by using the fuel for cooling before it goes to the fuel cells. Motor windings could be either superconducting or high-purity normal copper or aluminum. The electrical resistance of pure metals can drop to 1/100th or less of their room-temperature resistance at liquid hydrogen temperature. In either case, super or normal, much higher current density is possible in motor windings. This leads to more compact motors that are projected to produce 20 hp/lb or more in large sizes, in comparison to on the order of 2 hp/lb for large conventional motors. High power density is the major goal. To support cryogenic motor development, we have designed and built in-house a small motor (7-in. outside diameter) for operation in liquid nitrogen.

The motor is of the switched reluctance type. It can run both at room temperature and in liquid nitrogen. In early testing, we operated it in liquid nitrogen to 11,000 rpm and at room temperature to 16,000 rpm. The motor produced 10.6-kW (14.2-hp) power and 21 N·m (15.5 ft·lb)) torque with all of its 12 coils installed. Operating with only its own inertia as a load, the motor can accelerate from a 500 rpm idle to 8000 rpm in 0.23 sec. It is shown in the photograph submerged in liquid nitrogen. The haziness is due partly to the liquid nitrogen that covers the motor and partly to moisture from the room condensing in the cold nitrogen gas over the motor. Frost is also visible on some of the parts.

The maximum current density we have used is 30 A/mm^2, which is not sustainable at room temperature in a steady state. (Maximum room-temperature current density in steady state would be about 11 A/mm^2). However, in liquid nitrogen we have shown that maximum coil current densities of about 100 A/mm^2 (at the 50-percent duty cycle for coils in the motor) are possible in a steady state for coils that are specially configured for good heat transfer.

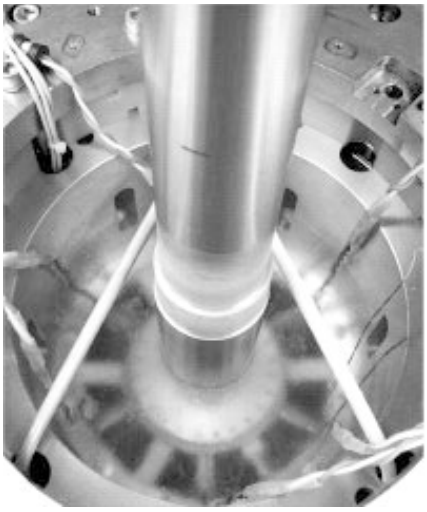

Switched reluctance motor submerged in liquid nitrogen (with 6 of 12 motor coils and a sensor coil installed).

Upgrading the power conditioning will extend the high torque produced at

low rpm to higher rpm. This will markedly increase the power production (and hence the specific power). The present limits of 160 V and 30 A per phase will be increased to 300 V and 100 A per phase in the first upgrade stage. A factor of 4 or more increase in power (from 14 kW) is predicted in the upgraded configuration.

The motor serves two purposes. It is a test bed for special motor winding configurations, and it will validate structural, electromagnetic, and heat transfer analysis and design procedures that can subsequently be applied to liquid-hydrogen-cooled motors.

Glenn contact:
Dr. Gerald V. Brown, 216–433–6047, Gerald.V.Brown@nasa.gov

Author: Dr. Gerald V. Brown

Headquarters program office: OAT

Programs/Projects:
Propulsion and Power, VSP, RAC

Design of Ultra-High-Power-Density Machine Optimized for Future Aircraft

The NASA Glenn Research Center's Structural Mechanics and Dynamics Branch is developing a compact, nonpolluting, bearingless electric machine with electric power supplied by fuel cells for future "more-electric" aircraft with specific power in the projected range of 50 hp/lb, whereas conventional electric machines generate usually 0.2 hp/lb. The use of such electric drives for propulsive fans or propellers depends on the successful development of ultra-high-power-density machines. One possible candidate for such ultra-high-power-density machines, a round-rotor synchronous machine with an engineering current density as high as 20,000 A/cm^2, was selected to investigate how much torque and power can be produced.

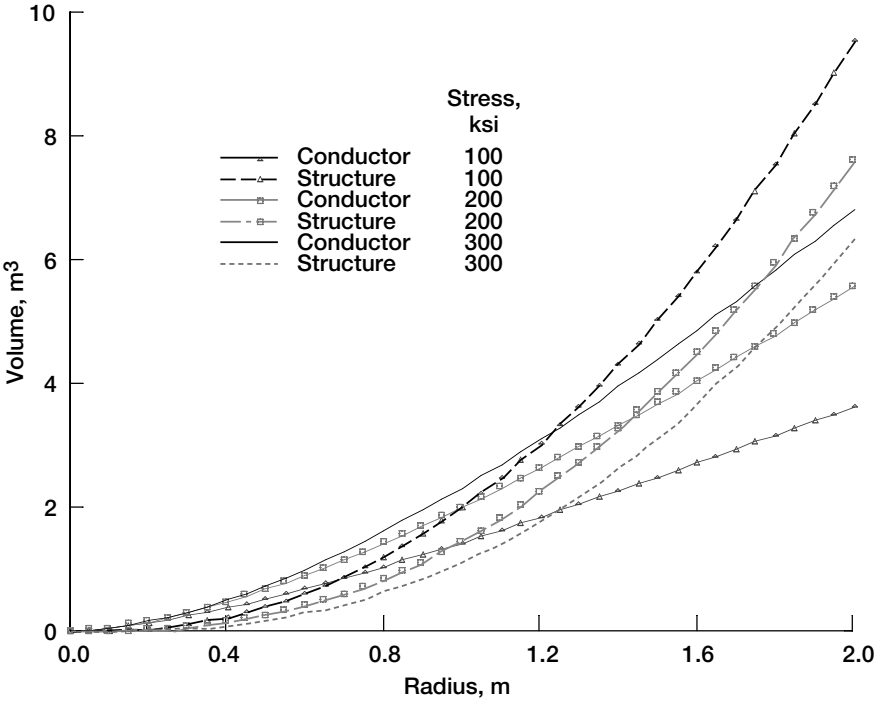

Volume per unit length of disk.

Last year we developed a code and finite element model for analyzing and optimizing the performance of ultra-high-power-density and high-specific-power machine that consists of rotor and stator windings and back-irons. This analytical code written in the MatLab language and a finite element model by AnSoft gave us the basic tools for optimal designs for synchronous round-motor machines.

This year we derived an improved electromagnetic model with carbon fiber structure on the rotor and implemented it into the current optimization code. At first we added a filament-wound structure to the rotor in proportion to local centrifugal stress, reducing the current density by the volume fraction occupied by the structure (see the graph to the left). Then, we optimized the results with respect to motor dimensions. At this point, the hoop stress due to electromagnetic tangential force was not considered because centripetal stress dominates in the rotor. Also the number of input and output parameters for the existing code variables for optimizing either specific power or power density was modified to provide more detailed quantitative results and to give the code the ability to determine optimal designs for synchronous round-motor

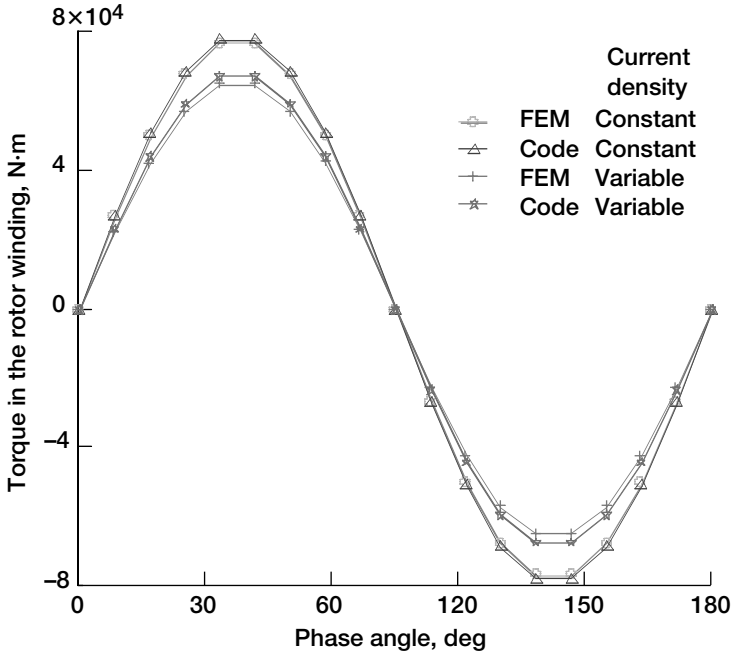

Torque in the four-pole synchronous motor with constant and variable current density.

machines. We also conducted a preliminary study to examine factors that influence the choice of motor length-to-diameter ratio, and we determined the optimum length-to-diameter ratio for best power density.

We enhanced our Electromagnetic Analysis of Synchronous Machine code and verified the results using an AnSoft (finite element software) model (see the graph to the left). This work showed the feasibility of using this technology for a future more-electric engine, making advances on the Ultra-High-Power-Density Motor project.

Glenn contacts:
Dr. Benjamin B. Choi, 216–433–6040, Benjamin.B.Choi@grc.nasa.gov; and Dr. Gerald V. Brown, 216–433–6047, Gerald.V.Brown@nasa.gov

Author: Dr. Benjamin B. Choi

Headquarters program office: OAT

Program/Projects: RAC

"Fan-Tip-Drive" High-Power-Density, Permanent Magnet Electric Motor and Test Rig Designed for a Nonpolluting Aircraft Propulsion Program

A scaled blade-tip-drive test rig was designed at the NASA Glenn Research Center. The rig is a scaled version of a direct-current brushless motor that would be located in the shroud of a thrust fan. This geometry is very attractive since the allowable speed of the armature is approximately the speed of the blade tips (Mach 1 or 1100 ft/s). The magnetic pressure generated in the motor acts over a large area and, thus, produces a large force or torque. This large force multiplied by the large velocity results in a high-power-density motor.

The goal of the test program is to maximize both the armature speed and the stator current density, thus producing a very high power density motor. The unique feature of the rig is that a generator provides the electrical current and voltage to drive the motor. The test motor and an auxiliary motor provide the

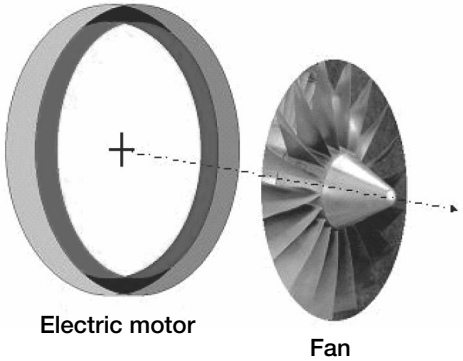

Blade tip fan drive.

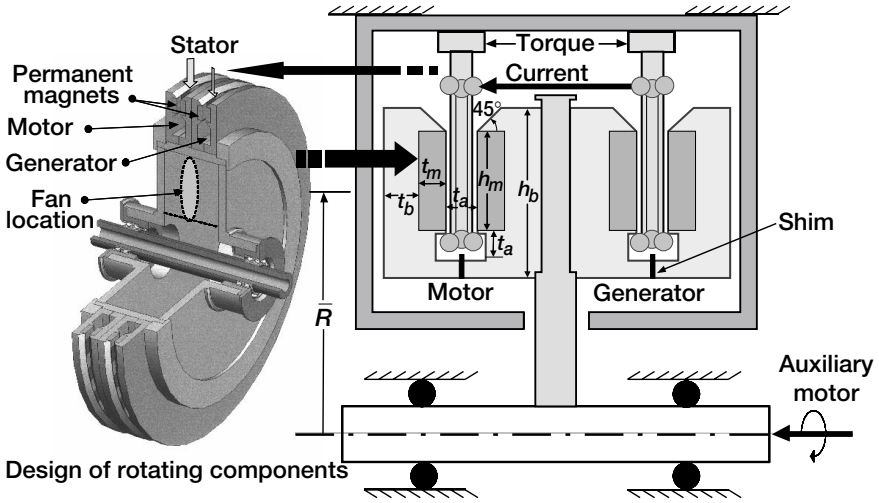

Operation of blade tip fan drive rig. Power, 115 kW; voltage, 576 V; current, 50 A; torque, 84.4 ft-lb; speed, 9550 rpm; radius of armature, R, 12 in.; thickness of back-iron, t_b, 0.5 in.; thickness of stator, t_a, 0.25 in.; thickness of magnets, t_m, 0.375 in.; height of magnets, h_m, 1.2 in.

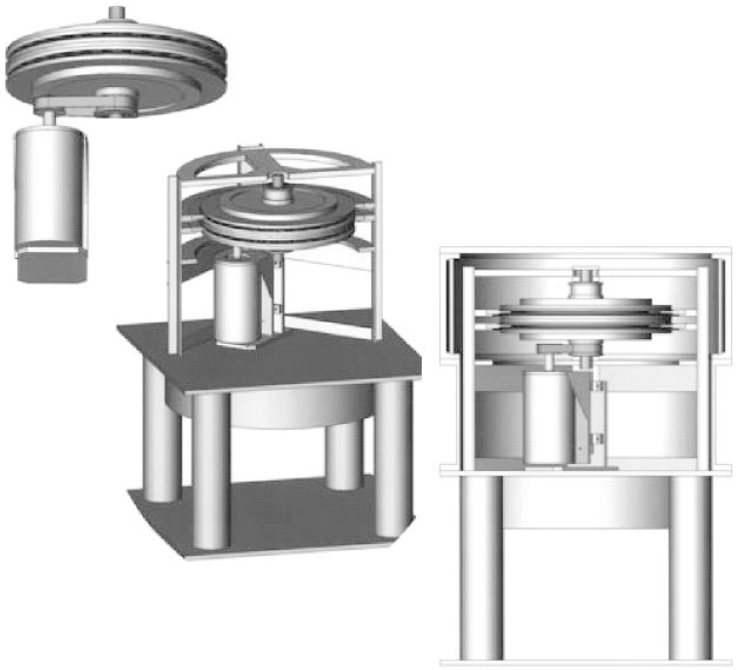

Assembly of blade tip fan drive rig.

torque to drive the generator. The auxiliary motor will also control the speed of the test rig. Later a pulse-width-modulated motor drive will be developed to drive the motor, and the torque will be absorbed by the generator.

Find out more about this research:
http://sdwww.grc.nasa.gov/5900website/5930/

Glenn contact:
Dr. Gerald V. Brown, 216–433–6047, Gerald.V.Brown@nasa.gov

U.S. Army Research Laboratory, Vehicle Technology Directorate at Glenn contact:
Albert F. Kascak, 216–433–6024, Albert.F.Kascak@grc.nasa.gov

Authors:
Dr. Gerald V. Brown and Albert F. Kascak

Headquarters program office: OAT

Programs/Projects: RAC

Method Developed for Noninterference Measurement of Blade Damping

Although noninterference optical instrumentation has been previously used to monitor and measure rotor blade vibrations, it has not been used at the NASA Glenn Research Center for the determination of damping. This article describes such a measurement in Glenn's Spin Rig facility. The optical system was chosen because installation of the slip rig for this particular configuration was not feasible, ruling out strain gauge instrumentation. The shaft in this facility was suspended with two radial magnetic bearings, and the excitation was supplied to the bearings by a signal generator. For the first mode, the direction of excitation force was always perpendicular to the blade as described by Morrison (ref. 1).

The graph on the left shows blade displacements, as measured by an optical probe during a frequency sweep designed to locate the first mode resonance. The resonance determines the frequency at which the shaft is excited. Because the sampling rate was fixed to only once per revolution with these transducers, and the first mode frequency was much larger than the rotational frequency, the data in this figure were undersampled with an apparent frequency that was only 1 Hz at the beginning of the sweep, about 14 Hz at the maximum amplitude, and about 20 Hz at the end of the sweep. The true excitation frequency varied during the sweep from 320 to 340 Hz, and the resonance occurred at 334 Hz.

Damping is determined by applying a frequency burst to the shaft. Upon cessation of the burst, the blade undergoes free decay. The apparent damping is then obtained by a least-squares fit of the theoretical cosine decay function through the experimental points. The graph on the right illustrates this procedure. Because of frequency aliasing, the apparent measured damping must be divided by the ratio of the true resonant frequency to the apparent measured frequency to obtain the true damping. Note that the contribution of the shaft vibration to the blade vibration could be neglected because it was shown that it is an order of magnitude smaller and that its decay is an order of magnitude faster.

The free decay method could not be applied for the higher torsional mode, because the displacements were smaller and frequency aliasing was higher, yielding an insufficient number of cycles for the decay fit. For this mode, damping was determined by the least-squares fitting of the theoretical forced frequency response function to the experimental data.

Reference

1. Morrison, Carlos R., et al.: Fully Suspended, Five-Axis, Three-Magnetic-Bearing Dynamic Spin Rig With Forced Excitation. NASA/TP—2004-212694, 2004. http://gltrs.grc.nasa.gov/cgi-bin/GLTRS/browse.pl?2004/TP-2004-212694.html

Glenn contacts:
Dr. Anatole P. Kurkov, 216–433–5695, Anatole.P.Kurkov@nasa.gov;
Andrew J. Provenza, 216–433–6025, Andrew.J.Provenza@nasa.gov; and
Carlos R. Morrison, 216–433–8447, Carlos.R.Morrison@nasa.gov

Author: Dr. Anatole P. Kurkov

Headquarters program office: OAT

Programs/Projects: QAT

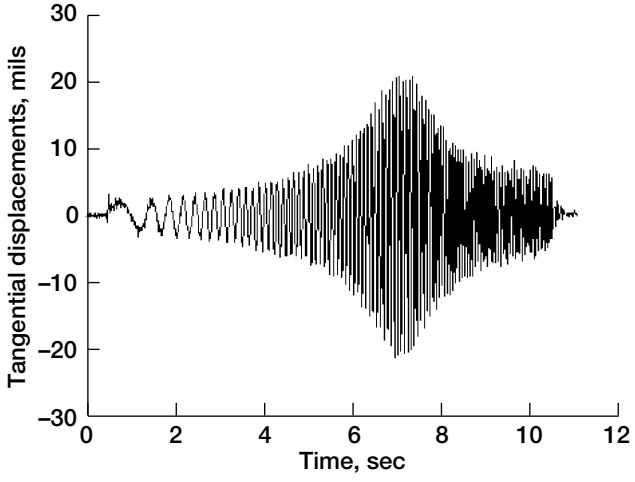

Frequency sweep through the resonance.

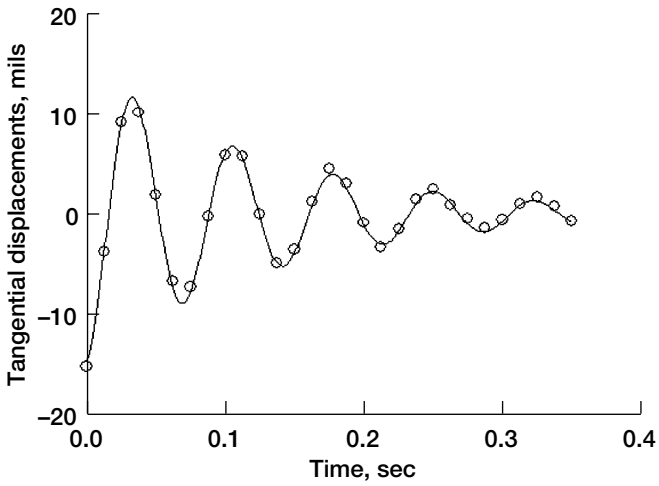

Least-squares fit of a decaying cosine function through experimental points.

New Tool Released for Engine-Airframe Blade-Out Structural Simulations

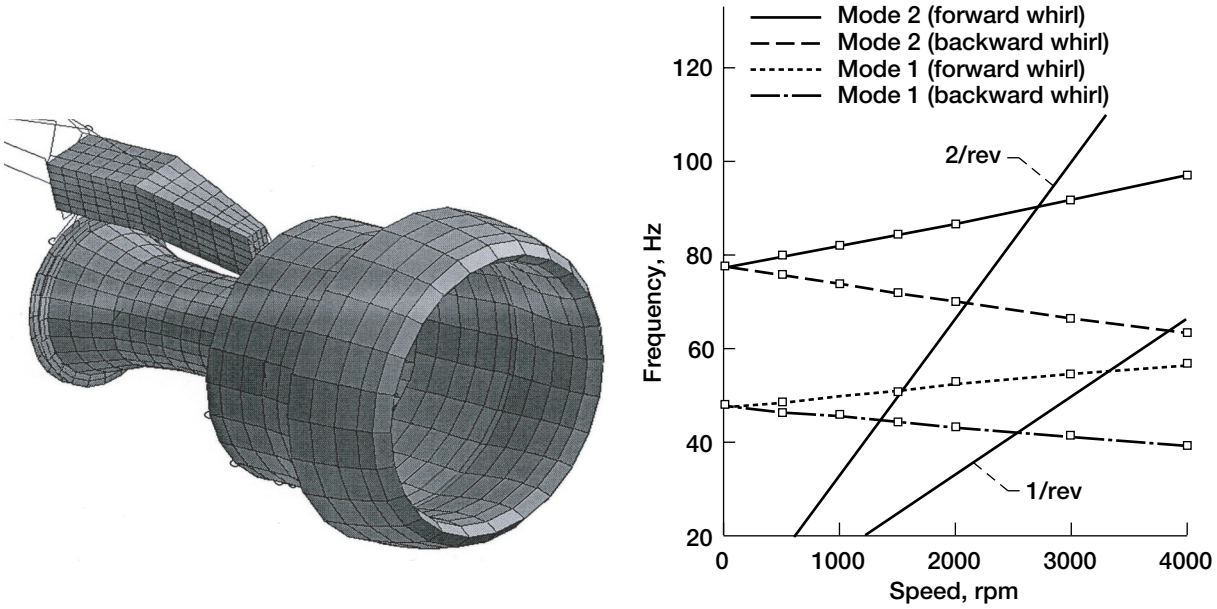

Detailed blade-fan-case interaction model. Left: Aircraft engine finite element model. Right: Natural vibration frequencies.

Researchers at the NASA Glenn Research Center have enhanced a general-purpose finite element code, NASTRAN, for engine-airframe structural simulations during steady-state and transient operating conditions. For steady-state simulations, the code can predict critical operating speeds, natural modes of vibration, and forced response (e.g., cabin noise and component fatigue). The code can be used to perform static analysis to predict engine-airframe response and component stresses due to maneuver loads. For transient response, the simulation code can be used to predict response due to bladeoff events and subsequent engine shutdown and windmilling conditions. In addition, the code can be used as a pretest analysis tool to predict the results of the bladeout test required for FAA certification of new and derivative aircraft engines.

Before the present analysis code was developed, all the major aircraft engine and airframe manufacturers in the United States and overseas were performing similar types of analyses to ensure the structural integrity of engine-airframe systems. Although there were many similarities among the analysis procedures, each manufacturer was developing and maintaining its own structural analysis capabilities independently. This situation led to high software development and maintenance costs, complications with manufacturers exchanging models and results, and limitations in predicting the structural response to the desired degree of accuracy. An industry-NASA team was formed to overcome these problems by developing a common analysis tool that would satisfy all the structural analysis needs of the industry and that would be available and supported by a commercial software vendor so that the team members would be relieved of maintenance and development responsibilities. Input from all the team members was used to ensure that everyone's requirements were satisfied and that the best technology was incorporated into the code. Furthermore, because the code would be distributed by a commercial software vendor, it would be more readily available to engine and airframe manufacturers, as well as to nonaircraft companies that did not previously have access to this capability.

The development team included MSC.Software, the developer of the commercial finite element code NASTRAN. As part of this team activity, MSC.Software incorporated a wide spectrum of unique features and innovations for engine-airframe simulation into NASTRAN. A summary of these features follows:

(1) *Multicomponent substructuring*. Engine-airframe structures are very large and complex, and they use finite element models often containing millions of degrees of freedom. Model reduction is required to practically implement these models for transient and steady-state analysis. The present code contains a full range of model-reduction capabilities that enables a large engine-airframe model to be condensed to

a reduced-order model without sacrificing the accuracy contained in the original full-fidelity model. The present code can reduce complex three-dimensional rotor models to simplified line models.

(2) *Gyroscopic terms in steady-state and transient solutions*. The analysis of engine-airframe structures requires the incorporation of the rotational effects generated by the rotating turbomachinery. Gyroscopic terms were added into the equations of motion for the steady-state and transient response to include rotational effects in the analysis code. Spooldown and windmilling effects can be simulated because the engine rotational speed is allowed to vary with time. Rotor internal damping and gyroscopic effects also were included in static analysis so that the loads resulting from aircraft maneuvers could be computed.

(3) *Multishaft systems*. Many aircraft engines, particularly larger size engines, consist of multishaft turbomachinery with each of the shafts rotating at different speeds. To accommodate this feature, the code incorporates the ability to model any number of spools, each rotating at arbitrary speeds.

(4) *Sudden blade loss and spooldown effects*. The ability to model the transient loading that occurs during a blade loss event is incorporated in the code by allowing for multiple blade mass unbalances to be applied at locations along the rotor at different rotor angles and times. Spooldown effects that occur after the blade loss has occurred and the engine is shut down and begins a windmilling phase are incorporated by allowing for the rotational speed to be a nonconstant time-varying parameter. In addition to the unbalance load normally associated with a blade loss, the change in rotor inertia properties resulting from blade loss and damage can be included as a parametric disturbance to the system. This effect may lead to self-excited instabilities and additional loadings.

(5) *Fan-case interaction models*. During a blade-off event, the large unbalance loads cause the rotor to exhibit large displacements that, in turn, cause the rotor blades to contact the casings. To model this occurrence, the code contains rub elements that apply a restoring force that pushes the rotor back into alignment and a friction force that opposes rotor rotation.

MSC.Software will market and distribute this version of NASTRAN worldwide. Every major commercial aircraft engine and airframe manufacturer in the world is committed to using this code. The new capabilities for rotating equipment simulation extend beyond aircraft structures and include applications in areas such as the automotive industry, space, military research and development, and power generation.

Glenn contacts:
Dr. Charles Lawrence, 216–433–6048, Charles.Lawrence-1@nasa.gov; and
Dr. Kelly S. Carney, 216–433–2386, Kelly.S.Carney@nasa.gov

Author: Dr. Charles Lawrence

Headquarters program office: OAT

Programs/Projects: PR&T, Ultra Safe

Prototype Morphing Fan Nozzle Demonstrated

Ongoing research in NASA Glenn Research Center's Structural Mechanics and Dynamics Branch to develop smart materials technologies for aeropropulsion structural components has resulted in the design of the prototype morphing fan nozzle shown in the photograph on the next page. This prototype exploits the potential of smart materials to significantly improve the performance of existing aircraft engines by introducing new inherent capabilities for shape control, vibration damping, noise reduction, health monitoring, and flow manipulation. The novel design employs two different smart materials, a shape-memory alloy and magnetorheological fluids, to reduce the nozzle area by up to 30 percent.

The prototype of the variable-area fan nozzle implements an overlapping spring leaf assembly to simplify the initial design and to provide ease of structural control. A single bundle of shape memory alloy wire actuators is used to reduce the nozzle geometry. The nozzle is subsequently held in the reduced-area configuration by using magnetorheological fluid brakes. This prototype uses the inherent advantages of shape memory alloys in providing large induced strains and of magnetorheologcal fluids in generating large resistive forces. In addition, the spring leaf design also functions as a return spring, once the magnetorheological fluid brakes are released, to help force the shape memory alloy wires to return to their original position. A computerized real-time control system uses the derivative-gain and proportional-gain algorithms to operate the system.

Prototype of a variable-area fan nozzle implementing overlapping spring leaf assembly, shape memory alloy wire actuators, and magnetorheological fluid locks.

This design represents a novel approach to the active control of high-bypass-ratio turbofan engines. Researchers have estimated that such engines will reduce thrust specific fuel consumption by 9 percent over that of fixed-geometry fan nozzles. This research was conducted under a cooperative agreement (NCC3–839) at the University of Akron.

Glenn contact:
Dr. Ho-Jun Lee, 216–433–3316, Ho-Jun.Lee-1@nasa.gov

Authors:
Dr. Ho-Jun Lee and Prof. Gangbing Song

Headquarters program office: OAT

Programs/Projects: RAC

Reduced-Order Blade Mistuning Analysis Techniques Developed for the Robust Design of Engine Rotors

The primary objective of this research program is to develop vibration analysis tools, design tools, and design strategies to significantly improve the safety and robustness of turbine engine rotors. Bladed disks in turbine engines always feature small, random blade-to-blade differences, or mistuning. Mistuning can lead to a dramatic increase in blade forced-response amplitudes and stresses. Ultimately, this results in high-cycle fatigue, which is a major safety and cost concern. In this research program, the necessary steps will be taken to transform a state-of-the-art

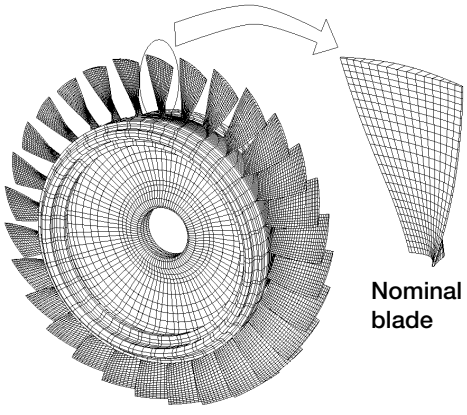

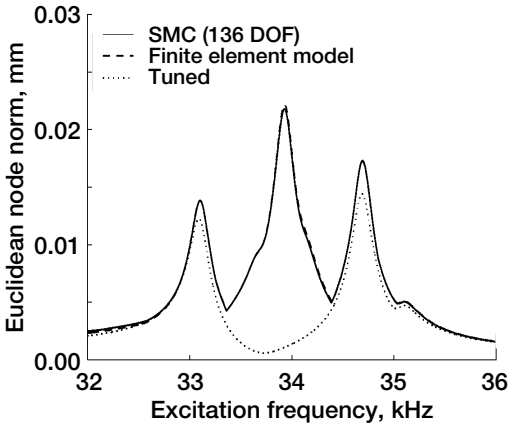

Prototype of a variable-area fan nozzle implementing an overlapping spring leaf assembly, shape-memory alloy wire actuators, and magnetorheological fluid locks. Significant decrease in degrees of freedom (DOF) is shown with the reduced-order modeling technique used in the Turbo-Reduce blade mistuning code. Left: 126,846 DOF in the full finite element model. Right: Forced response for tuned versus mistuned blades; 136 DOF for static mode compensation.

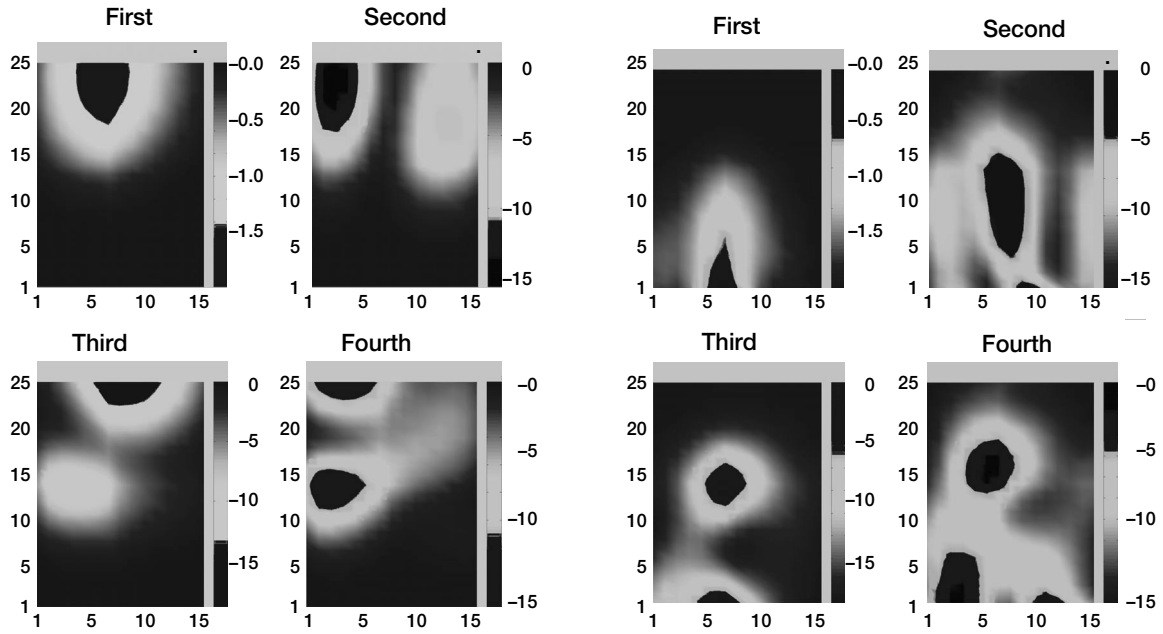

Effect of local blade property mistuning on natural frequencies: sensitivity maps showing the first through fourth natural frequencies. Left: Local mass mistuning. Right: Local stiffness mistuning. This figure is shown in color in the online version of this article (http://www.grc.nasa.gov/WWW/RT/2003/5000/5930min1.html).

vibration analysis tool, the Turbo-Reduce forced-response prediction code, into an effective design tool by enhancing and extending the underlying modeling and analysis methods. Furthermore, novel techniques will be developed to assess the safety of a given design. In particular, a procedure will be established for using eigenfrequency curve veerings to identify "danger zones" in the operating conditions—ranges of rotational speeds and engine orders in which there is a great risk that the rotor blades will suffer high stresses. This work also will aid statistical studies of the forced response by reducing the necessary number of simulations. Finally, new strategies for improving the design of rotors will be pursued. Several methods will be investigated, including the use of intentional mistuning patterns to mitigate the harmful effects of random mistuning, and the modification of disk stiffness to avoid reaching critical values of interblade coupling in the desired operating range. Recent research progress is summarized in the following paragraphs.

First, significant progress was made in the development of the component mode mistuning (CMM) and static mode compensation (SMC) methods for reduced-order modeling of mistuned bladed disks (see the figure on the preceding page). The CMM method has been formalized and extended to allow a general treatment of mistuning. In addition, CMM allows individual mode mistuning, which accounts for the realistic effects of local variations in blade properties that lead to different mistuning values for different mode types (e.g., mistuning of the first torsion mode versus the second flexural mode). The accuracy and efficiency of the CMM method and the corresponding Turbo-Reduce code were validated for an example finite element model of a bladed disk.

Second, SMC was developed for the modeling of large mistuning or geometric blade variations. A generalization of the CMM approach allows the modeling of large blade mistuning (e.g., a rogue blade) by using the so-called attachment modes from component mode synthesis to capture the effects of large mistuning on specified areas of the blade. An example of a bladed disk with one rogue blade was examined. This technique shows promise for modeling systems that incorporate intentional mistuning or geometric changes in the blade design.

Third, a comprehensive investigation was completed on modeling and predicting the effects of mass mistuning (see the images above). Traditionally, mass mistuning has been ignored in favor of simpler models incorporating only eigenvalue or stiffness mistuning. It was found that, relative to stiffness mistuning, mass mistuning widens the range of mistuned natural frequencies, and it also leads to a smaller response at lower frequencies and a greater response at higher frequencies for a given blade mode family. It was determined that the modal power of the blade modes is a metric that indicates the strength of mass mistuning. Furthermore, it was shown that a sensitivity analysis can be used to

map the variation of local blade properties to the mass or stiffness mistuning parameters used in the methods and the associated Turbo-Reduce code.

Fourth, enhancements and significant improvements were made in the Turbo-Reduce code for reduced-order modeling and analysis of mistuned bladed disks. The efficiency was increased, and the amount of computer memory needed to run the code was greatly reduced by improving the matrix storage and manipulation schemes used in the code. Enhanced models and simulation options for mistuning were implemented, including improved handling of mass mistuning based on the findings of the mass mistuning study mentioned earlier.

Fifth, key observations were made on frequency veering analysis for identifying critical operating conditions. It was observed that the calculation of continuous natural frequency curves provides physical insight because the actual nodal diameter modes are sampled points on the continuous curves. Furthermore, it was determined that the location of the nodal diameter modes relative to the frequency veerings indicates the relative amount of disk and blade participation in the vibration, and thus provides important information on the design: the strength of the interblade coupling, the sensitivity to mistuning, and possible effects of design changes. This work was performed under a grant by University of Michigan researchers in collaboration with NASA Glenn Research Center researchers.

Reference

1. Bladh, R.; and Pierre, C.: Component-Mode-Based Reduced Order Modeling Techniques for Mistuned Bladed Disks—Part I: Theoretical Models. J. Eng. Gas Turbines Power (ASME Paper 2003–GT–0360), vol. 123, no. 1, 2001, pp. 89–99.

Glenn contact:
Dr. James B. Min, 216–433–2587, James.B.Min@nasa.gov

Author: Dr. James B. Min

Headquarters program office: OAT

Programs/Projects:
Propulsion and Power, GUIDE

Vibration Characteristics Determined for Stainless Steel Sandwich Panels With a Metal Foam Core for Lightweight Fan Blade Design

The goal of this project at the NASA Glenn Research Center is to provide fan materials that are safer, weigh less, and cost less than the currently used titanium alloy or polymer matrix composite fans. The proposed material system is a sandwich fan construction made up of thin solid face sheets and a lightweight metal foam core. The stiffness of the sandwich structure is increased by separating the two face sheets by the foam layer. The resulting structure has a high stiffness and lighter weight in comparison to the solid face-sheet material alone. The face sheets carry the applied in-plane and bending loads (ref. 1). The metal foam core must resist the transverse shear and transverse normal loads, as well as keep the facings supported and working as a single unit. Metal foams have ranges of mechanical properties, such as light weight, impact resistance, and vibration suppression (ref. 2), which makes them more suitable for use in lightweight fan structures. Metal foams have been available for decades (refs. 3 and 4), but the difficulties in the original processes and high costs have prevented their widespread use. However, advances in production techniques and cost reduction have created a new interest in this class of materials (ref. 5).

The material chosen for the face sheet and the metal foam for this study was the aerospace-grade stainless steel 17–4PH. This steel was chosen because of its attractive mechanical properties and the ease with which it can be made through the powder metallurgy process (ref. 6). The advantages of a metal foam core, in comparison to a typical honeycomb core, are material isotropy and the ease of forming complex geometries, such as fan blades. A section of a 17–4PH sandwich structure is shown in this photograph.

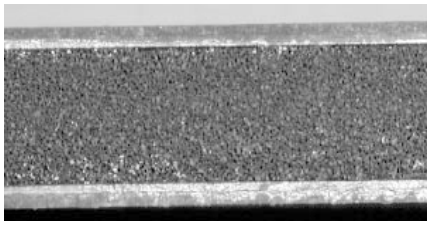

Side view of a 17–4 stainless steel foam panel with face sheets.

Part of process of designing any blade is to determine the natural frequencies of the particular blade shape. A designer needs to predict the resonance frequencies of a new blade design to properly identify a useful operating range. Operating a blade at or near the resonance frequencies leads to high-cycle fatigue, which

ultimately limits the blade's durability and life. So the aim of this study is to determine the variation of the resonance frequencies for an idealized sandwich blade as a function of its face-sheet thickness, core thickness, and foam density. The finite element method is used to determine the natural frequencies for an idealized rectangular sandwich blade. The proven Lanczos method (ref. 7) is used in the study to extract the natural frequency. The fan blade geometry and the mesh of the idealized plate are shown in the top figure.

The variation of the resonance frequency with foam-core thickness is shown in the center figure for a 6.3- by 3.25-in. plate with a 0.1-in. constant face-sheet thickness. The foam core assumed was a 17–4PH 80PPI[1] with a 6.0-percent relative density in comparison to a solid material. On the other hand, the results of varying the ratio of foam-core thickness to the face-sheet thickness to keep the overall thickness constant at 0.5 in. are shown for the first three resonance frequencies in the bottom figure. The variation of the frequency of an actual sandwich blade profile shown earlier is presented as a function of face-sheet thickness and foam-core density.

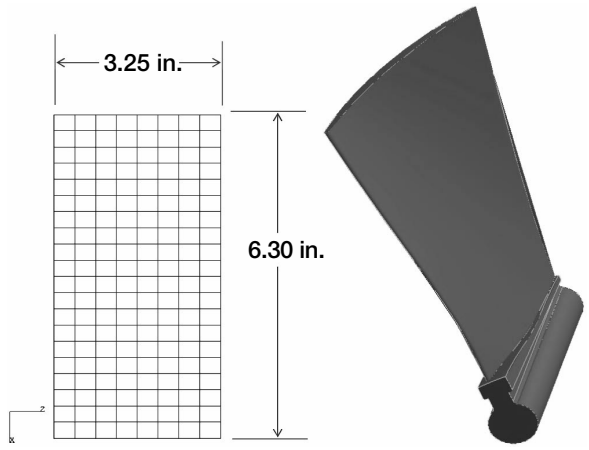

Left: Mesh of an idealized blade. Right: Typical fan blade geometry.

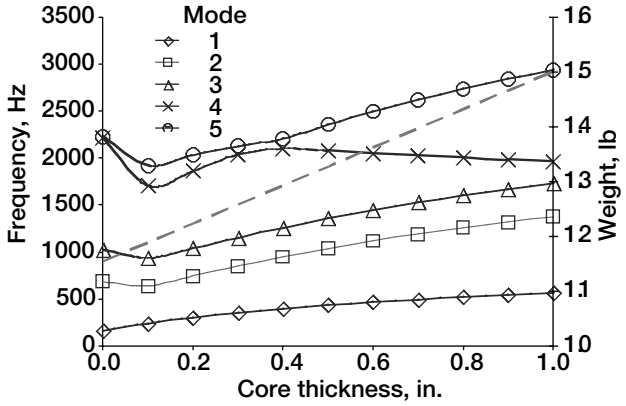

Variation of the five resonance frequencies as a function of the core thickness for a 6.3- by 3.25-in. plate with a 0.1-in. face-sheet thickness.

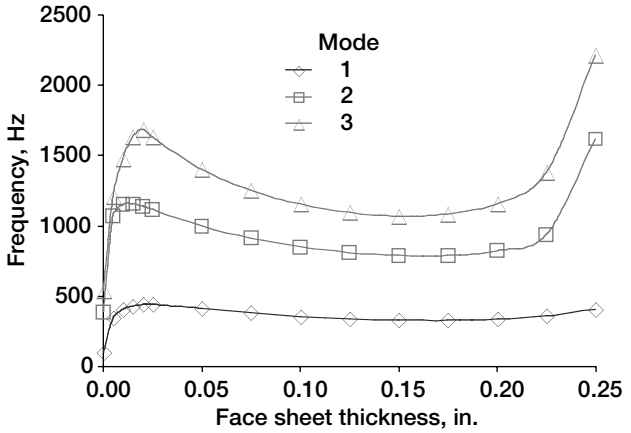

Variation of the resonance frequency as a function of the face-sheet thicknesses for a 6.3- by 3.25- by 0.5-in. constant-thickness plate.

References

1. Harte A.M.; Fleck, N.A.; and Ashby, M.F.: Sandwich Panel Design Using Aluminum Alloy Foam. Adv. Eng. Mat., vol. 2, no. 4, 2000, pp. 219–222.
2. Ashby, M.F., et al.: Metal Foams: A Design Guide. Butterworth-Heinemann, Woburn, MA, 2000.
3. Davies G.J.; and Zhen, S.: Metallic Foams—Their Production, Properties and Applications. J. Mater. Sci., vol. 18, no. 7, 1983, pp. 1899–1911.
4. Thornton, P.H.; and Magee, C.L.: Deformation Characteristics of Zinc Foam. Metall. T-A, vol. 6, no. 9, 1975, pp. 1801–1807.
5. Banhart J.: Manufacture, Characterisation and Application of Cellular Metals and Metal Foams. Prog. Mater. Sci., vol. 46, no. 6, 2001, pp. 559–632.
6. Porvair Fuel Cell Technology. Porvair's Advanced Materials. www.porvairfuelcells.com, select "M." Accessed January 13, 2004.
7. Hughes, Thomas J.R.: The Finite Element Method: Linear Static and Dynamic Finite Element Analysis. Prentice-Hall, Inc., Englewood Cliffs, NJ, 1987.

Glenn contact:
Dr. James B. Min, 216–433–2587, James.B.Min@nasa.gov

Ohio Aerospace Institute (OAI) contact:
Dr. Louis J. Ghosn, 216–433–3822,
Louis.J.Ghosn@grc.nasa.gov

Authors:
Dr. James B. Min, Dr. Louis J. Ghosn, Dr. Sai V. Raj,
Dr. Bradley A. Lerch, and Frederic A. Holland, Jr.

Headquarters program office: OAT

Programs/Projects: Ultra Safe

[1]Eighty pores per inch.

High-Temperature Hybrid Rotor Support System Developed

The Army Research Laboratory Vehicle Technology Directorate and the NASA Glenn Research Center demonstrated a unique high-speed, high-temperature rotor support system in September 2003. Advanced turbomachinery is on its way to surpassing the capabilities of rolling-element bearings and conventional dampers. To meet these demands, gas turbine engines of the future will demand increased efficiency and thrust-to-weight ratio, and reduced specific fuel consumption and noise. The more-electric engine replaces oil-lubricated bearings, dampers, gears, and seals with electrical devices. One such device is the magnetic bearing. The Vehicle Technology Directorate and Glenn have demonstrated the operation of a radial magnetic bearing in combination with a hydrostatic bearing at 1000 °F at 31,000 rpm (2.3 MDN[1]). This unique combination takes advantage of a high-temperature rub surface in the event of electrical power loss or sudden overloads. The hydrostatic bearings allow load sharing with the magnetic bearing. The magnetic-hydrostatic bearing combination eliminates wear and high contact stress from sudden acceleration of the rolling-element bearings and overheating. The magnetic bearing enables high damping, adaptive vibration control, and precise rotor positioning, diagnostics, and health monitoring. The illustration above shows a model of the test facility used at Glenn for this technology demonstration.

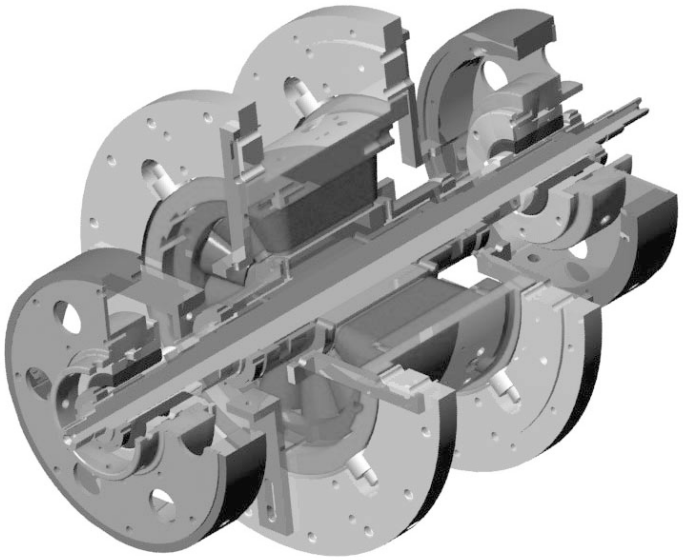

Model representation of test facility.

A high-temperature heteropolar radial magnetic bearing is located at the center of gravity of the test rotor. There is a 0.022-in. radial air gap between the rotor and stator. Two rub surface hydrostatic bearings were placed on either side of the magnetic bearing. The rotor is supported by a 0.002-in. hydrostatic air film and the magnetic field. The prototype active magnetic bearing cost $24,000 to design and fabricate and a set of four high-temperature, rub-surface, hydrostatic bearings cost $28,000. This work was funded by the Turbine-Based Combined Cycle program.

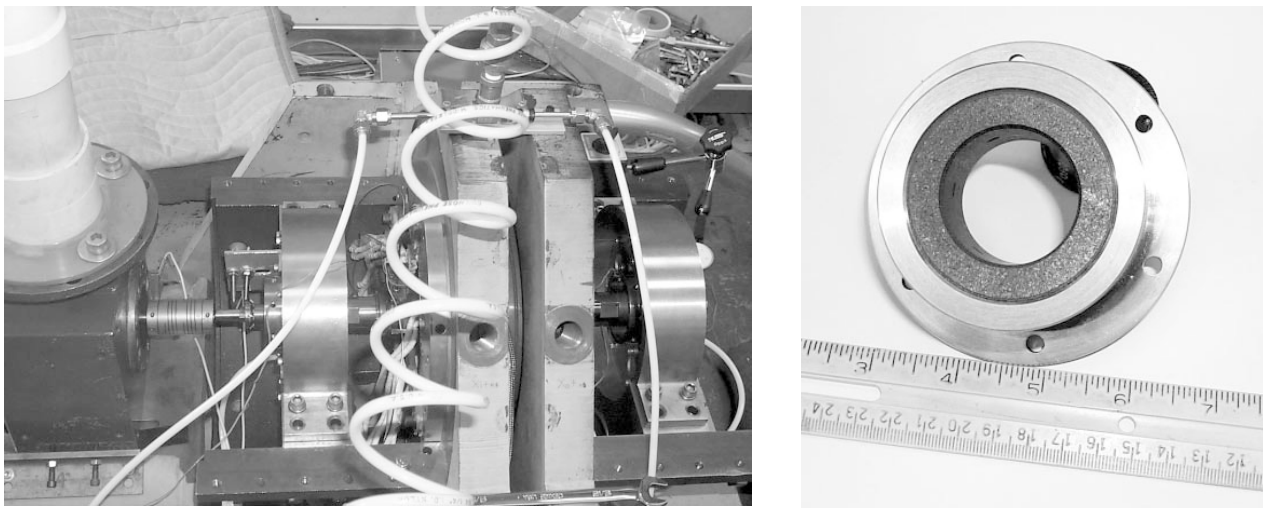

Left: High-temperature hydrostatic/magnetic bearing test facility. Right: High-temperature, rub surface hydrostatic bearing.

[1]One million × shaft diameter in millimeters × rotational speed in revolutions per minute.

Find out more about this research:

U.S. Army Research Laboratory, Vehicle Technology Directorate at Glenn:
http://www.grc.nasa.gov/WWW/army/

Glenn's Structural Mechanics and Dynamics Branch:
http://structures.grc.nasa.gov/5930/

U.S. Army Research Laboratory, Vehicle Technology Directorate at Glenn contact: Gerald T. Montague, 216–433–6252, Gerald.T.Montague@grc.nasa.gov

University of Toledo contact:
Mark J. Jansen, 216–433–6054, Mark.J.Jansen@grc.nasa.gov

Author: Gerald T. Montague

Headquarters program office:
OSF (Space Transportation)

Programs/Projects: TBCC

Special recognition:
2003 R&D 100 Award; American Helicopter Society International Best Paper Award in the Propulsion Session, "Experimental High Temperature Characterization of a Magnetic Bearing for Turbomachinery," May 6–8, 2003.

Bearingless Switched-Reluctance Motor Improved

The Morrison rotor, named after its inventor, is a hybrid rotor for use in a switched-reluctance electric motor. The motor is characterized as bearingless in the sense that it does not rely on conventional mechanical bearings: instead, it functions as both a magnetic bearing and a motor. Bearingless switched-reluctance motors are attractive for use in situations in which large variations in temperatures and/or other extreme conditions preclude the use of conventional electric motors and mechanical bearings.

In the Morrison motor, as in prior bearingless switched-reluctance motors, a multipole rotor is simultaneously levitated and rotated. In the prior motors, simultaneous levitation and rotation are achieved by means of two kinds of stator windings: (1) main motor windings and (2) windings that exert levitating forces on a multipole rotor. The multipole geometry is suboptimum for levitation because it presents a discontinuous surface to the stator pole faces, thereby degrading the vibration suppression capability of the magnetic bearing.

The Morrison rotor simplifies the stator design in that it contains only one type of winding. The rotor is a hybrid that includes both (1) a circular lamination stack for levitation and (2) a multipole lamination stack for rotation. Simultaneous levitation and rotation at 6000 rpm were achieved with a proto-

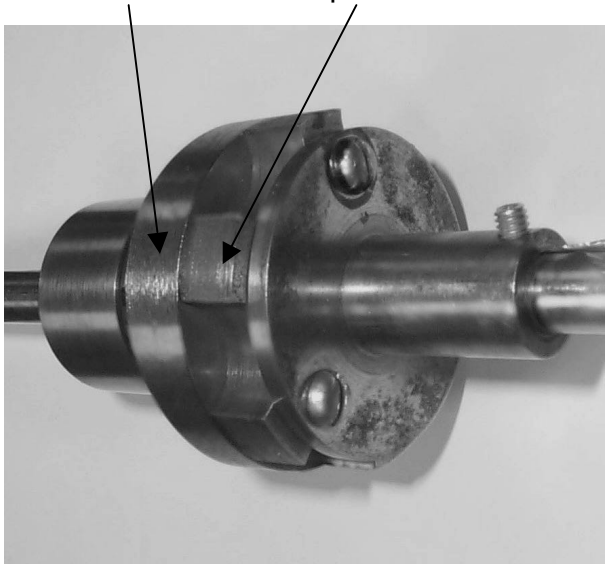

Prototype hybrid rotor.

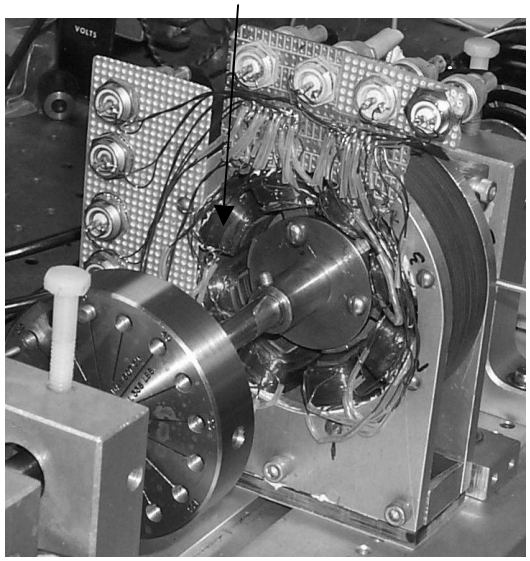

Rotor/stator ensemble.

type that included six rotor poles and eight stator poles (see the preceding photographs). During normal operation, two of the four pairs of opposing stator poles (each pair at right angles to the other pair) levitate the rotor. The remaining two pairs of stator poles exert torque on the six-pole rotor lamination stack to produce rotation.

The relative length of the circular and multipole lamination stacks on the rotor can be chosen to tailor the performance of the motor for a specific application. For a given overall length, increasing the length of the multipole stack relative to the circular stack results in an increase in torque relative to the levitation load capacity and vice versa.

Glenn contacts:
Carlos R. Morrison, 216–433–8447, Carlos.R.Morrison@nasa.gov; and
Dr. Gerald V. Brown, 216–433–6047, Gerald.V.Brown@nasa.gov

Author: Carlos R. Morrison

Headquarters program office: OAT

Programs/Projects:
PR&T, Ultra Safe

Subsonic Aircraft With Regression and Neural-Network Approximators Designed

At the NASA Glenn Research Center, NASA Langley Research Center's Flight Optimization System (FLOPS, ref. 1) and the design optimization testbed COMETBOARDS (ref. 2) with regression and neural-network-analysis approximators have been coupled to obtain a preliminary aircraft design methodology. For a subsonic aircraft, the optimal design, that is the airframe-engine combination, is obtained by the simulation. The aircraft is powered by two high-bypass-ratio engines with a nominal thrust of about 35,000 lbf. It is to carry 150 passengers at a cruise speed of Mach 0.8 over a range of 3000 n mi and to operate on a 6000-ft runway. The aircraft design utilized a neural network and a regression-approximations-based analysis tool, along with a multioptimizer cascade algorithm that uses sequential linear programming, sequential quadratic programming, the method of feasible directions, and then sequential quadratic programming again.

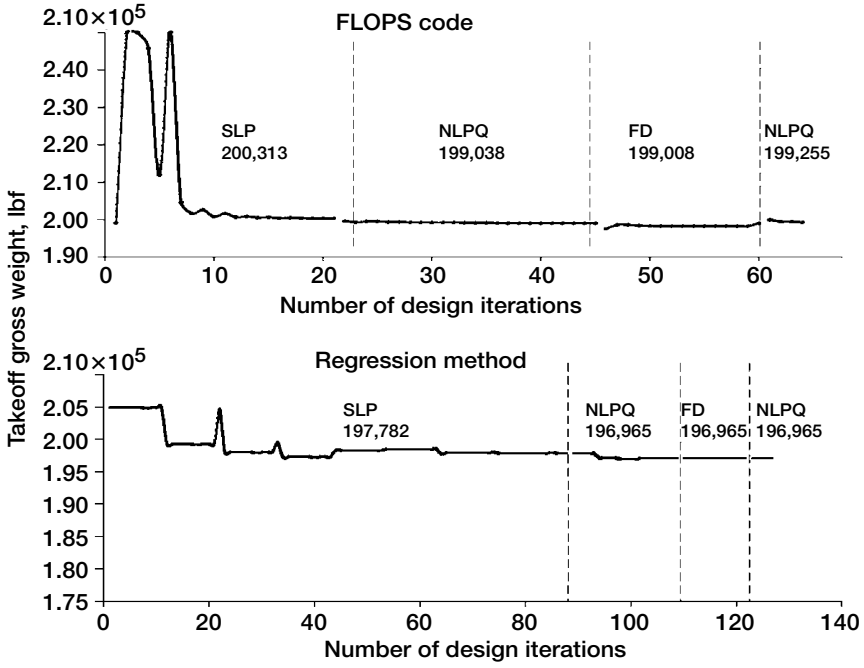

Optimum design of a subsonic aircraft. SLP, sequential linear programming; NLPQ, sequential quadratic programming; FD, method of feasible directions.

Optimal aircraft weight versus the number of design iterations is shown in the figure. The central processing unit (CPU) time to solution is given in the table. The figure shows that the regression-method-based analyzer exhibited a smoother convergence pattern than the FLOPS code. The optimum weight obtained by the approximation technique and the FLOPS code differed by 1.3 percent. Prediction by the approximation technique exhibited no error for the aircraft wing area and turbine entry temperature, whereas it was within 2 percent for most other parameters. Cascade strategy was required by FLOPS as well as the approximators. The regression method had a tendency to hug the data points, whereas the neural network exhibited a propensity to follow a mean path. The performance of the neural network and regression methods was considered adequate. It was at about the same level for small, standard, and large models with redundancy ratios (defined as the number of input-output pairs to the number of unknown coefficients) of 14, 28, and 57, respectively.

CPU TIME TO SOLUTION IN AN SGI OCTANE WORKSTATION

Task	Regression method			Neural network technique		
	Small	Standard	Large	Small	Standard	Large
Training, sec	0.2	0.4	0.8	59.1	136	538.8
Reanalysis,[a] msec	---	---	0.08	---	---	2.4
Reanalysis with closed-form gradient, msec	---	---	0.14	---	---	13.5
Design optimization, sec (percent of FLOPS solution time[b])	1.6 (0.78)	1.7 (0.84)	1.6 (0.78)	300.9 (15)	199.2 (9.8)	166.7 (8.2)

[a]Reanalysis with FLOPS, 3.1 sec.

[b]FLOPS solution time, 2031 sec.

In an SGI octane workstation (Silicon Graphics, Inc., Mountainview, CA), the regression training required a fraction of a CPU second, whereas neural network training was between 1 and 9 min, as given in the table. For a single analysis cycle, the 3-sec CPU time required by the FLOPS code was reduced to milliseconds by the approximators. For design calculations, the time with the FLOPS code was 34 min. It was reduced to 2 sec with the regression method and to 4 min by the neural network technique. The performance of the regression and neural network methods was found to be satisfactory for the analysis and design optimization of the subsonic aircraft.

References

1. McCullers, L.A.: Flight Optimization System, FLOPS. User's Guide, release 5.51, ViGyan, Inc., Hampton, VA, 1994.
2. Patnaik, S.N., et al.: Lessons Learned During Solutions of Multidisciplinary Design Optimization Problems. J. Aircr., vol. 39, no. 3, 2002, pp. 386–393.

Glenn contact:
Dale A. Hopkins, 216–433–3260, Dale.A.Hopkins@grc.nasa.gov

Authors: Dr. Surya N. Patnaik and Dale A. Hopkins

Headquarters program office: OAT

Programs/Projects:
Ultra Safe, UEET, HSR

New Dynamic Spin Rig Capabilities Used to Determine Rotating Blade Dynamics

The Dynamic Spin Rig Facility at the NASA Glenn Research Center is used to determine the structural response of rotating engine components without the effects of aerodynamic loading. Recently, this rig's capabilities were enhanced through the replacement of grease-lubricated ball bearings with magnetic bearings (see ref. 1). Magnetic bearings offer a number of advantages—the most important here being that they not only fully support the rotor system, but excite it as well. Three magnetic bearings support the rotor and provide five axes of controlled motion: an *x*- and *y*-axis translation at each of two radial bearings and a *z*-axis translation in the vertical or axial direction. Sinusoidal excitation (most commonly used) can be imparted on the rotor through the radial magnetic bearings in either a fixed or rotating frame of reference. This excitation is added directly to the magnetic bearing control output. Since the rotor is fully levitated, large translations and rotations of the rotor system can be achieved.

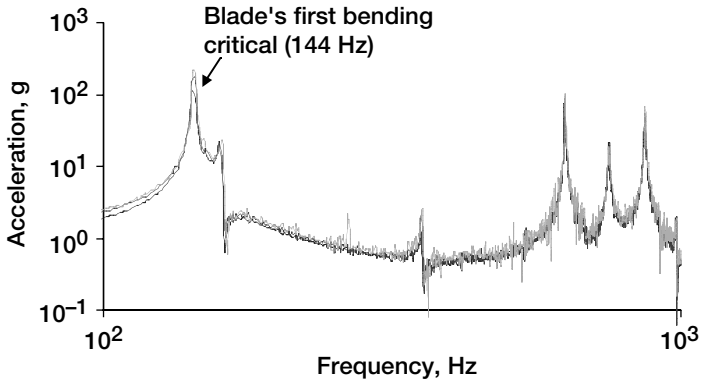

Titanium flat plate blade-tip acceleration magnitude versus frequency using swept sine excitations of 0.25, 0.5, and 1.0 A at 0 rpm.

Some of the capabilities of this excitation system were determined and reported in ref. 2. This graph shows the accelerations obtained at the tip of a titanium flat plate test article versus

the swept sine excitation sent to both radial bearings in phase and perpendicular to the plane containing the two blades. Recent tests required the excitation of fundamental bending and torsional blade resonances at rotor speeds up to 10,000 rpm. Successful fixed synchronous rotation of the excitation signal provided the best detectable blade resonant vibrations at excitation frequencies up to 1100 Hz for the particular blades of interest.

A noncontacting laser measurement system was used to collect blade-tip motions. From these data, the amplitude and frequency of the motion could be determined as well as the blade damping properties. Damping could be determined using two methods: (1) free decay and (2) curve fitting the vibration amplitude as a function of frequency in and around the resonance of interest and using the half-power method. The graph to the right shows the free decay of a composite blade vibrating at its first bending resonance while rotating at 3000 rpm.

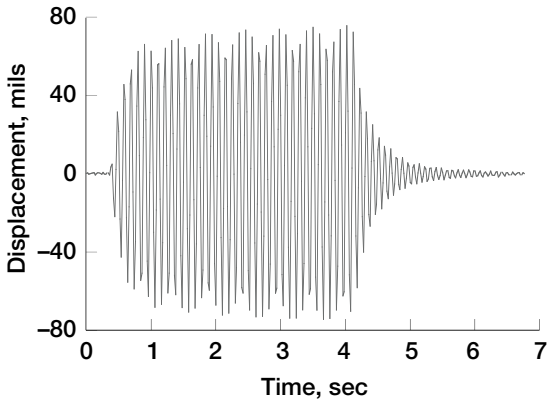

Blade excitation and free vibration decay at 3000 rpm.

This new system is currently being used to support the Efficient Low-Noise Fan project at Glenn. The damping properties of prototype hollow composite blades specially designed to reduce fan noise are currently being determined.

References

1. Morrison, Carlos R.; and Mehmed, Oral: Dynamic Spin Rig Upgraded With a Five-Axis-Controlled Three-Magnetic-Bearing Support System With Forward Excitation. Research and Technology 2002, NASA/TM—2003-211990, 2003, p. 168. http://www.grc.nasa.gov/WWW/RT2002/5000/5930morrison.html
2. Morrison, Carlos R., et al.: Fully Suspended, Five-Axis, Three-Magnetic-Bearing Dynamic Spin Rig With Forced Excitation. NASA/TP—2004-212694, 2004. http://gltrs.grc.nasa.gov/cgi-bin/GLTRS/browse.pl?2004/TP-2004-212694.html

Glenn contacts:
Andrew J. Provenza, 216–433–6025, Andrew.J.Provenza@nasa.gov;
Carlos R. Morrison, 216–433–8447, Carlos.R.Morrison@nasa.gov; and
Dr. Tony Kurkov, 216–433–5695, Anatole.P.Kurkov@nasa.gov

Author: Andrew J. Provenza

Headquarters program office: OAT

Programs/Projects:
SEC, QAT, UEET, ELNF

Linearized Aeroelastic Solver Applied to the Flutter Prediction of Real Configurations

A fast-running unsteady aerodynamics code, LINFLUX, was previously developed for predicting turbomachinery flutter. This linearized code, based on a frequency domain method, models the effects of steady blade loading through a nonlinear steady flow field. The LINFLUX code, which is 6 to 7 times faster than the corresponding nonlinear time-domain code, is suitable for use in the initial design phase. Earlier, this code was verified through application to a research fan, and it was shown that the predictions of work per cycle and flutter compared well with those from a nonlinear time-marching aeroelastic code, TURBO–AE. Now, the LINFLUX code has been applied to real configurations: fans developed under the Energy Efficient Engine (E-cubed) Program and the Quiet Aircraft Technology (QAT) project.

The LINFLUX code starts with a steady nonlinear aerodynamic flow field and solves the unsteady linearized Euler equations to calculate the unsteady aerodynamic forces on the turbomachinery blades. First, a steady aerodynamic solution is computed for given operating conditions using the nonlinear unsteady aerodynamic code TURBO–AE. A blade vibration analysis is done to determine the frequencies and mode shapes of the vibrating blades, and an interface code is used to convert the steady aerodynamic solution to a form required by LINFLUX. A preprocessor is used to interpolate the mode shapes from the structural dynamics mesh onto the computational fluid dynamics mesh. Then, LINFLUX is used to calculate the unsteady aerodynamic pressure distribution for a

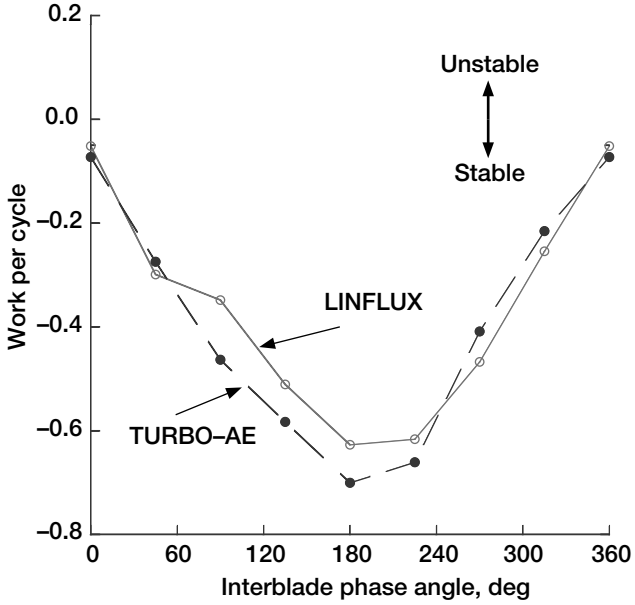

Work per cycle versus interblade phase angle for the first vibration mode of the E-cubed fan.

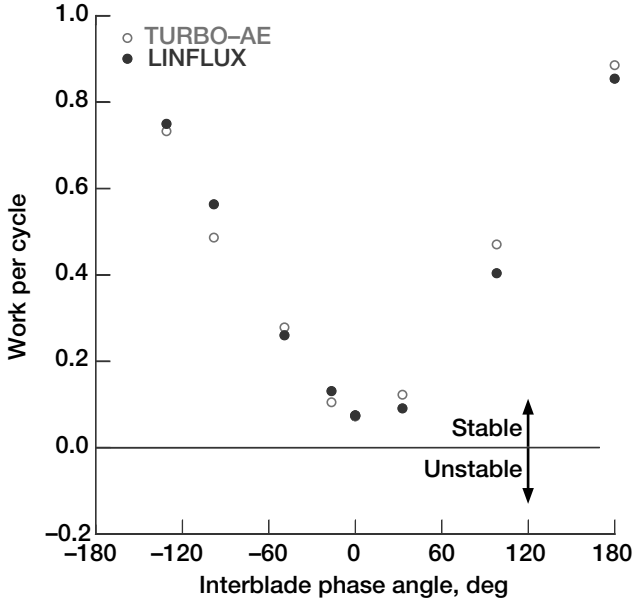

Work per cycle for the first vibration mode of the Quiet High Speed Fan.

given vibration mode, frequency, and interblade phase angle. Finally, a post-processor uses the unsteady pressures to calculate the generalized aerodynamic forces, eigenvalues, and response amplitudes. The eigenvalues determine the flutter frequency and damping.

Results of flutter calculations from the LINFLUX code are presented for (1) the E-cubed fan developed under the E-cubed program and (2) the Quiet High Speed Fan (QHSF) developed under the Quiet Aircraft Technology project. The results are compared with those obtained from the TURBO–AE code.

The graph on the left shows the work done per vibration cycle for the first vibration mode of the E-cubed fan. It can be seen that the LINFLUX results show a very good comparison with TURBO–AE results over the entire range of interblade phase angle. The graph on the right shows the work done per vibration cycle for the first vibration mode of the QHSF fan. Once again, the LINFLUX results compare very well with the results from the TURBO–AE code.

With the validation of the LINFLUX code through application to real configurations, it is now possible to apply this code for the aeroelastic calculations in the initial design of new turbomachinery blade rows. The aeroelastic development and calculations described here were performed under a NASA grant by University of Toledo researchers in collaboration with Glenn researchers.

University of Toledo contact:
Dr. T.S.R. Reddy, 216–433–6083, Tondapu.S.Reddy@grc.nasa.gov

Glenn contact:
Dr. Milind A. Bakhle, 216–433–6037, Milind.A.Bakhle@nasa.gov

Authors: Dr. Tondapu S. Reddy and Dr. Milind A. Bakhle

Headquarters program office: OAT

Programs/Projects:
PR&T, QAT, QHSF, E-cubed

Conical Magnetic Bearings Developed for Active Stall Control in Gas Turbine Engines

Active stall control is a current research area at the NASA Glenn Research Center that offers a great benefit in specific fuel consumption by allowing the gas turbine to operate beyond the onset of stall. Magnetic bearings are being investigated as a new method to perform active stall control. This enabling global aviation safety technology would result in improved fuel efficiency and decreased carbon dioxide emissions, as well as improve safety and reliability by eliminating oil-related delays and failures of engine components, which account for 40 percent of the commercial aircraft departure delays.

Active stall control works by perturbing the flow in front of the compressor stage such that it cancels the pressure wave, which causes the compressor to go into stall. Radial magnetic bearings are able to whirl the shaft so that variations in blade tip leakage would flow upstream causing a perturbation wave that could cancel the rotating stall cell. Axial or thrust magnetic bearings cannot be used to cancel the surge mode in the compressor because they have a very low bandwidth and thus cannot modulate at a high enough frequency. Frequency response is limited because the thrust runner cannot be laminated. To improve the bandwidth of magnetic thrust bearings, researchers must use laminations to suppress the eddy currents. A conical magnetic bearing can be laminated, resulting in increased bandwidth in the axial direction. In addition, this design can produce both radial and thrust force in a single bearing, simplifying the installation.

Conical magnetic bearing stator.

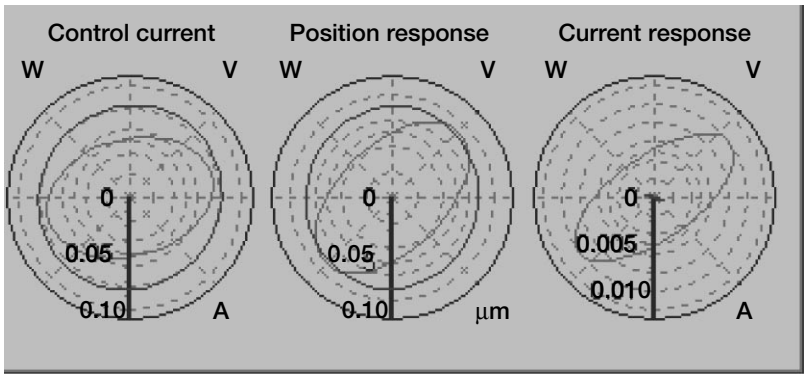

Filtered position and current response under current control. (V and W represent four of the five axes of control.)

The proposed solution combines the radial and thrust bearing into one design that can be laminated—a conical magnetic bearing. The new conical magnetic bearing test rig, funded by a Glenn fiscal year 2002 Director's Discretionary Fund, was needed because none of the existing rigs has an axial degree of freedom. The rotor bearing configuration will simulate that of the main shaft on a gas turbine engine. One conical magnetic bearing replaces the ball bearing in front of the compressor, and the second replaces the roller bearing behind the burner. The rig was made operational to 10,000 rpm under Smart Efficient Components funding, and both position and current adaptive vibration control have been demonstrated. Upon program completion, recommendations will be made as to the efficacy of the conical magnetic bearing for active stall control.

Glenn contact: Jeffrey J. Trudell, 216–433–5303, Jeffrey.J.Trudell@nasa.gov

U.S. Army Research Laboratory, Vehicle Technology Directorate at Glenn contact: Albert F. Kascak, 216–433–6024, Albert.F.Kascak@grc.nasa.gov

Authors: Jeffrey J. Trudell, Albert F. Kascak, Andrew J. Provenza, and Carl J. Buccieri

Headquarters program office: OA

Programs/Projects:
DDF, SEC, Flywheel Technologies

Nonlinear Acoustics Used To Reduce Leakage Flow

Leakage and wear are two fundamental problems in all traditional turbine seals that contribute to an engine's inefficiency. The solutions to seal leakage and wear conflict in the conventional design space. Reducing the clearance between the seal and rotating shaft reduces leakage but increases wear because of increased contact incidents. Increasing the clearance to reduce the contact between parts reduces wear but increases parasitic leakage. The goal of this effort is to develop a seal that restricts leakage flow using acoustic pressure while operating in a noncontacting manner, thereby increasing life.

In 1996, Dr. Timothy Lucas announced his discovery of a method to produce shock-free high-amplitude pressure waves. For the first time, the formation of large acoustic pressures was possible using dissonant resonators. A pre-prototype acoustic seal developed at the NASA Glenn Research Center exploits this fundamental acoustic discovery: a specially shaped cavity oscillated at the contained fluid's resonant frequency produces high-amplitude acoustic pressure waves of a magnitude approaching those required of today's seals.

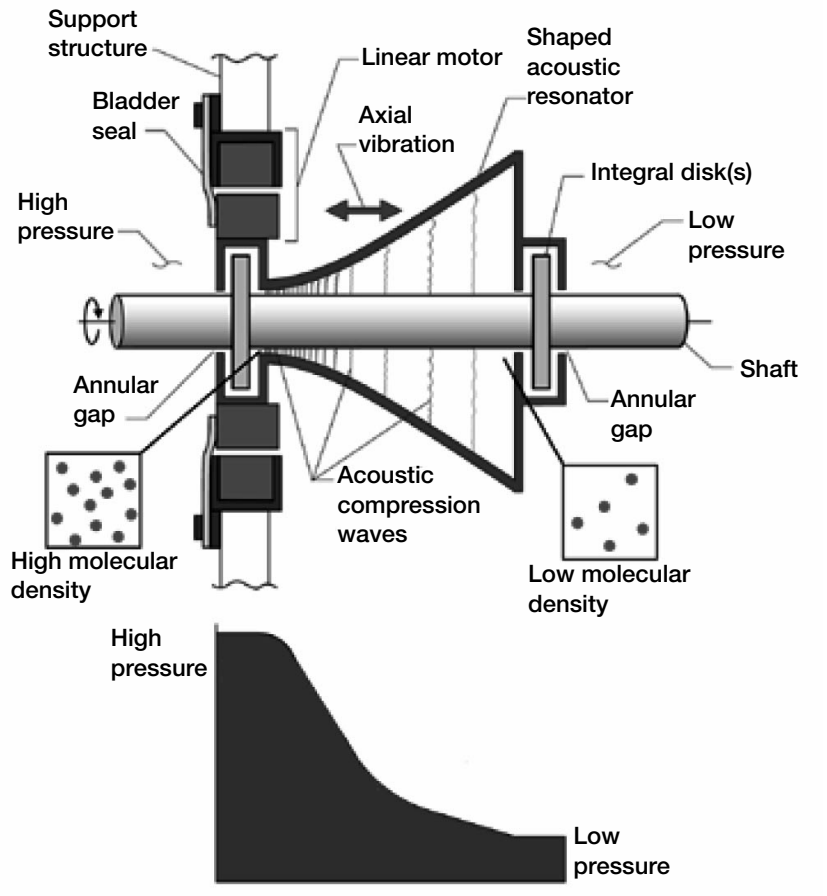

Top: Conceptual diagram of the acoustic seal. Bottom: Acoustically driven pressures are used to restrict flow through the seal.

While the original researchers are continuing their development of acoustic pumps, refrigeration compressors, and electronic thermal management systems using this technology, the goal of researchers at Glenn is to apply these acoustic principles to a revolutionary sealing device. When the acoustic resonator shape is optimized for the sealing device, the flow from a high-pressure cavity to a low-pressure cavity will be restricted by a series of high-amplitude standing pressure waves of higher pressure than the pressure to be sealed (see the figure to the left). Since the sealing resonator cavity will not touch the adjacent sealing structures, seal wear will be eliminated, improving system life.

Under a cooperative agreement between Glenn and the Ohio Aerospace Institute (OAI), an acoustic-based pre-prototype seal was demonstrated for the first time. A pressurized cavity was attached to one end of the resonator while the other end remained open to ambient pressure (see the following figure). Measurements were taken at several values of applied pressure with the assembly stationary, oscillated at an off-resonance frequency, and then oscillated on-resonance. The three cases show that the flow through the conical

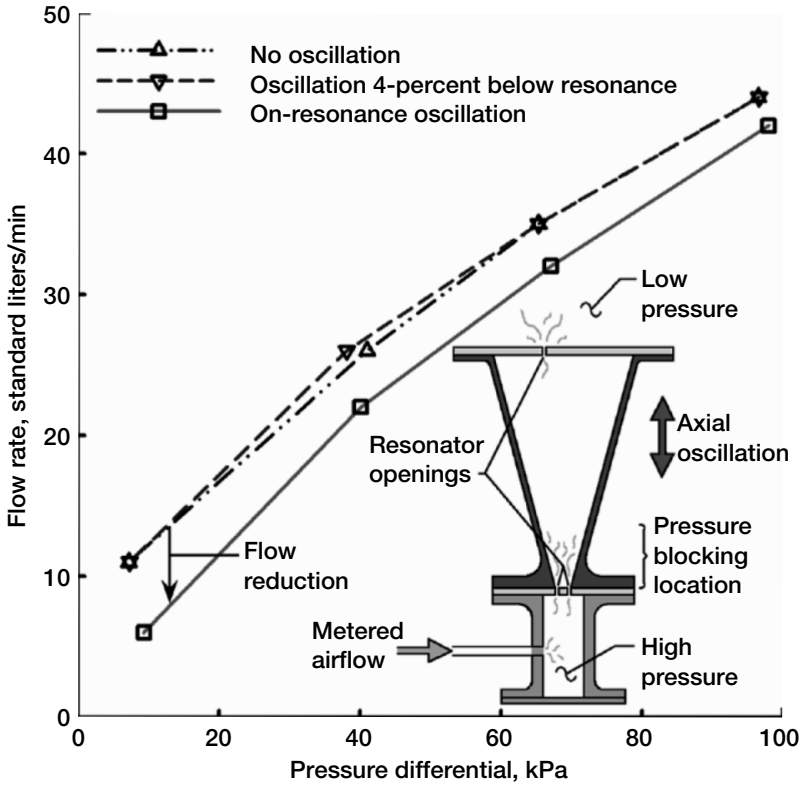

Experimental results showing flow reduction over the entire pressure range tested. Inset: Experimental pre-prototype acoustic seal used to assess leakage blocking capability.

resonator can be reduced by oscillating the resonator at the resonance frequency of the air contained within the cavity. The results are currently being compared with results obtained from a commercial computational fluid dynamics code. The objective is to improve the design through numerical simulation before fabricating a next-generation prototype sealing device. Future work is aimed at implementing acoustic seal design improvements to further reduce the leakage flow rate through the device and at reducing the device's overall size.

Find out more about this research:
http://www.grc.nasa.gov/WWW/TurbineSeal/TurbineSeal.html

University of Akron contact:
Dr. Christopher C. Daniels, 216–433–6714, Christopher.C.Daniels@grc.nasa.gov

Glenn contact:
Dr. Bruce M. Steinetz, 216–433–3302, Bruce.M.Steinetz@nasa.gov

Authors: Dr. Christopher C. Daniels and Dr. Bruce M. Steinetz

Headquarters program office: OAT

Programs/Projects:
Propulsion and Power

NASA Glenn's Seals Group Inaugurated a New State-of-the-Art High-Temperature Test Rig

The NASA Glenn Research Center is developing advanced control surface seals and propulsion system seals for future space and launch vehicles. To evaluate new seal designs, the Glenn Seals Team recently inaugurated a new state-of-the-art high-temperature seal test facility. The Hot Compression/Hot Scrub Rig can perform either high-temperature seal-compression tests or scrub tests at temperatures of up to 3000 °F by using different combinations of test fixtures made of monolithic silicon carbide (Hexoloy α-SiC), as shown in the figures at the top of the next page. For lower temperature tests (up to 1500 °F), Inconel X–750 test fixturing can be used.

The main components of this test rig are a servohydraulic load frame, an air furnace, and a noncontact laser extensometer (see the photograph at the bottom of the next page). The load frame has a top-mounted actuator that is connected to the appropriate fixturing and that can generate a load of 3300 lb over a 6-in. stroke. Dual servovalves control movement of the actuator at rates from 0.001 to 8 in./sec. This allows the actuator to move very slowly for the compression tests or quickly for the scrub tests. Computer control of the hydraulic system permits several loading profiles to be used, including monotonic, cyclic, stress relaxation, and mission-simulated duty cycles. A box furnace with a working volume that is 9 in. wide by 14 in. deep by 18 in. high is installed between the columns of the load frame. Kanthal Super 33 (Kanthal AB, Hallstahammar, Sweden) molybdenum disilicide ($MoSi_2$) heating elements heat the furnace to temperatures up to 3000 °F. The stationary base for each set of test fixtures rests on a tube that passes through an opening in the bottom of the furnace. A load cell (either 500 or 3300 lb) is attached to the base and

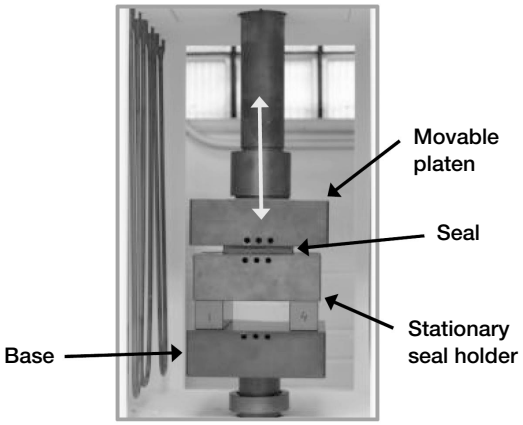

Compression test fixturing used in Glenn's Hot Compression/Hot Scrub Rig.

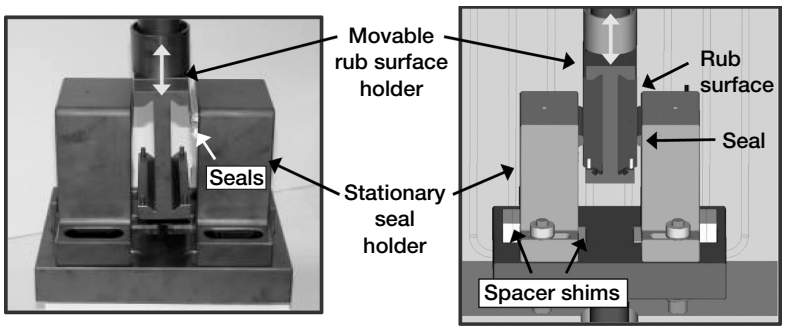

Photograph (left) and schematic (right) of scrub test fixturing used in Glenn's Hot Compression/Hot Scrub Rig (rub surfaces not shown on left).

stationary fixturing. The load cells are used to measure compressive loads applied to the seals during a compression test or frictional loads on the seals during scrub testing. Underneath the load cell is an alignment fixture that permits precise alignment of the load train.

Over the past year, the Hot Compression/Hot Scrub Rig was used to support many projects, including the testing of advanced preloader concepts (canted coil springs and Si_3N_4 compression springs) and evaluation of next-generation seals for propulsion applications. In addition, the Glenn Seals Team conducted tests on advanced thermal protection system seals for the Boeing/Air Force Air Vehicles Technology Integration Program and provided testing support for Glenn's Supersonic Parametric Inlet Project.

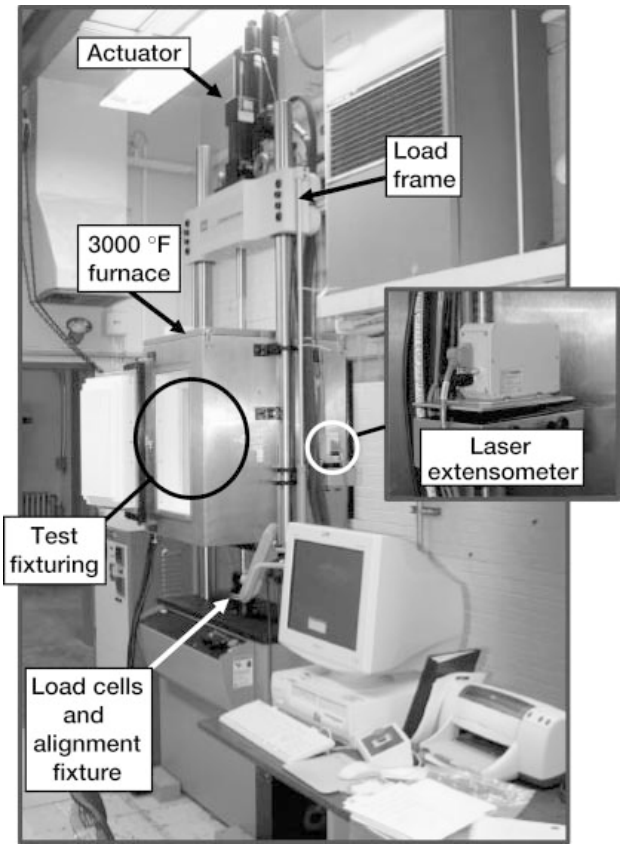

Major components of Glenn's Hot Compression/Hot Scrub Rig.

Bibliography

Dunlap, Patrick H., Jr.; Steinetz, Bruce M.; and DeMange, Jeffrey J.: Advanced Seal Development at NASA GRC for Future Space Vehicles. NASA/TM—2003-212478, 2003. Available from the NASA Center for AeroSpace Information.

Find out more about this research:

Structural seals and thermal barriers: http://www.grc.nasa.gov/WWW/structuralseal/

Glenn's Mechanical Components Branch: http://www.grc.nasa.gov/WWW/5900/5950/

University of Toledo contact:
Jeffrey J. DeMange, 216–433–3568, Jeffrey.J.DeMange@grc.nasa.gov

Glenn contacts:
Patrick H. Dunlap, Jr., 216–433–3017, Patrick.H.Dunlap@nasa.gov; and
Dr. Bruce M. Steinetz, 216–433–3302, Bruce.M.Steinetz@nasa.gov

Authors: Jeffrey J. DeMange, Patrick H. Dunlap, Jr., and Dr. Bruce M.Steinetz

Headquarters program office: OAT

Programs/Projects:
NGLT, RLV, PR&T, AVTIP, Supersonic Parametric Inlet Project

Atlas V Launch Incorporated NASA Glenn Thermal Barrier

In the Spring of 2002, Aerojet experienced a major failure during a qualification test of the solid rocket motor that they were developing for the Atlas V Enhanced Expendable Launch Vehicle. In that test, hot combustion gas reached the O-rings in the nozzle-to-case joint and caused a structural failure that resulted in loss of the nozzle and aft dome sections of the motor. To improve the design of this joint, Aerojet decided to incorporate three braided carbon-fiber thermal barriers developed at the NASA Glenn Research Center (see the top photograph). The thermal barriers were used to block the searing-hot 5500 °F pressurized gases from reaching the temperature-sensitive O-rings that seal the joint. Glenn originally developed the thermal barriers for the nozzle joints of the space shuttle solid rocket motors, and Aerojet decided to use them on the basis of the results of several successful ground tests of the thermal barriers in the shuttle rockets.

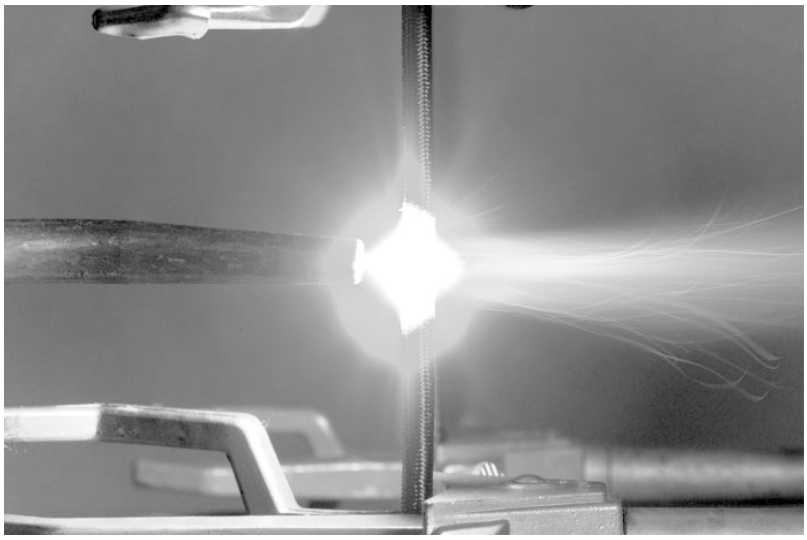

5500 °F oxyacetylene torch flame on braided carbon-fiber thermal barrier during testing at Glenn.

Final qualification test of the Aerojet solid rocket motor with Glenn thermal barriers installed (Dec. 11, 2002).

Aerojet undertook an aggressive schedule to redesign the rocket nozzle-to-case joint with the thermal barriers and to qualify it in time for a launch planned for the middle of 2003. They performed two successful qualification tests (Oct. and Dec. 2002) in which the Glenn thermal barriers effectively protected the O-rings (see the bottom photograph). These qualification tests saved hundreds of thousands of dollars in development costs and put the Lockheed-Martin/Aerojet team back on schedule.

On July 17, 2003, the first flight of an Atlas V boosted with solid rocket motors successfully launched a commercial satellite into orbit from Cape Canaveral Air Force Station (see the photograph on the next page). Aerojet's two 67-ft solid rocket boosters performed flawlessly, with each providing thrust in excess of 250,000 lbf. Both motors incorporated three Glenn-developed thermal barriers in their nozzle-to-case joints. The Cablevision satellite launched on this mission will be used to provide direct-to-home satellite television programming for the U.S. market starting in late 2003.

The Atlas V is a product of the military's Enhanced Expendable Launch Vehicle program designed to provide assured military access to space. It can lift payloads up to 19,100 lb to geosynchronous transfer orbit and was designed to meet Department of Defense, commercial, and NASA needs. The Atlas V and Delta IV are two launch systems being considered by NASA to launch the Orbital Space Plane/Crew Exploration Vehicle. The launch and rocket costs of this mission are valued at $250 million. Successful application of the Glenn thermal barrier to the Atlas V program was an enormous breakthrough for the program's technical and schedule success.

Reference

1. Steinetz, B.M.; and Dunlap, P.H.: Development of Thermal Barriers for Solid Rocket Motor Nozzle Joints. J. Propul. P. (NASA/TM—1999-209278), vol. 17, no. 5, 2001, pp. 1023–1034. http://gltrs.grc.nasa.gov/cgi-bin/GLTRS/browse.pl?1999/TM-1999-209278.html

Find out more about this research:

Structural seals and thermal barriers:
http://www.grc.nasa.gov/WWW/structuralseal/

High-temperature, flexible, fiber preform seal:
http://www.grc.nasa.gov/WWW/structuralseal/InventYr/1996Inv_Yr.htm

Glenn's Mechanical Components Branch:
http://www.grc.nasa.gov/WWW/5900/5950/

Glenn contacts: Patrick H. Dunlap, Jr., 216–433–3017, Patrick.H.Dunlap@nasa.gov; and Dr. Bruce M. Steinetz, 216–433–3302, Bruce.M.Steinetz@nasa.gov

Authors: Patrick H. Dunlap, Jr., and Dr. Bruce M. Steinetz

Headquarters program office: OAT

Programs/Projects: EELV, Space Shuttle Program

Special recognition: 2003 NorTech Innovation Award

Atlas V boosted by two Aerojet solid rocket motors incorporating Glenn thermal barriers (July 17, 2003).

Gear Performance Improved by Coating

Gears, bearings, and other mechanical elements transmit loads through contacting surfaces. Even if properly designed, manufactured, installed, and maintained, gears and bearings will eventually fail because of the fatigue of the working surfaces. Economical means for extending the fatigue lives of gears and bearings are highly desired, and coatings offer the opportunity to engineer surfaces to extend the fatigue lives of mechanical components. A tungsten-containing diamondlike-carbon coating exhibiting high hardness, low friction, and good toughness was evaluated for application to spur gears. Fatigue testing was done at the NASA Glenn Research Center on both uncoated and coated spur gears. The results showed that the coating extended the surface fatigue lives of the gears by a factor of about 5 relative to the uncoated gears.

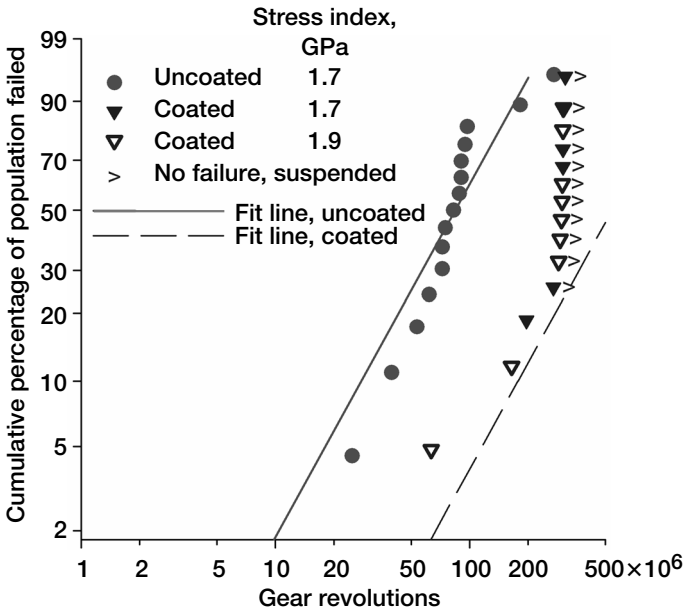

Weibull plot of fatigue test data for both uncoated and coated spur gears illustrates improved fatigue lives owing to the coating.

For the experiments, a lot of spur test gears made from AISI 9310 gear steel were case-carburized and ground to aerospace specifications. The geometries of the 28-tooth, 8-pitch gears were verified as meeting American Gear Manufacturing Association (AGMA) quality class 12. One-half of the gears were randomly selected for coating. The method of coating was selected to achieve desired adherence, toughness, hardness, and low-friction characteristics. First the gears to be coated were prepared by blasting (vapor honing) with Al_2O_3 particles and cleaning. Then, the gears were provided with a thin adhesion layer of elemental chromium followed by magnetron sputtering of the outer coating consisting of carbon (70 at.%), hydrogen (15 at.%), tungsten (12 at.%), and nickel (3 at.%) (atomic percent at the surface). In total, the coating thickness was about 2.5 to 3 μm. As compared with the steel substrate, the coated surface was harder by a factor of about 2 and had a smaller elastic modulus.

All gears were tested using a 5-centistoke synthetic oil, a 10,000-rpm rotation speed, and a hertzian contact stress of at least 1.7 GPa (250 ksi). Tests were run until either surface fatigue occurred or 300 million stress cycles were completed. Tests were run using either a pair of uncoated gears or a pair of coated gears (coated gears mated with uncoated gears were not evaluated). The fatigue test results, shown on Weibull coordinates in the graph, demonstrate that the coating provided substantially longer fatigue lives even though some of the coated gears endured larger stresses. The increase in fatigue life was a factor of about 5 and the statistical confidence for the improvement is high (greater than 99 percent). Examination of the tested gears revealed substantial reductions of total wear for coated gears in comparison to uncoated gears. The coated gear surface topography changed with running, with localized areas of the tooth surface becoming smoother with running. Theories explaining how coatings can extend gear fatigue lives are research topics for coating, tribology, and fatigue specialists. This work was done as a partnership between NASA, the U.S. Army Research Laboratory, United Technologies Research Corporation, and Sikorsky Aircraft.

Bibliography

Krantz, Timothy L., et al.: Increased Surface Fatigue Lives of Spur Gears by Application of a Coating. NASA/TM—2003-212463 (ARL–TR–2971), 2003. http://gltrs.grc.nasa.gov/cgi-bin/GLTRS/browse.pl?2003/TM-2003-212463.html

Find out more about this research:
http://www.grc.nasa.gov/WWW/5900/5950/

U.S. Army Research Laboratory, Vehicle Technology Directorate at Glenn contact:
Dr. Timothy L. Krantz, 216–433–3580, Timothy.L.Krantz@grc.nasa.gov

Author: Dr. Timothy L. Krantz

Headquarters program office: OAT

Programs/Projects:
VSP, UEET, Army Rotary Wing Vehicles

adwTools Developed—New Bulk Alloy and Surface Analysis Software for the Alloy Design Workbench

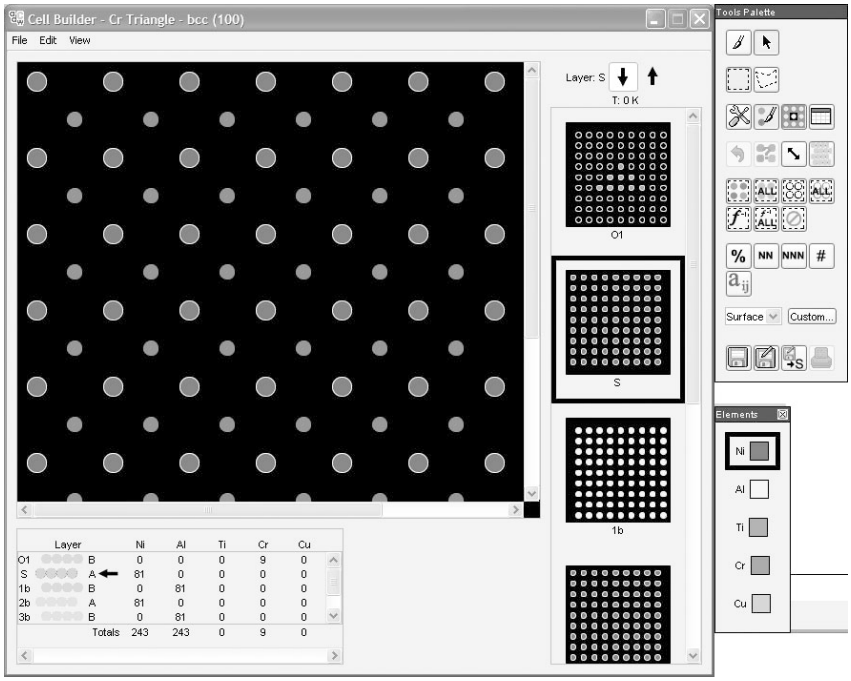

The starting point of adwTools is the cell builder, where arbitrary computational cells can be created using an extensive menu of options. These include several possible "Select" options for populating a lattice, as well as additional tools to make visualization easier. This figure is shown in color in the online version of this article (http://www.grc.nasa.gov/WWW/RT/2003/5000/5960bozzolo.html).

A suite of atomistic modeling software, called the Alloy Design Workbench, has been developed by the Computational Materials Group at the NASA Glenn Research Center and the Ohio Aerospace Institute (OAI). The main goal of this software is to guide and augment experimental materials research and development efforts by creating powerful, yet intuitive, software that combines a graphical user interface with an operating code suitable for real-time atomistic simulations of multicomponent alloy systems. Targeted for experimentalists, the interface is straightforward and requires minimum knowledge of the underlying theory, allowing researchers to focus on the scientific aspects of the work.

The centerpiece of the Alloy Design Workbench suite is the *adwTools* module (http://www.icmsc.org/RT/adwTools.html), which concentrates on the atomistic analysis of surfaces

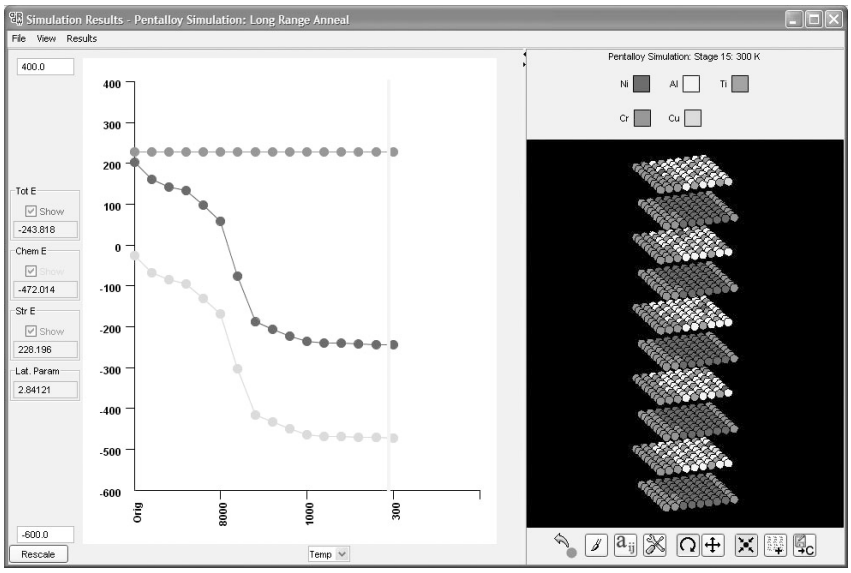

Currently adwTools performs two types of simulations: (1) Monte Carlo simulations based on the exchange of atoms of different species and (2) relaxation calculations where atoms vary their coordinates during the simulation according to different possible algorithms.This figure is shown in color in the online version of this article (http://www.grc.nasa.gov/WWW/RT/2003/5000/5960bozzolo.html).

and bulk alloys containing an arbitrary number of elements. An additional module, *adwParams*, handles ab initio input for the parameterization used in *adwTools*. Future modules planned for the suite include *adwSeg*, which will provide numerical predictions for segregation profiles to alloy surfaces and interfaces, and *adwReport*, which will serve as a window into the database, providing public access to the parameterization data and a repository where users can submit their own findings from the rest of the suite.

The entire suite is designed to run on desktop-scale computers. The *adwTools* module incorporates a custom OAI/Glenn-developed Fortran code based on the BFS (Bozzolo-Ferrante-Smith) method for alloys (http://www.icmsc.org/biblio.html, ref. 1). The heart of the suite, this code is used to calculate the energetics of different compositions and configurations of atoms.

The first step in using the *adwTools* module is to create a project (http://www.icmsc.org/RT/project.html), within which a user can define the structure and composition (http://www.icmsc.org/RT/structure.html) of computational cells, as illustrated in the screen capture on the preceding page. Projects contain two types of analytical tools: catalogs and simulations. Both utilize the cell builder module (http://www.icmsc.org/RT/cellBuilder.html), which provides tools (http://www.icmsc.org/RT/cellBuilderTools.html) for the creation of cells (e.g., multiple atom selection, layer selection, fill by species, random distributions, etc.). Layers can be added or removed, and antiphase boundaries can be created. Analysis tools (http://www.icmsc.org/RT/analysisTools.html) allow for atom-by-atom understanding of the energetics underlying the modeled behavior.

Within a catalog (http://www.icmsc.org/RT/catalog.html), a user can collect individually modified cells and compare their energies of formation. This analytical approach facilitates the comparison of different atomic configurations that can represent different compositions or atom locations. Energy calculations are done in real time (0.25 msec/atom in a standard Pentium III desktop personal computer). The results viewer displays all the cells in a catalog, along with an energy level spectrum that provides a ready reference for the difference in energy between different states (cells).

In addition to the analytical catalog approach to alloy bulk or surface energetics, adwTools provides several simulation tools (http://www.icmsc.org/RT/simulation.html). A simulation allows a user to create a cell and define a temperature cycle for a canonical ensemble exchange Monte Carlo algorithm leading to an equilibrium configuration, or relax the atomic coordinates via multiple relaxation algorithms. Each algorithm includes temperature dependence so that heating or annealing can be simulated. Simulation results (http://www.icmsc.org/RT/results.html) include a plot of the energy of the cell per stage and a three-dimensional cell viewer with numerous features to aid the analysis and visualization of the computational cell at each of the stages (e.g., rotation and translation tools, show/hide by atomic species, layer, etc.), as shown in the screen capture on this page. An AVI movie file of the entire simulation process can be created and then viewed outside of *adwTools* on any computer or shared via Internet. Full connectivity between catalogs and simulations allows intermediate simulation stages to be used in a catalog or to launch a new simulation.

Since its inception, *adwTools* has proven its versatility in a variety of applications (http://www.icmsc.org/RT/applications.html), including the study of alloy surfaces, surface alloys, and bulk alloy design (refs. 2 and 3). Images and animations demonstrating the capabilities of the *adwTools* software can be found in the expanded online version of this article (http://www.icmsc.org/RT/).

References

1. Bozzolo, G., et al.: Surface Segregation in Multicomponent Systems: Modeling of Surface Alloys and Alloy Surfaces. Comput. Mater. Sci., vol. 15, no. 2, 1999, pp. 169–195.
2. Woodruff, D.P.: Surface Alloys and Alloy Surfaces. Elsevier, Amsterdam, 2002.
3. Wilson, A., et al.: Experimental Verification of the Theoretical Prediction of the Phase Structure of a Ni-Al-Ti-Cr-Cu Alloy. Acta Mater., vol. 50, no. 11, 2002, pp. 2787–2800.

Find out more about this research:

International Computational Materials Science Consortium:
http://www.icmsc.org

Glenn's Tribology & Surface Science Branch:
http://www.grc.nasa.gov/WWW/SurfSci/

Ohio Aerospace Institute (OAI) contact:
Dr. Guillermo H. Bozzolo, 440–962–3103, Guillermo.H.Bozzolo@grc.nasa.gov

Glenn Research Center contacts:
Dr. Phillip B. Abel, 216–433–6063, Phillip.B.Abel@nasa.gov; and
Dr. Ronald D. Noebe, 216–433–2093, Ronald.D.Noebe@nasa.gov

Authors: Dr. Guillermo H. Bozzolo, Jeffrey A. Morse, Dr. Ronald D. Noebe, and Dr. Phillip B. Abel

Headquarters program office: OAT

Programs/Projects:
Propulsion and Power, HOTPC

Research Capabilities for Oil-Free Turbomachinery Expanded by New Rotordynamic Simulator Facility

A new test rig has been developed for simulating high-speed turbomachinery shafting using Oil-Free foil air bearing technology. Foil air journal bearings are self-acting hydrodynamic bearings with a flexible inner sleeve surface using air as the lubricant (see the illustration to the right). These bearings have been used in turbomachinery, primarily air cycle machines, for the past four decades to eliminate the need for oil lubrication. More recently, interest has been growing in applying foil bearings to aircraft gas turbine engines. They offer potential improvements in efficiency and power density, decreased maintenance costs, and other secondary benefits. The goal of applying foil air bearings to aircraft gas turbine engines prompted the fabrication of this test rig. The facility enables bearing designers to test potential bearing designs with shafts that simulate the rotating components of a target engine without the high cost of building actual flight hardware. The data collected from this rig can be used to make changes to the shaft and bearings in subsequent design iterations. The rest of this article describes the new test rig and demonstrates some of its capabilities with an initial simulated shaft system.

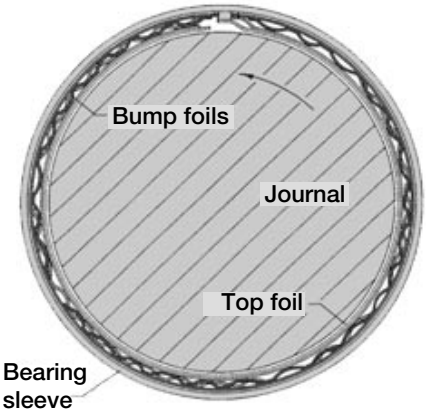

Foil bearing cross section.

The test rig has two support structures, each housing a foil air journal bearing (see the photograph on the next page). The structures are designed to accept any size foil journal bearing smaller than 63 mm (2.5 in.) in diameter. The bearing support structures are mounted to a 91- by 152-cm (3- by 5-ft) table and can be separated by as much as 122 cm (4 ft) and as little as 20 cm (8 in.) to accommodate a wide range of shaft sizes. In the initial configuration, a 9.5-cm (3.75-in.) impulse air turbine drives the test shaft. The impulse turbine, as well as virtually any number of "dummy" compressor and turbine disks, can be mounted on the shaft inboard or outboard of the bearings. This flexibility allows researchers to simulate various engine shaft configurations. The bearing support structures include a unique bearing mounting fixture that rotates to accommodate a laser-based alignment system. This can measure the misalignment of the bearing centers in each of 2 translational degrees of freedom and 2 rotational degrees of freedom. In the initial configuration, with roughly a 30.5-cm- (12-in.-) long shaft, two simulated aerocomponent disks, and two 50.8-cm (2-in.) foil journal bearings, the rig can operate at 65,000 rpm at room temperature.

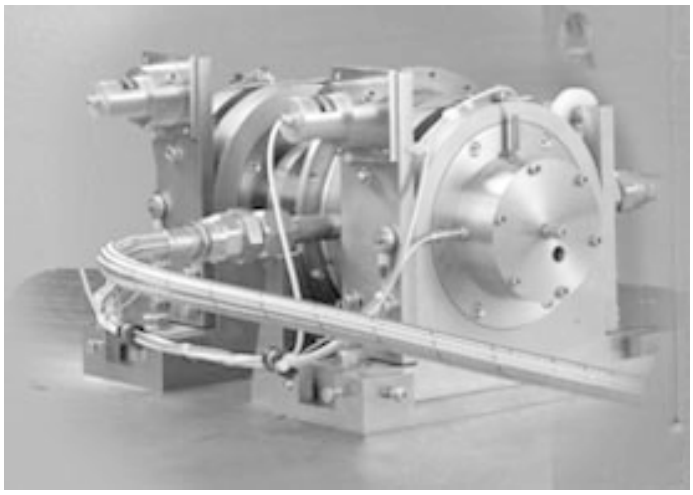

Rotordynamic simulator facility.

The test facility can measure shaft displacements in both the vertical and horizontal directions at each bearing location. Horizontal and vertical structural vibrations are monitored using accelerometers mounted on the bearing support structures. This information is used to determine system rotordynamic response, including critical speeds, mode shapes, orbit size and shape, and potentially the onset of instabilities (see the following images). Bearing torque can be monitored as well to predict the power loss in the foil bearings. All of this information is fed back and forth between NASA and the foil bearing designers in an iterative fashion to converge on a final bearing and shaft design for a given engine application.

In addition to its application development capabilities, the test rig offers several unique capabilities for basic bearing research. Using the laser alignment system mentioned earlier, the facility will be used to map foil air journal bearing performance. A known misalignment of increasing severity will be induced to determine the sensitivity of foil bearings to misalignment. Other future plans include oil-free integral starter generator testing and development, and dynamic load testing of foil journal bearings.

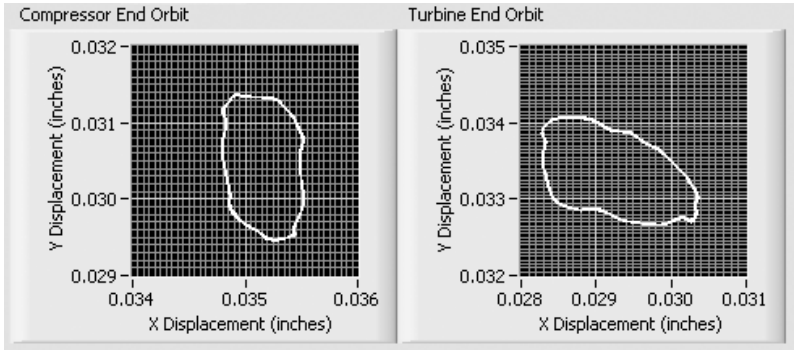

Sample shaft orbits at 15,000 rpm.

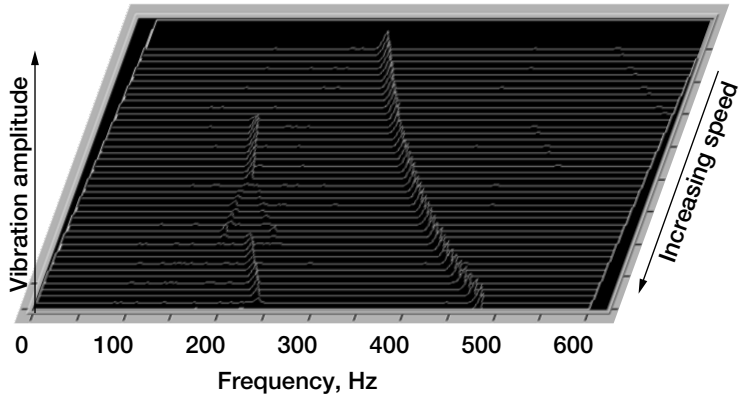

Waterfall plot showing synchronous and nonsynchronous vibration amplitudes.

Find out more about this research:
http://www.grc.nasa.gov/WWW/Oilfree/

Glenn contact:
Dr. Samuel A. Howard, 216–433–6076, Samuel.A.Howard@nasa.gov

Author: Dr. Samuel A. Howard

Headquarters program office: OAT

Programs/Projects: UEET

PS300 Tribomaterials Evaluated at 650 °C by Bushing Test Rig

A new facility has been developed to test the tribological behavior (friction and wear) of PS300 solid lubricant bushings at high temperatures. PS300 is a commercially available solid lubricant invented at the NASA Glenn Research Center. It can be prepared as a plasma spray coating or as a free-standing powder metallurgy component, designated PM300. PS300 and PM300 composites are designed to lubricate sliding components at temperatures above the capability of today's best oils, greases, and solid lubricants. One of the primary applications being pursued for PM300 is the development of bushings for use in high-temperature machinery. Examples include inlet guide vane bushings for gas turbines and conveyors, and bearings for industrial furnaces and ovens. Encouraging preliminary field trials indicate that PS300 and PM300 lubricant materials have been commercialized successfully in several industrial applications. However, the lack of laboratory performance data has hindered further commercialization especially for new applications that differ significantly from the established experience base.

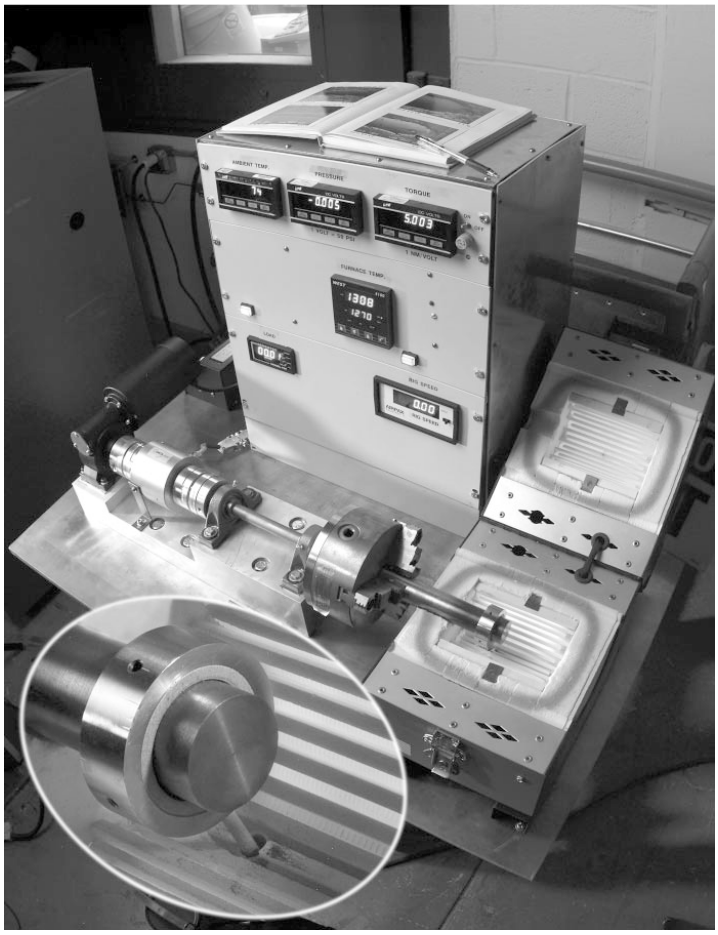

PM300 bushing loaded in bushing test rig.

The purpose of the newly developed bushing test rig will be to determine the performance characteristics of PM300, and other materials, under conditions closely matching intended applications. The data will be used to determine engineering friction and wear rates and to estimate the life expectancy of bushings for new applications. In the new rig, the bushing is loaded against a rotating shaft inside a furnace enclosure (see the photograph on this page). Loads can vary from 5 to 200 N, speeds from 1 to 400 rpm, and temperatures from 25 to 800 °C. Furnace temperature, bushing temperature, shaft speed, and torque are monitored during the test, and wear of both the bushing and the shaft is measured after testing is completed (see the photograph on the next page).

Initially, PM300 bushings will be evaluated and compared with lower temperature, traditional bushing materials like graphite and porous bronze. The baseline PM304 composition is 60 wt% NiCr (a binder), 20 wt% Cr_2O_3 (a hardener), 10 wt% BaF_2/CaF_2 (a high-temperature lubricant), and 10 wt% Ag (a low-temperature lubricant). Future research efforts will include determining the effects of load, sliding speed, and temperature on tribological performance and, possibly, tailoring composition for specific applications. We expect that the availability of measured performance data will enhance the market penetration of PM300 technology.

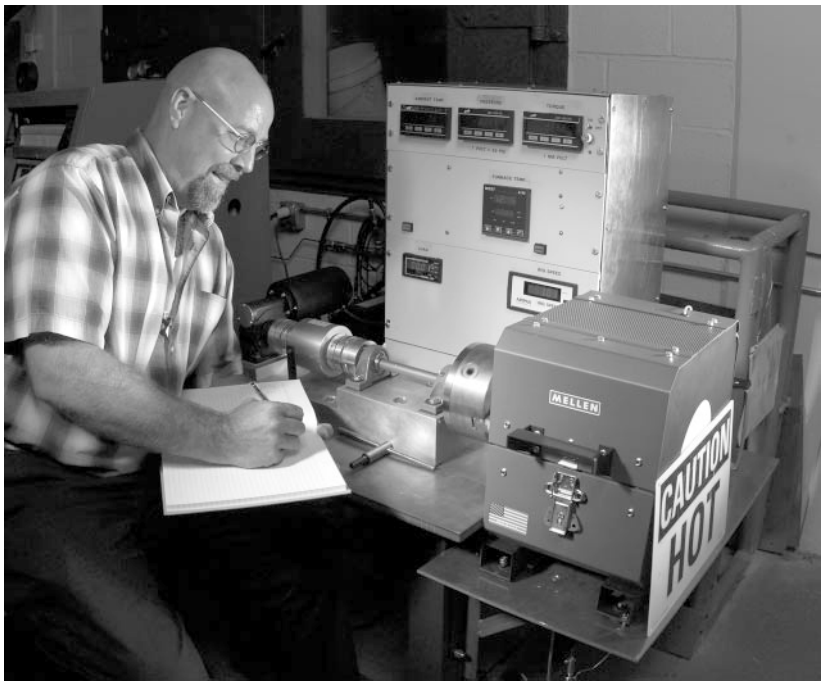

Measurements being recorded after testing with the bushing test rig.

Find out more about this research:
http://www.grc.nasa.gov/WWW/Oilfree/

U.S. Army Research Laboratory, Vehicle Technology Directorate at Glenn contact:
Don Striebing, 216–433–5558, Donald.R.Striebing@grc.nasa.gov

Glenn contact:
Dr. Chris DellaCorte, 216–433–6056, Christopher.DellaCorte@nasa.gov

Authors: Donald R. Striebing and Dr. Christopher DellaCorte

Headquarters program office: OAT

Programs/Projects: UEET

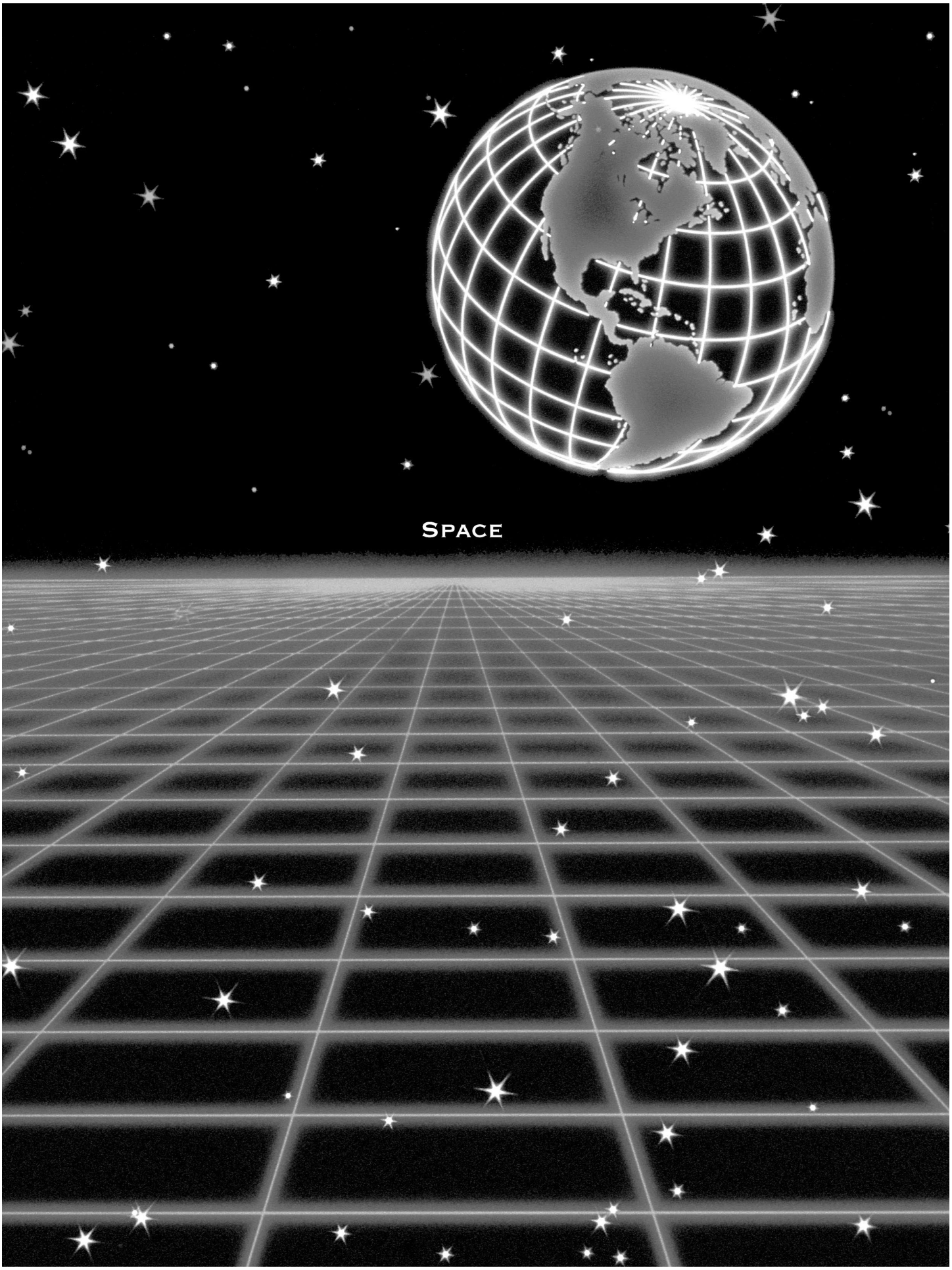
Space

Space Communications

Secure, Mobile, Wireless Network Technology Designed, Developed, and Demonstrated

The inability to seamlessly disseminate data securely over a high-integrity, wireless broadband network has been identified as a primary technical barrier to providing an order-of-magnitude increase in aviation capacity and safety. Secure, autonomous communications to and from aircraft will enable advanced, automated, data-intensive air traffic management concepts, increase National Air Space (NAS) capacity, and potentially reduce the overall cost of air travel operations. For the first time ever, secure, mobile, network technology was designed, developed, and demonstrated with state-of-the-art protocols and applications by a diverse, cooperative Government-industry team led by the NASA Glenn Research Center. This revolutionary technology solution will make fundamentally new airplane system capabilities possible by enabling secure, seamless network connections from platforms in motion (e.g., cars, ships, aircraft, and satellites) to existing terrestrial systems without the need for manual reconfiguration.

Called Mobile Router, the new technology autonomously connects and configures networks as they traverse from one operating theater to another. The Mobile Router demonstration aboard the Neah Bay, a U.S. Coast Guard vessel stationed in Cleveland, Ohio, accomplished secure, seamless interoperability of mobile network systems across multiple domains without manual system reconfiguration. The Neah Bay was chosen because of its low cost and communications mission similarity to low-Earth-orbiting satellite platforms. This technology was successfully advanced from technology readiness level (TRL) 2 (concept and/or application formation) to TRL 6 (system model or prototype demonstration in a relevant environment).

The secure, seamless interoperability offered by the Mobile Router and encryption device will enable several new, vehicle-specific and systemwide technologies to perform such things as remote, autonomous aircraft performance monitoring and early detection and mitigation of potential equipment malfunctions. As an additional benefit, team advancements were incorporated into open standards, ensuring technology transfer. Low-cost, commercial products incorporating the new technology are already available. Furthermore, these products are fully interoperable with legacy network technology equipment currently being used throughout the world.

Find out more about this research:

Bibliography:
http://roland.grc.nasa.gov/~ivancic/papers_presentations/papers.html

Secure mobile networking demonstration:
http://roland.grc.nasa.gov/~ivancic/secure_mobile_networks/smn.html

Glenn contacts:
William D. Ivancic, 216–433–3494, William.D.Ivancic@nasa.gov; and Phillip E. Paulsen, 216–433–6507, Phillip.E.Paulsen@nasa.gov

Authors:
William D. Ivancic and Phillip E. Paulsen

Headquarters program office: OES

Programs/Projects: Earth science; may benefit nearly all of NASA's future programs and projects. The equipment is mass, power, and volume efficient and can be used on nearly any mobile platform (trucks, cars, planes, helicopters, ships, spacecraft, etc.).

Special recognition:
NorTec Innovation Award (2003), TGIR (2003)

Microgravity Science

Thin-Filament Pyrometry Developed for Measuring Temperatures in Flames

Many valuable advances in combustion science have come from observations of microgravity flames. This research is contributing to the improved efficiency and reduced emissions of practical combustors and is benefiting terrestrial and spacecraft fire safety. Unfortunately, difficulties associated with microgravity have prevented many types of measurements in microgravity flames. In particular, temperature measurements in flames are extremely important but have been limited in microgravity. A novel method of measuring temperatures in microgravity flames is being developed in-house at the National Center for Microgravity Research and the NASA Glenn Research Center and is described here. Called thin-filament pyrometry, it involves using a camera to determine the local gas temperature from the intensity of inserted fibers glowing in a flame. It is demonstrated here to provide accurate measurements of gas temperatures in a flame simultaneously at many locations.

This photograph shows the experiment. The flame is a laminar gas jet diffusion flame fueled by methane (CH_4) flowing from a 14-mm round burner at a pressure of 1 atm. A coflowing stream of air is used to prevent flame flicker. Nine glowing fibers are visible. These fibers are made of silicon carbide (SiC) and have a diameter of 15 μm (for comparison, the average human hair is 75 μm in diameter). Because the fibers are so thin, they do little to disturb the flame and their temperature remains close to that of the local gas.

The flame and glowing filaments were imaged with a digital black-and-white video camera. This camera has an imaging area of 1000 by 1000 pixels and a wide dynamic range of 12 bits. The resolution of the camera and optics was 0.1 mm. Optical filters were placed in front of the camera to limit incoming light to 750, 850, 950, and 1050 nm.

Temperatures were measured in the same flame in the absence of fibers using 50-μm B-type thermocouples. These thermocouples provide very accurate temperatures, but they generally are not useful in microgravity tests because they measure temperature at only one location at a time. Thermocouple measurements at a height of 11 mm above the burner were used to calibrate the thin-filament pyrometry system at all four wavelengths.

This calibration was used to perform thin-filament pyrometry at other heights above the burner. One such profile is shown in the graph on the next page; this is for a height of 21 mm. The agreement between the pyrometry measurements and thermocouple results at this height is excellent in the range of 1000 to 2000 K, with an estimated uncertainty of ±50 K and an estimated upper limit of 2500 K. Neither the thermocouple nor the thin-filament pyrometry temperatures have been corrected for radiation, but the correction is expected to be nearly the same for both methods.

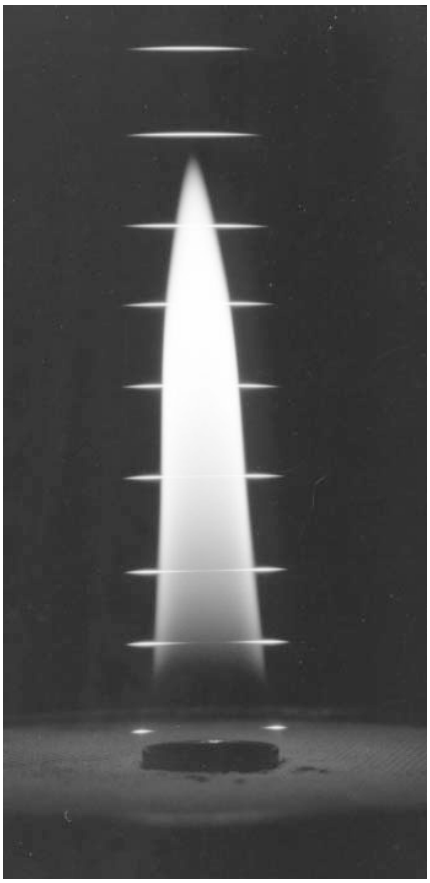

Image of the test flame and glowing fibers. The flame is about 70 mm long. The flame was observed in normal gravity with the flame tip up.

We anticipate that thin-filament pyrometry similar to that developed here will become an important diagnostic for studies of microgravity flames owing to its accuracy and its ability to simultaneously measure finely spaced temperatures.

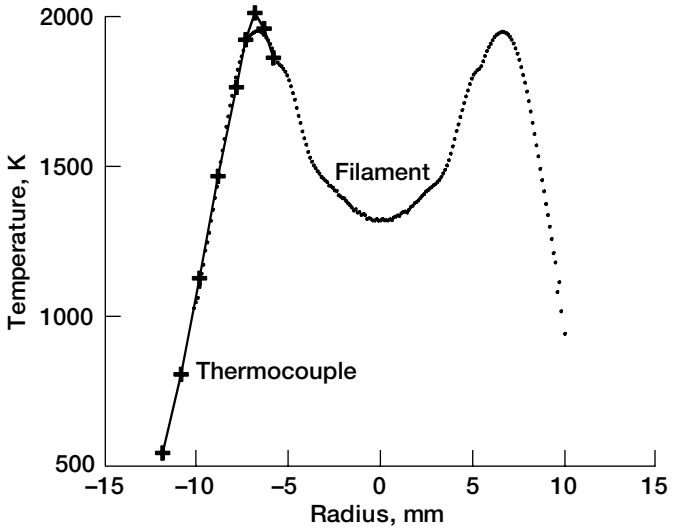

Temperature versus radius for the test flame as determined from both thin-filament pyrometry and thermocouples at a height of 21 mm above the burner. This height corresponds to the third fiber above the burner in the photograph.

Find out more about this research:

National Center for Microgravity Research: http://www.ncmr.org

Glenn's Microgravity Science Division: http://microgravity.grc.nasa.gov/

Glenn contact:
Dr. David L. Urban, 216–433–2835, David.L.Urban@nasa.gov

National Center for Microgravity Research contact:
Peter B. Sunderland, 216–433–8087, Peter.B.Sunderland@grc.nasa.gov

Author: Peter B. Sunderland

Headquarters program office: OBPR

Programs/Projects:
Microgravity Science

Edge Diffusion Flame Propagation and Stabilization Studied

In most practical combustion systems or fires, fuel and air are initially unmixed, thus forming diffusion flames. As a result of flame-surface interactions, the diffusion flame often forms an edge, which may attach to burner walls, spread over condensed fuel surfaces, jump to another location through the fuel-air mixture formed, or extinguish by destabilization (blowoff). Flame holding in combustors is necessary to achieve design performance and safe operation of the system. Fires aboard spacecraft behave differently from those on Earth because of the absence of buoyancy in microgravity. This ongoing in-house flame-stability research at the NASA Glenn Research Center is important in spacecraft fire safety and Earth-bound combustion systems.

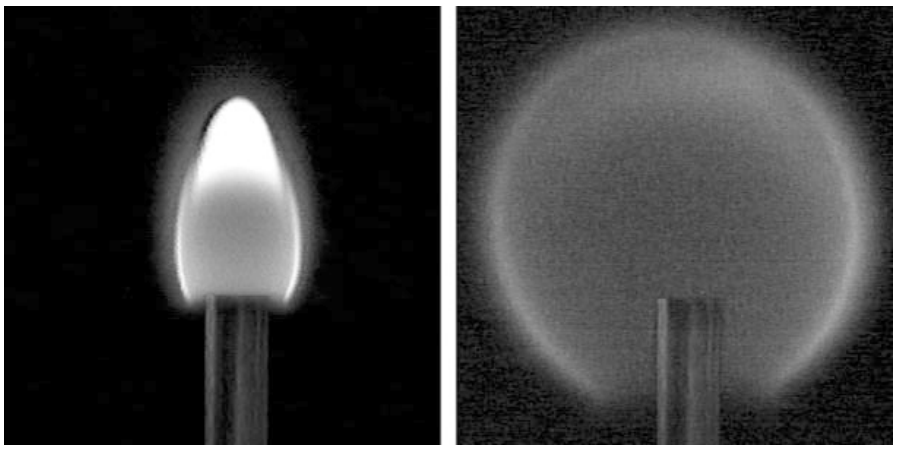

Video images of ethane jet diffusion flames in quiescent air. Burner tube inside diameter, i.d., 2.87 mm; mean fuel jet velocity, 7.5 cm/sec. Left: 1g. Right: μg.

Video observations of low-speed fuel jet diffusion flames have been made in normal Earth-gravity (1g) and in microgravity (μg) at the 2.2-Second Drop Tower at Glenn. The 1g flame was short and narrow, and the flame base was close to the burner rim as a result of buoyancy-induced flow. Intense blue emissions and a yellow-orange color indicated a vigorously burning flame zone and soot formation, respectively. By contrast, the μg flame was spherical and larger as a result of relatively slow fuel and oxygen molecular diffusion in every direction. The weak burning resulted in lower flame temperatures (thus reducing soot formation) and in a large quenched space near the burner wall.

Direct numerical simulations with a detailed reaction mechanism and radiative heat losses have revealed the flame structure in unsurpassed detail. Unlike previous work, these computations, which used a reaction mechanism including 33 species and

112 elementary steps, enabled genuine prediction of the flame propagation speed. In the simulations, a hydrocarbon fuel (methane, ethane, ethylene, acetylene, or propane) was injected into quasi-quiescent air in 1g or 0g for a short period (0.3 sec) and ignited downstream on the axis. The calculated flame propagation speed was independent of gravity and matched well with the stoichiometric laminar flame speed of each fuel.

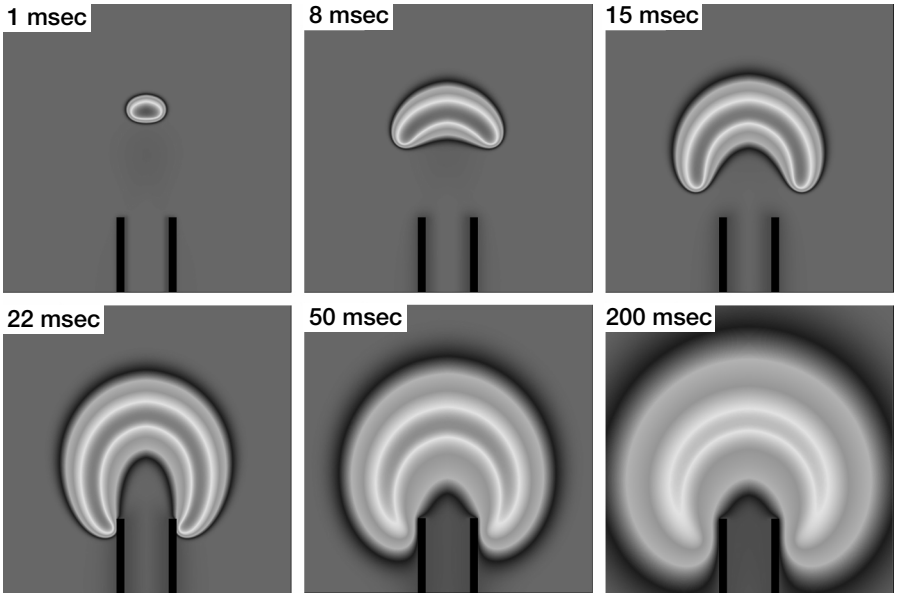

Temporal variations (from 1 to 200 msec) in the calculated temperature field of a propagating edge diffusion flame in an ethane jet in quasi-quiescent air in 0g. Burner tube i.d., 3 mm; mean fuel jet velocity, 6.86 cm/sec.

Computations revealed that a peak reactivity spot (i.e., a reaction kernel) was formed in the edge diffusion flame as a result of radical (H atom) back-diffusion into the high-oxygen-concentration region and subsequent chain-branching reactions. The reaction kernel in the propagating flame had characteristics of premixed flames in the direction of propagation. Once the edge diffusion flame attached to the burner rim, its premixed flame nature was lost because the flammable mixing layer became too narrow for propagation and its direction even became perpendicular to the incoming flow. Instead, vigorous reactions at the reaction kernel within an available residence time kept the trailing diffusion flame from blowoff. The 1g flame was stabilized at relatively high velocities because the reaction-kernel reactivity increased by "blowing." A linear correlation was found between the reaction-kernel reactivity and the velocity for each fuel. These new findings replace a conventional view of diffusion flame attachment based on premixed flames and may lead to better fire-extinguishing and flame-holding approaches.

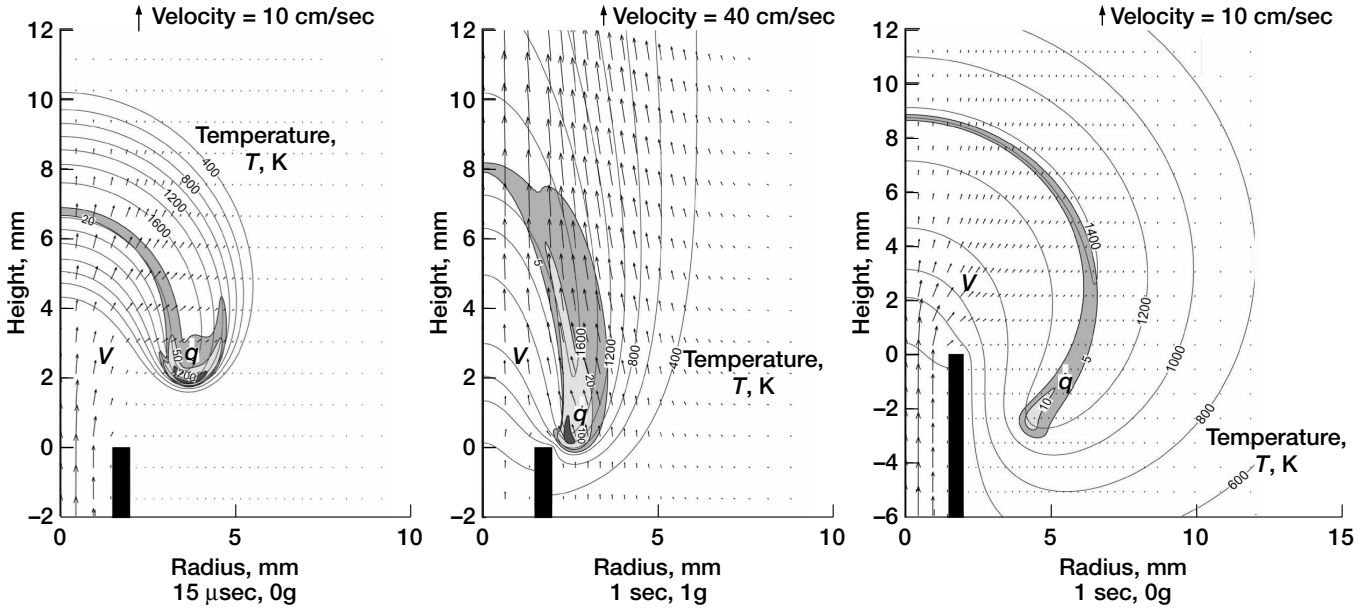

Calculated velocity vectors, v; temperature isotherms, T; and heat-release rate contours, q, in joules per cubic centimeter seconds. Burner tube i.d., 3 mm; mean fuel jet velocity, 6.86 cm/sec. Left: Propagating ethane flame in 0g. Center: Stabilized ethane jet diffusion flames in quasi-quiescent air in 1g. Right: Stabilized ethane jet diffusion flames in quasi-quiescent air in 0g.

References
1. Takahashi, F.; and Katta, V.R.: Reaction Kernel Structure and Stabilizing Mechanisms of Jet Diffusion Flames in Microgravity. Proc. Combust. Inst., part 2, vol. 29, 2002, pp. 2509–2518.
2. Takahashi, Fumiaki; and Katta, Viswanath R.: Propagation and Structure of Edge Diffusion Flames in Axisymmetric Hydrocarbon Fuel Jets. Proceedings of the 19th International Colloquium on the Dynamics of Explosions and Reactive Systems, Hakone, Japan, 2003.

National Center for Microgravity Research contact:
Dr. Fumiaki Takahashi, 216–433–3778, Fumiaki.Takahashi@grc.nasa.gov

Authors: Dr. Fumiaki Takahashi and Dr. Viswanath R. Katta

Headquarters program office: OBPR

Programs/Projects:
Microgravity Science

Carbon Dioxide Dispersion in the Combustion Integrated Rack Simulated Numerically

When discharged into an International Space Station (ISS) payload rack, a carbon dioxide (CO_2) portable fire extinguisher (PFE) must extinguish a fire by decreasing the oxygen in the rack by 50 percent within 60 sec. The length of time needed for this oxygen reduction throughout the rack and the length of time that the CO_2 concentration remains high enough to prevent the fire from reigniting is important when determining the effectiveness of the response and postfire procedures. Furthermore, in the absence of gravity, the local flow velocity can make the difference between a fire that spreads rapidly and one that self-extinguishes after ignition.

A numerical simulation of the discharge of CO_2 from PFE into the Combustion Integrated Rack (CIR) in microgravity was performed to obtain the local velocity and CO_2 concentration. The complicated flow field around the PFE nozzle exits was modeled by sources of equivalent mass and momentum flux at a location downstream of the nozzle. The time for the concentration of CO_2 to reach a level that would extinguish a fire anywhere in the rack was determined using the Fire Dynamics Simulator (FDS), a computational fluid dynamics code developed by the National Institute of Standards and Technology specifically to evaluate the development of a fire and smoke transport. The simulation shows that CO_2, as well as any smoke and combustion gases produced by a fire, would be discharged into the ISS cabin through the resource utility panel at the bottom of the rack (light gray region at the bottom of the CIR as shown in the bottom figure). These simulations will be validated by comparing the results with velocity and CO_2 concentration measurements obtained during the fire suppression system verification tests conducted on the CIR in March 2003.

Once these numerical simulations are validated, portions of the ISS labs and living areas will be modeled to determine the local flow conditions before, during, and after a fire event. These simulations can yield specific information about how long it takes for smoke and combustion gases produced by a fire to reach a detector location, how large the fire would be when the detector alarms, and the behavior of the fire until it has been extinguished. This new capability could then be used to optimize the location of fire detectors and fire-suppression ports as well as to evaluate the effectiveness of fire suppressants and response strategies. Numerical data collected from these simulations could also be used to develop a virtual reality fire event for crew training and fire safety awareness.

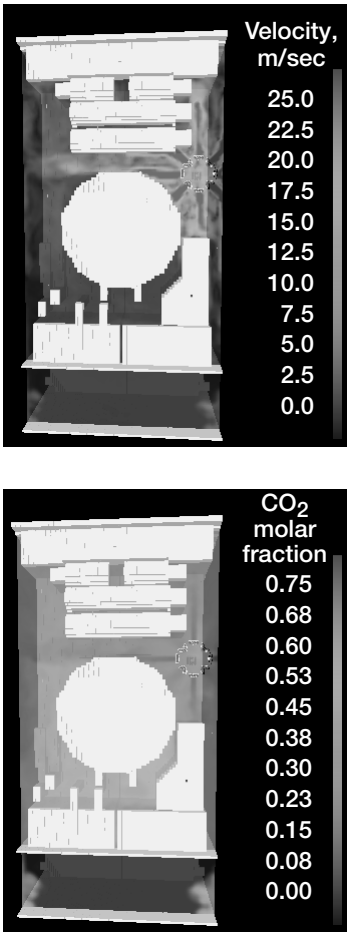

CO_2 after 8 sec of discharge from a PFE in the front section of the CIR. Top: Velocity. Bottom: Molar fraction. These figures are shown in color in the online version of this article (http://www.grc.nasa.gov/WWW/RT/6000/6711wu.html).

This work is funded by NASA's Bioastronautics Initiative, which has the objective of ensuring and enhancing the health, safety, and performance of humans in space. As part of this initiative, the Microgravity Combustion Science Branch at the NASA Glenn Research Center is conducting spacecraft fire safety research to significantly improve fire safety on inhabited spacecraft.

Find out more about this research: http://microgravity.grc.nasa.gov/combustion/

National Center for Microgravity Research contact:
Dr. Ming-Shin Wu, 216–433–3781, Ming-Shin.Wu@grc.nasa.gov

Glenn contact:
Dr. Gary A. Ruff, 216–433–5697, Gary.A.Ruff@nasa.gov

Authors:
Drs. Gary A. Ruff and Ming-Shin Wu

Headquarters program office: OBPR

Programs/Projects:
Microgravity Science

"Smart" Magnetic Fluids Experiment Operated on the International Space Station

InSPACE is a microgravity fluid physics experiment that was operated on the International Space Station (ISS) in the Microgravity Science Glovebox from late March 2003 through early July 2003. (InSPACE is an acronym for Investigating the Structure of Paramagnetic Aggregates From Colloidal Emulsions.) The purpose of the experiment is to obtain fundamental data of the complex properties of an exciting class of smart materials termed magnetorheological (MR) fluids. MR fluids are suspensions, or colloids, comprised of small (micrometer-sized) superparamagnetic particles in a nonmagnetic medium. Colloids are suspensions of very small particles suspended in a liquid. (Examples of other colloids are blood, milk, and paint.) These controllable fluids can quickly transition into a nearly solid state when exposed to a magnetic field and return to their original liquid state when the magnetic field is removed. Controlling the strength of the magnetic field can control the relative stiffness of these fluids. MR fluids can be used to improve or develop new seat suspensions, robotics, clutches, airplane landing gear, and vibration damping systems. The principal investigator for InSPACE is Professor Alice P. Gast of the Massachusetts Institute of Technology (MIT). The InSPACE hardware was developed at the NASA Glenn Research Center.

ISS Expedition Six Science Officer Don Petit operating the InSPACE investigation in the Microgravity Science Glovebox onboard the ISS.

The InSPACE samples were delivered to the ISS in November 2002, on the Space Shuttle Endeavour, on Space Station Utilization Flight UF–2/STS113. Operations began on March 31, 2003, with the processing of three different particle size samples at multiple test parameters. This investigation focused on determining the structural organization of MR colloidal aggregates when exposed to a pulsing magnetic field. On Earth, the aggregates take the shape of footballs with spiky tips. This characteristic shape may be influenced by the pull of gravity, which causes most particles initially suspended in the fluid to sediment, (i.e., settle and collect at the bottom of the cell). In the absence of sedimentation effects on the ISS, the behavior and shape of these MR aggregate structures are dominated exclusively by magnetic and surface tension forces. The microscopic detail of these structures was imaged under two

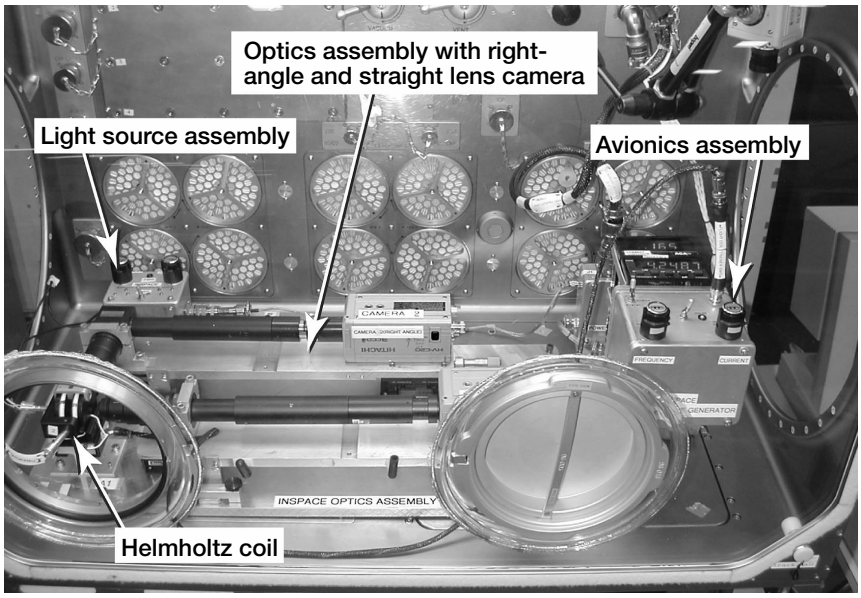

InSPACE experiment hardware mounted in the Microgravity Science Glovebox onboard the ISS. The hardware consists of the following components: a Helmholtz coil assembly that produces a uniform magnetic field in the sample mounted in the center of the coil, an MR fluid sample contained in a precision rectangular borosilicate glass vial (50-mm-long by 1-mm internal square), an avionics assembly that provides the capability for selecting a specified electrical current and frequency to produce the desired pulsed magnetic field inside the coil assembly, a light box assembly that illuminates the experiment so that it can be viewed, and an optics assembly that includes two video cameras for imaging the experiment from straight-on and right-angle views during the test runs.

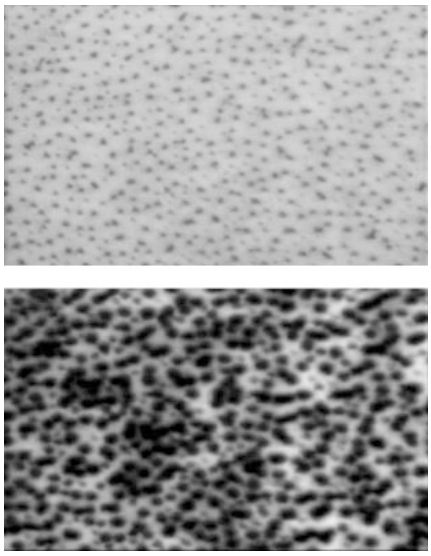

Early-stage structure generation. Top: Array of chain structures seen on end during steady magnetic field conditions (straight-on view looks in on the magnetic field lines); 0.66-μm particles at H = 1816 A/m (magnetic field). Bottom: The chain structures start to diffuse right after the magnetic field starts pulsing, but they will reorganize over time into a smaller number of large aggregates (straight-on view); 0.66-μm particles at H = 1816 A/m at 20 Hz.

orthogonal camera views. The video was downlinked to the InSPACE team at Glenn's Telescience Support Center and to MIT and also recorded onboard the ISS on videotapes that will be brought back to the ground by the space shuttles. The study examined the effect on the structure formation by varying the magnetic field strength and pulse frequency, and particle size. Fundamental data that characterized the structure formation were obtained.

InSPACE completed its last planned test run on July 2, 2003. Operations occurred on 21 days over approximately a 3-month period. Forty-one test points were completed during 26 test runs. During the initial testing, the procedures followed by the crew were modified to maximize the observation of some unexpected and interesting aggregate behavior. As a result Dr. Gast has reported on the formation of aggregate shapes that are more extended and diverse than those observed on the ground. Sheets of magnetic material folded over in a labyrinth pattern and large columnar aggregates with complex interfaces with the surrounding fluid are examples of the interesting structures that have been observed on the ISS. In light of these early findings, the understanding of the fundamental properties of MR fluids on the basis of ground-based observations may need to be reconsidered.

The experiments on the ISS have provided a vast amount of video data for analysis. While this analysis is ongoing, plans are being made for additional experimental runs. For this purpose, additional hardware and cells containing samples of different magnetic particles and sizes are being fabricated for a future launch to the ISS. The InSPACE hardware will remain on orbit until this testing is completed.

Reference

1. Promislow, J.H.E.; and Gast, A.P.: Magnetorheological Fluid Structure in a Pulsed Magnetic Field. Langmuir, vol. 12, no. 17, 1996, pp. 4095–4102.

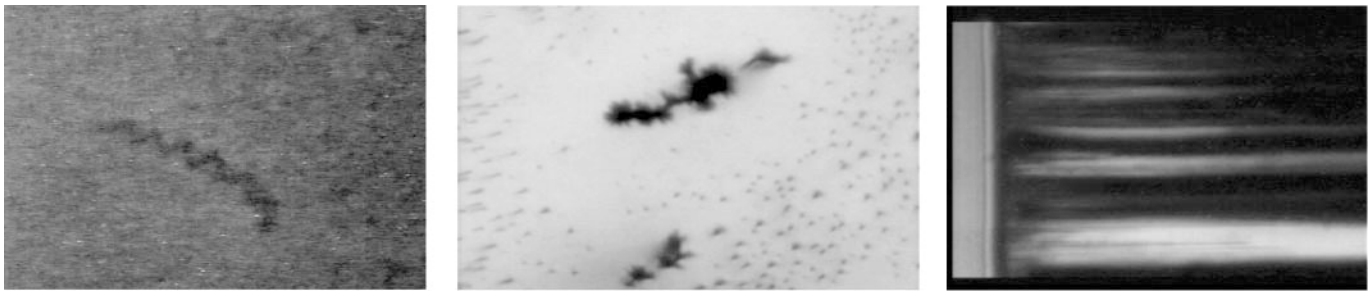

Late-stage structure development. Left: Labyrinth structure formed from the folding over of a two-dimensional sheet of magnetic particles (straight-on view); 0.66-μm particles at H = 1816 A/m (magnetic field) at 5 Hz. Center: Large aggregates forming complex interfaces with the surrounding fluid (straight-on view); 0.66-μm particles at H = 2082 A/m at 15 Hz. Right: Columnar aggregate structures imaged across the magnetic field (right-angle view); 0.66-μm particles at H = 2082 A/m at 20 Hz.

Find out more about this research:

Glenn's Microgravity Science Division: http://microgravity.grc.nasa.gov/

Microgravity Science Glovebox:
http://spaceresearch.nasa.gov/research_projects/ros/msg.html

ISS research overview: http://spaceresearch.nasa.gov/research_projects/ros/ros.html

InSPACE: http://microgravity.grc.nasa.gov/inspace

Dr. Alice P. Gast at MIT: http://web.mit.edu/cheme/people/faculty/gast.html

Amazing Magnetic Fluids (Science@NASA article):
http://science.nasa.gov/headlines/y2002/23aug_MRfluids.htm?list47209

Glenn contacts:
Dr. Juan H. Agui, 216–433–5409,
Juan.H.Agui@nasa.gov; and
Jack F. Lekan, 216–433–3459,
John.F.Lekan@nasa.gov

Authors:
Dr. Juan H. Agui and Jack F. Lekan

Headquarters program office: OBPR

Programs/Projects:
Microgravity Science

Calibration Experiments Conducted for Noninvasive Blood Glucose Sensing Through the Eye

There are more than 16 million diabetics in the United States and more than 100 million worldwide. Diabetes can lead to severe complications over time such as blindness, renal and cardiovascular diseases, and peripheral neuropathy in the limbs. Poor blood circulation in diabetics can lead to gangrene and the subsequent amputation of extremities. In addition, this pathology is the fourth leading cause of death in the United States. The most effective way to manage diabetes is frequent blood glucose monitoring performed by the patients themselves. However, because of pain, inconvenience, and the fear of developing infections from finger-prick blood tests or implants, many patients monitor their blood glucose levels less frequently than is recommended by their physicians. Therefore, a noninvasive, painless, and convenient method to monitor blood glucose would greatly benefit diabetics.

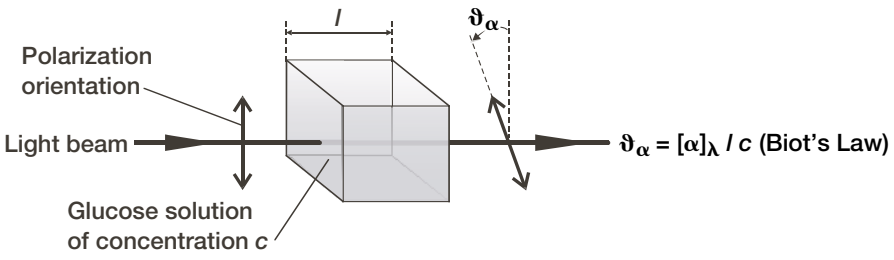

Principle of operation.

Likewise, detecting, preventing, and treating the untoward effects of prolonged space travel (e.g., a human mission to Mars) in real-time requires the development of noninvasive diagnostic technologies that are compact and powerful. As a "window to the body," the eye offers the opportunity to use light in various forms to detect ocular and systemic abnormalities long before clinical symptoms appear and to help develop preventative and therapeutic countermeasures early. The noninvasive feature of these technologies permits frequent repetition of tests, enabling an evaluation of the response to therapy.

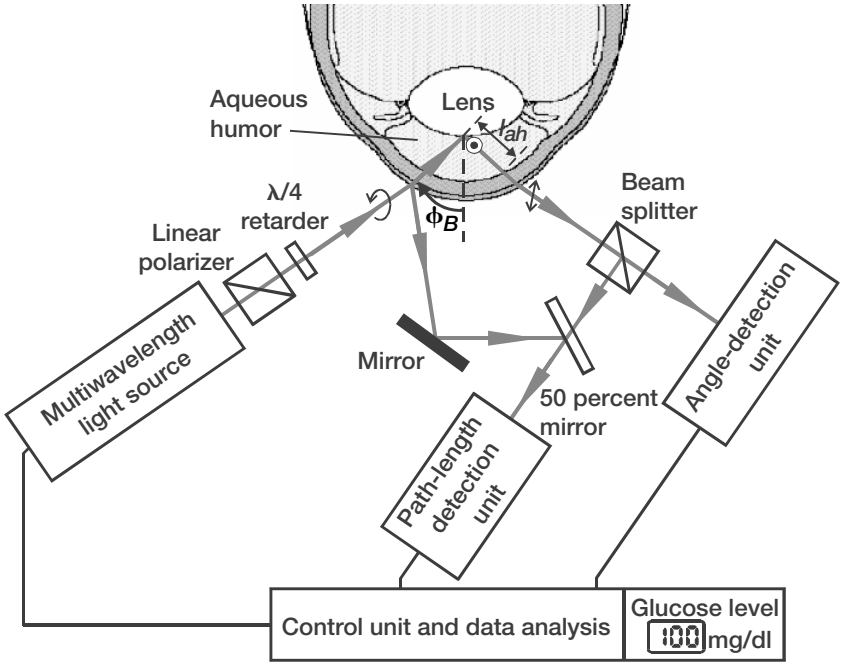

Schematic diagram of the apparatus. l_{ah}, reflected optical path length.

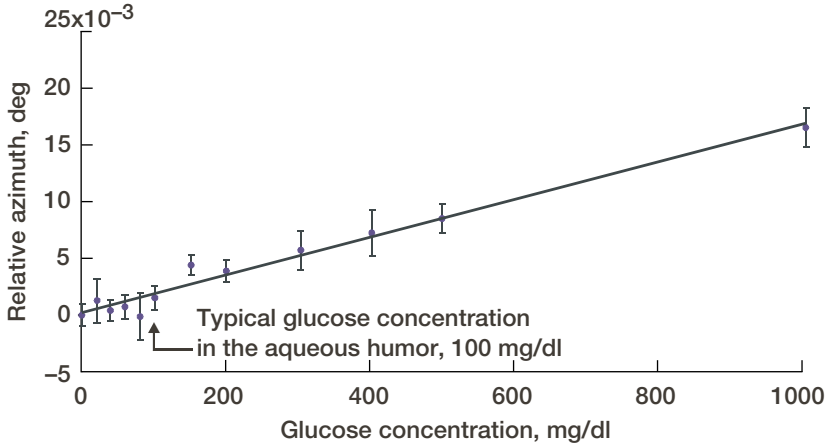

Instrument calibration.

Certain molecules (e.g., glucose) possess chiral properties: they will rotate a plane of polarized light to the right (clockwise). The rate of rotation is directly proportional to the amount of glucose present in a solution. The aqueous humor of the eye exhibits low scattering properties, and its glucose concentration closely matches blood glucose levels. A glucose molecule rotates the plane of polarization of incident polarized light by an angle ϑ_α that is proportional to the path length *l* and the concentration *c* in the sample. The substance-specific proportionality factor $[\alpha]_\lambda$ denotes the optical rotatory power, which is a function of the wavelength λ. By knowing this quantity at the wavelength and optical path length *l* used and by observing the polarization rotation ϑ_α, one can calculate the glucose concentration *c*.

The preferred test site for the polarimetric measurement of glucose concentration in the human body is the aqueous humor of the eye: the clear fluid between the cornea and crystalline lens in the eye's anterior chamber. This fluid is an ultrafiltrate of blood containing most of the molecules found in serum, including glucose, at concentrations that are reflective of serum levels in the human body. Therefore, the aqueous humor can act as an exceptional optical window to measure the glucose levels of diabetics without contact.

In our experimental setup, the aqueous humor is optically accessed with a circularly polarized light beam reflected at the Brewster's angle ϕ_B off the eye lens. On its way out of the eye, the resulting reflected linearly polarized light constitutes the measured quantity for the sensor. The application of a multiwavelength light source permits spectrally resolved signal detection by the angle-detection unit so that the device can benefit from the specific wavelength dependence of the optical rotatory power of glucose. Therefore, the influence of optically active confounders[1] and of changes in the polarization state induced by the geometry of the setup are mostly eliminated. For simultaneous measurement of the optical path length inside the aqueous humor, a path-length detection unit was built on the basis of low-coherence interferometry.

Preliminary proof-of-concept calibration experiments using aqueous glucose samples were conducted at the NASA Glenn Research Center. The results showed good linearity (correlation coefficient, r = 0.986) and high sensitivity (angle of rotation, σ = 1.38 millidegrees corresponding to a glucose concentration, *c*, of 77 mg/dl). Efforts are underway to further improve the sensitivity and repeatability and to reduce the size and cost of the sensor. The ultimate goal is a portable, easy-to-use, reliable measurement device for daily patient medical care and better diabetes management.

[1]Molecules other than glucose (e.g., albumins).

Reference

1. Ansari, Rafat R.; Böckle, Stefan; and Rovati, Luigi: New Optical Scheme for a Polarimetric-Based Glucose Sensor. J. Biomed. Opt., vol. 9, no. 1, 2004, pp. 103–115.

Glenn contact: Dr. Rafat R. Ansari, 216–433–5008, Rafat.R.Ansari@nasa.gov

Authors: Dr. Rafat R. Ansari, Dr. Stefan Bockle, Dr. Kwang I. Suh, and Dr. Luigi L. Rovati

Headquarters program office: OBPR

Programs/Projects:
Microgravity Science

Special recognition:
U.S. Patent 6,704,588 awarded March 9, 2004.

Operation of Packed-Bed Reactors Studied in Microgravity

The operation of a packed bed reactor (PBR) involves gas and liquid flowing simultaneously through a fixed-bed of solid particles. Depending on the application, the particles can be various shapes and sizes but are generally designed to force the two fluid phases through a tortuous route of narrow channels connecting the interstitial space. The PBR is the most common type of reactor in industry because it provides for intimate contact and high rates of transport between the phases needed to sustain chemical or biological reactions. The packing may also serve as either a catalyst or as a support for growing biological material. Furthermore, this type of reactor is relatively compact and requires minimal power to operate. This makes it an excellent candidate for unit operations in support of long-duration human space activities.

A NASA Research Announcement award to the University of Houston, Notre Dame University, and NASA Glenn Research Center is currently supporting research for fundamental studies of the PBR in a microgravity environment.

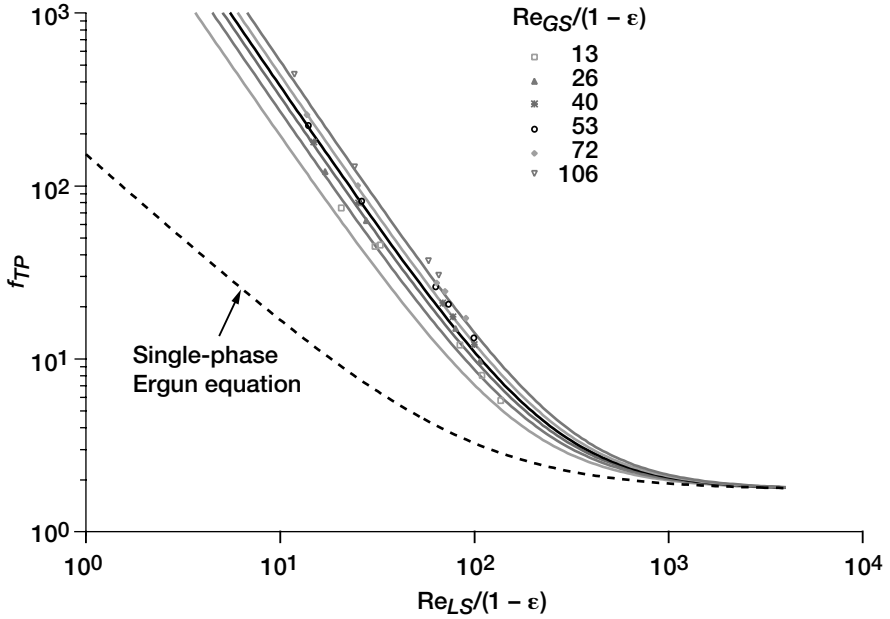

Pressure-drop model for microgravity operation for Suratman number Su = 146,000. Re_{GS} and Re_{LS}, Reynolds numbers for superficial gas and liquid flows, respectively; f_{TP}, modified two-phase friction factor.

Through this award, a series of experiments have flown on NASA's reduced-gravity aircraft. As a result of the experimental effort, models for pressure drop and flow regime transitions have been developed and recently published (ref. 1).

The graph on the left shows an example of the new pressure drop model for reduced gravity. The model is based on the well-known Ergun equation which is used to describe single-phase flow through porous media. The new model extends this equation by including a term to account for pressure losses associated with the interaction between the gas and liquid phases. This term could not be validated in a normal-gravity environment because of the masking effects of gravity.

A flow regime transition map was also developed for microgravity and is shown in the following graph. Through dimensional analysis, it was shown that the transition from bubbly flow to pulse flow (flow with alternating gas and liquid slugs) is a function of the gas and liquid Reynolds numbers and the Suratman number *Su*. This number arises in the analysis of capillary effects in small-diameter tubes and jets and is the ratio of the liquid Reynolds number to the capillary number. The transition occurs when the ratio of the Reynolds numbers for the superficial gas and liquid flows $(Re_{GS}/Re_{LS}) = 700 \times Su^{-2/3}$.

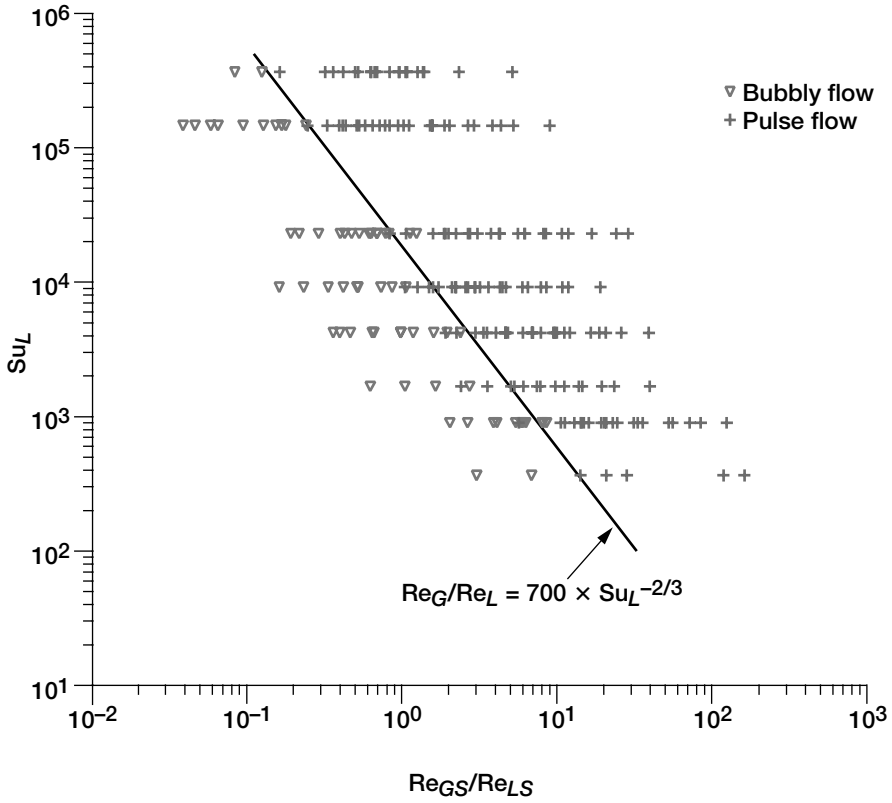

Transition map between bubbly and pulse flow for the microgravity environment. Su= Re/Ca; Suratman number of liquid, Su_L.

Future work is planned to study the effects of gravity on other parameters that affect the design and operation of the PBR. For example, the quasi-steady pulse characteristics are a strong function of gravity and greatly influence the mixing and mass transfer of the reactor. The goal of this research is to fully understand the operational characteristics of the PBR in microgravity. Then engineers may be able to take advantage of this environment to develop a reactor for space applications with an operational efficiency equal to or greater than the present levels found in terrestrial systems.

Reference

1. Motil, B.J.; Balakotaiah, V.; and Kamotani, Y.: Gas-Liquid Two-Phase Flows Through Packed Beds in Microgravity. AIChE J., vol. 49, no. 3, 2003, pp. 557–565.

Find out more about this research:
http://microgravity.grc.nasa.gov/6712/research.htm

Glenn contact:
Brian J. Motil, 216–433–6617, Brian.J.Motil@nasa.gov

Authors:
Brian J. Motil and Vemuri Balakotaiah

Headquarters program office: OBPR

Programs/Projects:
Microgravity Science

Two-Photon Fluorescence Microscopy Developed for Microgravity Fluid Physics

Recent research efforts within the Microgravity Fluid Physics Branch of the NASA Glenn Research Center have necessitated the development of a microscope capable of high-resolution, three-dimensional imaging of intracellular structure and tissue morphology. Standard optical microscopy works well for thin samples, but it does not allow the imaging of thick samples because of severe degradation caused by out-of-focus object structure. Confocal microscopy, which is a laser-based scanning microscopy, provides improved three-dimensional imaging and true optical sectioning by excluding the out-of-focus light. However, in confocal microscopy, out-of-focus object structure is still illuminated by the incoming beam, which can lead to substantial photobleaching. In addition, confocal microscopy is plagued by limited penetration depth, signal loss due to the presence of a confocal pinhole, and the possibility of live-cell damage.

Two-photon microscopy is a novel form of laser-based scanning microscopy that allows three-dimensional imaging without many of the problems inherent in confocal microscopy. Unlike one-photon microscopy, it utilizes the nonlinear absorption of two near-infrared photons. However, the efficiency of two-photon absorption is much lower than that of one-photon absorption because of the nonlinear (i.e., quadratic) electric field depen-

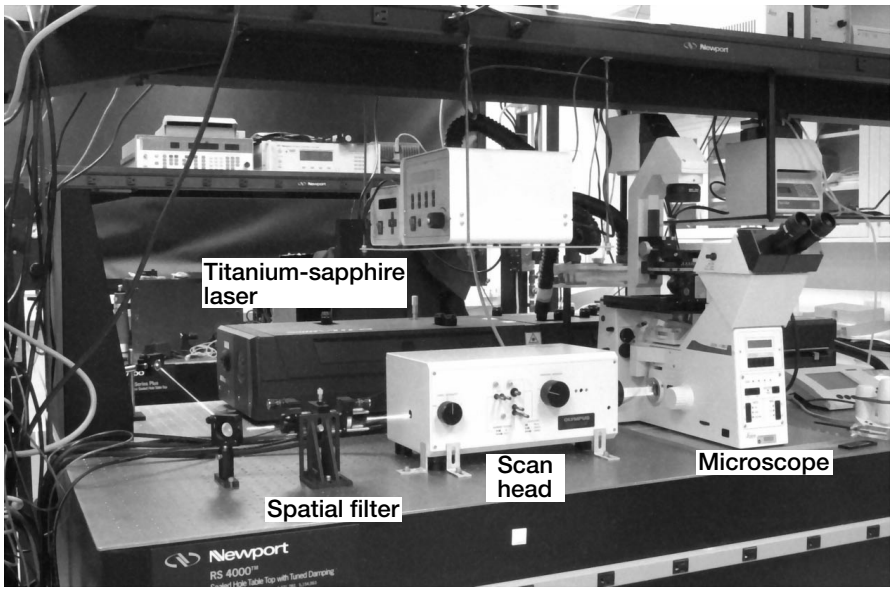

Optical system for two-photon fluorescence microscopy. This figure is shown in color in the online version of this article (http://www.grc.nasa.gov/WWW/RT/6000/6712fischer.html).

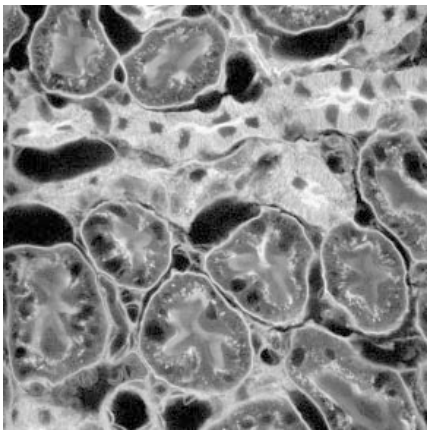

Multiple-channel two-photon fluorescence image of mouse kidney cells. The field of view is 134 μm square. This figure is shown in color in the online version of this article (http://www.grc.nasa.gov/WWW/RT/6000/6712fischer.html).

dence, so an ultrafast pulsed laser source must typically be employed. On the other hand, this stringent energy density requirement effectively localizes fluorophore excitation to the focal volume. Consequently, two-photon microscopy provides optical sectioning and confocal performance without the need for a signal-limiting pinhole. In addition, there is a reduction in photodamage because of the longer excitation wavelength, a reduction in background fluorescence, and a ×4 increase in penetration depth over confocal methods because of the reduction in Rayleigh scattering.

For these obvious advantages, a two-photon scanning microscope system was selected for development. The prohibitive cost of a commercial two-photon system, as well as a desired modularity, led to the construction of a custom-built system. It employs a Coherent mode-locked titanium:sapphire laser (Coherent, Inc., Santa Clara, CA) emitting 120 fsec pulses over a tuning range of 700 to 980 nm, allowing the excitation of a variety of targeted fluorophores. The ultrafast laser was interfaced with an Olympus (Tokyo, Japan) confocal scan head and a Leica Microsystems AG (Wetzlar, Germany) inverted microscope (shown in the photograph on the left), and optimal coupling of the hybrid system involved the design and optimization of both beam conditioning and transfer optics. In addition, an integrated software environment was developed for *x-y-z* scanning control as well as image acquisition and processing. A modular design was chosen to allow easy access to the optical train for future fluorescence correlation spectroscopy and fluorescence lifetime experiments. The spatial resolution of the microscope at an excitation wavelength of 780 nm was measured by scanning a 170-nm fluorescent bead throughout the focal region. The resolution was found to be 320 nm in the transverse direction and 740 nm in the longitudinal direction. The improved resolution and depth-sectioning capability of two-photon microscopy is illustrated in the photograph on the right, which shows a multiple-stained mouse kidney section that was imaged using two-channel spectral detection.

Glenn contacts:
Dr. David G. Fischer, 216–433–6379, David.G.Fischer@nasa.gov; and
Dr. Gregory A. Zimmerli, 216–433–6577, Gregory.A.Zimmerli@nasa.gov

Authors:
Dr. David G. Fischer, Dr. Gregory A. Zimmerli, and Marius Asipauskas

Headquarters program office: OBPR

Programs/Projects:
Microgravity Science

Reduced-Gravity Experiments Conducted to Help Bioreactor Development

The NASA Glenn Research Center and the NASA Johnson Space Center are collaborating on fluid dynamic investigations for a future cell science bioreactor to fly on the International Space Station (ISS). Project Manager Steven Gonda from the Cellular Biotechnology Program at Johnson is leading the development of the Hydrodynamic Focusing Bioreactor—Space (HFB–S) for use on the ISS to study tissue growth in microgravity. Glenn is providing microgravity fluid physics expertise to help with the design and evaluation of the HFB–S. These bioreactors are used for three-dimensional tissue culture, which cannot be done in ground-based labs in normal gravity. The bioreactors provide a continual supply of oxygen for cell growth, as well as periodic replacement of cell culture media with nutrients. The bioreactor must provide a uniform distribution of oxygen and nutrients while minimizing the shear stresses on the tissue culture.

The HFB–S is being developed with the ability to remove gas bubbles that may inadvertently enter the system during long-duration experiments (~1 to 3 months). The Rotating Wall Perfused Vessel (RWPV) has been used in the past with great success on shuttle flights and Mir missions, but it has occasionally experienced problems when gas bubbles entered the fluid-filled vessel. These bubbles are harmful to the cell science, and bubble removal in the rotating wall perfused vessel is problematic. The HFB–S has a central access port that has been designed to allow for bubble removal under specific operating conditions without detrimentally affecting the cell tissue. A detailed technical objective flight on the space shuttle is being planned to fully evaluate the HFB–S. In addition, ground-based activities are underway to quantify the characteristics of the HFB–S. Computational studies of the internal fluid flow of the HFB–S are being done at the University of Houston by Dr. Stanley Kleis to predict bubble motion as well as other operational parameters. Drs. Charles Niederhaus and Henry Nahra from Glenn's Microgravity Fluid Physics Branch and Dr. John Kizito at the National Center for Microgravity Research have been helping with the fluid analysis and experimental verification.

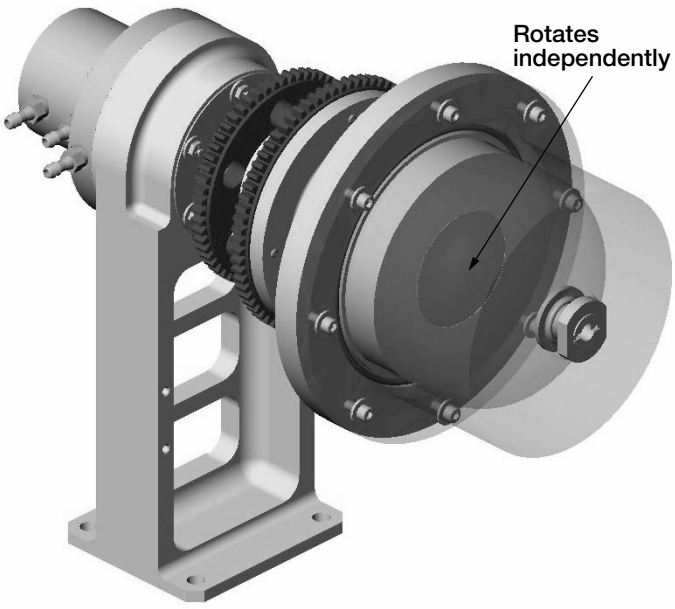

A CAD model of the proposed configuration of the HFB–S. The HFB–S has a dome-shaped top and a flat bottom. The inner part of the bottom (see arrow) rotates independently of the dome and acts as a weak centrifugal pump. The resulting flow inside the bioreactor resembles a vortex ring that is rotating about its central axis as well as rotating about the ring axis.

Experiments with the HFB–S were conducted in the microgravity environment on the KC–135 reduced-gravity aircraft operated by Johnson and flying out of Cleveland Hopkins International Airport and Houston Airport System's Ellington Field. The first set of flights in July 2002 provided useful data on bubble trajectories that are validating the computational predictions. The latest flights in January 2003 free-floated the apparatus and tested the most recent configuration of the bioreactor while focusing on the bubble removal process itself. These experiments showed that the bubble could be driven successfully to the removal port and purged in microgravity. The last day's experiments had an excellent microgravity environment because of calm air, and the experience gained in previous flights allowed successful bubble removal in 18 out of 35 tries—remarkable given the microgravity time constraints and the g-jitter on the KC–135.

John Yaniec and Sandra Geffert free-floating the HFB–S package. Stewart Robinson hangs onto the main console in the background while Charles Niederhaus operates the controls to remove the bubble.

Glenn contacts:
Dr. Charles E. Niederhaus, 216–433–5461, Charles.E.Niederhaus@nasa.gov; and Dr. Henry K. Nahra, 216–433–5385, Henry.K.Nahra@nasa.gov

National Center for Microgravity Research contact:
Dr. John P. Kizito, 216–433–2275, John.P.Kizito@grc.nasa.gov

Authors: Dr. Charles E. Niederhaus, Dr. Henry K. Nahra, and Dr. John P. Kizito

Headquarters program office: OBPR

Programs/Projects:
Microgravity Science

Compact Microscope Imaging System With Intelligent Controls Improved

The Compact Microscope Imaging System (CMIS) with intelligent controls is a diagnostic microscope analysis tool with intelligent controls for use in space, industrial, medical, and security applications. This compact miniature microscope, which can perform tasks usually reserved for conventional microscopes, has unique advantages in the fields of microscopy, biomedical research, inline process inspection, and space science. Its unique approach integrates a machine vision technique with an instrumentation and control technique that provides intelligence via the use of adaptive neural networks. The CMIS system was developed at the NASA Glenn Research Center specifically for interface detection used for colloid hard spheres experiments; biological cell detection for patch clamping, cell movement, and tracking; and detection of anode and cathode defects for laboratory samples using microscope technology.

This imaging system has many potential commercial uses, including automated inline inspection of precision parts, medical imaging, security industry applications (examination of currency in automated teller machines and fingerprint identification in secure entry locks), environmental industry applications (automated examination of soil and water samples), biomedical field applications (automated blood and cell analysis), and microscopy.

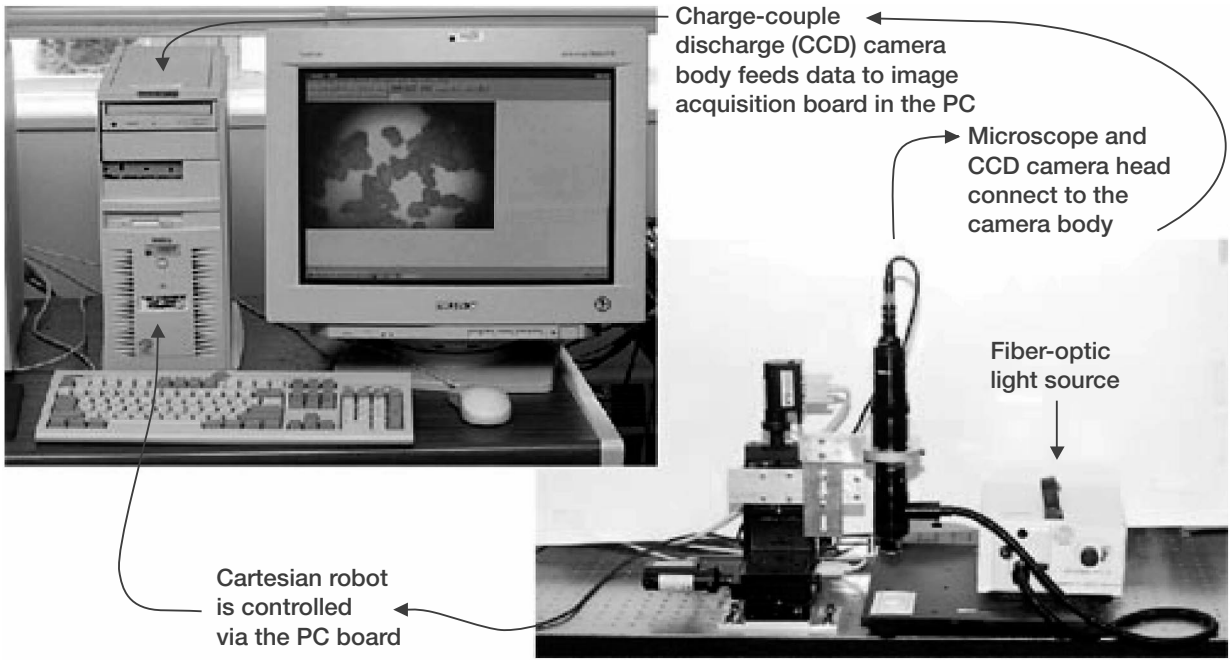

The CMIS system.

Find out more about this research: http://cmis.grc.nasa.gov

Glenn contact: Dr. Mark McDowell, 216–433–8161, Fax: 216–433–5033, drmm@easy.grc.nasa.gov

Author: Dr. Mark McDowell

Headquarters program office: OBPR

Programs/Projects: Microgravity Science

General-Purpose Stereo Imaging Velocimetry Technique Developed for Space and Industrial Applications

A new three-dimensional, full-field analysis technique has been developed for industrial and space applications. Stereo Imaging Velocimetry (SIV) will provide full-field analysis for three-dimensional flow data from any optically transparent fluid that can be seeded with tracer particles. The goal of SIV is to provide a means to measure three-dimensional fluid velocities quantitatively and qualitatively at many points. SIV is applicable to any optically transparent fluid experiment. Except for the tracer particles, this measurement technique is nonintrusive. Velocity accuracies are on the order of 95 to 99 percent of full-field. The system components of SIV include camera calibration, centroid determination, overlap decomposition, particle tracking, stereo matching, and three-dimensional velocity analysis. SIV has been used successfully for space shuttle experiments as well as for fluid flow applications for business and industry.

This technique provides a diagnostic tool for the quantitative and qualitative characterization of fluid flows. It permits direct comparisons between computed and experimentally measured three-dimensional flows. The PC-based SIV applications package is available for incorporation into existing experiments. Potential commercial uses for this technology include continuous casting, three-dimensional reconstruction, biofluid flow analysis (cell tracking), and inline process inspection.

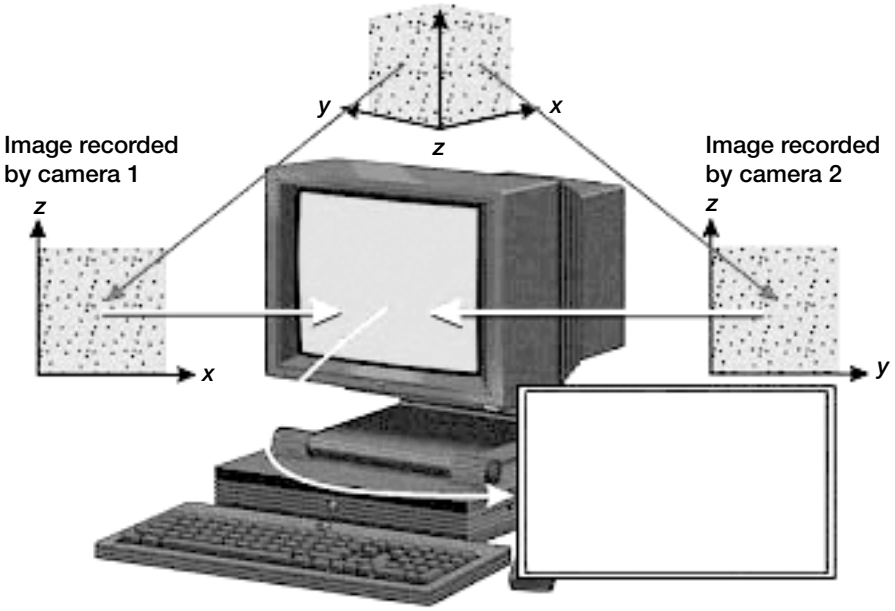

SIV experimental setup. Algorithms process image data to make three-dimensional, full-field, quantitative fluid flow measurements.

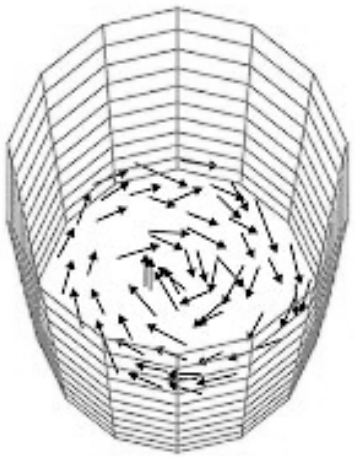

Fluid experiment seeded with tracer particles SIV vectors at Glenn (three-dimensional orthogonal view).

Find out more about this research: http://siv.grc.nasa.gov

Glenn contact:
Dr. Mark McDowell, 216–433–8161, Fax: 216–433–5033, drmm@easy.grc.nasa.gov

Author: Dr. Mark McDowell

Headquarters program office: OBPR

Programs/Projects:
Microgravity Science, continuous casting, three-dimensional reconstruction, biofluid flow analysis (cell tracking), inline process inspection

Special recognition:
U.S. Patents 6,603,535 and 5,905,568

Physics of Colloids in Space—Plus (PCS+) Experiment Completed Flight Acceptance Testing

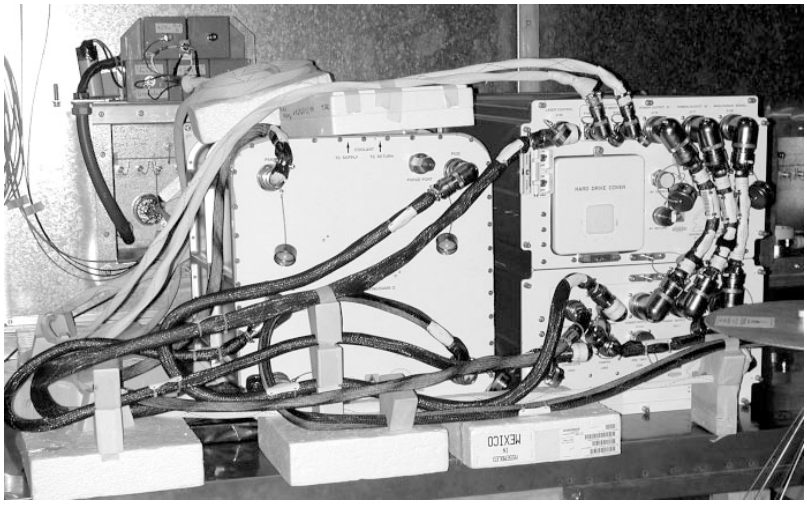

PCS+ hardware system (Test Section on left, Avionics Section on right) undergoing radiated emissions testing in Glenn's Electromagnetic Interference Laboratory.

The Physics of Colloids in Space—Plus (PCS+) experiment successfully completed system-level flight acceptance testing in the fall of 2003. This testing included electromagnetic interference (EMI) testing, vibration testing, and thermal testing. PCS+, an Expedite the Process of Experiments to Space Station (EXPRESS) Rack payload will deploy a second set of colloid samples within the PCS flight hardware system that flew on the International Space Station (ISS) from April 2001 to June 2002. PCS+ is slated to return to the ISS in late 2004 or early 2005.

PHYSICS OF COLLOIDS IN SPACE: SERIES OF EXPERIMENTS ON THE ISS IN EXPRESS RACK 2

	PCS	PCS+	PCS–3
Launch date	April 2001	Fall 2004 (est.)	Summer 2005 (est.)
Landing date	June 2002	Summer 2005 (est.)	Spring 2006 (est.)
Principal investigator(s)	David A. Weitz (Harvard Univ.)	Paul M. Chaikin (Princeton Univ.)	David A. Weitz (Harvard Univ.), Michael J. Solomon (Univ. of Michigan), and Eric R. Weeks (Emory Univ.)
Highlights and thrust of experiment	• 2400 hr on-orbit operations • Over 80 percent of science achieved • Four classes of colloids • Validation of experiment facility hardware and operations	• Relaunch of refurbished Avionics Section; relaunch of Test Section with new samples • Fundamental studies of colloidal hard sphere disorder-order transition and the properties of the resulting ordered phase	• Launch of completely new Test Section, enabling continuous operations of PCS "facility" • Avionics Section may remain on orbit after PCS–3

EMI testing, vibration testing, and thermal testing were conducted, respectively, in NASA Glenn Research Center's Electromagnetic Interference Laboratory, Structural Dynamics Laboratory, and Thermal Test Facility—three laboratories that are critical for ensuring space flight payload hardware integrity. Because of unanticipated alterations to the original PCS flight hardware system to replace and upgrade some electronic diagnostic components for PCS+, the EMI emissions test regimen was included to determine if the new equipment would negatively influence overall emission profiles. EMI emissions on ISS are undesirable because they generate both electric and magnetic fields, which can propagate into the ISS environment, affecting onboard ISS systems or other payloads. Testing proved that EMI emissions were virtually unchanged and that the hardware was acceptable for use on the ISS. Vibration and thermal testing (performed in both nonoperating and operating configurations) is required to ensure experiment integrity within prelaunch, launch, ISS operations, and deorbit environments as well as the quality of the reassembly workmanship. PCS+ also passed these tests.

PCS+ uses light-scattering techniques to extend the basic research in colloid physics that was begun under the Physics of Hard Spheres Experiment (PHASE) and the PCS experiment. Colloids are very small particles (about one hundredth of the thickness of a human hair) suspended in a liquid or a gas. Paint, ink, mayonnaise, milk, and even smoke are everyday examples of colloids. Colloids differ from other materials such as particles of sugar in water because they do not dissolve. Furthermore, the properties of these unique particle suspensions vary widely and often cannot be realized in other materials. Earth's gravity causes the heavier materials in a colloid to settle to the bottom (settling or sedimentation) and causes the lighter materials to go the top. Therefore, scientists cannot study many of the properties of these materials on Earth. On the ISS, where extended periods of microgravity exist, scientists can study the properties of colloids without any sedimentation or settling. The ordered colloids of PCS+ serve as a model for crystal growth, dendrite growth, and glass formation. These simplified model systems are furthering the fundamental knowledge of thermodynamic phase transitions, and this deeper knowledge could lead to novel drugs and materials. The principal investigator and coinvestigator for PCS+, respectively, are Prof. Paul M. Chaikin and Prof. William B. Russel (both of Princeton University).

The PCS flight hardware system is composed of a Test Section and an Avionics Section, which occupy four middeck locker spaces in ISS EXPRESS Rack 2. A third use of the PCS flight system has also been approved and is under development. This flight is called PCS–3. For PCS–3, the Avionics Section will be kept on-orbit after PCS+ operations are complete. A second Test Section will be fabricated for PCS–3 and will be populated with a third set of samples, which will be launched to the ISS approximately 10 months after the PCS+ launch. The principal investigators for PCS–3 are Prof. David Weitz, Prof. Michael Solomon (University of Michigan), and Prof. Eric Weeks (Emory University). The two Test Sections will be exchanged on-orbit. PCS–3 will initiate operations, whereas the PCS+ Test Section will be returned to Earth. The PCS+ experiment is being developed for launch by Zin Technologies under NASA contract NAS3–99154.

Find out more about this research:

Research description for Paul M. Chaikin, PCS+ principal investigator:
http://pupgg.princeton.edu/www/jh/research/Chaikin_paul.htmlx

Glenn Research Center's Electromagnetic Interference Laboratory:
http://facilities.grc.nasa.gov/emi/

Glenn's Structural Dynamics Laboratory: http://facilities.grc.nasa.gov/sdl/

Glenn's Thermal Test Facility: http://microgravity.grc.nasa.gov/thermalchambers/

Glenn's PCS research (includes data on a sample-by-sample basis): http://microgravity.grc.nasa.gov/6712/pcs.htm

Glenn's microgravity research: http://microgravity.grc.nasa.gov/

Glenn's fluid physics research: http://microgravity.grc.nasa.gov/MSD/MSD_htmls/fluids.html

Glenn contact:
Michael P. Doherty, 216–433–6641, Michael.P.Doherty@nasa.gov

Author: Michael P. Doherty

Headquarters program office: OBPR

Programs/Projects:
Microgravity Science

Special recognition:
The project team received a Space Act Award for their work on PCS.

Light Microscopy Module Imaging Tested and Demonstrated

The Fluids Integrated Rack (FIR), a facility-class payload, and the Light Microscopy Module (LMM), a subrack payload, are integrated research facilities that will fly in the U.S. Laboratory module, Destiny, aboard the International Space Station. Both facilities are being engineered, designed, and developed at the NASA Glenn Research Center by Northrop Grumman Information Technology. The FIR is a modular, multiuser scientific research facility that is one of two racks that make up the Fluids and Combustion Facility (the other being the Combustion Integrated Rack). The FIR has a large volume dedicated for experimental hardware; easily reconfigurable diagnostics, power, and data systems that allow for unique experiment configurations; and customizable software. The FIR will also provide imagers, light sources, power management and control, command and data handling for facility and experiment hardware, and data processing and storage. The first payload in the FIR will be the LMM. The LMM integrated with the FIR is a remotely controllable, automated, on-orbit microscope subrack facility, with key diagnostic capabilities for meeting science requirements—including video microscopy to observe microscopic phenonema and dynamic interactions, interferometry to make thin-film measurements with nanometer resolution, laser tweezers to manipulate micrometer-sized particles, confocal microscopy to provide enhanced three-dimensional visualization of structures, and spectrophotometry to measure the photonic properties of materials. Vibration disturbances were identified early in the LMM development phase as a high risk for contaminating the science microgravity environment. An integrated FIR–LMM test was conducted in Glenn's Acoustics Test Laboratory to assess mechanical sources of vibration and their impact to microscopic imaging. The primary purpose of the test was to characterize the LMM response at the sample location, the *x-y* stage within the microscope, to vibration emissions from the FIR and LMM support structures.

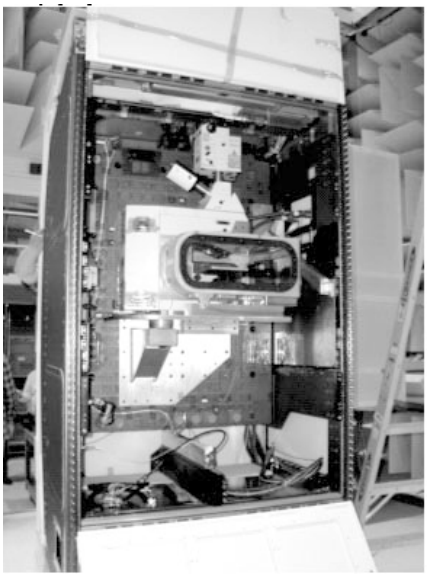

LMM and FIR integrated test configuration.

The imaging tests were performed, as close as possible, in an on-orbit configuration in the Acoustics Test Laboratory, as shown in the photograph. Launch bolts to the optics bench were removed, and the Air Thermal Control Unit (ATCU) was unlocked and supported by Lord isolators (Lord Corporation, Cary, North Carolina). Isolating foam was installed into the FIR, and all rack openings were closed and sealed to minimize acoustic disturbances. The LMM spindle assembly, the mechanism to structurally mount the LMM microscope, was bolted to the front of the optics bench. The FIR was configured with its various diagnostics and avionics as it would be during on-orbit operations with the LMM, and the LMM was mounted in its flightlike configuration onto the optics bench within the FIR. The main microgravity disturbers, fans located in the ATCU and the input/output processor, were on during the testing. Images of test target slides and sample cells mounted on the LMM *x-y* stage were captured while the FIR ATCU and input/output processor were running inside the FIR. Initial measurements indicated that the fans in the ATCU were the driving microgravity disturber. The ATCU was operated through the full range of

operating fan speeds, 1600 to 2600 rpm, while acquiring images at a frame rate of 30 Hz. In addition, with the FIR powered down to create a vibration-quiet environment, a small shaker was attached to the FIR optics bench to induce vibratory excitation so that frequency disturbances that cause image degradation could be determined.

The preliminary results revealed that, in general, the ATCU and small vibration shaker tests caused no image degradation. However, at a magnification of ×100, image degradation was observed above a frequency of 30 Hz with the ATCU operational, and with induced low-vibration excitations. At lower frequencies, the combined LMM–FIR configuration meets microgravity requirements. The test results have led the LMM team to design isolation techniques for the LMM *x-y* stage to prevent image degradation at high magnifications and at frequencies above 30 Hz.

Find out more about this research:

Light Microscopy Module (LMM):

http://www.cleveland.feddata.com/lmm/
http://microgravity.grc.nasa.gov/6712/lmm.html

Fluids and Combustion Facility: http://fcf.grc.nasa.gov/pages/project.html

Glenn's Acoustics Test Laboratory: http://www.grc.nasa.gov/WWW/AcousticalTest/

Glenn's Microgravity Science Division: http://microgravity.grc.nasa.gov/

Glenn contacts:
Susan M. Motil, 216–433–8589, Susan.M.Motil@nasa.gov;
Frank Gati, 216–433–2655, Frank.Gati-1@nasa.gov;
Dr. DeVon W. Griffin, 216–433–8109, Devon.W.Griffin@nasa.gov; and
John H. Snead, 216–433–2590, John.H.Snead@nasa.gov

Northrop Grumman Information Technology contacts:
John G. Eustace, 216–925–1244, jeustace@mrdoc.cc; and
Tony H. Haecker, 216–925–1094, thaecker@mrdoc.cc

Authors: Susan M. Motil and Frank Gati

Headquarters program office: OBPR

Programs/Projects:
Microgravity Science

Solid Fuel Delivery System Developed for Combustion Testing on the International Space Station

NASA initiated Bioastronautics and Human Research Initiatives in 2001 and 2003, respectively, to enhance the safety and performance of humans in space. The Flow Enclosure Accommodating Novel Investigations in Combustion of Solids (FEANICS) is a multiuser facility being built at the NASA Glenn Research Center to advance these initiatives by studying fire safety and the combustion of solid fuels in the microgravity environment of the International Space Station (ISS). One of the challenges for the FEANICS team was to build a system that allowed for several consecutive combustion tests to be performed with minimal astronaut crew interaction. FEANICS developed a fuel carousel that contains a various number of fuel samples, depending on the fuel width, and introduces them one at a time into a flow tunnel in which the combustion testing takes place. This approach will allow the science team to run the experiments from the ground, while only requiring the crew to change out carousels after several tests have been completed.

The combustion experiments using solid fuel on the ISS will be performed in a 100-liter combustion chamber on the Combustion Integrated Rack, which is also being developed at Glenn. Most of the FEANICS experiments require a controlled flow environment for testing. Consequently, a key component of the FEANICS hardware is a 30-cm-long flow tunnel. This takes up a significant portion of the combustion chamber, leaving reduced space for a mechanism to introduce the solid fuels for testing and remove them at completion. Many of the solid fuel experiments utilize large samples that are instrumented for temperature and radiometric readings, making them harder to maneuver. Another design challenge was to find a way to shield the crew from the burnt fuel samples while they remove the fuel holder mechanism and stow it. The fuel carousel was designed to meet these challenges and has been successfully built and tested by a FEANICS team of in-house and support service contractor researchers.

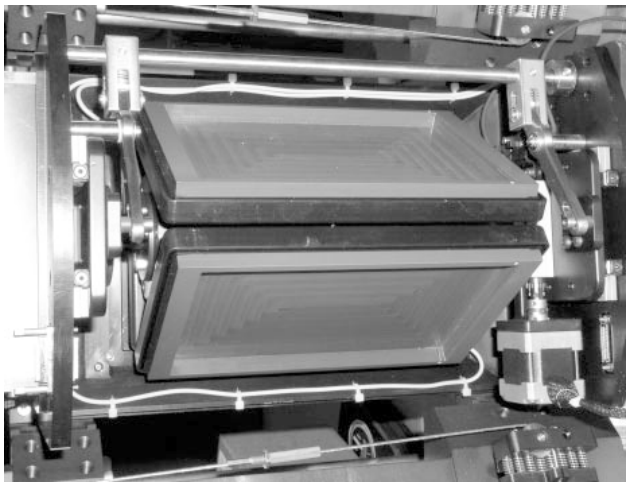

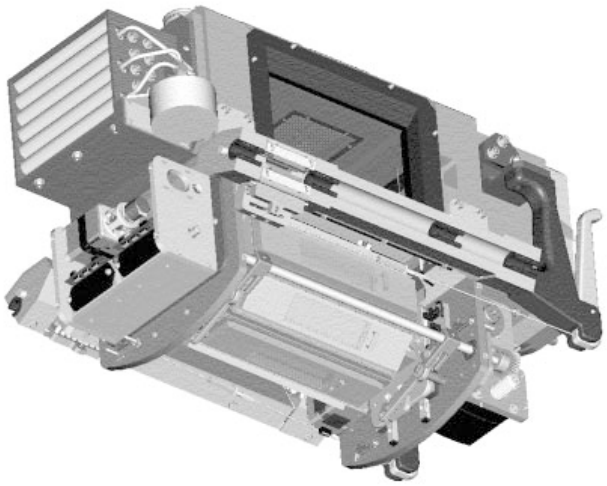

Left: A three-dimensional model of an eight-sided fuel carousel (without shroud) mounted to the FEANICS flow tunnel. Right: Underside of an engineering model of a three-sided fuel carousel with shroud removed. Two fuel trays are shown (no fuel installed).

The carousel is a rotating hub that can have a different number of sides, depending on the fuel width requirements. For example, for a 3-cm-wide fuel, an eight-sided carousel can be built, allowing eight consecutive tests without crew interaction. The carousel can accommodate a maximum fuel width of 11.5 cm, but this reduces the number of samples (carousel sides) to three. Each face of the carousel contains the fuel being tested, which is held by a nonflammable tray. This tray is equipped with an electrical connector that allows instrumentation and igniter power to be wired to each sample. The carousel has two modes of actuation. The translation mode allows the carousel to raise and lower a fuel into the flow tunnel for testing. The rotation mode allows the carousel to rotate from one sample to the next in between test runs. This entire carousel hub is enclosed in an aluminum shroud. Also, there is a motorized shutter at the top of the carousel that can cover the hole where the fuel is introduced in the tunnel. This serves two purposes. One is to completely seal the contents of the carousel during crew change-out, shielding them from any postcombustion particulate matter from the burnt sample, and the other is to provide a means to put out the flame on the fuel surface at the end of a test.

The FEANICS project is currently in the engineering model development phase. A three-sided carousel has been built and tested, and two others are being fabricated. The next stage will be to qualify the design and build the flight hardware.

Find out more about this research:
http://microgravity.grc.nasa.gov/combustion/feanics/feanics_index.htm

Glenn contact:
David T. Frate, 216–433–8329, David.T.Frate@nasa.gov

Author: David T. Frate

Headquarters program office: OBPR

Programs/Projects:
Microgravity Science

Combustion Module-2 Achieved Scientific Success on Shuttle Mission STS–107

The familiar teardrop shape of a candle is caused by hot, spent air rising and cool fresh air flowing behind it. This type of airflow obscures many of the fundamental processes of combustion and is an impediment to our understanding and modeling of key combustion controls used for manufacturing, transportation, fire safety, and pollution. Conducting experiments in the microgravity environment onboard the space shuttles eliminates these impediments. NASA Glenn Research Center's Combustion Module-2 (CM–2) and its three experiments successfully flew on STS–107/Columbia in the SPACEHAB module and provided the answers for many research questions. However, this research also opened up new questions.

The CM–2 facility was the largest and most complex pressurized system ever flown by NASA and was a precursor to the Glenn Fluids and Combustion Facility planned to fly on the International Space Station. CM–2 operated three combustion experiments: Laminar Soot Processes (LSP), Structure of Flame Balls at Low Lewis-Number (SOFBALL), and Water Mist Fire Suppression Experiment (Mist). Although Columbia's mission ended in tragedy with the loss of her crew and much data, most of the CM–2 results were sent to the ground team during the mission.

CM–2 systems and software engineers conduct final inspections of the CM–2 flight hardware at Glenn before it is shipped to the launch site.

The LSP experiment studied the formation of soot in flames so that methods for controlling soot can be devised to eliminate or mitigate significant public health problems caused by emissions of pollutant soot (e.g., soot causes 60,000 premature deaths per year). Observations of the LSP flames made during the *Columbia* flight were very successful, and the LSP results have already suggested new ways to reduce, and possibly even eliminate, emissions of pollutant soot from flames.

The objective of the SOFBALL experiment was to study weakly burning hydrogen and methane flames in oxygen-inert mixtures, resulting in "flame balls." Because flame balls are steady, symmetric, and occur in fuels with simple chemistry, they represent the simplest possible interaction of chemistry and transport in flames. The accomplishments of the experiment included (1) the weakest and leanest flames ever burned (0.5 W of thermal power and only 8 percent of the fuel usually needed for chemical balance) and (2) the longest-lived flame ever burned in space (81 min). Several totally new and unexpected results were found, including oscillating flame balls and flame balls drifting in a spiral or corkscrew pattern. The data obtained during the mission will help lead to the development of cleaner, more fuel-efficient engines as well as improved methods for assuring spacecraft fire safety.

The Mist experiment was motivated by the need to find a fire-extinguishing agent that would replace traditional chemical fire suppressants (halons), which have been banned because of their harmful effects to the ozone layer. Water mist, very small droplets like a fine fog, is a nontoxic, inexpensive,

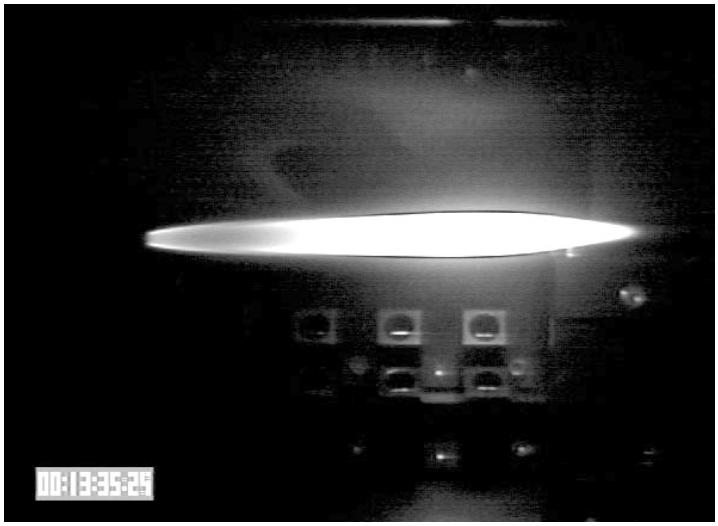

This LSP flame, which is an ethylene fuel burning in air at atmospheric pressure, is the longest laminar flame ever burned in microgravity.

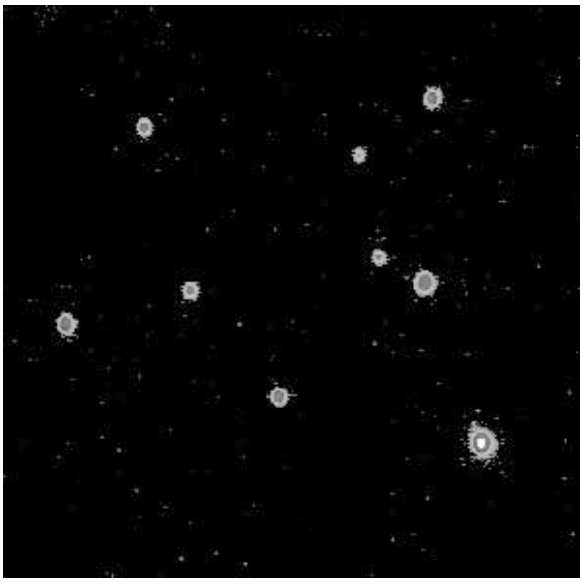

One of these nine color-enhanced SOFBALL flame balls burned for 81 min and set a new record for combustion in space. This figure is shown in color in the online version of this article (http://www.grc.nasa.gov/WWW/RT/2003/6000/6729over.html).

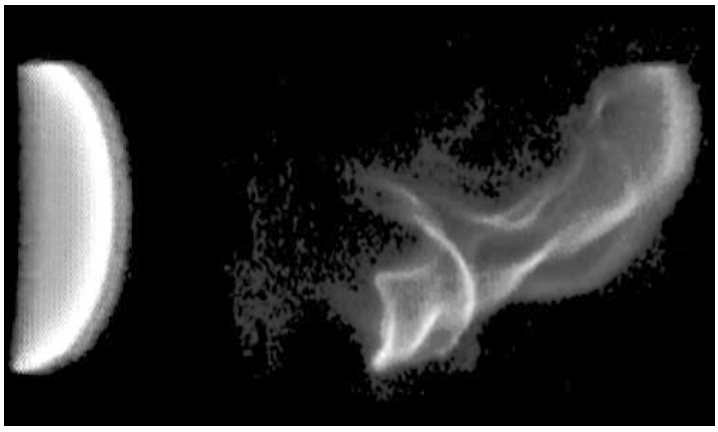

The sequence of two color-enhanced Mist propane flames shows a smooth, hemispherical flame in dry air, followed by a multilobed broken flame resulting from the interaction with the fine water mist. This figure is shown in color in the online version of this article (http://www.grc.nasa.gov/WWW/RT/2003/6000/6729over.html).

and efficient technology to replace halons while minimizing property damage. The results from the Mist experiment have provided crucial understanding of the physical and chemical mechanisms of how fine water droplets interact with and suppress flames. For example, small droplet sizes are consistently more effective for lean flame suppression than larger droplets. The results will be provided to manufacturers of fire suppression equipment to design the next generation of fire extinguishers that will be used in enclosed spaces such as airplanes, ships, libraries, museums, and residential homes. Water mist may also become a viable fire suppression system onboard orbiting spacecraft, such as the International Space Station.

Find out more about this research:
http://microgravity.grc.nasa.gov/combustion/

Glenn contacts:
Ann P. Over, 216–433–6535, Ann.P.Over@nasa.gov;
David T. Frate, 216–433–8329, David.T.Frate@nasa.gov; and
Dr. David L. Urban, 216–433–2835, David.L.Urban@nasa.gov

Author: Ann P. Over

Headquarters program office: OBPR

Programs/Projects:
Microgravity Combustion Science, Chemically Reacting Systems, Combustion Module-2

Power and Propulsion

International Space Station Nickel-Hydrogen Batteries Approached 3-Year On-Orbit Mark

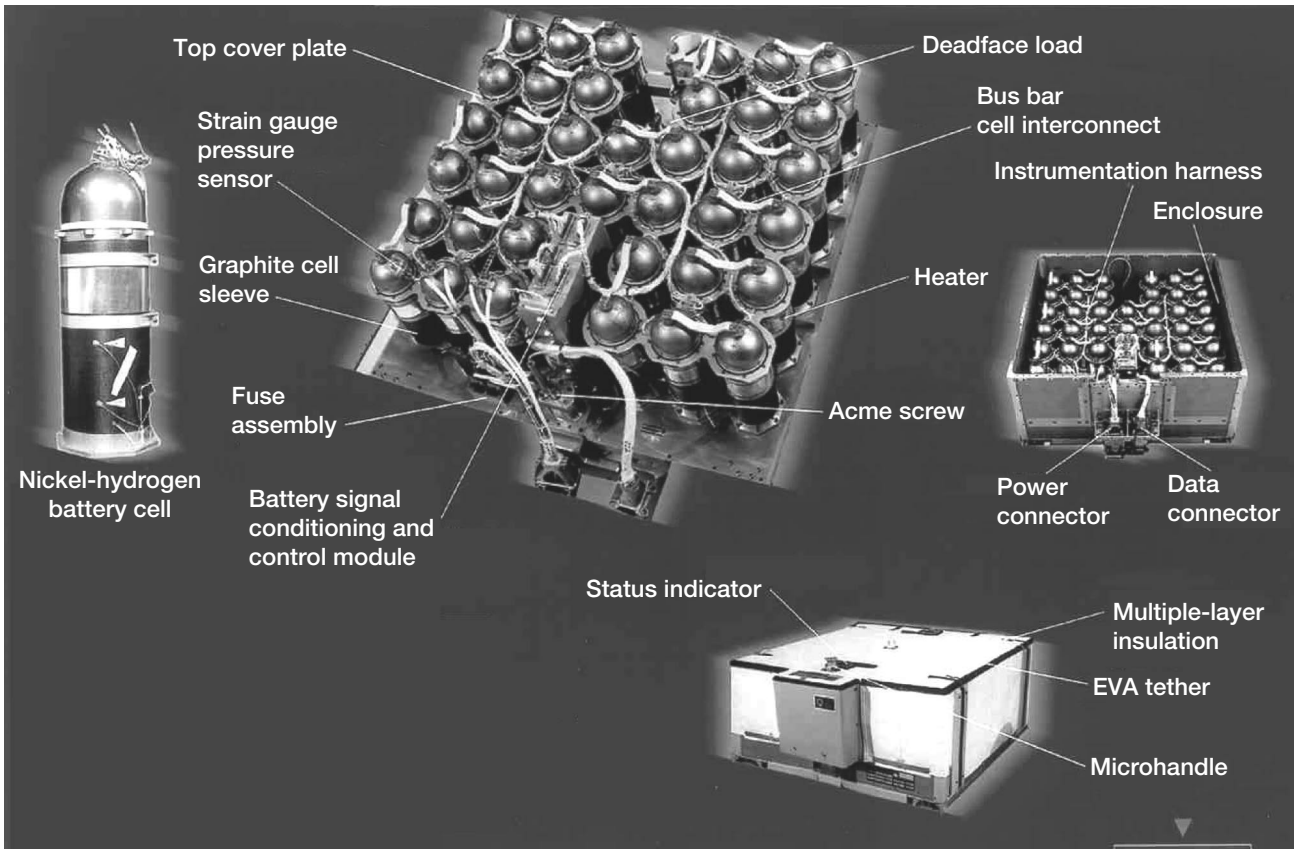

ISS battery subassembly ORU.

The International Space Station's (ISS) electric power system (EPS) employs nickel-hydrogen (Ni-H_2) batteries as part of its power system to store electrical energy. The batteries are charged during insolation and discharged, providing station power, during eclipse. The batteries are designed to operate at a maximum 35-percent depth of discharge during normal operation.

Thirty-eight individual pressure vessel Ni-H_2 battery cells are series-connected and packaged in an orbital replacement unit (ORU), and two ORUs are series-connected, using a total of 76 cells, to form one battery. When the ISS is in its assembly-complete form, the electrical power system will have a total of 24 batteries (48 ORUs) on-orbit. The ISS is the first application for low-Earth-orbit cycling of this quantity of series-connected cells.

Each battery ORU was designed to meet the following requirements:

- 6.5-year design life (38,000 charge-discharge cycles)
- 81-A·hr, 4-kW·hr nameplate capacity
- Contingency orbit capability consisting of one additional orbit at reduced power after a 35-percent depth of discharge without recharge
- 5-year mean time between failure
- Easy on-orbit replacement, utilizing the robotic arm

The cells selected for use in the battery ORUs are manufactured by Eagle Picher Technologies. They are RNH–81–5 EPI individual pressure vessel NiH_2 cells that have a back-to-back plate configuration. They were activated with a 31-wt% aqueous solution of potassium hydroxide electrolyte. The ORUs were assembled and acceptance tested by Space Systems/Loral.

The first set of 12 battery ORUs was integrated into the P6 (port side) integrated equipment assembly (IEA) and was successfully launched on November 30, 2000. The on-orbit battery cycling started in early December 2003. The remaining 36 battery ORUs have been delivered to the Kennedy Space Center and have been integrated into the next three IEAs, which are awaiting launch in 2004 and 2005.

The telemetered on-orbit data clearly show that the batteries are performing within their design specifications over the operational range. Because of the lower-than-anticipated power demands of the station, the P6 battery life is expected to meet or exceed the ISS 6.5-year life requirement.

All aspects of the ISS battery hardware, including design, development, assembly, test, and operation, are managed by the NASA Glenn Research Center. In addition to the current battery, Glenn is investigating advanced technologies as future replacements for the ISS.

Find out more about this research:

Glenn's energy storage publications:
http://ppoweb.grc.nasa.gov/ppo/publications/energystoreref.html

Glenn contact:
Penni J. Dalton, 216–433–5223, Penni.J.Dalton@nasa.gov

Author: Penni J. Dalton

Headquarters program office: OSF

Programs/Projects: ISS

Multifunctional Inflatable Structure Being Developed for the PowerSphere Concept

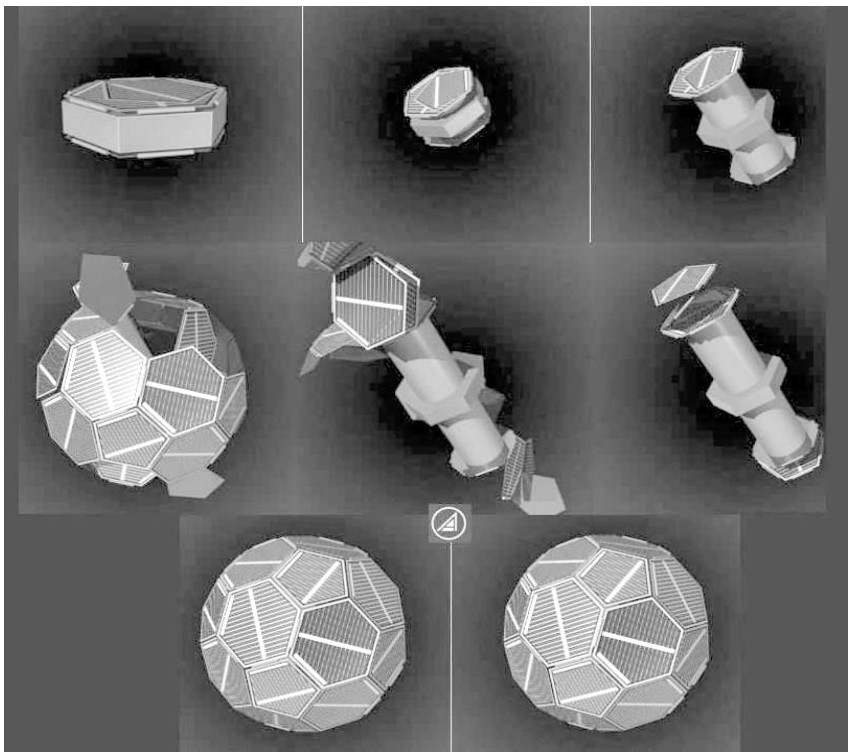

PowerSphere concept.

NASA has funded a collaborative team of The Aerospace Corporation, ILC Dover, Lockheed Martin, and NASA Glenn Research Center to develop the Multifunctional Inflatable Structure (MIS) for a "PowerSphere" concept through a NASA Research Announcement. This power system concept has several advantages, including a high collection area, low weight and stowage volume, and the elimination of all solar array pointing mechanisms. The current 3-year effort will culminate with the fabrication and testing of a fully functional engineering development unit.

The baseline design of the PowerSphere consists of two opposing semispherical domes connected to a central spacecraft. Each semispherical dome consists of hexagonal and pentagonal solar cell panels that together form a geodetic sphere. Inflatable

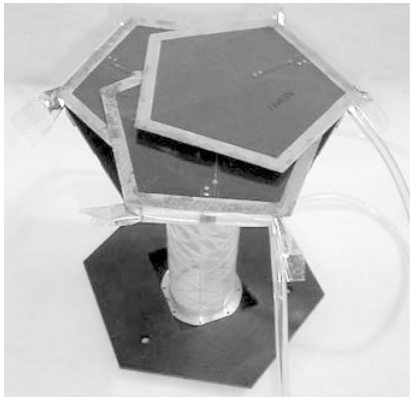


Left: Deployment test of thin-film panels (stowed). Right: Deployment test of thin-film panels (deployed).

ultraviolet (UV) rigidizable tubular hinges between the solar cell panels and UV rigidizable isogrid center columns with imbedded flex circuitry form the MIS. The reference configuration for the PowerSphere is a 0.6-m-diameter (fully deployed) spacecraft with a total mass budget of 4 kg (1 kg for PowerSphere, 3 kg for spacecraft) capable of producing 29 W of electricity with 10-percent-efficient thin-film solar cells. In a stowed configuration, the solar cell panels will be folded sequentially to the outside of the instrument decks. The center column will be z-folded between the instrument decks and the spacecraft housing for packaging. The instrument panel will secure the z-folded stack with launch ties. After launch, once the release tie is triggered, the center column and hinge tubes will inflate and be rigidized in their final configurations by ultraviolet radiation. The overall PowerSphere deployment sequence is shown pictorially in the illustration on the preceding page.

The PowerSphere MIS component technologies and system-level concept have matured sufficiently to begin engineering development unit fabrication in fiscal years 2003 and 2004 and testing in fiscal year 2004. Significant technology advances in thin-film photovoltaics, thin-film solar array flex circuitry, inflatable deployment systems, UV-rigidizable structures, coatings to protect polymer structures from electrostatic discharge and atomic oxygen, and distributed power management and distribution have been made through the second year of the overall 3-year effort. For example, the photographs on this page show prototype thin-film panel deployment tests recently performed at ILC Dover.

Potential NASA applications for the PowerSphere include Earth magnetotail surveys, solar flotilla missions, planetary protection, sample return missions, multiplatform planet surface science, and formation flying interferometric astronomy science missions. Follow-on efforts also are being proposed to further advance the PowerSphere technology readiness levels for these types of potential spaceflight demonstrations by incorporating a number of key power systems technologies.

References

1. Simburger, Edward J.: PowerSphere Concept. The Aerospace Corporation, Los Angeles, CA, 1999.
2. Simburger, E.J., et al.: Development of Flex Circuit Wiring Harness for the PowerSphere Concept. Paper presented at the 29th IEEE Photovoltaic Specialists Conference, New Orleans, LA, 2002, pp. 959–962.
3. Simburger, Edward J., et al.: Development, Design, and Testing of PowerSphere Multifunctional Ultraviolet-Rigidizable Inflatable Structures. AIAA Paper 2003–1897, 2003.

Glenn contacts:
Todd T. Peterson, 216–433–5350, Todd.T.Peterson@nasa.gov;
Tom Kerslake, 216–433–5373, Thomas.W.Kerslake@nasa.gov; and
Henry Curtis, 216–433–2231, Henry.B.Curtis@nasa.gov

Author: Todd T. Peterson

Headquarters program office: OAT

Programs/Projects:
Space Power Systems R&T, Power Systems R&T, Earth Science, Space Science, Human Spaceflight

Space Station Power Generation Investigated in Support of the Beta Gimbal Anomaly Resolution

The International Space Station (ISS) is the largest and most complex spacecraft ever assembled and operated in orbit. The first U.S. photovoltaic module, containing two solar arrays, was launched, installed, and activated in early December 2000. After the first week of continuously rotating the U.S. solar arrays, engineering personnel in the ISS Mission Evaluation Room observed higher than expected electrical currents on the drive motor in one of the Beta Gimbal Assemblies (BGA), the mechanism used to maneuver a U.S. solar array (see the on-orbit photograph below). The magnitude of the motor currents continued to increase over time on both BGAs, creating concerns about the ability of the gimbals to continue pointing the solar arrays towards the Sun, a function critical for continued assembly of the ISS. The BGA provides two critical capabilities to the ISS: (1) transfer of electrical power across a rotating joint and (2) positioning of the solar arrays. A number of engineering disciplines convened in May 2001 to address this on-orbit hardware anomaly. Over the course of a year, many scenarios were developed and used. Only two are discussed here: parked arrays and dual-angle mode.

In the first scenario, NASA Glenn Research Center personnel used Glenn's SPACE code (System Power Analysis for Capability Evaluation) to generate a set of power generation capabilities as a function of parked solar array position across the nominal solar β range. Using these data, the ISS power resource operations experts on the BGA Anomaly Resolution Team determined that if a subset of the electrical loads are transferred from one array to the other, only one BGA needs to rotate reliably for the next three assembly missions to be completed successfully.

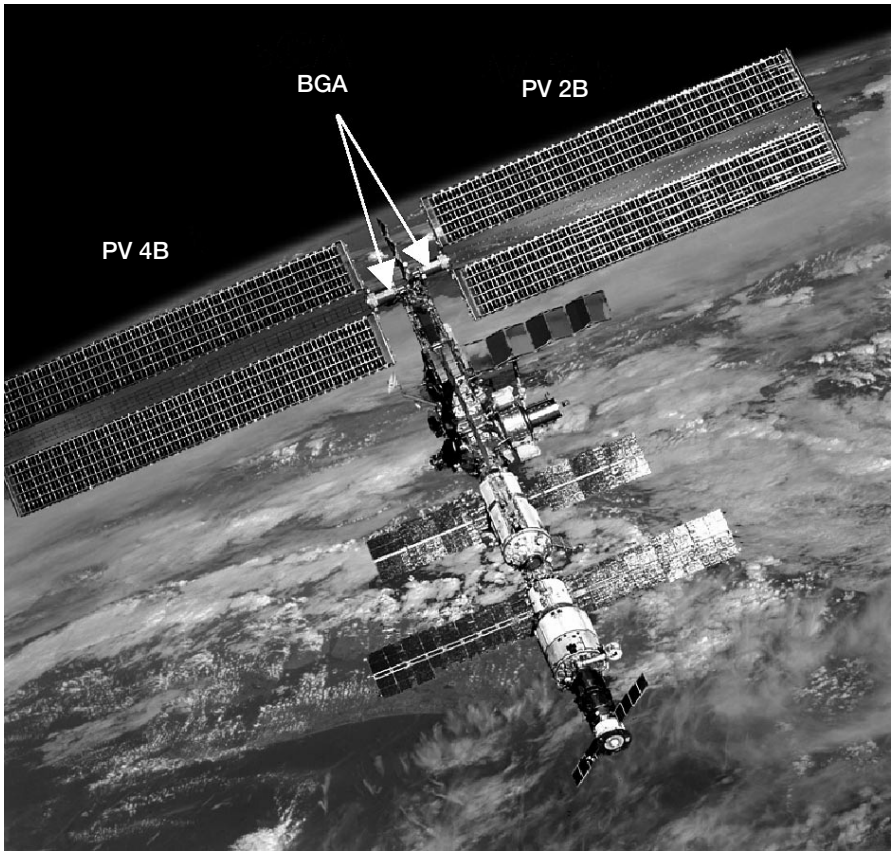

Location of the beta gimbal assemblies that rotate the U.S. photovoltaic arrays.

By June 2001, the root cause team had identified two possible data trends: (1) the long-duration unidirectional BGA motion appeared to exacerbate the high motor current anomaly, and (2) the motor current performance appeared to return to nominal levels after the direction of the BGA was reversed. Taking these observations into consideration, the BGA Anomaly Resolution Team developed the dual-angle-mode operational concept (see the diagram on the following page). This technique is unique in that, should the BGA stall or become stuck, the solar array position is guaranteed to be within a range of Sun-facing positions when the vehicle is in insolation, thus minimizing the potential impact on power generation. The SPACE results proved that the dual-angle-mode technique could generate 85 to 90 percent of the power realized from a Sun-tracking solar array in the nominal ISS solar β regime ($|\text{solar } \beta| < 37°$). SPACE analysis also showed the walkoff from using the same BGA target angles over the solar β range of 28° to –28°, indicating that the worst case loss would be 400 W out of a total capability of 10 kW. This analysis proved that a single set of BGA target angles could be used for dual-angle-mode tests lasting as long as 11 days with only a 4-percent loss in total power generation capability.

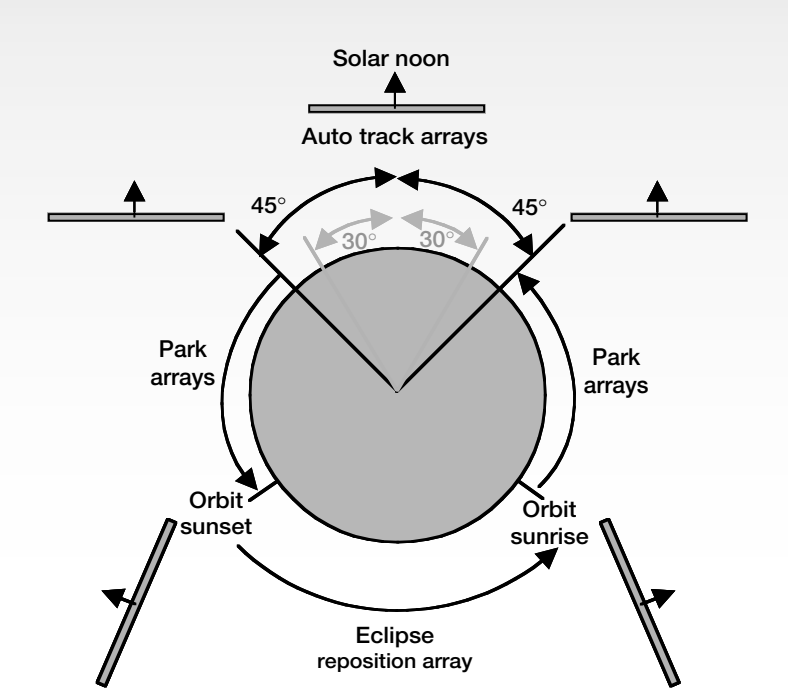

Dual-angle-mode operational concept (90° and 60° sweep).

The dual-angle technique continues to be used successfully. The operations team in conjunction with Glenn developed successful methods of managing ISS energy balance while supporting the overall team goal of minimizing cumulative BGA travel.

Find out more about this research:
http://space-power.grc.nasa.gov

Glenn contact:
Ann M. Delleur, 216–433–5519, Ann.M.Delleur@nasa.gov

Authors:
Ann M. Delleur and Timothy Propp

Headquarters program office: OSF

Programs/Projects:
ISS, Electrical Performance Modeling

Special recognition:
SPACE was a runner-up for NASA Software of the Year for 2003. Ann Delleur received a Silver Snoopy award for her BGA Anomaly Resolution Team work.

International Space Station Solar Array Wing On-Orbit Electrical Performance Degradation Measured

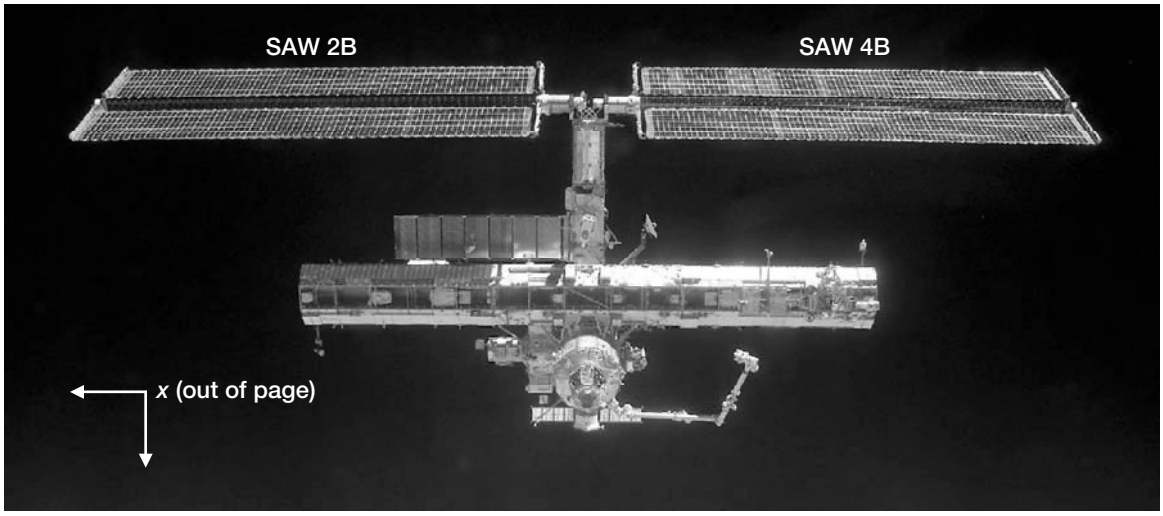

International Space Station showing coordinated system and solar array wing (SAW) nomenclature.

The port-side photovoltaic power module (P6) was activated on the International Space Station in December 2000. P6 provides electrical power to channels 2B and 4B to operate ISS power loads. A P6 is shown in the photograph above. This article highlights the work done at the NASA Glenn Research Center to calculate the on-orbit degradation of the P6 solar array wings (SAWs) using on-orbit data from December 2000 to February 2003.

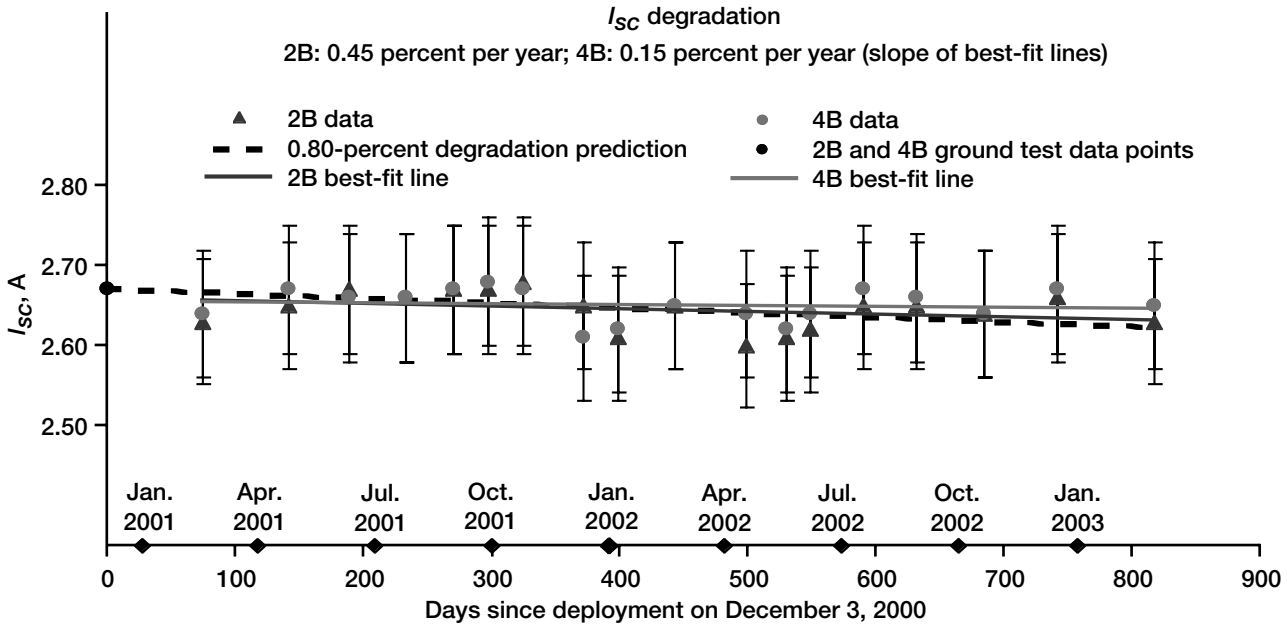

Measured on-orbit degradation of SAW string short-circuit current, I_{SC}.

During early ISS operations, the 82 strings of photovoltaic cells that make up a SAW can provide much more power than is necessary to meet the demand. To deal with excess power, a sequential shunt unit successively shunts the current from the strings. This shunt current was the parameter chosen for the SAW performance degradation study for the following reasons: (1) it is based on a direct shunt current measurement in the sequential shunt unit, (2) the shunt current has a low temperature dependence that reduces the data correction error from using a computationally derived array temperature, and (3) the SSU shunt current is essentially the same as the SAW short-circuit current on a per-string basis.

The major part of the analysis involved normalizing the shunt current to the reference conditions of equinox solar insolation, 28 °C operating temperature, no albedo current production, and no current loss from the shadowing of solar cells. This normalization allowed data from different dates and orbital conditions to be usefully compared with each other. Normalizing factors were calculated using the computer code SPACE (System Power Analysis for Capability Evaluation). The Glenn-developed SPACE code models the International Space Station's electric power system, and its accuracy has been validated with on-orbit data. For each shunt current data point, SPACE was used to correct for conditions that affect shunt current. These conditions can change on an orbit-to-orbit basis, such as solar insolation, or change within a given orbit, such as array temperature and Earth albedo.

After the shunt current was normalized, the shunt current per string of photovoltaic cells, equal to the string short-circuit current I_{SC}, was averaged over an orbit Sun period. This average value of I_{SC} was used for comparison over time. The process was repeated for several orbits over the time span of the analysis. A value for the percentage degradation per year can be calculated from the slope of a best fit line through the I_{SC} data points as shown in the graph above. The calculated I_{SC} degradation rates were 0.45 percent per year for SAW 2B and 0.15 percent per year for SAW 4B. This amount of degradation is much lower than the estimated data analysis uncertainty, ±3.2 percent, and is lower than the 0.8-percent-per-year I_{SC} degradation predicted by SPACE. Thus, we concluded that there has been no appreciable SAW I_{SC} degradation in the first 26 months of on-orbit operation. Glenn plans to continue monitoring degradation of P6 SAW currents as well as that of future photovoltaic power modules.

Bibliography

Kerslake, Thomas W.; and Gustafson, Eric D.: On-Orbit Performance Degradation of the International Space Station P6 Photovoltaic Arrays. NASA/TM—2003-212513 (AIAA Paper 2003–5999), 2003. http://gltrs.grc.nasa.gov/cgi-bin/GLTRS/browse.pl?/2003/TM-2003-212513.html

Glenn contacts:
Eric D. Gustafson, 216–433–3238, Eric.D.Gustafson@nasa.gov; and Thomas W. Kerslake, 216–433–5373, Thomas.W.Kerslake@nasa.gov

Authors: Eric D. Gustafson and Thomas W. Kerslake

Headquarters program office: OSF

Programs/Projects:
ISS, Electrical Performance Modeling

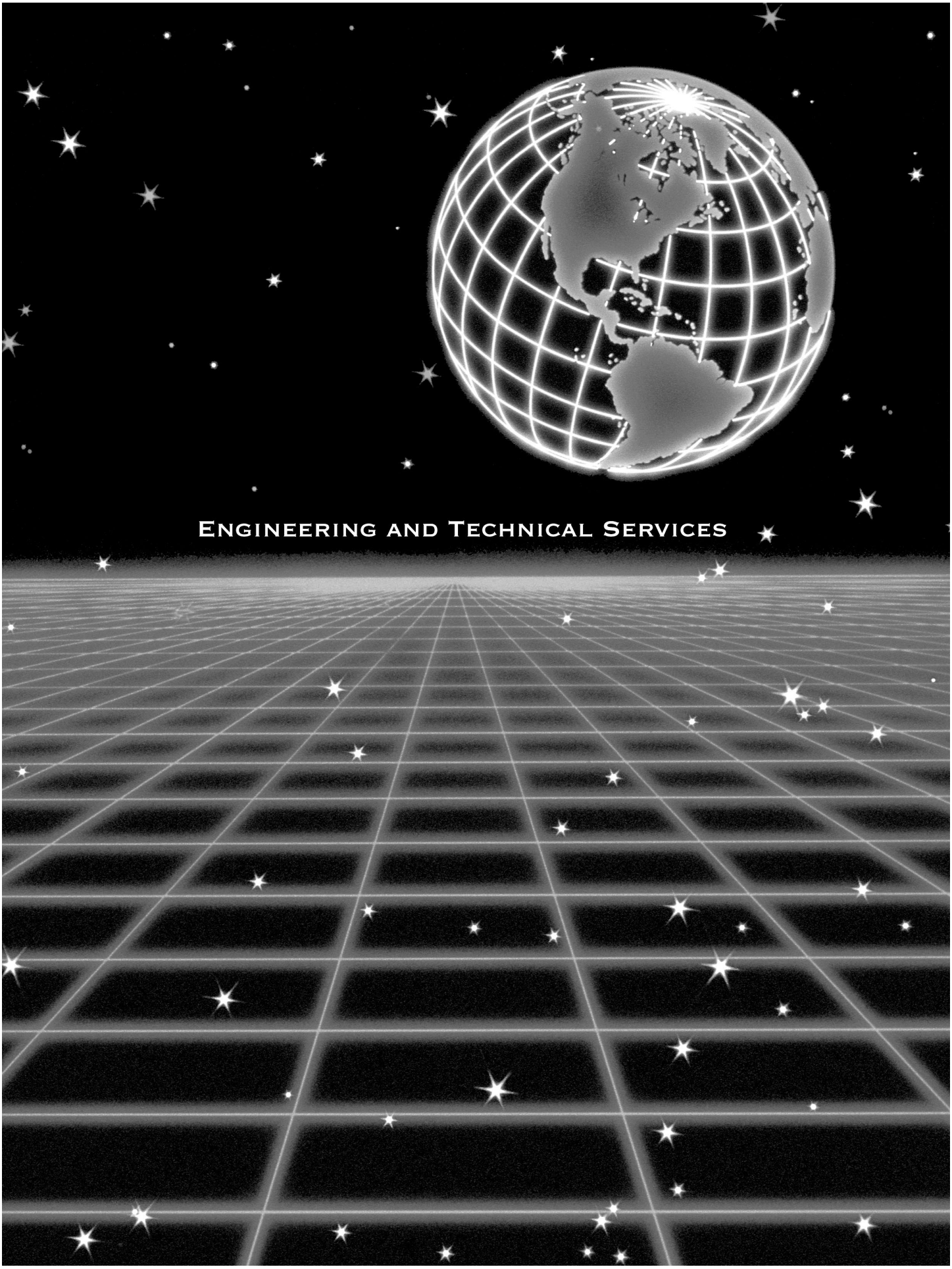
Engineering and Technical Services

Computer Services

User-Friendly Interface Developed for a Web-Based Service for SpaceCAL Emulations

A team at the NASA Glenn Research Center is developing a Space Communications Architecture Laboratory (SpaceCAL) for protocol development activities for coordinated satellite missions. SpaceCAL will provide a multiuser, distributed system to emulate space-based Internet architectures, backbone networks, formation clusters, and constellations. As part of a new effort in 2003, building blocks are being defined for an open distributed system to make the satellite emulation test bed accessible through an Internet connection.

The first step in creating a Web-based service to control the emulation remotely is providing a user-friendly interface for encoding the data into a well-formed and complete Extensible Markup Language (XML) document. XML provides coding that allows data to be transferred between dissimilar systems. Scenario specifications include control parameters, network routes, interface bandwidths, delay, and bit error rate. Specifications for all satellite, instruments, and ground stations in a given scenario are also included in the XML document.

For the SpaceCAL emulation, the XML document can be created using XForms, a Web-based forms language for data collection. Contrary to older forms technology, the interactive user interface makes the science prevalent, not the data representation. Required versus optional input fields, default values, automatic calculations, data validation, and reuse will help researchers quickly and accurately define missions. XForms can apply any XML schema defined for the test mission to validate data before forwarding it to the emulation facility. New instrument definitions, facilities, and mission types can be added to the existing schema.

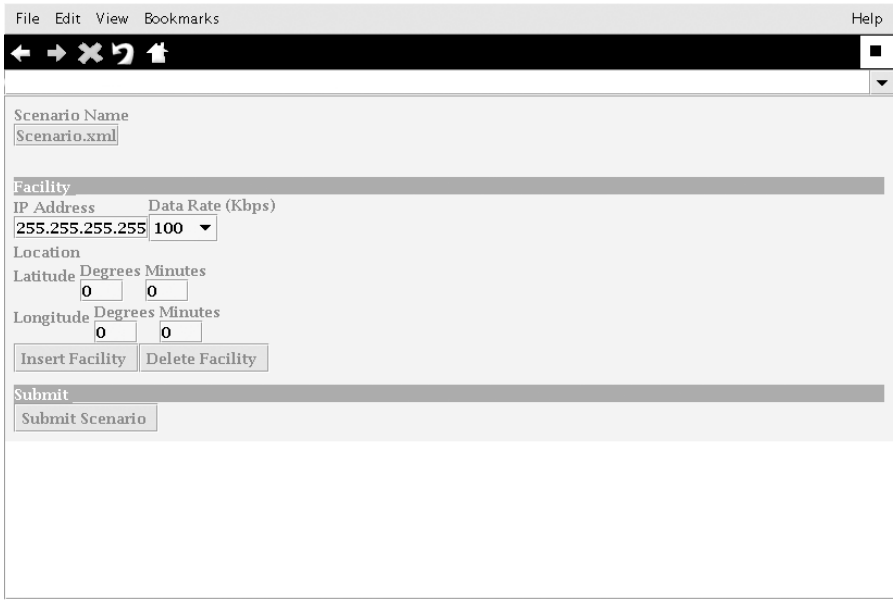

Sample Web-based form for scenario input.

The first prototype user interface incorporates components for interactive input and form processing. Internet address, data rate, and the location of the facility are implemented with basic form controls with default values provided for convenience and efficiency using basic XForms operations. Because different emulation scenarios will vary widely in their component structure, more complex operations are used to add and delete facilities.

Scenarios are submitted via a Common Gateway Interface (CGI) program. A Web server running in the SpaceCAL facility will need to execute the CGI program to validate user access rights and schedule emulation resources. These components are being put in place but are not complete yet. The next step in creating a next-generation distributed satellite emulation system will be to orchestrate lower-level Web services for interoperability and dynamic component testing. Incorporating standard protocols like the Simple Object Access Protocol (SOAP) will mean users do not need to change their development environment in order to use the emulation. The test-bed software should also allow users to generate a series of scripts to isolate one or more components (data collection satellites, high-speed communication satellites, ground stations, communication protocols, and onboard satellite software) and to replace default systems in the emulation system.

Find out more about this research: http://scp.grc.nasa.gov/portfolio/ia/scal.html

University of Akron contact:
Kathy J. Liszka, 216–433–5110, Kathy.J.Liszka@grc.nasa.gov

Glenn contacts:
Allen P. Holtz, 216–433–6005, Allen.P.Holtz@nasa.gov;
Charles W. Putt, 216–433–5204, Charles.W.Putt@nasa.gov; and
Karen A. Pischel, 216–433–5198, Karen.A.Pischel@nasa.gov

Authors:
Kathy J. Liszka and Allen P. Holtz

Headquarters program office:
OSF (SCO)

Programs/Projects:
CICT, Space Communications, Intelligent Architectures

Remote Arrhythmia Monitoring System Developed

Telemedicine is taking a step forward with the efforts of team members from the NASA Glenn Research Center, the MetroHealth campus of Case Western University, and the University of Akron. The Arrhythmia Monitoring System is a completed, working test bed developed at Glenn that collects real-time electrocardiogram (ECG) signals from a mobile or homebound patient, combines these signals with global positioning system (GPS) location data, and transmits them to a remote station for display and monitoring. Approximately 300,000 Americans die every year from sudden heart attacks, which are arrhythmia cases. However, not all patients identified at risk for arrhythmias can be monitored continuously because of technological and economical limitations. Such patients, who are at moderate risk of arrhythmias, would benefit from technology that would permit long-term continuous monitoring of electrical cardiac rhythms outside the hospital environment.

Embedded Web Technology developed at Glenn to remotely command and collect data from embedded systems using Web technology is the catalyst for this new telemetry system (ref. 1). In the end-to-end system architecture, ECG signals are collected from a patient using an event recorder and are transmitted to a handheld personal digital assistant (PDA) using Bluetooth, a short-range wireless technology. The PDA concurrently tracks the patient's location via a connection to a GPS receiver. A long distance link is established via a standard Internet connection over a 2.5-generation GSM/GPRS[1] cellular, wireless infrastructure. Then, the digital signal is transmitted to a call center for monitoring by medical professionals.

Three-lead ECG signal displayed at a call center along with real-time GPS tracking of a patient's location.

The call center is a personal computer with an Internet address that collects and displays the ECG signal in the traditional strip chart fashion. Because the GPRS network capacity is shared among many users in a given coverage area, data throughput varies. Software developed for the call center monitors the data rate, buffers the ECG signal as needed, and dynamically adjusts the display update to keep the strip chart in constant motion.

Non-ECG data are also transmitted from the patient event recorder to create a safer, viable system. The event recorder can display a low-battery

[1]Global System for Mobile Communications/ General Packet Radio Service.

indicator and send an alert to the call center to ensure the condition is acknowledged and addressed. In addition, a patient can send a noncritical medical alert to the call center by pressing a button on the event recorder when a heart flutter or other unusual feeling occurs. The time of the alert is marked in the ECG signal stream for later inspection by a cardiac specialist. Finally, a panic button is available to patients to send a critical alert for help. Call center personnel will be able to dispatch 911 services and provide them with the most recent GPS position to locate the patient.

References

1. Daniele, Carl J.: Embedded Web Technology: Internet Technology Applied to Real-Time System Control. Research & Technology 1997, NASA/TM—1998-206312, 1998, pp. 165–166. http://www.grc.nasa.gov/WWW/RT1997/7000/7750daniele.htm
2. York, David W.; and Ponyik, Joseph G.: New Web Server—the Java Version of Tempest—Produced. Research & Technology 1999, NASA/TM—2000-209639, 2000, pp. 177–178. http://www.grc.nasa.gov/WWW/RT1999/7000/7750york.html

Find out more about this research:

Embedded Web Technology:
http://live.grc.nasa.gov

Remote arrhythmia monitoring:
http://microgravity.grc.nasa.gov/grcbio/heart.html

Glenn contact:
David W. York, 216–433–3162, David.W.York@nasa.gov

Authors:
David W. York, Michael A. Mackin, Kathy J. Liszka, and Michael J. Lichter

Headquarters program office: OBPR

Programs/Projects: JGBEC, TTPO

Research Testing

NASA Glenn's Advanced Subsonic Combustion Rig Supported the Ultra-Efficient Engine Technology Project's Emissions Reduction Test

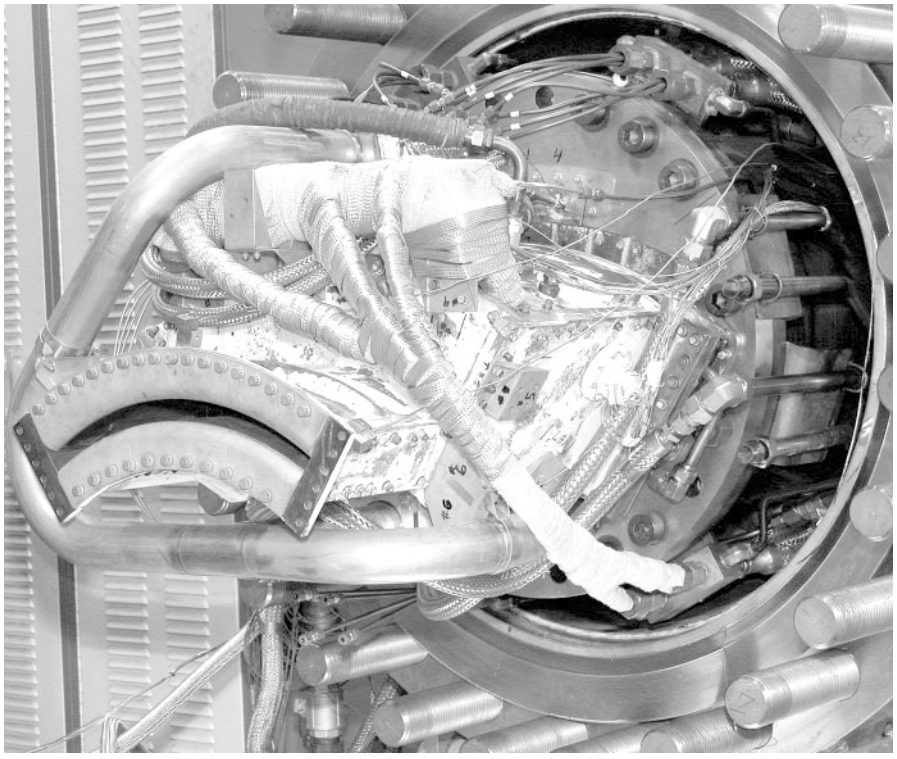

General Electric sector combustor mounted in the ASCR.

The Advanced Subsonic Combustor Rig (ASCR) is NASA Glenn Research Center's unique high-pressure, high-temperature combustor facility supporting the emissions-reduction element of the Ultra-Efficient Engine Technology (UEET) Project. The facility can simulate combustor inlet test conditions up to a pressure of 900 psig and a temperature of 1200 °F (non-vitiated). ASCR completed three sector tests in fiscal year 2003 for General Electric, Pratt & Whitney, and Rolls-Royce North America. This will provide NASA and U.S. engine manufacturers the information necessary to develop future low-emission combustors and will help them to better understand durability and operability at these high pressures and temperatures.

The UEET emissions reduction goal is to demonstrate landing and takeoff nitrogen oxides (NO_x) emission reductions of at least 70 percent of the 1996

International Civil Aviation Organization limits for future large and regional subsonic engines. This goal requires the ability to support testing at pressure ratios to 55:1 for large engines and to 30:1 for regional engines. To produce the higher pressures, ASCR has a dedicated high-pressure compressor that pressurizes Glenn's centrally supplied 450-psig combustion air up to 900 psig. The maximum facility airflow is 50 lb/sec, and the maximum combustor exhaust gas temperature is 3400 °F. These unique capabilities provide combustor test simulations at up to 60 atm, twice the capability of other combustor rigs in the United States.

In fiscal year 2003, ASCR completed three sector tests for aircraft engine companies evaluating combustor concepts for achieving UEET's 70-percent NO_x emissions-reduction goals. The success of these tests will help these companies develop technologies that can eventually be tested in a full annular combustor as part of UEET's longer-term project goals starting in fiscal year 2004. ASCR was instrumental in providing the high-pressure, high-temperature simulated engine test conditions necessary to provide NASA and U.S. engine manufacturers with the ability to quantify the effects of higher pressure on combustor emissions, durability, and operability.

Find out more about this research:

Research facilities at Glenn:
http://facilities.grc.nasa.gov

Aeronautics research at Glenn:
http://www.grc.nasa.gov/WWW/AERO/

Glenn contact:
Luis R. Beltran, 216–433–5678,
Luis.R.Beltran@nasa.gov

QSS Group, Inc., contact:
Susan E. Adkins, 216–433–5930,
Susan.E.Adkins@grc.nasa.gov

Author: Luis R. Beltran

Headquarters program office: OAT

Programs/Projects: UEET

NASA Glenn's Engine Components Research Lab, Cell 2B, Reactivated to Support the U.S. Army Research Laboratory T700 Engine Test

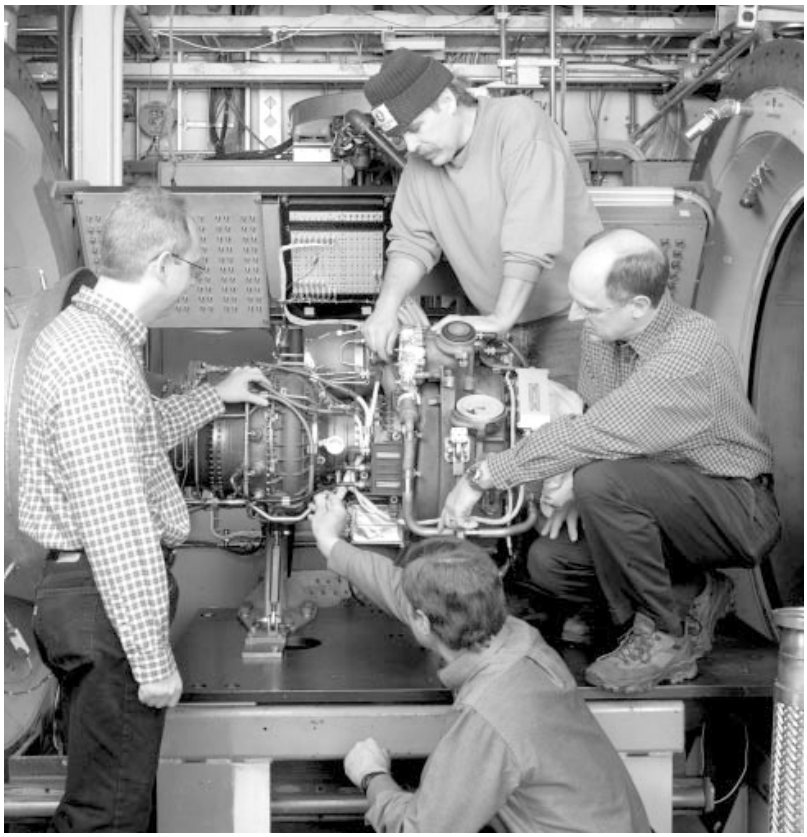

T700 engine mounted in ECRL 2B.

The U.S. Army Vehicle Technology Directorate at the NASA Glenn Research Center has been directed by their parent command, the U.S. Army Research Laboratory (ARL), to demonstrate active stall technology in a turboshaft engine as the next step in transitioning this technology to the Army and aerospace industry. Therefore, the Vehicle Technology Directorate requested the reactivation of Glenn's Engine Components Research Lab, Cell 2B, (ECRL 2B). They wanted to test a T700 engine that had been used previously for turboshaft engine research as a partnership between the Army and NASA on small turbine engine research. ECRL 2B had been placed in standby mode in 1997. Glenn's Testing Division initiated reactivation in May 2002 to support the new research effort, and they completed reactivation and improvements in September 2003.

As part of the reactivation, the facility underwent many upgrades to meet program goals and improve accuracy to make it a reliable, economical, and state-of-the-art facility. The dynamometer and the output shaft system were redesigned with new shafting and a torquemeter. The waterbrake was refurbished and will be used to apply load to the T700 engine. The control room was significantly enhanced with new operator stations and programmable logic controls. The electronic scanning pressure system was replaced with a higher accuracy processor, and all control panel loaders and pushbuttons were replaced with touch screens. The ECRL 2B rig can test turboshaft engines with shaft power outputs up to 2500 hp. T700, T800, and T55 engines have been tested to investigate performance, inlet temperature and pressure distortion, shaft vibrations, and automated stall recovery.

These enhancements will enable the more efficient use of the facility and improve data accuracy. We plan to start using the facility to support T700 research engine testing in fiscal year 2004.

Find out more about this research:
http://facilities.grc.nasa.gov

U.S. Army Research Laboratory, Vehicle Technology Directorate at Glenn contact:
Tom Griffin, 216–433–8536, Thomas.A.Griffin@grc.nasa.gov

Glenn contact:
Luis R. Beltran, 216–433–5678, Luis.R.Beltran@nasa.gov

Authors:
Thomas A. Griffin and Luis R. Beltran

Headquarters program office: ARL

Programs/Projects:
U.S. Army Vehicle Technology Directorate

NASA Glenn's Single-Stage Axial Compressor Facility Upgraded

NASA Glenn Research Center's Single-Stage Axial Compressor Facility was upgraded in fiscal year 2003 to expand and improve its research capabilities for testing high-speed fans and compressors. The old 3000-hp drive motor and gearbox were removed and replaced with a refurbished 7000-hp drive motor and gearbox, with a maximum output speed of 21,240 rpm. The higher horsepower rating permits testing of fans and compressors with higher pressure ratio or higher flow. A new inline torquemeter was installed to provide an alternate measurement of fan and compressor efficiency, along with the standard pressure and temperature measurements. A refurbished compressor bearing housing was also installed with bidirectional rotation capability, so that a variety of existing hardware could be tested. Four new lubrication modules with backup capability were installed for the motor, gearbox, torquemeter, and compressor bearing housing, so that in case the primary pump fails, the backup will prevent damage to the rotating hardware.

The combustion air supply line for the facility inlet air system was activated to provide dry air for repeatable inlet conditions. New flow conditioning hardware was installed in the facility inlet plenum tank, which greatly reduced the inlet turbulence. The new inlet can also be easily modified to accommodate 20- or 22-in.-diameter fans and compressors, so a variety of existing hardware from other facilities (such as Glenn's 9- by 15-Foot Low-Speed Wind Tunnel) can be tested in the Single-Stage Axial Compressor Facility. An exhaust line was also installed to provide bleed capability to remove the inlet boundary layer.

To improve the operation and control of the facility, a new programmable logic controller (PLC) was installed to upgrade from hardwired relay logic to software logic. The PLC also enabled the usage of human-machine interface software to allow for easier operation of the facility and easier reconfiguration of the facility controls when necessary. Finally, a new health-monitoring system was installed to measure shaft speed, shaft movement, and machine vibration on all of the rotating equipment. The system also provides automatic alarms and shutdown of the equipment when required.

An integrated systems test for checkout of the facility was completed on June 17, 2003. Research testing resumed on June 30 with data obtained in support of the Ultra-Efficient Engine Technology Project's Compressor Casing Treatment Project.

Find out more about this research:
http://facilities.grc.nasa.gov

Glenn contacts:
Richard A. Brokopp, 216–433–5676, Richard.A.Brokopp@nasa.gov; Gwynn A. Severt, 216–433–8310, Gwynn.A.Severt@nasa.gov; and Osvaldo Rivera, 216–433–5699, Osvaldo.Rivera-1@nasa.gov

Author: Richard A. Brokopp

Headquarters program office: OAT

Programs/Projects: UEET

New Acoustic Arena Qualified at NASA Glenn's Aero-Acoustic Propulsion Laboratory

A new acoustic arena has been qualified in the Aero-Acoustic Propulsion Laboratory (AAPL) at the NASA Glenn Research Center. This arena is outfitted specifically for conducting fan noise research with the Advanced Noise Control Fan (ANCF) test rig. It features moveable walls with large acoustic wedges (2 by 2 by 1 ft) that create an acoustic environment usable at frequencies as low as 250 Hz. The arena currently uses two dedicated microphone arrays to acquire fan inlet and exhaust far-field acoustic data. It was used successfully in fiscal year 2003 to complete three ANCF tests. It also allowed Glenn to improve the operational efficiency of the four test rigs at AAPL and provided greater flexibility to schedule testing.

There were a number of technical challenges to overcome in bringing the new arena to fruition. The foremost challenge was conflicting acoustic requirements of four different rigs. It was simply impossible to construct a static arena anywhere in the facility without intolerably compromising the acoustic test environment of at least one of the test rigs. This problem was overcome by making the wall sections of the new arena movable. Thus, the arena can be reconfigured to meet the operational requirements of any particular rig under test. Other design challenges that were encountered and overcome included structural loads of the large wedges, personnel access requirements, equipment maintenance requirements, and typical time and budget constraints.

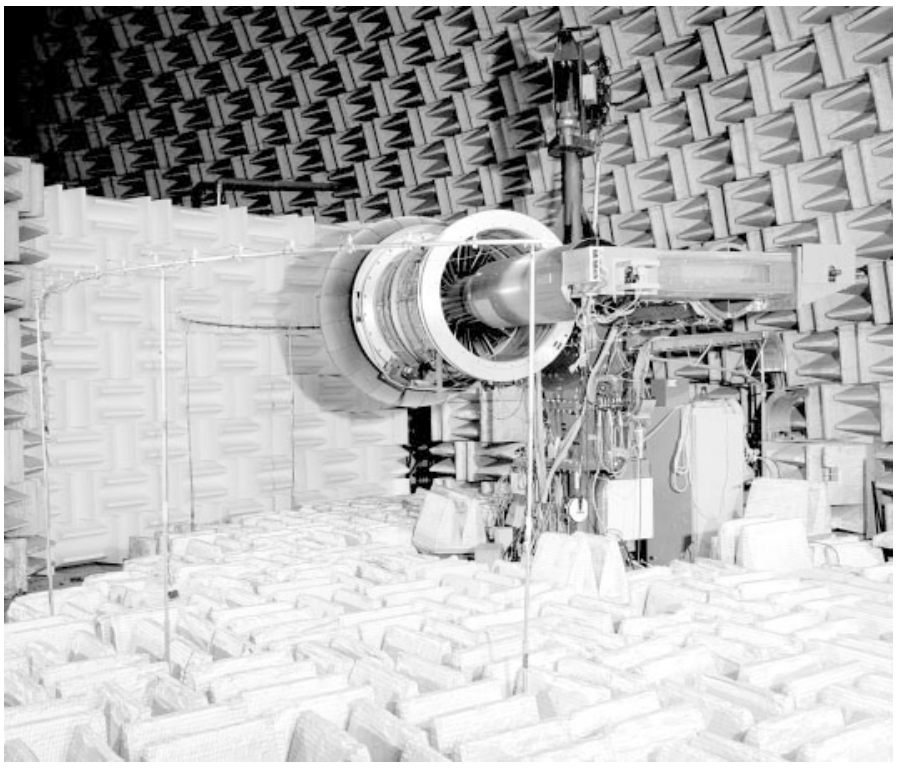

Advanced Noise Control Fan in compact acoustic arena.

The new acoustic arena improves operations at the AAPL facility in several significant ways. First, it improves productivity by allowing multiple rigs to operate simultaneously. Second, it improves research data quality by providing a unique test area within the facility that is optimal for conducting fan noise research. Lastly, it reduces labor and equipment costs by eliminating the periodic need to transport the ANCF into and out of the primary AAPL acoustic arena. The investment to design, fabricate, and install the new compact arena in fiscal year 2002 has paid dividends in fiscal year 2003 and will for many years to come. It has provided a dedicated, high-quality acoustic arena to support low-speed fan testing for ANCF while minimizing scheduling impacts and improving operational productivity in the AAPL facility.

Find out more about this research:
http://facilities.grc.nasa.gov

Glenn contacts:
Luis R. Beltran, 216–433–5678, Luis.R.Beltran@nasa.gov;
Dr. Dan L. Sutliff, 216–433–6290, Daniel.L.Sutliff@nasa.gov;
Steve P. Wnuk, 216–433–5748, Stephen.P.Wnuk@nasa.gov; and
Osvaldo Rivera, 216–433–5699, Osvaldo.Rivera-1@nasa.gov

Author: Stephen P. Wnuk

Headquarters program office: OAT

Programs/Projects:
Propulsion and Power (Fundamental Noise), UEET, QAT

Low-Pressure Capability of NASA Glenn's 10- by 10-Foot Supersonic Wind Tunnel Expanded

Extremely low dynamic pressure *Q* conditions are desired for space-related research including the testing of parachute designs and other decelerator concepts for future vehicles landing on Mars. Therefore, the low-pressure operating capability of the Abe Silverstein 10- by 10-foot Supersonic Wind Tunnel (10×10 SWT) at NASA Glenn Research Center was recently increased. Successful checkout tests performed in the fall of 2002 showed significantly reduced minimum operating pressures in the wind tunnel.

Using Glenn's central exhaust system, set up in a special seven-stage configuration and dedicated to the 10×10 SWT operation, the following test section conditions were run:

Mach number	Tunnel total pressure, P_t, psfa[a]
2.0 to 2.5	100
3.0 to 3.1	120
3.3	140
3.5	150

[a]Pounds per square foot, absolute.

This essentially reduced the minimum dynamic pressure operating line of the tunnel by about half. At each condition, the various wind tunnel subsystems were checked out—including the drive motors and compressors, coolers, and dew point. New low-pressure transducers installed in the wind tunnel control systems helped to maintain steady test section conditions in this continuous flow facility.

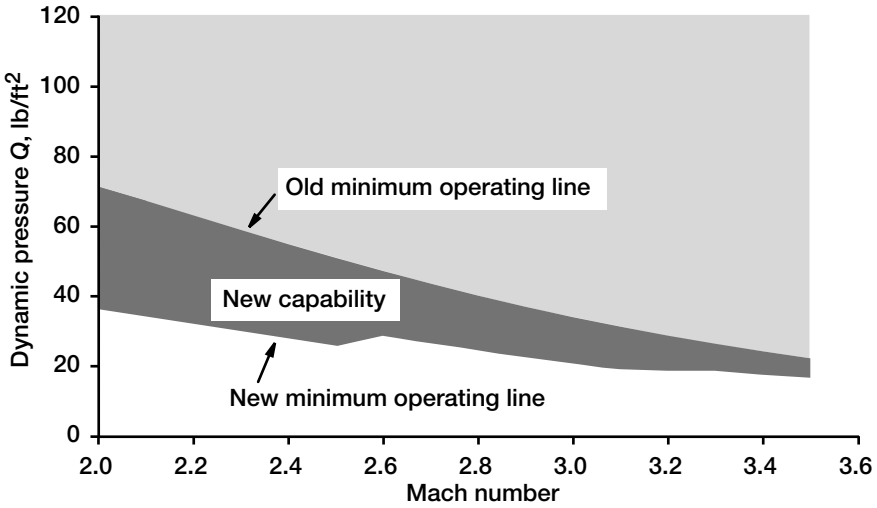

Increase in the minimum dynamic pressure capability in the 10×10 SWT.

In addition to successfully validating tunnel operations, we measured some test section conditions to determine if there were any flow quality issues at the extreme low pressures. This was not the case since the test section boundary layer was determined to be about 1 ft thick, essentially the same as at higher tunnel pressures; and the cross-sectional total temperature distribution in the test section appeared to be uniform.

A modified test section "calibration wedge" was also validated during this test. This tool is used to calibrate test section conditions—pressure, temperature, Mach number, and flow angle. Prior to this test, we determined that existing wedges could not be used at these low pressures (because of orifice size, line size, etc.). One wedge was modified and installed in the test section, and successful pressure measurements were obtained. This modified wedge design will be used for a future planned low-pressure calibration of the test section. Expanding the low-pressure capability of the 10×10 SWT will enhance its usefulness in furthering this Nation's space endeavors.

Find out more about this research:
http://facilities.grc.nasa.gov

Glenn contacts:
James Roeder, 216–433–5677, James.W.Roeder@nasa.gov;
David E. Stark, 216–433–2922, David.E.Stark@nasa.gov; and
Roger Chamberlin, 216–433–5726, Roger.Chamberlin-1@nasa.gov

Author: James W. Roeder

Headquarters program office: OAT

Programs/Projects:
PR&T, RLV, Space Transportation

Fuel Flexible Gas Turbine Combustor Flametube Facility Upgraded

In fiscal year 2003, test cell 23 of the Research Combustion Laboratory (RCL 23) at the NASA Glenn Research Center was upgraded with the addition of gaseous hydrogen as a working propellant and the addition of a 450-psig air-supply system. Test flexibility was further enhanced by upgrades to the facility control systems. RCL 23 can now test with gaseous hydrogen flow rates up to 0.05 lbm/sec and jet fuel flow rates up to 0.62 lbm/sec. Research airflow rates up to 3 lbm/sec are possible with the 450-psig supply system over a range of inlet temperatures. Nonvitiated, heated air is supplied from a shell and tube heat exchanger. The maximum nonvitiated facility air temperature is 1100 °F at 1.5 lbm/sec. Research-section exhaust temperatures are limited to 3200 °F because of material and cooling capacity limits.

A variety of support systems are available depending on the research hardware configuration. Test section ignition can be provided via either a hydrogen air torch system or an electronic spark system. Emissions measurements are obtained with either pneumatically or electromechanically actuated gas sample probes, and the electromechanical system allows for radial measurements at a user-specified axial location for measurement of emissions profiles. Gas analysis data can be obtained for a variety of species, including carbon monoxide (CO), carbon dioxide (CO_2), nitrogen oxides (NO and NO_x), oxygen (O_2), unburnt hydrocarbons, and unburnt hydrogen.

Facility control is accomplished with a programmable logic control system. Facility operations have been upgraded to a system based on graphical user interface control screens. A data system is available for real-time acquisition and monitoring of both measurements in engineering units and performance calculations.

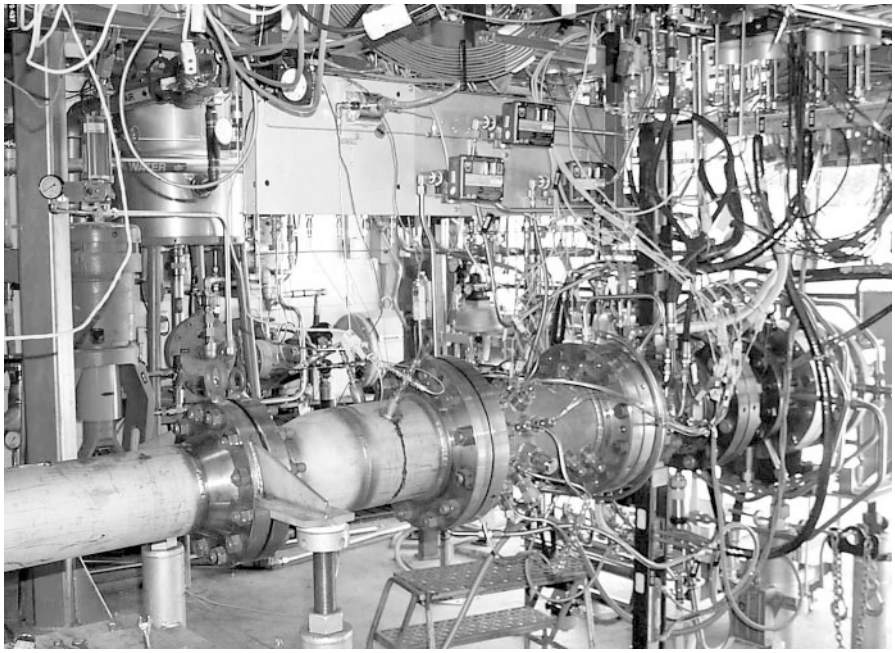

Typical flametube installation for RCL 23.

The upgrades have made RCL 23 a highly flexible facility for research into low-emissions gas turbine combustor concepts, and the flame tube configuration inherently allows for a variety of fuel nozzle configurations to be tested in a cost-effective manner. RCL 23 is poised to be a leading facility for developing modern low-emission fuel nozzles for use with jet fuel and alternative fuels.

Find out more about this research:

Glenn's Research Testing Division:
http://www.grc.nasa.gov/WWW/RTD/

Glenn's research facilities:
http://facilities.grc.nasa.gov/

QSS Group, Inc., contacts:
James E. Little, 216–433–3821, James.E.Little@grc.nasa.gov; and Steve A. Nemets, 216–433–6652, Steve.A.Nemets@grc.nasa.gov

Glenn contacts:
Tim D. Smith, 216–977–7546, Timothy.D.Smith@nasa.gov; Bruce J. Frankenfeld, 216–433–6456, Bruce.J.Frankenfeld@nasa.gov; and Robert Tornabene, 216–433–3045, Robert.T.Tornabene@nasa.gov

Authors:
James E. Little, Steve A. Nemets, Robert T. Tornabene, Timothy D. Smith, and Bruce J. Frankenfeld

Headquarters program office: OAT

Program/Projects:
Propulsion and Power, LEAP

Engineering Design and Analysis

Electrochemical Processes Enhanced by Acoustic Liquid Manipulation

Acoustic liquid manipulation is a family of techniques that employ the nonlinear acoustic effects of acoustic radiation pressure and acoustic streaming to manipulate the behavior of liquids. Researchers at the NASA Glenn Research Center are exploring new methods of manipulating liquids for a variety of space applications, and we have found that acoustic techniques may also be used in the normal Earth gravity environment to enhance the performance of existing fluid processes. Working in concert with the NASA Commercial Technology Office, the Great Lakes Industrial Technology Center, and Alchemitron Corporation (Elgin, IL), researchers at Glenn have applied nonlinear acoustic principles to industrial applications.

Collaborating with Alchemitron Corporation, we have adapted the devices to create acoustic streaming in a conventional electroplating process. As shown in the figure, an acoustic transducer is immersed in a tank of electroplating electrolyte. In this case, the process involves the selective gold plating of electronic circuit boards.

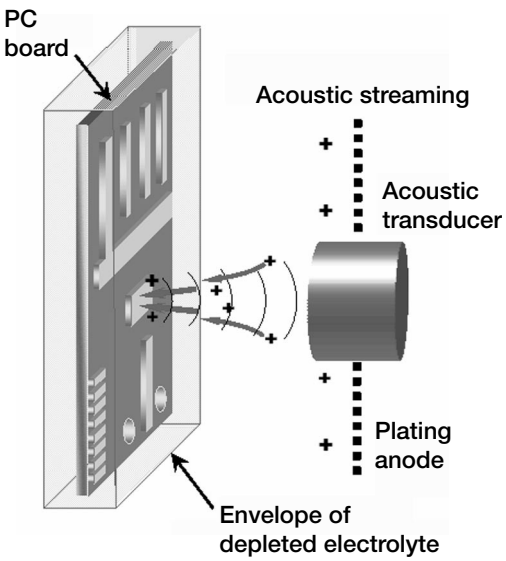

Acoustic streaming transducers can improve the controllability of an electroplating system, possibly eliminating the need for masking operations.

Normally the selective plating process would involve the use of masking tapes or masking coatings to distinguish the surface areas selected to be plated and to protect the nonselected areas. The masking process is the most labor- and tooling-intensive aspect of the plating process, and the disposable masking materials often become a substantial source of toxic waste. Substantial cost, health, and environmental issues motivate us to eliminate the masking process.

In a normal electroplating process, an electric field is used to deposit a metal onto a target part. The plating process is often impeded by the depletion of the electrolyte in the immediate vicinity of the part. The normal solution is to agitate the bath to eliminate the depleted layer that envelopes the part.

In the acoustically enhanced process, the bath is left quiescent and an envelope of depleted solution is allowed to form. We treat this depleted envelope as a virtual mask and use acoustic streaming to provide a low-speed liquid jet to penetrate the envelope with fresh "undepleted" electrolyte. The plating rate in the area where the acoustic beam impinges on the target is dramatically higher. Deposits are at least 10 times higher than in the area outside the beam. By careful manipulation and coordination of the electric current and the acoustically driven stream, we can control the shape, size, and deposition rate of the plated area.

Ongoing development and refinement of the process is expected to provide a viable maskless method of electroplating. In the future, we expect to employ acoustic phased-array techniques to provide electronic beam steering and focusing. Such a system will provide selective plating by raster scanning the acoustic beam to "paint out" preprogrammed patterns. This technology was recently patented and is available for licensing by commercial users.

Glenn contact:
Richard C. Oeftering, 216–433–2285, Richard.C.Oeftering@nasa.gov

Author: Richard C. Oeftering

Headquarters program office:
TTPO at Glenn

Programs/Projects: Commercial Technology, Microgravity Science, PR&T, Space Power Systems R&T

Special recognition: Awarded U.S. Patent 6,368,982, April 2002

Hybrid Power Management Program Evaluated Fuel Cell/ Ultracapacitor Combinations and Developed Other New Applications

In fiscal year 2003, the continuation of the Hybrid Power Management (HPM) Program through NASA Glenn Research Center's Commercial Technology Office resulted in several new successful applications of this pioneering technology. HPM is the innovative integration of diverse, state-of-the-art power devices in an optimal configuration for space and terrestrial applications. The appropriate application and control of the various power devices significantly improves overall system performance and efficiency. The advanced power devices include ultracapacitors, fuel cells, and photovoltaics. HPM has extremely wide potential, with applications from nanowatts to megawatts—including power generation, transportation systems, biotechnology systems, and space power systems. HPM has the potential to significantly alleviate global energy concerns, improve the environment, and stimulate the economy.

Fuel cells provide excellent efficiency and energy density, but do not have good power density. In contrast, ultracapacitors have excellent power density and virtually unlimited cycle life. To improve the power density of the fuel cell, the combination of fuel cells and ultracapacitors was evaluated. The addition of ultracapacitors significantly improved the power density of the system, thus providing a vastly improved transient response. An ultracapacitor is an excellent energy storage medium for fuel cell systems. Ultracapacitors can easily handle the high charge/discharge currents and have extremely long life in this application.

A typical cordless drill is powered by batteries. The batteries provide reduced performance over time, and eventually they need to be replaced and disposed of. Because batteries are not environmentally friendly, they must be disposed of carefully, and they have a memory that limits the energy that they provide to what was used previously. In contrast, the HPM cordless drill was recharged in 1 min and provided 3 min of continuous operation, or enough power to drive about 30 wood screws. The ultracapacitors provided consistent performance and worked well at low temperatures. In addition, they have no memory and will never need to be replaced.

An electric wheelchair normally is provided with lead acid batteries that require 6 hr to recharge. The range degrades over time, the batteries must be replaced after about 300 charging cycles, and the low-temperature performance of the batteries is greatly reduced. When a wheelchair was tested with ultracapacitors, it could be charged in 5 min and it provided 15 min of operation at full speed. Here too, the ultracapacitors had unlimited life and excellent low-temperature performance.

A two-wheeled human transportation system also is being evaluated. This vehicle is usually equipped with batteries that take 6 hr to recharge and must be replaced annually under normal use. For HPM, the vehicle is being equipped with maintenance-free ultracapacitors that have unlimited life and can be charged in minutes.

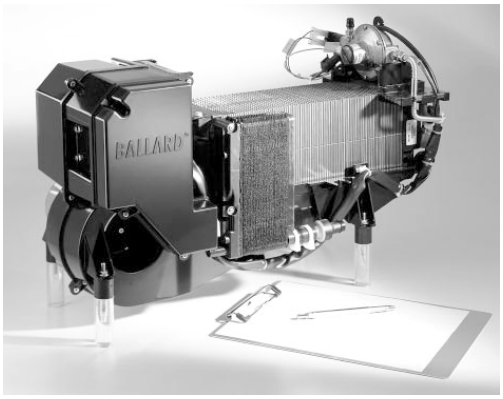

Hybrid Power Management (HPM) Program—exploring new power applications. Top: Cordless drills. Center: Electric wheelchair. Copyright Invacare; used with permission. Bottom: Fuel cells.

In addition, HPM is being considered for reliable, long-life energy storage systems, essential for space missions, such as the exploration of Mars, and for deep space missions, such as the exploration of the planet Jupiter's moon Europa. The technology also is being considered for various aeronautical electrical system applications.

Bibliography
Eichenberg, Dennis J.: Baseline Testing of the Club Car Carryall With Asymmetric Ultracapacitors. NASA/TM—2003-212705, 2003. http://gltrs.grc.nasa.gov/cgi-bin/GLTRS/browse.pl?2003/TM-2003-212705.html

Glenn contact:
Dennis J. Eichenberg, 216–433–8360, Dennis.J.Eichenberg@nasa.gov

Author: Dennis J. Eichenberg

Headquarters program office: OAT

Programs/Projects: TTPO

Magnetically Levitated Ducted Fan Being Developed as a Propulsor Option for Electric Flight

The NASA Glenn Research Center is developing a revolutionary engine concept called the Magnetically Levitated Ducted Fan. The objective of this work is to demonstrate the feasibility of a pollution-free electromagnetic propulsor for all-electric flight. This concept will help to reduce harmful emissions, to reduce the Nation's dependence on fossil fuels, and to mitigate many of the concerns and limitations encountered in conventional engine systems such as bearing wear, leaks, seal failure, and friction loss. The general concept is depicted in the following figure.

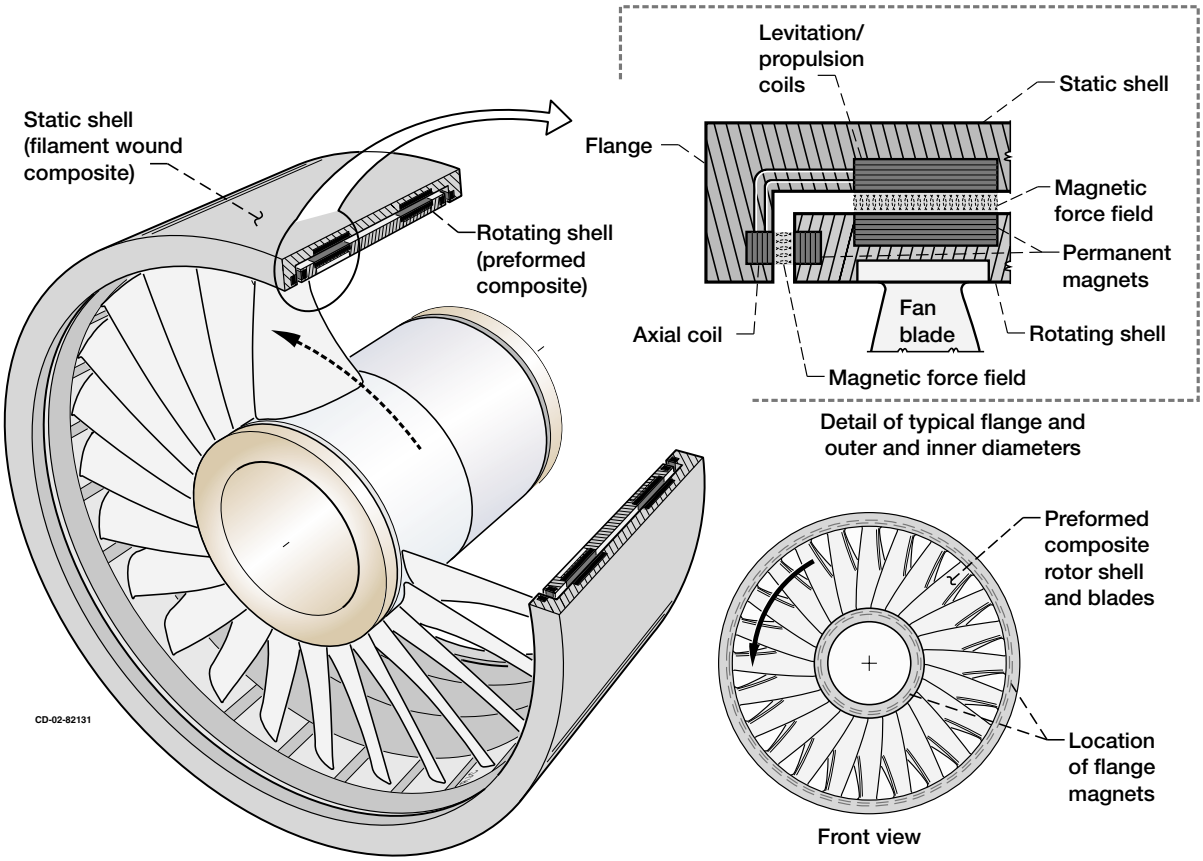

Early concept of the Magnetically Levitated Ducted Fan.

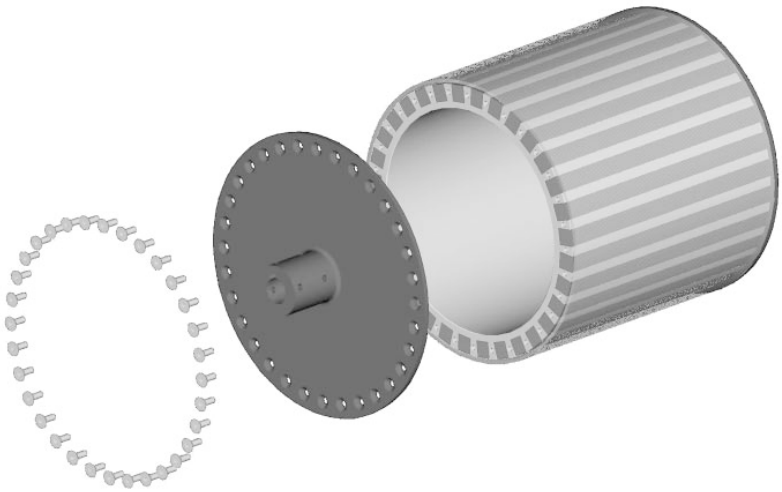

Small-scale levitation model rotor.

Small-scale levitation model stator.

This fully integrated system concept incorporates many advanced technologies into a new aeropropulsion system architecture. The innovative physical layout consists of a ducted fan drum rotor with blades attached at the outer diameter and supported by a stress tuner ring at the inner diameter. The drum rotor is made of composite material and is contained within a static shell assembly, or "stator." Magnetic fields suspend and support the rotor assembly within the stator. The rotor is driven by modulated electromagnetic fields between the rotor and the stator. Optimal modulation will be achieved via the controller and power electronic drive circuitry between the power source and the propulsor. This concept exploits unique physical dimensions and a large available surface area to optimize a custom, integrated electromagnetic system that provides both levitation and propulsion functions. Advanced technologies developed for particle accelerators, and currently under development for maglev trains and rocket launchers, served as pathfinders for adaptation into the application.

Development of this concept was funded through the Revolutionary Aeropropulsion Concepts (RAC) program beginning in 2003. During this first year, the focus of the work was on the development of the magnetic levitation system. The electromagnetic concept under investigation uses permanent magnet elements attached to the outer circumference of the rotor drum and wire coils placed in the stator shell. The permanent magnets are arranged in a Halbach configuration, which results in the production of a sinusoidally varying, periodic magnetic field in the vicinity of the stator coils. This magnetic array configuration was pioneered by Klaus Halbach for use in particle accelerators. When set in motion, the time-varying magnetic fields interact with the passive coils in the stator assembly to produce repulsive forces between the stator and the rotor, providing magnetic suspension. The beauty of this technique is that it is inherently stable once the rotor reaches a critical speed and, thus, requires no active feedback control or superconductivity as seen in many traditional implementations of magnetic suspension.

To date, theoretical calculations have been produced to predict the levitation forces developed by a cylindrical Halbach array and coil assembly. Early experimental hardware was successfully designed and developed that validated the basic principles and the theoretical work. On the basis of these findings, a small-scale system was designed that will serve as a levitation demonstration model. The rotor and stator of the demonstration model are shown in the preceding figures. The purpose of this model is to demonstrate stable suspension of a rotorlike body within a stator assembly.

The next step in the development process will be to further develop the electromagnetic propulsion concept and integrate both the magnetic suspension and propulsion function into a single multifunction assembly. In addition to aircraft engines, this technology has potential application in ultraefficient motors, computer memory systems, manufacturing equipment, and space power systems such as flywheels.

Glenn contact:
Dawn C. Emerson, 216–433–8901, Dawn.C.Emerson@nasa.gov

Author: Dawn C. Emerson

Headquarters program office: OAT

Programs/Projects: RAC

Composite Arbors Built and Tested to Improve the Specific Energy of Flywheel Batteries

Energy storage flywheels are quickly becoming an attractive alternative to electrochemical batteries. Their advantages of long cycle life, high turnaround efficiency, and insensitivity to operating temperatures have led to growing interest in terrestrial and space applications, including International Space Station and low-Earth-orbit satellites. This effort to develop composite arbor technology greatly increases the flywheel rotor specific energy potential and has the added advantage of relieving the high radial compressive stresses that limit durability, life, and operating temperature range.

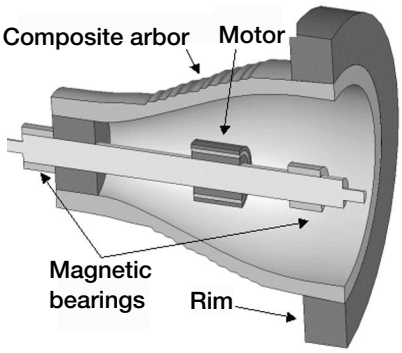

Conceptual cutaway view of composite arbor flywheel rotor.

Composite flywheels store energy by rapidly spinning a large wheel to ultrahigh speeds. This is made possible by the large load-carrying capacity of high-strength filament-wound composites (FWC). These composites are wound into large rings, focusing mass at the outer periphery to maximize the stored rotational energy. These large spinning rims must be mechanically connected to shafts, bearings, and motors and must interface with these metallic components without compromising on specific energy. Traditionally, the composite rims are pressed over metallic hubs, which also act as shafts for bearings and motors. Work has been ongoing at the University of Texas, Center for Electromechanics (CEM), under NASA Research Announcement funding to improve the interface between these rims and shafts. Composites are being used to traverse the small monolithic shaft to a larger rim while minimizing compressive stresses and achieving the full-speed operating temperature range of –45 to 85 °C necessary for satellite applications.

The arbor itself is an intricately wound FWC tube (see the illustraton above) smaller at one end to accept the metallic shaft and larger at the other end to interface with the main energy storing element, the composite rim. The shear, transverse, and hoop properties are traded off throughout the profile to efficiently optimize mechanical safety factors throughout. Plastic deformation was removed from the design by tailoring the winding angles and thicknesses of the helical layers. Both high-strength carbon fiber with tensile strength approaching 10^6 psi and intermediate strength carbon and glass fibers were interspersed in the arbor and rim builds to optimize mechanical properties in corresponding areas and stress states.

Prototype test rotor being lowered into the armored spin pit.

The recently completed year two of this 3-year development program saw several test arbors built and tested to anchor anisotropic modeling techniques and characterize material design allowables. Finally a prototypical arbor/rim spin test rotor (see the photograph) was spun to burst speed. The rotor was tested on September 3, 2003, and successfully reached 1337 m/sec (2990 mph) tip speed, corresponding to 60,070 rpm for the 16.7-in.-diameter wheel, which stored 1.4 kW·hr at that speed. This represents the highest known attained speed in any useable flywheel configuration. The specific energy of this rotor was 73 W·hr/kg, which rivals most present-day electrochemical battery units. Under year three of this program, further increases in specific energy will be realized as the shaft, arbor, and rim are optimized for additional reduced weight. The analytical results agreed quite well

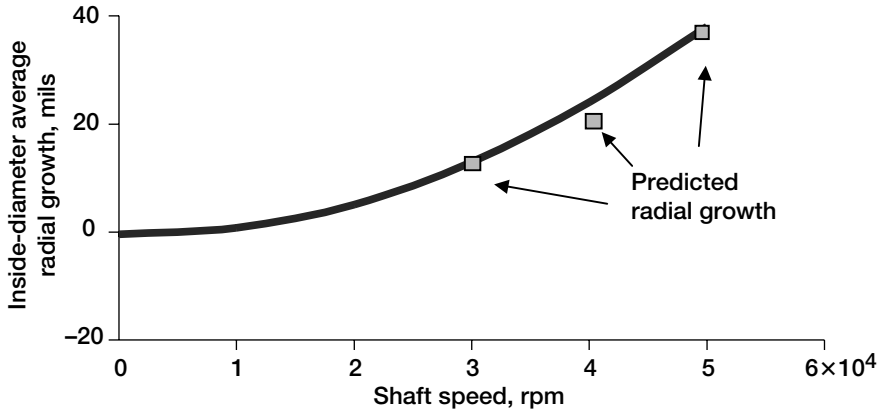

Analysis results and laser probe growth data of arbor during low-speed test run to 50,000 rpm.

with the strain response measured with eddy current and laser proximity probes around the rim and arbor (see the graph).

A further benefit of this program is a thorough understanding of the composite arbor's fundamental scalability, which will permit this technology to be useful in a broad range of applications. This technology is being used in a next-generation flywheel battery being designed and built at the NASA Glenn Research Center. In addition, a duplicate prototype arbor is being shipped to Glenn for cyclic spin testing and life verification.

Find out more about this research:
http://space-power.grc.nasa.gov/ppo/projects/flywheel/

Glenn contacts:
Kevin E. Konno, 216–433–8373, Kevin.E.Konno@nasa.gov;
Kerry L. McLallin, 216–433–5389, Kerry.L.McLallin@nasa.gov; and
Raymond F. Beach, 216–433–5320, Raymond.F.Beach@nasa.gov

CEM contact:
Richard C. Thompson, 512–232–1615, r.thompson@mail.utexas.edu

Authors: Kevin E. Konno and Richard C. Thompson

Headquarters program office: OAT

Programs/Projects:
Propulsion and Power, ISS

Fluids and Combustion Facility Acoustic Emissions Controlled by Aggressive Low-Noise Design Process

The Fluids and Combustion Facility (FCF) is a dual-rack microgravity research facility that is being developed by Northrop Grumman Information Technology (NGIT) for the International Space Station (ISS) at the NASA Glenn Research Center. As an on-orbit test bed, FCF will host a succession of experiments in fluid and combustion physics. The Fluids Integrated Rack (FIR) and the Combustion Integrated Rack (CIR) must meet ISS acoustic emission requirements (ref. 1), which support speech communication and hearing-loss-prevention goals for ISS crew. To meet these requirements, the NGIT acoustics team implemented an aggressive low-noise design effort that incorporated frequent acoustic emission testing for all internal noise sources, larger-scale systems, and fully integrated racks (ref. 2). Glenn's Acoustical Testing Laboratory (ref. 3) provided acoustical testing services (see the left photograph on the next page) as well as specialized acoustical engineering support as part of the low-noise design process (ref. 4).

Acoustic emissions of the CIR and FIR were estimated using analytical models that incorporated results from testing at the source and systems level as well as transmission loss tests of the rack envelope. These initial estimates indicated that the cooling system was the dominant contributor to the total rack noise and predicted that noise levels of the fully integrated CIR and FIR would exceed ISS acoustic emission limits at high fan speeds. Integrated rack-level testing of the CIR and the FIR helped to improve the validity of the analytical models and refine the acoustic emission estimates.

The NGIT acoustics team developed a comprehensive noise-control plan for each rack that included replacement of selected noise sources with low-noise components, addition of transmission loss to the rack envelope, and installation of absorptive material where needed to bring the rack into compliance. The application of flat,

FIR in Glenn's Acoustical Testing Laboratory with microphone array positioned for acoustic emission testing.

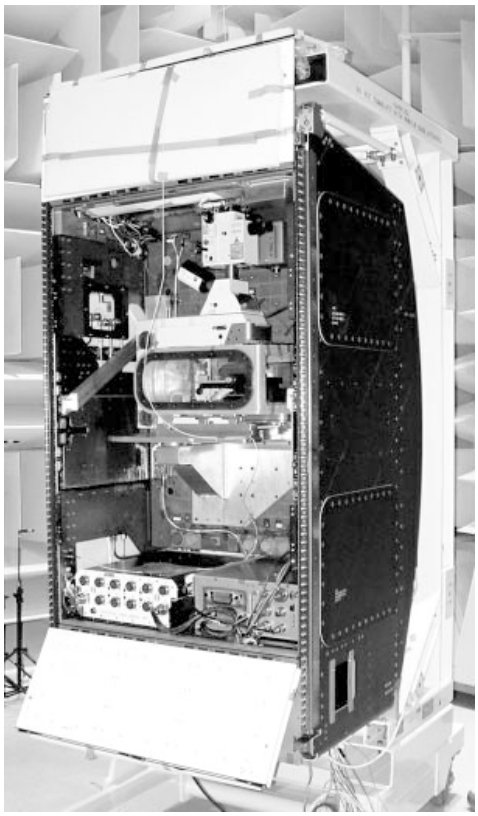

Open FIR, shown with application of acoustically absorptive melamine foam on upper and lower door panels.

white acoustically absorptive melamine foam to the side and rear panels of the rack, as well as to the rack doors and other selected areas is shown in the right photograph. A high-transmission-loss external "closeout" panel added below the door reduced the noise level to within a small margin of the requirement. Finally, the noise level was further reduced by operating the cooling system fans at lower speeds, while increasing water flow to meet thermal requirements.

This aggressive low-noise design approach allowed both the CIR and FIR to meet the acoustic emission requirement at fan speeds that correspond to the design point for cooling. The FCF noise-control plan calls for testing, before flying, all orbital replacement units expected to have significant noise emissions in order to maintain compliance with the ISS acoustic emissions requirements for the life of the FCF.

References

1. Pressurized Payloads Interface Requirements Document, International Space Station Program, NASA SSP–57000, Rev. E, Sect. 3.12.3.3 Acoustic Requirements, 2000.
2. Douzos, George G.; Krejsa, Gene; and Young, Judy: Testing and Noise Control for FCF Project Fluids and Combustion Facility (FCF): FIR and CIR. Proceedings of NOISE–CON 2003, Cleveland, OH, 2003.
3. Cooper, Beth A.: Design and Construction of a Convertible Hemi/Anechoic Acoustical Laboratory for Testing Space Flight Hardware at the NASA Glenn Research Center. Proceedings of NOISE–CON 2000, Newport Beach, CA, 2000.
4. Akers, James C.; Passe, Paul J.; and Cooper, Beth A.: Challenges in Acoustic Testing of ISS Payloads: Lessons Learned at the NASA Glenn Research Center Acoustical Testing Laboratory. Proceedings of NOISE–CON 2003, Cleveland, OH, 2003.

Find out more about this research:

Fluids and Combustion Facility (FCF):
http://fcf.grc.nasa.gov

Glenn's Acoustic Testing Laboratory:
http://www.grc.nasa.gov/WWW/AcousticalTest/

Glenn contact:
Beth Cooper, 216–433–3950,
Beth.A.Cooper@nasa.gov

Analex contact:
Judy Young, 216–925–1091,
Judith.A.Young@grc.nasa.gov

Authors:
Judith A. Young and Beth Cooper

Headquarters program office: OBPR

Programs/Projects:
Microgravity Science, FCF

NASA Glenn's Acoustical Testing Laboratory Awarded Accreditation by the National Voluntary Laboratory Accreditation Program

NASA Glenn Research Center's Acoustical Testing Laboratory (ATL) provides a comprehensive array of acoustical testing services, including sound pressure level, sound intensity level, and sound-power-level testing per ISO[1] 3744 (ref. 1). Since its establishment in September 2000, the ATL has provided acoustic emission testing and noise control services for a variety of customers, particularly microgravity space flight hardware that must meet International Space Station acoustic emission requirements (ref. 2).

The ATL consists of a 23- by 27- by 20-ft (height) convertible hemi/anechoic test chamber and a separate sound-attenuating test support enclosure (ref. 3). The ATL employs a personal-computer-based data acquisition system that provides up to 26 channels of simultaneous data acquisition with real-time analysis (ref. 4). Specialized diagnostic tools, including a scanning sound-intensity system, allow the ATL's technical staff to support its clients' aggressive low-noise design efforts to meet the space station's acoustic emission requirement.

From its inception, the ATL has pursued the goal of developing a comprehensive ISO 17025-compliant quality program that would incorporate Glenn's existing ISO 9000 quality system policies as well as ATL-specific technical policies and procedures. In March 2003, the ATL quality program was awarded accreditation by the National Voluntary Laboratory Accreditation Program (NVLAP) for sound-power-level testing in accordance with ISO 3744 (ref. 5). The NVLAP program is administered by the National Institutes of Standards and Technology (NIST) of the U.S. Department of Commerce and provides third-party accreditation for testing and calibration laboratories. There are currently 24 NVLAP-accredited acoustical testing laboratories in the United States. NVLAP accreditation covering one or more specific testing procedures conducted in accordance with established test standards is awarded upon successful completion of an intensive onsite assessment that includes proficiency testing and documentation review.

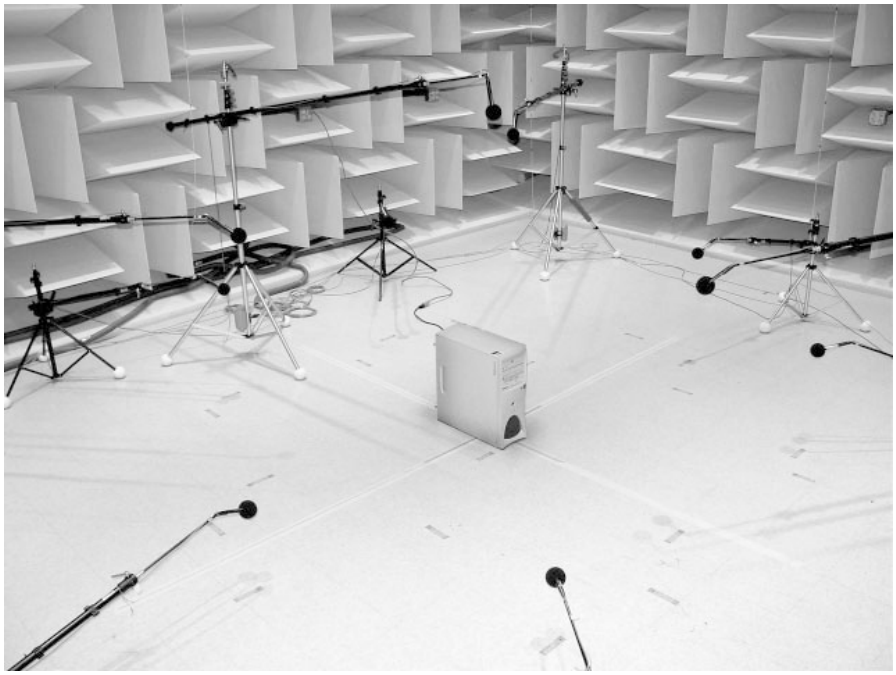

A hemispherical surface defines the microphone array required for sound power level testing in accordance with ISO 3744 (shown here for a computer hard drive).

The ATL NVLAP accreditation currently applies specifically to its ISO 3744 sound-power-level determination procedure (see the photograph) and supporting ISO 17025 quality system, although all ATL operations are conducted in accordance with its quality system. The ATL staff is currently developing additional procedures to adapt this quality system to the testing of space flight hardware in accordance with International Space Station acoustic emission requirements.

References

1. Acoustics—Determination of Sound Power Levels of Noise Sources Using Sound Pressure—Engineering Method in an Essentially Free Field Over a Reflecting Plane, International Standard ISO 3744, Second ed., 1994–05–1, 1994.
2. Pressurized Payloads Interface Requirements Document, International Space Station Program, NASA SSP–57000 Rev. E, Sect. 3.12.3.3 Acoustic Requirements, 2000.

[1]International Standards Organization.

3. Cooper, Beth A.: Design and Construction of a Convertible Hemi/Anechoic Acoustical Laboratory for Testing Space Flight Hardware at the NASA Glenn Research Center. Proceedings of NOISE–CON 2000, Newport Beach, CA, 2000.
4. Nelson, David A.: A Computer-Based Acoustical Measurement System for NASA Glenn Research Center. Proceedings of NOISE–CON 2003, Cleveland, OH, 2003.
5. Schmitt, Jeff G.: The Design of a Quality System to Support NASA Glenn Research Center Acoustical Testing Laboratory. Proceedings of NOISE–CON 2003, Cleveland, OH, 2003.

Find out more about this research:
http://acousticaltest.grc.nasa.gov

Glenn contact:
Beth Cooper, 216–433–3950,
Beth.A.Cooper@nasa.gov

Analex Corporation contact:
Jim Akers, 216–433–2169,
James.C.Akers@grc.nasa.gov

Authors:
James C. Akers and Beth Cooper

Headquarters program office: OBPR

Programs/Projects:
Microgravity Science, FCF

Finite Element Modeling Used to Study Stress Distribution on the Foot

A method to study the stress distribution inside the forefoot during walking was developed at the Cleveland Clinic Foundation by a researcher from the NASA Glenn Research Center. In this method, a semiautomated process was outlined to create a three-dimensional, patient-specific, finite element model (FEM) of the forefoot using magnetic resonance images (MRI). The images were processed in MATLAB using the k-nearest neighbor (k-NN) classification algorithm and Sobel edge detection to separate the different tissue types: bone, skin, fat, and muscle. This information was used to create curves and surfaces that were exported to an FEM preprocessor known as Truegrid. In Truegrid, eight-noded or brick elements were created by using surface mapping. The FEM was processed and postprocessed in Abaqus. Material properties of the models were obtained from past experiments such as fat pad confined compression, skin axial and biaxial tests, muscle in vivo compressive tests, and reference literature (bone properties). Nonlinear (hyperelastic) material models were used for the skin (epidermis and dermis), fat, and muscles; and a linear elastic model was used for the bones.

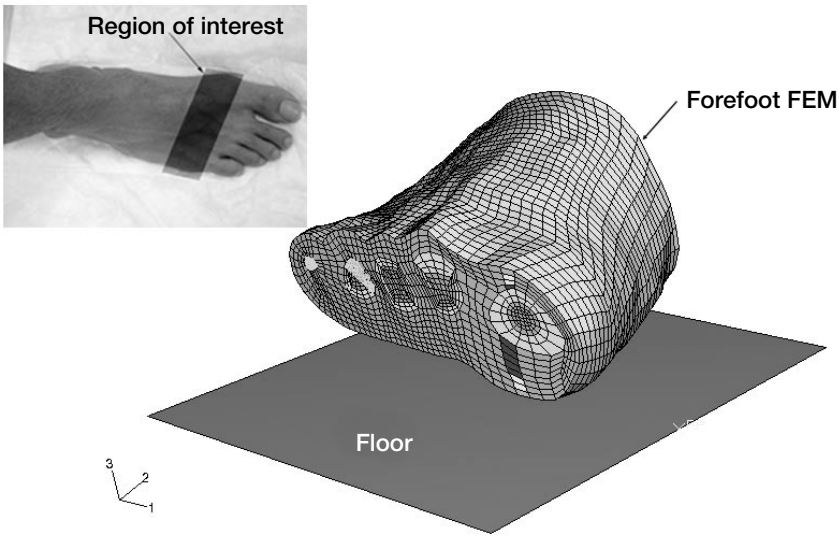

FEM configuration of the forefoot. Insert shows the region of interest in the forefoot for which the model was created. This figure is shown in color in the online version of this article (http://www.grc.nasa.gov/WWW/RT/2003/7000/7740morales.html).

Muscle activation during walking yielded uncertainties in the muscle material model since contracted muscles are stiffer than relaxed muscles. These uncertainties were resolved by performing a sensitivity analysis of the muscle material properties. The original properties were multiplied by arbitrary factors of 2, 3, 0.5, and 0.33. The strain and stress distributions, as well as the locations of peak values, were similar in all cases. The peak contact pressure P obtained for each case varied with respect to the applied factor f as follows:

$$P = 0.2563f + 0.3331 \ (R^2 = 0.9885)$$

where R^2 is the coefficient of determination.

The forefoot FEM was validated using a contact model in which a rigid surface (floor) was pressed against the bottom surface of the foot, as shown in the figure on the preceding page. This simulation captured the stance phase of the gait cycle. The contact pressure obtained from this model was compared with experimental pressure data. The pressure profiles for both cases were very similar even though the magnitudes were different (experimental data—0.295 MPa; FEM—0.624 MPa). The location of the peak values was similar in both cases. This difference could be due primarily to inaccuracies in modeling the muscle activation levels. Also, other inaccuracies may exist since the material models were obtained using tests with loads different than the loads during walking (experimental data—uniaxial tension; simulation—three-dimensional tension, compression, and shear).

After validation, peak loads were applied to study the interaction between tissue layers. The following figure shows the results of this simulation. Although all these different tasks were done using a nondiabetic foot model, the same could be repeated for a diabetic foot model if the appropriate material properties were adjusted accordingly. After repeating similar tasks for a diabetic case and comparing them with a nondiabetic case, we found that the internal Von Mises stresses were much higher in the diabetic case (4 MPa vs. 0.6 MPa) even though peak pressure loads were 30-percent higher in the diabetic case (0.9 MPa vs. 0.7 MPa).

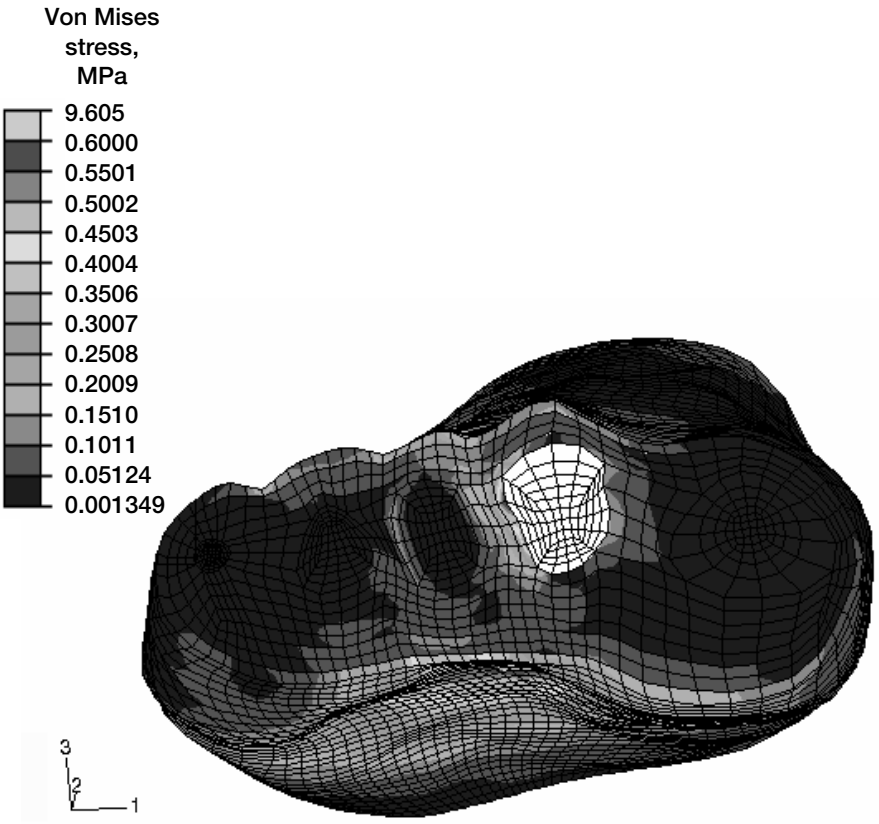

Von Mises stress distribution inside the forefoot region. Average criterion, 75 percent. This figure is shown in color in the online version of this article (http://www.grc.nasa.gov/WWW/RT/2003/7000/7740morales.html).

Bibliography
Morales, Nelson: Stress Distribution Study on the Foot Using Finite Element Modelling. Master of Science Thesis, Case Western Reserve University, 2003.

Find out more about this research:

John Glenn Biomedical Engineering Consortium:
http://microgravity.grc.nasa.gov/grcbio/bec.html

Lerner Research Institute, Department of Biomedical Engineering:
http://www.lerner.ccf.org/bme/

Lerner, Musculoskeletal Biomechanics projects: http://www.lerner.ccf.org/bme/biomechanics/

Lerner, Device for Simultaneous Measurement of Pressure and Shear Force Distribution on the Plantar Surface of the Foot: http://www.lerner.ccf.org/bme/biomechanics/simultaneous_measurement_device.php

Glenn contact:
Nelson Morales, 216–977–7050, Nelson.Morales-1@nasa.gov

Authors: Nelson Morales, Brian Davis, and Azita Tajaddini

Headquarters program office: OBPR

Programs/Projects:
JDRF, John Glenn Biomedical Engineering Consortium, BEGIN

Advanced Manufacturing Techniques Demonstrated for Fabricating Developmental Hardware

NASA Glenn Research Center's Engineering Development Division has been working in support of innovative gas turbine engine systems under development by Glenn's Combustion Branch. These one-of-a-kind components require operation under extreme conditions. High-temperature ceramics were chosen for fabrication was because of the hostile operating environment. During the designing process, it became apparent that traditional machining techniques would not be adequate to produce the small, intricate features for the conceptual design, which was to be produced by stacking over a dozen thin layers with many small features that would then be aligned and bonded together into a one-piece unit. Instead of using traditional machining, we produced computer models in Pro/ENGINEER (Parametric Technology Corporation (PTC), Needham, MA) to the specifications of the research engineer. The computer models were exported in stereolithography standard (STL) format and used to produce full-size rapid prototype polymer models. These semiopaque plastic models were used for visualization and design verification. The computer models also were exported in International Graphics Exchange Specification (IGES) format and sent to Glenn's Thermal/Fluids Design & Analysis Branch and Applied Structural Mechanics Branch for profiling heat transfer and mechanical strength analysis.

In addition, the computer models of the design were used to produce full-scale, two-dimensional drawings, which were in turn used to manufacture negative photolithographs for high-resolution chemical etching of the many small features into the

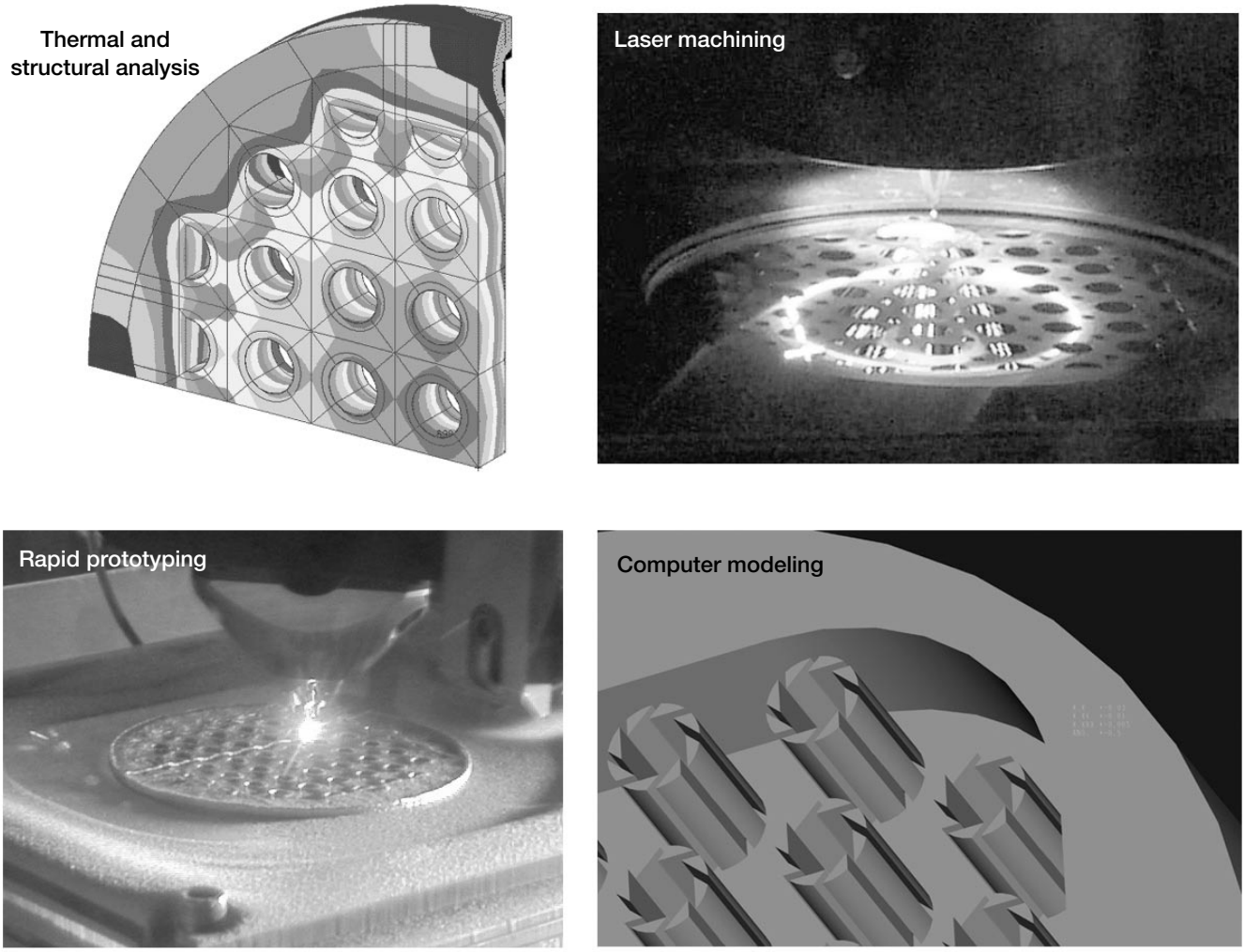

Advanced manufacturing techniques for fabricating developmental hardware.

ceramic components. However, not all of the components could be produced in this manner, which was the original goal, because of the time and budget constraints of the project. Instead, diamond core drilling was used to manufacture some larger features in the thicker sections. Also, one section of the design had many small turning vanes that had to be manufactured using electrical discharge machining, and the housing for the vanes was manufactured with computer numerical control (CNC) milling machining.

As development continued on the components, we decided to produce a working, full-scale stainless steel version to demonstrate the operation and verify the flow characteristics of the analytical models. The layers were cut from thin sheets (0.010 and 0.020 in.) of 300 series stainless steel using a 300-W yttrium-aluminum-garnet (YAG) laser cutting system. The plates received a thin copper coating on one side by a vapor deposition process called sputtering. Afterward, they were aligned and stacked on a fixture and compressed in a vacuum furnace to bond the assembly into a sealed unit.

Other components were produced using another rapid prototype process called Laser Engineered Net Shaping (LENS) which uses powdered metal fed into a laser beam and melted into a pattern of overlapping layers. The part required some secondary machining and then was ready for brazing to the rest of the system.

The planning and developing of this new hardware has only been possible through the hard work of the skilled technicians using the advanced manufacturing techniques and state-of-the-art equipment available at Glenn.

Find out more about this research:
http://www.grc.nasa.gov/WWW/EDD/

Glenn contact:
Chip Redding, 216–433–3468,
Chip.Redding@nasa.gov

Author: Chip Redding

Headquarters program office: OAT

Programs/Projects: SEC

Multiscale Extended Kalman Method Developed for Active Combustion Control

As researchers work toward drastically reducing particulate and NO_x emissions, future aeroengine combustors will likely have lean-burning front ends. However, as the ground-based gas-turbine field has experienced, lean-burning combustors are more susceptible to combustion instabilities. Thermoacoustic resonances can produce large pressure oscillations inside the combustor, leading to premature mechanical failures. Consequently, active control of combustion instabilities was identified as an enabling technology for superior engine performance. Among the

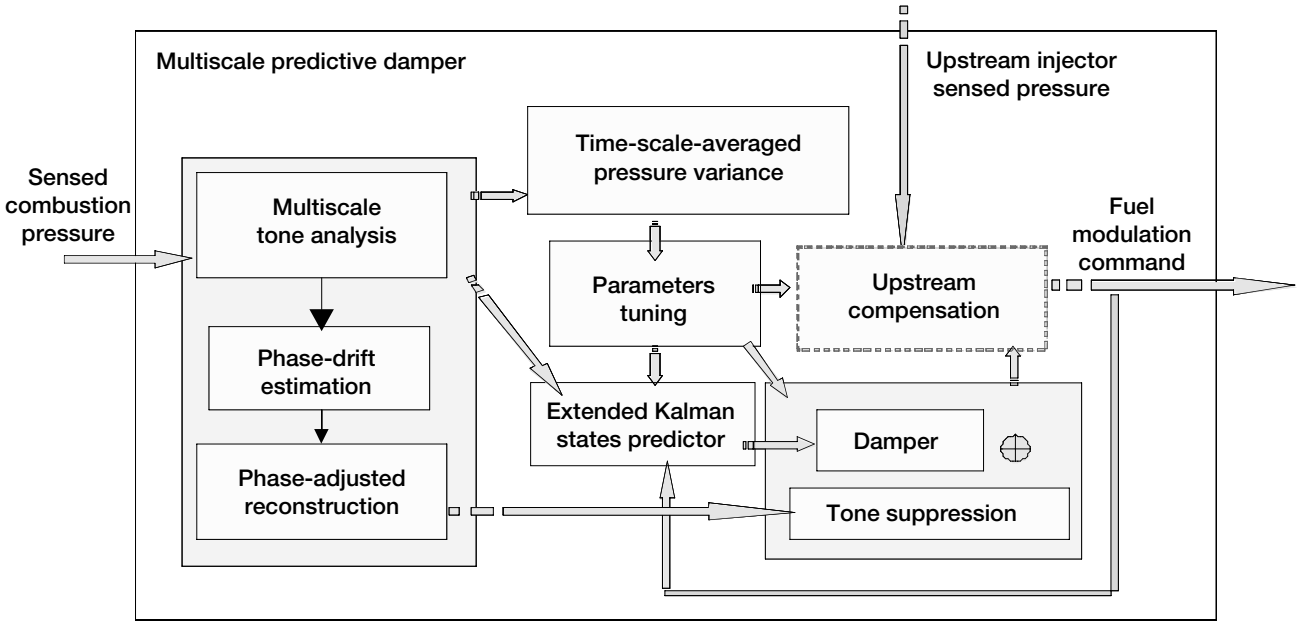

MSEK logic for combustion instability suppression by fuel modulation.

many control mechanisms investigated, properly phased fuel modulation to regulate the combustion heat release has been recognized as a very promising, and possibly the most practical way, to suppress combustion instabilities in aeroengines. Toward this end, the multiscale extended Kalman (MSEK) method—a novel, model-based control approach developed in-house at the NASA Glenn Research Center—was successfully used in the design of fuel-modulation logic for the demonstration of an active combustion control technique. The digital control logic formulated in this approach demonstrated steady suppression of a high-frequency (>500-Hz) combustion instability emulated in a liquid-fuel combustion test rig operating with realistic engine conditions.

Effective fuel modulation for combustion instabilities suppression has been known to be a very challenging control problem because of the large time delay in the fuel flow mechanism and heat-release dynamics and because of the noisy environment of the combustor. The MSEK controller (see the figure on the preceding page) combines a waveletlike multiscale analysis of combustion pressure perturbations and an extended Kalman observer (a state predictor) to predict the thermoacoustic states to make up for the severe delay in the effects of fuel modulation on heat release. The commanded fuel modulation is composed of a broadband acoustics damping action based on the predicted states, and a tone-suppression action based on an estimation of thermal excitations and other transient disturbances. The multiscale analysis logic also calculates a type of time-scale-averaged pressure variance of the combustion zone that the controller minimizes by performing automatic adjustments to the control gains and phases.

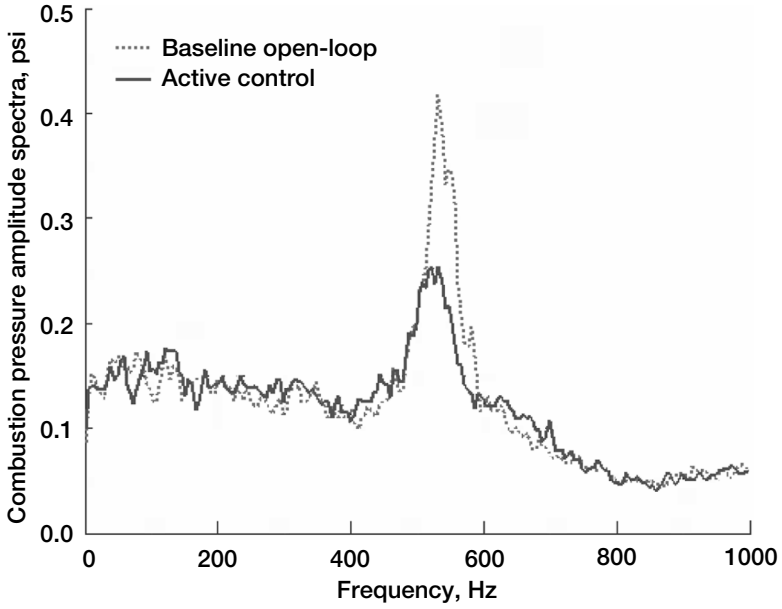

Amplitude spectra showing the effects of active combustion control by the MSEK method over the combustion instability peak pressure oscillations (Sept. 11, 2002, test).

In demonstrations of active combustion control on the rig in June and September 2002 at the United Technologies Research Center, this controller was shown to consistently perform automatic self-tuning and to suppress the oscillation amplitude peak by 30 percent (see the graph below). This accomplishment completed an important milestone in the Smart Efficient Components program being conducted by Glenn in collaboration with Pratt & Whitney and United Technologies. High-fidelity simulations done in 2003 showed that this controller could possibly suppress the instability peak down to the "noise-floor" if the background disturbances were at a (lower) level comparable to that seen in an actual, low-emission engine under study (ref. 1). It has potential applications at Glenn to lean-direct-injection combustors and can be generalized for effective model-based control of many challenging types of acoustic dynamics, structural dynamics, or even rotordynamics.

Reference

1. Le, Dzu K.; DeLaat John C.; and Chang, Clarence T.: Control of Thermo-Acoustics Instabilities: The Multi-Scale Extended Kalman Approach. NASA/TM—2003-212536 (AIAA–2003–4934), 2003. http://gltrs.grc.nasa.gov/cgi-bin/GLTRS/browse.pl?2003/TM-2003-212536-REV1.html

Find out more about this research:
http://www.grc.nasa.gov/WWW/cdtb/projects/combustor/

Glenn contacts:
Dr. Dzu K. Le, 216–433–5640, Dzu.K.Le@nasa.gov; and
John C. DeLaat, 216–433–3744, John.C.DeLaat@nasa.gov

Author: Dr. Dzu K. Le

Headquarters program office: OAT

Programs/Projects:
SEC, SRF (fiscal years 2001 to 2003)

Definitions of NASA Headquarters Program Offices

ARL U.S. Army Research Laboratories

DDF Director's Discretionary Fund at the NASA Glenn Research Center

OA Office of the Administrator

OAT Office of Aerospace Technology

- **TTPO** Technology Transfer and Parnership Office

OBPR Office of Biological and Physical Research

OES Office of Earth Science

OSF Office of Space Flight

- **SCDS** Space Communications and Data Systems
- **SCO** Space Communications Office
- Space Transportation

OSMA Office of Safety and Mission Assurance

- Safety in Operation of Ground Test Facilities

OSS Office of Space Science

Definitions of Programs and Projects

AATT	Advanced Air Transportation Technologies
AFFT	Alternate Fuels Foundation Technologies
AFCPS	Aircraft Fuel Cell Power Systems
ASTP	Advanced Space Transportation Program
AvSP	Aviation Safety Program
AVTIP	Boeing/Air Force Air Vehicles Technology Integration Program
BEGIN	Bioscience and Engineering Glenn Initiative
CICT	Computing Information and Communications Technology Program
CVCCE	Constant Volume Combustion Cycle Engine
DARPA	Defense Advanced Research Program Agency
DDF	Director's Discretionary Fund at the NASA Glenn Research Center
DOD	Department of Defense
E-cubed	Energy-Efficient Engine
ECS	Engineering for Complex Systems
EELV	Enhanced Expendable Launch Vehicle
ELNF	Efficient Low-Noise Fan
ERAST	Environmental Research Aircraft and Sensor Technology
FCF	Fluids and Combustion Facility
Gen 2	Second Generation Reusable Launch Vehicles
Gen 3	Third Generation Reusable Launch Vehicles
GUIDE	Government, Universities, and Industry Consortium
HiPEP	High Power Electric Propulsion
HOTPC	High Operating Temperature Propulsion Components
HSR	High-Speed Research
ICDPS/ICD	Intelligent Control & Diagnostics for Propulsion Systems/Intelligent Controls & Diagnostics
IHPTET	Integrated High Performance Turbine Engine Technology
ISS	International Space Station
JDRF	Juvenile Diabetes Research Foundation
JGBEC	John Glenn Biomedical Engineering Consortium
JIMO	Jupiter Icy Moons Orbiter
JWST	James Webb Space Telescope
LEAP	Low Emissions, Alternative Power Project
NEPAG	NASA Electronic Parts Assurance Group
NEXT	NASA's Evolutionary Xenon Thruster

NExTNAS	NASA Exploratory Technology for National Air Space
NGLT	Next Generation Launch Technology
NorTec	Northeast Ohio Technology Coalition
NPSS	Numerical Propulsion System Simulation
OSP	Orbital Space Plane
PR&T	Propulsion Systems Research and Technology
QAT	Quiet Aircraft Technology
QHSF	Quiet High-Speed Fan
RAC	Revolutionary Aeropropulsion Concepts
RASC	Revolutionary Aerospace Systems Concept
RLV	Reusable Launch Vehicles
RTA	Revolutionary Turbine Accelerator
SCDS	Space Communications and Data Systems Project
SEC	Smart Efficient Components
SLEP	Service Life Extension Program
SLI	Strategic Launch Initiative
SRF	Glenn's Strategic Research Fund
SRG	Stirling Radioisotope Generator
SSP	Space Solar Power
TBCC	Turbine-Based Combined Cycle
TGIR	Turning Goals Into Reality
TTPO	Technology Transfer and Partnership Office
UEET	Ultra-Efficient Engine Technology
Ultra Safe	Ultra Safe Propulsion
VAATE	Versatile, Affordable, Advanced Technology Engine
VSP	Vehicle Systems Program

Index of Authors and Contacts

Both authors and contacts are listed in this index. Articles start on the page numbers following the names.

X

Y

Z

REPORT DOCUMENTATION PAGE

Form Approved
OMB No. 0704-0188

1. AGENCY USE ONLY (*Leave blank*)	2. REPORT DATE	3. REPORT TYPE AND DATES COVERED
	May 2004	Technical Memorandum

4. TITLE AND SUBTITLE

Research & Technology 2003

5. FUNDING NUMBERS

None

6. AUTHOR(S)

7. PERFORMING ORGANIZATION NAME(S) AND ADDRESS(ES)

National Aeronautics and Space Administration
John H. Glenn Research Center at Lewis Field
Cleveland, Ohio 44135–3191

8. PERFORMING ORGANIZATION REPORT NUMBER

E–14254

9. SPONSORING/MONITORING AGENCY NAME(S) AND ADDRESS(ES)

National Aeronautics and Space Administration
Washington, DC 20546–0001

10. SPONSORING/MONITORING AGENCY REPORT NUMBER

NASA TM—2004-212729

11. SUPPLEMENTARY NOTES

Responsible person, Walter S. Kim, organization code 9400, 216–433–3742.

12a. DISTRIBUTION/AVAILABILITY STATEMENT

Unclassified - Unlimited
Subject Categories: 01 and 31 Distribution: Nonstandard

Available electronically at http://gltrs.grc.nasa.gov
This publication is available from the NASA Center for AeroSpace Information, 301–621–0390.

12b. DISTRIBUTION CODE

13. ABSTRACT ***(Maximum 200 words)***

This report selectively summarizes NASA Glenn Research Center's research and technology accomplishments for fiscal year 2003. It comprises 170 short articles submitted by the staff scientists and engineers. The report is organized into four major sections: Aeronautics, Research and Technology, Space, and Engineering and Technical Services. A table of contents and author index have been developed to assist readers in finding articles of special interest. This report is not intended to be a comprehensive summary of all the research and technology work done over the past fiscal year. Most of the work is reported in Glenn-published technical reports, journal articles, and presentations prepared by Glenn staff and contractors. In addition, university grants have enabled faculty members and graduate students to engage in sponsored research that is reported at technical meetings or in journal articles. For each article in this report, a Glenn contact person has been identified, and where possible, a reference document is listed so that additional information can be easily obtained. The diversity of topics attests to the breadth of research and technology being pursued and to the skill mix of the staff that makes it possible. For more information about research at Glenn, visit us on the World Wide Web (http://www.grc.nasa.gov). This document is available online (http://www.grc.nasa.gov/WWW/RT). For publicly available reports, visit the Glenn Technical Reports Server (http://gltrs.grc.nasa.gov).

14. SUBJECT TERMS	15. NUMBER OF PAGES
Aeronautics; Aerospace engineering; Space flight; Space power; Materials; Structures; Electronics; Space experiments	261
	16. PRICE CODE

17. SECURITY CLASSIFICATION OF REPORT	18. SECURITY CLASSIFICATION OF THIS PAGE	19. SECURITY CLASSIFICATION OF ABSTRACT	20. LIMITATION OF ABSTRACT
Unclassified	Unclassified	Unclassified	